THE JOURNAL
OF
CHEMICAL PHYSICS

VOLUME 18, NUMBER 9 SEPTEMBER, 1950

Notice

Formation of a Division of Chemical Physics in the American Physical Society

IN 1945 the Council of the American Physical Society appointed a committee to organize a Division of Chemical Physics, but for various reasons the committee did not act. At its February, 1950, meeting the Council again appointed the same persons (O. Beeck; F. G. Brickwedde; J. E. Mayer; O. K. Rice; R. S. Mulliken, *Chairman*) as a new Organizing Committee. Subsequent to the recent greatly regretted death of Dr. Beeck, the committee has been enlarged by the addition of J. G. Kirkwood and H. H. Nielsen.

As stated in the draft of a set of by-laws drawn up by the committee for submission to the Council at its next meeting: "The principal objective of the new Division shall be the advancement of understanding in subjects of chemical interest whose development depends strongly on modern physical theories or techniques."

The draft by-laws further state: "The Members of the Division shall consist of *those Members and Fellows of the Physical Society* who have made written application for enrollment in the Division and have paid an initiation fee of two dollars. Application for membership together with initiation fee shall be sent to the Treasurer of the Division." Pending the appointment of a Treasurer, applications for membership accompanied by initiation fee may be sent to R. S. Mulliken, Physics Department, University of Chicago, Chicago 37, Illinois. Interested persons who are *not now* members of the American Physical Society should first seek the sponsorship of two members of the Society for nomination to membership. (Nomination blanks can be secured from K. K. Darrow, Secretary of the American Physical Society, Columbia University, New York 27, New York.) Members of the Physical Society are entitled to obtain *The Journal of Chemical Physics* at reduced subscription rates. For the present, no annual dues are contemplated for membership in the Division of Chemical Physics, but only an initiation fee.

According to present tentative plans, the inaugural meeting of the Division will be held as a part of the Pittsburgh meeting of the American Physical Society in March, 1951; it will comprise a symposium on molecular structure and valence theory, and symposia on other topics involving statistical mechanics. Prospective members are invited to make suggestions as to speakers and topics for these symposia; these should be sent promptly to Dr. Mulliken with the applications for enrollment.

Since the Division is in a formative stage, its precise scope is still under discussion. Proposals have been made that it should include "appropriate aspects of such subjects as the following: chemical binding and valence phenomena, chemical kinetics, chemical thermodynamics and statistical mechanics, optical, dielectric, and magnetic properties of molecules and crystals, molecular spectra of all kinds from Raman and radiofrequency to vacuum ultraviolet spectra, mass spectroscopy of molecules, radiation chemistry, isotopic and other exchange phenomena, and radiochemistry". Interested persons are invited to communicate their views on the proper scope of the Division when they apply for enrollment.

The Thermodynamics of Some Non-Isothermal Systems

L. DALLAS TUCK
The University of California College of Pharmacy, San Francisco, California
(Received May 22, 1950)

The thermodynamic theory of non-isothermal systems of liquid solutions is treated by the method of Tolman and Fine, which method includes consideration of the irreversible processes in calculating the conditions of the steady state.

The concept *entropy of transfer* of a dissolved molecule is discussed in terms of the interaction of the molecule with the solution. The method of Tolman and Fine is then applied in the derivations of the Soret "equilibrium" and the e.m.f. of a thermocell. It is shown that the irreversible transport of heat down the temperature gradient has no effect upon the steady-state conditions, even for finite values of the gradient.

I. INTRODUCTION

THERE are a number of relations referring to non-isothermal systems which have been derived by appeal to the equilibrium form of the laws of thermodynamics, or "thermostatics," as Eckart has dubbed it.[1] These include the Kelvin treatment of the thermoelectric effect and Eastman's treatments of the Soret equilibrium and thermocell electromotive force.

As has been pointed out frequently, these derivations involve the assumption, foreign to classical thermodynamics, that the final "equilibrium" state is independent of irreversible processes which may be occurring owing to the incomplete state of equilibrium.[1–6] Yet at the same time, the derivations seem to arrive at the right answers, furnishing empirical justification for ignoring the irreversible processes.[5,7]

The thermostatic method is based on the rigorous conditions of equilibrium, which may be expressed by the equalities,

$$\Sigma dE=0, \quad \Sigma dS=0, \tag{1}$$

where dE and dS represent virtual variations of all energies and entropies. In the case of the non-existence of thermal equilibrium a condition corresponding to these equations is impossible to obtain without ignoring irreversible effects. This means that any virtual process occurring must correspond to a conservation of energy but an increase of entropy in accordance with the non-equilibrium conditions of Clausius,

$$\Sigma dE=0, \quad \Sigma dS>0. \tag{2}$$

Tolman and Fine[8] have shown that the inequality in some particular cases of non-equilibrium processes may be replaced by an equality by including the appropriate irreversible increases in entropy, dS_{irr}. We may express the inequality in (2) by the equation

$$\Sigma dS=\Sigma dS_{irr}. \tag{3}$$

In what follows, we shall refer to Eq. (3) as the Second Law equation. The First Law of Thermodynamics has the form

$$\Sigma dE=0 \tag{3a}$$

with emphasis on the requirement that it must include the energies of both reversible and irreversible processes, in contrast with the usual application to non-isothermal systems.

In the present study we derive expressions for the electromotive force of a thermocell and Soret equilibrium, both of which require the understanding of the concept of the *entropy of transfer*. We discuss first the latter, in which the entropy of transfer figures in a more direct way.

II. SORET EFFECT AND ENTROPY OF TRANSFER

If two vessels originally containing the same solution are joined by a bridge of the solution, and each is held at a different temperature, in general diffusion of the solute will occur until the relative concentrations reach a steady-state characteristic of the temperature interval (and the average concentration and temperature). The steady state is called the "Soret equilibrium," though it was first described by Ludwig in 1856.[9] The more general term "thermal diffusion" includes the whole field of processes involving diffusion induced by a thermal gradient, whether in gas, liquid, or solid. The Soret effect, on the other hand, signifies thermal diffusion in liquid solutions. It excludes systems complicated by convection or other effects arising from external forces, such as the Clusius-Dickel process. This is not to imply that it is a trivial special case, however,

[1] C. Eckart, Phys. Rev. **58**, 267 (1940).
[2] L. Boltzmann, Sitz. Ber. Akad. Wiss. Wien, Math.-naturw. Klasse, Abt. II, **96**, 1258 (1887).
[3] N. Bohr, "Studier over Metallernes Elektronteori," Dissertation, Copenhagen, 1911, p. 72.
[4] L. Onsager, Beretn. Skand. Naturforskermøde, 18th meeting, Copenhagen, 1929, pp. 440–1; Phys. Rev. **37**, 405 (1931); **38**, 2265 (1931).
[5] P. W. Bridgman, *The Thermodynamics of Electrical Phenomena in Metals* (Macmillan Company, New York, 1934), pp. 49–50; *The Nature of Thermodynamics*, (Harvard University Press, Cambridge, 1941), pp. 133–140.
[6] H. B. G. Casimir, Rev. Mod. Phys. **17**, 343 (1945).
[7] Another point of view, not inconsistent with ours, is expressed in the derivations by the principle of microscopic reversibility, referred to in references 4 and 6.
[8] R. C. Tolman and P. C. Fine, Rev. Mod. Phys. **20**, 51 (1948).
[9] C. Ludwig, Sitz. ber. Akad. Wiss. Wien **20**, 539 (1856); C. Soret, Ann. chim. et phys. (5) **22**, 293 (1881); see also historical note and bibliography in S. R. De Groot, "L'Effet Soret," thesis, Amsterdam, 1945.

for the Soret effect is the unit process upon which the theory of all liquid thermal diffusion is based.

A thermodynamic study of the Soret effect was first made by Eastman[10] and again by Wagner,[11] the latter on the basis of a thermodynamic cycle. More recently an independent derivation was developed on the basis of microscopic reversibility by De Groot.[12] The present derivation is an application of the method of Tolman and Fine.[8]

As will be shown below, the existence of a concentration gradient due to the temperature gradient hinges on the existence of a quantity S^*, which Eastman called *entropy of transfer*; we discuss this concept below in some detail.

Entropy of Transfer

The entropy of transfer is a property of a dissolved molecule derivable from certain energy phenomena which occur when it diffuses from one region in the solution to another. The molecule which is of interest is the entity which actually diffuses through the solution, the solvated molecule, which is not necessarily the bare solute molecule.

This aspect has been emphasized by Eastman in his discussion of the nature of the entropy of transfer.[10] While he discussed the case of an ion in water the effect will be qualitatively the same (though perhaps not so striking) in the case of a non-electrolyte solute.

Thus, in what follows, when we speak of the diffusing molecule, we refer to the entire diffusing ensemble. It may be argued that the thermal forces will constantly be adding or removing solvent molecules and that the solvated molecule will not be the same from one moment to the next. This creates no difficulty, for we can, in principle at least, consider a statistical model which simulates the behavior of the actual diffusing molecule.

The "internal" energy of a dissolved molecule in the thermodynamic sense may be considered to consist of two parts. First, there are the kinetic and potential energies of the (solvated) molecule caused by its translational, rotational, and vibrational energy states. And second, there are the potential energies due to long-range intermolecular forces such as van der Waals' forces between the solute and solvent molecules, the energy of interaction of dipolar solute molecules with one another, the electrostatic energy in the case of ions due to the alignment of the surrounding dipolar solvent molecules, the Debye and Hückel-type energy of interaction of an ion with its ion-atmosphere, etc. When the solute moves from one region of a solution to another, the first type of energy remains with the solute molecule. The second type, on the other hand, since it is due to an interaction of the molecule with the body of the solution, is subject to a relaxation upon the removal of the molecule and its long-range field effects.

Because of the adjustments of the potential energy there are changes in the entropy of the system. If we think about these in the customary way in terms of the freedom of the system, it is apparent that the entropy effects in which we are interested, *viz.* those corresponding to the long-range forces, are due to alteration in the freedom of motion of the solvent molecules or of the solution as a whole surrounding the solute molecules.[13] This is analogous to the cooling effect which accompanies demagnetization, except that in the latter there is negligible interaction among the atomic magnets. The complication due to the interaction of the electrical dipoles (permanent or induced) of the solvent molecules makes it difficult to predict *a priori* even the sign of the present effect.

If the field of the solute molecule reduces the freedom of the surrounding molecules then upon relaxation, energy will be absorbed by the region of the solution in question. Conversely, if the presence of the field causes on the whole an increase in their freedom, upon removal of the solute molecule heat will be evolved.

The latter case is difficult to imagine if we think of the solvent as made up of independent molecules. In any actual liquid solvent, however, the interaction between molecules is considerable, and the net effect of the solute will be the sum of the decreases in entropy due to alignment of the solvent in its field and an increase due to the breaking up of the associations which undoubtedly exist, particularly in polar liquids.[14,15]

It should be noted, as Rice has done in a similar connection, that the entropy effect in question should contain no contribution from restriction of the freedom of the ion (or molecule) itself, but only from that part "that is due to the effect of the ions [molecules] on the solvent."[16]

Let us picture the mechanism of transfer of a molecule from one region to another. We know that between jumps a molecule (of the same approximate size as the solvent molecule) will vibrate many thousand times in a "cage" of solvent molecules and will move only when a "hole" is vacated by one of them.[17] Such a process obviously requires a kinetic energy of activation. This energy of activation in general may include in part the long-range effects listed in an earlier paragraph. There will be additional energy terms owing to the necessity of breaking liquid bonds between solvent molecules.

---

[10] E. D. Eastman, J. Am. Chem. Soc. **48**, 1482 (1926); **50**, 283 (1928); see also criticism by W. Rodebush and reply *ibid.* **49**, 792 (1927).

[11] C. Wagner, Ann. der Physik (5) **3**, 629 (1929); **6**, 370 (1930).

[12] S. R. De Groot, J. phys. radium (8) **8**, 193 (1947).

[13] An excellent elementary discussion germane to this point is given in O. K. Rice, *Electronic Structure and Chemical Binding* (McGraw-Hill Book Company, Inc., New York, 1940), Chapter 19.

[14] H. S. Frank and M. W. Evans, J. Chem. Phys. **13**, 507 (1945).

[15] A. Eucken, Nachr. Akad. Wiss. Göttingen, Math.-Phys. Klasse, 1947, p. 33; Zeits. f. Elektrochemie **51**, 6 (1948); **52**, 255 (1948); **53**, 102 (1949).

[16] A. Eucken, Zeits. f. Elektrochemie **53**, 412 (1949).

[17] M. J. Polissar, J. Chem. Phys. **6**, 833 (1938); Glasstone, Laidler, and Eyring, *Theory of Rate Processes* (McGraw-Hill Book Company, Inc., New York, 1941).

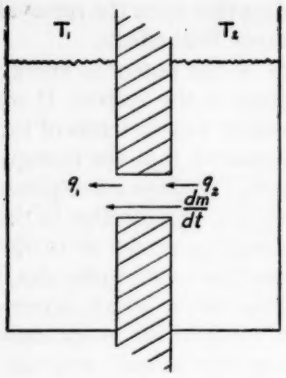

FIG. 1. Schematic diagram of a Soret cell, indicating the conventional rates of flow of heat and solute.

The activation energy may be thought of as an energy absorbed from the surroundings *before* the transfer occurs. The entropy effects considered in the previous paragraph are effects which occur *after*. Though they may in some details involve breaking or relaxing the same forces, the activation effect involves directly energy terms, while the "after" effects are fundamentally entropy terms, i.e. terms dependent upon the temperature coefficient of energy terms. This is true because the transfer occurs reversibly, in which case the heat absorbed is the product of gain in entropy for the process and the temperature.

When there is a net diffusion from one region to another, there will be a net heat effect caused by the sum of the two contributions mentioned. It is this sum to which we refer as the "heat of transfer."[18]

We imagine a vessel S containing a solution at temperature T in thermal equilibrium with a reservoir R of infinite heat capacity. Assume that the solute molecules diffuse out through a thermally insulating plug into a region in thermal equilibrium with a second heat reservoir.

We define the heat of transfer of the solute Q^* as the heat absorbed by the system S from the reservoir R for each mole of solute diffusing out of system S. The entropy of transfer is then defined by the quotient Q^*/T.

It follows conversely, of course, that the amount of heat *absorbed by* the region from which the molecule diffuses is *evolved by* the region into which it diffuses, provided that the conditions of temperature and concentration (and other variables) are identical with those in the original system.

The presence of the insulating plug is actually not necessary to the definition. It is used in the above discussion to emphasize that heat effects outside the region of S are not to be included in the concept of entropy of transfer. In any actual case, superimposed upon the entropy of transfer effect there will be an additional effect due to the conduction of heat down thermal gradients. As will be shown presently, this irreversible effect has no influence on the final condition of equilibrium.

[18] H. J. V. Tyrrell and G. L. Hollis (Trans. Faraday Soc. **45**, 411 (1949)) have treated the heat of transfer as made up entirely of the energy of activation. This does not seem to this author to be valid.

The Soret Effect

Consider a cell of the type illustrated schematically in Fig. 1, placed such that each side is in perfect thermal contact with a thermostat of infinite heat capacity, where $T_2 > T_1$. We shall now calculate the conditions of the steady state from Eqs. (3) and (3a), rewritten as time derivatives:

$$\frac{dE_R}{dt}+\frac{dE_S}{dt}=0, \quad \frac{dS_R}{dt}+\frac{dS_S}{dt}=\frac{dS_{irr}}{dt}. \tag{4a, b}$$

The processes which occur in the cell are the following: (1) the solute may diffuse from one side of the cell to the other, and (2) heat flows from T_2 to T_1.

The heat exchange between the cell and the reservoir must include that due to the entropy of transfer as well as that which flows down the gradient. Assuming a diffusion of solute from T_2 to T_1 the energy absorbed per unit time *from* the reservoir at T_2 may be expressed as

$$q_2+Q_2^*(dm/dt),$$

where q_2 is the rate of heat flow into the bridge at the hot end, Q_2^* is the heat of transfer under the conditions existing at T_2, and dm/dt represents the rate of diffusion of the solute (e.g., in moles per second). The rate of heat *gained* by the low temperature half of the reservoir is

$$q_1+Q_1^*(dm/dt),$$

q_1 being taken as the rate of heat flow out of the bridge at the cold end. The difference of these two terms represents the net rate of gain of energy of the heat *reservoirs*,

$$dE_R/dt=q_1-q_2+(Q_1^*-Q_2^*)(dm/dt). \tag{5}$$

This expression may be simplified by noting that the rate of heat flow q past an arbitrary point in the gradient increases in accordance with the differential equation,

$$dq=-d\bar{H}(dm/dt), \tag{6a}$$

or the integral form

$$q_1-q_2=(dm/dt)(\bar{H}_2-\bar{H}_1), \tag{6b}$$

$\bar{H}$ being the partial molal heat content of the solute. Equation (5) then becomes

$$\begin{aligned} dE_R/dt&=(Q_1^*-Q_2^*+\bar{H}_2-\bar{H}_1)(dm/dt)\\ &=(T_1S_1^*-T_2S_2^*+\bar{H}_2-\bar{H}_1)(dm/dt). \end{aligned} \tag{7}$$

The rate of gain of energy of the *system*, which consists in the contents of the cell, may be calculated from the initial and final states. At constant pressure this is

$$dE_S/dt=(\bar{H}_1-\bar{H}_2)(dm/dt). \tag{8}$$

From (4a), (7), and (8) we obtain for the consequence

of the First Law of Thermodynamics

$$T_1S_1^*-T_2S_2^*=0, \tag{9}$$

which has the differential form

$$d(TS^*)=TdS^*/dT+S^*=0. \tag{10}$$

Equations (9) and (10) do not imply that $Q_1^*=Q_2^*$ for the two temperatures in a solution of uniform concentration. Rather, the implication is that at Soret equilibrium the concentration so adjusts its gradient that this condition applies. That is, Eq. (10) implies only

$$(\partial Q^*/\partial c)dc+(\partial Q^*/\partial T)dT=0.$$

Evaluation of the left side of Eq. (4b) is similar to the above, leading to

$$dS_R/dt+dS_S/dt=q_1/T_1-q_2/T_2 +(S_1^*-S_2^*+\bar{S}_1-\bar{S}_2)(dm/dt). \tag{11}$$

Since each half of the cell taken by itself is isothermal and otherwise homogeneous and in thermal equilibrium with the reservoir, no irreversible processes occur except those in the thermal (and concentration) gradient. We must examine the gradient for evaluation of the term on the right side of Eq. (4b).

The two processes occurring in the gradient (in the absence of convection or other purely mechanical processes) are the diffusion of the solute and the flow of heat. The former process is reversible, as we may consider our system to be infinitely near to the steady-state concentration gradient. The heat flow under the constraint of a temperature gradient is irreversible, and in this case it is the only irreversible process.

In each element of the gradient the rate of production of entropy is expressed[8] by $(q/T^2)dT$, where q is the rate of heat flow past an arbitrary point in the gradient. The total rate of irreversible entropy production must then be obtained by integration over the temperature integral,

$$\frac{dS_{irr}}{dt}=\int_{T_1}^{T_2}\frac{q}{T^2}dT=-\int_{T_1}^{T_2}d\left[\frac{q}{T}\right]+\int_{T_1}^{T_2}\frac{dq}{T},$$

which by Eq. (6a) becomes

$$=q_1/T_1-q_2/T_2-(dm/dt)\int_{T_1}^{T_2}(d\bar{H}/T). \tag{12}$$

Combining (4b), (11), and (12) we obtain the integral equation of the Second Law,

$$S_1^*-S_2^*+\bar{S}_1-\bar{S}_2=-\int_{T_1}^{T_2}(d\bar{H}/T) \tag{13}$$

$$S_2^*-S_1^*=-\int_{T_1}^{T_2}\left(d\bar{S}-\frac{d\bar{H}}{T}\right)=\int_{c_1}^{c_2}\frac{1}{T}\frac{\partial\bar{F}}{\partial c}dc, \tag{13a}$$

whose differential form is

$$\frac{dS^*}{dT}=\frac{1}{T}\frac{\partial\bar{F}}{\partial c}\frac{dc}{dT}. \tag{14}$$

It is to be noted that the integral equation of neither (9) nor (13) contains terms in q; they are thereby proved to be independent of the irreversible heat flow down the temperature gradient. These equations may be combined to produce an equation for the Soret equilibrium for a finite temperature gradient, whose evaluation requires only the knowledge of the activity coefficient of the solute as a function of temperature and concentration in the region of the gradient. The resulting equations are of the form

$$S_1^*/T_2=S_2^*/T_1=\frac{-1}{T_2-T_1}\int_{c_1}^{c_2}\frac{1}{T}\frac{\partial\bar{F}}{\partial c}dc \tag{15}$$

in terms of the concentration coefficient of the partial molal free energy. Evidently when T_2 approaches T_1 these two equations approach the same equation,

$$(\partial\bar{F}/\partial c)(dc/dT)=-S^*, \tag{16}$$

which also follows from (10) and (14).

This is the equation derived by Eastman using thermostatic methods. This equation is not yet in terms of the usual measured Soret coefficient, $-(1/c)(dc/dT)$. Where thermodynamic activities of the solute are available, the Soret coefficient may be expressed in the form

$$K_s=-\frac{1}{c}\frac{dc}{dT}=\frac{S^*}{cRT(d\log a/dc)}. \tag{17}$$

For a solute whose activity coefficient is independent of the concentration, (e.g., in infinitely dilute solutions) the Soret coefficient turns out to have the following simple forms: For a non-dissociating solute it is S^*/RT. For the general case of a solute which dissociates in solution into N molecules (ions) the coefficient is simply S^*/NRT, where S^* is now defined as

$$S^*=\Sigma_i n_i S_i^*,$$

corresponding to the chemical equation of the dissocia-

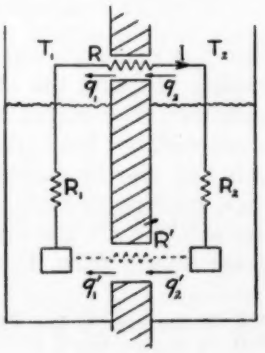

FIG. 2. Schematic diagram of a thermocell, indicating the conventional flow of positive current and heat.

tion,

$$M=\Sigma_i n_i M_i,$$

where M_i stands for the chemical formula of the ith component, and n_i is its coefficient in the chemical equation.

In the general case the Soret coefficient is related to the entropy of transfer through partial derivatives of the activity coefficient with respect to concentration. For the simple non-dissociating solute it is

$$K_s=S^*/RT(1+c(\partial \log\gamma/\partial c)),$$

while for the general case it becomes

$$K_s=\frac{S^*}{RT\left[N+\sum_i c_i\frac{\partial \log\gamma_i}{\partial c}\right]}, \tag{18}$$

which at infinite dilution becomes

$$K_{s0}=S_0^*/NRT.$$

The Soret coefficient for a finite gradient may easily be derived from Eq. (15). It appears to be of no particular value, practical or theoretical. Our purpose in carrying the integral form as far as we did was to show the independence of the steady state upon incidental irreversible processes.

III. THERMOCELL E.M.F.

By a *thermocell* we mean a galvanic cell composed of identical half-cells, deriving its electromotive force from the fact that the two halves are at different temperatures.[10,19] As an example we use a cell of the type

$$\underset{T_1\cdots\cdots T_2}{\mathrm{Ag|AgCl|\ 0.01}\ m\ \mathrm{NaCl\ |AgCl|Ag}},$$

where the dotted line represents a temperature gradient within the otherwise uniform solution.

If effects occurring at the temperature gradient due to the transfer of ions could be ignored, the electromotive force of the cell would measure the entropy of the half reaction

$$\mathrm{Ag}+\mathrm{Cl}^-=\mathrm{AgCl}+e^-,$$

i.e.

$$f(d\epsilon/dT)=\Delta S=S_{\mathrm{AgCl}}+\bar{S}_e-S_{\mathrm{Ag}}-\bar{S}_{\mathrm{Cl}^-}, \tag{19}$$

where f is Faraday's constant, $d\epsilon$ is the e.m.f. of the complete cell, and the other terms have their usual significance. The partial molal entropy of electrons in the silver $\bar{S}_e$ has been calculated from Thomson coefficients and also by considerations of electron-gas statistical mechanics; both methods yield a value of the order of 0.05 e.u.[20] The entropies of the solids AgCl and Ag are known from Third Law measurements. This means that the measured e.m.f. would yield by difference the partial molal entropy of chloride ion for the solution in question.

Tabulated values of $\bar{S}$ for individual ions are always based on the convention that the $\bar{S}$ for hydrogen ion is zero. It is easy to see that the value derivable from Eq. (19) depends on no such assumption and would thus be an absolute partial molal entropy.

Unfortunately for the simplicity of the system, the reversible effects due to transfer across the temperature gradient add an extra term to Eq. (19) which is a function of the transfer of the ions present. Ignoring irreversible effects, Eastman found the expression for the e.m.f. to be

$$f(d\epsilon/dT)=\Delta S+\Delta S^*, \tag{20}$$

where ΔS^* is the net entropy of transfer accompanying a virtual transfer of one faraday of (positive) electricity up the temperature gradient in the circuit external to the cell. It is defined for a binary electrolyte solution by

$$\Delta S^*=t_c S_c^*-t_a S_a^*, \tag{21}$$

where the t's are transference numbers and a and c refer, respectively, to anion and cation.

As we have argued in an earlier paragraph, the neglect of irreversible effects appears to be justifiable. This section is devoted to a proof of this assertion in the case of thermocell electromotive force.[21]

Placing our thermocell in the usual way in contact with two infinite heat reservoirs, one at temperature T_2, the other at $T_1(<T_2)$, for simplicity we insulate thermally the electrolytic bridge and the wire joining the two electrodes, as indicated schematically in Fig. 2. We shall lump the various electrical resistances in the cell shown letting R_1 and R_2 represent, respectively, the total resistances in each half cell, exclusive of those in the temperature gradient, the latter being represented by R and R', where the primed quantity refers to the resistance in the electrolytic bridge.

Consider first the energy of the heat reservoir. Let q_2 be the heat conducted into the wire per unit time at T_2 and q_1 that *flowing out* at T_1 due to the temperature gradient. Let q be the rate of heat flow through the wire at an arbitrary point in the gradient. Assuming the electric current to travel up the temperature gradient (which is the same as assuming the half-reaction to go forward at the higher temperature), the Thomson effect causes the current to absorb heat reversibly from q at the rate of $I\sigma dT$ for each element in the gradient. At the same time the resistance of each element of wire in the gradient will cause an irreversible dissipation of power I^2dR, which will tend to increase q_1 over q_2.[8] Hence, the heat delivered at T_1 will differ from that

[19] E. D. Eastman, J. Am. Chem. Soc. **50**, 292 (1928).
[20] R. G. Preston and L. D. Tuck, unpublished calculations.
[21] This proof first appeared in the author's doctoral thesis, University of California, 1948. It is somewhat modified and improved in this report.

absorbed at T_2 by the amount

$$q_1-q_2=\int_{T_2}^{T_1} dq=\int_{T_2}^{T_1}(I^2dR+I\sigma dT)$$

$$=I^2R+\int_{T_2}^{T_1} I\sigma dT. \quad (22)$$

A similar consideration of the mechanism of electrical and thermal transport at the electrolytic bridge, where the Thomson coefficient is replaced by the partial molal specific heats of the transferred ions, yields

$$q_1'-q_2'=\int_{T_2}^{T_1}\left(I^2dR'-\frac{I}{f}\Delta\bar{C}dT\right)$$

$$=I^2R'-\int_{T_2}^{T_1}\frac{I}{f}\Delta\bar{C}dT. \quad (22a)$$

In this equation $\Delta\bar{C}$ represents the expression

$$t_c\bar{C}_c-t_a\bar{C}_a,$$

where the t's are the transference numbers of the respective ions and the $\bar{C}$'s are their partial molal specific heats. Because of the molal character of $\bar{C}$ it is necessary to express the current in "moles of electricity" per second by dividing the current in amperes by Faraday's constant.

To the above heat effects we add the heat *evolved* at the electrodes during the reversible electrode reaction, *viz.*, $T_1\Delta S_1$ at T_1 and $-T_2\Delta S_2$ at T_2. We shall add a further heat effect due to the heat of transfer, which has been defined and discussed in a previous section. The heat evolved by the solution at T_1 is expressed as $T(t_cS_c^*-t_aS_a^*)$, or by Eq. (21), $T_1\Delta S_1^*$. The corresponding effect at T_2 is $-T_2\Delta S_2^*$. Add also the heat dissipated in R_1 and R_2.

The rate of gain of energy of the reservoir may thus be expressed as

$$dE_R/dt=q_1-q_2+q_1'-q_2'+T_1\Delta S_1 -T_2\Delta S_2+T_1\Delta S_1^*-T_2\Delta S_2^*+I^2(R_1+R_2).$$

By consideration of Eqs. (22) and (22a)

$$dE_R/dt=I^2(R_1+R_2+R+R')+I\int_{T_2}^{T_1}\left(\sigma-\frac{\Delta\bar{C}}{f}\right)dT$$

$$+\frac{I}{f}(T_1\Delta S_1-T_2\Delta S_2+T_1\Delta S_1^*-T_2\Delta S_2^*).$$

Since the total reaction which occurs when a faraday of electricity passes through the cell must include materials transferred in the process as well as the chemical reaction at the electrodes, we obtain for the net rate of gain of the system

$$dE_S/dt=(I/f)(\Delta H_2-t_c\bar{H}_{c2}+t_a\bar{H}_{a2}) -(\Delta H_1-t_c\bar{H}_{c1}+t_a\bar{H}_{a1}).$$

Noting that

$$\int_{T_1}^{T_2}\Delta\bar{C}dT=t_c(\bar{H}_{c2}-\bar{H}_{c1})-t_a(\bar{H}_{a2}-\bar{H}_{a1})$$

and

$$\Delta\epsilon=I(R+R'+R_1+R_2),$$

where $\Delta\epsilon$ is the electromotive force of the circuit, we obtain what appears to be the simplest integral equation resulting from application of the First Law,

$$-f\Delta\epsilon=\Delta F_2-\Delta F_1-T_2\Delta S_2^*+T_1\Delta S_1^*-\int_{T^1}^{T_2}\sigma f dT. \quad (23)$$

Differentiation produces the corresponding differential equation

$$f(d\epsilon/dT)=\Delta S+\frac{d(T\Delta S^*)}{dT}+f\sigma$$

$$=\Delta S+\Delta S^*+T(d\Delta S^*/dT)+f\sigma. \quad (24)$$

We now proceed to consideration of the terms going into the equation of the Second Law, Eq. (4b).

The ΔS_S term is simply the total change of entropy of the system,

$$(I/f)[\Delta S_2-\Delta S_1-t_c(\bar{S}_{c2}-\bar{S}_{c1})+t_a(\bar{S}_{a2}-\bar{S}_{a1})].$$

The ΔS_R term is also simple; it includes entropy changes arising from heat furnished in the two reservoirs. At T_2 these total

$$(1/T_2)[-q_2-(I/f)(\Delta S_2+\Delta S_2^*)T_2-q_2'+I^2R_2] \quad (25a)$$

while at T_1 they give

$$(1/T_1)[q_1+(I/f)(\Delta S_1+\Delta S_1^*)T_1+q_1'+I^2R_1]. \quad (25b)$$

Somewhat more complicated are the irreversible entropy increases. They include first of all the two I^2R terms caused by R_1 and R_2. The other irreversible entropy effects occur in the temperature gradient.

Considered in each element of the gradient, the irreversible entropy increase includes (a) the entropy increase due to the dissipated ohmic power (I^2dR/T), and (b) the entropy increase due to the irreversible passage of heat down the gradient dT, which at variable T in the gradient amounts to $-(q/T^2)dT$. The entropy increase in the wire, integrated over the interval, is

$$\int_{T_2}^{T_1}\left(\frac{I^2dR}{T}-\frac{q}{T^2}dT\right).$$

By the differential form of Eq. (22) we may eliminate dR to get

$$\int_{T_2}^{T_1}\left(\frac{dq}{T}-\frac{q}{T^2}dT-\frac{I\sigma}{T}dT\right).$$

The first two terms of the integrand reduce to the exact differential $d(q/T)$, leading to

$$\frac{q_1}{T_1}-\frac{q_2}{T_2}+\int_{T_1}^{T_2}\frac{I\sigma}{T}dT. \quad \text{(Note reversal of limits.)}$$

With similar considerations as regards the electrolyte bridge we obtain for the total irreversible entropy increase

$$\frac{dS_{irr}}{dt}=I^2\left(\frac{R_2}{T_2}+\frac{R_1}{T_1}\right)-\frac{q_2}{T_2}+\frac{q_1}{T_1}-\frac{q_2'}{T_2}+\frac{q_1'}{T_1}+\int_{T_1}^{T_2}\left(I\sigma-\frac{I}{f}\Delta\bar{C}\right)\frac{dT}{T}. \quad (26)$$

We are now ready to write our complete Second Law equation from Eq. (4b), making the obvious cancellations,

$$(I/f)[-t_c(\bar{S}_{c2}-\bar{S}_{c1})+t_a(\bar{S}_{a2}-\bar{S}_{a1})-(\Delta S_2^*-\Delta S_1^*)]=(I/f)\int_{T_1}^{T_2}(f\sigma-\Delta\bar{C})(dT/T).$$

This may be simplified by the relationship

$$\int_{T_1}^{T_2}\Delta\bar{C}(dT/T)=t_c(\bar{S}_{c2}-\bar{S}_{c1})-t_a(\bar{S}_{a2}-\bar{S}_{a1}),$$

to yield the integral result of the Second Law,

$$\Delta S_2^*-\Delta S_1^*+f\int_{T_1}^{T_2}\sigma(dT/T)=0, \quad (27)$$

and its differential form

$$d\Delta S^*/dT+f\sigma/T=0. \quad (28)$$

It should be noted here again, as in the Soret case, that the fact that the integral Eqs. (23) and (27) contain no terms in ohmic dissipation or heat conduction proves that the irreversible processes have no effect on the steady state.

Combining Eqs. (23) and (27) produces two integral equations for the e.m.f.,

$$f\Delta\epsilon=\Delta F_1-\Delta F_2+(T_2-T_1)\Delta S_1^*+f\int_{T_1}^{T_2}\sigma\left(1-\frac{T_2}{T}\right)dT,$$
$$f\Delta\epsilon=\Delta F_1-\Delta F_2+(T_2-T_1)\Delta S_2^*+f\int_{T_1}^{T_2}\sigma\left(1-\frac{T_1}{T}\right)dT. \quad (29)$$

These equations reduce to the differential equation

$$fd\epsilon/dT=\Delta S+\Delta S^*, \quad (30)$$

in agreement with Eastman's result, Eq. (20).

In the present derivation we have chosen to dissipate the electrical energy produced by the cell as ohmic power. Another approach to the derivation would be to include in the First Law equation (4b) a term representing electrical energy removed reversibly. This procedure would necessitate a modification in treatment of the resistive dissipation. It is evident, however, that it leads to the same result, both in the integral and the differential equations, because as it turns out the irreversible effects are eliminated in combining the terms into the individual Eqs. (4).

Near Ultraviolet Absorption Spectrum of Hydroquinone, Resorcinol, and Catechol*

CARL A. BECK
Department of Physics, The Catholic University of America, Washington, D. C.
(Received June 12, 1950)

The near ultraviolet absorption spectra of the three dihydroxybenzenes in the vapor state are measured. 0,0 values are chosen and compared with benzene. Frequency differences of the main bands are given and some vibrational assignments made.

I. INTRODUCTION

THE absorption spectrum of benzene and several singly and doubly substituted benzenes[1] in the near ultraviolet region of 2600A have been discussed during recent years. Phenol[2] with one OH substitution has also been investigated in this region and it was of interest to see the effect of the double substitution. This was done with the hope of finding the amount of pure electronic excitation, also vibrational frequencies in the ground and upper electronic states.

It can be shown from symmetry considerations that the electronic transition observed in this region is, for the three di-hydroxy-benzenes, thus described:

$C_6H_4(OH)_2$(1,4) Hydroquinone (V_h symmetry), $A_{1g}\rightarrow B_{3u}$

$C_6H_4(OH)_2$(1,3) Resorcinol (C_{2v} symmetry), $A_1\rightarrow B_1$

$C_6H_4(OH)_2$(1,2) Catechol (C_{2v} symmetry), $A_1\rightarrow A_1$.

From symmetry, these transitions are allowed. From the work of Klingstedt[3] on this u.v. absorption of these molecules in hexane solution, each of the three molecules show about ten times the total absorption strength of benzene. It is also to be expected, then, that these spectra in the vapor will show the features (Sponer-Teller[1]) of an allowed transition, namely, a strong 0,0 band and excitation of totally symmetrical vibrations, with non-totally symmetrical vibrations appearing as 0,0 1,1 $\cdots$ $v-v$ transitions, and more weakly as $\Delta v=2$, 4, etc., and one would not expect the features of a forbidden transition to appear with any prominence. Unlike the case of substitution by a single atom, these three molecules do not strictly possess a V_h and probably not a C_{2v} type of symmetry, respectively. However, the change in electronic wave function should not be expected to be great.

Existing data comprise work[4] on the vapor spectrum

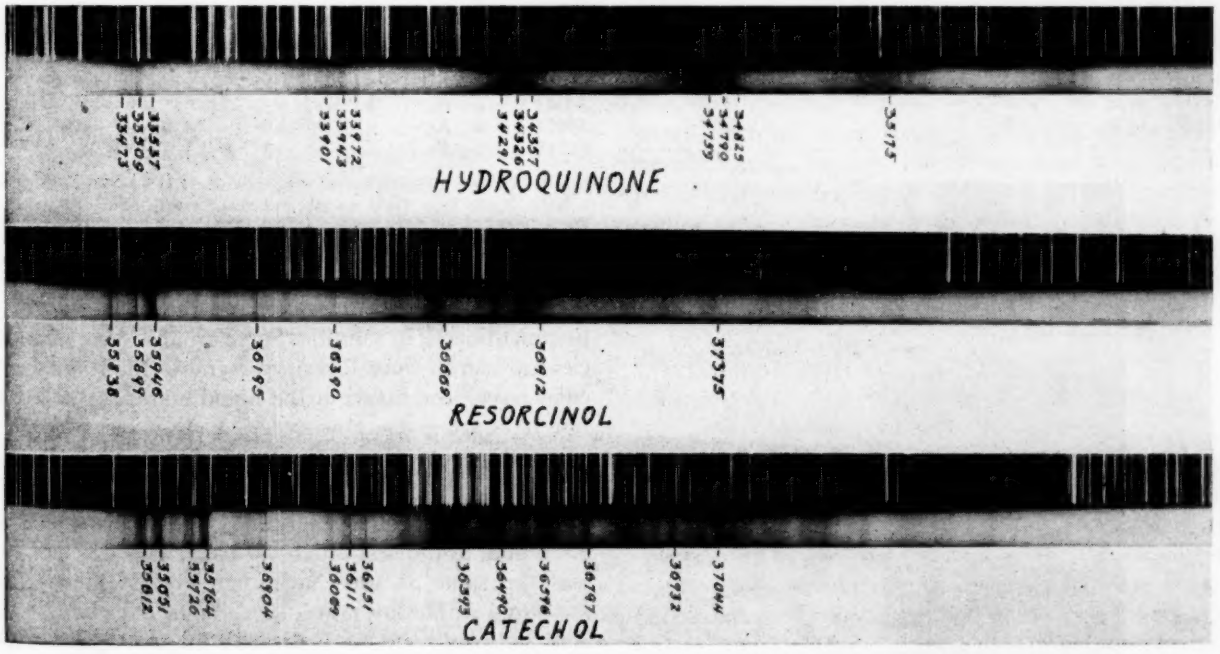

FIG. 1. Absorption spectra of hydroquinone, resorcinol, and catechol.

* This research was aided by the ONR Contract N6onr-255.
[1] H. Sponer and E. Teller, Rev. Mod. Phys. **13**, 115 (1941); H. Sponer, Rev. Mod. Phys. **14**, 224 (1942).
[2] N. Ginsburg and F. A. Matsen, J. Chem. Phys. **13**, 167 (1945); M. B. Hall, Duke University, Ph.D. thesis, 1942.
[3] F. W. Klingstedt, Comptes Rendus **175**, 365 (1922).
[4] W. N. Hartley and A. G. G. Leonard, J. Chem. Soc. London **95**, 34 (1909), (Hydroq.); P. K. Seshan, Ind. Acad. Sci. **3**, 172 (1936), (Hydroq.); J. E. Purvis and N. R. McCleland, J. Chem. Soc. London **103**, 1088 (1913), (Catechol).

TABLE I. Hydroquinone.

Wave number (cm^{-1})	Intensity	No. of readings	Assignment
33009	*w vBr*	2	0−528
33017		2	
33029	*w Br*	2	
33038	*w*	2	
33046	*w*	2	
33054	*w vBr*	2	0−483
33075	*w*	2	0−462
33167	*w*	1	0−370
33177	*w*	2	
33197	*w vBr*	1	
33230	*w vBr*	2	
33251	*w Br*	1	
33261	*m*	3	0−276
33277	*w vBr*	1	
—			
33391	*w Br*	1	0−146
33422	*w Br*	3	
33432	*w Br*	1	
33441	*w Br*	4	0−96
33450	*w*	2	
33458	*w Br*	2	
33473	*m Br*	3	0−64
33502 }	*s*	4	0−35
33509 }	*m*	4	
33518	*w Br*	1	
33527 }	*m Br*	2	
33537 }	*s*	4	0−0
33553	*w Br*	3	
33570	*w sh*	2	
33589	*w sh*	3	
33614	*w vBr*	3	
33626	*w vBr*	3	
33641	*w vBr*	4	
33668	*w vBr*	4	
33724	*w vBr*	1	
—			
33757	*w Br*	2	
—			
33791	*w vBr*	2	
33812	*w Br*	2	
33827	*w*	4	

TABLE I.—*Continued.*

Wave number (cm^{-1})	Intensity	No. of readings	Assignment
33855	*m Br*	5	
33868	*w Br*	3	0+331
33878	*m Br*	3	
33893	*m Br*	4	
33908	*s*	4	0+435−64
33937 }	*s*	4	
33943 }	*s*	4	0+435−36 (?); 0+400
33953	*w*	1	
33959	*w*	3	
33968	*w*	1	
33972 }	*s*	3	0+435
33986 }	*w Br*	1	
34262	*w Br*	2	
34277	*w vBr*	2	
34291	*m*	4	0+820−64
34314	*w*	2	
34326	*m*	2	0+820−36
34333	*w Br*	1	
34346 }	*m*	1	
34357 }	*s*	3	0+820
34372	*w*	3	
34385	*w*	3	0+850
34578	*w*	2	
34727	*w vBr*	4	0+820−64+435; 0−97+435+850
34759	*m Br*	4	0+435−36+820; 0−64+435+850
34779	*w Br*	4	
34790	*s vBr*	4	0+435+820; 0−35+435+850
34826	*m*	4	0+435+850
35140	*w*	3	0+2×820−36
35167	*m*	4	
35175	*m Br*	3	0+2×820
35195	*w Br*	4	0+848+820
35213		4	
35224	*m Br*	4	0+2×850
35259	*w*	2	
35558	*m*	4	
35608	*m*	4	0+435+2×820
35642	*m*	4	0+435+850+820
36011	*w Br*	4	
36042	*w Br*	4	
36074	*w Br*	4	
36111	*w Br*	2	

Note: Bands from 33473 up taken at about 115°C. Lower value bands taken progressively between 124°C and 138°C. Number of readings give some idea about difficulty of measurement because of diffuse and weak appearance.

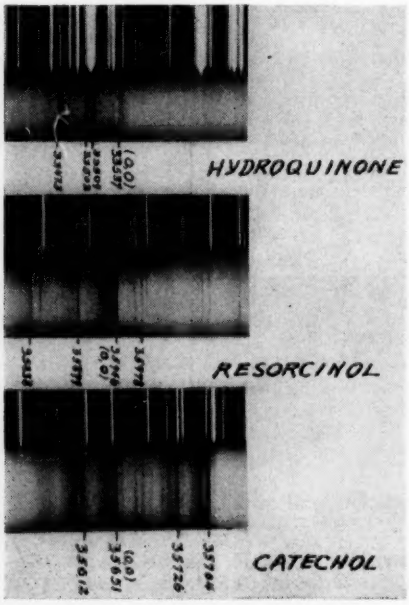

FIG. 2. Indicated 0,0 and surrounding region for hydroquinone, resorcinol, and catechol.

of hydroquinone and catechol and that of Klingstedt,[3] just mentioned, in solution. Some ground-state frequencies are known since Raman spectra[5] of the three molecules have been taken in the liquid state. No polarization data are given. however.

II. EXPERIMENTAL METHODS

A five-meter concave grating with a dispersion of 3.5A/mm, in the first order was used. The arrangement was the same as used in earlier work.[6] Bands were measured with a low power (9×) binocular microscope. The samples were of Eastman's highest grade. The bands were checked carefully for the presence of bands of phenol and the other two isomers in each case, and none were detected. A further check consisted in three

[5] K. W. F. Kohlrausch and A. Pongratz, Wien. Ber. **143**, 358 (1934); Mh. Chem. **65**, 6 (1935).
[6] W. F. Radle and C. A. Beck, J. Chem. Phys. **8**, 507 (1940).

TABLE II. Resorcinol.

Wave number (cm^{-1})	Intensity		No. of readings	Assignment
35102	*vw*		2	
35108	*vw*		2	
35152	*w*		2	
35200	*w*		2	0−746
35398	*w*		2	0−548
35435	*w*		4	0−511
35448	*w*		2	0−498
35546	*vw*		1	
35564	*s*		4	0−382
35598	*w*		1	0−348
35675			1	
35687	*w*		1	
35730	*m*		4	
35735	*w*		4	0−211
35747	*w*		4	
35780	*m*		4	
35792	*w*		4	
35801	*w*		4	
35838	*m*		4	0−108
35851	*m*		4	
35899	*m*		4	0−47
35940	*m*		4	
35946	*vs*		4	0−0
35968	*m*		4	
35978	*m*		4	0−210+250 (?)
35986	*w*		4	
35999	*w*	*Br*	4	
36014	*w*	*Br*	4	
36045	*w*	*Br*	2	0−99
36051	*w*		4	
36059	*w*		4	0−210+333 (?)
36098	*m*		4	0+152
36147	*w*		4	0+250−47
36169		*Br*	4	
36188	*w*		2	
36195	*m*		4	0+250

TABLE II.—*Continued*.

Wave number (cm^{-1})	Intensity		No. of readings	Assignment
36219	*w*	*Br*	4	
36226			4	0+332−47
36269	*m*		4	
36277	*w*		4	0+331
36312			1	
36344	*w*		1	
36354	*w*		1	
36390	*w*		4	0+444
36502	*vw*		2	
36518			2	
36532	*vw*		4	
36542	*vw*		4	0+703−108
36562	*w*		4	0+723−108
36576	*vw*	*Br*	1	
36589	*vw*		1	
36597	*w*		1	0+703−52
36623	*w*		4	0+723−47
36649	*m*		4	0+703
36669	*m*		4	0+723
36804	*m*	*vvBr*	4	0+966−108
36865	*w*		3	0+966−47
36906	*w*	*Br*	4	
36912	*s*		4	0+966
37108		*Br*	2	
37135	*vw*		1	
37156	*m*		3	0+1210
37178	*w*		3	0+1232 (?)
37245		*Br*	4	
37355		*Br*	1	0+2×703
37376	*w*		4	0+2×723 (?)
37486	*w*		2	
37613		*vvBr*	1	0+703+966
37638		*Br*	4	0+723+966
37867		*Br*	2	
37881	*vw*	*Br*	3	0+2×966

Note: Strongest bands of 0,0 and below measured at about 95°C. Bands lower than 0,0 measured progressively at temperatures between 95°C and 110°C.

times recrystallizing the benzene, after which the spectra appeared the same as before.

The whole cell with side arm was kept successively at the following temperatures and corresponding vapor pressures:

Hydroquinone 115 125 130 140°C
at 0.02 0.6 1.0 2.0 mm Hg.

Resorcinol 70 80 90 100 110 135°C
with pressures from roughly 0.1 to 5 mm.

Catechol 60 70 80 90°C
with maximum pressure about 2 mm.

Values of precise vapor pressures at the required temperatures were not found in the literature, so those given were roughly estimated from data given by Stull.[7] Above these temperatures, it was not thought possible to bring out more bands to the red from 0,0 because of the increasing diffuseness of the spectrum.

Spectra at approximately liquid air temperature were taken with a special Dewar arrangement built by the Naval Research Laboratory, for taking absorption spectra at low temperatures. It was held immediately before the slit and consisted of two parts. Liquid air was poured into one part, the copper end of which almost completely (i.e., except for the openings necessary for the light beam and insertion) surrounded the specimen, melted previously between two quartz plates. This part rested in a ground glass seal inside the other part containing quartz windows. The space between the two parts could then be evacuated.

[7] D. R. Stull, Ind. Eng. Chem. **39**, 517 (1947).

III. RESULTS AND DISCUSSION

The general appearance of the spectra, seen in Fig. 1, shows that the bands become gradually more diffuse toward the high frequency side of the spectrum. This is much more pronounced than in benzene. Also, a continuous absorption seems to cover a large part of the spectrum, and this makes it more difficult to observe the bands. Surely for the bands of very diffuse appearance, and, also, for others, relatively sharper, frequency values are not easily measured with great accuracy. Overlapping of bands also is a source of some difficulty. The wave-number values of heads, given to the nearest unit, are accurate to about one wave number for the sharpest bands, but other bands may have an uncertainty of two or three or even more in some cases. The band edges become sharper in the contrast of prints, and

this seems to lead to a greater possibility of seeing rather broad bands. Very roughly estimated intensities are given in a column beside the wave numbers. Not much attempt to bracket close-lying bands, suggesting some closer relationship, as rotational branches, has been thought feasible. Due to the appearance of some bands, there is little doubt but that they, as in benzene, are composed of two or even in some cases three branches. Generally, the branch, lying to shorter wave-lengths which usually is the strongest has been taken in computing frequency differences. The bands for which this can be detected, degrade to the red in catechol and resorcinol, as in benzene, but to the violet in hydroquinone, so for the latter the setting is taken on the long wave-length edge for all bands. This unusual behavior in hydroquinone is discussed later.

Spectra of all three molecules were taken at the low temperature partly to aid in substantiating 0,0 values. The spectra are very broad but the whole pattern did indicate the same general trend as in the vapor, the whole spectrum simply being shifted to the red. These liquid air spectra are not reproduced, because they are of such a broad character with only a few main maxima showing.

A. Hydroquinone

About 85 band heads have been measured. The spectrum is shown in Fig. 1. The bands appear at about 100°C and there is complete take-out of the central region at about 130°C. The position of the whole band system is displaced to longer wave-lengths from that of benzene (Table IV, 0,0 transitions) and there is a considerable region of relative transparency between this system and a band system around 2000A. Many of the bands have a diffuse appearance although this does not seem to be as marked here as in catechol and resorcinol. This diffuseness in general increases with decreasing wave-length. For several reasons, including diffuseness, difficulty of locating the proper band head (double and triple branches), anharmonicity and overlapping, it is not always possible to give very accurate and unambiguous frequency assignments.

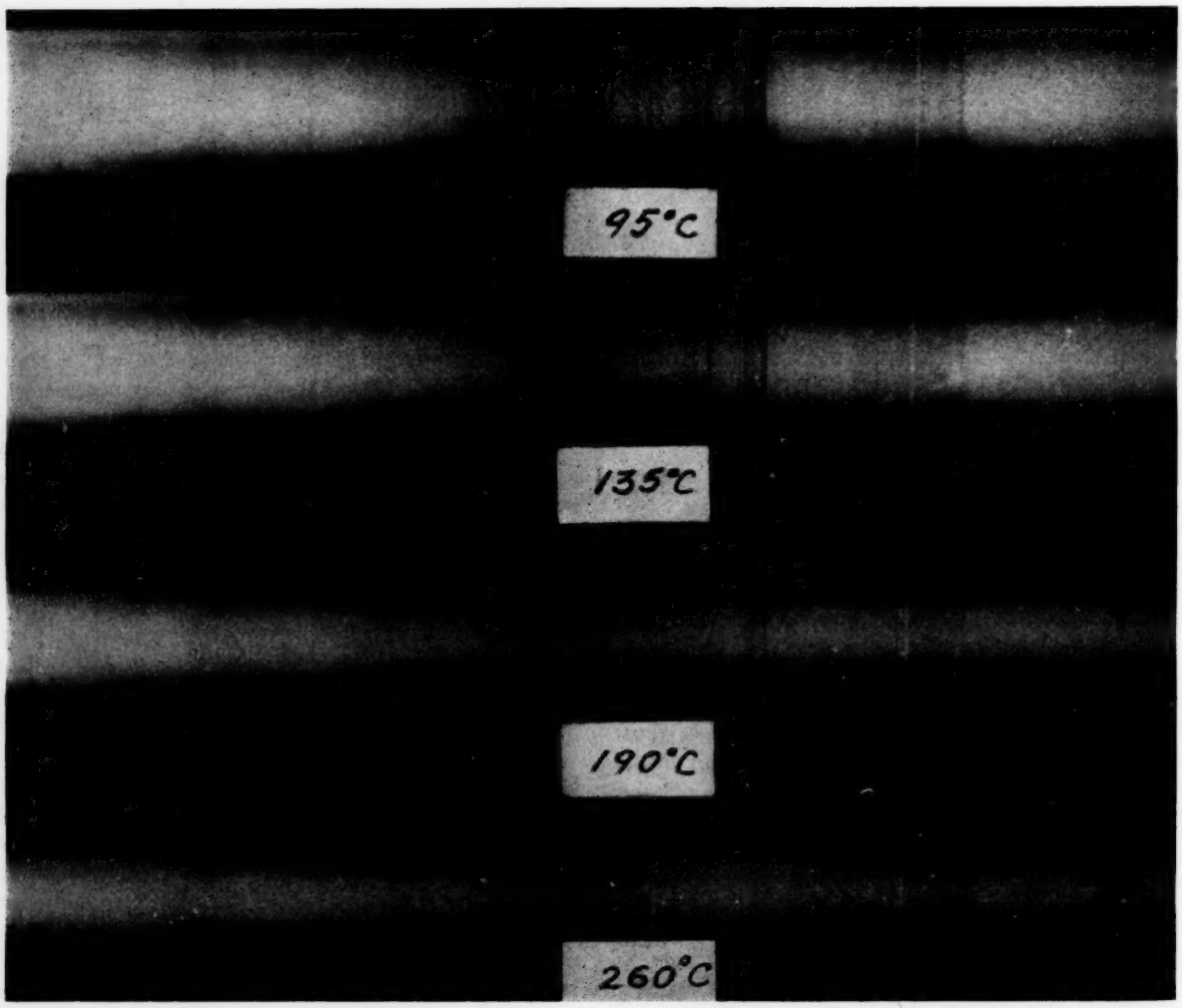

FIG. 3. Spectra of catechol with constant number of molecules at various temperatures.

TABLE III. Catechol.

Wave number (cm^{-1})	Intensity	No. of readings	Assignment
34883	*m Br*	2	0−768
34996	*m*	2	0−768+113
35050	*w Br*	2	
35058	*m Br*	2	
35079	*m Br*	2	0−572
35144	*m Br*		
35179	*w Br*	2	0−572+100
35343	*m*	2	0−308
35383	*m*	4	0−268
35395	*w Br*	2	
35449	*m*	4	0−202
35459	*m*	2	0−308+116
35485	*vw*	2	
35528	*m Br*	4	0−123
35569	*m*	4	0−82
35601	*s*	6	
35608	*s*	2	
35611	*s*	6	0−40
35630	*m vBr*	2	
35643	*m Br*	2	
35651	*vs*	6	0−0
35659	*s*	6	
35675	*w*	6	
35685	*w*	2	0+113−80
35692	*w Br*	2	
35708	*m*	2	
35716	*m*	2	
35726	*s*	6	0+113−36
35756	*m*	6	
35764	*vs*	6	0+113
35771	*m*	4	
35843	*m Br*	4	0+192
35861	*vw vvBr*	2	
35869	*vw Br*	2	
35877	*m*	4	0+227
35880		4	
35894	*m*	2	
35904	*s*	6	0+253
35917	*w*	2	
35948	*vw vBr*	4	0+300
35991	*w vBr*	2	
36018	*vvBr*	2	

TABLE III.—*Continued.*

Wave number (cm^{-1})	Intensity	No. of readings	Assignment
36054	*w vBr*	2	
36068	*m vvBr*	4	0+500−83
36111	*m vvBr*	4	0+500−41
36122	*w vBr*	2	0+476
36136	*w vBr*	2	
36151	*m*	4	0+500
36174		2	
36206		2	
36255	*m vBr*	2	0+2×300 (?)
36294	*m vBr*	4	
36333	*m*	2	
36352	*m*	4	
36375	*m Br*	2	
36382	*w*	4	
36393	*m*	6	0+742
36453	*w vvBr*	2	
36490	*m*	6	0+839
36557	*m vBr*	2	
36596	*m vvBr*	2	0+945 (2×476)?
36643	*m vBr*	2	0+2×500
36675	*m vBr*	2	
36703	*w vBr*	2	
36759	*m*	2	
36797	*m*	6	0+1146
36859	*m vBr*	2	
36897	*w vBr*	4	
36932	*m*	6	0+1280
37035	*w Br*	2	
37044	*m*	2	0+1280+113
37087	*m vBr*	2	
37097	*m Br*	2	
37135	*m*	2	0+2×742
37182	*m*	2	
37225	*m vBr*	2	
37273	*w*	2	
37342	*m*	2	
37434	*m vBr*	2	
37538	*vw Br*	2	0+2×945
37573	*vw Br*	2	
37767	*w vvBr*	2	

Note: Strong bands from 35600 up measured at 60°C. Weaker bands measured at 70°C. Bands below 35600 measured progressively at three temperatures ranging between 70°C and 90°C.

The gas spectrum contains four groups of bands. The high frequency bands in these four groups are located at 33537 cm^{-1}, 33972 (33537+435) cm^{-1}, 34357 (33537+820) cm^{-1}, 34790 (33537+435+820) cm^{-1}; the first two are much weaker than the last two. The 0,0 transition is taken to be 33537 cm^{-1}. If this interpretation is correct, the fact that the bands involving 0,820 and 0,435+820 transitions have higher intensity indicates a change in internuclear distance in the excited state. A very rough calculation leads to a change of the same order of magnitude as in benzene. In solution, the first strong peaks from the red lie at about 33000 cm^{-1}, with three or four following to shorter wave-length; the published data are not good enough to measure frequency differences, but do not contradict the estimate of about 400, 800, and 1200. As in the gas, the first two peaks are weaker than the next two.

The low temperature spectrum obtained was very broad and peaks were not clearly visible, so from this source the 0,0 is not established with certainty. The red end of the spectrum is shifted about 1100 cm^{-1} toward the red from the assumed 0,0 transition in the gas.

The frequency assignments in Table I refer mainly to transitions from the vibrationless ground state. With the temperatures used, bands to about only 500 cm^{-1} to the red from 0,0 were observed with sufficient intensity or clearness. For the purpose of correlation the papers of Sponer and Kirby-Smith[8] and the diagrams of Kohlrausch[9] were mainly used.

From the 0,0 group there is a group 435 cm^{-1} to the violet, but it appears only once. We recall that there arise two components from the degenerate 606 vibration in benzene, one totally symmetrical and the other non-totally symmetrical. Kohlrausch[5,9] ascribes the 468 Raman line (value in liquid) to the symmetrical one. It is possible that the 435 frequency is of this type. We expect the other, non-totally symmetrical component to have a higher value. This is seen for example, in

[8] H. Sponer and Kirby-Smith, J. Chem. Phys. **9**, 667 (1941).
[9] K. W. F. Kohlrausch, Ramanspektren, Hand. und Jahrbuch der Chem. Phys. **9**, 367 (1943).

TABLE IV. Frequency values of 0,0 transitions of hydroquinone, resorcinol catechol, and differences Δ from benzene.

	Vapor		Liquid		Solid	
Benzene	38089 (calc.)		37750		37828 (calc.)	
		Δ		Δ		Δ
Hydroquinone (*p*)	33537	4552	33000	4750	32500	5330
Resorcinol (*m*)	35946	2143	35800	1950	35900	1930
Catechol (*o*)	35764	2325	35200	2550	34000	3830

mono-deutero and para-deutero-benzene,[10] in mono-chloro[11] and the di-chloro-benzenes.[12] This other frequency may be the Raman 531; there is also a band, 33009, shifted to the red by about this amount.

The 406 in benzene splits in V_h symmetry into an A_{2u} and a B_{2u} but for neither are transitions $0-1$ or $1-0$ allowed.

In phenol the Raman frequency 810 is ascribed[13] to the totally symmetrical C−OH, the frequency 830 to some type of ring vibration.[14] One should expect that the corresponding frequencies in hydroquinone are not very different. 829 and 853 are found,[5] and it would seem right to ascribe the latter to the ring vibration (this agrees with a rough estimate from the square root ratio of the masses). In ortho- and meta-chloro-fluoro benzenes also the ring vibration is chosen[15] as the higher of the two. It is now very curious that in our spectrum there are two bands at 820 and 850 cm^{-1} to the violet of the 0,0 transition respectively. Both form progressions which, however, because of diffuseness cannot be followed much beyond the second members. 820 and 850 are practically identical with the above Raman frequencies, but refer to vibrations in the excited state. In no case up to now, for benzene or substituted benzenes, have the upper state frequencies been found to be so close to the ground state frequencies, but they were found to be 30 to 90, rarely more, wave numbers lower.

As is usual there is the recurring pattern of small frequency differences, probably *n*,*n* transitions. The difference 36 might be explained by the 370 vibration (33167) dropping in the upper state to 331 (band at 33868) or by 462 dropping to 435, although the latter difference being 9 cm^{-1} off may not be plausible.

In benzene and in all the singly and doubly substituted benzenes which have come to our attention to date, the degradation of the bands is to the red. This means, of course, that at least one moment of inertia is higher in the excited state than in the ground state. Here, however, all those bands for which it is possible to observe a sharp edge (many bands are very diffuse) behave oppositely. This is observed in an even more pronounced manner in para-chlorophenol, on which substance work by Y. C. Kao is in progress in this laboratory. This means that, for these substituted benzenes at one moment of inertia is lower in the excited state than in the ground state. The structural appearance of the bands is not uniform. For example, the 0,0 band has a different structure (2 branches only) than the band at 0,0−35 (3 branches). The latter looks somewhat like a mirror image of the A_0^0 of benzene (0,0+520).

B. Resorcinol

The vapor spectrum contains three outstanding groups of bands, the violet band of each is located at 35946, 36663, and 36912. The first one was chosen for the 0,0 transition (Table II).

In the low temperature spectrum, three peaks apparently corresponding to these three groups appear to be present. This substantiates the choice of the 0,0 position. All peaks were displaced by a rather constant small amount, roughly less than 400 cm^{-1} to the red from the corresponding position in the gas.

In searching on the red side of the 0,0 for frequencies found in the Raman spectrum there is a band displaced by 748 cm, the value given by Kohlrausch, which is probably the totally symmetrical C−OH vibration. In the upper state there are two bands at 36649 (0+703) and 36669 (0+723), both fairly strong. They probably correspond to the Raman 724 and the above 748.

The symmetrical ring vibration corresponds probably to the strong 1000 Raman frequency, which may drop in value to 966 in the upper electronic state. (Strong band at 36912.) Since bands to the red from the 0,0 of more than 850 cm^{-1} were not in these spectra, the ground-state frequency was not observed.

A broad Raman line is reported at 531. There are bands to the red for 500, 513, and 550, and the Raman value may be an average of these. The relatively strong bands at 35735 (0−211) and 35564 (0−382) probably contain non-totally symmetrical vibrations and are considerably weaker than a mere Boltzmann decrease would predict.

On the violet side, other differences appear in prominent bands: 152, 250, 444, and others at 1210 and 1232 in bands not so strong. In the Raman spectra, there are in the region around 1000 several totally symmetrical vibrations which are rather independent of substituent, among which are 1000 and 1290. 1000 may drop in the higher state to 966 as stated above and 1290 to 1210.

Several small frequency shifts appear, e.g., 47 and 108, connected probably with 1,1 transitions. This could however be confirmed if bands belonging to $0-1$ and $1-0$ transitions with satisfactory frequency values were found. This is not the case, from which one may conclude that the vibrations involved are non-totally symmetrical.

[10] A. Langseth and R. C. Lord, Det. Kgl. Danske Vidensk. Selskab. **16**, No. 6 (1943).
[11] H. Sponer and S. H. Wollman, J. Chem. Phys. **9**, 816 (1941).
[12] H. Sponer, Rev. Mod. Phys. **14**, 229 (1942).
[13] J. Lecomte, J. de phys. et rad. **8**, 489 (1937).
[14] K. W. F. Kohlrausch, Physik. Zeits. **37**, 68 (1936).
[15] A. M. Bass, Duke University, M.S. thesis, 1943.

C. Catechol

Many bands towards shorter wave-lengths become extremely diffuse so that it becomes impossible to follow the progressions to higher frequencies. Many of the bands are diffuse on both sides, but the measurements were taken on the violet edge (Table III).

The spectrum contains two groups of bands; (Fig. 2) the group towards the red contains four bands, about 41 cm^{-1} distant from each other, the group of shorter wave-length surely two and perhaps also four bands, also 41 cm^{-1} apart. The wave number difference between the groups is 113 cm^{-1}. It was expected that one of these bands corresponded to the 0−0 transition. To ascertain whether any ground-state vibration is involved, a series of exposures (Fig. 3) were taken, with a constant amount of the material (about one milligram) placed in the cell, and the temperature was raised from 60°C to 250°C. It was evident that at about 75°C all the material had evaporated. Above that temperature all the bands seemed to get weaker, but the edges seem fairly sharp even at elevated temperatures. At the same time a continuous background appears; its intensity increasing with temperature, so that at first glance the spectrum appears more diffuse. Since these results did not give decision on the 0,0 transition, spectra of a thin solid layer were taken next at liquid air temperature. While no separate bands are visible, there seem to be two broad maxima, about 100 cm^{-1} apart and of equal intensity (as are the two groups 113 cm^{-1} apart in the vapor state). There is no absorption further to the red, therefore it seems reasonable to identify these two peaks with the two groups of bands in the vapor state and conclude that they start from the vibrationless ground state. Accordingly it was concluded that the violet band of the band group located to larger wave-length, with a wave number of 35651, is the 0,0 band, while the other bands of this and the other band group, with wave-number differences of about 41, are probably *n,n* transitions (see the remarks at the end of the discussion on resorcinol). There are two possible explanations of the wave-number differences, 113 cm^{-1} between the two band groups: It may be a vibration frequency in the excited state, or an electronic doublet. A vibration frequency as low as 113 is not very probable.

From polarization data and the correlation diagram,[8] 202 seems to be non-totally symmetrical and weak as expected. If the 113 in the upper state represents this vibration, the difference gives 89 instead of 81 which is observed. This may be too far off to be plausible. The bands in general have more than one branch and an error of 20 cm^{-1} or even more could be made by a measurement to points which do not correspond to the same branch. Here, branches of corresponding, strong, intensity towards the violet side are taken.

The 308 does not seem to be a totally symmetrical vibration, and the band containing it is weak. The vibration 572 is probably a totally symmetrical one, and appears with fairly good intensity. The Raman frequency 768 is probably the totally symmetric C−OH valence vibration in the ground state. To it corresponds the band at 34883; considering the small Boltzmann factor involved, this band is fairly strong.

To the violet side of the 0,0 transition there lies another group of four bands (with differences of 41 cm^{-1} as described before). Its violet band lies at 36151, and is interpreted as (0,0+500). There is another band at 35904 (0,0+253). One might think that $500=2\times253$. However this band does not form part of a group of four; therefore it seems more probable that the two bands are of different origin. No interpretation for the two frequencies 253 and 500 is given.

The totally symmetric ring vibration is probably the Raman frequency 1036. There are two bands, 839 and 945 cm^{-1} respectively shifted to shorter wave-lengths from the 0,0 transition. Either 839 or 945 may be the totally symmetric ring vibration in the excited state. To decide between the two it would be useful to find the 1,1 transition, but this should be very weak because of the small Boltzmann factor.

Other bands to the violet, with frequency differences against 0,0 of 1146 and 1280 are observed. Because of the strength of these bands, the corresponding vibrations would seem to be totally symmetric. 1146 may be the excited state vibration corresponding to the Raman line 1263.

Band groups with small frequency differences of approximately 41 appear besides the three mentioned earlier. While it is probable that $n-n$ transitions are involved, it has not been possible definitely to assign them to any particular vibration. If the transitions belonged to the ground-state frequencies 202 or 306, there ought to be 0−1 transitions at $35764+202-40=35926$ or $35764+308-40=36032$. These bands are not visible on the plates. For the Raman frequency 454, the corresponding band would be at $35764+454-40=36188$; this region is masked by several closely lying bands.

SUMMARY

In conclusion we wish to emphasize that the assignments here included, are not final in many cases because of the difficulties of setting up a complete unambiguous correlation table of vibration frequencies.

Table IV gives the comparison between assigned 0,0 transition values, measured in vapor, and very roughly estimated in solution[3] and solid, and the corresponding value in benzene. Here we notice a change from the usual order *p.m.o.*[16] This and also a general difficulty of interpretation may be related to a deviation from a true C_{2v} or V_h symmetry.

The various peaks in a given liquid appear to shift by approximately the same amount from their position

[16] Miller and Thompson find in the substituted benzo-trifluorides the order of *p* and *m* to be reversed. C. H. Miller and H. W. Thompson, J. Chem. Phys. **17**, 845 (1949).

in the vapor. The same relation seems to hold also between solid and vapor.

Choice of 0,0's is greatly aided by low temperature spectra, and it is intended to include these spectra taken at lower temperatures in our future program.

The occurrence of degradation to the violet is of great interest, but the whole problem of the band shape is larger than could be contained in the scope of this paper.

Finally I wish to acknowledge the aid of Mr. Y. C. Kao in the experimental work of taking the plates; also, Mr. Elias Burstein, of the Naval Research Laboratory, Washington, D. C., for kindly allowing us the use of the Dewar absorption apparatus; the invaluable and extremely generous assistance of Dr. Hertha Sponer for discussion and helpful criticism and the constant interest and aid of Dr. K. F. Herzfeld.

THE JOURNAL OF CHEMICAL PHYSICS VOLUME 18, NUMBER 9 SEPTEMBER, 1950

The C—Br Bond Dissociation Energy in Benzyl Bromide and Allyl Bromide

M. SZWARC, B. N. GHOSH, AND A. H. SEHON
Chemistry Department, University of Manchester, England

(Received March 21, 1950)

The pyrolysis of organic bromides in a stream of toluene is described as a method for the determination of the C—Br bond dissociation energies. The technique used makes it possible to discriminate between two mechanisms of decomposition:

$$R.Br \rightarrow R\cdot + Br \quad (a)$$

$$R.Br \rightarrow \text{olefin} + HBr. \quad (b)$$

It was found that both benzyl and allyl bromide decomposed according to mechanism (a), the bromine atoms reacting readily with toluene to give hydrobromic acid. The rate of the primary dissociation process was measured by the rate of formation of HBr. It was proved that the thermal decompositions of benzyl and allyl bromide were homogeneous gas reactions obeying first order kinetics. The activation energies were calculated at 50.5±2 kcal./mole and 47.5±2 kcal./mole, and identified with $D(C_6H_5.CH_2-Br)$ and $D(CH_2{:}CH.CH_2-Br)$, respectively.

The fate of the allyl radical is discussed, and a rough estimate of the activation energy for the reaction

$$CH_2{:}CH.CH_2\cdot + C_6H_5.CH_3 \rightarrow CH_2{:}CH.CH_3 + C_6H_5CH_2\cdot$$

leads to a value of 14–17 kcal./mole.

The problem of ionic contribution in the C—Br bonds is discussed.

The estimation of the dissociation energies of the C—Br bonds of various organic bromides is of great interest since the values for these dissociation energies, combined with the heats of formation of the relevant bromides in the gaseous state, make it possible to determine the heats of formation of various organic radicals. Furthermore, the latter data in conjunction with the heats of formation of hydrocarbons enable us to calculate the various C—H and C—C bond dissociation energies and the resonance energies of the relevant radicals.

THE METHOD OF DETERMINATION OF THE C—Br BOND DISSOCIATION ENERGY

IT was deduced by Baughan and Polanyi[1] that the C—Br bond dissociation energies are much lower than the respective dissociation energies of C—H or C—C bonds. In consequence one might expect that the thermal decomposition of an organic bromide RBr would result in rupturing the weakest C—Br bond with the formation of a radical R and a bromine atom, i.e.,

$$R.Br \rightarrow R + Br. \quad (1)$$

The estimation of the rate of reaction (1) by a suitable experimental technique would lead to the determination of the C—Br bond dissociation energy. That has been achieved in our work by investigating the pyrolysis of organic bromides in a stream of toluene. As was shown in previous communications[2] toluene is very effective in removing various radicals which react with it according to Eq. (2)

$$C_6H_5.CH_3 + R \rightarrow C_6H_5.CH_2\cdot + HR. \quad (2)$$

The relatively stable benzyl radicals produced in this type of reaction dimerise to give dibenzyl which is one of the products of pyrolysis.

If the pyrolysis of RBr takes place according to the above scheme, then each decomposed molecule of RBr will give rise to one molecule of HBr, of RH, and of dibenzyl; and the rate of the primary dissociation process of the organic bromide could be measured by the rate of formation of HBr, RH, or dibenzyl. It is possible, however, that a molecule of an organic bromide could decompose into HBr and the corresponding olefin.[3] This case can be easily distinguished from the former, for although HBr would again be a product of pyrolysis, no dibenzyl would be produced. Hence, using toluene as a carrier gas one would be able to measure for an organic bromide both the rate of decomposition into radicals according to Eq. (1), and into HBr and olefin according to Eq. (3)

$$RBr \rightarrow HBr + \text{olefin}, \quad (3)$$

even if these reactions occurred simultaneously. The

---

[1] E. C. Baughan and M. Polanyi, Nature **146**, 685 (1940).

[2a] M. Szwarc, J. Chem. Phys. **17**, 432 (1949). [b] M. Szwarc, J. Chem. Phys. **17**, 505 (1949) and Proc. Roy. Soc. **A198**, 267 and 285 (1949).

[3] E. T. Lessig, J. Phys. Chem. **36**, 2335 (1932). E. L. Vernon and F. Daniels, J. Am. Chem. Soc. **55**, 922 (1933). P. Fugassi and F. Daniels, *ibid.* **60**, 771 (1938). F. Daniels and P. L. Veltman, J. Chem. Phys. **7**, 756 (1939).

rate of reaction (1) would be measured by the rate of formation of dibenzyl, whereas the sum of the rates of both reactions (1) and (3) would be measured by the rate of formation of HBr.

EXPERIMENTAL

Apparatus and Technique

The experimental set-up for liquid bromides was essentially similar to that used in the investigation of the decomposition of ethyl-benzene[2a] and of hydrazine,[2b] whilst that for gaseous bromides, e.g. methyl bromide, resembled closely that used for the pyrolysis of butene-1.[4] In consequence only a brief description of the technique as applied to the study of benzyl and allyl bromides will be given here.

The diagram of the apparatus is given in Fig. 1. The vapor of the bromide, introduced through a fine capillary K_1, streamed into a large excess of toluene vapor. The gaseous mixture of both compounds maintained under a pressure of a few mm Hg was made to flow continuously through a silica reaction vessel *R* heated by means of an electric furnace. The products of pyrolysis and the undecomposed toluene and bromide were led through a glass tube and a glass capillary K_2* (both heated by nichrome winding to about 80°C) into a small trap, *U*, cooled by ice. The scarcely volatile products (e.g., dibenzyl) were deposited mainly in this trap. The undecomposed toluene and bromide, small amounts of dibenzyl, and other products of pyrolysis such as HBr were condensed in the large trap *H* cooled to −180°C. The non-condensable gases produced (hydrogen and methane) were continuously removed by a system of two diffusion pumps P_1 and P_2, and pumped into a storage vessel *S* connected to a McLeod gauge. The pressure of the gases collected was measured at the end of the run, and then part of the gases collected was admitted into an analytical system for the estimation of the hydrogen to methane ratio.

At the end of each run taps 1 and 2 were closed, the Dewar flask containing the liquid air around trap *H* was lowered for a period of about 45 min. so as to enable the previously condensed materials in trap *H* to migrate to the bottom of the trap. Then trap *H* was re-immersed completely in liquid air, the ground joint socket *G* was forced up, and distilled water was injected into trap *H* through *G* flooding all the condensed material. The liquid air container was then removed quickly so as to prevent all the water from freezing out. The contents of this trap kept at 0°C were titrated iodometrically for HBr against standard sodium thiosulphate solutions. Blank analyses proved that under these conditions, i.e. in presence of toluene and at 0°C, there was hardly any hydrolysis of the bromides.

In order to recover the dibenzyl which had passed into trap *H*, after titration for HBr, the hydrocarbon layer was distilled in vacuum at 0°C, and the weight of the residue was added to the weight of the bulk of dibenzyl isolated in the *U*-tube.

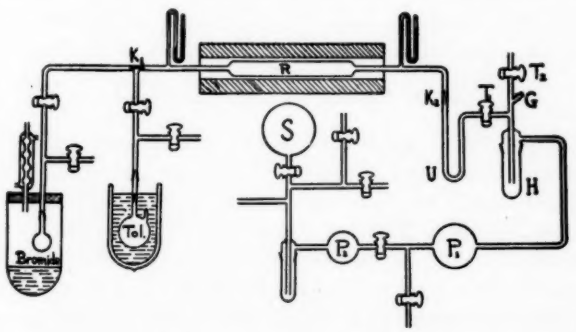

FIG. 1. Apparatus diagram.

TABLE I.

Run	T°K	Ratio of (dibenzyl)/(HBr)
30*P*	768	0.85
29	781	1.0
33	803	0.94
19	823	1.2
18	823	1.0
10	823	1.18
6	823	0.97
17	823	1.0
16	823	0.94
11	823	1.0
15	823	1.0
2	823	0.85
7	824	1.15
12	824	1.0
14	825	1.0
9	829	1.26
36*P*	843	0.92
37*P*	856	1.0
38	860	1.0
22	870	1.0
20	872	1.0
21	872	1.27
23	872	1.0

Materials

The benzyl bromide used for this investigation was obtained commercially. It was distilled in vacuum, the middle fraction being collected into a dark bottle and kept over mercury. The allyl bromide, also commercially obtained, was purified by distillation in a similar way. The toluene was prepared as in previous studies by the repeated pyrolysis of "sulphur-free" toluene at about 820°C followed by a careful distillation over sodium.

BENZYL BROMIDE

Results

The thermal decomposition of benzyl bromide was investigated over the temperature range 768° to 872°K. Before each experiment a blank run for the pyrolysis

[4] A. H. Sehon and M. Szwarc, Proc. Roy. Soc. **A202**, 263 (1950).
* The time of contact could be varied by sealing various capillaries K_2 into the system.

TABLE II.

Run[a]	T°K	$\frac{(CH_4+H_2)}{HBr}$%
30*P*	768	15.
31*P*	774	3.
24	774	0.
25	774	1.
28	781	4.
29	781	5.
32	781	4.
26	783	6.
27	783	6.
33	803	1.
8	816	4.
19	823	5.
18	823	10.
5	823	4.
10	823	5.
6	823	7.
17	823	10.
16	823	14.
11	823	7.
15	823	15.
2	824	4.
4	824	4.
7	824	4.
12	824	11.
14	825	12.
34	825	4.
9	829	5.
35*P*	839	13.
36*P*	843	6.
37*P*	856	8.
38	860	9.
22	870	4.
20	872	10.
21	872	5.
23	872	10.

[a] *P* denotes the runs carried out in the packed reaction vessel.

TABLE III.

Run[a]	T°K	K.10² sec.⁻¹	K_{774}.10² sec.⁻¹
30*P*	768	5.7	7.3
31*P*	774	6.9	6.9
24	774	7.5	7.5
25	774	7.2	7.2
32	781	9.2	6.8
			K_{843}.10² sec.⁻¹
14	825	52.	100.
34	825	67.	129.
9	829	65.	107.
35*P*	839	90.	105.
36*P*	843	96.	96.
37*P*	856	156.	99.
38	860	203.	108.

[a] Runs denoted by *P* were carried out in the packed reaction vessel.

of toluene was carried out, and the appropriate corrections for its decomposition, if any, were introduced.

Hydrobromic acid and dibenzyl were the main products of the decomposition of benzyl bromide. From Table I it is readily seen that within experimental error the molar ratio of HBr to dibenzyl was 1:1, suggesting that the dissociation of benzyl bromide is represented by Eq. (1).

In addition to HBr and dibenzyl, small amounts of non-condensable gases were formed, their analysis showing that it was a mixture of constant proportion of 60 percent hydrogen to 40 percent methane. As indicated in Table II the ratio of the amount of gases produced to HBr varied from experiment to experiment, but never exceeded 15 percent.

TABLE IV.

Run	T°K	$P_{\text{benzyl bromide}} \times 10^3$ in mm Hg	K.10² sec.⁻¹
18	823	14	55.
2	824	17.5	59.
5	823	18	55.
10	823	19	53.
4	824	19	59.
6	823	22	56.
7	824	22.5	56.
11	823	38.5	57.
12	824	40	58.
14	825	161	52.
15	823	2300	59.

Kinetics

The decomposition of benzyl bromide measured by the rate of formation of either HBr or dibenzyl was proved to be a homogeneous gas reaction of the first order.

Variation of the surface to volume ratio by a factor of about 4 to 5,* as shown in Table III, had no effect on the first order rate constant. Tables IV and V prove that the first order rate constant was not affected by a change of the partial pressure of benzyl bromide by a factor of 200, and of the time of contact by a factor of 3. Similarly, the results listed in Table VI demonstrate that the unimolecular rate constant is independent of the partial pressure of toluene. The variation of the rate constant over the whole temperature range from 768° to 872°K is given in Table VII. The plot of $\log k$ against $1/T$ is represented in Fig. 2 the straight line corresponding to an activation energy of 50.5±2 kcal./mole and a frequency factor of 1.10^{13} sec.$^{-1}$.

Discussion

It follows from the above results that the thermal decomposition of benzyl bromide is a unimolecular dissociation into benzyl radicals and bromine atoms

$$C_6H_5.CH_2Br \rightarrow C_6H_5.CH_2. + Br.$$

The products obtained are in accordance with the scheme suggested earlier in this paper, the 1:1 ratio of HBr to dibenzyl being the strongest argument in its favor. This is further supported by the first order kinetics of the decomposition and by the theoretically expected frequency factor of the order of 10^{13} sec.$^{-1}$.

Making our usual assumption that the recombination of benzyl radicals and bromine atoms involves no activation energy we conclude that the observed

* The surface to volume ratio was increased by packing the reaction vessel with silica wool.

TABLE V.

Run	T°K	Time of contact secs.	K.10² sec.⁻¹
26	783	0.51	9.0
27	783	0.51	10.5
32	781	0.92	10.5
28	781	1.17	8.5
29	781	1.17	9.2
19	823	0.49	48.
18	823	1.04	55.
10	823	1.15	53.
17	823	1.21	53.
16	823	1.22	52.

activation energy for the decomposition process, i.e., 50.5±2 kcal./mole is equal to the C−Br bond dissociation energy in benzyl bromide. This conclusion may be checked in the following way. The direct determination of the C−H bond dissociation energy in toluene[5] gives 77.5±1.3 kcal./mole for $D(C_6H_5CH_2-H)$. Therefore, the difference between $D(C_6H_5CH_2-H)$ and $D(C_6H_5CH_2-Br)$ is equal to 27±3.3 kcal. On the other hand this difference was estimated at 29±3 kcal. by calorimetric measurements carried out by Gellner and Skinner.[6] The satisfactory agreement between these two differences strengthens our confidence in the value of 50.5±2 kcal./mole for $D(C_6H_5CH_2-Br)$.

It must be mentioned, however, that the formation of small amounts of hydrogen and methane cannot be explained by the above mechanism. The very fact that the molar ratio of hydrogen to methane is 1.5 to 1, which is identical with that found in the pyrolysis of toluene,[5] indicates that some secondary reaction producing atomic hydrogen—and not molecular hydrogen—is responsible for the formation of the observed gases according to Eqs. (4), (5a), and (5b).

$$C_6H_5.CH_2.+H_2 \quad (60\ \text{percent}) \qquad (4)$$

$$C_6H_5.CH_3+H \nearrow \quad \downarrow$$

$$\left\{\begin{array}{l} C_6H_6+CH_3. \\ C_6H_5.CH_3+CH_3.\rightarrow \\ C_6H_5.CH_2.+CH_4 \end{array}\right\} (40\ \text{percent}) \qquad (5a)\ (5b)$$

Although, as seen from Table II, there is no conclusive evidence that the production of gases depends on the stationary concentration of dibenzyl and bromine atoms, we suggest tentatively that atomic hydrogen might be produced by either reactions (6a) and (6b), or (7) and (6b).*

$$C_6H_5.CH_2.CH_2.C_6H_5+Br\rightarrow C_6H_5.CH_2.CH.C_6H_5+HBr, \qquad (6a)$$

$$C_6H_5.CH_2.CH.C_6H_5\rightarrow C_6H_5.CH{:}CH.C_6H_5+H, \qquad (6b)$$

$$C_6H_5.CH_2.CH_2.C_6H_5\rightarrow C_6H_5.CH_2.CH.C_6H_5+H. \qquad (7)$$

[5] M. Szwarc, J. Chem. Phys. 16, 128 (1948).
[6] O. H. Gellner and H. A. Skinner, J. Chem. Soc. 1145 (1949).
* Reactions (6a) and (6b) would not change the 1:1 ratio of HBr to dibenzyl, whereas reactions (7) and (6b) would lead to some small increase of the dibenzyl to HBr ratio.

TABLE VI.

Run	T°K	P_{tot} in mm Hg	K.10² sec.⁻¹
19	823	8.7	48
17	823	9.5	53
16	823	9.6	52
10	823	14.4	53
18	823	15.2	55

TABLE VII.

Run	T°K	P_{tot} in mm Hg	$P_{\text{benzyl bromide}}$ ×10³ mm Hg	Time of contact sec.	% decomposition	K.10² sec.⁻¹
30*P*	768	10.5	166.	0.98	5.4	5.7
31*P*	774	10.7	158.	0.99	6.5	6.9
24	774	9.5	10.	0.52	3.9	7.5
25	774	9.5	10.	0.52	3.7	7.2
28	781	14.5	17.	1.17	9.4	8.5
29	781	14.5	18.	1.17	10.3	9.2
32	781	10.5	149.	0.92	9.3	10.5
26	783	9.6	25.	0.51	4.7	9.0
27	783	9.5	18.	0.51	5.0	10.5
33	803	10.0	39.	0.86	16.7	22.
8	816	14.5	23.	1.13	34.5	37.
19	823	8.7	10.	0.49	22.2	48.
18	823	15.2	13.	1.04	43.7	55.
5	823	14.4	18.	1.09	45.0	55.
10	823	14.4	19.	1.15	44.5	53.
6	823	14.4	22.	1.05	46.5	56.
17	823	9.5	23.	1.21	47.6	53.
16	823	9.6	32.	1.22	47.2	52.
11	823	13.4	38.	1.06	45.6	57.
15	823	15.2	2300.	1.09	47.8	59.
2	824	14.3	17.	1.10	48.0	59.
4	824	14.4	19.	1.07	46.8	59.
7	824	14.4	22.	1.14	46.8	56.
12	824	14.5	40.	1.07	46.5	58.
14	825	14.5	161.	1.08	42.0	52.
34	825	10.2	115.	0.85	43.7	67.
9	829	14.5	23.	1.12	52.0	65.
35*P*	839	10.9	332.	0.83	52.4	90.
36*P*	843	10.7	121.	0.87	57.4	96.
37*P*	856	10.2	99.	0.87	74.1	156.
38	860	10.2	121.	0.85	81.8	203.
22	870	9.5	10.	0.46	74.0	287.
20	872	9.5	14.	0.45	65.5	236.
21	872	9.5	10.	0.45	72.5	285.
23	872	9.6	16.	0.47	71.5	268.

ALLYL BROMIDE

Results

The pyrolysis of allyl bromide was investigated over the temperature range 732 to 865°K. In contrast to the rather simple mechanism of decomposition for benzyl bromide, the pyrolysis of allyl bromide exhibited peculiar complications. First of all the amount of dibenzyl isolated, as shown in Table VIII, was much lower than the quantity of HBr produced. Furthermore, we noticed that the amounts of hydrogen and methane formed, as well as the hydrogen to methane ratio, increased with increasing temperature. The relative quantities of gases to HBr and their composition are listed in Table IX, in which we indicated also the other variable factors such as time of contact, packing effect, and the molar ratio of allyl bromide to toluene.

In addition to these products of pyrolysis we isolated

TABLE VIII.

Run[a]	T°K	Dibenzyl / HBr
1*P*	766	0.23
8	766	0.23
7	777	0.23
9	809	0.31
10	809	0.31
5	857	0.34
6	858	0.34
3*P*	860	0.40
4*P*	865	0.40

[a] The runs denoted by *P* represent experiments carried out in the packed reaction vessel.

from the contents of the *H* trap a gaseous material amounting to about 20–30 percent of the quantity of HBr produced. It was proved by infra-red analysis that this material was propylene, the allene content being less than 1 percent of the propylene formed.†

Kinetics

The extent of the decomposition of allyl bromide was measured by the rate of formation of HBr, and it was found that the pyrolysis of allyl bromide was a first order homogeneous gas reaction.

The homogeneity of the reaction was proved by changing the surface to volume ratio by a factor of 4–5, which had no effect on the rate constant at low temperatures (see Table X). We observed, however, a slight decrease in the rate of decomposition in the packed reaction vessel at higher temperatures, this trend being particularly noticeable for high percentages of decomposition (see Table XI).*

The first order character of the kinetics was demonstrated by changing the time of contact by a factor of 4 (see Table XII), by varying the partial pressures of allyl bromide by a factor of 4 (see Table XIII), and by varying the partial pressure of toluene by a factor of 3 (see Table XIV). The temperature dependence of the rate constant over the whole temperature range is given in Table XV. The plot of log$k$ against $1/T$ is given in Fig. 3 the straight line corresponding to an activation energy of 47.5±2 kcal./mole, and a frequency factor of 5.10^{12} sec.$^{-1}$.

Discussion

The fact that the amount of dibenzyl isolated was much lower than that expected on the basis of HBr opens the question as to which of the two possible mechanisms of decomposition operates in the case of allyl bromide. The two possible modes of decomposition are represented by Eqs. (8) and (9).

$$CH_2{:}CH.CH_2.Br \rightarrow CH_2{:}CH.CH_2. + Br, \quad (8)$$

$$CH_2{:}CH.CH_2.Br \rightarrow CH_2{:}C{:}CH_2 + HBr. \quad (9)$$

Reaction (9) is ruled out, however, since no allene was formed in the pyrolysis of allyl bromide.*[7,8] Hence, the formation of HBr is attributed to reaction (8) only, and in this case the rate of formation of HBr measures the rate of the unimolecular dissociation of allyl bromide into allyl radicals and bromine atoms. This conclusion is supported by the fact that the kinetics of decomposition obeys the first order law, and also by the magnitude of the frequency factor which agrees well with the theoretically expected value of the order of 10^{13} sec.$^{-1}$.

Further evidence for the "radical" split is brought out by the formation of dibenzyl. However, the deficiency of this product from the expected amounts calculated on the basis of the HBr formed indicates that not all allyl radicals are removed by the reaction (10)

$$CH_2{:}CH.CH_2. + C_6H_5CH_3 \rightarrow CH_2{:}CH.CH_3 + C_6H_5CH_2. \quad (10)$$

and that a considerable fraction of these radicals react in some other way. This point is dealt with more fully in the next section.

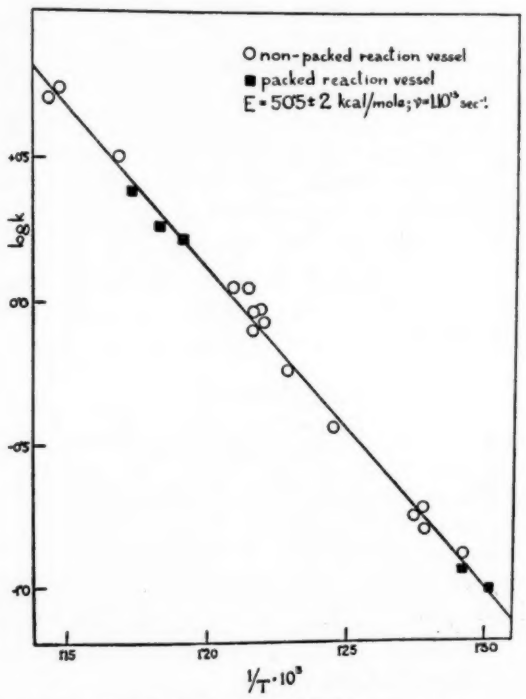

FIG. 2. Benzyl bromide. Plot of log$k$ against $1/T$ for benzyl bromide.

† We are indebted to Messrs. I. C. I. Blackley for the results of the infra-red analysis.

* It seems that some recombination of allyl radicals and Br atoms takes place on the surface, this reaction being of some importance at high stationary concentrations of the respective species.

* It has to be emphasized that the results of the pyrolyses of propylene (see reference 7) and isobutene (see reference 8), in which allene was formed and readily identified, suggest that we could have hardly failed in detecting allene in the present case, had it actually been produced.

[7] M. Szwarc, J. Chem. Phys. **17**, 284 (1949).

[8] M. Szwarc, J. Chem. Phys. **17**, 292 (1949).

TABLE IX.

Run[a]	T°K	$\frac{CH_4+H_2}{HBr}$ percentage	H_2%	Time of contact sec.	Molar ratio of allyl bromide / toluene
14	732	no gas	—	0.62	1:19
21	744	0.7	—	0.58	1:24
1*P*	766	1.7	—	0.59	1:11
8	766	no gas	—	0.56	1:22
2*P*	769	1.4	—	0.60	1:15
7	777	no gas	—	0.56	1:19
11	796	4.0	—	0.56	1:18
9	809	5.1	53	0.52	1:20
10	809	6.0	58	0.54	1:23
18	814	13.3	69	0.55	1:11
15	815	9.8	64	0.56	1:14
20	817	19.0	60	0.81	1:18
17	820	6.5	60	0.56	1:34
16	822	7.9	58	0.50	1:29
19	824	1.1	—	0.18	1:51
12	834	18.9	67	0.54	1:19
13	846	23.3	72	0.54	1:20
5	857	27.3	70	0.51	1:21
6	858	28.2	69	0.50	1:24
4*P*	860	29.2	72	0.53	1:17
3*P*	865	33.6	75	0.53	1:17

[a] *P* denotes the runs carried out in the packed reaction vessel.

Assuming, as usually, that the recombination of radicals involves no activation energy, we conclude that the observed activation energy, attributed to the primary dissociation process (8), can be identified with the C−Br bond dissociation energy in allyl bromide, i.e. $D(CH_2{:}CH.CH_2{-}Br)=47.5\pm2$ kcal./mole. This conclusion can be checked as in the case of benzyl bromide. The directly estimated values for D(C−H) in propylene and D(C−Br) in allyl bromide are 76.5 kcal./mole[4] and 47.5±2 kcal./mole respectively. This leads to

$$D(CH_2{:}CH.CH_2{-}H)-D(CH_2{:}CH.CH_2{-}Br)\simeq 29 \text{ kcal./mole.}$$

On the other hand this difference was estimated at 32±3 kcal./mole by calorimetric measurements of Gellner and Skinner.[6]

The Fate of the Allyl Radical

The allyl radical is stabilized by its high resonance energy† to at least the same extent as the benzyl radical. It is reasonable to expect, therefore, that this radical is not sufficiently reactive to extract readily a hydrogen atom from toluene. This is confirmed by the small amount of propylene formed, i.e. only 20–30 percent of the expected amount on the basis of HBr.

The activation energy for the reaction between toluene and methyl radicals

$$CH_3.+C_6H_5CH_3\rightarrow CH_4+C_6H_5CH_2. \qquad (11)$$

was recently estimated at 12±2 kcal./mole.[9] While this reaction is exothermic to the extent of about 24 kcal./mole, the analogous reaction (10) between allyl radicals and toluene is thermoneutral or even endothermic to the extent of about 1 kcal./mole. We expect, therefore, the activation energy of the latter reaction to be still higher than that required for the reaction of toluene with methyl radicals.

TABLE X.

Run[a]	T°K	K.10^3 sec.$^{-1}$	$K_{766}.10^3$ sec.$^{-1}$
1*P*	766	14.4	14.4
8	766	16.8	16.8
2*P*	769	16.2	14.3

[a] *P* denotes the runs carried out in the packed reaction vessel.

TABLE XI.

Run[a]	T°K	K.10^3 sec.$^{-1}$	$K_{818}.10^3$ sec.$^{-1}$
5	857	415	425
6	858	368	368
4*P*	860	336	305
3*P*	865	333	262

[a] *P* denotes the runs carried out in the packed reaction vessel.

We can give a rough estimate for the activation energy of reaction (10) on the basis of the results obtained from the analysis of the products of decomposition of allyl bromide. The fraction of allyl radicals which reacts with toluene to give propylene is given by the ratio of propylene to HBr formed, the actual ratio being $\frac{1}{3}$–$\frac{1}{5}$. Using the equation

$$[CH_2{:}CH.CH_3]=k_1\cdot[CH_2{:}CH.CH_2.]\cdot[C_6H_5CH_3]\cdot t$$

where $[CH_2{:}CH.CH_3]$ represents the concentration of propylene formed, i.e. $\frac{1}{3}$–$\frac{1}{5}$ of the concentration of allyl radicals,

$$[CH_2{:}CH.CH_2.]=2.10^{-9} \text{ moles/cc},$$
$$[C_6H_5.CH_3]=2.10^{-7} \text{ moles/cc},$$

where t is the time of contact (about 0.5 sec.), we derive that the rate constant k_1 of the reaction responsible for the formation of propylene is given by $k_1=2.5\times10^6$ cc/moles sec. If the steric factor for the reaction between allyl radicals and toluene is "normal"[10] (0.01−0.1), the collision frequency of this reaction becomes $10^{10}-10^{11}$ cc/moles sec. and the activation energy 14–17 kcal./mole. These values seem quite reasonable in view of the activation energy of 12±2 kcal./mole required for reaction (11).

The allyl radicals which are not removed by the reaction with toluene (10) may either dimerise or associate with benzyl radicals.‡ Thus, the inertness of

† The resonance energy of the allyl radical was estimated at about 25 kcal./mole.

[9] M. Szwarc and J. S. Roberts, Trans. Faraday Soc. (in press).

[10] M. G. Evans and M. Szwarc, Trans. Faraday Soc. 45, 940 (1949).

‡ The dibenzyl formed in the pyrolysis of allyl bromide was definitely contaminated by some impurities, and a particularly impure product was obtained in experiments in which the percentage of decomposition was high. It seems that this phenomenon was caused by the formation of an association product between allyl and benzyl radicals. Similar observations were made in pyrolysis of butene −1 (see reference 4).

TABLE XII.

Run	T°K	Time of contact secs.	K.10² sec.⁻¹	K_{824}.10² sec.⁻¹
19	824	0.18	139	139
12	834	0.54	220	153
17	820	0.56	136	157
20	817	0.81	109	139

TABLE XIII.

Run	T°K	$P_{\text{allyl bromide}}$ ×10² mm Hg	K.10² sec.⁻¹	K_{815}.10² sec.⁻¹
19	824	16	139	102
17	820	30	136	121
10	809	45	93.5	116
9	809	48	83.1	103
20	817	58	109	101

TABLE XIV.

Run	T°K	P_{tot} in mm Hg	K.10² sec.⁻¹	K_{815}.10² sec.⁻¹
15	815	6.3	104	104
19	824	8.1	139	102
9	809	10.3	83.1	103
10	809	10.3	93.5	116
17	820	10.4	136	121
16	822	18.0	161	126

the allyl radicals and their possible association with benzyl radicals easily account for the low dibenzyl to HBr ratios observed. Under our experimental conditions the possibility of allyl radicals' dissociating into allene and hydrogen is excluded because of the relatively high value of 68.5 kcal./mole for $D(CH_2{:}C.CH_2.)$.[4,7]

H

The formation of hydrogen and methane can be accounted for by reactions (6a), (6b), and (7). However, since the amount of gases and their hydrogen content were definitely higher than those observed in the pyrolysis of benzyl bromide, we conclude that some additional reactions responsible for this phenomenon must participate in the pyrolysis of allyl bromide. We suggest tentatively that the decomposition of ω̆-phenyl butene-1 or diallyl produces the additional quantity of hydrogen atoms or molecules. This conclusion is supported by the observation that the amount of gases and their hydrogen content increases with increasing concentration of products* (see Table IX).

COMPARISON OF THE C–Br BOND DISSOCIATION IN BENZYL AND ALLYL BROMIDE

We concluded earlier that the determination of activation energies of the respective unimolecular dissociation processes leads to

$$D(C_6H_5.CH_2-Br)=50.5\pm2 \text{ kcal./mole}$$

and

$$\nu_1=1.10^{13} \text{ sec.}^{-1}$$

and

$$D(CH_2{:}CH.CH_2-Br)=47.5\pm2 \text{ kcal./mole}$$

and

$$\nu_2=0.5.10^{13} \text{ sec.}^{-1};$$

ν_1 and ν_2 denoting the respective frequency factors. These values lead to

$$D(C_6H_5CH_2-Br)-D(CH_2{:}CH.CH_2-Br)=3\pm4 \text{ kcal./mole.}$$

An alternative method of estimating this difference is to assume that the frequency factors of both dissociation processes are identical. The experimental errors involved in the determination of activation energies prevent us from confirming or rejecting this assumption. Nevertheless, if we accept it we can estimate the required difference in bond dissociation energies from the equation

$$D(C_6H_5.CH_2-Br)-D(CH_2{:}CH.CH_2-Br)=RT.\ln.(k_2/k_1),$$

where k_1 and k_2 denote the unimolecular rate constants for the dissociation process of benzyl and allyl bromide respectively. Thus we obtain

$$D(C_6H_5.CH_2-Br)-D(CH_2{:}CH.CH_2-Br)=1.5 \text{ kcal./mole.}$$

In this connection it is worth while mentioning that the calorimetric measurements of Gellner and Skinner[6] indicate that

$$\{D(C_6H_5.CH_2-Br)-D(CH_2{:}CH.CH_2-Br)\}-\{D(C_6H_5.CH_2-H)-D(CH_2{:}CH.CH_2-H)\}\simeq3 \text{ kcal./mole,}$$

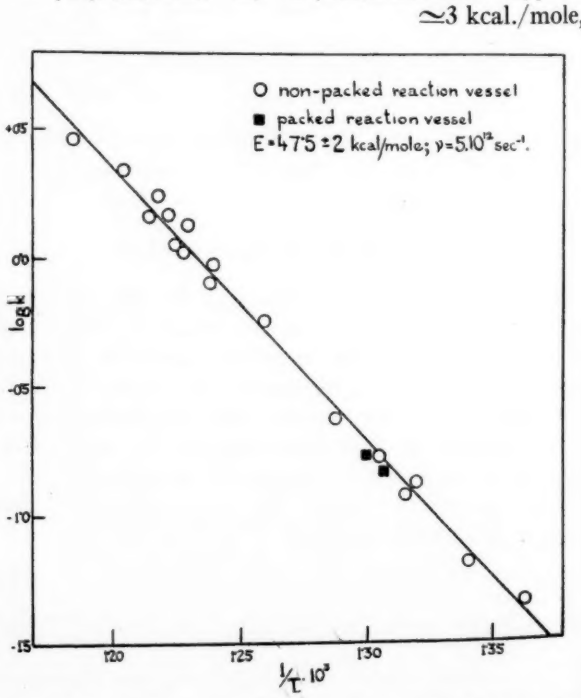

FIG. 3. Allyl bromide. Plot of log$k$ against $1/T$ for allyl bromide.

* We attempted to obtain some information about the nature of the additional products by *u.v.* analysis. The minute quantities and the complex nature of these prevented us, however, from getting any conclusive evidence.

which means that the decrease between the respective C–H and C–Br bond dissociation energies is about 3 kcal./mole greater in the case of allyl compounds than in the case of benzyl compounds.

THE PROBLEM OF IONIC CONTRIBUTION

The concept of ionic-covalent resonance was introduced by Pauling[11] and further discussed by Baughan, Evans, and Polanyi.[12] According to these authors the increase in ionic contribution should reveal itself by an increase in the bond dissociation energy.

The C–Br bond dissociation energy in methyl bromide may be estimated either from thermochemical data using $D(CH_3-H)=102$ kcal./mole,[13] or from the results of pyrolysis of methyl bromide.† Both methods lead to $D(CH_3-Br)=67$–68 kcal./mole. We can compare, therefore, the differences of the C–H and C–Br bond dissociation energies in the corresponding hydrocarbons and bromides:

$$D(CH_3-H)-D(C_6H_5.CH_2-H)=24.5 \text{ kcal./mole}$$
$$D(CH_3-Br)-D(C_6H_5.CH_2-Br)=17\text{–}18 \text{ kcal./mole}.$$

The decrease in the C–H bond dissociation energy is attributed to the resonance energy of the benzyl radical. The smaller decrease in the C–Br bond dissociation energy means, therefore, that some additional factor is responsible for the increase of the C–Br bond dissociation energy in benzyl bromide. Similar conclusions can be drawn for allyl bromide. Our general knowledge of the chemical behavior of methyl bromide and benzyl bromide suggests that the ionic character of the C–Br bond is stronger in the latter compound. If one accepts this argument one has to conclude that the increase in ionic character increases the bond dissociation energy. Baughan, Evans, and Polanyi[12] arrived at a similar conclusion on the basis of the results obtained for various C–I bond dissociation energies.

TABLE XV.

Run	T°K	P_{tot} in mm Hg	$P_{\text{allyl bromide}}$ $\times 10^3$ in mm Hg	Time of contact secs.	% decomposition	K.10 sec.$^{-1}$
14	732	10.5	55	0.62	2.6	4.3
21	744	10.7	44	0.58	3.6	6.4
1*P*	766	11.0	90	0.59	8.2	14.4
8	766	10.1	45	0.56	9.05	16.8
2*P*	769	10.8	66	0.60	9.25	16.2
7	777	10.3	51	0.56	12.5	23.8
11	796	10.6	56	0.56	28.	59.2
9	809	10.3	48	0.52	35.	83.1
10	809	10.3	45	0.54	40.	93.5
18	814	10.7	101	0.55	51.	129
15	815	6.3	43	0.56	44.	104
20	817	10.6	58	0.81	59.	109
17	820	10.4	30	0.56	53.	136
16	822	18.0	45	0.50	55.	161
19	824	8.1	16	0.18	22.	139
12	834	10.2	51	0.54	70.	220
13	846	10.3	49	0.54	79.	287
5	857	10.2	46	0.51	88.	415
6	858	10.1	41	0.50	84.5	368
4*P*	860	10.4	59	0.53	83.	336
3*P*	865	10.6	61	0.53	83.	333

[11] L. Pauling, *The Nature of the Chemical Bond* (Cornell University Press, Ithaca, N. Y., 1945).

[12] Baughan, Evans, and Polanyi, Trans. Faraday Soc. **37**, 377 (1941).

[13] G. B. Kistiakowsky and E. R. Van Artsdalen, J. Chem. Phys. **12**, 479 (1944).

† Unpublished results of A. H. Sehon and M. Szwarc.

THE JOURNAL OF CHEMICAL PHYSICS VOLUME 18, NUMBER 9 SEPTEMBER, 1950

Quantum-Mechanical Resonance between Identical Molecules

HERBERT JEHLE
University of Nebraska, Lincoln, Nebraska
(Received February 20, 1950)

The process of synapsis of chromosomes in meiosis and the process of self-duplication of genes in mitosis reveal the existence of a highly specific attraction between pairs of large molecules provided they are identical and rigid. We shall investigate the quantum-mechanical behavior of a pair of molecules which interact with each other by means of vibrating electric dipole moments which are thermally excited. Because of resonance between equal frequency modes or commensurable modes of vibration, each one of the molecules shows a statistical preference for certain phase relations between these modes (using the language of the correspondence principle). A pair of molecules interacts strongly if it is an identical pair because of these phase preferences.

INTRODUCTION

SEVERAL investigators have examined the characteristic properties of the interaction forces which are at work in synapsis of chromosomes and in autosynthesis of genes. It became clear that these specific interaction forces cannot be accounted for by ordinary chemical bond formation. This does not mean, however, that they do not fit into the scheme of intermolecular forces which quantum mechanics is able to explain.

A statement of the biological problem is given in Sections I and II. In Section III we discuss the types of interaction between a pair of thermally excited vibrators. In the remaining sections the interaction by means of vibrating electric dipole moments will be investigated in view of an explanation of a specific attraction between identical large molecules. Classical statistical mechanics cannot account for the specificity in question (Section IV). Also quantum statistics of a pair of simple vibrators does not show an attraction which would be particularly strong if the vibrators are identical (Section V). On the other hand, two large molecules will show a strong attraction toward each other if both have the same commensurabilities in between many of their modes, and they therefore show the same phase preferences between the vibrations of their commensurable modes.

We proceed first to give a qualitative argument in terms of the correspondence principle (Sections VI and VII). Then, in order to check this argument and in order to outline a straightforward quantum-mechanical treatment of the problem, we calculate the quantum-mechanical partition function for a simplified model. After noting what corresponds to classical phase preferences in quantum-mechanical language (Section VIII), we give a short review of quantum-mechanical resonance between commensurable modes in a molecule (Section IX).

The simplified model consists of a pair of molecules, each having but two modes between which there is some coupling (parameter λ). In Section X some of the eigenfunctions, and first- and second-order energy level perturbations are given. The attraction is calculated by means of the partition function. It is of the same type as dispersion forces.[1] An extension of the calculation for large molecules (Section XI) shows an attraction which increases very strongly with the coupling parameter λ and with the number of commensurable modes, in analogy to the effect of phase preferences discussed in Section VII.

In order to illustrate the kind of specificity of this strong attraction, we detune the model in various ways (Section XII) and find that the strong attraction depends upon the presence of the same kind of phase preferences in both molecules of the pair. Such corresponding phase preferences evidently prevail if the two molecules are identical.

I. SPECIFICITY PROBLEMS IN BIOLOGY

In a number of biological phenomena we encounter highly specific interactions between molecules. We have to distinguish between two entirely different phenomena. On the one hand two like or unlike atoms or molecules may combine with each other rather than with another atom or compound available in the surrounding medium, just because of chemical affinity. On the other hand there are several very general types of specific interactions which, for various reasons, cannot be accounted for by chemical bond formation. These we would like to investigate here.

We shall discuss specific interactions as they occur in the process of synapsis of homologous chromosomes (in meiosis) and in the very remarkable process of self-duplication of chromosomes (in mitosis), the specificity of the processes depending on a pair of large molecules being identical, or almost identical. These phenomena are so general that they demand some explanation which will not be dependent upon detailed assumptions about the model by which we hope to explain them.

Synapsis is a stage of meiosis (reduction division leading to the formation of gametes). Before the diploid cell can divide into two haploid cells, the 48 chromosomes (in man) of the diploid cell have to conjugate into 24 pairs of homologous chromosomes so that in the subsequent reduction 24 different chromosomes keep company. Here is a phenomenon in which homologous,

[1] F. London, Proc. Faraday Soc. (1937).

that is, almost identical gene complexes of two chromosomes line up with each other because of their identity. This is most beautifully evidenced in inverted synapsis. Compared with self-duplication, synapsis is much more a macrophenomenon, involving much larger molecules and larger distances, and it is not quite so highly specific as self-duplication.

The phenomenon of *self-duplication* of the genes is one stage in the reproduction process of chromosomes during mitosis (ordinary somatic cell division). Self-duplication occurs before the double chromosome splits by longitudinal division into two daughter chromosomes. A chromosome is a long fibre-like structure containing a row of genes or gene complexes. Each gene is made up of many large "constituent molecules" linked together by chemical bonds. (We leave it open whether in the following a "constituent molecule" is to be understood as a protein, a nucleic acid, a nucleoprotein molecule, or rather only part of all these, e.g., a peptide ring.) A duplicated chromosome consists of two such fibrous structures which lie parallel close to each other. Their distance, however, is of a larger order of magnitude than the usual distance between chemically bound atoms.

The current view about self-duplication is as follows. The building up of a duplicate by the original gene is understood as a gradual collection of molecules which are readily available from the surrounding medium, and which happen to be identical with the constituent molecules of the original gene. It is a selective attraction of the proper molecules into the neighborhood of the constituent molecules in the original gene. Thereafter, the constituent molecules of the daughter gene have a chance to join together by chemical bond-formation and so provide for the synthesis of a complete daughter gene. If one can show a specific attraction to exist between identical large molecules, one has taken the main hurdle.

We started with the description of synapsis as it involves only the specific interaction (auto-attraction) of almost identical macromolecules, whereas self-duplication (autosynthesis) involves not only the phenomenon of auto-attraction and of bond formation in the daughter genes, but also the assumption that the constituent molecules are readily available in the surrounding medium.[2] The problem of synthesis of the "readily available" constituent molecules (together with many other molecules which are not used in building the genes) is likely to be a much simpler problem, as these molecules are simpler and of a much smaller variety, e.g., such as peptides. In this note we shall, for brevity, use the word "constituent molecules" (or sometimes just "molecules") for both the big macromolecules involved in synapsis (the rigid genes or gene-complexes of which a chromosome thread is made) and the much smaller molecules which are being attracted in the process of self-duplication of a gene.

II. BASIC FACTS BEARING UPON SELF-DUPLICATION

Let us try to explain the specificity involved in the above described phenomena, looking at chromosomes and their constituent genes and smaller parts as unsophisticated molecules, and see how far we are able to go before we consider them as servomechanisms.

What is particularly characteristic about these phenomena? As H. J. Muller has pointed out, synapsis and even more so self-duplication are very general processes of unbelievable versatility. These processes work for all kinds of genes to the extent that even mutations become accurately inheritable through self-duplication. Furthermore, there is the enormous accuracy which makes exact self-duplication usually not fail in the sequence of many chromosome generations through which identical replicas of a gene are transmitted.

What would happen if there were an occasional mistake in self-duplication, meaning a production and (in the case of sex cells) a handing down of a defective set of chromosomes to the next generation? The result would be similar to that when a gene changes by itself (lethal or non-lethal change). We have thus two different types of mutations. We understand the latter mutations (in particular their mutation rates in their dependence on temperature and on radiation) to behave like a monomolecular reaction of the individual gene by itself;[3] the mistakes in self-duplication on the other hand behave differently. Therefore we have some means of discriminating between the two types' share in the total mutation rate. Experimental work is now going on to determine the relative number of mistakes in self-duplication compared with the monomolecular gene mutations.

The versatility and accuracy of the self-duplication process make it hopeless to look for explanations which involve chain reactions[4] because they present the difficulty that a different reaction would have to be invoked for every different gene.

Also in other respects this specificity does not fit into the pattern of ordinary chemical bond formation. It does not seem very promising to consider self-duplication as a surface phenomenon in which exact replica formation of a gene is explained on the hypothesis that the gene is a surface structure and that the shape of the new molecules' surface is to fit exactly that of the original molecule. Steric effects are not sufficient to explain the accuracy of self-duplication. Furthermore, it is artificial to assume that self-duplicating genes are an almost monatomic layer. This they

[2] H. J. Muller, Sci. Monthly 44, 212 (1937).

[3] N. W. Timofeeff-Ressovsky and M. Delbrück, Goettinger Nachrichten, (Biologie), p. 189, (1935).

[4] M. Delbrück, Cold Spring Harbor Symposium 9, 1941.

would have to be if steric effects were to account for the formation of exact replicas.

The distance between a pair of molecules which shows specific interaction is usually very large compared with the range of chemical bonds. In the case of self-duplication of a gene this interaction force must at least act over a range equal to the distance between corresponding constituent molecules of a gene and its self-duplicated daughter gene, a distance of the order of the diameter of a gene. In synapsis it will even have to act over a range equal to the distance between the center lines of the two chromosome threads, a distance large compared with interatomic distances. Specific interaction of corresponding genes during synapsis, particularly in the case of inverted synapsis, is the most interesting evidence for a fairly long-range specific interaction in the cell.

III. COUPLED THERMAL VIBRATIONS OF A PAIR OF IDENTICAL MOLECULES

Let us follow up some suggestions brought up by H. J. Muller.[5] We shall investigate how the interaction between a pair of large molecules is influenced by the circumstance that at least part of their vibrational modes are identical for the two molecules. By identical we understand that the vibrational spectrum, the preferred phase-relationships between commensurable modes, and the relative orientations of the vibrational modes of one of the molecules are the same as those of the other molecule.

It is reasonable to investigate thermal vibrations as the cause of specificity because of the fact that the genes in whose interaction we are interested are molecules which perform well-defined vibrations, as they have a very definite structure. X-ray investigations of some proteins by Bernal and others have shown such enormous numbers of Fourier components that even without knowing their structure we know that every atom is located at a well-defined place. This well-defined structure and the rigidity of the molecules exist as long as they are not denatured or dehydrated. (Rigidity is also often inferred from entropy changes with denaturation, or from behavior of viscosity.) Protein molecules are extraordinary in this respect.[6]

A different kind of argument can be advanced for the fixed structure of the genes. Organic molecules in the cell are usually forming and breaking bonds at a considerable rate. If a long chain molecule breaks into two, there may be several possibilities of the two broken ends joining other different molecules, rather than healing with each other again. The healing process is unlikely because of the small probability of the broken ends returning into each other's spheres of influence. On the contrary, if a molecule has a well-defined structure with little or no possibility of performing internal rotations about single bonds, any bond will have a high probability of healing up again after it was broken. This circumstance will bring about a high stability for such a molecule. Conversely, a gene must owe its notorious stability, besides other factors, to its rigidly defined molecular structure (necessary condition for stability).

We shall assume that the smaller constituent molecules of which a gene is built up (e.g. peptide rings) are rigid also.

Each molecule of a pair of constituent molecules is assumed to vibrate as an independent unit. The interaction of the internal vibrational modes of these molecules with the surrounding medium or with the adjacent constituent molecules are both assumed to be small. The interaction of the surrounding medium with the pair of molecules amounts to a weak coupling of the Brownian motion of the temperature bath provided by the medium with the thermal vibrations of the two molecules.

The range of frequencies and amplitudes of mechanical vibrations are discussed in the appendix. We know the vibrational spectrum to be as high as 3000 cm^{-1} or 300 cm^{-1}. From there on, of course, we have many lower frequencies just as a solid has in Debye's theory of specific heat. Remembering that $kT/hc \sim 200$ cm^{-1} we have level spacings of vibrational modes both $>$ and $< kT$. The vibrational amplitudes range in the order of 10^{-9} cm.

We come now to the problem: what forces provide for the interaction between the vibrations of one molecule and those of another, i.e., what are the coupling forces between a pair of vibrators? We have to consider the following properties of various forces when deciding which ones are responsible.:

(1) Their range.

As a cause for the coupling it excludes exponentially decreasing forces such as direct chemical bonds between the pair.

(2) Their relaxation time.

Forces which involve an adjustment towards a statistical equilibrium distribution cannot follow the frequencies of a vibrating molecule. So the Debye-Hückel forces and the orientation effect contributions to Van der Waals forces (Keesom) take too much time to provide for vibrational coupling.

(3) The effect of the medium between the pair of molecules on the coupling force.

The coupling of the vibrations of the two molecules with the mechanical vibrations of the medium is small. Otherwise it would be difficult to understand why the experiments show that a molecule's vibrational spectrum is so little dependent on it being in solution or not. If this were not the case, it would also not be explainable why two molecules are supposed to be able to recognize each other with high accuracy on account of their having an identically same frequency spectrum. We there-

[5] Proc. Roy. Soc. **B134**, 1 (1947). Cold Spring Harbor Symposium **9**, 290 (1941). The Am. Naturalist **56**, (1922).

[6] I. Langmuir, Proc. Phys. Soc. **51**, 592 (1939). J. D. Bernal and I. Fankuchen, J. Gen. Physiol. **25**, 111.

fore do not expect hypersonic vibrations transmitted through the medium to be responsible for the coupling. A further difficulty would come up if the interaction were provided by vibrations of the medium. The Brownian movement in the medium would cause much noise to be superimposed on interaction forces and actually jam them, because the interaction energy is small compared with the vibrational energy of the thermally excited pair of molecules, and very small compared with the energy of the noise.

Let us therefore consider electric dipole-dipole interactions between the pair; the mechanical vibrations of each of the two molecules will evidently be accompanied by vibrations of their charge distributions. For simplicity we take just the electric dipole moment of the vibrational modes in considering their interaction, though actually quadrupole and higher moments are important too. Every kind of vibrational mode will usually have some electric dipole moment associated with it. As the highest frequencies have an electromagnetic wave-length between (1/300) cm and (1/3000) cm, we usually need not take into account retardation effects. We shall not consider the Debye induction effect because it is not specific.

So far we have discussed the vibrating electric charge distribution (of the electronic shells and of the nuclei) which accompanies the mechanical vibrations of the nuclei. But perhaps this may not be the most important source of vibrating charge distributions. It may be that vibrations of the hydrogen bridges or extended electronic oscillators[7] or even ordinary electronic transitions provide the essential contribution to the molecules' electric dipole vibrations. For the following sections, however, it is of but secondary importance which of these phenomena provide the source for the electric vibrations.

If we want to explain specific interaction, we have to see how the interaction of an identical pair differs from that of an almost identical pair and of a non-identical pair of molecules. We want to find out how the interaction depends on the coupling between the dipole pairs, i.e. on the distance R between the molecules. We want to investigate first a pair of simple vibrators and afterwards a pair of molecules represented by two orchestras of vibrators. The word "orchestra" does not mean that we represent a molecule by a set of independent vibrators, but that we think of the coupling between the modes of a molecule. This is a generalization essential for the understanding of specificities. Finally, we want to study the dependence of the effect on h/T.

IV. CLASSICAL LIMIT (ABSENCE OF SPECIFIC EFFECTS)

In the following we like to use the work "specific attraction" as denoting an attraction which depends on identical vibrational behavior of the pair of molecules.

[7] F. London, AAAS Publication No. 21, 141 (1943).

Consider a pair of linear harmonic vibrators, e.g. two negatively charged mass points vibrating about two positively charged centers a distance R apart. The vibration goes along the line connecting the centers, with displacements, z_I, z_{II}. I, II stand for molecules I and II. Their Hamiltonian is

$$\mathcal{T}+\mathcal{U}=\tfrac{1}{2}(m_I^{-1}p_{zI}^2+m_{II}^{-1}p_{zII}^2)+\tfrac{1}{2}(k_I^2z_I^2+k_{II}^2z_{II}^2)-2e^2R^{-3}z_Iz_{II}. \quad (4.1)$$

Therefore the partition function

$$Z=\int\int \exp(-\mathcal{T}/kT)dp_{zI}dp_{zII} \times\int\int \exp(-\mathcal{U}/kT)dz_Idz_{II} \quad (4.2)$$

will contain the masses m_I, m_{II} only through the first double integral, i.e. as factors in Z. Thus the attractive force $-kT\partial \log Z/\partial R$ is independent of the masses, i.e., independent of whether the frequencies of the pair are identical or not.

V. QUANTUM-MECHANICAL RESONANCE OF A PAIR OF SIMPLE VIBRATORS

Let us first study what would happen if only one of the vibrational modes of each molecule were excitable. We represent them by coordinates q_I, q_{II}; normal coordinates can be defined for small q if we can neglect anharmonic terms. In the one dimensional case we define $q_I=m_I^{\frac{1}{2}}z_I$ and we use the abbreviation $\kappa_I=m_I^{-\frac{1}{2}}k_I$. The x, y axes shall be perpendicular to the line connecting the two molecules. Then the molecules' orientation with respect to the axes may be described by stating that the components of the electric dipole moments which accompany the two linear mechanical vibrations q_I, q_{II} are

$$\mu_{zI}q_I,\ \mu_{yI}q_I,\ \mu_{zI}q_I,\ \mu_{zII}q_{II},\ \mu_{yII}q_{II},\ \mu_{zII}q_{II}. \quad (5.1)$$

We consider first the interaction for a given fixed orientation; the ratios of the μ's are regarded as parameters which describe orientation effects to be discussed later.

The Hamiltonian is

$$H=\tfrac{1}{2}(\dot{q}_I^2+\dot{q}_{II}^2)+\tfrac{1}{2}(\kappa_I^2q_I^2+\kappa_{II}^2q_{II}^2)+\text{anharmonic terms}+R^{-3}[\mu_{zI}\mu_{zII}+\mu_{yI}\mu_{yII}-2\mu_{zI}\mu_{zII}]q_Iq_{II}. \quad (5.2)$$

The equations of motion yield, in the harmonic limit, a secular equation for the frequencies ω_+ and ω_- of the inphase and the antiphase vibrations,

$$\omega_\pm^4-\omega_\pm^2(\kappa_I^2+\kappa_{II}^2)+\kappa_I^2\kappa_{II}^2-R^{-6}[\mu\mu]^2=0. \quad (5.3)$$

The well-known solution of this equation is

$$\omega_\pm^2=\omega^2(1\pm\epsilon),\quad \omega_\pm=\omega(1\pm\tfrac{1}{2}\epsilon-\tfrac{1}{8}\epsilon^2\pm\tfrac{1}{16}\epsilon^3-(5/128)\epsilon^4) \quad (5.4)$$

where

$$\omega^2=\tfrac{1}{2}(\kappa_I^2+\kappa_{II}^2) \tag{5.5}$$

$$\epsilon=\{(\kappa_I^2-\kappa_{II}^2)^2+4R^{-6}[\mu\mu]^2\}^{\frac{1}{4}}(\kappa_I^2+\kappa_{II}^2)^{-1}. \tag{5.6}$$

ϵ is small compared with unity; the signature of the square root is to be equal to the signature of $[\mu\mu]$ of Eq. (5.2).

$$\left.\begin{aligned}&\tfrac{1}{2}(\omega_++\omega_-)\sim\omega(1-\tfrac{1}{8}\epsilon^2-(5/128)\epsilon^4),\\&\tfrac{1}{2}(\omega_+-\omega_-)\sim\omega(\tfrac{1}{2}\epsilon+\tfrac{1}{16}\epsilon^3).\end{aligned}\right\} \tag{5.7}$$

For identical or almost identical vibrators we have

$$|2R^{-3}[\mu\mu]|\gg|\kappa_I^2-\kappa_{II}^2| \tag{5.8}$$

$$\left.\begin{aligned}&\epsilon^2\sim 4R^{-6}[\mu\mu]^2(\kappa_I^2+\kappa_{II}^2)^{-2}\\&\omega_\pm^2\sim\tfrac{1}{2}(\kappa_I^2+\kappa_{II}^2)\pm R^{-3}[\mu\mu]\end{aligned}\right\}. \tag{5.9}$$

For dissimilar vibrators we have

$$|2R^{-3}[\mu\mu]|\ll|\kappa_I^2-\kappa_{II}^2| \tag{5.10}$$

$$\left.\begin{aligned}&\epsilon^2\sim\{1+4R^{-6}[\mu\mu]^2(\kappa_I^2-\kappa_{II}^2)^{-2}\}\\&\qquad\times(\kappa_I^2-\kappa_{II}^2)^2(\kappa_I^2+\kappa_{II}^2)^{-2}.\\&\text{If we let } \kappa_I \text{ be larger than } \kappa_{II} \text{ we can write}\\&\omega_\pm^2\sim\tfrac{1}{2}(\kappa_I^2+\kappa_{II}^2)\pm\tfrac{1}{2}(\kappa_I^2-\kappa_{II}^2)\\&\qquad\pm R^{-3}[\mu\mu]\{R^{-3}[\mu\mu](\kappa_I^2-\kappa_{II}^2)^{-1}\},\end{aligned}\right\} \tag{5.11}$$

with the understanding that the upper and lower signs, respectively, on the right-hand side correspond to ω_+ and ω_-, respectively, if $[\mu\mu]$ is positive, and to ω_- and ω_+, respectively, if $[\mu\mu]$ is negative. We find (5.9) and (5.11) plotted in Herzberg.[8] Note that even far away from exact resonance, i.e. $\kappa_I-\kappa_{II}\sim|R^{-3}[\mu\mu](\kappa_I^2+\kappa_{II}^2)^{-\frac{1}{2}}|$, the resonance effect $\omega_--\kappa_I=\kappa_{II}-\omega_+$ still is of the order of $|R^{-3}[\mu\mu](\kappa_I^2+\kappa_{II}^2)^{-\frac{1}{2}}|$. The quantum states of these harmonic vibrators are

$$E_{n_+n_-}=\hbar\{(n_++\tfrac{1}{2})\omega_++(n_-+\tfrac{1}{2})\omega_-\}. \tag{5.12}$$

We see from Fig. 1 immediately[9] that (for $[\mu\mu]<0$) n_+ predominates over n_- among thermally accessible quantum states, i.e. we get attraction.

Let us discuss the eigenfunctions in the case of identical pairs of vibrators, see Section VIII. Dots represent ψ functions which are symmetric functions of q_I and q_{II}, circles represent antisymmetric functions. Instead of this representation of ψ as a product of inphase ψ and antiphase ψ, i.e.

$$\psi_{n_+n_-}=\psi_{n_+}(q_+)\psi_{n_-}(q_-),\quad q_\pm=q_I\pm q_{II} \tag{5.13}$$

we could have used, in this case of close resonance, a "resonance" representation whose zero-order eigenfunction is

$$\psi_{nm}{}^{(0)}=2^{-\frac{1}{2}}(\psi_n(q_I)\psi_m(q_{II})\pm\psi_m(q_I)\psi_n(q_{II})). \tag{5.14}$$

[8] G. Herzberg, *Infared and Ramanspectra* (D. Van Nostrand Company, Inc., New York, 1945), p. 216; L. Pauling, *Chemical Bonds* (Cornell University Press, Ithaca, New York, 1940), p. 18, or H. Jehle, Proc. Nat. Ac. Sci. **36**, 242 (1950).

[9] See W. Heisenberg, Zeits. f. Physik **38**, 415 (1926).

The partition function Z for the pair of harmonic vibrators gives

$$\begin{aligned}\log Z=-\{&\tfrac{1}{2}\hbar\omega_+/kT+\log(1-\exp(-\hbar\omega_+/kT))\\&+\tfrac{1}{2}\hbar\omega_-/kT+\log(1-\exp(-\hbar\omega_-/kT))\}.\end{aligned} \tag{5.15}$$

In the classical limit $\hbar\omega/kT\ll1$

$$\begin{aligned}\log Z\to&-\log\hbar\omega_+/kT-\log\hbar\omega_-/kT\\&=-\log\{(1-\epsilon^2)^{\frac{1}{2}}(\hbar\omega/kT)^2\}\end{aligned} \tag{5.16}$$

$$\partial\log Z/\partial R\to\tfrac{1}{2}(1-\epsilon^2)^{-1}\partial\epsilon^2/\partial R. \tag{5.17}$$

In the other limit $\hbar\omega/kT\gg1$

$$\begin{aligned}\log Z\to&-\tfrac{1}{2}\hbar\omega_+/kT-\tfrac{1}{2}\hbar\omega_-/kT\\&+\exp(-\hbar\omega_+/kT)+\exp(-\hbar\omega_-/kT)\\&=-(1-\tfrac{1}{8}\epsilon^2-(5/128)\epsilon^4)(\hbar\omega/kT)\\&+(2+\tfrac{1}{4}\epsilon^2(\hbar\omega/kT)+\tfrac{1}{4}\epsilon^2(\hbar\omega/kT)^2)\\&\qquad\times\exp(-\hbar\omega/kT)\end{aligned} \tag{5.18}$$

$$\begin{aligned}\partial\log Z/\partial R\to&\{\tfrac{1}{8}(1+\tfrac{5}{8}\epsilon^2)(\hbar\omega/kT)\\&+(\tfrac{1}{4}(\hbar\omega/kT)+\tfrac{1}{4}(\hbar\omega/kT)^2)\\&\qquad\times\exp(-\hbar\omega/kT)\}\partial\epsilon^2/\partial R.\end{aligned} \tag{5.19}$$

The attractive force between the pair of vibrators which is proportional to $\partial\log Z/\partial R$ is non-specific in both limits because $\partial\epsilon^2/\partial R$ does not depend on $(\kappa_I^2-\kappa_{II}^2)$ (i.e. on the coincidence of κ_I and κ_{II}); the factors $(1-\epsilon^2)^{-1}$ and $(1+\frac{5}{8}\epsilon^2)$ are both of the order of magnitude one. In the classical limit we have proved this already in Section IV. In the other limit we have actually the case of London's dispersion forces before us.

VI. A MOLECULE CONSIDERED AS A SET OF COUPLED VIBRATORS (CORRESPONDENCE TREATMENT)

In a large molecule we may have many repetitions of the same radicals or atoms which, if they were noninteracting ("unperturbed"), would perform similar vibrations with identical or almost identical frequencies. Actually they interact because of their vibrating electric dipole-dipole coupling and because they all are attached to the main body of the molecule.

In a large molecule we also have many radicals or atoms which perform commensurable vibrations. Anharmonic terms in the potential energy of the restoring forces bring about coupling between "modes" with commensurable or almost commensurable frequencies. In the case of a molecule with anharmonicities we can talk about vibrational modes only in the approximation of infinitely small vibrational amplitudes. Let q_1 and q_2 denote two "normal coordinates." The word "modes" then implies that there are no bilinear terms q_1q_2 in the Hamiltonian, but among cubic and higher terms there are perturbing coupling terms between the modes q_1 and q_2. These coupling terms may be very strong since q_1 and q_2 are modes of a single molecule.

If the unperturbed modes q_1 and q_2 have the same or almost the same frequency, or if they have commensurable or almost commensurable frequencies, then the eigenfunctions of the coupled system correspond to different phase relations between the phases of the

unperturbed "modes." In the simplest case this would imply inphase and antiphase relations if we express the coupled system in terms of the zero-order wave functions of the uncoupled modes, see the analysis of an analogous case in Section VIII. The energy difference of these different eigenfunctions, due to coupling, is strongest in this case of resonance. It is advantageous to carry through at least the qualitative considerations in terms of the corresponding Bohr quantum theory. Speaking in terms of the correspondence principle, we get, because of the Boltzmann factor $\exp(-E/kT)$, a statistical preference for certain phase relations which we may call "inphase," whatever the commensurability ratio may be.

The establishment of preferred phase relations will be particularly strong if we have a great number n of commensurable modes in one molecule. Such a molecule will, in the course of the period of lowest mode (most of the time), perform a fairly well-defined motion. The large molecule can therefore be cautiously replaced by a single macroscopic "representative vibrator" vibrating, say, with the frequency of the lowest mode and with a very large representative amplitude. We have to keep in mind only that this molecule's number of quantum states, or phase space volume which it occupies while performing vibrations of a given representative amplitude, increases very strongly with a small rise of this amplitude. This is because the number of neighboring states all belonging to the same representative amplitude goes up enormously with increasing amplitudes.

Let us point to a well-known analogous phenomenon which, strictly speaking, belongs to the domain of self-excited rather than free vibrations. If you sing a clear tone before a microphone, the acoustic system of the singer plus the microphone causes oscillations with various overtones. These have phase relationships established among themselves. This becomes evident from inspection by means of an oscilloscope connected to the microphone. Just these phase relationships permit a distinct pattern to be seen on the screen during many sweeps of the oscilloscope. The strong coupling between the various "modes" of one molecule brings about such phase related motion also in the thermally excited vibrations of a molecule.

In order to simplify this qualitative description we may momentarily make a crude assumption which certainly will not satisfy the actual case. We assume that instead of phase preferences we have true phase locking in between the modes of a large molecule.

VII. THE PAIR OF MOLECULES

Such a molecule behaves somewhat like a large amplitude vibrator when interacting with another identical molecule. This it does for the following reason. If the lowest modes of the pair of molecules are inphase, then because of the phase locking between the various modes of each one of the molecules, all other modes are pairwise inphase too, and they all add up to a strong dipole-

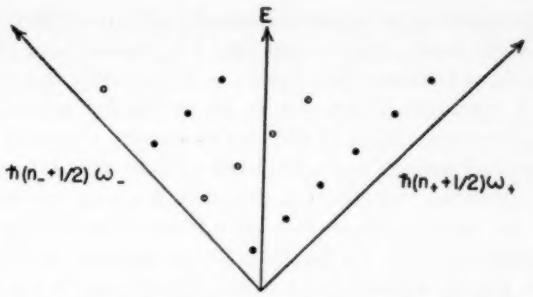

FIG. 1. Energy states for negative $[\mu\mu]$, e.g. parallel aligned dipoles vibrating in the Z direction.

dipole interaction energy between the pair of molecules. Other phase relations between the pair of lowest modes, of course, do not give this strong interaction energy. The phase relations between the pair of molecules *I*, *II* correspond to eigenfunctions which are symmetric or antisymmetric with respect to *I*, *II*. Though under the influence of Brownian motion there is always intercombination between symmetric and antisymmetric states and thus between different phase relations of molecules *I* and *II*, we have a strong statistical preference for the energetically lower inphase vibrations, inphase in the case of z components in dipole-dipole coupling. The situation may be represented by a diagram similar to Fig. 1, representing the thermally accessible quantum states with the modification that higher statistical weights will have to be attributed to higher quantum states. More precisely, a state $n_+=3$, $n_-=1$ which indicates a strong excitation of the inphase mode and a weak excitation of the other mode will, in this picture, have the same statistical weight as a state $n_+=1$, $n_-=3$; the statistical weights will very strongly increase with higher quantum numbers of this representative pair of large amplitude vibrators. Thermal accessibility on the other hand, can be represented by a horizontal line $E=$constant, limiting the region of accessible states. Consequently, the thermal excitation of the inphase mode will be overwhelming compared with that of the antiphase mode, i.e. the number of thermally excited states in which n_+ dominates over n_- is much larger than that in which $n_->n_+$. The net effect of the contribution of all quantum states amounts to a decrease of the free energy, which means that it amounts to an attraction.

If we consider phase preferences instead of strict phase locking inside the molecules, we will get a similar effect but of a smaller order. In the classical limit $h/T\to 0$, resonance effects and specific attraction disappear. In order for this effect to arise, quite an orchestra of modes of one of the molecules has to correspond to that of the other, i.e. the two molecules have to show the same vibrational commensurabilities in between their modes. This is likely to happen only if the two molecules are structurally identical.[10] A slight difference

[10] I. Langmuir once suggested that a cumulative effect of many small interaction energies be responsible for specificity.

in between the two molecules usually will cause differences in their mode orientations and frequencies, and phase relations between their modes so as to nullify the effect.

A condition which has to be satisfied concerns the relative orientation of the two molecules. Consider two identical molecules in the same mutual orientation as, for example, two identical closed books lying one on top of the other with each book's front cover facing upwards, but with the bindings facing opposite directions (cf. Fig. 2). Let the z axis in this illustration be vertical, i.e. in the direction connecting the centers of the two molecules. If each of the molecules vibrates *en bloc* with established phase relationships and if the pair of molecules vibrates in synchronism, we have a form of motion in which the z_I, z_{II} components of vibration all vibrate e.g. inphase and therefore all x_I, x_{II} components of vibration and all y_I, y_{II} components vibrate in antiphase. So all three components contribute an attractive perturbation potential through $[\mu\mu]$ cf. Eq. (5.2).

The peculiar kind of mutual orientation mentioned is caused by the same anharmonic resonance effect as the attraction itself: The pair has lower energy if orientated in that way. Brownian motion will bring about an orientation of lowest energy.

VIII. CORRESPONDENCE BETWEEN THE QUANTUM-MECHANICAL DESCRIPTION AND THE OLD QUANTUM THEORETICAL DESCRIPTION

Let us recall some simple correspondence arguments. Consider the simple one-dimensional problem of a pair of identical linear harmonic vibrators I and II, a distance R apart, and vibrating along the axis connecting them. The effect of a perturbing interaction energy $-2z_Iz_{II}e^2R^{-3}$ causes resonance between the pair. The classical and old quantum theoretical description states that the classical frequency suffers a shift up or down depending on the classical phase relations between the two vibrations (inphase or antiphase). We can introduce an inphase and an antiphase mode which will stay normal in the perturbed system.

From the unperturbed individual eigenfunctions

$$\psi_n(z_I, t) \quad \text{and} \quad \psi_m(z_{II}, t),$$

the wave mechanical description of this resonance phenomenon builds a symmetric and an antisymmetric wave function.

$$\psi_{nm}{}^{(0)} = 2^{-\frac{1}{2}}(\psi_n(z_I, t)\psi_m(z_{II}, t) \pm \psi_m(z_I, t)\psi_n(z_{II}, t)). \quad (8.1)$$

The first-order term of the perturbation of the energy can be written

$$-2e^2R^{-3}\int\int \psi_{nm}{}^{(0)*}z_Iz_{II}\psi_{nm}{}^{(0)}dz_Idz_{II}$$

$$= \mp 2e^2R^{-3}\int \psi_n{}^*(z_I, t)z_I\psi_m(z_I, t)dz_I$$

$$\times \int \psi_m{}^*(z_{II}, t)z_{II}\psi_n(z_{II}, t)dz_{II}$$

$$+\text{conj. complex.} \quad (8.2)$$

The upper sign refers to the synchronous inphase vibration of $\langle n|z_I|m\rangle$ with $\langle m|z_{II}|n\rangle$ in the correspondence description, the lower sign to the antiphase. (The product of the two integrals is time independent.) Instead of this resonance description we could have used $\psi_{n_+n_-} = \psi_{n_+}(z_+)\psi_{n_-}(z_-)$ where $z_\pm = z_I \pm z_{II}$; even or odd values of n_- represent symmetric or antisymmetric wave functions, respectively.

From this well-known relation between classical and wave mechanical description it follows that arguments in correspondence language, based on classical phase relations or phase-preferences, have their quantum-mechanical counterpart in arguments about stationary states of the pair, made up from symmetric or antisymmetric combinations of resonating quantum states. (The perturbation integral of a stationary state of the pair reveals resonating transitions of the systems I and II.) To get the statistical effect of phase-preferences we have, in the classical picture, inphase domains occupying a larger phase-space volume than antiphase domains of the same energy. In quantum statistics the effect of phase-preferences is completely registered in the level shifts of the *stationary* states of the pair, brought about by the above calculated perturbation energy.

Transitions between different stationary states of the pair give a non-vanishing z_I+z_{II} if a symmetric state combines with a symmetric neighbor state or if an antisymmetric one combines with an antisymmetric neighbor. They give a non-vanishing z_I-z_{II} if a symmetric state combines with an antisymmetric neighbor state. For a pair of large molecules imbedded in a liquid medium, the Brownian motion in the medium causes both kinds of transitions.

Analogous considerations hold for pairs of modes in a single molecule where the interaction between the "modes" originates in anharmonic terms.

IX. QUANTUM-MECHANICAL RESONANCE BETWEEN COMMENSURABLE MODES

Placzek[11] presented the detailed theory of resonance between two commensurable vibrations in one molecule, anharmonic terms providing the coupling. He considered the case in which there are just two non-degenerate "modes" in the molecule and $2\kappa_1 \sim \kappa_2$. Using the abbreviations

$$\kappa_2 + 2\kappa_1 = 4\kappa, \quad \kappa_2 - 2\kappa_1 = 4\delta \quad (9.1)$$

one starts with a Hamiltonian which contains the essential interaction term

$$H = \tfrac{1}{2}[\dot{q}_1{}^2 + \dot{q}_2{}^2 + \kappa_1{}^2q_1{}^2 + \kappa_2{}^2q_2{}^2] + a_{112}q_1{}^2q_2$$
$$\sim \tfrac{1}{2}[\dot{q}_1{}^2 + \dot{q}_2{}^2 + 4\kappa^2(q_2{}^2 + \tfrac{1}{4}q_1{}^2)]$$
$$+ 4\kappa\delta(q_2{}^2 - \tfrac{1}{4}q_1{}^2) + a_{112}q_1{}^2q_2. \quad (9.2)$$

[11] G. Placzek, *Handbuch der Radiologie*, edited by Marx, second edition, vol. VI, p. 319, Akad. Verlag. Leipzig. Cf. also E. Fermi, Zeits. f. Physik **71**, 250, (1931), and D. M. Dennison, Phys. Rev. **41**, 304 (1932).

The terms in the square bracket are independent of δ. One considers them as describing the unperturbed system whose levels (2, 0) and (0, 1) coincide exactly. The first-order perturbation theory with the remaining two terms furnishes the two energy levels (energies with reference to the ground level)

$$2\hbar\{\kappa\pm(\delta^2+2p^2)^{\frac{1}{2}}\},\quad p=\tfrac{1}{8}\kappa^{-\frac{1}{2}}a_{112}\hbar^{\frac{1}{2}}, \tag{9.3}$$

and the two eigenfunctions

$$\left.\begin{aligned}&(2\xi)^{-\frac{1}{2}}\{(\xi+|\delta|)^{\frac{1}{2}}\psi_{01}\pm(\xi-|\delta|)^{\frac{1}{2}}\psi_{20}\}\\ \text{and}\quad&(2\xi)^{-\frac{1}{2}}\{(\xi-|\delta|)^{\frac{1}{2}}\psi_{01}\mp(\xi+|\delta|)^{\frac{1}{2}}\psi_{20}\}\end{aligned}\right\}, \tag{9.4}$$

where $\xi=(\delta^2+2p^2)^{\frac{1}{2}}$ and the upper and lower signs have to be taken according to whether p and δ have equal signature or not, respectively. For $\delta^2\ll p^2$ the two energy levels become

$$2\hbar\{\kappa\pm 2^{\frac{1}{2}}p(1+\delta^2/4p^2)\}, \tag{9.5}$$

and for $\delta^2\gg p^2$ they become

$$2\hbar\{\kappa\pm\delta(1+p^2/\delta^2)\}, \tag{9.6}$$

which equals

$$\hbar(\kappa_2+2p^2/\delta) \tag{9.6a}$$

and

$$\hbar(2\kappa_1-2p^2/\delta). \tag{9.6b}$$

Cf. the similar situation, Sections V and X. It is clear that anharmonicity, i.e., p causes a repulsion between the two levels (9.3) and therefore in thermal equilibrium it causes a predominance of one eigenfunction over the other, in analogy to the phase preferences discussed above.

X. QUANTUM-MECHANICAL CALCULATION OF THE INTERACTION BETWEEN AN IDENTICAL MOLECULE PAIR

We mentioned in Section VI that, in a complicated molecule, we may have many radicals or atoms which, if vibrating each one by itself, unperturbed by the others, would show the same or almost same frequencies. They actually resonate with each other by virtue of some coupling $\lambda q_{1I}q_{2I}$, or some more complicated λ terms, cf. (11.1). We shall occasionally call q_{1I}, q_{2I} pseudomodes because $\lambda q_{1I}q_{2I}$ could be transformed away by a principal axes transformation. We shall, however, describe our system in terms of these coordinates q_{1I}, q_{2I} etc. of the unperturbed systems as we want to investigate the effect of the interaction parameters λ and μ (10.2), (11.1) on the attraction between the molecule pair.

Furthermore we have resonance between commensurable vibrations, causing level shifts (between e.g. symmetric and antisymmetric combinations of resonating function ψ_{01} and ψ_{20}). These level shifts are the stronger, the stronger the anharmonic coupling coefficient, the closer the commensurability, and the larger the number of resonating modes (cf. Section XI). Instead of following through the fairly complicated elaboration of Section IX for a pair of complicated molecules, let us make the rough assumption that the essential features of this situation can again be represented by an interaction $\lambda q_{1I}q_{2I}$ and $\lambda q_{1II}q_{2II}$ of two harmonic pseudomodes of exactly equal frequency, inside each of the identical molecules I and II. Indeed, the effects discussed above in terms of the correspondence principle, do not much depend on the kind of coupling which is assumed to exist between the modes of each one of the molecules. $\lambda q_{1I}q_{2I}$, just like $\lambda q_{1I}{}^2q_{2I}$, has the effect of pushing two resonating levels in molecule I apart.

q_{1I} and q_{2I} may be parallel oriented, and we assume λ to be negative which of course might not be the case. As we look for a quantum effect, and as we want the calculations to be as simple as possible we assume that, apart from the ground level 0, practically only the next two bunches of levels 1 and 2 are thermally excited. We calculate the ground level and the bunches 1 and 2 up to second-order perturbation which means that we have to take into account the influence of the levels up to the 4th bunch. The unperturbed energies of the ground level 0 and of the bunches 1 and 2 have the values

$$E_0^{(0)}=4\cdot\tfrac{1}{2}\hbar\kappa=2\hbar\kappa,\quad E_1^{(0)}=3\hbar\kappa,\quad E_2^{(0)}=4\hbar\kappa. \tag{10.1}$$

In order to calculate the electric dipole-dipole interaction of a pair of molecules, we assume a perturbation function

$$\begin{aligned}H_1=&\lambda(q_{1I}q_{2I}+q_{1II}q_{2II})\\&+\mu(q_{1I}q_{1II}+q_{1I}q_{2II}+q_{2I}q_{1II}+q_{2I}q_{2II})\end{aligned} \tag{10.2}$$

where μ is some expression of the type

$$R^{-3}[(\mu_{zI}\mu_{zII}+\mu_{yI}\mu_{yII}-2\mu_{zI}\mu_{zII}]. \tag{10.3}$$

H_1 is symmetric with respect to permutations (12) and with respect to (I II). As unperturbed wave functions we may take the set (10.4)

$$\begin{aligned}\psi_{00}=\psi_0(q_{1I})\psi_0(q_{2I})\psi_0(q_{1II})\psi_0(q_{2II})\equiv(0000)\\ =\text{sym. (12), sym. (}I\ II\text{)}\end{aligned}$$

for the ground state,

$$\begin{aligned}\psi_{10}=\tfrac{1}{2}\{(0100)+(1000)+(0001)+(0010)\}\\ =\text{sym. (12), sym. (}I\ II\text{)}\\ \psi_{11}=\tfrac{1}{2}\{(0100)+(1000)-(0001)-(0010)\}\\ \text{sym. (12), antis. (}I\ II\text{)}\\ \psi_{12}=\tfrac{1}{2}\{(0100)-(1000)+(0001)-(0010)\}\\ =\text{antis. (12), sym. (}I\ II\text{)}\\ \psi_{13}=\tfrac{1}{2}\{(0100)-(1000)-(0001)+(0010)\}\\ =\text{antis. (12), antis. (}I\ II\text{)}\end{aligned}$$

for the first bunch,

$$\psi_{20}=\tfrac{1}{4}\{(0200)+(2000)+(0002)+(0020)\}$$
$$+2^{-\frac{1}{2}}\{(1100)+(0011)\}$$
$$+2^{-\frac{1}{2}}\{(0101)+(0110)+(1001)+(1010)\}$$
$$\psi_{21}=\tfrac{1}{4}\{(0200)+(2000)+(0002)+(0020)\}$$
$$+2^{-\frac{1}{2}}\{(1100)+(0011)\}$$
$$-2^{-\frac{1}{2}}\{(0101)+(0110)+(1001)+(1010)\}$$
$$\psi_{22}=2^{-1}\{(0200)+(2000)+(0002)+(0020)\}$$
$$-\tfrac{1}{2}\{(1100)+(0011)\}$$
$$\psi_{23}=\tfrac{1}{2}\{(0101)-(0110)-(1001)+(1010)\}$$
all sym. (12), sym. (*I II*),
$$\psi_{24}=2^{-1}\{(0200)+(2000)-(0002)-(0020)\}$$
$$+\tfrac{1}{2}\{(1100)-(0011)\}$$
$$\psi_{25}=-2^{-1}\{(0200)+(2000)-(0002)-(0020)\}$$
$$+\tfrac{1}{2}\{(1100)-(0011)\}$$
both sym. (12), antis. (*I II*),
$$\psi_{26}=2^{-1}\{(0200)-(2000)+(0002)-(0020)\}$$
$$+\tfrac{1}{2}\{(0101)-(1010)\}$$
$$\psi_{27}=-2^{-1}\{(0200)-(2000)+(0002)-(0020)\}$$
$$+\tfrac{1}{2}\{(0101)-(1010)\}$$
both antis. (12), sym. (*I II*),
$$\psi_{28}=2^{-1}\{(0200)-(2000)-(0002)+(0020)\}$$
$$+\tfrac{1}{2}\{(0110)-(1001)\}$$
$$\psi_{29}=-2^{-1}\{(0200)-(2000)-(0002)+(0020\ \}$$
$$+\tfrac{1}{2}\{(0110)-(1001)\}$$
both antis. (12), antis. (*I II*),

for the second bunch.

As we use the higher levels only for the purpose of calculating second-order perturbations of the ground level and the first and second bunches, we simply choose the wave functions

(3000), (0300), (0030), (0003), (2100), (1200), (0021), (0012), (2010), (2001), (1020), (0120), (0210), (0201), (1002), (0102), (1110), (1101), (1011), (0111) 3rd

for the third bunch. And we choose

(4000), (0400), (0040), (0004), (3100), (1300), (0031), (0013), (3010), (3001), (1030), (0130), (0310), (0301), (1003), (0103), (2020), (2002), (0220), (0202), (2200), (0022), (2110), (2101), (1021), (0121), (1210), (1201), (1012), (0112), (2011), (0211), (1120), (1102), (1111)

for the fourth bunch.

The only non-vanishing off-diagonal elements of the hermitian H_1 which connect the ground level or the first or the second bunch of levels among each other or with any other bunch are the following.

Elements connecting the ground level with other levels:

$$\left.\begin{aligned}\langle 00|H_1|20\rangle&=2^{-\frac{1}{2}}(\lambda+2\mu)\hbar/2\kappa\\ \langle 00|H_1|21\rangle&=2^{-\frac{1}{2}}(\lambda-2\mu)\hbar/2\kappa\\ \langle 00|H_1|22\rangle&=-\lambda\hbar/2\kappa.\end{aligned}\right\}\tag{10.5}$$

The 4 states of the first bunch are on speaking terms only with 16 out of the 20 states of the third bunch, there are 64 non-vanishing matrix elements. These are all the elements which connect the first bunch with some other. The 10 states of the second bunch are on speaking terms with 31 out of the 35 states of the fourth bunch, there are 257 non-vanishing matrix elements. Furthermore, 3 states of the second bunch speak to the ground level, cf. (10.5). These are all the elements which connect the second bunch with some other.

With the choice (10.4) of eigenfunctions, H_1 is a diagonal matrix inside the first bunch and it is a diagonal matrix inside the second bunch. Therefore the first order perturbation theory is already carried through, we have only to list these diagonal elements of H_1, they are

$$\begin{aligned}&E_{00}^{(1)}=0,\\ &E_{10}^{(1)}=(\lambda+2\mu)\hbar/2\kappa, && E_{11}^{(1)}=(\lambda-2\mu)\hbar/2\kappa, && E_{12}^{(1)}=E_{13}^{(1)}=-\lambda\hbar/2\kappa,\\ &E_{20}^{(1)}=2(\lambda+2\mu)\hbar/2\kappa, && E_{21}^{(1)}=2(\lambda-2\mu)\hbar/2\kappa, && E_{24}^{(1)}=2\lambda\hbar/2\kappa,\\ &E_{22}^{(1)}=E_{23}^{(1)}=E_{25}^{(1)}=-2\lambda\hbar/2\kappa, && E_{26}^{(1)}=E_{28}^{(1)}=2\mu\hbar/2\kappa, && E_{27}^{(1)}=E_{29}^{(1)}=-2\mu\hbar/2\kappa.\end{aligned}\tag{10.6}$$

In order to carry through the second-order perturbations for this degenerate system, we use Van Vleck's method[12] which becomes particularly simple in the present case. For the ground level we get

$$E_0^{(2)}=\sum_{j''}\langle 00|H_1|2j''\rangle\langle 2j''|H_1|00\rangle/(E_0^{(0)}-E_2^{(0)})$$
$$=-\hbar\kappa(\tfrac{1}{4}\lambda^2+\tfrac{1}{2}\mu^2)/\kappa^4.\tag{10.7}$$

For the first bunch of levels the second-order perturbations yield a matrix

$$\langle 1j|G_2|1j'\rangle$$
$$=0-\sum_{j''}\langle 1j|H_1|3j''\rangle\langle 3j''|H_1|1j'\rangle/2\hbar\kappa,\tag{10.8}$$

in Kemble's notation. This matrix, however, is already diagonal, the second-order perturbations of the energy levels are these diagonal elements

$$\begin{aligned}E_{10}^{(2)}&=-\hbar\kappa(\tfrac{3}{8}\lambda^2+\tfrac{1}{2}\lambda\mu+\mu^2)/\kappa^4,\\ E_{11}^{(2)}&=-\hbar\kappa(\tfrac{3}{8}\lambda^2-\tfrac{1}{2}\lambda\mu+\mu^2)/\kappa^4,\\ E_{12}^{(2)}&=E_{13}^{(2)}=-\hbar\kappa(\tfrac{3}{8}\lambda^2+\tfrac{1}{2}\mu^2)/\kappa^4.\end{aligned}\tag{10.9}$$

Similarly, for the second bunch, the matrix

$$\langle 2j|G_2|2j'\rangle=0-\sum_{j''}\langle 2j|H_1|4j''\rangle\langle 4j''|H_1|2j'\rangle/2\hbar\kappa$$
$$+\langle 2j|H_1|00\rangle\langle 00|H_1|2j'\rangle/2\hbar\kappa\tag{10.10}$$

is diagonal. The calculations give

$$\begin{aligned}E_{20}^{(2)}&=-\hbar\kappa(\tfrac{1}{2}\lambda^2+\lambda\mu+\tfrac{3}{2}\mu^2)/\kappa^4\\ E_{21}^{(2)}&=-\hbar\kappa(\tfrac{1}{2}\lambda^2-\lambda\mu+\tfrac{3}{2}\mu^2)/\kappa^4\\ E_{24}^{(2)}&=-\hbar\kappa(\tfrac{1}{2}\lambda^2+\tfrac{3}{2}\mu^2)/\kappa^4\\ E_{22}^{(2)}&=E_{23}^{(2)}=E_{25}^{(2)}=-\hbar\kappa(\tfrac{1}{2}\lambda^2+\tfrac{1}{2}\mu^2)/\kappa^4\\ E_{26}^{(2)}&=E_{28}^{(2)}=-\hbar\kappa(\tfrac{1}{2}\lambda^2+\tfrac{1}{2}\lambda\mu+\mu^2)/\kappa^4\\ E_{27}^{(2)}&=E_{29}^{(2)}=-\hbar\kappa(\tfrac{1}{2}\lambda^2-\tfrac{1}{2}\lambda\mu+\mu^2)/\kappa^4.\end{aligned}\tag{10.11}$$

We form the partition function Z by means of (10.1), (10.6), (10.7), (10.9), (10.11). We finally arrive to the

[12] E. C. Kemble, *Quantum Mechanics* (McGraw-Hill Book Company, Inc., New York, 1937), pp. 388–396.

following expression for the attractive force

$$-kT\frac{\partial \log Z}{\partial R}=-kT\frac{d\mu}{dR}Z^{-1}\frac{\partial Z}{\partial \mu}=-kT\frac{d}{dR}\left(\frac{\mu}{\kappa^2}\right)\frac{\mu}{\kappa^2}\frac{\hbar\kappa}{kT}$$
$$\times\left[1+\exp\left\{-\left(1+\frac{1}{2}\frac{\lambda}{\kappa^2}-\frac{1}{8}\frac{\lambda^2}{\kappa^4}\right)\frac{\hbar\kappa}{kT}\right\}\right.$$
$$\cdot\left(2+2\frac{\hbar\kappa}{kT}-2\frac{\lambda}{\kappa^2}\frac{\hbar\kappa}{kT}+\frac{1}{2}\frac{\lambda^2}{\kappa^4}\frac{\hbar\kappa}{kT}\right)$$
$$+\exp\left\{-\left(2+\frac{\lambda}{\kappa^2}-\frac{1}{4}\frac{\lambda^2}{\kappa^4}\right)\frac{\hbar\kappa}{kT}\right\}$$
$$\left.\cdot\left(2+4\frac{\hbar\kappa}{kT}-4\frac{\lambda}{\kappa^2}\frac{\hbar\kappa}{kT}+\frac{\lambda^2}{\kappa^4}\frac{\hbar\kappa}{kT}\right)\right]. \quad (10.12)$$

In working out this expression we made use of the relation $\mu\ll\lambda$, but of course only after the differentiation of Z with respect to μ. This relation means that the coupling between two modes of one molecule is strong compared with the coupling between two modes, one in the one molecule, the other in the other molecule. The formula (10.12) checks with the corresponding one in reference 8, l.c., if we drop the higher order perturbation terms from (10.12).

We see that the attractive force depends on $\hbar$, we have a quantum-mechanical resonance effect. The force of this dipole-dipole interaction depends on $\mu d\mu/dR$, i.e., it is proportional to R^{-7}. The first term 1 in the square bracket represents the ground levels contribution to London's dispersion force. The exponential terms in the square bracket interest us most of all because they register the influence of the excited states toward the attraction. They are therefore the terms in which the effect of phase preferences show up. They contain a factor

$$\exp\left\{-\frac{1}{2}\frac{\lambda}{\kappa^2}\frac{\hbar\kappa}{kT}\right\}$$

and

$$\exp\left\{-\frac{\lambda}{\kappa^2}\frac{\hbar\kappa}{kT}\right\}, \quad \text{respectively,} \quad (10.13)$$

which means that for strong coupling between the modes of each one of the molecules (and $\lambda<0$), we get an exponential multiplicative factor in the expression for the attractive force. Although for molecules with only two modes, this factor has not much influence, for molecules with many (n) modes it becomes important, as shown in the following section. (If $E_{12}^{(1)}=E_{13}^{(1)}$ would have been $=+\lambda h/2\kappa$, i.e. if we would not have had phase preferences, then the expression for Z^{-1} would have been different, and the result (10.12) would not have given this strong attraction effect.)

This result (10.12) is interesting for some more reasons. We assumed λ to be negative. (Let us note en passant that the exponential functions are each multiplied by a sum of four positive quantities, the quantities in round parantheses.) The exponential functions in (10.12) have an exponent which is larger than $-\hbar\kappa/kT$, larger by an amount determined by λ/κ^2. Other exponential functions like $\exp\{-[1-\frac{1}{2}(\lambda/\kappa^2)-\frac{1}{8}(\lambda^2/\kappa^4)](\hbar\kappa/kT)\}$ and similar ones referring to the second bunch of levels, cancelled out altogether in the formation of the attractive force. We see therefore that the second order perturbation terms $+\frac{1}{8}(\lambda^2/\kappa^4)(\hbar\kappa/kT)$ and $+\frac{1}{4}(\lambda^2/\kappa^4)(\hbar\kappa/kT)$ in the exponents of the exponential functions have the same positive signature as the first order terms, $-\frac{1}{2}(\lambda/\kappa^2)(\hbar\kappa/kT)$ and $-(\lambda/\kappa^2)(\hbar\kappa/kT)$. First-order perturbation theory alone will therefore give an effect (10.13) in the same direction as this complete second-order theory. This is important for the calculations done in the following sections by first-order theory only. In order to estimate the order of magnitude of the attraction term, we compare it with the above mentioned London force term. For this purpose we evidently needed to carry through the second-order perturbation theory.

Another observation can be made with (10.12). The second bunch of levels has an influence on the attraction force, an influence similar to that of the first bunch. For complicated molecules the higher bunches become more and more in thermal reach, and difficulties of calculation make but the lowest bunches accessible to even first-order perturbation calculations. So it is good to know in this example that the first-order perturbation of the first bunch already characterizes the over-all effect given by the λ dependence of the square bracket in (10.12).

This is the effect of phase preferences on the attraction. Our argumens in Section VII show that in the case of commensurable rather than equal frequency modes, specific attraction has its cause in corresponding phase preferences in the pair of molecules—and those corresponding phase preferences depend on the identity of the pair.

XI. LARGE MOLECULES

We should like to see how this attraction effect depends on the number of modes, i.e., on the size of the molecules. Therefore, we shall look at a more complicated model, one which more closely resembles the case of molecules with many commensurable modes. Consider the case of molecules I and II each having 4 modes of equal frequency, and let us calculate the first order perturbation of the first bunch of levels above the ground level

$$\psi_{00}=\psi_0(q_{1I})\cdots\psi_0(q_{4II})$$
$$=(0000\ 0000)\sim(\langle 1234\rangle)(\langle I\ II\rangle)$$

by which symbol we mean complete symmetry in 1, 2, 3, 4 and in I, II.[13]

[13] E. Fues, Quantenmech., *Handb. d. Expphys. Ergaenzungswerk*, Vol. II, p. 167 (1935). F. Hund, *Handb. der Phys.* 24.1, p. 585 (1933).

We assume a perturbation function

$$\begin{aligned}H_1=\lambda&(q_{1I}q_{2I}+q_{2I}q_{3I}+q_{3I}q_{4I}\\&+q_{4I}q_{1I}+q_{1I}q_{3I}+q_{2I}q_{4I})\\&+\lambda(q_{1II}q_{2II}+\cdots+q_{2II}q_{4II})\\&+\mu(q_{1I}q_{1II}+q_{1I}q_{2II}+q_{1I}q_{3II}\\&+q_{1I}q_{4II}+\cdots+q_{4I}q_{4II}).\end{aligned}\quad(11.1)$$

Let us find the eigenfunctions and levels of each of the molecules by themselves, e.g. of molecule I. For the levels of bunch 1, in which case all but one mode are in the ground state, we have four orthonormal eigenfunctions:

$$\begin{aligned}\psi_{10}{}^I&=\tfrac{1}{2}\{(0100)+(1000)\\&\qquad+(0001)+(0010)\}\sim(\langle 1234\rangle)\\\psi_{11}{}^I&=\tfrac{1}{2}\{(0100)+i(1000)\\&\qquad-(0001)-i(0010)\}\sim(\langle 134\rangle,2)\\\psi_{12}{}^I&=\tfrac{1}{2}\{(0100)-(1000)\\&\qquad+(0001)-(0010)\}\sim(\langle 134\rangle,2)\\\psi_{13}{}^I&=\tfrac{1}{2}\{(0100)-i(1000)\\&\qquad-(0001)+i(0010)\}\sim(\langle 134\rangle,2).\end{aligned}\quad(11.2)$$

(In the table of Fues these are the only non-vanishing eigenfunctions in the case of four identical modes.) The first order perturbations of the levels of the first bunch are

$$\begin{aligned}&\langle 10|H_1{}^I|10\rangle=3\lambda\hbar/2\kappa\\&\langle 11|H_1{}^I|11\rangle=\langle 12|H_1{}^I|12\rangle=\langle 13|H_1{}^I|13\rangle\\&\qquad\qquad=-\lambda\hbar/2\kappa.\end{aligned}\quad(11.3)$$

The off diagonal elements vanish. This shows already that the first symmetrical state is, because of the Boltzmann factor $\exp(-E/kT)$, the statistically most preferred one ($\lambda<0$), which is in accordance with the phase preference argument.

For a pair of molecules, the orthonormal eigenfunctions for the first bunch of levels are

$$\begin{aligned}&2^{-\frac{1}{2}}(\psi_{10}{}^I\psi_{00}{}^{II}\pm\psi_{00}{}^I\psi_{10}{}^{II}),\\&2^{-\frac{1}{2}}(\psi_{11}{}^I\psi_{00}{}^{II}\pm\psi_{00}{}^I\psi_{11}{}^{II}),\\&2^{-\frac{1}{2}}(\psi_{12}{}^I\psi_{00}{}^{II}\pm\psi_{00}{}^I\psi_{12}{}^{II}),\\&2^{-\frac{1}{2}}(\psi_{13}{}^I\psi_{00}{}^{II}\pm\psi_{00}{}^I\psi_{13}{}^{II}).\end{aligned}\quad(11.4)$$

The diagonal elements of H_1 are

$$(3\lambda+4\mu)\hbar/2\kappa,\quad(3\lambda-4\mu)\hbar/2\kappa,\quad(11.5)$$

and six equal elements $-\lambda\hbar/2\kappa$. The quantity μ again shows up in the level shifts of the phase-preferred first pair of states and therefore has a strong influence on the attractive force.

Finally, let us consider the general case of a pair of identical molecules each having n modes of identical frequency, and let us calculate the first-order perturbation of the first bunch of levels. We rewrite the above example for $n=4$. We may choose as eigenfunctions the eight functions

$$(1000\ 0000),\ (0100\ 0000),\ \cdots,\ (0000\ 0001).\quad(11.6)$$

The diagonal elements $E^{(1)}\equiv\epsilon\hbar/2\kappa$ of the perturbation function H_1 [Eq. (11.1)] are the roots of

$$0=\begin{vmatrix}-\epsilon&\lambda&\lambda&\lambda&\mu&\mu&\mu&\mu\\\lambda&-\epsilon&\lambda&\lambda&\mu&\mu&\mu&\mu\\\lambda&\lambda&-\epsilon&\lambda&\mu&\mu&\mu&\mu\\\lambda&\lambda&\lambda&-\epsilon&\mu&\mu&\mu&\mu\\\mu&\mu&\mu&\mu&-\epsilon&\lambda&\lambda&\lambda\\\mu&\mu&\mu&\mu&\lambda&-\epsilon&\lambda&\lambda\\\mu&\mu&\mu&\mu&\lambda&\lambda&-\epsilon&\lambda\\\mu&\mu&\mu&\mu&\lambda&\lambda&\lambda&-\epsilon\end{vmatrix}.\quad(11.7)$$

It is easily seen that the roots are the ones given by (11.5). Indeed, we add the rows 2, 3, 4, 5, 6, 7, 8 to row 1 and realize that the determinant has a factor $(-\epsilon+3\lambda+4\mu)$. Then we add the rows 2, 3, 4 and subtract rows 5, 6, 7, 8 from row one and see that the determinant has also a factor $(-\epsilon+3\lambda-4\mu)$. To prove that the remaining six roots ϵ are all equal to $-\lambda$, we subtract the second column from the first, the third from the second, the fourth from the third, the seventh from the eighth, the sixth from the seventh, and the fifth from the sixth. The resulting determinant has $(\epsilon+\lambda)^6$ as a factor.

In the general case the first-order perturbations of the energy levels are $((n-1)\lambda+n\mu)\hbar/2\kappa$, $((n-1)\lambda-n\mu)\hbar/2\kappa$ and there are $2n-2$ equal levels with perturbation $-\lambda\hbar/2\kappa$.

Forgetting second-order perturbation terms and neglecting all but the first excited bunch of levels, we have, analogous to (10.12),

$$\begin{aligned}Z\sim&\exp\{-n\hbar\kappa/kT\}\\&+\exp\{-[(n+1)+(\tfrac{1}{2}(n-1)\lambda+\tfrac{1}{2}n\mu)/\kappa^2]\hbar\kappa/kT\}\\&+\exp\{-[(n+1)+(\tfrac{1}{2}(n-1)\lambda-\tfrac{1}{2}n\mu)/\kappa^2]\hbar\kappa/kT\}\\&+(2n-2)\exp\{-[(n+1)-\tfrac{1}{2}\lambda/\kappa^2]\hbar\kappa/kT\}.\end{aligned}\quad(11.8)$$

$$\begin{aligned}-kT\frac{d\mu}{dR}Z^{-1}\frac{\partial Z}{\partial\mu}\sim&-kT\frac{d}{dR}\left(\frac{\mu}{\kappa^2}\right)\cdot\frac{n^2}{2}\frac{\mu}{\kappa^2}\left(\frac{\hbar\kappa}{kT}\right)^2\\&\times\exp\left\{-\left(1+\frac{n-1}{2}\frac{\lambda}{\kappa^2}\right)\frac{\hbar\kappa}{kT}\right\}.\end{aligned}\quad(11.9)$$

This shows the influence of λ on the attractive force; $-(n-1)\lambda/2\kappa^2$ can become large compared with unity.

In a macromolecule with large n we certainly have to take into account the perturbations of the higher bunches of levels. This is very complicated to do, and the correspondence description is more adequate. In the case of $n=2$ we can, however, already see the influence of perturbations of the levels of bunch two, cf. Eq. (10.12).

XII. SPECIFICITY

Let us look at the calculations of Section X in case of a pair of molecules which has been detuned (verstimmt). This should, at least for this particular model, tell us something about the specificity of interaction. To get a deeper insight, however, one has to carry out

these calculations for a pair of molecules which have many anharmonically coupled modes.

We are going to detune the frequency κ of the modes by amounts δ. We want to study the behavior of the ground and first bunch of levels in first-order perturbation theory in order to find out the influence of δ on the partition function and on the attractive force. We work in the neighborhood of resonance $\delta=0$, i.e. small values $\delta \ll \kappa$ because we are interested in the comparison of an identical pair with a nearly identical pair. (A comparison with large values of δ is meaningless as such case would represent an altogether different situation.) Therefore, we may neglect terms δ^2 compared with terms $\kappa\delta$. Our notation is made so that $\delta \geq 0$.

When detuning, we shall shift as many frequencies upwards as we shift downwards, by the same amount δ, so that the mean value of the frequencies is not changed. (A change of this mean value would cause a change in attraction, but this effect is again not what we are interested in.)

We study four kinds of detuning. In every case we split $H=H_0+H_1$ with

$$H_0=\tfrac{1}{2}(\dot{q}_{1I}{}^2+\dot{q}_{2I}{}^2+\dot{q}_{1II}{}^2+\dot{q}_{2II}{}^2) +\tfrac{1}{2}\kappa^2(q_{1I}{}^2+q_{2I}{}^2+q_{1II}{}^2+q_{2II}{}^2). \quad (12.1)$$

Detuning A

$$\kappa_{1I}=\kappa_{2I}=\kappa+\delta, \quad \kappa_{1II}=\kappa_{2II}=\kappa-\delta$$
$$H_1=\kappa\delta(q_{1I}{}^2+q_{2I}{}^2)-\kappa\delta(q_{1II}{}^2+q_{2II}{}^2)+\lambda(\cdot)+\mu(\cdot). \quad (12.2)$$

where the λ and μ terms are as in (10.2). For $\kappa^2\delta^2 \ll \mu^2$ there is no change compared with the calculation in Section X. For $\kappa^2\delta^2 \gg \mu^2$ the first-order perturbations are

$$E_0{}^{(1)}=0; \quad E_{10}{}^{(1)}, E_{11}{}^{(1)}=\{\lambda \mp (2\kappa\delta+\mu^2/\kappa\delta)\}\hbar/2\kappa;$$
$$E_{12}{}^{(1)}, E_{13}{}^{(1)}=\{-\lambda \mp 2\kappa\delta\}\hbar/2\kappa. \quad (12.3)$$

The first bunch of eigenfunctions are of course no longer (10.4). The attractive force becomes

$$-kT\frac{d\mu}{dR}Z^{-1}\frac{\partial Z}{\partial \mu}=-kT\frac{d}{dR}\left(\frac{\mu}{\kappa^2}\right)\cdot\frac{\mu}{\kappa^2}\frac{\hbar\kappa}{kT} \times\left[2\frac{\hbar\kappa}{kT}\exp\left\{-\left(1+\frac{\lambda}{2\kappa^2}\right)\frac{\hbar\kappa}{kT}\right\}\right]. \quad (12.4)$$

(12.4) is identical with (10.12) when the second-order perturbation of the groundlevel is ignored. We conclude that in this particular model the detuning A does not affect the attraction, in analogy to the simple oscillator pair, Eq. (5.19).

Detuning B

$$\kappa_{1I}=\kappa+\delta, \quad \kappa_{1II}=\kappa-\delta, \quad \kappa_{2I}=\kappa_{2II}=\kappa$$
$$H_1=\kappa\delta q_{1I}{}^2-\kappa\delta q_{1II}{}^2+\lambda(\cdot)+\mu(\cdot) \quad (12.5)$$

For $\kappa^2\delta^2 \gg \lambda^2$ we get

$$E_0{}^{(1)}=0; \quad E_{10}{}^{(1)}, E_{11}{}^{(1)}=\pm(2\kappa\delta+\tfrac{3}{4}\mu^2/\kappa\delta)\hbar/2\kappa;$$
$$E_{12}{}^{(1)}, E_{13}{}^{(1)}=\pm(\mu^2\kappa\delta/\lambda^2)\hbar/2\kappa \quad (12.6)$$

and the attractive force

$$-kT\frac{d}{dR}\left(\frac{\mu}{\kappa^2}\right)\cdot\frac{\mu}{\kappa^2}\frac{\hbar\kappa}{kT} \times\left[\frac{\hbar\kappa}{kT}\left(\frac{3}{2}+\frac{\mu^2\kappa^2\delta^2}{\lambda^4}\right)\exp\left\{-\frac{\hbar\kappa}{kT}\right\}\right]. \quad (12.7)$$

The term (10.13) which causes the strong attraction between large molecule pairs, has disappeared.

Detuning C

$$\kappa_{1I}=\kappa+\delta, \quad \kappa_{2I}=\kappa-\delta, \quad \kappa_{1II}=\kappa_{2II}=\kappa$$
$$H_1=\kappa\delta q_{1I}{}^2-\kappa\delta q_{2I}{}^2+\lambda(\cdot)+\mu(\cdot) \quad (12.8)$$

For $\kappa^2\delta^2 \gg \lambda^2$ we get

$$E_0{}^{(1)}=0;$$
$$E_{10}{}^{(1)}=(\lambda-2\lambda\mu^2/\kappa^2\delta^2)\hbar/2\kappa, \quad E_{11}{}^{(1)}=-\lambda\hbar/2\kappa \quad (12.9)$$
$$E_{12}{}^{(1)}, E_{13}{}^{(1)}=\pm(2\kappa\delta+\lambda^2/4\kappa\delta+\mu^2/\kappa\delta)\hbar/2\kappa$$

and the attractive force

$$-kT\frac{d}{dR}\left(\frac{\mu}{\kappa^2}\right)\cdot\frac{\mu}{\kappa^2}\frac{\hbar\kappa}{kT} \times\left[\left(2\frac{\lambda}{\delta^2}\exp\left\{-\frac{\lambda}{2\kappa^2}\frac{\hbar\kappa}{kT}\right\} +2\frac{\hbar\kappa}{kT}\right)\exp\left\{-\frac{\hbar\kappa}{kT}\right\}\right]. \quad (12.10)$$

Here the term (10.13) has been slashed (the factor of (10.13) in (10.12) is large compared with that in (12.10)). This is a particularly interesting detuning as it shows that if phase preference is established only in molecule II then specific attraction is gone. In other words it shows that (10.12) is not just a cumulative effect of two level lowerings in the two molecules.

Detuning D

$$\kappa_{1I}=\kappa_{1II}=\kappa+\delta, \quad \kappa_{2I}=\kappa_{2II}=\kappa-\delta$$
$$H_1=\kappa\delta(q_{1I}{}^2+q_{1II}{}^2)-\kappa\delta(q_{2I}{}^2+q_{2II}{}^2) +\lambda(\cdot)+\mu(\cdot). \quad (12.11)$$

For $\kappa^2\delta^2 \gg \lambda^2$ we get

$$E_0{}^{(1)}=0;$$
$$E_{10}{}^{(1)}, E_{11}{}^{(1)}=\{2\kappa\delta+\lambda^2/4\kappa\delta \pm \mu(1+\lambda/2\kappa\delta)\}\hbar/2\kappa$$
$$E_{12}{}^{(1)}, E_{13}{}^{(1)}=\{-2\kappa\delta-\lambda^2/4\kappa\delta \pm \mu(1-\lambda/2\kappa\delta)\}\hbar/2\kappa \quad (12.12)$$

and the attractive force

$$-kT\frac{d}{dR}\left(\frac{\mu}{\kappa^2}\right)\cdot\frac{\mu}{\kappa^2}\frac{\hbar\kappa}{kT}\left[\frac{1}{2}\frac{\hbar\kappa}{kT}\left\{\left(1+\frac{\lambda}{\kappa\delta}\right)\right.\right. \times\exp\left\{-\left(1+\frac{1}{2\kappa^2}\left[2\kappa\delta+\frac{\lambda^2}{4\kappa\delta}\right]\right)\frac{\hbar\kappa}{kT}\right\}+\left(1-\frac{\lambda}{\kappa\delta}\right) \times\left.\left.\exp\left\{-\left(1-\frac{1}{2\kappa^2}\left[2\kappa\delta+\frac{\lambda^2}{4\kappa\delta}\right]\right)\frac{\hbar\kappa}{kT}\right\}\right\}\right]. \quad (12.13)$$

Again the term (10.13) is missing; the present influence of λ is of a smaller order of magnitude than that in (10.12). The attractive force (10.12) is specific with respect to the changes B, C, D performed on the molecule pair. The absence of corresponding phase preferences causes the lack of strong attraction.

XIII. DISCUSSION

The argument for specificity depends on the presence of a great number of identical pairs of vibrational modes (all with the same or commensurable frequencies) in a pair of rigid molecules. If the pair is not quite identical, because in one of the partners some change has been made, such change is likely to alter the set of phase-related vibrational modes of this molecule. Thus the changed molecule will no longer match the unchanged molecule and specificity will be lost.

An experimental test of the vibrational cause for specificity might be tried on this basis. The surrounding medium of a self-duplicating chromosome has, of course, to contain constituent molecules of the right chemical composition, but in some of these molecules one or several atoms may have been replaced by isotopes (e.g. isotopes at location where they do not walk out of the molecule or into it).[14] The resulting molecules will be chemically, but no longer vibrationally identical with the original ones. Thus they will be discriminated against when it comes to being attracted by the original chromosome. The change of vibrational behavior by substitution of isotopes is, however, small compared to a change of vibrational behavior caused by a chemical or structural change of the molecule. Inactivation of viruses may perhaps be understood on the basis of a change of vibrational properties.

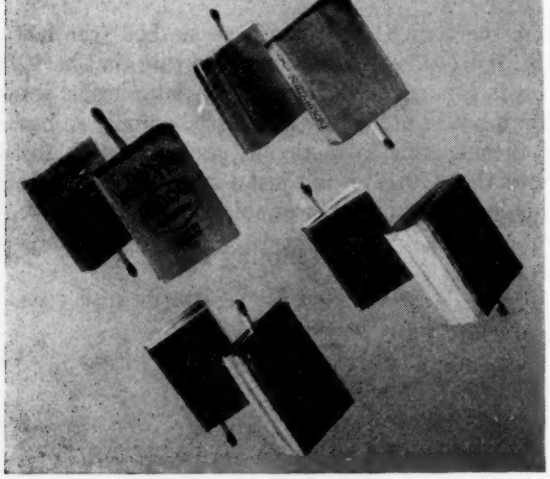

FIG. 2. Orientation of eight identical macromolecules if specific forces alone determine their orientation. The matches are used to indicate the top end of the pages.

After a pair of molecules has come close together in the energetically most favorable orientation, the dipole field of the pair is altogether different from that of an individual molecule. It will make it difficult for them to match a third identical molecule which is alone. Hence triplets are not so easily formed. However, another *pair* may be attracted. This is in agreement with the fact that we observe only doublets, quadruplets, octuplets, etc. among chromosomes.

Also the mutual orientation of very large crystal-forming molecules may be influenced by this orientation effect. Figure 2 shows 8 molecules in such a preferential orientation. The whole crystal will be a multiple repetition of this octuplet. Such an orientation effect in crystals may show up provided the other intermolecular forces are too small to be influential.

Another fundamental phenomenon fits into this theory of self-duplication. This is the fact that laevo configurations of proteins always reproduce laevo. This has been a particular puzzle to the mould theory (explanation of specificity by steric effects) which tries to explain what is called a complementary structure. But it is evident from the orientation argument discussed above that a laevo configuration particularly strongly attracts another laevo configuration. A short discussion of various mutual orientations between laevo molecules and dextro molecules shows that they fail to be strongly attracted.

While a constituent gene in the chromosome is attracting an identical gene, the pair of genes has the orientation described above (end of Section VII). The adjacent genes of the original chromosome may have already built up identical replicas from the surrounding medium. Now the genes of the daughter chromosomes, being close together, may be bound to each other by means of the chromosome material into which the genes are imbedded. This is done in just the same way as with the genes in the original chromosome. To establish this pearlstring alignment properly, the individual genes which are going to form the daughter chromosome either have each to turn 180° around the z axis (cf. Fig. 3), whereby they become oriented parallel to the genes of the original chromosome, or without changing their absolute orientation in space (cf. Fig. 3), they may align in antiparallel orientation. In the first case the x and y components of vibration cause repulsion after the rotation so that the strong attraction between the pair of genes is practically nullified. Let us now look into the second case (antiparallel xy alignment). If the chromosome section is elongated, such an alignment makes the distances be-

[14] Experiments have been done in this direction by K. F. Bonhoeffer and collaborators. Zeits. f. Physik. Chemie **172A**, 370–378 (1935); **175A**, 459 (1936); **176A**, 202 (1936); **180A**. Among other problems, the influence of deuterium on the growth of yeast is investigated. Careful distinction is made between hydrogen atoms so located in the organic compounds of yeast that they are easily exchangeable (Austausch) with deuterium present in the surrounding D_2O, and hydrogen atoms at locations where they are built in (Einbau), i.e. not exchangeable with D if brought in contact with pure D_2O. The difficulty arose that even in the latter case such H atoms get occasionally exchanged with D atoms of compounds present in a nutrient solution.

tween corresponding genes very large and alters the angles of relative orientation of the lines connecting pairs of genes (new z axis) to the gene axes, so that the resulting attraction is diminished. If the chromosome section is not elongated, e.g. if we consider only one gene complex, the "or" configuration still results in some strong attraction. It might also be that the genes imbedded in the chromosome material can easily turn and so preserve the energetically most favorable orientation with respect to daughter genes.

Self-duplicated and synapsed chromosomes separate again at later stages in the respective processes. This may have various causes, e.g. changes in the constitution of the surrounding aqueous medium. The reorientation of the genes might help in permitting the chromosome pairs to go apart. Figure 3 illustrates the reorientation of genes in a daughter chromosome while the genes join together as in a string of beads. The strings are indicated by dotted lines; lines connecting corresponding genes are dashed. The original chromosome (consisting of 2 genes in this picture) is on the left, the daughter chromosome is on the right.

The theory requires us to regard the constituent molecules in a gene as being vibrationally independent units with little vibrational coupling between neighboring constituent molecules of the gene. This should be so because the molecule in the original gene is supposed to perform the same vibrations as the free molecule which is being attracted from the surrounding medium. That point should be understood more clearly.

We might remark in concluding that the problem of specific attraction between identical or almost identical macromolecules certainly has several aspects of which vibrational compatibility seems to be the most important. But one should understand clearly the limitations of this phenomenon and attempt some experimental investigations of it. It would go beyond the scope of this note if we would discuss the possible relations of this specific attraction phenomenon to polymerization, antigen antibody specificity and related fields.[14]

APPENDIX

Frequencies, Velocities, and Amplitudes of the Low Frequency Vibrations in Macromolecules

The highest frequencies in molecular vibrations are known to be of the order $\nu = 10^{14}$ to 10^{13} sec.$^{-1}$. This is above the equipartition value $kT/h = 0.6 \cdot 10^{13}$ sec.$^{-1}$, and is important for specific interactions.

In this Appendix we should like to get oriented about the thermal excitation of the lower frequency vibrations of a "constituent molecule" of a gene. We can imagine such a macromolecule as vibrating as a solid does in Debye's theory of specific heats. Let us calculate

[14] P. Jordan, Naturwiss. **29**, 89 (1941).

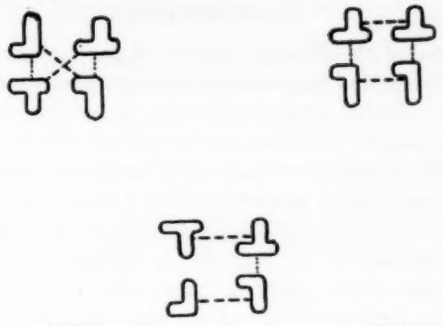

FIG. 3. Above: Orientation before daughter genes are strung up. Below: Orientation afterwards.

velocities and amplitudes of vibrations of smaller and larger parts of the macromolecule. These low frequency vibrations usually do not play the predominant role in specific interaction.

Let m_0 be the average atomic weight of the atoms in the "constituent molecule" and let M be the total mass of the molecule, measured in atomic units, and let m (in the same units) be the mass of a part of this molecule, a part in whose motion as a subunit we are interested. For simplicity, let us imagine M and m to be cubical in shape, and let us assume that practically all thermal energy is vibrational.

First approach

Since we are interested in the average motion of the atoms of a certain part of the molecule, we assume that this part moves as an independent unit, performing vibrations of such a form as if it were a section $\lambda/2$ of a standing wave, whereas the rest of the molecule moves differently and there were no interdependence between the motion of the different "parts" of the molecule. A hydrogen atom with kinetic energy $\frac{1}{2}kT$ (considering the motion in one direction, say x direction) has a velocity of 160,000 cm/sec. Therefore, our part m has a thermal root mean square velocity

$$\sim 160{,}000/m^{\frac{1}{2}} \qquad \text{(A1)}$$

("mean" over space and time).

If we approximate the motion of our part by a harmonic motion, the equivalent frequency with which this part moves may be about that of an acoustic vibration whose $\lambda/2$ is about equal to the linear extension of the part *viz.*

$$\lambda/2 \sim (m/m_0)^{\frac{1}{3}} 2 \cdot 10^{-8}.$$

Therefore, the equivalent frequency ν becomes

$$\nu \sim 10^5/\lambda \sim 0.15 \cdot 10^{13} (m_0/m)^{\frac{1}{3}}.$$

And the vibrational amplitude = time maximum of velocity$/2\pi\nu$ = $2^{\frac{1}{2}}$ root mean square velocity$/2\pi\nu$

$$\sim 2^{\frac{1}{2}} 160{,}000/2\pi \cdot 0.25 \cdot 10^{13} m_0^{\frac{1}{3}} m^{1/6}. \qquad \text{(A2)}$$

Second approach

Instead of considering the part of the molecule which we are interested in as moving independently, we calculate its velocity and amplitudes by adding up, with random phases, velocities and amplitudes of the normal modes of vibrations of the whole molecule. We add up only those normal modes which actually contribute to the motion of our part m as a whole and we assume that to the motion of the part m as a subunit only those modes contribute whose $\lambda/2$ are larger than the linear extension $(m/m_0)^{\frac{1}{3}}2\cdot10^{-8}$ of the part m. The modes of shorter wave-length contribute to internal differential motions inside the part m. We are not interested in them. Let us calculate the r.m.s. velocity and amplitude of vibration in one mode. As the whole molecule participates in the mode, the thermal r.m.s. velocity

$$\sim 160{,}000/M^{\frac{1}{2}}.$$

And its vibrational amplitude

$$= 2^{\frac{1}{2}} \text{ r.m.s. velocity}/2\pi\nu \sim 2^{\frac{1}{2}}160{,}000/2\pi\nu M^{\frac{1}{2}}.$$

In the summation of the contributions of the various modes, the mode with lowest frequency is determined by

$$\lambda_l/2 = (M/m_0)^{\frac{1}{3}}2\cdot10^{-8}$$
$$\nu_l \sim 10^5/\lambda_l = 0.25\cdot10^{13}(m_0/M)^{\frac{1}{3}},$$

the highest frequency mode by

$$\lambda_h/2 = (m/m_0)^{\frac{1}{3}}2\cdot10^{-8}$$
$$\nu_h \sim 0.25\cdot10^{13}(m_0/m)^{\frac{1}{3}}.$$

There are altogether $3(4\pi/3\cdot8)\cdot(\nu_h/\nu_l)^3$ modes between ν_l and ν_h, the factor 3 stands for 2 transverse plus 1 longitudinal modes; only $\frac{1}{3}$ of these modes have motion in the x direction, so we have to add $(\pi/6)(\nu_h/\nu_l)^3$ modes' contributions with random phases. To calculate the thermal r.m.s. velocity of the part m, each contribution has the same amount, $160{,}000/M^{\frac{1}{2}}$. Therefore the sum with random phases is thermal r.m.s. velocity of m

$$\sim(160{,}000/M^{\frac{1}{2}})\Big(\sum_{\nu_l}^{\nu_h} 1^2\Big)^{\frac{1}{2}}$$
$$= (160{,}000/M^{\frac{1}{2}})[(\pi/6)(\nu_h/\nu_l)^3]^{\frac{1}{2}}$$
$$= (160{,}000/M^{\frac{1}{2}})(\pi/6)^{\frac{1}{2}}(M/m)^{\frac{1}{2}}$$
$$= (\pi/6)^{\frac{1}{2}}160{,}000/m^{\frac{1}{2}}. \quad \text{(A3)}$$

For such an approximate calculation this is a good agreement with the previous calculation (A1). In a similar way we calculate, by the method of the second approach, the resulting amplitude. The contributions of the various modes, $2^{\frac{1}{2}}\cdot160{,}000/2\pi\nu M^{\frac{1}{2}}$ are different for the different modes. The summation with random phases is given, as above, by the evaluation of

$$(2^{\frac{1}{2}}\cdot160{,}000/2\pi M^{\frac{1}{2}})\Big(\sum_{\nu_l}^{\nu_h}(1/\nu^2)\Big)^{\frac{1}{2}}.$$

In the interval ν to $\nu+\nu_l$ there are about $(4\pi/8)(\nu/\nu_l)^2$ modes contributing to motion in the x direction. Therefore

$$\sum_{\nu_l}^{\nu_h}\left(\frac{1}{\nu}\right)^2 = \int \frac{1}{\nu^2}\frac{4\pi}{8}\frac{\nu^2}{\nu_l^2}\frac{d\nu}{\nu_l}$$

$$= \frac{\pi}{2}\frac{\nu}{\nu_l^3}\Bigg|_{\nu_l}^{\nu_h} = \frac{\pi}{2\nu_l^2}\left(\frac{\nu_h}{\nu_l}-1\right) \sim \frac{\pi\nu_h}{2\nu_l^3}.$$

Thus we get for the vibrational amplitude

$$\sim(2^{\frac{1}{2}}\cdot160{,}000/2\pi M^{\frac{1}{2}})(\pi\nu_h/2\nu_l^3)^{\frac{1}{2}}$$
$$= (\pi/2)^{\frac{1}{2}}2^{\frac{1}{2}}160{,}000/2\pi\cdot0.25\cdot10^{13}m_0^{\frac{1}{3}}m^{1/6} \quad \text{(A4)}$$

(cf. (A2)). Particularly interesting in this result is the small dependence of the vibrational amplitude upon the mass m of the part of the molecule.

Accordingly the thermal velocities of vibration and amplitudes of vibration assume the following orders of magnitude (m is the mass of the part of the molecule whose vibration as a subunit we consider)

m in atomic mass units	10	100	1000	10000
thermal velocity in cm/sec.	$3\cdot10^4$	10^4	$3\cdot10^3$	10^3
amplitude in cm	$4\cdot10^{-9}$	$3\cdot10^{-9}$	$2\cdot10^{-9}$	$1.4\cdot10^{-9}$

It is a great pleasure to me to express my gratitude to many colleagues who through patient criticism and encouragement have made this investigation possible.

THE JOURNAL OF CHEMICAL PHYSICS VOLUME 18, NUMBER 9 SEPTEMBER, 1950

X-Ray Dose Determinations with Chloral Hydrate

HOWARD L. ANDREWS AND PARKHURST A. SHORE
Experimental Biology and Medicine Institute of the National Institutes of Health, Bethesda, Maryland
(Received May 15, 1950)

The chemical effects of x-rays on aqueous solutions of chloral hydrate ($CCl_3CH(OH)_2$) have been studied. The primary reaction is the conversion of the organic halogen to HCl and the resulting changes in electrical conductance have been used for the determination of x-ray dosage. The change in conductance is linear with x-ray dose and independent of dose-rate over a wide range. This compound has been used to determine the total output and depth-dose curves from a high intensity beryllium window x-ray tube.

THE development of high intensity, beryllium window x-ray tubes has provided an extremely useful tool for work in radiation chemistry, but accurate determinations of the energy delivered to test samples cannot be made by conventional means. Thin-wall ionization chambers can be constructed for use at relatively low photon energies but even with these chambers the correction factors are rather large[1] and they are not suitable for determining the energy delivered to a solution. Because of the low quantum energies the dose delivered to a test sample will vary sharply with depth and it appears that chemical dosimetry can be used to advantage. The specification of x-ray output in terms of roentgens does not give a true measure of the potentialities of a tube for work in radiation chemistry since here the important quantity is the total energy (which may be expressed in gram-roentgens) that can be delivered to a sample. This can be readily determined with chemical dosimetry.

Radiation effects on solutions of organic halogen compounds are particularly easy to follow with measurements of electrical conductance since the main reaction consists in general in the conversion of the very slightly ionized organic molecule to a highly ionized inorganic halide. Chloral hydrate, $CCl_3CH(OH)_2$, is an inexpensive, readily available compound. It is readily soluble in water and has a sufficiently high chlorine content to provide the necessary sensitivity to radiation.

Chloral hydrate, C.P., from Eastman was used without further purification and before irradiation showed specific conductances ranging from 7.5×10^{-6} mho/cm for 1.0 molar to 4.6×10^{-6} mho/cm for 0.001 molar, all solutions being made up in conductivity water from a Pyrex or silica still. All conductance measurements were made at 25°C using an a.c. bridge and an amplifier. Preliminary experiments showed a continuous change in conductance following irradiation which was traced to the catalytic action of the platinized electrodes in the conductance cell. This effect was completely eliminated by the use of tungsten electrodes.

The solutions were calibrated against calibrated ionization chambers using a Villard circuit x-ray unit operating at 100–200 KVP with a 0.25 mm copper filter. The solutions were then used to study the radiation from a Machlett type AEG-50T beryllium window tube operated at 50 kv constant potential.

The reactions involved have not been completely determined but it seems reasonable to expect HCl to be one of the main products. Measurements of conductivity, *p*H, chloride ion content and total acid content were made on a series of irradiated solutions. From these data the quantity of HCl formed was calculated on the assumption that it was the only ionized reaction product. The results on three solutions receiving different amounts of radiation, shown in Table I, are in reasonable agreement considering the analytical errors involved in determining the low concentrations, and indicate that HCl is the chief ionizable product formed. The conductance data for HCl tabulated by Harned and Owen[2] were used in all calculations of chemical equivalents formed by the reaction. The uniformly higher values found for total acid suggest the presence of a weakly ionized acid, but this has not been identified.

The dependence of yield upon concentration and dose was determined with 200 KVP x-rays at a dose rate of 150 r per minute. Figure 1 shows the HCl yield for five concentrations of chloral hydrate. The 0.5 M curve is not linear with dose and this appears to be a true effect since repeated runs under different experimental conditions yielded the same result.

Although the specific yield increases with increasing concentration there is no evidence to suggest that the main radiation effect is a direct effect upon the solute molecules. Assuming that the energy loss is due entirely to the Compton effect the relative energy expenditures in solute and solvent can be calculated. Over the concentration range studied the energy input to the solute ranged from 0.015 percent to 15 percent of that received by the water but the specific yield increased only about tenfold. This suggests strongly that the reaction takes place mainly through the interaction of activated water molecules with the solute. The observed increase of specific yield with concentration can be explained by the increased probability of a reaction at the higher concentrations between activated solvent and solute.

[1] F. H. Day, "Thimble-chamber calibration on soft x-rays," J. Research Nat. Bur. Stand. **40**, 295 (1948).

[2] Harned and Owen, *The Physical Chemistry of Electrolytic Solutions* (Reinhold Publishing Company, New York, 1950), p. 537.

TABLE I. Analyses of irradiated solutions.

HCl from conductance	Cl^- from analysis	H^+ from pH	Total acid from titration
3.72×10^{-3} M	3.78×10^{-3} M	3.7×10^{-3} M	4.70×10^{-3} M
1.75×10^{-3}	1.79×10^{-3}	1.65×10^{-3}	2.32×10^{-3}
1.19×10^{-3}	1.23×10^{-3}	1.22×10^{-3}	1.54×10^{-3}

It is recognized that calculations of ionic yield (molecules of product formed per ion pair) are of questionable significance but it is of interest to determine the relative values as a function of concentration. Figure 2 shows a plot of ionic yields calculated on the assumption that one ion pair is formed for every 33 ev expended. At every concentration studied the ionic yield is substantially greater than unity and in a 1 M solution rises to 79. At this concentration the yield corresponds to an expenditure of 0.42 ev per molecule of HCl formed.

If a chemical reaction is to be used to determine radiation doses it is highly desirable that the yield be independent of dose-rate. This has been studied up to the maximum obtainable from the AEG-50T tube operated at 50 KV and 50 ma. Within the experimental error the yield of HCl is independent of dose-rate up to 6000 r/min. and hence no corrections are necessary for varying dose-rates throughout the depth of a solution.

Figure 3 shows the total output of unfiltered radiation from the tube as a function of voltage. The data for this curve were obtained by using a volume of solution sufficient to absorb over 99 percent of the x-ray beam. The curve is linear over the region measured in agreement with the equation developed by Beatty[3] but it does not pass through the origin because of absorption in the window at low photon energies. Assuming a uniform spacial distribution and neglecting window absorption and electron scattering the value of the

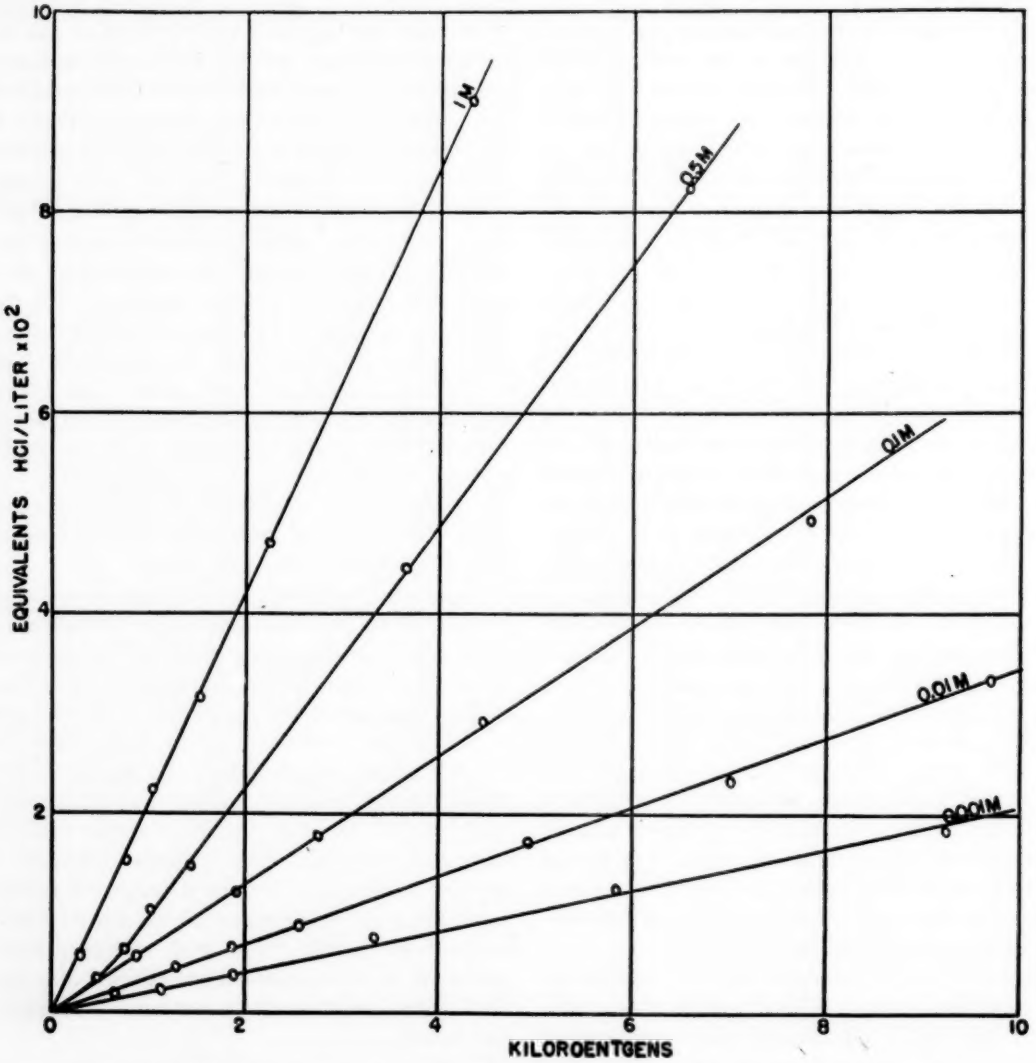

FIG. 1. Yield of HCl from x-ray irradiated chloral hydrate as calculated from conductance data.

[3] R. T. Beatty, "The energy of roentgen rays," Proc. Roy. Soc. A89, 314 (1913).

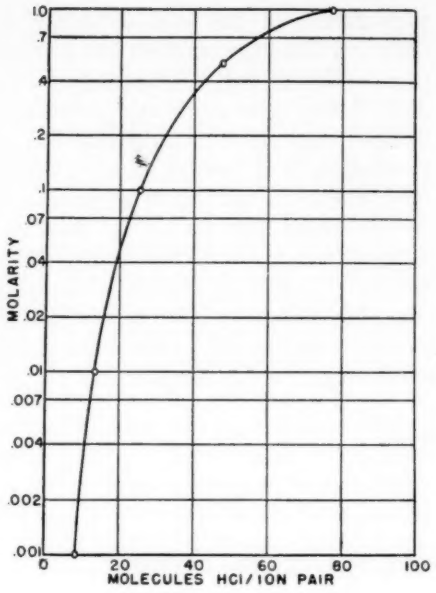

FIG. 2. Ionic yield of HCl from irradiated chloral hydrate.

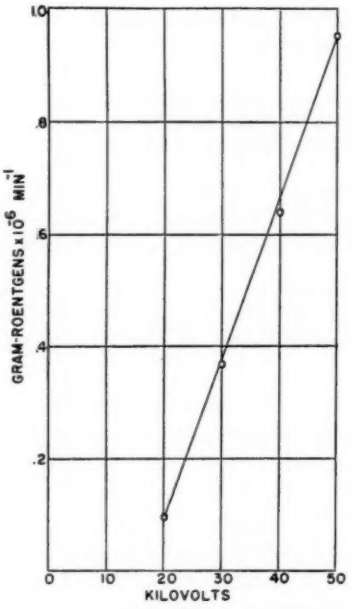

FIG. 3. X-ray beam energy of beryllium window tube as a function of applied voltage.

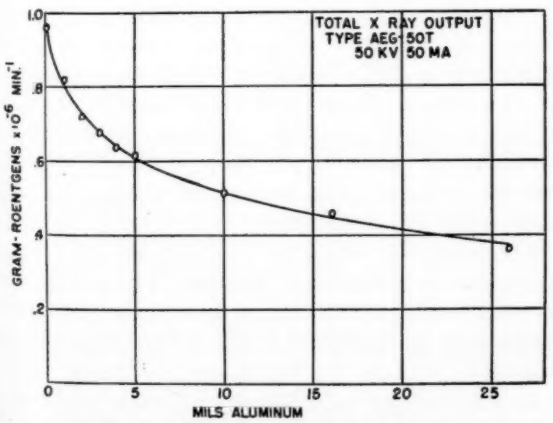

FIG. 4. Effect of filtration on the total beam energy of a beryllium window tube.

constant k in the Beatty equation, using our data, is 0.66×10^{-9}/volt. This is lower than the value 1.1×10^{-9}/volt given by Compton and Allison[4] as the best value but is in reasonable agreement since the beam is known

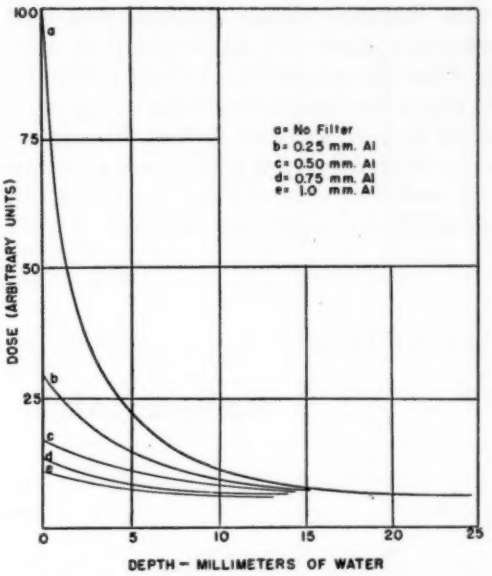

FIG. 5. Depth-dose data in water with a beryllium window tube. 25 cm focal distance.

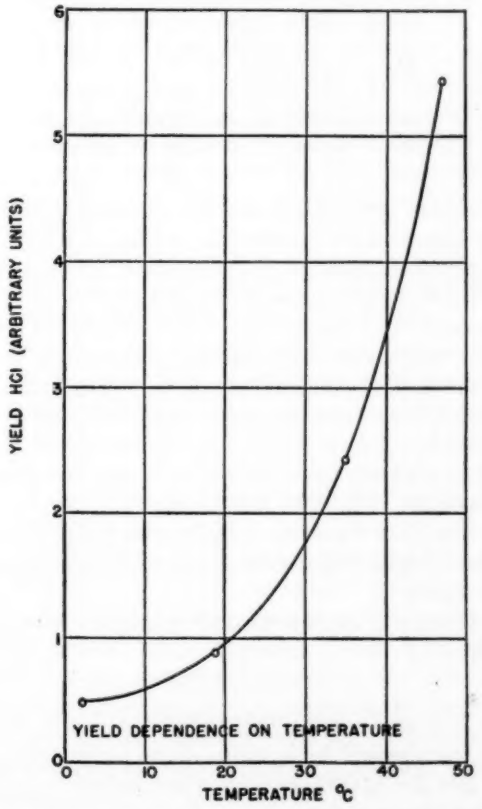

FIG. 6. Temperature coefficient of the reaction producing HCl.

[4] Compton and Allison, *X-rays in Theory and Experiment* (D. Van Nostrand and Company, Inc., New York, 1935), p. 90.

to be non-uniform and we have applied no correction factors. The effects of added filtration on the total output of the tube operating at 50 KV and 50 ma are shown in Fig. 4.

Depth dose determinations were made with a 1 mm cell with stretched rubber windows 0.04 mm thick cemented to a plastic ring. In obtaining the data shown in Fig. 5 the cell was placed in a water bath of sufficient size to insure equilibrium conditions at the cell.

Chloral hydrate solutions 0.01 M have proved very useful in determining the photon energy delivered to samples under conditions where ionization chambers are not applicable. Care must be taken to control the temperature of the solution during the exposure to radiation since the reaction has a substantial temperature coefficient, Fig. 6. Chloral hydrate solutions deteriorate slowly upon standing, particularly when exposed to light, and show an increased conductance prior to irradiation. It is possible to work with solutions two or three weeks old but fresher solutions are to be preferred for low doses because of the smaller corrections for initial conductance. Other organic halogens react similarly to radiation and will be reported on later but chloral hydrate appears to be the most useful compound for practical dosimetry because of the ease of handling, sensitivity, and relative stability.

THE JOURNAL OF CHEMICAL PHYSICS VOLUME 18, NUMBER 9 SEPTEMBER, 1950

Molecular Orbital Predictions of Organic Spectra*

JOHN R. PLATT
Department of Physics, University of Chicago, Chicago, Illinois
(Received April 25, 1950)

The energies of the first two to five electronic transitions of 16 conjugated molecules are predicted as simple one-electron LCAO molecular orbital transitions (with overlap included). Assignments of the observed levels to the predicted levels are made. Qualitative agreement is good when $S=0.25$ and $\beta=23{,}000$ cm^{-1} for ring systems.

It is shown that configuration interaction must be introduced to modify these energy predictions and to account for the intensities in some molecules ("round-field") such as benzene, triphenylene, coronene, and porphine. This interaction is less important in other molecules ("long-field") such as pyrene, biphenyl, and tetrahydroporphine.

Empirical groupings of intensities and luminescence lifetimes are shown for the different singlet-singlet and singlet-triplet band types of round-field hydrocarbons and for related molecules containing conjugated hetero-atoms. The alteration of these groupings in long-field molecules, and under *jj*-coupling, is described.

IT does not seem to be generally realized how accurate the simple LCAO molecular orbital calculations of the π-electronic spectra of a conjugated system can be. They have commonly been used to predict the one or two longest wave-length transitions only. A comparison between calculated and observed frequencies in non-polar solvents of the first two to five observed transitions of 16 molecules is given in Table I and in Figs. 1, 2, and 3.

The predictions have all been made by the following prescription:

(1) Compute the roots, x, of the simple LCAO secular equation, neglecting overlap, setting all α's equal and all β's equal.

(2) Compute the one-electron energies corrected for overlap

$$y=x/(1+Sx),$$

where S is the overlap integral, taken equal to 0.25.[1] These energies will be in units of the parameter, β.

(3) Set $\beta=32{,}000$ cm^{-1} for short polyenes; $-23{,}000$ cm^{-1} for ring systems.

(4) The lowest transition frequencies are then given approximately by $[y$ (low empty orbital$)-y$ (high filled orbital$)]\beta$, which is the energy of a one-electron jump. The polarizations will be determined by the symmetries of the initial and final orbitals.

(5) This procedure predicts the center-of-gravity of singlet-triplet pairs.[2] If the approximate singlet-triplet separation, δ, is known, $\frac{1}{2}\delta$ may be added to the prediction to locate the singlet more accurately; or subtracted to locate the triplet. The value of δ for one low pair in naphthalene is about 14,000 cm^{-1}.[3] This correction has not been made in Table I and Fig. 1 since it is known in only a few cases; this may be the main reason (as in the polyacenes) for some of the discrepancies between the predicted centers-of-gravity and the observed singlet-singlet transition frequencies.

This procedure neglects "electron interaction" or "configuration interaction." Analogy with the benzene spectrum and its interpretation showed that such interactions must be important in all cata-condensed hydro-

* This work was assisted in part by the ONR under Task Order IX of Contract N6ori-20 with the University of Chicago.

[1] G. W. Wheland, J. Am. Chem. Soc. **63**, 2025 (1941).

[2] For non-degenerate cases. For degenerate cases, it predicts the center of gravity of a whole set of singlets and triplets, i.e., of a *configuration*. For example, see benzene in Table I and Fig. 1.

[3] H. B. Klevens and J. R. Platt, J. Chem. Phys. **17**, 470 (1949).

carbons,[4] azulene,[5] and benzazulenes.[6] This has been confirmed by theoretical computation on naphthalene[7] and by a more elaborate treatment of benzene.[8]

Nevertheless, the method outlined here seems to give for many molecules a useful prediction of the number, sequence, and position of the strong transitions up to about 60,000 cm^{-1}. Some elementary semi-empirical arguments may be used to determine the probable polarizations of some observed transitions and their correspondence with the predicted transitions.[9] When this is done, the sequence of the observed transitions for a molecule sometimes disagrees with the sequence of the predicted transitions (naphthalene, Fig. 2; azulene, Fig. 3). This fact makes it risky to assign the lowest frequency observed transition to the lowest predicted transition, the second lowest observed to the second predicted, and so on, without making sure that these assignments are supported by additional polarization arguments or by the resemblances of the bands to assigned bands of the proper types in related molecules. Tentative assignments have nevertheless been made on

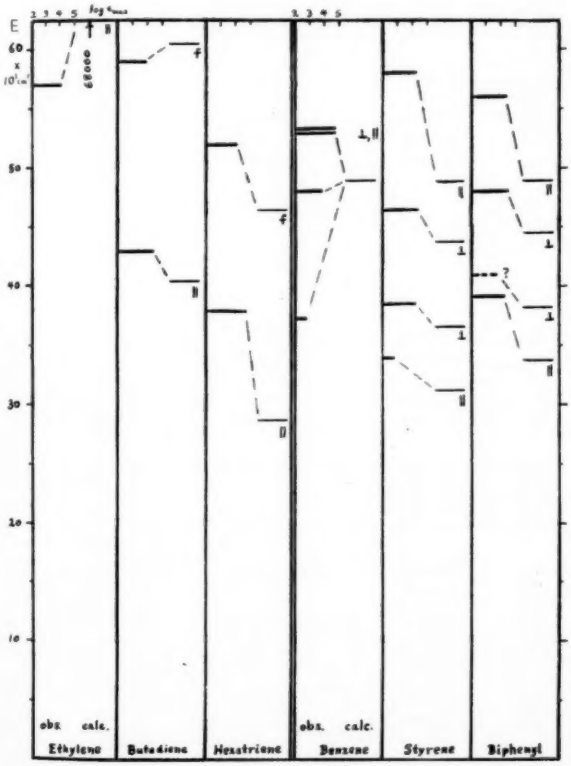

FIG. 1. Calculated centers of gravity and observed singlet excited states in polyenes and phenyl systems. (Vibrational structure omitted for simplicity. Length of horizontal lines in "observed" columns indicates intensity of transition from ground state according to scale at the top of the figure.)

[4] J. R. Platt, J. Chem. Phys. **17**, 484 (1949).
[5] Mann, Platt, and Klevens, J. Chem. Phys. **17**, 481 (1949).
[6] H. B. Klevens (to be published).
[7] J. Jacobs, Proc. Phys. Soc. (London) **62**, 710 (1949).
[8] D. P. Craig, J. Chem. Phys. **17**, 1358 (1949).
[9] J. R. Platt, "Iso-Conjugate molecules and vari-conjugate sequences" (to be published).

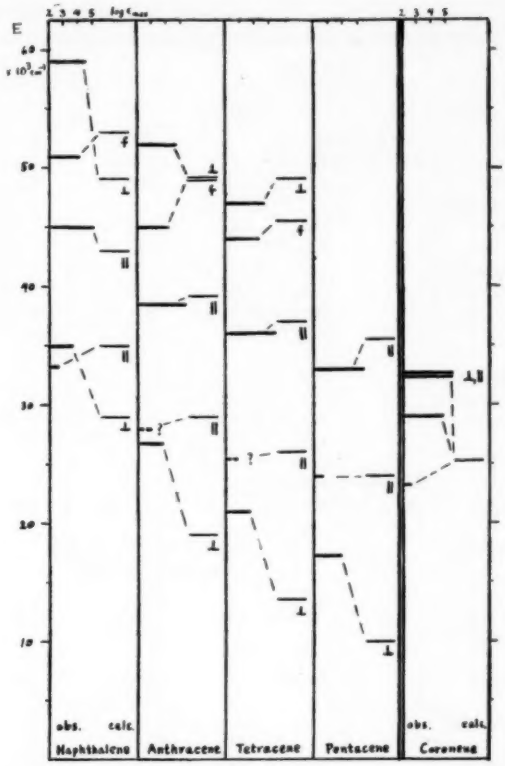

FIG. 2. Calculated centers of gravity and observed singlet excited states in polyacenes and coronene. (See note under Fig. 1.)

essentially this basis alone in biphenyl (Fig. 1), fulvene and tetrahydroporphine (Fig. 2), since in these cases the confirmatory evidence is unavailable or uncertain.

If the assignments shown in Table I and in Figs. 1 to 3 are correct, the agreement between the predictions and observations is within 10,000 cm^{-1} in almost all cases.

EFFECT OF CONFIGURATION INTERACTION ON GENERAL SPECTRAL TYPE

Configuration interaction seems to be the most important correction which must be applied to these simple one-electron predictions to obtain good correspondence between the predicted and observed transitions. This interaction is one which changes the energies and wave functions of two neighboring molecular states which have the same parity and symmetry. The familiar quantum-mechanical result is that the total wave functions of such states mix, so that each state becomes a hybrid; the lower state has its energy lowered further, and the upper state has its energy raised. These effects are stronger the closer the two states are together. If they have the same energy and are mutually degenerate in the one-electron approximation, as in benzene, the interaction removes the degeneracy and has an especially large effect.

These effects are shown schematically in Fig. 4. This figure is drawn for a conjugated system with V_h symmetry, but the reasoning is probably applicable to any

TABLE I. Predicted and observed π-electron absorption bands.

Molecule	Transition	Pol.	Predicted trans. energy β	Predicted trans. energy cm^{-1}	Observed singlets cm^{-1}	Correction cm^{-1}
Polyenes: $\beta=-32{,}000$ cm^{-1}						
Ethylene	$N\rightarrow V_1$ ^1B_b	∥[a]	2.133[b]	68,000	57,000[c,d]	−11,000[e]
Butadiene (*trans-*)	$N\rightarrow V_1$ ^1B_b	∥	1.266[b]	40,500	43,000[c,f]	+2500
	$N\rightarrow V_2$ ^1C_b	forb. in *trans-*	1.883[b]	60,500	59,000[c,f]	−1500
Hexatriene (*trans-*)	$N\rightarrow V_1$ ^1B_b	∥	0.899[b]	28,700	38,000[c,g]	+9500[e]
	$N\rightarrow V_2$ ^1C_b	forb. in *trans-*	1.450[b]	46,500	52,000[c,g]	+5500[e]
Ring systems: $\beta=-23{,}000$ cm^{-1}						
Pyrrole	(fourfold degen. in this approximation)		3.252[h]	75,000	>57,000[i] (c. g. of singlets)	?
Fulvene[j]		⊥	0.808	18,600	27,000[k]	+8500
		∥	1.073	24,700	35,500[m]	+11,000
		∥	1.657	38,000	54,000(?)[m]	+16,000
Azulene[n]	^1L_b	⊥	0.871	20,000	14,400	−5500
	^1L_a	∥	1.171	27,000	27,500	+500
	^1B_b	∥	1.331	30,600	34,000	+3500
	^1C_b	∥	1.917	44,000	41,000	−3000
	^1B_a	⊥	1.630	37,500	48,000	+10,500
Benzene[o]	^1L_b; $A_g\rightarrow{}^1B_{2u}$ ^1L_a; $A_g\rightarrow{}^1B_{1u}$ ^1B; $A_g\rightarrow{}^1E_u$ (fourfold degen. in this approximation)	∥, ⊥	2.133	49,100	48,000 (c. g. of singlets)	−1000
Diphenyl[p]	^1L_a?	∥	1.47	33,800	39,200[m]	+5500
	^1L_b?	⊥	1.66	38,200	(41,000 est.)	+3000
		⊥	1.93	44,400	48,000	+3500
		∥	2.13	49,000	56,000	+7000
Styrene[q]		∥	1.362	31,300	34,000[m]	+3000
		⊥	1.594	36,700	38,500	+2000
		⊥	1.901	43,800	46,500	+3000
		∥	2.133	49,000	58,000	+9000
Naphthalene[r]	^1L_a	⊥	1.265	29,000	35,000	+6000
	^1L_b	∥	1.530	35,000	32,200	−3000
	^1B_b	∥	1.868	43,000	45,000	+2000
	^1C_b	forb.	2.315	53,000	51,000(?)	−2000
	^1B_a	⊥	2.133	49,000	59,000	+10,000
Anthracene[s]	^1L_a	⊥	0.836	19,000	26,700	+8000
	^1L_b	∥	1.261	29,000	(28,000 est.)	(−1000)

ring structure where the conjugated system extends in two dimensions.

There are two extreme cases: where the configuration interaction is important; and where it is relatively unimportant. Which case we have seems to depend on the molecular geometry in such a way that it is convenient to call spectra exhibiting strong configuration interaction "round-field spectra" and those showing little interaction "long-field spectra."

"Round-Field" Spectra

In near ultraviolet spectra, configuration interaction is especially important when low excited states of the same total symmetry are degenerate, or nearly so, in the one-electron approximation. This happens when the highest filled molecular orbitals and the lowest unfilled orbitals are in pairs, degenerate, or almost so (left side of Fig. 4). The highest filled pair and the lowest unfilled

TABLE I.—*Continued.*

Molecule	Transition	Pol.	Predicted trans. energy β	Predicted trans. energy cm^{-1}	Observed singlets cm^{-1}	Correction cm^{-1}
Anthracene[r]	^1B_b	∥	1.708	39,300	38,500	−1000
	^1C_b	forb.	2.133	49,000	45,000	−4000
	^1B_a	⊥	2.133	49,000	52,000	+3000
Tetracene[r]	^1L_a	⊥	0.587	13,500	21,000	+7500
	^1L_b	∥	1.115	26,000	(25,500 est.)	(−1000)
	^1B_b	∥	1.605	37,000	36,000	−1000
	^1C_b	forb.	1.983	45,500	44,000	−1500
	^1B_a	⊥	2.133	49,000	47,000	−2000
Pentacene[r]	^1L_a	⊥	0.441	10,000	17,300	+7000
	^1L_b	∥	1.033	24,000	24,000(?)	0
	^1B_b	∥	1.538	35,500	33,000	−2500
	^1B_a	⊥	2.133	49,000	—	—
Coronene[s]	^1L_b; $A_g-{}^1B_{2u}$ ^1L_a; $A_g-{}^1B_{1u}$ ^1B; $A_g-{}^1E_u$ (fourfold degen. in this approximation)	⊥, ∥	1.097	25,200	29,000 (c. g. of singlets)	+4000
Porphine	$A_{2u}-E_g$ ($^1L_{a,b}$?)	⊥, ∥ (doub. degen.)	0.391[t] (0.627)[u]	9000 (14,500)	16,000[v]	+7000
	$A_{1u}-E_g$ ($^1B_{a,b}$?)	⊥, ∥ (doub. degen.)	0.927 (0.718)	21,300 (16,500)	23,200	+2000
Tetrahydro-porphine	$B_{1u}-B_{3g}$; ^1L_a(?)	⊥	0.380[t] (0.573)[u]	8700 (13,200)	13,000[v]	+4000
	A_u-B_{3g}; ^1L_b(?)	∥	0.700 (0.449)	16,100 (10,300)	16,300	0
	$B_{1u}-B_{3g}$;	⊥	0.963 (0.915)	22,200 (21,000)	19,000(?)	−3000
	$B_{1u}-B_{2g}$; ^1B_b(?)	∥	1.003 (1.181)	23,000 (27,200)	24,000	+1000
	A_u-B_{2g}	⊥	1.322 (1.056)	30,400 (24,300)	—	—

[a] ∥ and ⊥ mean with respect to the longest axis in the molecule.
[b] From the usual formula for LCAO energies of polyenes: $x_n=2\cos n\pi/(N+1)$; $n=1, 2, \cdots, N$ where N is the number of atoms in the conjugate chain.
[c] Reduced 2000 cm^{-1} for comparison with solution prediction.
[d] Platt, Klevens, and Price, J. Chem. Phys. **17**, 466 (1949).
[e] See reference 3 and H. Kuhn, J. Chem. Phys. **17**, 1198 (1949) for discussion of systematic errors in prediction of polyene frequencies as function of length.
[f] W. C. Price and A. D. Walsh. Proc. Roy. Soc. **174A**, 220 (1940).
[g] W. C. Price and A. D. Walsh, Proc. Roy. Soc. **185A**, 182 (1946).
[h] See Tables II and XIII of reference 12. The Coulomb integral on N is taken equal to that on C.
[i] $N\rightarrow V$ bands at 45,000 and 57,000 cm^{-1}. Two higher bands from this configuration not found.
[j] The secular equation for fulvene gives the lowest four energy levels at $x=2.115$, 1.00, 0.618, and −0.255. The lowest transitions are from the first three of these (filled) to the fourth (unfilled).
[k] Estimated from Stark *et al.*, Physik. Zeits. **9**, 661 (1908).
[m] H. B. Klevens and J. R. Platt (unpublished).
[n] See reference 5.
[o] See reference 4.
[p] E. Hückel, Zeits. f. Physik **76**, 628 (1932).
[q] Secular equations given by W. G. Penney and G. J. Kynch, Proc. Roy. Soc. London **A164**, 409 (1938).
[r] See reference 3. Predictions from C. A. Coulson, Proc. Phys. Soc. **60**, 257 (1948).
[s] Molecular orbital energies derived from W. E. Moffitt and C. A. Coulson, Proc. Phys. Soc. **60**, 309 (1948); Spectra from J. W. Patterson, J. Am. Chem. Soc. **64**, 1485 (1942), and Fromberg, Thaler, and Wolf, Zeits. f. Elektrochemie **49**, 387 (1943).
[t] See reference 12. From energies x, with nitrogen Coulomb integral equal to carbon.
[u] See reference 12. Values in brackets are from energies x', nitrogen Coulomb integral >carbon.
[v] Observations as summarized by E. Rabinowitch, Rev. Mod. Phys. **16**, 226 (1944).

pair are normally of opposite parity (for the V_h case) if the molecule forms a closed-shell chemically stable type of ground state. In such a situation the lowest transition, neglecting spin, is fourfold degenerate (or almost degenerate) and allowed, in this approximation. Configuration interaction partially removes the degeneracy, producing two relatively weak long-wavelength singlet "multipole" transitions (^1L_a, ^1L_b) and two higher singlet strong allowed dipole transitions (^1B_a, ^1B_b). (See the states under "elect. int." in Fig. 4.) Both these pairs are degenerate, or almost so. The interaction produces an equal number of triplet transitions which may lie lower and which may also be of two types: relatively weak (multiply forbidden) (^3L_a, ^3L_b) and relatively strong (singly forbidden) (^3B_a, ^3B_b).[4]

The total spread of the states produced by this electron or configuration interaction amounts to 30,000 cm^{-1} in the case of benzene. Some additional effects may be specific to the structure of the molecule, such as removal of the remaining degeneracy or the further

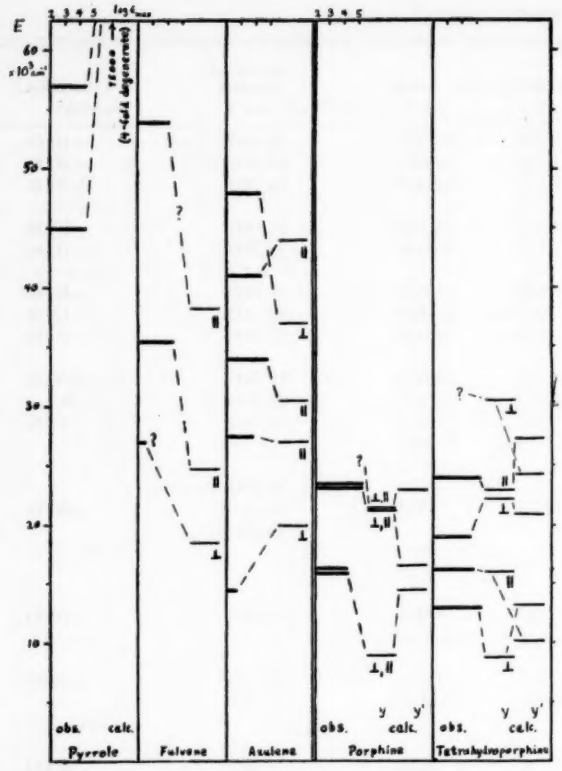

FIG. 3. Calculated centers of gravity and observed singlet excited states in 5-ring systems and in porphines. (See note under Fig. 1.)

splitting of a close pair of states. (See the states under "nuclear field" in Fig. 4.) But these specific effects will be small compared to the configuration interaction. Consequently the general intensity distribution and sequence of the observed transitions is remarkably similar in such molecules as benzene, triphenylene, coronene, and porphine. The cata-condensed hydrocarbons are also surprisingly close to this extreme case. Since the specific structural effects in these spectra are so small, this may be called a "weak-field case"; or, since this case is typical of molecules having symmetry D_{3h} or higher, a better name might be the "round-field case."

In short, for this case the observed transitions should be farther apart in both position and intensity than the simple LCAO-predicted one-electron transitions. Configuration interaction will be important for determining transition frequency, and essential for predicting intensities.

The maximum extinction coefficients of the several types of "round-field" transitions lie in very limited ranges. In Fig. 5, the empirical ranges of values of the molar extinctions, oscillator strengths and luminescence lifetimes (seconds) of different singlet-singlet π-transition types[3] are shown. Also the characteristic ranges of these quantities for the different triplet types and for some non-bonding transitions of different types in aza and keto polycyclics are given, as taken from the work of M. Kasha and from the literature. (The non-bonding transitions are given a new terminology—^1W,[3] W, ^1U, ^3U—consistent with the π-electron terminology, to facilitate future discussion.)

The scales in Fig. 5 are empirical for the long-wave transitions of systems of 2 to 20 conjugated carbon atoms in the visible and near ultraviolet. They do not apply to Rydberg bands and some other types of transitions found near 2000A and below in systems of four carbons or less. The f-values are roughly proportional to ϵ because the band width is roughly constant. The lifetimes, τ, are almost but not quite inversely proportional to f because they depend also on frequency, and the observed weak bands are always at lower frequency than the observed strong bands. Evidently, the identity and character of many bands of "round-field" molecules can be determined by a simple measurement of ϵ_{max}.**

Figure 5 is valid only for extreme LS-coupling, that is to say, low spin-orbit interaction, as in light atoms. McClure has shown that heavy substituents transform the spectra toward jj-coupling, and give triplets more

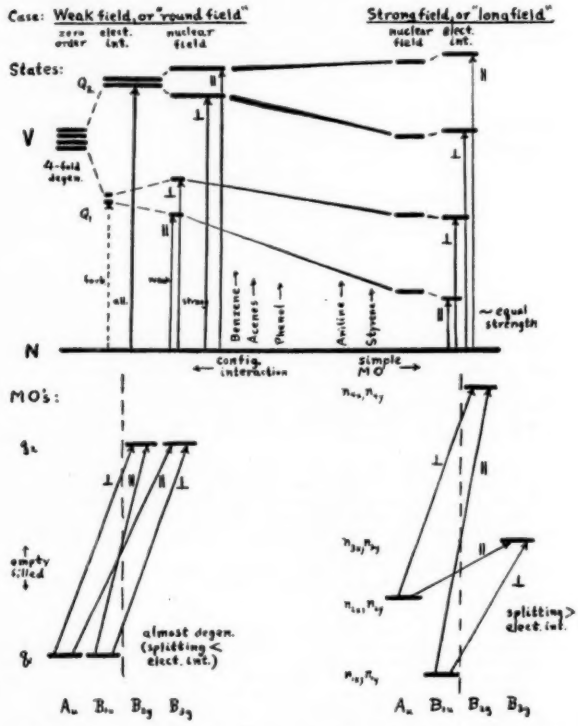

FIG. 4. Effect of configuration interaction on "round-field" and "long-field" spectra.

** Here we must enter a caveat in the use of the terms "forbidden," "multipole," "multiply forbidden," etc., in the above paragraphs and in Fig. 5. These terms apply to the *electronic* character of a transition for the *equilibrium* nuclear configuration only. In polyatomic molecules, the observed transitions are always "made allowed" by vibrations, except when spin-forbidden. The character of the radiation is then "allowed dipole" for some *non*-equilibrium configuration, and the transitions are more intense than the terms "forbidden" and so on normally indicate when used in atomic spectra. In spite of this, these terms indicate useful classifications of transition types, as is shown in Fig. 5. They may be safely applied to polyatomic molecules if this special meaning is generally understood.

singlet character.[10] Kasha has suggested that the spin-orbit coupling may also be greater for non-bonding electrons than for bonding σ- or π-electrons even in light atoms.[11] This would account for the fact that the non-bonding singlet-triplet separation in Fig. 5 is less than the π-singlet-triplet separation.

"Long-Field" Spectra

Turning to the other extreme case, the right side of Fig. 4 shows the situation when configuration interaction is relatively unimportant. This occurs when the molecular geometry separates the two highest filled orbitals by amounts large compared with the electron interaction energy. This is a "strong-field case," or more accurately, a "long-field case." The simple LCAO-predictions of position and intensity will be reasonably accurate (see the states under "nuclear field" in Fig. 4), and electron interaction will be only a small correction (see the states under "elect. int."). The distinction between "multipole" and dipole transitions will disappear, and intensities will become roughly equal. The L bands of Fig. 5 will take on B character. The energy levels will be more separated than in the "round-field" case, and the first absorption bands will in general lie at longer wave-lengths than in the latter case.

The transition from the "round-field" to the "long-field" case parallels the change in the eigenstates which would occur if we adiabatically transformed a two-dimensional circular box into a rectangular box of the same area. In the round box an angular momentum number, q, is a good quantum number, but not a linear momentum number, n_x or n_y. In the rectangular box the degeneracies are removed and the reverse is true; the states are also closer together. So in the round field case, the individual q's are good quantum numbers; in the long field case, the individual n_x or n_y's.

The transition from the toluene to the aniline spectrum is no doubt of this type; as is also the transition

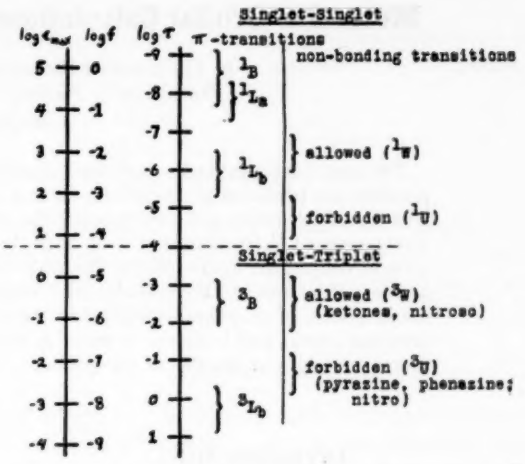

FIG. 5. Approximate extinctions, oscillator strengths, and luminescence lifetimes for different band types. (Compiled with the help of M. Kasha.)

from porphine to tetrahydroporphine.[12] The spectra of other molecules may have intermediate character, some closer to one case, some to the other, as suggested for the molecules in the middle of Fig. 4. Because the electron interaction energy is always so large there is probably no pure "long-field" type of molecule.

The pyrene spectrum is more "long-field"[13] than the anthracene spectrum. Qualitatively this seems strange since pyrene is the rounder molecule. Perhaps this means that the cross-links help preserve the "round field" character in the cata-condensed hydrocarbons (anthracene), while they distort it toward the "long-field" case in the peri-condensed compounds (pyrene), regardless of the shape of the perimeter of the molecule.

As the distinction between L and B bands disappears in "long-field" molecules, so there may be other classes of molecules in which the distinction between the U and W bands of Fig. 5 will also disappear.

[10] D. McClure, J. Chem. Phys. **17**, 905 (1949).
[11] M. Kasha, private communication.
[12] Longuet-Higgins, Rector, and Platt, J. Chem. Phys., **18**, 1174 (1950).
[13] H. B. Klevens and J. R. Platt (unpublished results).

Molecular Orbital Calculations on Porphine and Tetrahydroporphine*

H. C. LONGUET-HIGGINS,† C. W. RECTOR,†† AND J. R. PLATT
Department of Physics, University of Chicago, Chicago, Illinois

(Received April 25, 1950)

The first three electronic transitions of porphine and the first five electronic transitions of tetrahydroporphine are predicted as simple one-electron *LCAO* molecular orbital transitions (with overlap included). The electron densities and bond orders in the ground states are also computed. The observed levels are tentatively assigned to the predicted levels with the help of comparisons with spectra of other aza-amine derivatives of conjugated hydrocarbons. Probable degeneracies and polarizations are determined. The blue shift and loss of intensity of the first electronic transition, in going from tetrahydroporphine to the larger conjugated system of porphine, is typical of the change from a "long-field" to a "round-field" molecule (see previous paper) and is shown to occur in several other "long-field" systems when additional conjugated atoms are added at the side of the system.

INTRODUCTION

THE wide occurrence of porphine derivatives in nature, and their essential role in photosynthesis, makes the understanding of their electronic structures a most important matter.

In this paper we shall investigate the electronic structures of porphine (I) and tetrahydroporphine (II), using molecular orbital theory in its simplest form. We shall attempt to interpret certain interesting features of their electronic spectra on the assumption that their ground state and excited states are adequately described by single electron configurations. The notation used will be that of Coulson and Longuet-Higgins.[1]

A theoretical discussion of the structure of these molecules has been recently given by Simpson, using the free-electron model.[2] Also Rabinowitch earlier brought together experimental data on the spectra of these and related compounds (porphyrins, chlorins, and bacterio-chlorophyll) and discussed the interpretation of their spectra.[3] Further references may be found in these two papers.

THEORY

It is assumed that the longest wave-length electronic bands of I and II arise from transitions involving the π electrons, not the σ electrons. Attention will therefore be restricted to the former.

TABLE I. A_{2u} *MO* in porphine.

x	2.39138	0.77287	0.00000	−2.16425
c_1	0.17070	−0.29912	0.00000	0.06615
c_2	0.23750	0.06794	0.00000	−0.20933
c_3	0.19863	0.17581	0.35355	0.19344
c_{21}	0.19863	0.17581	−0.35355	0.19344

It is convenient to express the molecular orbitals (*MO*) of the electrons as linear combinations of suitable atomic orbitals (*LCAO*). Each *MO* is then written in the form

$$\psi=\sum_r c_r\phi_r, \tag{1}$$

where ϕ_1 to ϕ_{24} are the $2pz$ orbitals of atoms 1 to 24. For simplicity it is assumed that the atomic orbitals (*AO*) are orthogonal and normalized, *viz.*

$$\int \phi_r\phi_s d\tau=1 \text{ if } r=s, \text{ 0 if } r\neq s. \tag{2}$$

On these assumptions, the energy of an electron in ψ is given by the usual secular equations

$$(\alpha_r-\epsilon)c_r+\sum_{s\neq r}\beta_{rs}c_s=0, \qquad (r=1, 2, \cdots, 24), \tag{3}$$

where

$$\phi_r=\int \phi_r H\phi_r d\tau, \qquad \beta_{rs}=\int \phi_r H\phi_s d\tau. \tag{4}$$

In solving these equations for the molecules under investigation we assume that

$$\beta_{rs}=\begin{cases}\beta & \text{if atoms } r \text{ and } s \text{ are bonded,}\\ 0 & \text{otherwise,}\end{cases} \tag{5}$$

where β has the same value for all CC and CN bonds. We also assume that α_r has the same value α for all the atoms. This is, of course, not correct: nitrogen is more electronegative than carbon, and will certainly have a lower value of α_r. However, it is most convenient to begin by assuming all the α's equal, and to correct the resulting energies later, using the equation

$$\partial\epsilon/\partial\alpha_r=c_r^2. \tag{6}$$

TABLE II. B_{2u} *MO* in porphine.

x	2.00000	0.618034	−1.618034
c_1	0.22361	−0.25583	0.09972
c_2	0.22361	0.09972	−0.25583
c_{21}	0.22361	0.31623	0.31623

* This work was assisted in part by the ONR under Task Order IX of Contract N6ori-20 with the University of Chicago.

† Present address: Department of Theoretical Chemistry, University of Manchester, Manchester, England.

†† Present address: Department of Chemistry, Massachusetts Institute of Technology, Cambridge 39, Massachusetts.

[1] C. A. Coulson and H. C. Longuet-Higgins, Proc. Roy. Soc. (London) **A191**, 39 (1947).

[2] W. T. Simpson, J. Chem. Phys. **17**, 1218 (1949).

[3] E. Rabinowitch, Rev. Mod. Phys. **16**, 226 (1944).

TABLE III. A_{1u} *MO* in porphine.

x	0.61803	−1.61803
c_1	0.18587	−0.30075
c_2	0.30075	0.18587

With these assumptions, the secular equations take the form

$$(\alpha-\epsilon)c_r+\sum_{s \text{ bonded to } r}\beta c_s=0, \tag{7}$$

or, more briefly,

$$-xc_r+\sum_{s \text{ bonded to } r}c_s=0, \tag{8}$$

where $x=(\epsilon-\alpha)/\beta$.

MOLECULAR ORBITALS IN PORPHINE

The symmetry group of porphine is D_{4h}. The π *MO* are, by definition, all antisymmetric with respect to the molecular plane, and therefore belong to the species A_{2u}, B_{2u}, A_{1u}, B_{1u}, and E_g.

Species A_{2u}

The molecular orbitals of species A_{2u} may be written in the form

$$\begin{aligned}\psi(A_{2u})=&c_1(\phi_1+\phi_5+\phi_6+\phi_{10}+\phi_{11}+\phi_{15}+\phi_{16}+\phi_{20})\\&+c_2(\phi_2+\phi_4+\phi_7+\phi_9+\phi_{12}+\phi_{14}+\phi_{17}+\phi_{19})\\&+c_3(\phi_3+\phi_8+\phi_{13}+\phi_{18})\\&+c_{21}(\phi_{21}+\phi_{22}+\phi_{23}+\phi_{24}).\end{aligned}$$

The secular Eqs. (8) demand that

$$\begin{aligned}-xc_1+c_1+c_2&=0\\-xc_2+c_1+c_3+c_{21}&=0\\-xc_3+2c_2&=0\\-xc_{21}+2c_2&=0.\end{aligned}$$

Eliminating the coefficients c_r we obtain

$$\begin{vmatrix}1-x, & 1, & 0, & 0\\ 1, & -x, & 1, & 1\\ 0, & 2, & -x, & 0\\ 0, & 2, & 0, & -x\end{vmatrix}=0=x^4-x^3-5x^2+4x.$$

This equation has four real roots $x_j(j=1, 2, 3, 4)$, so there are 4 *MO* of species A_{2u}, with energies $\epsilon_j=\alpha+\beta x_j$. The ratios of the coefficients c_r for each of these are obtained by substituting the appropriate x_j back into the equations; and their absolute magnitudes are fixed by the condition that the *MO* be normalized, *viz.*,

$$8c_1^2+8c_2^2+4c_3^2+4c_{21}^2=1.$$

The values of x_j and the corresponding values of c_r are given in Table I below.

Species B_{2u}

The *MO* of species B_{2u} have nodal planes through atoms 3, 8, 13, and 18. They have the general form

$$\begin{aligned}\psi(B_{2u})=&c_1(\phi_1-\phi_5-\phi_6+\phi_{10}+\phi_{11}-\phi_{15}-\phi_{16}+\phi_{20})\\&+c_2(\phi_2-\phi_4-\phi_7+\phi_9+\phi_{12}-\phi_{14}-\phi_{17}+\phi_{19})\\&+c_{21}(\phi_{21}-\phi_{22}+\phi_{23}-\phi_{24}).\end{aligned}$$

TABLE IV. B_{1u} *MO* in porphine.

x	1.618034	−0.618034	−2.000000
c_1	0.09972	−0.25583	0.22361
c_2	0.25583	−0.09972	−0.22361
c_3	0.31623	0.31623	0.22361

The fact that c_3 etc., are zero means that the *MO* in this species satisfy the secular equations for an isolated 5-membered ring of unsaturated atoms. The solutions are given in Table II.

Species A_{1u}

The orbitals of this species have nodal planes through the nitrogen atoms as well as through the corner carbon atoms. They therefore satisfy the secular equations for butadiene. Their general form is

$$\begin{aligned}\psi(A_{1u})=&c_1(\phi_1-\phi_5+\phi_6-\phi_{10}+\phi_{11}-\phi_{15}+\phi_{16}-\phi_{20})\\&+c_2(\phi_2-\phi_4+\phi_7-\phi_9+\phi_{12}-\phi_{14}+\phi_{17}-\phi_{19}).\end{aligned}$$

The energies and normalized *AO* coefficients are given in Table III below.

Species B_{1u}

The orbitals of this species are of the general form

$$\begin{aligned}\psi(B_{1u})=&c_1(\phi_1+\phi_5-\phi_6-\phi_{10}+\phi_{11}+\phi_{15}-\phi_{16}-\phi_{20})\\&+c_2(\phi_2+\phi_4-\phi_7-\phi_9+\phi_{12}+\phi_{14}-\phi_{17}-\phi_{19})\\&+c_3(\phi_3-\phi_8+\phi_{13}-\phi_{18}).\end{aligned}$$

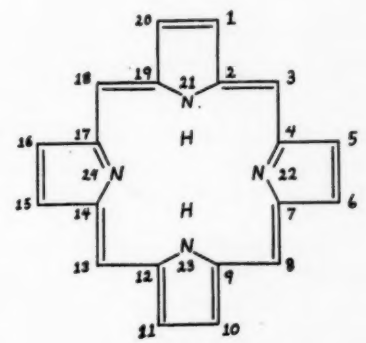

(I) Porphine

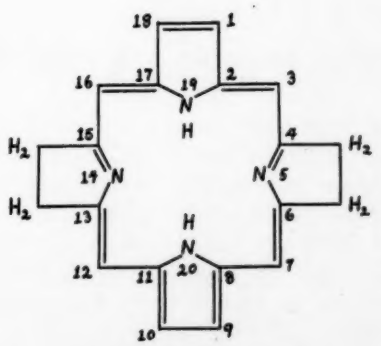

(II) Tetrahydroporphine

FIG. 1. Structure of porphine and tetrahydroporphine.

TABLE V. E_g *MO* in porphine.

x	2.25619	1.18994	0.61803	−0.35650	−1.61803	−2.08963
c_1	0.25427	0.22432	−0.34409	0.03958	0.08132	0.08811
c_2	0.31940	0.04261	0.13143	−0.05368	−0.21290	−0.27221
c_3	0.18324	−0.24524	0.00000	−0.32161	0.00000	0.22018
c_4	0.09401	−0.33442	−0.13143	0.16833	0.21290	−0.18789
c_5	0.02887	−0.15271	−0.08123	0.26160	−0.34448	0.22454
c_{21}	0.28314	0.07161	0.42533	0.30117	0.26316	0.26054

TABLE VI. π-electron densities and mobile bond orders in porphine.

$q_1=1.0846$	$p_{20,1}=0.785$
$q_2=1.0711$	$p_{1,2}=0.472$
$q_3=0.9656$	$p_{2,3}=0.575$
$q_{21}=1.2231$	$p_{2,21}=0.579$

Since they have nodal planes through the nitrogen atoms, they satisfy the secular equations for a twenty-membered ring, and are relatively easily obtained. The solutions are given in Table IV.

Species E_g

The *MO* of species E_g occur in degenerate pairs, and though the energy of each pair is determinate, there is a certain freedom of choice in the forms of the *MO*. We shall use the following real forms:

$$\psi(E_g)=c_1(\phi_1-\phi_{10}-\phi_{11}+\phi_{20})+c_2(\phi_2-\phi_9-\phi_{12}+\phi_{19})+c_3(\phi_3-\phi_8-\phi_{13}+\phi_{18})+c_4(\phi_4-\phi_7-\phi_{14}+\phi_{17})+c_5(\phi_5-\phi_6-\phi_{15}+\phi_{16})+c_{21}(\phi_{21}-\phi_{23})$$

and

$$\psi'(E_g)=c_1(\phi_5+\phi_6-\phi_{15}-\phi_{16})+c_2(\phi_4+\phi_7-\phi_{14}-\phi_{17})+c_3(\phi_3+\phi_8-\phi_{13}-\phi_{18})+c_4(\phi_2+\phi_9-\phi_{12}-\phi_{19})+c_5(\phi_1+\phi_{10}-\phi_{11}-\phi_{20})+c_{21}(\phi_{22}-\phi_{24}).$$

The symmetry properties of ψ and ψ' are most easily seen by referring to the diagram (Fig. 2). The secular equations, for both ψ and ψ', are as follows:

$$\begin{aligned} -xc_1+c_1+c_2&=0, & -xc_4+c_3+c_5&=0,\\ -xc_2+c_1+c_3+c_{21}&=0, & -xc_5+c_4-c_5&=0,\\ -xc_3+c_2+c_4&=0, & -xc_{21}+2c_2&=0. \end{aligned}$$

When expanded, the secular determinant factorizes into a quartic and a quadratic. The orbital energies and coefficients are as follows:

ELECTRON DENSITIES AND BOND ORDERS IN PORPHINE

It must be re-emphasized that the above values of the energy parameter x and the *AO* coefficients c_r have been calculated on the assumption that the nitrogen atoms and the carbon atoms all have the same Coulomb integral α. With this assumption in mind, let us calculate the electron densities and mobile bond orders for the molecule in its ground state. These are defined by the equations

$$q_r(=\text{electron density in } \phi_r)=2\sum c_r^2, \text{ and}$$
$$p_{rs}(=\text{mobile order of bond } rs)=2\sum c_r c_s,$$

the summations being taken over the 13 *molecular* orbitals of lowest energy, since the molecule has altogether 26 π electrons. These 13 *MO* include the 12 *MO* of positive x (6 of these are non-degenerate, and 3 pairs are doubly degenerate), and the one *MO* (of species A_{2u}) for which $x=0$. Summing over these orbitals we obtain for the electron densities and bond orders the values given in Table VI.

It is interesting to note that the π-electron density comes out highest on atoms 21, 22, 23, 24, even though no allowance has been made in the calculations for the greater electron affinity of nitrogen than carbon. This suggests two things. First, that the great stability of porphine is largely due to the presence of nitrogen atoms at points in the skeleton where, for purely *geometrical* reasons, the π-electrons tend to congregate. Secondly, this piling up of the electrons may reduce the effective electron affinity of the nitrogen atoms to a value not very far from that of the carbon atoms; and, if this is so, then it may not be such a bad approximation to set the Coulomb integrals of the nitrogen atoms in porphine equal to those of the carbon atoms.

Table VI also shows that positions 3, 8, 13, and 18 have the lowest π-electron densities. In porphine, therefore, these positions should be the initial points of attack by nucleophilic reagents.

The bond orders call for little comment. The external bond of the five-membered rings appears to have the highest mobile order, but this difference would be

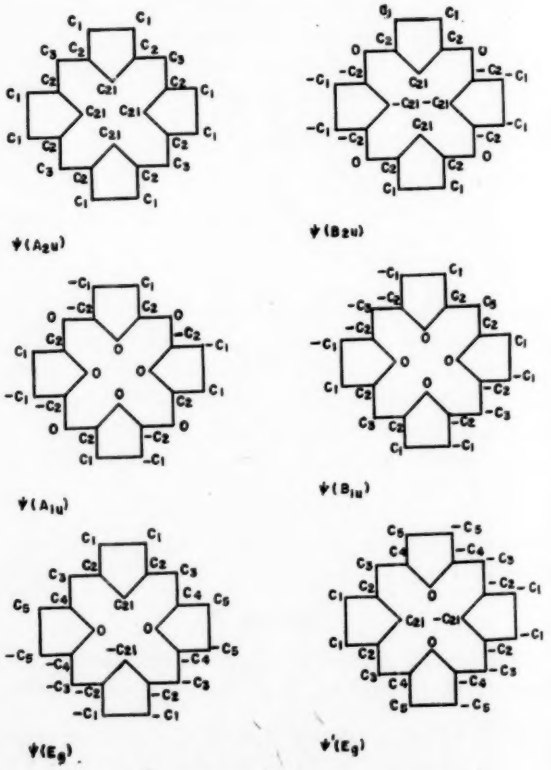

FIG. 2a. Molecular orbital species of porphine.

lessened if one assigned the nitrogen atoms a larger Coulomb integral than the carbon atoms.

MOLECULAR ORBITALS IN TETRAHYDROPORPHINE

The symmetry group of tetrahydroporphine is D_{2h}, and the π *MO* are of species B_{1u}, B_{2g}, B_{3g}, and A_u. The numbering of the *AO* is shown in Fig. 1.

Species B_{1u}

The *MO* of this species have the form

$$\psi(B_{1u})=c_1(\phi_1+\phi_9+\phi_{10}+\phi_{18})+c_2(\phi_2+\phi_8+\phi_{11}+\phi_{17})+c_3(\phi_3+\phi_7+\phi_{12}+\phi_{16})+c_4(\phi_4+\phi_6+\phi_{13}+\phi_{15})+c_5(\phi_5+\phi_{14})+c_{19}(\phi_{19}+\phi_{20}).$$

The *AO* coefficients and energies in these *MO* are found to be:

Species B_{2g}

The orbitals of this species have nodes through atoms 5 and 14. They are of the general form:

$$\psi(B_{2g})=c_1(\phi_1-\phi_9-\phi_{10}+\phi_{18})+c_2(\phi_2-\phi_8-\phi_{11}+\phi_{17})+c_3(\phi_3-\phi_7-\phi_{12}+\phi_{16})+c_4(\phi_4-\phi_6-\phi_{13}+\phi_{15})+c_{19}(\phi_{19}-\phi_{20}).$$

The *AO* coefficients and energy parameters are:

Species B_{3g} and A_u

These *MO* are of the forms

$$\psi(B_{3g})=c_1(\phi_1+\phi_9-\phi_{10}-\phi_{18})+c_2(\phi_2+\phi_8-\phi_{11}-\phi_{17})+c_3(\phi_3+\phi_7-\phi_{12}-\phi_{16})+c_4(\phi_4+\phi_6-\phi_{13}-\phi_{15})+c_5(\phi_5-\phi_{14}).$$

$$\psi(A_u)=c_1(\phi_1-\phi_9+\phi_{10}-\phi_{18})+c_2(\phi_2-\phi_8+\phi_{11}-\phi_{17})+c_3(\phi_3-\phi_7+\phi_{12}-\phi_{16})+c_4(\phi_4-\phi_6+\phi_{13}-\phi_{15}).$$

The *MO* of both these species have nodal planes through

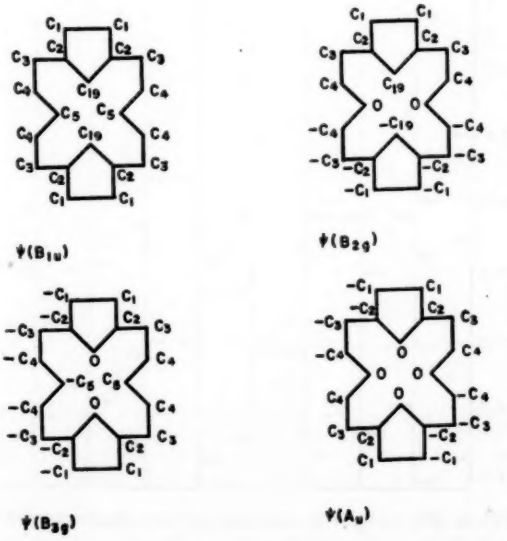

FIG. 2b. Molecular orbital species of tetrahydroporphine.

TABLE VII. B_{1u} orbitals in tetrahydroporphine.

x	2.28618	1.63047	0.68163	0.00000	−1.50203	−2.09625
c_1	0.23801	−0.17437	0.38333	0.00000	−0.08515	0.09356
c_2	0.30612	−0.10994	−0.12205	0.00000	0.21305	−0.28969
c_3	0.19404	0.12997	−0.10843	−0.35355	0.04883	0.23731
c_4	0.13748	0.32185	0.04814	0.00000	−0.28640	−0.20777
c_5	0.12027	0.39480	0.14124	0.35355	0.38134	0.19823
c_{19}	0.26780	−0.13485	−0.35809	0.35355	−0.28369	0.27639

TABLE VIII. B_{2g} orbitals in tetrahydroporphine.

x	2.24698	1.00000	0.55496	−0.80194	−2.00000
c_1	0.25838	−0.28868	0.28747	0.06668	−0.11323
c_2	0.32220	0.00000	−0.12794	−0.12015	0.33968
c_3	0.17881	0.28868	0.10259	−0.26998	−0.22646
c_4	0.07958	0.28868	0.18487	0.33665	0.11323
c_{19}	0.28678	0.00000	−0.46106	0.29965	−0.33968

atoms 19 and 20. They therefore satisfy the secular equations for a closed 18-membered ring, and the values of x and c_r are readily obtained. The solutions are given in Table IX.

ELECTRON DENSITIES AND BOND ORDERS IN TETRAHYDROPORPHINE

From the above values of the coefficients, we can calculate, as for porphine itself, the values that the electron densities and bond orders would have if the nitrogen and carbon atoms had equal Coulomb integrals.

There are 22 π-electrons, and so in the ground state the 10 *MO* of positive x will contain 2 electrons each, and there will also be two electrons in the *MO* for which $x=0$. Summation of $2c_r^2$ and $2c_rc_s$ over these *MO* leads to the following values for the electron densities and bond orders (see Table XI).

As in porphine itself, the calculated electron densities are highest on atoms 19 and 20, though no allowance has been made in the calculation for the fact that these are nitrogen and not carbon atoms. The bond orders show a trend similar to that in porphine, but here again the calculated difference in mobile order between the external bonds are probably too large.

MO ENERGIES IN PORPHINE AND TETRAHYDROPORPHINE

Up to this point, no account has been taken in the theory of the difference in the Coulomb integral of nitrogen and of carbon. We shall now examine how this difference affects the calculated *MO* energies.

Coulson and Longuet-Higgins[1] showed that if the Coulomb integral of atom r is altered by a small amount $\delta\alpha_r$, then the change in energy of any *MO* involving that atom is given by

$$\delta\epsilon=c_r^2\delta\alpha_r, \tag{9}$$

where c_r is the coefficient of ϕ_r in the *MO* under discussion. Now $\alpha_n-\alpha_c$ is of the order of β;[4] and although β

[4] H. C. Longuet-Higgins, J. Chem. Phys. **18**, 275 (1950).

TABLE IX. B_{3g} orbitals in tetrahydroporphine.

x	1.87939	1.00000	−0.34730	−1.53209	−2.00000
c_1	0.05788	−0.16667	0.25535	−0.31323	0.23570
c_2	0.16667	−0.33333	0.16667	0.16667	−0.23570
c_3	0.25535	−0.16667	−0.31323	0.05788	0.23570
c_4	0.31323	0.16667	−0.05788	−0.25535	−0.23570
c_5	0.33333	0.33333	0.33333	0.33333	0.23570

TABLE X. A_u orbitals in tetrahydroporphine.

x	1.53209	0.34730	−1.00000	−1.87939
c_1	0.11401	−0.21726	0.00000	−0.32827
c_2	0.28868	−0.28868	0.00000	0.28868
c_3	0.32827	0.11401	−0.35535	−0.21726
c_4	0.21726	0.32827	0.35355	0.11401

TABLE XI. Electron densities and bond orders caused by π-electrons in tetrahydroporphine.

$q_1=1.1135$	$p_{1,2}=0.5034$
$q_2=1.0928$	$p_{2,3}=0.5256$
$q_3=1.0617$	$p_{3,4}=0.6796$
$q_4=1.0564$	$p_{4,5}=0.6207$
$q_5=1.0750$	$p_{1,18}=0.7534$
$q_{19}=1.2759$	$p_{2,19}=0.5838$

is not small Eq. (9) will at least give a rough idea how the *MO* energies are modified by the nitrogen atoms. Denoting by x' the modified values of x, we have the following approximate relations:

(for porphyrin) $x'=x+c_{21}^2+c_{22}^2+c_{23}^2+c_{24}^2$,
(for tetrahydroporphyrin) $x'=x+c_{19}^2+c_{20}^2$.

The values of x, and the corresponding values of x', are listed in Table XII, and presented graphically in Fig. 3.

COMPARISON WITH OBSERVED SPECTRA: PORPHINE

In another paper[5] it is shown how fairly accurate spectroscopic predictions can be obtained from LCAO orbital energies for a whole series of molecules. We may apply this procedure to porphine and tetrahydroporphine. First, the orbital energies, x and x', are corrected for overlap, using $S=0.25$.[5,6] The corrected energies, y and y', in units of β are given in Table XIII and the highest filled and lowest unfilled levels are shown with corrected energies in Fig. 4. This figure also indicates the lowest allowed transitions in the two molecules, with their polarizations. Using $\beta=-23{,}000$ cm^{-1} these transition energies then should give the approximate location of the centers of gravity of singlet-triplet pairs in the spectrum.

The observed singlet energy states of the molecules[3] and the computed centers-of-gravity are compared in Table XIV and in Fig. 5. When we consider how accurate the number, sequence, and position of energy levels is predicted in other molecules by this method,[5] it becomes quite probable that the 6000A transition of porphine is doubly degenerate in the approximation used here, and that the 4000A transition or "Soret band" is also doubly degenerate. These general conclusions hold whether we adopt the set of levels y or y'. A choice between the two sets is not possible because each fits the data about as well as do other predictions made by this method. M. Kasha has independently arrived at the conclusion that the 6000A bands involve at least two electronic transitions,[7] from the variable appearance of their envelopes under different substitutions[3] in the porphyrines, which are porphine derivatives. This probably means that the degeneracy is removed and the two component transitions are separated different amounts by the different substitutions. Conceivably the degeneracy is removed even in porphine itself by the presence of the two central hydrogens, since they must slightly distort the D_{4h} symmetry of the conjugated system. These bands may also be in different positions, as Simpson supposes,[2] in the two tautomers in which these central hydrogens are located (a) on opposed, or (b) on adjacent nitrogens.

The 6000A bands of porphine are relatively weak, even though they represent a formally allowed transition in the simple LCAO scheme used here. This means that there must be configuration interaction between the upper state of these bands and the upper state of the Soret bands. Porphine is thus another typical in-

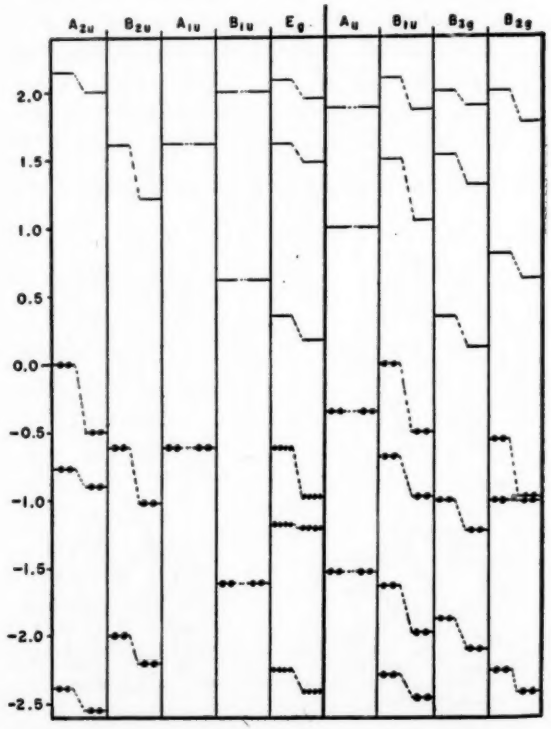

FIG. 3. *MO* energies in porphine and tetrahydroporphine.

[5] John R. Platt, J. Chem. Phys. **18**, 1168 (1950).
[6] G. W. Wheland, J. Am. Chem. Soc. **63**, 2025 (1941).
[7] M. Kasha, private communication.

stance of the "round-field" type of spectra[1] found in benzene, triphenylene, and coronene. The configuration interaction does not seem to alter the LCAO-predicted positions of bands as much as it alters their intensities.

This interpretation of the porphine bands is substantially equivalent to that given by Simpson.[2] However, he used an oversimplified model for the conjugated system, a closed 18-atom ring, neglecting two double bonds in the molecule and the effect of the two amino nitrogens. On considering electron interaction, he then obtained a weak doubly degenerate low transition and a strong higher one, just as here. But the oversimplification is dangerous, since it is hard to know in advance when it will be justified; and it is unnecessary, since the low frequency bands will be weak in any "round-field" molecule,[5] such as porphine or coronene, regardless of whether we can draw a closed ring through most of the conjugated atoms or not. Kuhn[8] has made a qualitative interpretation similar to Simpson's, but says he has a more accurate discussion in press. Neither author gives such detailed predictions of the different bands as are given by the present method.

COMPARISON WITH OSBSERVED SPECTRA: TETRAHYDROPORPHINE

In tetrahydroporphine, the situation is less clear than in porphine. If the nitrogen Coulomb integral is about equal to that of carbon (*MO* energies, y), a perpendicularly polarized transition is lowest in the LCAO scheme; otherwise (y'), a parallel transition. Furthermore, in either case, crossovers could occur, as they do in the polyacenes,[5,9] between the predicted center-of-gravity

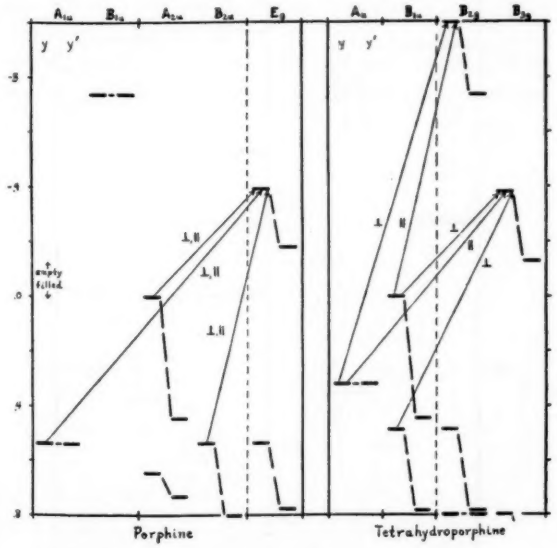

FIG. 4. Lowest allowed transitions in porphine and tetrahydroporphine. (The symbol $\perp$, $\parallel$ indicates double degeneracy. The symbols $\perp$ and $\parallel$ indicate polarization, with respect to the longest axis of the conjugated system in tetrahydroporphine.)

[8] H. Kuhn, Zeits. f. Elektrochimie **53**, 165 (1949); an English translation has appeared in J. Chem. Phys. **17**, 1198 (1949).
[9] John R. Platt, J. Chem. Phys. **17**, 484 (1949).

TABLE XII. *MO* energies in porphine and tetrahydroporphine, uncorrected (x) and corrected (x').

	Porphine			Tetrahydroporphine	
	x	x'		x	x'
A_{2u}	−2.16425	−2.01457	B_{1u}	−2.09625	−1.86508
	0.00000	0.50000		−1.50203	−1.05023
	0.77287	0.89651		0.00000	0.50000
	2.39138	2.54919		0.68163	0.97798
				1.63047	1.97857
B_{2u}	−1.61803	−1.21803		2.28618	2.45853
	0.61803	1.01803			
	2.00000	2.20000	B_{2g}	−2.00000	−1.76923
				−0.80194	−0.62236
A_{1u}	−1.61803	−1.61803		0.55496	0.98011
	0.61803	0.61803		1.00000	1.00000
				2.24698	2.41147
B_{1u}	−2.00000	−2.00000			
	−0.61803	−0.61803	B_{2g}	−2.00000	−1.88889
	1.61803	1.61803		−1.53209	−1.30987
				−0.34730	−0.12508
E_g	−2.08963	−1.95387		1.00000	1.22222
	−1.61803	−1.47952		1.87939	2.10161
	−0.35650	−0.17509			
	0.61803	0.97984	A_u	−1.87939	−1.87939
	1.18994	1.20020		−1.00000	−1.00000
	2.25619	2.41653		0.34730	0.34730
				1.53209	1.53209

sequence and the observed sequence of singlets, because of different singlet-triplet separations in the two low states.

In this situation, empirical analogies may help us to infer the probable polarization. Tetrahydroporphine is a C_{18} conjugated loop with two carbons replaced by aza-nitrogens and with two amine substituents. The spectrum of a simple C_{18} conjugated loop is not known. The closest known approximation may be the spectrum of the C_{18} ring system, tetracene, which has cross links.[9] The tetrahydroporphine spectrum may therefore be related to the tetracene spectrum somewhat as the amino and diamino-acridine spectra studied by Craig and Short[10] are related to the spectrum of their parent C_{14} hydrocarbon, anthracene (Fig. 6).

Aza substitution in ring systems slightly modifies the π-electron spectra in intensity and position, and no doubt adds weak bands of extinctions 1000 or less, though these seem to be hidden by the strong π-bands in acridine. But these changes are small compared with those introduced by amino substitution. This has the effect of mixing the π-electron intensities, producing strong red-shifts, and adding a strong new band to the spectrum as seen in Fig. 6. Probably a second band is added in the diamino case, but is blended with the first or with one of the other bands.

This is indeed also the general description of changes in going from the tetracene spectrum to that of tetrahydroporphine.

These changes with amino substitution seem to be less profound with increasing size of the substituted molecule and might be expected to become negligible for very large molecules. Consequently it is tempting to

[10] D. P. Craig and L. N. Short, J. Chem. Soc., 419 (1945).

TABLE XIII. *MO* energies from Table XII corrected for overlap ($S=0.25$).

	Porphine			Tetrahydroporphine	
	y	y'		y	y'
A_{1u}	−2.71714	−2.71714	A_u	−3.54501	−3.54501
	0.53531	0.53531		−1.33333	−1.33333
				0.31955	0.31955
B_{1u}	−4.00000	−4.00000		1.10778	1.10778
	−0.73097	−0.73097			
	1.15202	1.15202	B_{1u}	−4.40444	−3.49442
				−2.40521	−1.42415
A_{2u}	−4.71575	−4.05868		0.00000	0.44444
	0.00000	0.44444		0.58238	0.78584
	0.64771	0.73236		1.15831	1.32377
	1.49663	1.55694		1.45473	1.52265
B_{2u}	−2.71714	−1.75132	B_{2g}	−4.00000	−3.17242
	0.53531	0.81149		−1.00302	−0.73703
	1.33333	1.41935		0.48734	0.78721
				0.80000	0.80000
E_g	−4.37536	−3.81973		1.43876	1.50447
	−2.71714	−2.34803			
	−0.39137	−0.18310	B_{3g}	−4.00000	−3.57893
	0.53531	0.78704		−2.48321	−1.94767
	0.91711	0.92287		−0.38031	−0.12911
	1.44253	1.50644		0.80000	0.93617
				1.27862	1.37774

TABLE XIV. Comparison of calculated centers of gravity with observed singlets.

Molecule	Trans. type	Pol.	Calculated trans. energy[a] β	Calculated trans. energy[a] cm^{-1}	Observed singlets[b] cm^{-1}	Correction
Porphine	$A_{2u}-E_g$	⊥, ∥ doub. degen.	0.391 (0.627)	9000 (14,500)	16,000	+7000
	$A_{1u}-E_g$	⊥, ∥ doub. degen.	0.927 (0.718)	21,300 (16,500)	23,200	+2000
	$B_{2u}-E_g$	⊥, ∥ doub. degen.	0.927 (0.994)	21,300 (23,000)	?	?
Tetrahydroporphine	$B_{1u}-B_{3g}$	⊥	0.380 (0.573)	8700 (13,200)	13,000	+4000
	A_u-B_{3g}	∥	0.700 (0.449)	16,100 (10,300)	16,300	0
	$B_{1u}-B_{3g}$	⊥	0.963 (0.915)	22,200 (21,000)	19,000(?)	−3000
	$B_{1u}-B_{2g}$	∥	1.003 (1.181)	23,000 (27,200)	24,000	+1000
	A_u-B_{2g}	⊥	1.322 (1.056)	30,400 (24,300)	?	?

[a] Predicted energies in brackets are between orbitals y' of Table XIII and Fig. 4. The others are between orbitals y.
[b] See reference 3.

relate the 19,000 and 34,000 cm^{-1} bands of 2,6-diaminoacridine to the 26,000 and 39,000 cm^{-1} bands of anthracene respectively. It is even more tempting, because the symmetry is preserved, to relate the 12,000 and 24,000 cm^{-1} bands of tetrahydroporphine to the 21,000 and 36,000 cm^{-1} bands of tetracene, and to say that they are polarized ⊥ and ∥ to the longer axis of the system respectively, as the latter bands are believed to be.[9]

Some other arguments support this assignment. One is that the position of the Soret band (24,000 cm^{-1}) is but little changed in going from porphine to the dihydro compound (chlorins[3]) and then to the tetrahydro compound. This suggests the band is polarized ∥, along the unchanged, or long, axis of the latter system. If this is the case, it seems improbable that the 12,000 cm^{-1} band in the tetrahydro system would have so much intensity unless it had the opposite, or transverse (⊥), polarization.

Another argument is that the 12,000 cm^{-1} band may be related to the low bands in dihydroporphine (chlorins), which are stronger than in porphines and so are probably polarized in this same ⊥ direction (transverse to the long axis, or parallel to the C_{2v} axis in dihydroporphine); because a permanent dipole in this direction is created in going from porphine to the chlorins.

The two strong bands in tetrahydroporphine are therefore assigned as indicated in Fig. 5. The remaining bands are tentatively assigned to the nearest remaining predicted levels. Tetrahydroporphine appears to give a typical and even an extreme example of the "long-field" type of spectrum, in which the lowest transition is very strong.[5]

The dihydroporphine bands are intermediate in position and intensity between those in porphine and in the tetrahydro compound,[3] as seems reasonable. No doubt they have a sequence of assignments and polarizations similar to that in the latter compound, but simply

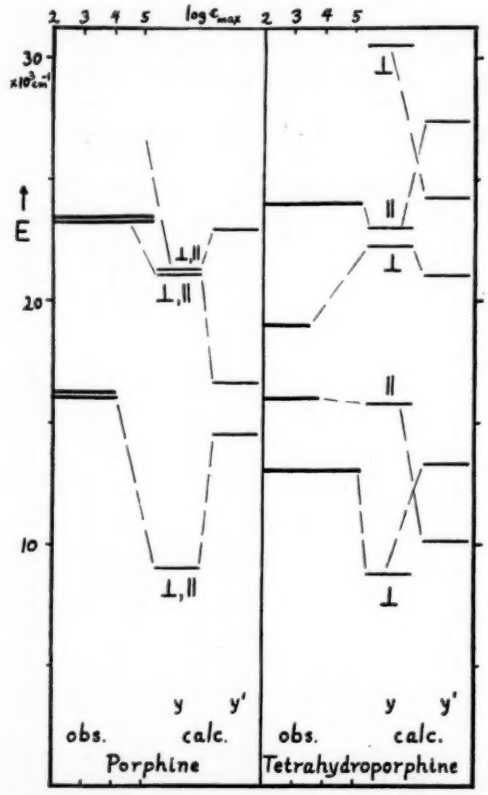

FIG. 5. Comparison of calculated with observed electronic energy states. (Vibrational structure omitted for simplicity. Length of the horizontal lines in the "observed" column indicates approximate intensity of transition from the ground state. Double lines indicate presumed double degeneracy.)

represent an intermediate type of field. This interpretation would relate the longest wave-length bands in the three compounds to each other, in contradiction to Rabinowitch's interpretation[3] which seeks to relate

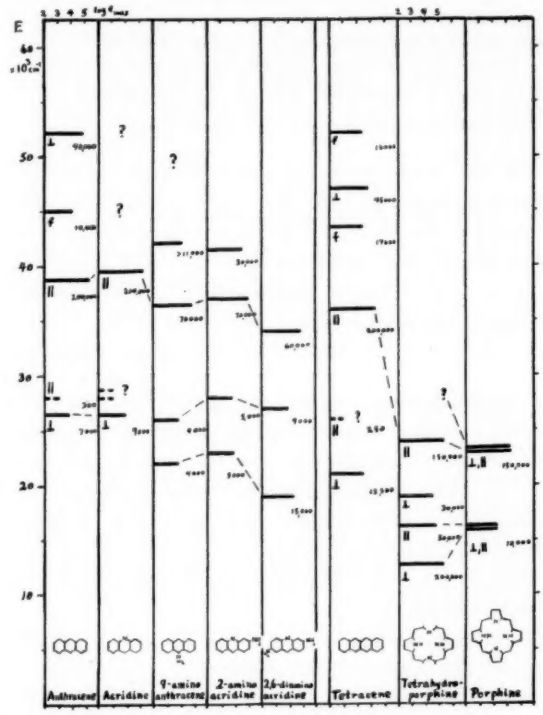

FIG. 6. Effect of aza and amino substitution on spectra of ring systems. (See note under Fig. 5. Numbers near horizontal lines indicate $\epsilon_{max.}$)

bands which have nearly the same position and intensity in the three compounds.

It has occasioned some surprise that there should be a *blue* shift of the long wave bands in adding conjugated

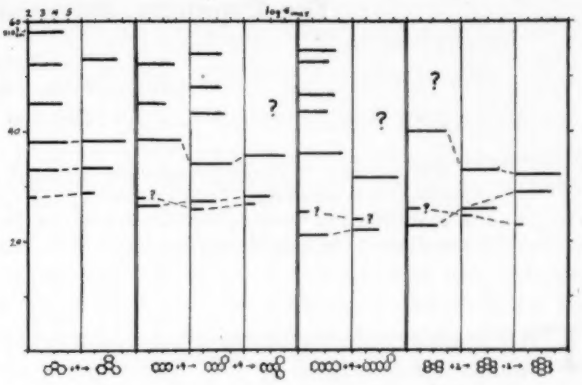

FIG. 7. Blue shifts produced by adding conjugated atoms to the sides of a long conjugated system.

atoms to a conjugated system, as in going from tetrahydroporphine to porphine itself.[3] However, such blue shifts are fairly common when the additional atoms are at the sides of an initially elongated system, as is shown by several examples in Fig. 7.[11] They seem to be associated, as here, with the change from a "long-field" to a "round-field" type of spectrum, and are more prominent in larger molecules where the normal red shift associated with the simple increase of molecular size from the additional atoms is not so important.

The qualitative parallel between the spectral changes in the porphine→dihydroporphine→tetrahydroporphine sequence and those in the coronene→dihydrocoronene→tetrahydrocoronene (perylene) sequence shown in Fig. 7 is especially remarkable.

[11] The data in Fig. 7 are principally from: E. Clar, *Aromatische Kohlenwasserstoffe* (Verlag. Julius Springer, Berlin, 1941), with some additional spectra from Fromberg, Thaler, and Wolf, Zeits. f. Elektrochemie **49**, 387 (1943), (coronene); H. B. Klevens and J. R. Platt, J. Chem. Phys. **17**, 470 (1949), (short wave-length cata-condensed spectra).

The Repulsive Potential of Normal Helium Atoms*

PHILIP ROSEN
Rensselaer Polytechnic Institute, Troy, New York
(Received April 26, 1950)

The repulsive potential between two normal helium atoms is calculated using the bond eigenfunction method. It is found that Slater's potential, $V(R)=770\exp(-2.43R/a_0)\times10^{-12}$ ergs, must be multiplied by a factor of 2.1 in the region of the minimum of the total potential. By extrapolating to $R=0$, the energy of beryllium in the ground state is found to be -29.4 Rhc units.

THE repulsive potential between two normal helium atoms was calculated by J. C. Slater[1] and it was found that $V(R)=770\exp(-2.43R/a_0)\times10^{-12}$ ergs is a good approximation for the potential as a function of the internuclear separation, R. N. Rosen[2] also computed this potential and obtained lower values than Slater. However, there is evidence that Slater's repulsive potential is too low.[3-5] Kistemaker and Keesom[5] state that the total potential A, of Buckingham, Hamilton and Massey which is:

$$(977\exp(-2.434R/a_0)-1.50/R^6-2.51/R^8)\times10^{-12}\text{ ergs}\quad(R\text{ in }A^0)\quad(1)$$

yields almost the correct behavior of the second virial coefficient at very low temperatures. This potential was fitted to the best data known at the time. Recently Schneider and Intema[6] have found that the total potential which yields the best fit for the experimental behavior of the second virial coefficient at high temperatures is:

$$(1200\exp(-2.496R/a_0)-1.24/R^6-1.89/R^8)\times10^{-12}\text{ ergs}\quad(R\text{ in }A^0).\quad(2)$$

One's interest is aroused in this problem because at present it is not possible to determine by comparing virial coefficient measurements with calculated values whether helium obeys Bose-Einstein or Fermi-Dirac statistics.[5] This is so because the total potential is not known with sufficient accuracy.

In Slater's calculation a very accurate atomic eigenfunction was used, but certain multiple exchange integrals were neglected, and several integrals were approximated. This invalidates the results because all exchange integrals are found to be important.[7] Therefore a simpler but less accurate eigenfunction was chosen for this work so that all integrals could be evaluated.

The unsymmetrized atomic functions,[8]

$$a(1)\cdot b(2)=(Z_1^3/\pi)^{\frac{1}{2}}\exp(-Z_1A_1)\cdot(Z_2^3/\pi)^{\frac{1}{2}}\exp(-Z_2A_2)$$
$$c(3)\cdot d(4)=(Z_1^3/\pi)^{\frac{1}{2}}\exp(-Z_1B_3)\cdot(Z_2^3/\pi)^{\frac{1}{2}}\exp(-Z_2B_4)\quad(3)$$

were chosen with $Z_1=2.15$ and $Z_2=1.19$. A_1 is the distance of electron 1 from nucleus A, B_3 is the distance of electron 3 from nucleus B, etc. The functions $a(1)$ and $b(2)$ are hydrogenic functions centered about nucleus A; the functions $c(3)$ and $d(4)$ belong to nucleus B. Function (3) yields a ground-state energy for helium of -5.7508 Rhc units (observed energy $=-5.80736$ Rhc).

The unsymmetrized function for the helium molecule with spin included will therefore be:

$$\varphi_1=a(1)\alpha(1)\cdot b(2)\beta(2)\cdot c(3)\alpha(3)\cdot d(4)\beta(4).\quad(4)$$

From (4) we can construct four Pauli determinants which are written in the form:

$$\psi_1=|a\alpha\ \ b\beta\ \ c\alpha\ \ d\beta|,\quad\psi_2=|a\alpha\ \ b\beta\ \ c\beta\ \ d\alpha|$$
$$\psi_3=|a\beta\ \ b\alpha\ \ c\alpha\ \ d\beta|,\quad\psi_4=|a\beta\ \ b\alpha\ \ c\beta\ \ d\alpha|.$$

The bond eigenfunction[9] for a "bond" between electrons 1 and 2 and between electrons 3 and 4 is:

$$\psi_A=\psi_1-\psi_2-\psi_3+\psi_4.$$

That is, we make the total eigenfunction antisymmetric upon the interchange of the spins of electrons 1 and 2 or electrons 3 and 4. The total energy, E, will then be:

$$E=\frac{H_{AA}}{\Delta_{AA}}=\frac{\int\psi_A^*H\psi_Ad\tau}{\int\psi_A^*\psi_Ad\tau}.$$

The matrix element H_{AA} becomes:

$$H_{AA}=H_{11}+H_{22}+H_{33}+H_{44}-2H_{12}-2H_{13}+2H_{14}+2H_{23}-2H_{24}-2H_{34},\quad(5)$$

* This research was supported by the Rensselaer Polytechnic Institute Research Fund.

[1] J. C. Slater, Phys. Rev. **32**, 349 (1928).
[2] N. Rosen, Phys. Rev. **38**, 255 (1931).
[3] H. S. W. Massey and R. A. Buckingham, Proc. Roy. Soc. **A169**, 205 (1938).
[4] Buckingham, Massey, Hamilton, Proc. Roy. Soc. **A179**, 103 (1941).
[5] J. Kistemaker and W. H. Keesom, Physica **12**, 227 (1946).
[6] National Research Council of Canada. Private communication from Professor H. Margenau, Yale University.
[7] H. Margenau, Phys. Rev. **63**, 131 (1943).
[8] L. Pauling and E. B. Wilson, *Introduction to Quantum Mechanics* (McGraw-Hill Book Company, Inc., New York, 1935).
[9] Eyring, Walter, and Kimball, *Quantum Chemistry* (John Wiley and Sons, Inc., New York, 1944).

where

$$H_{11}=\int \psi_1^* H \psi_1 d\tau$$

$$=\sum_\mu (-1)^{p\mu}\int a(1)\alpha(1)b(2)\beta(2)c(3)\alpha(3)d(4)\beta(4)$$

$$HP_\mu[a(1)\alpha(1)b(2)\beta(2)c(3)\alpha(3)d(4)\beta(4)]d\tau,$$

and the other matrix elements are obtained in a similar fashion. The permutation operator, P_μ, is any operator of the symmetric group of permutations on 4 particles: (1)(2)(3)(4); (12), (34), (13), (23), (14), (24); (123), (124), (134), (132), (234), (243), (143), (142); (12)(34), (13)(24), (14)(23); (1234), (1324), (1243), (1342), (1432), (1423); p_μ is 1 for odd permutations and 2 for even permutations.

If the Hamiltonian does not contain any spin orbit interaction, Eq. (5) becomes:

$$H_{AA}=4Q-2([13]+[14]+[23]+[24]-2[12]-2[34])-2([134]+[243]+[123]+[142]+[124]+[132]+[234]+[143])+4([(13)(24)]+[(14)(23)]+[(12)(34)])-2([1234]+[1432]+[1243]+[1342]-2[1423]-2[1324]),$$

where

$$Q=\int a(1)b(2)c(3)d(4)Ha(1)b(2)c(3)d(4)d\tau$$

$$[12]=\int a(1)b(2)c(3)d(4)Ha(2)b(1)c(3)d(4)d\tau,$$

and so forth. Δ_{AA} can be obtained by replacing H by unity. Thus our problem resolves itself to computing exchange integrals.

The Hamiltonian for the helium molecule in natural units (unit length $=a_0$, the radius of the hydrogen atom) is:

$$H=-\sum_i \nabla_i^2-4\left(\frac{1}{A_1}+\frac{1}{A_2}+\frac{1}{B_1}+\frac{1}{B_2}+\frac{1}{A_3}+\frac{1}{A_4}+\frac{1}{B_3}+\frac{1}{B_4}\right)+2\sum_{i\neq j}\frac{1}{r_{ij}}+\frac{8}{R},$$

where r_{ij} is the distance from the ith to the jth electron. We can put H into the form: $H=H_0+H_1$ where $H_1=-4(1/A_3+1/A_4+1/B_1+1/B_2)+2\sum_{i\neq j}1/r_{ij}+8/R$ and $H_0^1+H_0^2+H_0^3+H_0^4=H_0$; with $H_0=-\nabla_1^2-4/A_1$, $H_0^2=-\nabla_3^2-4/B_3$, etc. It is also convenient to put the H_0^{i}'s in the form

$$H_0^1=\bar{H}_0^1+\frac{2Z_1-4}{A_1} \qquad H_0^3=\bar{H}_0^3+\frac{2Z_1-4}{B_3}$$

$$H_0^2=\bar{H}_0^2+2Z_2-4/A_2 \qquad H_0^4=\bar{H}_0^4+2Z_2-4/B_4,$$

where

$$\bar{H}_0^1 a(1)=-Z_1^2 a(1) \quad \bar{H}_0^3 c(3)=-Z_1^2 c(3)$$
$$\bar{H}_0^2 b(2)=-Z_2^2 b(2) \quad \bar{H}_0^4 d(4)=-Z_2^2 d(4).$$

EVALUATION OF EXCHANGE INTEGRALS

Many of the integrals needed here are tabulated by S. Weinbaum;[10] to change to our notation we make the substitutions: $\psi\to a$, $\xi\to b$, $\varphi\to c$, $\eta\to d$, $Z\to Z_1$, $Z'\to Z_2$, $\epsilon=Z_2/Z_1$, and $\rho=Z_1R$. To save space we shall not repeat his table of integrals but we shall only tabulate integrals which are not given there. We shall use the symbols, s, t_0, t and the F's as Weinbaum uses them. The F's can be written as $F(\epsilon,\rho)$ or $F(\rho)$ as the case may be. The table of integrals is in the Appendix.

The results can be put in a simple form if we let:

$$\Sigma[ij]=[13]+[14]+[23]+[24]-2[12]-2[34]$$
$$\Sigma[ijk]=[134]+[243]+[123]+[142]+[124]+[132]+[234]+[143]$$
$$\Sigma[(ij)(kl)]=[(13)(24)]+[(14)(23)]+[(12)(34)]$$
$$\Sigma[ijkl]=[1234]+[1432]+[1243]+[1342]-2[1423]-2[1324].$$

We find:

$$Q=2(Z_1^2+Z_2^2-4Z_1-4Z_2)-8Z_1F_1-8Z_2F_1'+2(Z_1F_{11}+Z_2F_{11}')+2(K+K')+4Z_1u+8/R$$

$$\Sigma[ij]=2s^2(Z_2^2-4Z_2-Z_1^2)+2s_\epsilon^2(Z_1^2-4Z_1-Z_2^2)-8(Z_1+Z_2)t^2+16(Z_1+Z_2)t_0^2-8(t^2+s_\epsilon^2-2t_0^2)Z_1F_1-8(t^2+s^2-2t_0^2)Z_2F_1'+4(Z_1-4)sZ_1F_2+4(Z_2-4)s_\epsilon Z_2F_2'+2(Z_1F_6+Z_2F_6')-8(Z_1+Z_2-4)t_0Z_1F_7+32t_0Z_1F_8+(2Z_2-8)t[Z_1F_9+Z_2F_{10}']+(2Z_1-8)t[Z_1F_{10}+Z_2F_9']+2t^2[Z_1F_{11}+Z_2F_{11}']-\frac{32t_0\epsilon^{\frac{3}{2}}}{(1+\epsilon)^2}\left[Z_1F_{11}^{(2)}+Z_1F_{11}^{(3)}+\frac{2\epsilon}{1+\epsilon}Z_1F_{11}^{(4)}+\frac{2}{1+\epsilon}Z_1F_{11}^{(5)}\right]+\frac{8s_\epsilon^3}{(2\epsilon-1)^{\frac{1}{2}}}Z_1F_{15}^{(2)}+\frac{8s_\epsilon}{\epsilon^2\left(\frac{2}{\epsilon}-1\right)^{\frac{1}{2}}}Z_1F_{15}^{(3)}+8t(Z_1F_{17}+Z_2F_{17}')+2(s_\epsilon^2K+s^2K')-\frac{160Z_1\epsilon^5}{(1+\epsilon)^5}-8t_0^2Z_1u+4Z_1F_{13}+\frac{8}{R}(s^2+s_\epsilon^2+2t^2-4t_0^2),$$

$$\Sigma(ijk)=-8(Z_1^2+2Z_2)st_0t-8(Z_2^2+2Z_1)s_\epsilon t_0t-16s_\epsilon t_0tZ_1F_1-16st_0tZ_2F_1'+4(2Z_1-8)t_0tZ_1F_2+4(2Z_2-8)t_0tZ_2F_2'+4(Z_1+Z_2-4)(ts+ts_\epsilon)Z_1F_7-16(ts+ts_\epsilon)Z_1F_8+(2Z_2-8)(t_0s_\epsilon+t_0s)(Z_1F_9+Z_2F_{10}')+(2Z_1-8)(t_0s_\epsilon+t_0s)(Z_1F_{10}+Z_2F_9')+\frac{16\epsilon^{\frac{3}{2}}}{(1+\epsilon)^2}t\left(sZ_1F_{11}^{(2)}+s_\epsilon Z_1F_{11}^{(3)}+\frac{2\epsilon}{1+\epsilon}sZ_1F_{11}^{(4)}+\frac{2}{1+\epsilon}s_\epsilon Z_1F_{11}^{(5)}\right)+8t(Z_1F_{15}+Z_2F_{15}')+\frac{8tt_0\epsilon^3}{(2\epsilon-1)^{\frac{1}{2}}}Z_1F_{15}^{(2)}+\frac{8tt_0}{\epsilon^2\left(\frac{2}{\epsilon}-1\right)^{\frac{1}{2}}}Z_1F_{15}^{(3)}+8t_0(sZ_1F_{17}+s_\epsilon Z_2F_{17}')+8(sZ_1F_{18}+s_\epsilon Z_2F_{18}')+8t_0(Z_1F_{19}+Z_2F_{19}')+\frac{8}{R}[4t_0t(s+s_\epsilon)],$$

$$\Sigma[(ij)(kl)]=-2(Z_1^2+Z_2^2)[t_0^4+t^4+s^2s_\epsilon^2]+4(Z_1-4)s_\epsilon^2sZ_1F_2+4(Z_2-4)s^2s_\epsilon Z_2F_2'+2(s_\epsilon^2Z_1F_6+s^2Z_2F_6')+4(Z_1+Z_2-4)t_0^2Z_1F_7-16t_0^2Z_1F_8+(2Z_2-8)t^2[Z_1F_9+Z_2F_{10}']+(2Z_1-8)t^2[Z_1F_{10}+Z_2F_9']+8ss_\epsilon Z_1F_{14}+8t_0^2Z_1F_{16}+\frac{80Z_1\epsilon^5}{(1+\epsilon)^5}t_0^2+12t^2Z_1F_{13}+\frac{8}{R}(s^2s_\epsilon^2+t^4+t_0^4),$$

[10] S. Weinbaum, J. Chem. Phys. **3**, 547 (1935).

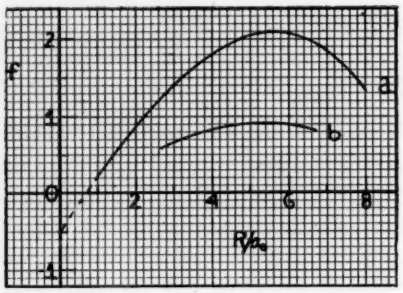

FIG. 1(a). The ratio, $E'/770\exp(-2.43(R/a_0))\times 10^{-12}$, the factor f, is plotted as a function of R/a_0; (b) the ratio of the results of N. Rosen to Slater's results is plotted as a function of R/a_0.

$$\Sigma[ijkl]=-4(Z_1^2+Z_2^2)[t_0^2f^2+t_0^2ss_\epsilon-2f^2ss_\epsilon]$$
$$+4(Z_1-4)(t_0^2s_\epsilon-2f^2s_\epsilon)Z_1F_2+4(Z_2-4)(t_0^2s-2f^2s)Z_2F_2'$$
$$+4(Z_1+Z_2-4)(f^2t_0+t_0ss_\epsilon)Z_1F_7-16(f^2t_0+ss_\epsilon t_0)Z_1F_8$$
$$+2(Z_2-4)(t_0^2t-2tss_\epsilon)[Z_1F_9+Z_2F_{10}']$$
$$+2(Z_1-4)(t_0^2t-2tss_\epsilon)[Z_1F_{10}+Z_2F_9']+4(t_0^2-2f^2)Z_1F_{14}$$
$$+8t_0(s_\epsilon Z_1F_{15}+sZ_2F_{15}')+4(f^2+ss_\epsilon)Z_1F_{16}+8t_0t(Z_1F_{18}+Z_2F_{18}')$$
$$+(4t_0^2-8ss_\epsilon)Z_1F_{13}-16ts_\epsilon Z_1F_{19}-16tsZ_2F_{19}'$$
$$+\frac{16}{R}(t_0^2f^2+t_0^2ss_\epsilon-2f^2ss_\epsilon).$$

Furthermore:

$$\Delta_{AA}=4-2(s^2+s_\epsilon^2+2f^2-4t_0^2)-8(tt_0s+tt_0s_\epsilon)$$
$$+4(s^2s_\epsilon^2+t^4+t_0^4)-4(t_0^2f^2+t_0^2ss_\epsilon-2f^2ss_\epsilon).$$

If R becomes infinite the expression for H_{AA} is:

$$H_{AA\infty}=8(Z_1^2+Z_2^2-4Z_1-4Z_2)$$
$$+16(Z_1+Z_2-4)(t_0^3+t_0)Z_1F_7$$
$$+16(Z_1u+20Z_1\epsilon^3/(1+\epsilon)^5)(t_0^2+1)$$
$$-8[4(Z_1+Z_2)t_0^2+(Z_1^2+Z_2^2)t_0^4]$$

with

$$\Delta_{AA\infty}=4+8t_0^2+4t_0^4.$$

Then the energy of two helium atoms, E is:

$$E_\infty=\frac{H_{AA\infty}}{\Delta_{AA\infty}}=-5.7508\ \text{Rhc}.$$

Thus the interaction energy, E', becomes:

$$E'=H_{AA}/\Delta_{AA}-H_{AA\infty}/\Delta_{AA\infty}$$
$$=[\Delta_{AA\infty}H_{AA}-H_{AA\infty}\Delta_{AA}]/\Delta_{AA}\Delta_{AA\infty}$$

Now $H_{AA}=H_{AA}'+H_{AA\infty}$. That is H_{AA}' contains the terms which vanish at $R=\infty$. We can then put E' into the form:

$$E'=[\Delta_{AA\infty}H_{AA}'+H_{AA\infty}(\Delta_{AA\infty}-\Delta_{AA})]/\Delta_{AA}\Delta_{AA\infty}$$

with

$$\Delta_{AA\infty}-\Delta_{AA}=2(s^2+s_\epsilon^2+2f^2)+8tt_0(s+s_\epsilon)$$
$$-4(s^2s_\epsilon^2+t^4)+4(t_0^2f^2+t_0^2ss_\epsilon-2f^2ss_\epsilon).$$

For good numerical accuracy it is necessary to avoid the subtraction of two large terms. The large terms are the ones which contain no exponentials and we find that these cancel each other. Finally, after eliminating these terms, we find:

$$H_{AA}'=4Q'-2\Sigma'[ij]-2\Sigma'[ijk]$$
$$+4\Sigma'[(ij)(kl)]-2\Sigma'[ijkl]$$

where

$$Q'=-8Z_1f_1-8Z_2f_1'+2Z_1f_{11}+2Z_2f_{11}'+2(k+k'),$$
$$\Sigma'[ij]=2s^2(Z_2^2-4Z_2-Z_1^2)+2s_\epsilon^2(Z_1^2-4Z_1-Z_2^2)$$
$$-8f^2(Z_1+Z_2)-8(f^2+s_\epsilon^2-2t_0^2)Z_1f_1-8(f^2+s^2-2t_0^2)Z_2f_1'$$
$$+4(Z_1-4)sZ_1F_2+4(Z_2-4)s_\epsilon Z_2F_2'+2(Z_1F_6+Z_2F_6')$$
$$+32t_0Z_1f_8+2(Z_2-4)t[Z_1F_9+Z_2F_{10}']+2(Z_1-4)t[Z_1F_{10}+Z_2F_9']$$
$$+2f^2(Z_1F_{11}+Z_2F_{11}')-\frac{32t_0\epsilon^{\frac{1}{2}}}{(1+\epsilon)^2}\Big[Z_1f_{11}^{(2)}+Z_1f_{11}^{(3)}$$
$$+\frac{2\epsilon}{1+\epsilon}Z_1f_{11}^{(4)}+\frac{2}{1+\epsilon}Z_1f_{11}^{(5)}\Big]+\frac{8s\epsilon^3}{(2\epsilon-1)^{\frac{1}{2}}}Z_1F_{15}^{(2)}+\frac{8s_\epsilon Z_1F_{15}^{(3)}}{\epsilon^2\left(\frac{2}{\epsilon}-1\right)^{\frac{1}{2}}}$$
$$+8t(Z_1F_{17}+Z_2F_{17}')+2(s_\epsilon^2K+s^2K')+4Z_1F_{13},$$
$$\Sigma'[ijk]=-8(Z_1^2+2Z_2)st_0t-8(Z_2^2+2Z_1)s_\epsilon t_0t-16s_\epsilon t_0tZ_1f_1$$
$$-16st_0tZ_2f_1'+2(4Z_1-16)t_0tZ_1F_2+2(4Z_2-16)t_0tZ_2F_2'$$
$$+4(Z_1+Z_2-4)(ts+ts_\epsilon)Z_1F_7-16(ts+ts_\epsilon)Z_1f_8$$
$$+(2Z_2-8)(t_0s_\epsilon+t_0s)[Z_1F_9+Z_2F_{10}']$$
$$+(2Z_1-8)(t_0s_\epsilon+t_0s)[Z_1F_{10}+Z_2F_9']$$
$$+\frac{16\epsilon^{\frac{1}{2}}}{(1+\epsilon)^2}t\Big[sZ_1F_{11}^{(2)}+s_\epsilon Z_1F_{11}^{(3)}+\frac{2\epsilon}{1+\epsilon}sZ_1F_{11}^{(4)}+\frac{2}{1+\epsilon}s_\epsilon Z_1F_{11}^{(5)}\Big]$$
$$+8t[Z_1F_{15}+Z_2F_{15}']+\frac{8t_0\epsilon^3}{(2\epsilon-1)^{\frac{1}{2}}}Z_1F_{15}^{(2)}+\frac{8t_0}{\epsilon^2\left(\frac{2}{\epsilon}-1\right)^{\frac{1}{2}}}Z_1F_{15}^{(3)}$$
$$+8t_0(sZ_1F_{17}+s_\epsilon Z_2F_{17}')+8(sZ_1F_{18}+s_\epsilon Z_2F_{18}')$$
$$+8t_0[Z_1F_{19}+Z_2F_{19}'],$$
$$\Sigma'[(ij)(kl)]=-2(Z_1^2+Z_2^2)(t^4+s^2s_\epsilon^2)+(4Z_1-16)s_\epsilon^2sZ_1F_2$$
$$+(4Z_2-16)s^2s_\epsilon Z_2F_2'+2s_\epsilon^2Z_1F_6+2s^2Z_2F_6'-16t_0^3Z_1f_8$$
$$+(2Z_2-8)t^2[Z_1F_9+Z_2F_{10}']+(2Z_1-8)t^2[Z_1F_{10}+Z_2F_9']$$
$$+8ss_\epsilon Z_1F_{14}+8t_0^2Z_1f_{16}+12f^2Z_1F_{13}+\frac{8}{R}(s^2s_\epsilon^2+t^4),$$
$$\Sigma'[ijkl]=-4(Z_1^2+Z_2^2)(t_0^2f^2+t_0^2ss_\epsilon-2f^2ss_\epsilon)$$
$$+4(Z_1-4)(t_0^2s_\epsilon-2f^2s_\epsilon)Z_1F_2+4(Z_2-4)(t_0^2s-2f^2s)Z_2F_2'$$
$$+4(Z_1+Z_2-4)(f^2t_0+t_0ss_\epsilon)Z_1F_7-16(f^2t_0+t_0ss_\epsilon)Z_1f_8$$
$$+(2Z_2-8)(t_0^2t-2tss_\epsilon)[Z_1F_9+Z_2F_{10}']$$
$$+(2Z_1-8)(t_0^2t-2tss_\epsilon)[Z_1F_{10}+Z_2F_9']$$
$$+4(t_0^2-2f^2)Z_1F_{14}+8t_0(s_\epsilon Z_1F_{15}+sZ_2F_{15}')+4(f^2+ss_\epsilon)Z_1F_{16}$$
$$+8t_0t(Z_1F_{18}+Z_2F_{18}')+(4t_0^2-8ss_\epsilon)Z_1F_{13}-16ts_\epsilon Z_1F_{19}$$
$$-16tsZ_2F_{19}'-(32/R)f^2ss_\epsilon.$$

The small letters f_1, f_1', f_8, f_{11}, f_{11}', $f_{11}^{(2)}$, $f_{11}^{(3)}$, $f_{11}^{(4)}$, $f_{11}^{(5)}$, f_{16}, k, and k' mean that the $1/\rho$ term has been removed from the corresponding functions F_1, F_1' etc.

NUMERICAL RESULTS

The final results are shown in Fig. 1a, where the interaction energy divided by Slater's interaction energy is plotted against R/a_0. At $R=0$, the value of the energy is found by extrapolation to be about $-0.5\times770\times10^{-12}$ erg or -17.9 Rhc units. If one then adds this to the ground state energy of two helium atoms (-11.5 Rhc), we obtain -29.4 Rhc units, which is in excellent agreement with the ground state energy of beryllium.[11] Since

[11] F. Seitz, *Modern Theory of Solids* (McGraw-Hill Book Company, Inc., New York, 1940).

this is an extrapolation, we do not expect this to be accurate but it is significant as a check on our work.

In the region $5 \leqslant R/a_0 \leqslant 7$, where the minimum of the total potential falls we see that the ratio of E' to Slater's value is fairly constant and equal to about 2. This is another check because as was shown by Born and Mayer[12] and by Buckingham[13] an exchange potential can be approximated over a limited range of R by $V=C_1\exp(-C_2R)$, where C_1 and C_2 are constants. Margenau[7] also found that such a potential is valid for the problem of two hydrogen molecules, in the important regions of interaction.

To determine the effect of neglecting higher order exchange integrals, the contribution due to the permutations $(ij)(kl)$ and $(ijkl)$ were neglected for $R/a_0=6$ and it was found that E' was reduced from 2.1 to 1.3 times Slater's value.

Also shown in Fig. 1 are the results of N. Rosen plotted as a ratio to Slater's values. In his calculation, N. Rosen used an atomic wave function of the form $c_1\exp(-c_2r)$ for both electrons. This function was calculated from a Hartree charge distribution and it turned out to be too low in the inner part of the atom. This was compensated by imagining additional electronic charge concentrated at the center of the atom. This introduces an additional approximation the effect of which is difficult to estimate.

G. Gentile[14] in his calculation of the repulsive force used a one parameter atomic function of the form $\psi\sim\exp(-Zr)$. This is the simplest function one can use but it is not very accurate. The graphs in his paper are disfigured but he states that he agrees with Slater for R greater than $1A^0$.

The author in concluding wishes to express his appreciation to Professor Henry Margenau of Yale University for suggesting this problem and for the generous advice and encouragement he has given him.

APPENDIX

Most of the integrals are evaluated without much difficulty except for Z_2F_{19}' which was evaluated by Sugiura's method.

$$\int\frac{a^2(1)b^2(2)d\tau}{r_{12}}=Z_1\left(1-\frac{1}{(1+\epsilon)^2}-\frac{\epsilon}{(1+\epsilon)^3}\right)=Z_1u$$

$$\int\frac{a^2(1)c^2(2)d\tau}{r_{12}}=\frac{1}{R}\left[1-\exp(-2\rho)\left(1+\frac{11}{8}\rho+\frac{3}{4}\rho^2+\frac{\rho^3}{6}\right)\right]=K(\rho)$$

$$\int\frac{b^2(1)d^2(2)d\tau}{r_{12}}=K(\epsilon\rho)=K';\quad F_1(\epsilon\rho)=F_1';\quad F_2(\epsilon\rho)=F_2';$$

$$F_0\left(\frac{1}{\epsilon},\epsilon\rho\right)=F_0';\qquad F_9\left(\frac{1}{\epsilon},\epsilon\rho\right)=F_9';\qquad F_{10}\left(\frac{1}{\epsilon},\epsilon\rho\right)=F_{10}';$$

$$F_{11}\left(\frac{1}{\epsilon},\epsilon\rho\right)=F_{11}';\quad F_{15}\left(\frac{1}{\epsilon},\epsilon\rho\right)=F_{15}';\quad F_{13}\left(\frac{1}{\epsilon},\epsilon\rho\right)=F_{13}'=\frac{Z_1}{Z_2}F_{13}.$$

$$\int\frac{a(1)b(1)a(2)b(2)d\tau}{r_{12}}=20Z_1\epsilon^5/(1+\epsilon)^5$$

$$\int\frac{a(1)b(1)d^2(2)d\tau}{r_{12}}=\frac{4\epsilon^5}{(1+\epsilon)^2}Z_1F_{11}\left(\frac{2\epsilon}{1+\epsilon},\frac{1+\epsilon}{2}\rho\right)=\frac{4\epsilon^5}{(1+\epsilon)^2}Z_1F_{11}^{(2)}$$

$$\int\frac{a(1)b(1)c^2(2)d\tau}{r_{12}}=\frac{4\epsilon^5}{(1+\epsilon)^2}Z_1F_{11}\left(\frac{2}{1+\epsilon},\frac{1+\epsilon}{2}\rho\right)=\frac{4\epsilon^5}{(1+\epsilon)^2}Z_1F_{11}^{(3)}$$

$$\int\frac{b^2(1)c(2)d(2)d\tau}{r_{12}}=\frac{8\epsilon^{5/2}}{(1+\epsilon)^3}Z_1F_{11}\left(\frac{1+\epsilon}{2\epsilon},\epsilon\rho\right)=\frac{8\epsilon^{5/2}}{(1+\epsilon)^3}Z_1F_{11}^{(4)}$$

$$\int\frac{a^2(1)c(2)d(2)d\tau}{r_{12}}=\frac{8\epsilon^5}{(1+\epsilon)^3}Z_1F_{11}\left(\frac{1+\epsilon}{2},\rho\right)=\frac{8\epsilon^5}{(1+\epsilon)^3}Z_1F_{11}^{(5)}$$

$$\int\frac{a(1)d(1)b(2)c(2)d\tau}{r_{12}}=Z_1F_{13}.$$

$$\int\frac{a(1)c(1)b^2(2)d\tau}{r_{12}}=\int\frac{a(1)c(1)d^2(2)d\tau}{r_{12}}=\frac{\epsilon^3}{(2\epsilon-1)^{\frac{1}{2}}}Z_1F_{15}(2\epsilon-1,\rho)$$

$$=\frac{\epsilon^3}{(2\epsilon-1)^{\frac{1}{2}}}Z_1F_{15}^{(2)}$$

$$\int\frac{a^2(1)b(2)d(2)d\tau}{r_{12}}=\int\frac{c^2(1)b(2)d(2)d\tau}{r_{12}}$$

$$=\frac{1}{\epsilon^2[(2/\epsilon)-1]^{\frac{1}{2}}}Z_1F_{15}\left(\frac{2}{\epsilon}-1,\epsilon\rho\right)=\frac{1}{\epsilon^2[(2/\epsilon)-1]^{\frac{1}{2}}}Z_1F_{15}^{(3)}$$

$$\int\frac{a(1)d(1)b^2(2)d\tau}{r_{12}}=\int\frac{b(1)c(1)d^2(2)d\tau}{r_{12}}=Z_1F_{17}=\frac{8Z_1\epsilon^{5/2}}{(1-\epsilon^2)^2\rho}\exp(-\rho)$$

$$+2Z_1\exp(-\epsilon\rho)\left[\frac{\epsilon^{5/2}(4+28\epsilon+32\epsilon^2)}{(1+\epsilon)^2(1-\epsilon)(1+3\epsilon)^2}+\frac{1}{\epsilon^{\frac{1}{2}}\rho}\right.$$

$$\left.\times\left(\frac{1+8\epsilon+17\epsilon^2}{(1+3\epsilon)^3}+\frac{1-2\epsilon}{(1-\epsilon)^2}-\frac{2+5\epsilon+\epsilon^2}{(1+\epsilon)^3}\right)\right]-2Z_1\exp[-(1+2\epsilon)\rho]$$

$$\times\left\{\frac{4\epsilon^{7/2}}{(1+\epsilon)^2(1+3\epsilon)^2}-\frac{1}{\epsilon^{\frac{1}{2}}(1+\epsilon)^3(1+3\epsilon)^3\rho}\right.$$

$$\left.\times[(1+3\epsilon)^3(1+2\epsilon-\epsilon^2)-(1+\epsilon)^3(1+8\epsilon+17\epsilon^2]\right\}$$

$$\int\frac{c^2(1)a(2)d(2)d\tau}{r_{12}}=\int\frac{a^2(1)b(2)c(2)d\tau}{r_{12}}=Z_2F_{17}\left(\frac{1}{\epsilon},\epsilon\rho\right)=Z_2F_{17}'$$

$$\int\frac{a(1)b(1)b(2)c(2)d\tau}{r_{12}}=\int\frac{a(1)d(1)c(2)d(2)d\tau}{r_{12}}=Z_1F_{19}=16Z_1\epsilon^5$$

$$\times\left\{\frac{\exp(-\epsilon\rho)}{\rho}\left[\frac{1}{(1+\epsilon)^5}+\frac{1}{(1+\epsilon)^4}+\frac{1}{(1+\epsilon)^3(1-\epsilon)}+\frac{1}{(1+\epsilon)^3(1-\epsilon)^2}\right]\right.$$

$$-\exp(-\rho)\left[\left(\frac{3}{8(1+\epsilon)^4}+\frac{1}{(1+\epsilon)^3(1-\epsilon)}+\frac{1}{8\epsilon^2(1+\epsilon)^2}+\frac{1}{2\epsilon(1+\epsilon)^3}\right)\right.$$

$$-\frac{1}{\rho}\left(\frac{1}{8\epsilon^3(1+\epsilon)^2}+\frac{1}{4\epsilon^2(1+\epsilon)^3}-\frac{1}{2\epsilon(1+\epsilon)^3}-\frac{1}{8\epsilon^3(1+\epsilon)^2}-\frac{5}{8(1+\epsilon)^5}\right.$$

$$\left.\left.-\frac{1}{(1+\epsilon)^3(1-\epsilon)^2}-\frac{3}{8(1+\epsilon)^4}-\frac{1}{(1+\epsilon)^3(1-\epsilon)}\right)\right]$$

$$+\exp[-(2\epsilon-1)\rho]\left[\left(\frac{1}{4\epsilon(1+\epsilon)^2}-\frac{1}{8\epsilon^2(1+\epsilon)^2}-\frac{1}{4(1+\epsilon)^3}-\frac{1}{8(1+\epsilon)^4}\right)\right.$$

$$\left.\left.+\frac{1}{\rho}\left(\frac{1}{8\epsilon^2(1+\epsilon)^2}+\frac{1}{2\epsilon(1+\epsilon)^3}-\frac{1}{8\epsilon^3(1+\epsilon)^2}-\frac{1}{4\epsilon^2(1+\epsilon)^3}\right.\right.\right.$$

$$\left.\left.\left.-\frac{5}{8(1+\epsilon)^4}-\frac{3}{8(1+\epsilon)^5}\right)\right]\right\}.$$

$$\int\frac{a(1)d(1)a(2)b(2)d\tau}{r_{12}}=Z_2F_{19}\left(\frac{1}{\epsilon},\epsilon\rho\right)=Z_2F_{19}'$$

$$=\int\frac{b(1)c(1)c(2)d(2)d\tau}{r_{12}}$$

[12] Born and Mayer, Zeits. f. Physik **75**, 1 (1932).
[13] R. A. Buckingham, Proc. Roy. Soc. **A168**, 264 (1938).
[14] G. Gentile, Zeits. f. Physik **63**, 795 (1930).

$$\int \frac{a(1)d(1)b(2)d(2)d\tau}{r_{12}} = \int \frac{b(1)d(1)b(2)c(2)d\tau}{r_{12}} = Z_2F_{19}'$$

$$= \frac{Z_2(\epsilon\rho)^2}{8\epsilon^3}\Big\{[s_\epsilon E_i(-2\epsilon\rho\alpha) - s_\epsilon' E_i(-2\epsilon\rho\gamma)]\exp(\epsilon\rho\alpha)$$

$$\times\left[\frac{72c}{(\epsilon\rho\alpha)^5} - \frac{72c}{(\epsilon\rho\alpha)^4} + \frac{(34c-6d-4a)}{(\epsilon\rho\alpha)^3} - \frac{(10c-6d-4a)}{(\epsilon\rho\alpha)^2} + \frac{(2c-2d-2a+2b)}{\epsilon\rho\alpha}\right] + \left[s_\epsilon' E_i(-2\epsilon\rho) - s_\epsilon\left(\ln\frac{2\epsilon\rho\alpha}{\gamma} + C\right)\right]$$

$$\times\exp(-\epsilon\rho\alpha)\left[\frac{72c}{(\epsilon\rho\alpha)^5} + \frac{72c}{(\epsilon\rho\alpha)^4} + \frac{(34c-6d-4a)}{(\epsilon\rho\alpha)^3} + \frac{(10c-6d-4a)}{(\epsilon\rho\alpha)^2} + \frac{(2c-2d-2a+2b)}{\epsilon\rho\alpha}\right] + \exp(-\epsilon\rho\gamma)\left[\frac{6d-6c}{\epsilon\rho\gamma} + \frac{6d-18c}{(\epsilon\rho\gamma)^2} - \frac{(\epsilon\rho\gamma)^3}{36c} - \frac{36c}{(\epsilon\rho\gamma)^4} + \frac{(2b+2d-2a-2c)}{\gamma} - \frac{4a+4c}{\epsilon\rho\gamma^2} - \frac{4a+4c}{(\epsilon\rho)^2\gamma^3}\right]$$

$$+ s_\epsilon'\exp(-\epsilon\rho\delta)\left[\frac{72c}{(\epsilon\rho)^5\alpha^4\gamma} + \frac{36c}{(\epsilon\rho)^5\alpha^3\gamma^2} + \frac{24c}{(\epsilon\rho)^5\alpha^2\gamma^3} + \frac{18c}{(\epsilon\rho)^5\alpha\gamma^4} + \frac{12c}{(\epsilon\rho)^4\alpha^2\gamma^2} + \frac{12c}{(\epsilon\rho)^4\alpha\gamma^3} + \frac{(10c-6d-4a)}{(\epsilon\rho)^3\alpha^2\gamma} + \frac{(5c-3d-2a)}{(\epsilon\rho)^3\alpha\gamma^2}\right]$$

$$- s_\epsilon\exp(-\epsilon\rho\alpha)\left[\frac{18c}{(\epsilon\rho)^5\alpha\gamma^4} + \frac{24c}{(\epsilon\rho)^5\alpha^2\gamma^3} + \frac{36c}{(\epsilon\rho)^5\alpha^3\gamma^2} + \frac{72c}{(\epsilon\rho)^5\alpha^4\gamma} + \frac{24c}{(\epsilon\rho)^4\alpha\gamma^3} + \frac{36c}{(\epsilon\rho)^4\alpha^2\gamma^2} + \frac{72c}{(\epsilon\rho)^4\alpha^3\gamma} + \frac{(16c-3d-2a)}{(\epsilon\rho)^3\alpha\gamma^2} + \frac{(34c-6d-4a)}{(\epsilon\rho)^3\alpha^2\gamma} + \frac{(10c-6d-4a)}{(\epsilon\rho)^2\alpha\gamma} - \frac{144c}{(\epsilon\rho)^4\alpha^4} - \frac{72c}{(\epsilon\rho)^3\alpha^3} - \frac{(28c-12d-4a)}{(\epsilon\rho)^2\alpha^2} - \frac{6c-6d}{\epsilon\rho\alpha}\right]\Big\},$$

where

$$a = \frac{\exp(\epsilon\rho\beta)-\exp(-\epsilon\rho\beta)}{\epsilon\rho\beta}, \quad a' = \frac{\exp(\epsilon\rho\beta)+\exp(-\epsilon\rho\beta)}{\epsilon\rho\beta}$$

$$b = \left[1+\frac{2}{(\epsilon\rho\beta)^2}\right]a - \frac{2a'}{\epsilon\rho\beta}, \quad c = \left[1+\frac{3}{(\epsilon\rho\beta)^2}\right]a - \frac{3}{\epsilon\rho\beta}a'$$

$$d = \left[1+\frac{17}{(\epsilon\rho\beta)^2}+\frac{36}{(\epsilon\rho\beta)^4}\right]a - \left[\frac{5}{\epsilon\rho\beta}+\frac{36}{(\epsilon\rho\beta)^3}\right]a'$$

$$\alpha = \tfrac{1}{2}\left(\frac{Z_1}{Z_2}+1\right), \quad \beta = \tfrac{1}{2}\left(\frac{Z_1}{Z_2}-1\right), \quad \gamma = \alpha+1, \quad \delta = \alpha+2$$

C = Euler's Constant, $s' = \exp(\rho)(1-\rho+\frac{1}{3}\rho^2)$, $s_\epsilon' = \exp(\epsilon\rho)[1-\epsilon\rho+\frac{1}{3}(\epsilon\rho)^2]$.

$$\int \frac{a(1)c(1)b(2)c(2)d\tau}{r_{12}} = \int \frac{a(1)d(1)a(2)c(2)}{r_{12}} = Z_1F_{19}.$$

For Z_1F_{19} replace Z_2 by Z_1 and Z_1 by Z_2 and $\epsilon\rho$ by ρ in the formula for Z_2F_{19}'.

THE JOURNAL OF CHEMICAL PHYSICS VOLUME 18, NUMBER 9 SEPTEMBER, 1950

Optical Rotatory Power of Benzoin

TING-CHANG KWOH AND HENRY EYRING
University of Utah, Salt Lake City, Utah

(Received April 21, 1950)

The procedure for calculating the optical rotatory power due to one electron transitions in an asymmetric field is simplified and systematized. The necessary transformations of functions to elliptic coordinates is carried through explicitly and the method of calculation is outlined. Extensive tables and graphs were prepared which greatly simplify the calculations. The method is applied to benzoin and the results are compared with the published experimental results which vary characteristically with the solvent. Representing transitions by eigenfunctions involving changes in more than one electron is the next natural but difficult improvement in this type of treatment.

ONE hundred and thirty-six years ago, Jean Baptiste Biot discovered the optical rotation of quartz. In 1860 Louis Pasteur had already reached the conclusion that "dissymmetry" is necessary for molecular rotation. However, with a hundred years of verification, there are still theoretical problems remaining.

Many classical mechanical theories have been suggested.[1] Notable among these are the coupled oscillator theories of Born, Oseen, and Kuhn.[2] Quantum-mechanical investigations reveal the presence of optical rotation associated with one-electron transitions—a non-existent effect in classical theory. Optical rotation is the algebraic sum of the effects due to individual electronic transitions. A transition is usually interpreted as the jumping of a single electron from a lower to a higher level. Actually this is a decided oversimplification since the jump of one electron will cause the other electrons to simultaneously reorganize. Kirkwood and we both start from the Rosenfeld equation[3] which is exact. However, Kirkwood has been especially interested in exploring the multiple electron jump aspect of the transition while we calculate the effect to be expected from the jump of the chromophoric electron ignoring the simultaneous reorganization of other electrons.

[1] For a brief summary, see Lowry, *Optical Rotatory Power* (Longmans, London, 1935); Jean-Paul Mathieu, *Les Theories Moleculaires du Pouvoir Rotatovire Naturel* (Société Journal de Physique, Paris, 1946); also, Born, *Optik* (Verlag. Julius Springer, Berlin, 1933).

[2] Born, Physik. Zeits. **16**, 251 (1915); Ann. d. Physik **55**, 177 (1918); Oseen, Ann. d. Physik **48**, 1 (1915); Gray, Phys. Rev. **7**, 472 (1916); Kuhn, Zeits. f. Physik **4**, 14 (1929); also Kuhn's many published papers.

[3] Rosenfeld, Zeits. f. Physik **52**, 161 (1928); Condon, Altar, and Eyring, J. Chem. Phys. **5**, 753 (1937); E. U. Condon, Rev. Mod. Phys. **9**, 432 (1937); J. G. Kirkwood, J. Chem. Phys. **5**, 479 (1937).

The experimental result should be compared roughly with the sum of the two effects. This is only approximately correct since our method of estimation slightly overlaps his and there are additional supposedly small effects not treated in either estimate. In the present paper we report very considerable simplication in the still laborious one-electron jump approximation and present new results for the molecule benzoin.

I. TRANSFORMATIONS OF COORDINATES FOR HYDROGEN-LIKE EIGENFUNCTIONS

The Rodrigues' formula for associated Legendre polynomials is:

$$P_l^{|m|}(\cos\theta)=\frac{(\sin\theta)^{|m|}}{2^l l!}\frac{d^{l+|m|}}{d(\cos\theta)^{l+|m|}}(\cos^2\theta-1)^l. \tag{1}$$

Expanding $(\cos^2\theta-1)^l$ by the binomial theorem differentiating $l+|m|$ times, and replacing the index on $\cos\theta$ by σ, we obtain:

$$P_l^{|m|}(\cos\theta)=\frac{(\sin\theta)^{|m|}}{2^l l!}\sum_{\sigma=0^+}^{l-|m|}(-)^{\frac{1}{2}(3l+|m|+\sigma)}{}_lC_{\frac{1}{2}(\sigma+l+|m|)}\frac{(\sigma+l+|m|)!}{\sigma!}(\cos\theta)^\sigma. \tag{2}$$

Equation (2) represents two cases. When $l-|m|$ is odd, σ is summed over odd values from 1 to $l-|m|$; when $l-|m|$ is even, σ is summed over even values from 0 to $l-|m|$. In Cartesian coordinates (2) becomes:

$$P_l^{|m|}(x,y,z)=\frac{1}{2^l l!}\left(\frac{r^2-z^2}{r^2}\right)^{|m|/2}\sum_{\sigma=0^+}^{l-|m|}(-)^{\frac{1}{2}(3l+|m|+\sigma)}{}_lC_{\frac{1}{2}(\sigma+l+|m|)}\frac{(\sigma+l+|m|)!}{\sigma!}\left(\frac{z}{r}\right)^\sigma \tag{3}$$

where

$$r^2=x^2+y^2+z^2.$$

Now, for the angular part of a hydrogen-like eigenfunction we have

$$Y_l^{\pm m}=\left[\frac{2l+1}{4\pi}\frac{(l-|m|)!}{(l+|m|)!}\right]^{\frac{1}{2}}P_l^{|m|}(\cos\theta)e^{\pm im\varphi}.$$

Therefore, for $m=0$, Y_l^0 has the form:

$$Y_l^0=\left[\frac{2l+1}{4\pi}\right]^{\frac{1}{2}}\frac{1}{2^l l!}\sum_{\sigma=0^+}^{l}(-)^{\frac{1}{2}(3l+\sigma)}{}_lC_{\frac{1}{2}(\sigma+l)}\frac{(\sigma+l)!}{\sigma!}\left(\frac{z}{r}\right)^\sigma. \tag{4}$$

For $m\neq 0$, $Y_l^{\pm m}$ is as usual replaced by the combinations

$$Y_l^{\pm m}(+)\equiv 2^{-\frac{1}{2}}(Y_l^{+m}+Y_l^{-m})$$

$$Y_l^{\pm m}(-)\equiv(2i)^{-\frac{1}{2}}(Y_l^{+m}-Y_l^{-m}).$$

Using Eq. (3) and taking $e^{\pm im\varphi}=(x\pm iy)^m/r^m\sin^m\theta$, followed by simple expansion and collecting terms, one obtains

$$Y_l^{\pm m}(+)=\frac{1}{2^l l!}\left[\frac{2l+1}{2\pi}\frac{(l-|m|)!}{(l+|m|)!}\right]^{\frac{1}{2}}\sum_{s=0}^{m^-/2}\sum_{\sigma=0^+}^{l-|m|}(-)^{\frac{1}{2}(2s+3l+\sigma+|m|)}{}_{|m|}C_{2s}\cdot{}_lC_{\frac{1}{2}(\sigma+l+|m|)}\cdot\frac{(\sigma+l+|m|)!}{\sigma!}\frac{(x^{|m|-2s}y^{2s}z^\sigma)}{r^{\sigma+|m|}} \tag{5}$$

and

$$Y_l^{\pm m}(-)=\frac{1}{2^l l!}\left[\frac{2l+1}{2\pi}\frac{(l-|m|)!}{(l+|m|)!}\right]^{\frac{1}{2}}\sum_{s=1}^{m^+/2}\sum_{\sigma=0^+}^{l-|m|}(-)^{\frac{1}{2}(2s+3l+\sigma+|m|-2)}$$

$$\cdot{}_{|m|}C_{2s-1}\cdot{}_lC_{\frac{1}{2}(\sigma+l+|m|)}\frac{(\sigma+l+|m|)!}{\sigma!}\frac{(x^{|m|-2s+1}y^{2s-1}z^\sigma)}{r^{\sigma+|m|}}. \tag{6}$$

In both (5) and (6) there are two cases depending on whether m is odd or even. If m is odd then m^- stands for $m-1$, while m^+ stands for $m+1$; otherwise m^- and m^+ stand for m.

Equations (4) to (6) can be combined into one expression:

$$Y_l^{\pm m}\begin{pmatrix}0\\ \pm\end{pmatrix}=\frac{1}{2^{l+\delta}l!}\left[\frac{2l+1}{2\pi}\frac{(l-|m|)!}{(l+|m|)!}\right]^{\frac{1}{2}}\sum_{s=\gamma}^{m^{\mp}/2}\sum_{\sigma=0^+}^{l-|m|}(-)^{\frac{1}{2}(2s+3l+\sigma+|m|)-\gamma}$$
$$\cdot{}_{|m|}C_{2s-\gamma}\cdot i^{C}{}_{\frac{1}{2}(\sigma+l+|m|)}\frac{(\sigma+l+|m|)!}{\sigma!}\frac{(x^{|m|-2s+\gamma}y^{2s-\gamma}z^{\sigma})}{r^{\sigma+|m|}} \tag{7}$$

where $\delta=\frac{1}{2}$ when $m=0$, and 0 when $m\neq 0$; and the γ is 0 for $Y_l^0(0)$ and $Y_l^{\pm m}(+)$, and 1 for $Y_l^{\pm m}(-)$.

For some purposes, we need to transform the (x, y, z) coordinates of the hydrogen-like function by a pure rotation into a new Cartesian set (ξ, η, ζ) as follows:

$$\begin{bmatrix}x\\ y\\ z\end{bmatrix}=\begin{bmatrix}\alpha_{11}&\alpha_{12}&\alpha_{13}\\ \alpha_{21}&\alpha_{22}&\alpha_{23}\\ \alpha_{31}&\alpha_{32}&\alpha_{33}\end{bmatrix}\begin{bmatrix}\xi\\ \eta\\ \zeta\end{bmatrix}.$$

The process is straightforward. Equation (7) becomes

$$Y_l^{\pm m}\begin{pmatrix}0\\ \pm\end{pmatrix}=\frac{1}{2^{l+\delta}l!}\left[\frac{2l+1}{2\pi}\frac{(l-|m|)!}{(l+|m|)!}\right]^{\frac{1}{2}}\sum_{s=\gamma}^{m^{\mp}/2}\sum_{\sigma=0^+}^{l-|m|}\sum_{(p_1q_1t_1)=0}^{|m|-2s+\gamma}\sum_{(p_2q_2t_2)=0}^{2s-\gamma}\sum_{(p_3q_3t_3)=0}^{\sigma}$$
$$\cdot(-)^{\frac{1}{2}(2s+3l+\sigma+|m|)-2\gamma}\frac{|m|!\,l!\,(\sigma+l+|m|)!\,\alpha_1\alpha_2\alpha_3}{[\frac{1}{2}(\sigma+l+|m|)]![\frac{1}{2}(l-\sigma-|m|)]!\,p_1!\,p_2!\,p_3!\,q_1!\cdots t_3!}\frac{(\xi^{\Sigma p}\eta^{\Sigma q}\zeta^{\Sigma t})}{r^{\sigma+|m|}} \tag{8}$$

where

$$\alpha_i\equiv\alpha_{i1}{}^{p_i}\alpha_{i2}{}^{q_i}\alpha_{i3}{}^{t_i} \tag{9}$$

$$\left.\begin{aligned}\Sigma p&\equiv p_1+p_2+p_3\\ \Sigma q&\equiv q_1+q_2+q_3\\ \Sigma t&\equiv t_1+t_2+t_3\end{aligned}\right\}. \tag{10}$$

The parenthesis on p_i, q_i, t_i in $\sum_{(p_iq_it_i)=0}^{x}$ means that the sum is to be taken from $p_i=0$ to $p_i=x$; $q_i=0$ to x; and t_i from 0 to x, but for each combination, $p_i+q_i+t_i$ must be equal to x. And the other symbols in (8) have the same meaning defined earlier.

Next we transform to elliptic coordinates as follows:

$$\left.\begin{aligned}\xi&=\tfrac{1}{2}R[(u^2-1)(1-v^2)]^{\frac{1}{2}}\cos\phi\\ \eta&=\tfrac{1}{2}R[(u^2-1)(1-v^2)]^{\frac{1}{2}}\sin\phi\\ \zeta&=\tfrac{1}{2}R(1+uv)\end{aligned}\right\}\qquad\left.\begin{aligned}r_a&=\tfrac{1}{2}R(u+v)\\ r_b&=\tfrac{1}{2}R(u-v)\end{aligned}\right\}.$$

Equation (8) finally yields the following expressions for the Y's in elliptical coordinates.

$$Y_l^{\pm m}\begin{pmatrix}0\\ \pm\end{pmatrix}=N(Y)\sum_i K_i(-)^x(u+v)^{-(\sigma+|m|)}[(u^2-1)(1-v^2)]^{\frac{1}{2}(\Sigma p+\Sigma q)}(1+uv)^{\Sigma t}\cdot(\cos\phi)^{\Sigma p}(\sin\phi)^{\Sigma q} \tag{11}$$

where

$$N(Y)\equiv\frac{1}{2^{l+\delta}l!}\left[\frac{2l+1}{2\pi}\frac{(l-|m|)!}{(l+|m|)!}\right]^{\frac{1}{2}} \tag{12}$$

$$\sum_i\equiv\sum_{s=\gamma}^{m^{\mp}/2}\sum_{\sigma=0^+}^{l-|m|}\sum_{(p_1q_1t_1)=0}^{|m|-2s+\gamma}\sum_{(p_2q_2t_2)=0}^{2s-\gamma}\sum_{(p_3q_3t_3)=0}^{\sigma} \tag{13}$$

$$K_i\equiv\frac{l!\,|m|!\,(\sigma+l+|m|)!\,\alpha_1\alpha_2\alpha_3}{[\frac{1}{2}(\sigma+l+|m|)]![\frac{1}{2}(l-\sigma-|m|)]!\,p_1!\,p_2!\,p_3!\,q_1!\,q_2!\cdots t_3!} \tag{14}$$

$$x\equiv\tfrac{1}{2}(2s+3l+|m|+\sigma)-\gamma. \tag{15}$$

Now, the transformed hydrogen-like eigenfunctions can be obtained at once in terms of elliptical coordinates, or, in other words, in polynomials involving u, v, ϕ etc. provided we use the explicit form for the associated Laguerre polynomials.[4]

[4] See any text of quantum mechanics, for example, Eyring, Walter, and Kimball, *Quantum Chemistry* (John Wiley and Sons, Inc., New York, 1947).

II. NUMERICAL COMPUTATION OF MATRIX ELEMENTS

Consider now the matrix elements $(n_1/V_i/n_2)$. Here, the n_1 and n_2 of course stand for the whole sets of quantum numbers n_1, l_1, m_1 and n_2, l_2, m_2, respectively. V_i in general is a function of r_b, the distance from the perturbing atom to the electron in question. Let us

take the incomplete screening field as a generally useful example. V_i can be expressed as

$$V_i=\sum_k\left[e^2\int\frac{\varphi_{ik}^2}{r_{ik}}d\tau_k-\frac{Ze^2}{r_i}\right] \tag{16}$$

for a Hartree field.[5] For simplicity, we take also the Slater-type function,[6]

$$\varphi_{ik}=N_r r_k^{n^*-1}\exp[-(Z-s)r/n^*a_0]Y(l,m)$$

and using the well-known Neumann expansion

$$\frac{1}{r_{ik}}=\sum_{l=0}^{\infty}\sum_{m=-l}^{m=l}\frac{(l-|m|)!}{(l+|m|)!}\frac{r_<^l}{r_>^{l+1}}P_l^{|m|}(\cos\theta_i)P_l^{|m|}(\cos\theta_k)\exp[im(\varphi_i-\varphi_k)] \tag{17}$$

obtain:

$$\int\frac{\varphi_{ik}^2}{r_{ik}}d\tau_k=N_r^2\sum_{l=0}^{\infty}\sum_{m=-l}^{m=l}\int\frac{r_k^{2n^*}r_<^l}{r_>^{l+1}}\exp\left[-\frac{2(Z-s)r_k}{n^*a_0}\right]dr_k$$
$$\cdot\int Y_{(l,m)}^2P_l^{|m|}(\cos\theta_i)P_l^{|m|}(\cos\theta_k)\exp[im(\varphi_i-\varphi_k)]\sin\theta_k d\theta_k d\varphi_k. \tag{18}$$

By considering the properties of associated Legendre polynomials, only a few terms in (17) give non-zero results. Thus

$$\frac{1}{r_{ik}}=\frac{1}{r_>}+\sum_l\frac{r_<^l}{r_>^{l+1}}\left\{P_l^0(\cos\theta_i)P_l^0(\cos\theta_k)+\frac{(l-|2m_0|)!}{(l+|2m_0|)!}P_l^{|2m_0|}(\cos\theta_i)P_l^{|2m_0|}(\cos\theta_k)\exp[2im_0(\varphi_i-\varphi_k)]\right\} \tag{19}$$

where n_0, l_0, m_0 are the quantum numbers in φ_{ik}.

After integration of (18), (16) has the general form*

$$V_i=-\sum_k e^2N_r^2\exp(-b'r_k)\left[\sum_{s=1}^{2n_0^*}\frac{s(2n_0^*-1)!}{(2n_0^*-s)!}\frac{r_k^{2n_0^*-s-1}}{b^{s+1}}\right]-e^2\sum_k\sum_l\frac{(2l_0+1)(l_0-|m_0|)!}{2(l_0+|m_0|)!}$$
$$\times\left\{\exp(-b'r_k)\left[\sum_{s=1}^{2n_0^*-l-1}\left(\frac{(2n_0^*+l)!}{(2n_0^*+l-s)!}-\frac{(2n_0^*-l-1)!}{(2n_0^*-l-s-1)!}\right)\frac{r_k^{2n_0^*-s-1}}{b'^{s+1}}+\sum_{s=2n_0^*-l}^{2n_0^*+l}\frac{(2n_0^*+l)!}{(2n_0^*+l-s)!}\frac{r_k^{2n_0^*-s-1}}{b'^{s+1}}\right]\right.$$
$$\left.-\frac{(2n_0^*+l)}{r_k^{l+1}b'^{2n_0^*+l+1}}\right\}\left\{I_\theta^0P_l^0(\cos\theta_i)+\frac{(l-|2m_0|)!}{(l+|2m_0|)!}I_\theta^m\cos2m_0\varphi_iP_l^{|2m_0|}(\cos\theta_i)\right\}, \tag{20}$$

with

$$N_r^2\equiv b'^{2n_0^*+1}/\Gamma(2n_0^*+1), \tag{20a}$$

$$b'\equiv2(Z-s')/n_0^*a_0, \tag{20b}$$

$$I_\theta^0\equiv\int_0^\pi P_l^0P_{l_0}^{m_0}P_{l_0}^{m_0}\sin\theta d\theta, \tag{20c}$$

$$I_\theta^m\equiv\int_0^\pi P_l^{2m_0}P_{l_0}^{m_0}P_{l_0}^{m_0}\sin\theta d\theta. \tag{20d}$$

For spherical symmetry of perturbing atoms, only the first line of (20) gives a contribution. Writing this term in elliptical coordinates gives:

$$V_i=-e^2\exp\left[-\frac{b'R(u-v)}{2}\right]\sum_k\sum_{s=1}^{2n_0}\left\{\frac{sb'^{2n_0^*-s}(\tfrac{1}{2}R)^{2n_0^*-s-1}(u-v)^{2n_0^*-s-1}}{2n_0^*(2n_0^*-s)!}\right\}_k. \tag{21}$$

Using (11), (21), and the explicit form of the radial functions we can write

$$(n_1|V_i|n_2)=-e^2N_1N_2S_aI_aI_\phi, \tag{22}$$

[5] Gorin, Walter, and Eyring, J. Chem. Phys. **6**, 825 (1938).
[6] Slater, Phys. Rev. **36**, 57 (1930).
* Using this equation, we have calculated the effective field of C, H, and O. The results agree with many earlier one-electron calculations except for the coefficient of the first term of the angular part of V_i for oxygen. We find it to be 15.99 instead of 19.75 obtained by Gorrin, Kauzmann, and Walter, J. Chem. Phys. **7**, 327 (1939).

with

$$N_i \equiv N_i(r)N_i(Y) = \frac{1}{2^{l_i+\delta} l_i!}\left[\frac{2l_i+1}{2\pi}\frac{(l_i-|m_i|)!}{(l_i+|m_i|)!}\frac{(n_i-l_i-1)!}{2n_i\{(n_i+l_i)!\}^3}\left(\frac{2Z_i}{n_i a_0}\right)^3\right]^{\frac{1}{2}}, \tag{23}$$

$$I_a \equiv \int \exp[-Au-Bv](u+v)^a(u-v)^b(1+uv)^c(u^2-1)^d(1-v^2)^d du dv, \tag{24}$$

$$I_\phi \equiv \int_0^{2\pi} (\cos\phi)^{\Sigma p}(\sin\phi)^{\Sigma q} d\phi, \tag{25}$$

$$A \equiv \left[\frac{Z_1}{n_1}+\frac{Z_2}{n_2}+\frac{2(Z_0-s')}{n_0^*}\right]\frac{R}{2a_0}, \tag{26}$$

$$B \equiv \left[\frac{Z_1}{n_1}+\frac{Z_2}{n_2}-\frac{2(Z_0-s')}{n_0^*}\right]\frac{R}{2a_0}, \tag{27}$$

$$a \equiv 1+l_1+l_2+k_1+k_2-(\sigma_1+\sigma_2+m_1+m_2), \tag{28}$$

$$b \equiv 2n_0^*-s, \tag{29}$$

$$C \equiv \Sigma t, \tag{30}$$

$$d \equiv \tfrac{1}{2}(\Sigma p+\Sigma q), \tag{31}$$

$$S_a \equiv \sum_k \sum_{s=1}^{2n_0^*} \frac{sb'^{2n_0^*-s}}{2n_0^*(2n_0^*-s)!}(\tfrac{1}{2}R)^{2n_0^*-s+2} \sum_{k_1=0}^{n_1-l_1-1}\sum_{k_2=0}^{n_2-l_2-1}\sum_{s_1=\gamma_1}^{m_1\mp/2}\sum_{s_2=\gamma_2}^{m_2\mp/2}$$

$$\cdot \sum_{\sigma_1=0^+}^{l_1-|m_1|}\sum_{\sigma_2=0^+}^{l_2-|m_2|}\sum_{(p_{11}q_{11}t_{11})=0}^{|m_1|-2s_1+\gamma_1}\sum_{(p_{12}q_{12}t_{12})=0}^{|m_2|-2s_2+\gamma_2}\sum_{(p_{21}q_{21}t_{21})=0}^{2s_1-\gamma_1}\sum_{(p_{22}q_{22}t_{22})=0}^{2s_2-\gamma_2}\sum_{(p_{31}q_{31}t_{31})=0}^{\sigma_1}\sum_{(p_{32}q_{32}t_{32})=0}^{\sigma_2}$$

$$\cdot \frac{[(n_1+l_1)!(n_2+l_2)!]^2(-2R/n_1a_0)^{l_1+k_1}(-2R/n_2a_0)^{l_2+k_2}(-)^{x_1+x_2} l_1!l_2!|m_1|!|m_2|!}{(n_1-l_1-1-k_1)!(2l_1+1+k_1)!k_1!(n_2-l_2-1-k_2)!(2l_2+1+k_2)!k_2!}$$

$$\cdot \frac{(\sigma_1+l_1+m_1)!(\sigma_2+l_2+m_2)!(\alpha_1\alpha_2\alpha_3)_1(\alpha_1\alpha_2\alpha_3)_2}{\left(\frac{l_1-m_1-\sigma_1}{2}\right)!\left(\frac{l_1+m_1+\sigma_1}{2}\right)!\left(\frac{l_2+m_2+\sigma_2}{2}\right)!\left(\frac{l_2-m_2-\sigma_2}{2}\right)! p_{11}!p_{21}!p_{31}!\cdots t_{32}!}. \tag{32}$$

Σp and Σq signify summation over all p's and q's for $\psi_{n_1}{}^0$ and $\psi_{n_2}{}^0$, the α's involved in (32) are

$$\alpha_{11}{}^{p_{11}+p_{12}}\alpha_{12}{}^{q_{11}+q_{12}}\cdots\alpha_{33}{}^{t_{31}+t_{32}}.$$

The first subscript on the p, q, and t are defined in Eq. (9). The second subscript indicates the state—either the initial state or the final state. 0 indicates the quantity arising from the perturbing function. R is the distance between the perturbing atom and the chromophoric center.

TABLE I. Coordinates of atoms in benzoin. (Chromophoric center, O of =CO.)

Atom	x	y	z	R	$\alpha_{13}=\frac{x}{R}$	$\alpha_{23}=\frac{y}{R}$	$\alpha_{33}=\frac{z}{R}$
O_3	0	0	0	0	0	0	0
C_7	−1.258	−2.025	−2.542	3.485	−0.3610	−0.5811	−0.7294
C_8	−1.475	−3.272	−3.117	4.755	−0.3108	−0.6881	−0.6555
C_9	−2.613	−3.490	−3.889	5.843	−0.4472	−0.5973	−0.6656
C_{10}	−2.528	−2.463	−4.087	5.400	−0.4681	−0.4561	−0.7569
C_{11}	−3.308	−1.217	−3.511	4.975	−0.6649	−0.2446	−0.7057
C_{12}	−2.173	−0.998	−2.740	3.637	−0.5975	−0.2744	−0.7534
H_6	0.874	−1.950	−2.280	3.125	0.2797	−0.6240	−0.7296
H_9	−2.783	−4.449	−4.332	6.806	−0.4089	−0.6537	−0.6365
H_9	−0.774	−3.753	−3.348	5.090	−0.1521	−0.7373	−0.6578
H_{10}	−4.402	−2.631	−4.681	6.944	−0.6339	−0.3789	−0.6741
H_{11}	−4.012	−0.426	−3.663	5.450	−0.7361	−0.0878	−0.6721
H_{12}	−2.004	−1.552	−3.519	4.336	−0.4622	−0.3579	−0.8116

I_ϕ can be easily integrated. The fact that if either Σp or Σq is odd, $I_\phi=0$, and I_ϕ is unchanged if $(\frac{1}{2}\pi-\phi)$ is substituted for ϕ, and further the fact that the relations

$$\sum_{i=1}^{3}\alpha_{ij}{}^2=\sum_{j=1}^{3}\alpha_{ij}{}^2=1$$

$$\sum_{\substack{i=1\\ j\neq k}}^{3}\alpha_{ij}\alpha_{ik}=\sum_{\substack{j=1\\ i\neq k}}^{3}\alpha_{ij}\alpha_{kj}=0$$

holds will further simplfy the relation (22).

Concerning I_a, we can further expand and write

$$I_a=\sum_\nu \int \Omega_\nu \int u^\nu \exp[-Au-Bv]dudv, \tag{33}$$

where Ω_ν is calculated to be:†

$$\Omega_\nu=(1-v^2)^d\sum_{\mu=0}^{a}\sum_{\tau=0}^{b}\sum_{\Delta=0}^{c}\sum_{\varepsilon=0}^{d}(-)^{b+d+\tau+\varepsilon}$$

$$\times {}_aC_\mu\cdot{}_bC_\tau\cdot{}_cC_\Delta\cdot{}_dC_\varepsilon V^{(a+b)-\nu+2(\Delta+\varepsilon)}\equiv D_jV^j. \quad (34)$$

Now, let us define

$$U_{nA}\equiv\int_1^\infty u^n e^{-Au}du \quad (35)$$

$$V_{nB}\equiv\int_{-1}^{1} v^n e^{-Bv}dv. \quad (36)$$

Hence,

$$(n_1|V_i|n_2)=-e^2N_1N_2S_a I_\phi\sum_{a,j}[D_jV_{jB}\cdot U_{aA}]. \quad (37)$$

The entry U_{nA} and V_{nB} are calculated and given at length in the first author's thesis. These values are plotted against A and B, respectively, for different n's. Then every U_{nA} and V_{nB} is known by direct reading from the appropriate graphs.

An example for numerical computation of matrix elements will be given in Section III.

III. OPTICAL ROTATORY POWER OF BENZOIN

Benzoin has two oxygens which may be expected to be chromophoric centers, one from the hydroxyl group; and the other from the carbonyl group. But we must decide which group makes the most important contribution to the optical rotation of benzoin. The absorption of the hydroxyl group has a maximum around 2600A; while that for the carbonyl group is about 2950A.[7] The latter is closer to the visible region of the spectrum and this will tend to make it give large contributions. Important support for the importance of the carbonyl is Peter Preiswerk's experiments on the absorption and rotation of benzoin and its derivatives in the ultraviolet.[8] The rotation dispersion curve rises, then falls abruptly around the carbonyl region. The first peak of ultraviolet absorption is about 3150A.

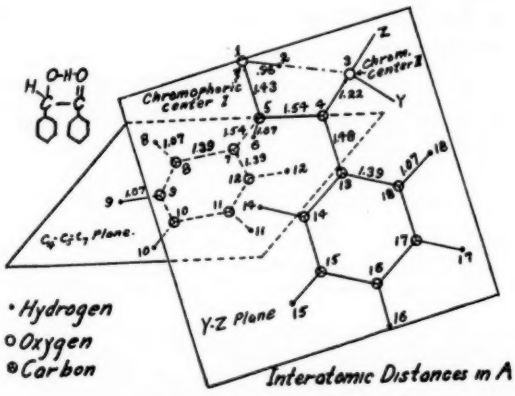

FIG. 1. Conformation of benzoin.

† A more convenient method has been developed for writing Ω_ν in the first author's thesis and extensive tables and graphs may be secured for the cost of photographic reproductions.

[7] Scheibe and Grieneisen, Zeits. f. physik. Chemie **B26**, 52 (1934); Herzberg and Scheibe, *ibid.* **B7**, 390 (1930).

TABLE II. Quantum numbers of $\psi_n{}^0$.

$\psi_n{}^0$	Z	n	l	m	$Y_l^{\pm m}\binom{0}{\pm}$	δ	γ
$\psi_{2Py}{}^0$	1.80	2	1	±1	$Y_1^{\pm1}(-)$	0	1
$\psi_{2Pz'}{}^0$	1.44	2	1	0	$Y_1^0(0)$	$\frac{1}{2}$	0
$\psi_{3dxy}{}^0$	1.44	3	2	±2	$Y_2^{\pm2}(-)$	0	1

TABLE III.[a] C_i.

Atom	$\alpha_{11}\alpha_{22}\alpha_{33}$	$(2P_z'\|V_i\|3d_{xy})a_0/e^2$	C_i
C_7	−0.1530	-2.655×10^{-2}	-2.821×10^{-2}
C_8	−0.1402	-4.151×10^{-3}	-4.041×10^{-3}
C_9	−0.1778	-7.793×10^{-4}	-9.622×10^{-4}
C_{10}	−0.1616	-1.459×10^{-3}	-1.637×10^{-3}
C_{11}	−0.1148	-3.126×10^{-3}	-2.492×10^{-3}
C_{12}	−0.1235	-2.252×10^{-2}	-1.931×10^{-2}
H_6	0.1273	-8.637×10^{-3}	7.635×10^{-3}
H_8	−.07377	-5.896×10^{-4}	-3.020×10^{-4}
H_9	−0.1791	-3.219×10^{-5}	-3.803×10^{-5}
H_{10}	−0.1619	-2.515×10^{-5}	-2.828×10^{-5}
H_{11}	−.03867	-3.189×10^{-4}	-8.562×10^{-5}
H_{12}	−0.1343	-1.812×10^{-3}	-1.690×10^{-3}
		$C=\Sigma_iC_i=-0.0512$	

[a] $C_i=-0.144\alpha_{11}\alpha_{22}\alpha_{33}(2P_z'|V_i|3d_{z.y})$. Since $1/(E_{2Pz'}{}^0-E_{3dxy}{}^0)=-0.144$.

Since benzoin exists in several conformations, we are forced to calculate its most probably conformation. There are several possible rotations about single bonds. If these take place, the calculations become extremely complicated. We should average over all possible conformations. However, we expect a hydrogen bond to be formed between the hydroxyl group and the carbonyl group. The observations from infra-red absorption proves that this hydrogen bond actually exists.[9] We assume that the benzene ring, attached to the carbonyl carbon, is in the yz-plane. The other benzene ring is in the plane containing the C_7-C_5 and C_5-C_4 bonds. This assumption will not lead to any serious mistake because the average contribution due to rotation will be small and effect atoms on the benzene ring which are far away from the chromophoric center. See Fig. 1. Based on this assumption, the coordinates of the atoms of benzoin are calculated as in Table I.

The eigenfunctions for the carbonyl oxygen as the chromophoric centers are:[10]

$$\Psi_a=\psi_{2Py}{}^0,$$
$$\Psi_b=\psi_{2Pz'}{}^0+C\psi_{3dxy}.$$

For the initial state we take $Z_1=1.80$, because the ionization potential of the non-bonding electron, $2P_y$,

[8] Peter Preiswerk, Helv. Phys. Acta **7**, 203 (1933).

[9] Hilbert, Wulf, Hendricks, and Liddel, J. Am. Chem. Soc. **58**, 548 (1938); Linus Pauling, *ibid.* 96 (1936).

[10] R. S. Mulliken, J. Chem. Phys. **3**, 564 (1935); Kauzmann, Walter, and Eyring, Chem. Rev. **26**, 339 (1940).

TABLE IV. Optical rotatory power of 1-benzoin in different solvents.

Solvent	Dipole moment, μ	$n_D^{20°}$	$[\alpha]_D^{20°}$	β
Acetaldehyde	2.7	1.332	−106.5	-3.62×10^{-34}
Acetone	2.8	1.359	−119.2	-3.97×10^{-34}
Acetonitrile	3.2	1.344	−157.8	-5.32×10^{-34}
Nitromethane	3.0	1.381	−162.0	-5.32×10^{-34}
Methanol	1.7	1.328	−163.0	-5.56×10^{-34}
Methylene chloride	1.5	1.424	−208.9	-6.62×10^{-34}
Chloroform	1.0	1.446	−212.3	-6.66×10^{-34}
Acetic acid	1.7	1.372	−225.7	-7.46×10^{-34}
Methyl iodide	1.3	1.530	−240.5	-7.11×10^{-34}
Acetophenone	2.9	1.533	−175.6	-5.18×10^{-34}
Nitrobenzene[a]	3.9	1.550	−86.9	-2.62×10^{-34}
Benzaldehyde	217	1.545	−194.7	-5.69×10^{-34}
Benzonitrile	318	1.528	−202.2	-5.98×10^{-34}
Toluene	0.4	1.501	−218.5	-6.59×10^{-34}
Bromobenzene	1.5	1.560	−118.2	-3.42×10^{-34}
Chlorobenzene	1.5	1.525	−240.6	-7.13×10^{-34}
Anisole	1.2	1.516	−248.7	-7.42×10^{-34}
Iodobenzene	1.2	1.618	−268.4	-7.47×10^{-34}
Carbon tetrachloride	0	1.416	−247.7	-7.94×10^{-34}
Carbon disulfide	0	1.628	−410.0	-11.3×10^{-34}
Mesitylene	0	1.496	−103.0	-3.12×10^{-34}
Benzene	0	1.501	−218.9	-6.60×10^{-34}

[a] $t=21.5°$.

of the carbonyl group is observed to be 11.3 ± 0.5 volts,[11] or 10.83 ± 0.1 volts.[12] For the excited state we take $Z_2=1.44$. This comes from Peter Preiswerk's observed value of the absorption peak for the benzoin.

Now, the optical rotatory power of benzoin is obtained by simple substitution in the equation:

$$\beta=\frac{c}{3\pi h}\sum_a \rho_a \sum_b \frac{Im\{(a|R|b)\cdot(b|M|a)\}}{\nu_{ba}{}^2-\nu^2}, \tag{38}$$

i.e.,

$$\beta=\frac{c}{3\pi h}\cdot\frac{C}{\nu_{ba}{}^2-\nu^2}(2P_y|x|3d_{xy})(2P_z'|1|2P_z)$$

with the following calculated values:

$$(2P_y|x|3d_{xy})=0.868\times10^{-8}\text{ cm}$$
$$(2P_{z'}|1|2P_z)=0.969$$
$$\nu=\nu_D \quad =0.509\times10^{15}\text{ sec.}^{-1}$$
$$\nu_{ba} \quad =0.952\times10^{15}\text{ sec.}^{-1}$$

[11] T. N. Jewitt, Phys. Rev. **46**, 616 (1934).
[12] W. C. Price, Phys. Rev. **46**, 529 (1934).

and

$$C=\Sigma_i C_i=-0.0512,$$

where

$$C_i=\frac{\alpha_{13}\alpha_{23}\alpha_{33}}{E_{2P_z}{}^0-E_{3d_{xy}}{}^0}(2P_z'|V_i|3d_{xy}).$$

Every matrix element in C is calculated by Eq. (37). The required quantum numbers and results are given in Tables II and III, respectively.

Hence, we have

$$\beta=1.43\times10^{-34}.$$

The specific rotation of l- and d-benzoin are given as $-118.6°$ in acetone and alcohol, and $120.5°$ in acetone, respectively.[13] In other words, these give $\beta=4.04\times10^{-34}$ and -3.97×10^{-34}, respectively. A series of measurements of rotation of l-benzoin in the different solvents was performed by Rule and Crawford.[14] Using their data, we calculate the β's which are tabulated in Table IV.

We readily see that our theoretical value is quite reasonably comparable to the experimental ones. However, we still want to point out that the numerous solvent effects make it difficult to make more direct comparison.

IV. SUMMARY

It is very necessary in ordinary quantum mechanical calculations, that some simplification should be made. In this paper, we transform the hydrogen-like eigenfunctions, generalize the incomplete screening field, and in this way, develop a more expeditious numerical computation of the matrix element.

The optical rotatory power of benzoin has been calculated. The result is found to be comparable to the experimental ones.

Finally, the authors want to express their debt to Dr. Chyong-Tsong Kwoh who made part of the calculations and checked the extensive tables on which the calculations are based.

[13] See I. C. T., Vol. VII, p. 362.
[14] Rule and Crawford, J. Chem. Soc., 138 (1937), Rule and Chambers, *ibid.*, 145 (1937).

THE JOURNAL OF CHEMICAL PHYSICS VOLUME 18, NUMBER 9 SEPTEMBER, 1950

Dielectric Constants of Non-Polar Fluids. I. Theory

WILLIAM FULLER BROWN, JR.
Sun Physical Laboratory, Newtown Square, Pennsylvania
(Received April 27, 1950)

The dielectric constant of a classical fluid, composed of spherically symmetric molecules with dipole-dipole interactions, is calculated by a method that leads to formulas previously derived by Yvon but is more direct and yields additional results. The relations of the formulas of Lorentz, Yvon, Kirkwood, and Böttcher to one another are clarified. An accurate calculation of the deviation from the Clausius-Mosotti formula requires knowledge of molecular distribution functions of various orders, but an approximate calculation is possible on the basis of the radial distribution function alone. It is shown that the success of Böttcher's approximation is partly the result of an approximate cancellation of errors, and that a practically equivalent formula can be obtained by another method that lends itself more readily to improvement. The distinctive feature of the present calculation is the introduction of quantities $\mathbf{p}_i^{(h)}$, the mean moment of molecule i when the positions of it and of $h-1$ other molecules are specified; Lorentz's formula corresponds to the approximation $\mathbf{p}_1^{(2)}=\mathbf{p}_1^{(1)}$, and other formulas to various approximate evaluations of the difference $\mathbf{p}_1^{(2)}-\mathbf{p}_1^{(1)}$.

1. INTRODUCTION

NON-POLAR fluids under high pressure show significant deviations from the Clausius-Mosotti formula for the variation of the static dielectric constant ϵ with density d.[1] According to this formula, $(\epsilon-1)/[(\epsilon+2)d]$ should, for a given substance, be independent of density. The usual derivation is based on Lorentz's formula for the mean electric field intensity acting on a molecule;[2] this is only an approximation, and its failure in the case of polar fluids is well known.[3] For non-polar fluids, formulas intended to supersede Lorentz's have been derived by Yvon,[4] by Kirkwood,[5] and by Böttcher.[6] Yvon's and Kirkwood's calculations are based on rigorous molecular theory and lead to series formulas, of which Yvon's have a wider range of validity because fewer special assumptions are introduced. Böttcher's calculation is based on the Onsager model, in which one molecule is treated explicitly and the rest are replaced by a continuum; it leads to a formula in closed form, but the errors inherent in the model are difficult to estimate.

The problem will be treated here by a method that is based on the same physical assumptions as that of Yvon and of Kirkwood, but differs in procedure and leads to more complete results. The distinctive feature of the method is the introduction of a set of quantities $\mathbf{p}_i^{(1)}$, $\mathbf{p}_{i;j}^{(2)}$, etc., representing respectively the mean electric moment of molecule i without further specification, the mean moment of molecule i when the position of a second molecule j with respect to it is specified, etc. By this device it proves possible to obtain directly formulas that otherwise would require inversion of a series, to see more clearly the relations of previous formulas to each other, and to analyze Böttcher's theory critically.

2. DEFINITIONS AND NOTATION

A homogeneous fluid containing N identical molecules is assumed to occupy a volume V. The molecules are assumed to interact mechanically according to a law of intermolecular force consistent with spherical symmetry but otherwise arbitrary, and to interact electrostatically as point dipoles with constant, isotropic polarizability α.

The field intensity at point O due to a dipole of moment $\mathbf{p}$ at point P is, in Gaussian units, $[-\mathbf{p}+3\mathbf{1}\cdot\mathbf{p}]/r^3$, where $\mathbf{r}$ is the vector from O to P, of magnitude r and in the direction of the unit vector $\mathbf{1}$. This field intensity may be written $\mathbf{A}\cdot\mathbf{p}$, where $\mathbf{A}$ represents the linear operator (dyadic)

$$\mathbf{A}\equiv[-1+3\mathbf{1}\mathbf{1}]/r^3; \qquad (2\text{-}1)$$

here $\mathbf{1}$ represents a unit vector along $\mathbf{r}$, whereas 1 represents the operator that leaves the operand unchanged (idem factor).

The macroscopic field intensity $\mathbf{E}$ is calculated by adding to the applied field intensity $\mathbf{E}_0$ (due to external sources) a term due to the polarized fluid. This latter term is the Coulomb (inverse-square-law) field intensity of a fictitious distribution of charges of volume density $-\mathrm{div}\mathbf{P}$ and surface density $\mathbf{n}\cdot\mathbf{P}$, where $\mathbf{P}$ is the macroscopic polarization (electric moment per unit volume) and $\mathbf{n}$ is the outward normal to the surface of the dielectric. At points outside the fluid and distant from it by a distance large on the molecular scale, $\mathbf{E}$ as so defined is equal to $\mathbf{E}_0+\int\mathbf{A}\cdot\mathbf{P}d\tau$ (where $d\tau$ is a volume element) and may be interpreted as the actual force per unit charge accessible to macroscopic observation; but

[1] S. S. Kurtz, Jr., and A. L. Ward, J. Franklin Inst. **222**, 563–592 (1936); **224**, 583–601 and 697–728 (1937).
[2] H. A. Lorentz, *Theory of Electrons* (B. G. Teubner, Leipzig, 1909), pp. 137ff.
[3] See Ann. N. Y. Acad. Sci. **40**, 289–482 (1940); Trans. Faraday Soc. **42A**, 1–256 (1946); H. Fröhlich, *Theory of Dielectrics: Dielectric Constant and Dielectric Loss* (Oxford University Press, London, 1949).
[4] J. Yvon, *Recherches sur la Théorie Cinétique des Liquides: I, Fluctuations en Densité; II, La Propagation et la Diffusion de la Lumière. Actualités Scientifiques et Industrielles, Nos. 542 and 543* (Hermann et Cie., Paris, 1937). Yvon's thesis (Paris, 1937) contains the same material. For a brief summary of the dielectric constant calculation, see Jacques Yvon, Comptes Rendus **202**, 35–37 (1936).
[5] John G. Kirkwood, J. Chem. Physics **4**, 592–601 (1936).
[6] C. J. F. Böttcher, Physica **9**, 937–944 and 945–953 (1942); *The Theory of the Dielectric Constant* (announced by Elsevier Publishing Company, New York, as in press, 1949).

at internal points, $\mathbf{E}$ is best regarded as having only mathematical significance. To simplify the calculations, the body of fluid will be assumed ellipsoidal in shape, with principal axes along the coordinate axes and with depolarizing (demagnetizing) factors L_1, L_2, L_3.[7] Then if $\mathbf{P}$ is uniform, its contribution to $\mathbf{E}$ will be uniform within the fluid. Such a uniform state will be assumed; whether it can actually be maintained is a question to be answered by the subsequent analysis, and therefore $\mathbf{E}_0$ will not be assumed in advance to be a uniform field or even a physically producible one. Under the assumed conditions $\mathrm{div}\mathbf{P}=0$, and $E_x=E_{0x}-L_1P_x$ etc.; or

$$\mathbf{E}=\mathbf{E}_0-\boldsymbol{\lambda}\cdot\mathbf{P}, \tag{2-2}$$

where the dyadic $\boldsymbol{\lambda}$ has a diagonal matrix with elements L_1, L_2, L_3.

For the evaluation of averages over a statistical ensemble, it is convenient to introduce molecular distribution functions, or simultaneous densities,[8-11] for which a slight modification of Yvon's notation will be used. The probability of finding h specified, infinitesimal volume elements $d\tau_1, d\tau_2, \cdots, d\tau_h$ simultaneously occupied by the centers of h distinct, but unspecified, molecules will be written $\nu_{12}^{(h)\cdots h}\,d\tau_1 d\tau_2\cdots d\tau_h$; the subscripts will sometimes be omitted, in which case $\nu^{(3)}$ is to be understood as meaning $\nu_{123}^{(3)}$ rather than, for instance, $\nu_{124}^{(3)}$.[12] In general $\nu^{(h)}$ is a function of the h position vectors $\mathbf{r}_1, \mathbf{r}_2, \cdots, \mathbf{r}_h$ of the specified volume elements; but for a fluid under homogeneous equilibrium conditions, $\nu^{(1)}$ (the number density of molecules) is independent of position, except very near the surface of the fluid, and $\nu_{12}^{(2)}$ is a function only of $r_{12}\equiv|\mathbf{r}_2-\mathbf{r}_1|$. The probability of finding the centers of *h specified molecules*, numbers 1, 2, $\cdots$, h, in $d\tau_1, d\tau_2, \cdots, d\tau_h$ respectively is $[(N-h)!/N!]\nu^{(h)}d\tau_1 d\tau_2\cdots d\tau_h$. The conditional probability of finding molecule $h+1$ in $d\tau_{h+1}$, given that molecules 1, 2, $\cdots$, h are in $d\tau_1, d\tau_2, \cdots, d\tau_h$, respectively, is therefore $\nu^{(h+1)}d\tau_{h+1}/(N-h)\nu^{(h)}$, and

$$\int_V \nu^{(h+1)}d\tau_{h+1}=(N-h)\nu^{(h)}. \tag{2-3}$$

The mean number density of molecules other than 1, at distance r_{12} from the center of 1, is $\nu_{12}^{(2)}/\nu^{(1)}$. When r_{12} is large on a molecular scale, this density has a constant value that differs from $\nu^{(1)}$ by terms of order $1/N$. The ratio of the value at distance r to the limiting value at large r will be represented by $\rho(r)$; by definition, therefore, $\rho(\infty)=1$ exactly. The term "radial distribution function," as used here, will refer to this function $\rho(r)$, which differs from $\nu^{(2)}/[\nu^{(1)}]^2$ by terms of order $1/N$, and which satisfies the relation[13]

$$4\pi\int_0^\infty [\rho(r)-1]r^2dr=kT\kappa-1/\nu^{(1)}, \tag{2-4}$$

where k and T have their usual meaning and κ is the compressibility. Terms of order $1/N$ are important in Eq. (2-4) but may be neglected in certain integrals that will occur later.

A useful approximation, introduced by Kirkwood,[8] expresses $\nu^{(3)}$ in terms of $\nu^{(1)}$ and $\nu^{(2)}$:

$$\nu_{123}^{(3)}=\nu_{12}^{(2)}\nu_{23}^{(2)}\nu_{31}^{(2)}/[\nu^{(1)}]^3. \tag{2-5}$$

Here terms of order $1/N$ have been disregarded.

The mean electric moment of molecule 1, when the positions of it and of $h-1$ other molecules 2, 3, $\cdots$, h are specified, will be written $\mathbf{p}_{1;2,3,\cdots,h}^{(h)}$; again subscripts will at times be omitted, and then $\mathbf{p}_1^{(3)}$, $\mathbf{p}_2^{(3)}$, $\mathbf{p}_3^{(3)}$ will mean $\mathbf{p}_{1;2,3}^{(3)}$, $\mathbf{p}_{2;3,1}^{(3)}$, $\mathbf{p}_{3;1,2}^{(3)}$ respectively. Successive $\mathbf{p}^{(h)}$'s satisfy the relation

$$\int_V \nu^{(h+1)}\mathbf{p}_1^{(h+1)}d\tau_{h+1}=(N-h)\nu^{(h)}\mathbf{p}_1^{(h)}. \tag{2-6}$$

For a homogeneous fluid, the mean moment $\mathbf{p}^{(1)}$ of a molecule with only its own position specified is independent of that position, except at positions very close to the surface; and the macroscopic polarization is

$$\mathbf{P}=\nu^{(1)}\mathbf{p}^{(1)}. \tag{2-7}$$

3. FORMULATION OF THE PROBLEM

When all the positions are specified, the moments $\mathbf{p}^{(N)}$ are determined by the N vector equations

$$\mathbf{p}_i^{(N)}=\alpha\{\mathbf{E}_0+\sum_{\substack{j=1\\ \neq i}}^{N}\boldsymbol{\Lambda}_{ij}\cdot\mathbf{p}_j^{(N)}\};\quad i=1, 2, \cdots, N. \tag{3-1}$$

$\boldsymbol{\Lambda}_{ij}$ is given by (2-1) with $\mathbf{r}=\mathbf{r}_{ij}=\mathbf{r}_j-\mathbf{r}_i$. The method of Yvon and of Kirkwood is to solve these equations by successive approximations, on the assumption that $\mathbf{p}_i^{(N)}$ can be expressed as a power series in α, and then to average the result over all configurations, with proper statistical weights. Instead, let us average Eq. (3-1) as it stands over all configurations of molecules $h+1$, $h+2$, $\cdots$, N, the positions of molecules

---

[7] J. C. Maxwell, *Treatise on Electricity and Magnetism*, 3d edition (Oxford University Press, London, 1904), Vol. 2, pp. 66–72.

[8] John G. Kirkwood, J. Chem. Physics **5**, 300–313 (1935); John G. Kirkwood and Elizabeth Monroe Boggs, J. Chem. Physics **10**, 394–402 (1942).

[9] J. Yvon, *La Théorie Statistique des Fluides et l'Équation d'État. Actualités Scientifiques et Industrielles, No. 203* (Hermann et Cie., Paris, 1935). See also reference 4.

[10] Joseph E. Mayer and Elliott Montroll, J. Chem. Phys. **9**, 2–16 (1941).

[11] M. Born and H. S. Green, Proc. Roy. Soc. **A188**, 10–18 (1946).

[12] $\nu_{123}^{(3)}=\nu_{123}$ (Yvon) $=n_3^{(123)}$ (Born and Green) $=N(N-1)\times(N-2)V^{-3}F_3\{3\}$ (Montroll and Mayer) $=N(N-1)(N-2)V^{-3}\times\exp\{-[W_3(\mathbf{R}_1, \mathbf{R}_2, \mathbf{R}_3)-W_0]/kT\}$ or $N(N-1)(N-2)V^{-3}\cdot\rho_2(\mathbf{R}_1, \mathbf{R}_2)\cdot{}^{12}\rho_3(\mathbf{R}_1, \mathbf{R}_2, \mathbf{R}_3)$ (Kirkwood and Boggs).

[13] L. Ornstein and F. Zernike, Physik. Zeits. **27**, 761 (1926); J. Yvon, reference 4.

1, 2, $\cdots$, h being specified. This gives

$$\mathbf{p}_i^{(h)}=\alpha\Big\{\mathbf{E}_0+\sum_{\substack{j=1\\ \neq i}}^{h}\mathbf{A}_{ij}\cdot\mathbf{p}_j^{(h)} +\frac{1}{\nu^{(h)}}\int_V \nu^{(h+1)}\mathbf{A}_{i,\,h+1}\cdot\mathbf{p}_{h+1}^{(h+1)}d\tau_{h+1}\Big\} \quad (3\text{-}2)$$

$$(i=1, 2, \cdots, h;\quad h=1, 2, \cdots, N-1).$$

Here the integral, which is the sum of $N-h$ identical contributions by molecules $h+1$, $h+2$, $\cdots$, N, has been expressed as $(N-h)$ times the contribution of molecule $(h+1)$.

For $h>1$ the applied field may be eliminated by subtracting from Eq. (3-2) the corresponding equation with $h=1$, after renumbering the variable of integration in the latter equation $h+1$. This gives

$$\mathbf{p}_i^{(h)}-\mathbf{p}^{(1)}=\alpha\sum_{\substack{j=1\\ \neq i}}^{h}\mathbf{A}_{ij}\cdot\mathbf{p}_j^{(h)}+\alpha\int\mathbf{A}_{i,\,h+1}\cdot\Big\{\frac{\nu^{(h+1)}}{\nu^{(h)}}\mathbf{p}_{h+1}^{(h+1)}-\frac{\nu_{i,\,h+1}^{(2)}}{\nu^{(1)}}\mathbf{p}_{h+1;\,i}^{(2)}\Big\}d\tau_{h+1} \quad (3\text{-}3)$$

$$(i=1, 2, \cdots, h;\quad h=2, 3, \cdots, N-1).$$

For large $|\mathbf{r}_{h+1}|$ the interactions of molecule $h+1$ with molecules 1, 2, $\cdots$, h become negligible; the two $\mathbf{p}$'s in the integrand become equal, and their coefficients in the braces become $\nu^{(1)}$ to within terms of order $1/N$. The quantity in braces therefore vanishes, to within terms of order $1/N$, as $r_{i,\,h+1}\to\infty$, and the integrand vanishes faster than $1/r_{i,\,h+1}{}^3$. For $h\cong 1$ the terms of order $1/N$ may be disregarded. (They contribute a shape-dependent integral of order $\alpha\mathbf{p}^{(1)}/V$; its ratio to either term on the left is of order $\alpha/V\cong a^3/V$, where a is the radius of the molecular sphere of exclusion.) The integral in Eq. (3-3) may then be extended over all space.

Equation (3-2) for $h=1$ requires a different treatment. This equation is

$$\mathbf{p}^{(1)}=\alpha\Big\{\mathbf{E}_0+\int_V\frac{\nu_{12}^{(2)}}{\nu^{(1)}}\mathbf{A}_{12}\cdot\mathbf{p}_{2;\,1}^{(2)}d\tau_2\Big\}. \quad (3\text{-}4)$$

In the integral, write $\mathbf{p}_{2;\,1}^{(2)}=\mathbf{p}^{(1)}+[\mathbf{p}_{2;\,1}^{(2)}-\mathbf{p}^{(1)}]$. The integral containing $\mathbf{p}_{2;\,1}^{(2)}-\mathbf{p}^{(1)}$ may be extended over all space as before. The integral containing $\mathbf{p}^{(1)}$ depends on the shape of the fluid body; it is the electrostatic field intensity of a continuous distribution of dipole sources of polarization $\nu_{12}^{(2)}\mathbf{p}^{(1)}/\nu^{(1)}$. Everywhere except in the vicinity of the point 1, this polarization is constant and equal, to within an error of order $1/N$, to $\nu^{(1)}\mathbf{p}^{(1)}=\mathbf{P}$; at point 1, it vanishes strongly because of the factor $\nu_{12}^{(2)}$. This factor insures convergence of the integral and permits its calculation from the equivalent charge densities, which reduce in this case to a surface density $\mathbf{n}\cdot\mathbf{P}$ on the ellipsoidal surface of the fluid and a volume density $-\mathrm{div}[\nu_{12}^{(2)}\mathbf{p}^{(1)}/\nu^{(1)}]$ in the neighborhood of point 1. The corresponding field intensities are $-\boldsymbol{\lambda}\cdot\mathbf{P}$ and $4\pi\mathbf{P}/3$. The value of the latter is dependent on the fact that $\nu_{12}^{(2)}$ is a function only of r_{12}, vanishes at $r_{12}=0$, and attains the constant value $\nu^{(1)2}$ (to within error of order $1/N$) at some value of r_{12} well inside the fluid surface; it is independent of the other properties of this function.

Since $\mathbf{E}_0-\boldsymbol{\lambda}\cdot\mathbf{P}$ is the macroscopic field intensity $\mathbf{E}$, Eq. (3-4) becomes

$$\mathbf{p}^{(1)}=\alpha\Big\{\mathbf{E}+\frac{4}{3}\pi\mathbf{P} +\nu^{(1)}\int\rho(r_{12})\mathbf{A}_{12}\cdot[\mathbf{p}_{2;\,1}^{(2)}-\mathbf{p}_1]d\tau_2\Big\}; \quad (3\text{-}5)$$

the integration may be extended over all space, and the approximation $\nu_{12}^{(2)}=\nu^{(1)2}\rho(r_{12})$ introduces negligible error.

If the approximation $\mathbf{p}_{2;\,1}^{(2)}=\mathbf{p}^{(1)}$ is made, the integral in Eq. (3-5) drops out and the expression in braces reduces to Lorentz's expression for the "local field." The Lorentz formula, then, assumes that the mean moment of a molecule known to be at a specified position with respect to another molecule is the same as the mean moment of a molecule without such specification. In the usual derivation of Lorentz's formula, this assumption enters at the point where it is argued that the field intensity due to molecules within a "physically small" sphere about a given molecule must vanish. It is seldom stated explicitly and is sometimes adroitly concealed—as in the "proof" of Lorentz's lemma given by Fowler.[14]

Equation (3-5) can be reduced to scalar form. By linearity and symmetry,

$$\mathbf{p}_{1;\,2}^{(2)}=\mathbf{p}_{2;\,1}^{(2)}=\{1+\boldsymbol{\Pi}_{12}\}\cdot\mathbf{p}^{(1)}, \quad (3\text{-}6)$$

where $\boldsymbol{\Pi}_{12}=\boldsymbol{\Pi}(\mathbf{r}_{12})$ is a dyadic of the form

$$\boldsymbol{\Pi}(\mathbf{r})=g(r)+[f(r)-g(r)]\mathbf{11}. \quad (3\text{-}7)$$

This may be seen by resolving $\mathbf{p}^{(1)}$ into components along and transverse to $\mathbf{r}_{12}$ and considering each separately. (Eq. (2-6) for $h=1$ is not exactly satisfied by this form of $\mathbf{p}^{(2)}$; but on the basis of the behavior of $\boldsymbol{\Pi}(\mathbf{r})$ at large r deduced later, the fractional error is of order α/V.) The product $\mathbf{A}_{12}\cdot\boldsymbol{\Pi}_{12}$ contains a term in 1 and a term in $\mathbf{11}$; the average of the latter over angles is $\frac{1}{3}$, and therefore the integral in Eq. (3-5) ultimately reduces to a scalar times $\nu^{(1)}\mathbf{p}^{(1)}$ or $\mathbf{P}$. This form of the equation shows that the vectors $\mathbf{E}$ and $\mathbf{P}$ (or $\mathbf{p}^{(1)}$) have the same direction and justifies the definition of a scalar dielectric constant ϵ. Solution for $\mathbf{E}$ and hence for

[14] R. H. Fowler, *Statistical Mechanics*, 2d edition (The Macmillan Company, New York, 1936), p. 440.

the ratio $E/P=4\pi/(\epsilon-1)$ gives

$$\frac{1}{\epsilon-1}=\frac{1}{4\pi\nu^{(1)}\alpha}-\tfrac{1}{3}(1+2C), \tag{3-8}$$

where

$$C=\int_0^\infty \rho(r)[f(r)-g(r)]r^{-1}dr. \tag{3-9}$$

Since the relation of $\mathbf{E}$ to $\mathbf{P}$ is independent of position, uniform $\mathbf{P}$ implies uniform $\mathbf{E}$ within the fluid and can, by (2-2), be maintained by a uniform $\mathbf{E}_0$.

Equation (3-8) may be written

$$\frac{\epsilon+2}{\epsilon-1}=\frac{3}{4\pi\nu^{(1)}\alpha}-2C, \tag{3-10}$$

which reduces to the Clausius-Mosotti formula for $C=0$. The correction to the Clausius-Mosotti formula is determined by the integral (3-9). Evaluation of this integral requires knowledge of the radial distribution function $\rho(r)$ and of the functions $f(r)$ and $g(r)$ that appear in the dyadic $\mathbf{\Pi}(\mathbf{r})$, i.e., in the expression for $\mathbf{p}^{(2)}$ as a linear vector function of $\mathbf{p}^{(1)}$. Determination of this function requires solution of the system of Eqs. (3-3).

4. SERIES SOLUTION

Since all the $\mathbf{p}^{(h)}$'s become equal to $\mathbf{p}^{(1)}$ when the r_{ij}'s are large in comparison with $\alpha^{\frac{1}{3}}$, i.e., when the quantities α/r_{ij}^3 are small, it is reasonable to assume series expansions

$$\mathbf{p}_i^{(h)}=\mathbf{p}^{(1)}+\sum_{s=1}^{\infty}\mathbf{p}_i^{(h)(s)}\alpha^s \tag{4-1}$$

in which the leading term is $\mathbf{p}^{(1)}$. In contrast, Yvon's and Kirkwood's calculations are based on expansions in which the leading term is $\alpha\mathbf{E}_0$. Choice of the form (4-1) implies choice of $\mathbf{p}^{(1)}$ or $\mathbf{P}$, rather than of $\mathbf{E}_0$ or $\mathbf{E}$, as independent variable; this choice is consistent with the form already chosen for Eq. (3-8) or (3-10).

If the series (4-1) is substituted in Eqs. (3-3) and coefficients of α^s are equated, the result is

$$\mathbf{p}_i^{(h)(1)}=\sum_{\substack{j=1\\ \neq i}}^{h}\mathbf{A}_{ij}\cdot\mathbf{p}^{(1)} + \int\left[\frac{\nu^{(h+1)}}{\nu^{(h)}}-\frac{\nu_{i,h+1}^{(2)}}{\nu^{(1)}}\right]\mathbf{A}_{i,h+1}\cdot\mathbf{p}^{(1)}d\tau_{h+1}; \tag{4-2}$$

$$\mathbf{p}_i^{(h)(s)}=\sum_{\substack{j=1\\ \neq i}}^{h}\mathbf{A}_{ij}\cdot\mathbf{p}_j^{(h)(s-1)} + \int\mathbf{A}_{i,h+1}\cdot\left[\frac{\nu^{(h+1)}}{\nu^{(h)}}\mathbf{p}_{h+1}^{(h+1)(s-1)} - \frac{\nu_{i,h+1}^{(2)}}{\nu^{(1)}}\mathbf{p}_{h+1;i}^{(2)(s-1)}\right]d\tau_{h+1}, \quad s>1. \tag{4-3}$$

Given the distribution functions $\nu^{(h)}$, any desired accuracy in $\mathbf{\Pi}$ can in principle be attained by an iterative procedure based on these formulas. Evaluation of $\mathbf{\Pi}$ or $\mathbf{p}^{(2)}$ (and hence of C) to the first order in α requires only the zero-order approximation, $\mathbf{p}^{(1)}$, to $\mathbf{p}^{(3)}$; evaluation of $\mathbf{\Pi}$ to the second order requires the first-order approximation to $\mathbf{p}^{(3)}$, which in turn requires only the zero-order approximation to $\mathbf{p}^{(4)}$; and so on. However, present knowledge of the higher order distribution functions is too scanty to permit calculation, by this method, of approximations beyond the first. Equation (4-2) for $h=2$ gives the first-order approximation

$$\mathbf{\Pi}_{12}=\alpha\left\{\mathbf{\Lambda}_{12}+\int\left[\frac{\nu_{123}^{(3)}}{\nu_{12}^{(2)}}-\frac{\nu_{13}^{(2)}}{\nu^{(1)}}\right]\mathbf{\Lambda}_{13}d\tau_3\right\}, \tag{4-4}$$

and this can be used directly if $\nu^{(3)}$ is approximated by means of Kirkwood's formula (2-5).

Let $\mathbf{r}=\mathbf{r}_{12}$, $\mathbf{t}=\mathbf{r}_{13}$, $\mathbf{s}=\mathbf{r}_{23}$, $\mathbf{1}_r=\mathbf{r}/r$ etc., $\theta=\cos^{-1}(\mathbf{1}_t\cdot\mathbf{1}_r)$: then in polar coordinates $(r,\ \theta,\ \phi)$, the average of $[-1+3\mathbf{1}_t\mathbf{1}_t]$ over ϕ is $[-1+3\mathbf{1}_r\mathbf{1}_r]P_2(\cos\theta)$. Therefore (4-4) may be written

$$\mathbf{\Pi}(\mathbf{r})=\alpha[-1+3\mathbf{1}_r\mathbf{1}_r][r^{-3}+\nu^{(1)}\Phi(r)], \tag{4-5}$$

where

$$\Phi(r)=\int\frac{\nu_{13}^{(2)}}{\nu^{(1)2}}\left[\frac{\nu^{(1)}\nu_{123}^{(3)}}{\nu_{12}^{(2)}\nu_{13}^{(2)}}-1\right]P_2(\cos\theta)\frac{1}{t^3}d\tau_3. \tag{4-6}$$

Equation (4-5) implies

$$\tfrac{1}{2}f(r)=-g(r)=\alpha[r^{-3}+\nu^{(1)}\Phi(r)], \tag{4-7}$$

and therefore

$$C=3\alpha\int_0^\infty\rho(r)[r^{-3}+\nu^{(1)}\Phi(r)]dr/r. \tag{4-8}$$

Insertion of (4-6) in (4-8) and of the result in (3-8) or (3-10) gives the correction to the Clausius-Mosotti formula in a form already given by Yvon.[4]

Use of Kirkwood's approximation (2-5) with neglect of terms of order $1/N$ gives

$$C=3\alpha A+6\pi\nu^{(1)}\alpha B \tag{4-9}$$

with

$$A=\int_0^\infty\rho(r)dr/r^4, \tag{4-10}$$

$$B=\int_0^\infty\int_0^\infty\int_{|t-r|}^{t+r}\rho(r)\rho(t)[\rho(s)-1] \times P_2(\cos\theta)sdsdtdr/t^2r^2, \tag{4-11}$$

since $d\tau_3=2\pi t^2\sin\theta d\theta dt=2\pi sdsdtdr/r$ with $0\leq\theta\leq\pi$ or $|t-r|\leq s\leq t+r$. B can also be evaluated by use of Fourier transforms. The results to be given in Section 5 were calculated by both methods.

5. WORKING FORMULAS BASED ON THE FIRST-ORDER APPROXIMATION

The triple integration of Eq. (4-11) can be reduced to a single integration, for approximate calculations, by the following method. As a first approximation, $\rho(r)$ may be replaced by the step function

$$\rho_0(r)=0, \quad r<a; \qquad =1, \quad r>a. \tag{5-1}$$

Then for a better approximation

$$\rho(r)=\rho_0(r)+\rho_1(r), \tag{5-2}$$

where the correction $\rho_1(r)$ is appreciable only in the neighborhood of $r=a$. The constant a is an effective molecular diameter, whose value is to some extent arbitrary. An approximate value of the integral in (4-11) may now be obtained by neglecting terms of order higher than the first in $\rho_1(r)$. When all the integrations have been carried out that do not require knowledge of the function $\rho_1(r)$, the result is

$$\frac{\epsilon+2}{\epsilon-1}=\frac{1}{z}-c_0+c_1 z, \tag{5-3}$$

where

$$z\equiv 4\pi\nu^{(1)}\alpha/3, \tag{5-4}$$

and

$$c_0=2\alpha/a^3+6\alpha\int_0^\infty \rho_1(r)dr/r^4 \tag{5-5}$$

(exact),

$$c_1=15/16+(1/a)\int_0^\infty \rho_1(r)g(r/a)dr \tag{5-6}$$

(to the first order in $\rho_1(r)$), with

$$g(x)=(3/8)(6-17x^2+12x^3-x^5), \quad x<2; \qquad =12/x^4, \quad x>2. \tag{5-7}$$

For gases at not too high densities it may be permissible to use Kirkwood's[5] distribution function for rigid spheres of radius a subject to van der Waals attractive forces. For $r>a$ the intermolecular potential energy is $-C'/r^6$; if $C'/kTa^6\ll 1$ and if ternary encounters are neglected,

$$\rho_1(r)=0, \quad r<a; \qquad =\mu/r^6, \quad r>a, \tag{5-8}$$

with

$$\mu=C'/kT. \tag{5-9}$$

Equations (5-5) and (5-6) give

$$c_0=(2\alpha/a^3)(1+\mu/3a^6), \tag{5-10}$$

$$c_1=(15/16)[1+(2/5)(\mu/a^6)(32/45-\ln 2)] =(15/16)[1+0.007186\mu/a^6]. \tag{5-11}$$

To get a formula directly comparable with Kirkwood's, the reciprocal of the right member of Eq. (5-3) (or of the equivalent formula for $1/(\epsilon-1)$) must be expanded as a series in α through the term in α^3. The resulting formula for $(\epsilon-1)/(\epsilon+2)$ (or for $\epsilon-1$) is identical with Kirkwood's except that he neglected the effect of $\rho_1(r)$ on c_1—an effect that is in fact, according to Eq. (5-11), negligibly small.

For liquids an approximate formula can be derived by a method due to Yvon.[4] This consists in replacing $\rho_1(r)$ by a constant times $\delta(r-a)$ (where $\delta(x)=0$ for $x\neq 0$, but $\int_{-\epsilon'}^{\epsilon'}\delta(x)dx=1$ for $\epsilon'>0$) and evaluating the constant by means of Eq. (2-4), with the term in κ neglected. This gives

$$c_0=4\alpha/a^3-3\alpha/2\pi\nu^{(1)}a^6, \tag{5-12}$$

$$c_1=15/16. \tag{5-13}$$

In observations of the variation of ϵ with density, the second term in c_0 will combine with the term $1/z$ in (5-3) to give a variation according to the law

$$\frac{\epsilon+2}{\epsilon-1}=\frac{1}{z'}-c_0'+c_1'z' \tag{5-14}$$

with

$$z'=(4\pi\nu^{(1)}\alpha/3)/(1+2\alpha^2/a^6), \tag{5-15}$$

$$c_0'=4\alpha/a^3, \tag{5-16}$$

$$c_1'=(15/16)(1+2\alpha^2/a^6). \tag{5-17}$$

In general, the integrals in (5-5) and (5-6) will be density- and temperature-dependent. If, therefore, the data at constant temperature are fitted to a formula of the form (5-14) with

$$z'\equiv d/d_0, \tag{5-18}$$

and with d_0, c_0', and c_1' constants, the precise interpretation of these constants requires evaluation of the integrals by use of detailed information about the function $\rho_1(r)$. In order of magnitude, however, $c_0'\cong c_0\cong 2\alpha/a^3$ and $c_1'\cong c_1\cong 1$. If a is taken just small enough so that $\rho(r)$ practically vanishes for $r<a$, then as r increases from a the function $\rho_1(r)$ has a positive maximum followed by a less pronounced minimum;[15] for liquids the minimum is negative.[8] The function $g(x)$ is negative and small for $1<x<1.35$, positive and considerably larger for $1.35<x<2$. The net effect of $\rho_1(r)$ on c_0 and c_1 is therefore likely to be positive; and since Eq. (5-17) suggests $c_1'>c_1$, probably $c_1'>15/16$. For a molecule pictured as a conducting sphere of diameter a, $\alpha=a^3/8$, so that $c_0'\cong\frac{1}{4}$ is to be expected.

The empirical formula of Eykman,[16] as applied to dielectric constant data by Kurtz and Ward,[1] assumes the following form when its constant is evaluated by use of the relation $(\epsilon-1)/4\pi\nu^{(1)}\alpha\to 1$ as $\nu^{(1)}\to 0$:

$$(\epsilon-1)/(\epsilon^{\frac{1}{2}}+0.4)=(3/1.4)z. \tag{5-19}$$

Expansion of this formula in the form (5-3) gives $c_0=1/14$, $c_1=45/56$. The signs and orders of magnitude

[15] Elliott W. Montroll and Joseph E. Mayer, J. Chem. Phys. 9, 626–637 (1941), Fig. 3.

[16] J. F. Eykman, Rec. Trav. Chim. 14, 185 (1895).

agree with those deduced from molecular theory; no more theoretical standing than this can be claimed for the formula.

6. INTEGRAL EQUATION METHOD

Since the functions $\nu^{(4)}$, $\nu^{(5)}$, etc., are not well known, an approximate method of calculating $\mathbf{\Pi}(\mathbf{r})$ will now be developed which requires no knowledge of them. The basis of this method is the introduction of an approximate formula for $\mathbf{p}_1^{(3)}$ in terms of $\mathbf{p}^{(1)}$ and $\mathbf{p}_1^{(2)}$, analogous to Kirkwood's formula for $\nu^{(3)}$. Such a formula can be obtained by assuming that the change in the mean moment of molecule 1 that results from specification of the positions of molecules 2 and 3 (with respect to it) can be found, with sufficient accuracy, by superposing the changes due to specification of 2 and 3 separately. This assumption can be justified by arguments similar to those used to justify Kirkwood's approximation (2-5). It leads to the formula

$$\mathbf{p}_{1;2,3}^{(3)}=\{1+\mathbf{\Pi}_{12}+\mathbf{\Pi}_{13}\}\cdot\mathbf{p}^{(1)}, \tag{6-1}$$

and insertion of this and of (2-5) in Eq. (3-3) for $h=2$ gives the following integral equation for $\mathbf{\Pi}$:

$$\begin{aligned}\mathbf{\Pi}_{12}=&\alpha\mathbf{A}_{12}\cdot[1+\mathbf{\Pi}_{12}]\\&+\nu^{(1)}\alpha\int\rho_{13}(\rho_{23}-1)\mathbf{A}_{13}\cdot[1+\mathbf{\Pi}_{31}]d\tau_3\\&+\nu^{(1)}\alpha\int\rho_{13}\rho_{23}\mathbf{A}_{13}\cdot\mathbf{\Pi}_{32}d\tau_3.\end{aligned} \tag{6-2}$$

If a solution is assumed in the form

$$\mathbf{\Pi}_{ij}=\sum_{s=1}^{\infty}\mathbf{\Pi}_{ij}^{(s)}\alpha^s, \tag{6-3}$$

then by equating coefficients of α^s it is found that

$$\mathbf{\Pi}_{12}^{(1)}=\mathbf{A}_{12}+\nu^{(1)}\int\rho_{13}(\rho_{23}-1)\mathbf{A}_{13}d\tau_3, \tag{6-4}$$

$$\begin{aligned}\mathbf{\Pi}_{12}^{(s)}=&\mathbf{A}_{12}\cdot\mathbf{\Pi}_{12}^{(s-1)}\\&+\nu^{(1)}\int\rho_{13}(\rho_{23}-1)\mathbf{A}_{13}\cdot\mathbf{\Pi}_{31}^{(s-1)}d\tau_3\\&+\nu^{(1)}\int\rho_{13}\rho_{23}\mathbf{A}_{13}\cdot\mathbf{\Pi}_{32}^{(s-1)}d\tau_3,\quad(s>1).\end{aligned} \tag{6-5}$$

The first-order solution (6-4) is the same as that obtained by the method of Section 4. The higher order terms have been considerably simplified.

This approximation may be regarded as the second in a series of successively better approximations, of which Lorentz's is the first. For quantities $\Delta\mathbf{p}^{(h)}$ may be defined by the equations

$$\mathbf{p}_{1;2}^{(2)}=\mathbf{p}^{(1)}+\Delta\mathbf{p}_{1;2}^{(2)}, \tag{6-6}$$

$$\mathbf{p}_{1;2,3}^{(3)}=\mathbf{p}^{(1)}+\Delta\mathbf{p}_{1;2}^{(2)}+\Delta\mathbf{p}_{1;3}^{(2)}+\Delta\mathbf{p}_{1;2,3}^{(3)}, \tag{6-7}$$

where the last term in each case takes account of effects that are appreciable only when all the molecules considered in the equation are close together. The Lorentz approximation is $\Delta\mathbf{p}^{(2)}=0$ and the present approximation $\Delta\mathbf{p}^{(3)}=0$; a still better approximation could be obtained by retaining $\Delta\mathbf{p}^{(3)}$ but neglecting a similarly defined term $\Delta\mathbf{p}^{(4)}$.

For the simplified distribution function $\rho_0(r)$, the integrations give

$$\frac{\epsilon+2}{\epsilon-1}=\frac{1}{z}-c_0+c_1z-c_2z^2+\cdots, \tag{6-8}$$

where

$$c_0=(2/3)\ln[(1+x)/(1-2x)], \tag{6-9}$$

$$c_1=\frac{15}{16}\left[1+\left(\frac{29}{15}-\frac{2}{5}\ln 2\right)x+\cdots\right] \tag{6-10}$$

$$=0.9375+1.55257x+\cdots,$$

$$c_2=\frac{80{,}071}{107{,}520}+\cdots=0.744708+\cdots, \tag{6-11}$$

with

$$x=\alpha/a^3, \tag{6-12}$$

$$z=4\pi\nu^{(1)}\alpha/3\equiv d/d_0. \tag{6-13}$$

The results (6-10) and (6-11) are presented with less assurance than the other results of this article; they have been checked, but not by a method completely independent of the original calculation method. The calculation, with checks, filled about 100 pages, each 17 in.×22 in.; that size of paper (with the long dimension horizontal) permits writing each step in a single line and is recommended to anyone who undertakes to verify the integrations—which, while tedious, are elementary.

The precision of present data on ϵ *vs.* d and on $\rho(r)$ does not justify carrying these calculations further.

7. CRITICAL ANALYSIS OF BÖTTCHER'S THEORY

Böttcher calculates the moment of molecule 1 by supposing that it is at the center of a spherical cavity of radius a, outside of which is a continuum whose dielectric constant ϵ is that of the actual dielectric. Now the moment is given rigorously by Eq. (3-4), in which the integral may be regarded as the field intensity of a continuous polarization

$$\begin{aligned}\mathbf{P}'=&\nu_{12}^{(2)}\mathbf{p}_{2;1}^{(2)}/\nu^{(1)}=\rho(r_{12})\nu^{(1)}\mathbf{p}_{2;1}^{(2)}[1+0(1/N)]\\=&\rho(r_{12})[1+\mathbf{\Pi}_{12}]\cdot\mathbf{P},\end{aligned} \tag{7-1}$$

with neglect of terms in $1/N$. In Böttcher's calculation, therefore, $\mathbf{P}'$ is replaced by 0 for $r<a$ and is evaluated for $r>a$ as if molecule 1 were a dipole at the center of a macroscopic cavity.

It is clear that if this method has any strict justifica-

tion, that justification can apply only to the special distribution function $\rho(r)=\rho_0(r)$ of Eq. (5-1), with a the radius of the molecular sphere of exclusion. Comparison of Eq. (7-1) with the continuum polarization calculated by Böttcher's method then shows that Böttcher's theory is equivalent to the assumption

$$\mathbf{\Pi}_{12}=C''\mathbf{\Lambda}_{12} \tag{7-2}$$

with

$$C''=\frac{\epsilon-1}{2\epsilon+1}\left[\frac{3}{4\pi\nu^{(1)}}-a^3\right]; \tag{7-3}$$

and in fact if this formula is used in Eqs. (3-9) and (3-10), it leads to Böttcher's final formula, which may be written

$$z=\frac{4\pi\nu^{(1)}\alpha}{3}=\frac{\epsilon-1}{9\epsilon}\left\{(2\epsilon+1)-2(\epsilon-1)\frac{\alpha}{a^3}\right\}. \tag{7-4}$$

If this formula is solved for $(\epsilon+2)/(\epsilon-1)$ and the result is expanded in the form (5-3), it gives $c_0=2\alpha/a^3$, $c_1=2$. For $\rho(r)=\rho_0(r)$ the correct values are $2\alpha/a^3$ and 15/16 respectively. Böttcher's approximation therefore gives an error in the term of order 1 in the polarizability. In this respect it is inferior to the approximation of Section 6, which is exact to the first order in α and which furthermore permits the introduction of an arbitrary radial distribution function $\rho(r)$.

The success of Böttcher's formula in fitting experimental data may be attributed to the approximate cancellation of two errors. The use of the simplified distribution function $\rho_0(r)$ would, by itself, result in too low a value (15/16) of c_1 by omitting the integral in Eq. (5-6); but in the calculation of the local field a further error is made, which raises the too low value 15/16 to a value 2 that may be approximately correct.

The use of macroscopic concepts in calculating the electrostatic effect of molecule 1 on the surrounding fluid is legitimate in a region where $\mathbf{E}$ and $\mathbf{P}$ are varying slowly, but not in the region $r\cong a$, where they are varying fast. The form (7-2) is therefore valid for $r\gg a$ but not for $r\cong a$; and because it gives incorrect values of $\mathbf{P}'$ in the region $r\cong a$, its use in this region probably results in an erroneous estimate of the "shielding effect" of near molecules on the field at large r, and therefore of the value of C'' in the region where the general form (7-2) is valid. This latter error, however, is probably small; the chief error is in the estimation of $\mathbf{P}'$ at $r\cong a$ and therefore of the contribution of this region to the local field acting on molecule 1.

A partial verification of these ideas can be obtained as follows. The method of Section 6 has been seen to involve no error in the term of first order in α. Let us now, in this method, commit an error similar to Böttcher's and observe the result. An asymptotic solution of the integral equation (6-2), valid at large r, can be found for $\rho(r)=\rho_0(r)$ by assuming the form (7-2), evaluating the integrals, and neglecting terms that vanish at infinity faster than $1/r^3$. This gives

$$C''=\alpha\frac{1-4\pi\nu^{(1)}a^3/3}{1+4\pi\nu^{(1)}\alpha/3}. \tag{7-5}$$

The two values of C'', (7-3) and (7-5), are not exactly equal (if they are equated, the result is the Clausius-Mosotti formula); and since each is based on approximations, it cannot be easily decided which value is better. If the form (7-2), with the value (7-5) of C'', is now used in the formula (3-9) as if it were valid over the entire region $r>a$, the following formula is obtained:

$$\frac{\epsilon+2}{\epsilon-1}=\frac{3}{4\pi\nu^{(1)}\alpha}-\frac{2\alpha}{a^3}\frac{1-4\pi\nu^{(1)}a^3/3}{1+4\pi\nu^{(1)}\alpha/3}; \tag{7-6}$$

and to the first order in α, this is identical with the result obtained by expanding Böttcher's formula. It therefore appears that the chief error is not the incorrect evaluation of the constant in the long-range effect of molecule 1, but the incorrect evaluation of the mean moments in its immediate neighborhood.

8. GENERAL REMARKS

I am indebted to Mr. S. S. Kurtz, Jr. for directing my attention to this problem, and to other members of the Sun Oil Company staff, especially Dr. Eugene J. Rosenbaum, for many stimulating discussions. I am also indebted to Professor Joseph E. Mayer of the Institute of Nuclear Studies, University of Chicago, for a very helpful discussion of the statistical mechanical aspects of the problem.

To the experimentalist who is primarily interested in finding a formula on which he can rely, it is confusing to find in the literature a number of apparently incompatible formulas, derived independently by different authors. I hope that the discussion given here will help to clarify the relations of the formulas of Lorentz, Yvon, Kirkwood, and Böttcher to each other. I wish particularly to call attention to Yvon's work, which has seldom been cited in English-language publications. His discussion of dielectric properties[4] includes, besides the material already mentioned, a detailed analysis of the dynamical behavior at optical frequencies; and his treatment of distribution functions[9] contains a number of results that have since been rederived by other authors.

A complete theory would have to take account of several factors disregarded here: anisotropy of the molecules,[5,17] variation of the polarizability of a molecule with distance from its neighbors,[18] and quantum-mechanical aspects of the problem.[19] It seems to me, however, that these matters can be treated more satis-

[17] C. V. Raman and K. S. Krishnan, Proc. Roy. Soc. **A117**, 589–599 (1928); see also P. O. John, Phil. Mag. **22**, 274–281 (1936).
[18] Michels, de Boer, and Bijl, Physica **4**, 981–994 (1937); S. R. de Groot and C. A. ten Seldam, Physica **13**, 47–48 (1947).
[19] J. H. Van Vleck, J. Chem. Phys. **5**, 556–558 and 991 (1937).

factorily if the error in the Lorentz local field formula has first been examined in the case in which the other factors are not present, so that there is less danger of attributing to them effects due to it. It also seems to me that the concept of molecular distribution functions is a more fruitful one with which to attack the local field problem than are such concepts as the cybotactic lattice[20] and the classification of molecules as nearest neighbors, next-nearest, and so on.[21]

It is occasionally contended that the local field is **E**.[22,23] (If this were so, and if the molecular polarizability α were independent of density, then for a given substance $(\epsilon-1)/d$ rather than $(\epsilon-1)/[(\epsilon+2)d]$ should be independent of density.) The arguments by which this contention is supported involve the supposition that **E** (interpreted perhaps as the field intensity inside a needle-shaped Kelvin cavity) can be somehow related to the mean field intensity acting on a molecule, without explicit consideration of molecular distribution functions. If this supposition were correct, then in a detailed statistical mechanical treatment the final formulas would turn out to be independent of the molecular distribution functions. This they do not in the present treatment, which is based on a spherically symmetric model of the molecule. It is possible that the distribution functions might drop out in a treatment based on an extreme model such as a needle-molecule, but there is no reason for expecting such a simple result in the case of a realistically anisotropic model.

The empirical finding that $(\epsilon-1)/d$ is approximately constant *for a group of isomers*[1] is a different matter, which can be elucidated only by means of an atomic theory of the molecular polarizability.

Experimental data will be analyzed in another article.

[20] H. Mueller, Phys. Rev. **50**, 547 (1936).
[21] G. Jaffé, J. Chem. Phys. **8**, 879–888 (1940); Phys. Rev. **57**, 558 (1940).
[22] G. B. Brown, Nature **150**, 661–662 (1942).
[23] Jatkar, Iyengar, and Sathe, J. Ind. Inst. Sci. **28** A (Pt. II), 1–15 (1946). The starting point of these authors is: "The concept of a dipole is that it is a highly anisotropic body having a needle shape." From a Kelvin cavity calculation they conclude that the local field is **E**. The resulting formula is stated to be correct "for all liquids, solids, and solutions."

THE JOURNAL OF CHEMICAL PHYSICS VOLUME 18, NUMBER 9 SEPTEMBER, 1950

Dielectric Constants of Non-Polar Fluids. II. Analysis of Experimental Data

WILLIAM FULLER BROWN, JR.
Sun Physical Laboratory, Newtown Square, Pennsylvania
(Received April 27, 1950)

Although the formulas of Part I do not apply strictly to actual gases and liquids, they suggest a possibly useful method of analyzing data on the variation of dielectric constant ϵ with density d under high pressure at constant temperature. The method is to express $(\epsilon+2)d/(\epsilon-1)$ as a polynomial in d; the variable terms represent the deviation from the Clausius-Mosotti formula. This method has been tested, and compared with alternative procedures based on more specialized formulas, by analysis of data on carbon disulfide (Chang, Danforth) and on carbon dioxide (Michels and Kleerekoper). It is concluded that the proposed method is an efficient one for representing the data, that the values of the coefficients are consistent with the approximate values estimated from the simplified theory, and that there is no advantage in the use of more specialized formulas. The precision of present ϵ *vs.* d data and of present knowledge of molecular distribution functions does not justify any more detailed conclusions.

1. INTRODUCTION

IN I[1] under this title, formulas were derived for the dielectric constant ϵ of a non-polar fluid under pressures sufficiently high to reveal measurable departures from the Clausius-Mosotti relation. The more reliable of these formulas, some of which were derived earlier by Yvon,[2] require a knowledge of various molecular distribution functions and a triple integration; but by introduction of some reasonable approximations, simplified formulas were obtained that require knowledge only of the radial distribution function $\rho(r)$ and only a single integration. Even this function is imperfectly known, either theoretically or experimentally, for most actual fluids; but on the basis of approximations discussed in I, it seems likely that if the data at constant temperature are fitted to a formula

$$\frac{\epsilon+2}{\epsilon-1}=\frac{d_0}{d}-c_0'+c_1'\frac{d}{d_0}-c_2'\left(\frac{d}{d_0}\right)^2+\cdots, \qquad (1\text{-}1)$$

where d is the density, the constants c_n' will be positive and of order of magnitude 1. The constant d_0 should be at least approximately equal to $3m_0/4\pi\alpha$, where m_0 is the mass of a molecule and α its polarizability; the constant c_0' should be 2 to 4 times the ratio α/a^3, where a is an effective molecular diameter. These conclusions are consistent with formulas derived by Kirkwood[3] and by Böttcher[4] on the basis of more

[1] William F. Brown, Jr., J. Chem. Phys. **18**, 1193 (1950).
[2] J. Yvon, *Actualités Scientifiques et Industrielles*, Nos. 542 and 543 (Hermann et Cie., Paris, France, 1937).
[3] John G. Kirkwood, J. Chem. Phys. **4**, 592–601 (1936).
[4] C. J. F. Böttcher, Physica **9**, 937–944 and 945–953 (1942).

specialized assumptions; their formulas can also be derived from the general formulas of I by methods described there.

The molecules were assumed to be spherically symmetric in their mechanical and electrical properties and to interact electrostatically as point dipoles. For molecules with any resemblance to spherical symmetry these approximations are probably admissible, if the radial distribution function and polarizability are interpreted as averages over all orientations; the neglect of quadruple and higher moments introduces appreciable error only for molecules very close together. But for highly asymmetric molecules, the averaging of the properties of two molecules individually before they are allowed to interact, rather than of the properties of the interacting pair (or of clusters of higher order), no doubt introduces a serious error. Furthermore there are cases in which the electrostatic interactions are so far from being of a dipole-dipole nature that it is not even permissible to regard the molecule as equivalent to a dipole plus a quadruple and so on; this is obviously true of long chain molecules.

For these reasons, Yvon was reluctant to apply his formulas to any substances except monatomic ones and a few others; the number of measurements remaining for analysis was small indeed, and no very conclusive test of the formulas was possible. Kirkwood and Böttcher applied their formulas to cases in which data were plentiful, and by suitable choice of the constants in the formulas succeeded in fitting the data better than by use of the Clausius-Mosotti formula; but this is also no very conclusive test, for Kurtz and Ward[5] accomplished as much by use of purely empirical formulas.

The application to actual liquids and gases of specific formulas based on the spherical molecule is not a step that I wish to defend; but the formulas based on this model do suggest the form (1–1) as a possibly suitable form in which to represent the observed data analytically. If it turns out that the data generally lend themselves to this mode of representation, and if the constants have the orders of magnitudes predicted by the simple theory, then the goal of a more ambitious theory becomes more specific: to calculate the magnitudes of these constants for actual substances. The values of the constants also indicate, more definitely than the original data, to what degree any actual substance departs from the idealized behavior assumed in the simple theory.

I will present here the results of a numerical analysis of representative data, based primarily on the formula (1–1). A direct fit to some of the more specialized formulas has also been made, for comparison. The conclusions are that the more specialized formulas, such as Böttcher's, have no advantage over the general formula (1–1); and that in order to detect and study deviations of the substances studied from the behavior predicted by the spherical molecule theory, it would be necessary to have available both detailed knowledge of the (average) radial distribution and more precise data on the dielectric constant.

The left member of (1–1) is the reciprocal of the quantity which, according to the Clausius-Mosotti formula, should be proportional to the density. In the right member, therefore, the terms after the first represent the deviation from the Clausius-Mosotti formula. The left member as it stands is the ratio of the Lorentz local field intensity $E+4\pi P/3$ to $4\pi P$ (E = macroscopic electric field intensity, P = polarization). By subtraction of 1 and division by 3 it becomes $1/(\epsilon-1)$, the ratio of the macroscopic field intensity to $4\pi P$; by addition of 2 and division by 3 it becomes $\epsilon/(\epsilon-1)$, the ratio of the electric displacement $D=E+4\pi P$ to $4\pi P$. Either of these ratios or any linear combination of them might be used instead of the one chosen here, and essentially only the value of c_0' would be affected.

The calculations reported here were exploratory, and their primary object was to establish satisfactory procedures for analysis of data rather than to carry out an extensive analysis. Only a few sets of data have been analyzed, but they have been analyzed systematically and quite completely. Numerical, not graphical, methods have been used in order that the relative success of different formulas might be judged as accurately as possible; and the estimates of the success achieved take account of the number of disposable constants in each formula.

The special formulas tested, in addition to the general one (1–1), are:

(a) The empirical Eykman formula, (5–19) of I:

$$\frac{\epsilon-1}{\epsilon^{\frac{1}{2}}+0.4}=\frac{3}{1.4}\frac{d}{d_0}. \tag{1–2}$$

(b) Böttcher's formula, (7–4) of I:

$$\frac{d}{d_0}=\frac{\epsilon-1}{9\epsilon}\left\{(2\epsilon+1)-2(\epsilon-1)\frac{\alpha}{a^3}\right\}. \tag{1–3}$$

(c) Formula (5–3) of I for the simple distribution function $\rho_0(r)$ (Kirkwood's non-attracting spheres):

$$\frac{\epsilon+2}{\epsilon-1}=\frac{d_0}{d}-\frac{2\alpha}{a^3}+\frac{15}{16}\frac{d}{d_0}=\frac{d_0}{d}-c_0+\frac{15}{16}\frac{d}{d_0}. \tag{1–4}$$

(d) The higher order approximation (6–8) of I for the same distribution function:

$$\frac{\epsilon+2}{\epsilon-1}=\frac{d_0}{d}-c_0+c_1\frac{d}{d_0}-c_2\left(\frac{d}{d_0}\right)^2, \tag{1–5}$$

with

$$\begin{aligned} c_0&=(2/3)\ln[(1+x)/(1-2x)],\\ c_1&=0.9375+1.55257x,\\ c_2&=0.744708,\\ x&=\alpha/a^3. \end{aligned} \tag{1–6}$$

[5] S. S. Kurtz, Jr. and A. L. Ward, J. Franklin Inst. **222**, 563–592 (1936); **224**, 583–601 and 697–728 (1937).

The Clausius-Mosotti formula itself is (1–1) with only one term retained. Reference will also be made to the basic theoretical formula from which (1–1) is derived, Eq. (3–10) of I:

$$\frac{\epsilon+2}{\epsilon-1}=\frac{d_0}{d}-2C, \tag{1–7}$$

where C (not a constant) is given by an integral involving the radial distribution function $\rho(r)$ and other functions, Eq. (3–9) of I.

Formula (1–4) received more attention in these calculations than it deserves in any subsequent ones. When the calculations were made, the importance of the correction term in Eqs. (5–6) of I was underestimated.

The data will be discussed in the chronological order of the measurements.

2. CARBON DISULFIDE

As representative data on a liquid I have taken the data on carbon disulfide under high pressure at 30°C. Two sets of data have been published, by Chang[6] and by Danforth.[7] Both sets were taken in Bridgman's laboratory; Bridgman[8] states that Chang's, though published later, were taken earlier.

Chang gives 11 values of dielectric constant ϵ at known density d; for definiteness I have used the values at frequency 2000 c.p.s.[9] The range of pressure is 1 to 12,000 kg/cm², of density 1.247 to 1.687 g/cm³, and of dielectric constant 2.624 to 3.580. An accuracy of 1/10 percent is claimed in the dielectric constant, but it is not stated what precision measure this is (whether standard deviation or "probable error") or how it was estimated. The densities at given pressures are derived from older data of Bridgman.[10]

The first step is to obtain a reliable estimate of the random error in the value of ϵ at given d; this can be obtained by least squares analysis of the data themselves. If the function $\epsilon(d)$ is expressed analytically by means of an approximating function containing s adjustable constants, such as a polynomial of degree $s-1$, and if the constants are evaluated by a least squares fit to n points (where n considerably exceeds the minimum number s necessary to determine all the constants), an estimate of the variance σ^2 of the data (mean square error for many experiments) may be obtained by dividing the sum of the squares of the deviations by $n-s$.[11] If this process is carried out successively for $s=1, 2, \cdots$, then on the average for many repetitions of the experiment the corresponding variance estimates should at first decrease with increasing s and then become constant at a value equal to the actual variance of the data; after this constant value has been reached, further increase in the degree of the approximating polynomial serves only to fit the errors more faithfully and not to give a better representation of the physical relations. In any single experiment, of course, the variance estimates do not decrease in a regular manner with s but exhibit irregular fluctuations superposed on the general decrease to a constant value.

For simplicity it has been assumed throughout that all values of ϵ in any one set of data have the same variance σ^2; the analysis would be only slightly modified if weighting factors were introduced to correspond, for instance, to equal mean square percentage errors in ϵ (or in $\epsilon-1$).

When Chang's 11 points are fitted successively by polynomials $\epsilon(d)$ of degrees 0, 1, 2, 3, the resulting estimates of the standard deviation σ (square root of the variance) of the data are 0.32, 0.019, 0.0058, 0.0063 respectively. We may conclude that a second-degree approximating polynomial is all that is warranted by the data and that the root-mean-square random error in ϵ at a specified d is about 0.006. To fit the data within experimental error by use of a polynomial requires only three constants: therefore an equally good fit by means of any other three-constant function justifies no conclusion in regard to the theoretical significance of the function; but if a one- or two-constant formula can be made to fit the data equally well, that result may have significance.

The straightforward method of testing a formula of the form (1–1) is to carry out for the function yd, where

$$y=(\epsilon+2)/(\epsilon-1), \tag{2–1}$$

the same procedure just described for the function ϵ, but with weights

$$W=\left(\frac{1}{d}\frac{d\epsilon}{dy}\right)^2 \tag{2–2}$$

assigned to the points in order that the quantity minimized may still be the sum of the squares of the deviations in ϵ. If this gives an approximating polynomial

$$yd=A_0+A_1d+A_2d^2+\cdots, \tag{2–3}$$

then the constants of (1–1) are

$$d_0=A_0, \quad c_0'=-A_1, \quad c_1'=A_0A_2, \quad c_2'=-A_0^2A_3. \tag{2–4}$$

This procedure applied to Chang's data gives, for polynomials of degrees 0, 1, 2, 3, the estimates $\sigma=0.027$, 0.0063, 0.0064, 0.0068 respectively; the individual deviations for the first three of these are shown in Table I. It must be concluded that only two constants are significant: the data support the form (1–1) or (1–7) as an efficient representation of the relations, and

[6] Z. T. Chang, Chinese J. Phys. **1**, 1–55 (1934).
[7] W. E. Danforth, Jr., Phys. Rev. **38**, 1224–1235 (1931).
[8] P. W. Bridgman, Rev. Mod. Phys. **18**, 1–93 (1946), p. 71.
[9] With correction of an obvious misprint in the value at 5000 kg/cm².
[10] P. W. Bridgman, Proc. Am. Acad. **49**, 1–114 (1913), Table XI, p. 62.
[11] E. T. Whittaker and G. Robinson, *The Calculus of Observations*, 4th editon (Blackie and Sons, Ltd., London, 1944), p. 245; A. C. Aitken, *Statistical Mathematics*, 4th edition (Oliver and Boyd, Edinburgh and London; Interscience Publishers, Inc., New York, 1945), p. 116.

TABLE I. Carbon disulfide at 30°C: data of Chang.

d Density g/cm³	ϵ Dielectric constant	Deviation of ϵ from calculated value[a] P_0	P_1	P_2	E	B	(1-4)	(1-5)
1.247	2.624	+0.0439	+0.0063	+0.0035	−0.0427	+0.0185	+0.0132	+0.0088
1.297	2.717	+0.0381	+0.0047	+0.0033	−0.0399	+0.0105	+0.0081	+0.0057
1.336	2.784	+0.0250	−0.0045	−0.0049	−0.0448	−0.0031	−0.0035	−0.0044
1.398	2.914	+0.0219	−0.0001	+0.0007	−0.0310	−0.0041	−0.0023	−0.0011
1.447	3.005	+0.0023	−0.0125	−0.0110	−0.0337	−0.0191	−0.0163	−0.0140
1.487	3.107	+0.0103	+0.0023	+0.0041	−0.0100	−0.0053	−0.0021	+0.0006
1.522	3.177	−0.0050	−0.0062	−0.0045	−0.0096	−0.0136	−0.0107	−0.0078
1.565	3.287	−0.0038	+0.0042	+0.0056	+0.0142	−0.0012	+0.0009	+0.0032
1.603	3.378	−0.0126	+0.0046	+0.0051	+0.0273	+0.0025	+0.0031	+0.0042
1.647	3.487	−0.0243	+0.0050	+0.0042	+0.0449	+0.0089	+0.0070	+0.0060
1.687	3.580	−0.0456	−0.0040	−0.0067	+0.0535	+0.0075	+0.0027	−0.0013
σ[b]		0.0273	0.0063	0.0064	0.0368	0.0115	0.0089	0.0070
Constants used:								
A_0 or d_0		3.61458	3.31569	3.09979	3.25939	4.48135	3.85114	3.68790
A_1		—	0.19558	0.48789	—	—	—	—
A_2		—	—	−0.09814	—	—	—	—
α/a^3		—	—	—	—	0.66859	0.26476	0.18860

[a] P_n, fit of $(\epsilon+2)d/(\epsilon-1)$ to polynomial of degree n in d (P_0 is the Clausius-Mosotti formula); E, Eykman formula (1-2); B, Böttcher formula (1-3); (1-4) and (1-5), see these equations in the text.
[b] Standard deviation of ϵ estimated from the deviations on the assumption that the formula is adequate.

they give clear evidence that a non-vanishing correction term $-2C$ is necessary, but they are capable of yielding only an average value of this correction term for the whole range and are not precise enough to give, by themselves, any reliable information about its variation over the range.

The two-constant fit gives

$$d_0=A_0=(3.316\pm0.022)\ \text{g/cm}^3,$$
$$-c_0'=A_1=0.196\pm0.015.$$

The uncertainty estimates are standard deviations computed by the usual method[12] from the standard deviation 0.0063 of ϵ. The errors in A_0 and A_1 are correlated; the coefficient of correlation (defined as the ratio of the mean product of the two errors to the product of the two standard deviations) is

$$\rho_{01}=-0.9964.$$

The net correction $-2C$ in (1-7) is clearly positive, but its separation into density-independent and density-dependent terms by this method is impossible or at least very uncertain. The three-constant fit gives

$$A_0=(3.10\pm0.26)\ \text{g/cm}^3,$$
$$A_1=0.49\pm0.34,$$
$$A_2=-0.10\pm0.12\ \text{cm}^3/\text{g},$$

with correlation coefficients

$$\rho_{01}=-0.9989,$$
$$\rho_{12}=-0.9991,$$
$$\rho_{20}=+0.9961.$$

The signs of A_1 and A_2 are both opposite to what one would expect from Section 1; but from the indicated standard deviations, there is no overwhelming assurance that the signs are right, even if the measurements are subject only to random error. Systematic error, if present, is not detected by this analysis.

For the same substance, Danforth gives eight points over about the same range; his ϵ-values are given only to two decimal places, whereas Chang's are given to three. We may forego the polynomial fit to ϵ and proceed to the polynomial fit to yd: degrees 0, 1, 2, 3 give[13] $\sigma=0.067, 0.018, 0.015, 0.018$ respectively (see Table II). Again the data are incapable of yielding much information except the average value of the correction to the Clausius-Mosotti formula. The two-constant fit gives

$$d_0=A_0=(2.971\pm0.068)\ \text{g/cm}^3,$$
$$-c_0'=A_1=0.429\pm0.045;$$

the correlation coefficient of the errors is

$$\rho_{01}=-0.9954.$$

The deviations between these values and those based on Chang's data are well outside the random error: if the samples were identical chemically then at least one set of measurements was subject to systematic error. The three-constant fit gives

$$d_0=A_0=(4.15\bar{}\pm0.66)\ \text{g/cm}^3,$$
$$c_0'=-A_1=+1.17\pm0.91,$$
$$A_2=(0.54\pm0.30)\ \text{cm}^3/\text{g},$$

with correlation coefficients

$$\rho_{01}=-0.9990,$$
$$\rho_{12}=-0.9991,$$
$$\rho_{20}=+0.9964.$$

[12] See E. T. Whittaker and G. Robinson, reference 11, pp. 241, 246. A similar formula, expressing the mean product of the errors in two unknowns in terms of non-diagonal elements A_{ij}, is easily derived: see D. Brunt, *The Combination of Observations* (Cambridge University Press, London, 1917), pp. 116-117.

[13] σ^2 is the sum of a term σ_1^2 due to experimental error and a term $\sigma_2^2=(1/12)\times10^{-4}$ due to rounding to the second decimal place; the latter is negligible.

TABLE II. Carbon disulfide at 30°C: data of Danforth.

d Density g/cm³	ϵ Dielectric constant	Deviation of ϵ from calculated value[a] P_0	P_1	P_2	E	B	(1–4)
1.241	2.61	+0.042	−0.036	−0.022	−0.037	−0.026	−0.029
1.291	2.74	+0.074	+0.006	+0.012	+0.003	+0.011	+0.009
1.332	2.82	+0.070	+0.012	+0.012	+0.008	+0.013	+0.012
1.394	2.94	+0.057	+0.017	+0.010	+0.013	+0.013	+0.014
1.487	3.11	+0.014	+0.007	−0.004	+0.004	−0.001	+0.002
1.550	3.23	−0.022	+0.001	−0.009	−0.001	−0.005	−0.004
1.601	3.33	−0.055	−0.006	−0.010	−0.004	−0.010	−0.007
1.689	3.52	−0.111	−0.006	+0.010	+0.003	−0.001	+0.002
σ[b]		0.067	0.018	0.015	0.015	0.015	0.015
Constants used:							
A_0 or d_0		3.61508	2.97082	4.14562	3.27199	3.99702	3.54361
A_1		—	0.42890	−1.17462	—	—	—
A_2		—	—	0.54183	—	—	—
α/a^3		—	—	—	—	0.54132	0.17670

[a] P_n, fit of $(\epsilon+2)d/(\epsilon-1)$ to polynomial of degree n in d (P_0 is the Clausius-Mosotti formula); E, Eykman formula (1–2); B, Böttcher formula (1–3); (1–4), see this equation in the text.
[b] Standard deviation of ϵ estimated from the deviations on the assumption that the formula is adequate.

Hence[14]

$$c_1' = A_0 A_2 = 2.2 \pm 1.6.$$

The constants c_0' and c_1' now have the right signs to be identified with c_0 and c_1 in Section 5 of I; the value $c_1 = 2.2 \pm 1.6$ is consistent with the approximate values 15/16 and 2 derived in I, but the value $c_0 = 1.17 \pm 0.91$ is larger than the estimate $2\alpha/a^3 = 1/4$ or $4\alpha/a^3 = 1/2$ for conducting spheres. These facts are perhaps worth mentioning, but their significance is doubtful. The only conclusions that can be drawn with any certainty are (1) that the deviations from the Clausius-Mosotti formula are significant, (2) that Eq. (1–1) or (1–7) is a satisfactory form for exhibiting the deviations, and (3) that the data are capable only of evaluating α and a mean value of $2C$ and not capable of revealing, with any certainty, the variation of C with density.

If, however, some knowledge of the general nature of this variation is provided by theory, the data may be capable of discriminating between various specific possibilities. Thus if a one- or two-constant formula is fitted to the data, and if the variance of the data is estimated as before, agreement of this estimate with the one obtained by use of polynomials of various degrees indicates that the formula is capable of fitting the data within experimental error. If the formula has a theoretical basis, the theory must be regarded as at least pragmatically successful; if it has no theoretical basis, it may still be useful as an empirical representation of the data. If it significantly fails to meet this test, it must be rejected.

The data already discussed have been fitted in this manner to several formulas; in each case such weighting factors were used that the quantity minimized was the sum of the squares of the deviations in ϵ. In the case of a formula such as (1–4), where the constants do not enter linearly, it is necessary to use a successive approximation method: provisional values of the constants are used to compute the deviations; the linear equations connecting the first-order changes in these with the changes in the constants are used in a least-squares adjustment of the constants;[15] the new values of the constants are used to compute (directly, without approximation) new values of the deviations; and so on, until successive approximations coincide. In each case σ^2 is estimated by dividing the sum of the squares of the deviations in ϵ by $n-s$, where n is the number of points and s the number of constants; values of σ are therefore directly comparable for one- and two-constant formulas, whereas the deviations themselves would not be.

Chang's data on carbon disulfide at 30°C, when treated thus, yield the following estimates of σ (cf. Table I): Clausius-Mosotti formula (fit of yd with polynomial of degree 0, see above), 0.027; Eykman formula (1–2), 0.037, actually worse than Clausius-Mosotti; Böttcher's formula (1–3), 0.012; formula (1–4), 0.0089; formula (1–5), 0.0070. In view of the discrepancies between Chang's and Danforth's data, it is quite possible that the improvement on going from (1–4) to (1–5) is fortuitous.

Danforth's data on the same substance at the same temperature give for σ (see Table II): Clausius-Mosotti, 0.067; Eykman, 0.015, better in this case; Böttcher and formula (1–4), both 0.015. His data on the same substance at 75°C give: Clausius-Mosotti, 0.044; Eykman, 0.017; Böttcher and formula (1–4), both 0.007. The data at the two temperatures were treated independently.

[14] The standard deviation σ_c of c_1' is calculated from those of A_0 and A_2, σ_0 and σ_2, and from their coefficient of correlation ρ_{20}, by means of the formula $\sigma_c^2 = A_0^2\sigma_2^2 + 2\rho_{20}A_2A_0\sigma_2\sigma_0 + A_2^2\sigma_0^2$. This formula is obtained from the first-order formula for the error in a single experiment, $\Delta c_1' = A_0\Delta A_2 + A_2\Delta A_0$, by squaring and averaging over many experiments. The correlation between the errors in A_0 and A_2 has therefore been taken into account; but since the error in A_2 is almost as large as A_2 itself, the first-order formula is not very reliable.

[15] See E. T. Whittaker and G. Robinson, reference 11, p. 214.

TABLE III. Carbon dioxide at 50°C: data of Michels and Kleerekoper.

d Density Amagat[b]	ϵ Dielectric constant	Deviation of ϵ from calculated value[a] P_0	P_1	P_2	P_3	E	B	(1–4)
24.28	1.02486	−0.00029	−0.00065	−0.00002	+0.00016	−0.00054	+0.00010	−0.00027
34.86	1.03578	−0.00046	−0.00097	−0.00011	+0.00012	−0.00083	+0.00005	−0.00045
44.37	1.04566	−0.00062	−0.00125	−0.00022	+0.00005	−0.00110	−0.00003	−0.00063
61.20	1.06343	−0.00078	−0.00163	−0.00033	−0.00003	−0.00147	−0.00009	−0.00084
72.09	1.07513	−0.00080	−0.00177	−0.00035	−0.00004	−0.00162	−0.00009	−0.00091
81.93	1.08574	−0.00085	−0.00194	−0.00041	−0.00011	−0.00181	−0.00014	−0.00102
92.19	1.09712	−0.00067	−0.00187	−0.00026	+0.00002	−0.00175	+0.00002	−0.00090
104.99	1.11124	−0.00063	−0.00197	−0.00029	−0.00003	−0.00189	−0.00001	−0.00095
116.87	1.12444	−0.00061	−0.00207	−0.00035	−0.00014	−0.00204	−0.00008	−0.00103
143.31	1.15457	−0.00024	−0.00029	−0.00022	−0.00011	−0.00202	+0.00002	−0.00089
157.11	1.17057	+0.00001	−0.00177	−0.00013	−0.00008	−0.00195	+0.00009	−0.00078
174.50	1.19098	+0.00034	−0.00155	−0.00003	−0.00006	−0.00184	+0.00016	−0.00063
200.97	1.22261	+0.00091	−0.00111	+0.00016	+0.00001	−0.00160	+0.00028	−0.00035
231.23	1.25991	+0.00197	−0.00015	+0.00072	+0.00046	−0.00086	+0.00076	+0.00037
258.13	1.29328	+0.00242	+0.00027	+0.00074	+0.00041	−0.00063	+0.00070	+0.00055
303.98	1.35175	+0.00322	+0.00116	+0.00087	+0.00050	−0.00003	+0.00071	+0.00098
324.61	1.37793	+0.00279	+0.00083	+0.00019	−0.00014	−0.00046	+0.00001	+0.00044
350.40	1.41189	+0.00288	+0.00109	+0.00006	−0.00020	−0.00028	−0.00016	+0.00047
373.61	1.44240	+0.00233	+0.00075	−0.00059	−0.00076	−0.00064	−0.00083	−0.00006
395.02	1.47205	+0.00281	+0.00148	−0.00009	−0.00015	+0.00012	−0.00032	+0.00053
419.83	1.50571	+0.00205	+0.00106	−0.00067	−0.00059	−0.00019	−0.00088	+0.00002
444.32	1.54043	+0.00212	+0.00152	−0.00022	−0.00001	+0.00049	−0.00040	+0.00047
470.70	1.57801	+0.00160	+0.00151	−0.00008	+0.00025	+0.00081	−0.00019	+0.00055
490.64	1.60671	+0.00095	+0.00130	−0.00002	+0.00037	+0.00094	−0.00008	+0.00051
520.11	1.64971	−0.00032	+0.00078	+0.00013	+0.00051	+0.00108	+0.00016	+0.00039
549.90	1.69318	−0.00272	−0.00074	−0.00032	−0.00011	+0.00045	−0.00019	−0.00048
572.36	1.72744	−0.00381	−0.00109	+0.00045	+0.00037	+0.00095	+0.00065	−0.00015
595.89	1.76244	−0.00658	−0.00299	+0.00003	−0.00053	+0.00009	+0.00030	−0.00116
σ[c]		0.00221	0.00146	0.00039	0.00033	0.00123	0.00040	0.00070
Constants used:								
A_0 or d_0		2920.52	2877.82	2959.87	2988.37	2893.57	2977.49	2927.23
A_1		—	0.0899206	−0.348629	−0.638717	—	—	—
$A_2\times10^4$		—	—	5.30918	13.7168	—	—	—
$A_3\times10^8$		—	—	—	−73.6745	—	—	—
α/a^3		—	—	—	—	—	0.23604	0.08722

[a] P_n, fit of $(\epsilon+2)d/(\epsilon-1)$ to polynomial of degree n in d (P_0 is the Clausius-Mosotti formula); E, Eykman formula (1–2); B, Böttcher formula (1–3); (1–4), see this equation in the text.
[b] The Amagat unit is so chosen, for each substance, that the density is unity at 0°C and atmospheric pressure.
[c] Standard deviation of ϵ estimated from the deviations on the assumption that the formula is adequate.

Chang's 75° data, fitted with formula (1–4), give $\sigma=0.0076$, as compared with 0.0088 at 30°, the data at each temperature being treated independently. When the whole group of data is fitted to a single curve the fit is appreciably worse: $\sigma=0.0098$.

3. CARBON DIOXIDE

As representative data on a gas at high pressure, I have used the data of Michels and Kleerekoper[16] on carbon dioxide at 49.71°C. Here there are 28 points; the number of points and the precision of the data are sufficient to yield more conclusive results than in the previous cases. The polynomial fit to yd gives, for degrees 0, 1, 2, and 3, $\sigma=0.0022$, 0.0015, 0.00039, and 0.00033 respectively (see Table III). The improvement by going from degree 1 to degree 2 is clearly significant, and the improvement from degree 2 to degree 3 probably so (the deviations for degree 2 show a systematic trend; see Table III). Degree 2 (3 constants) gives

$$d_0= A_0=2959.9\pm4.8 \text{ Amagat},$$
$$c_0'=-A_1=0.349\pm0.024,$$
$$A_2=(5.31\pm0.28)\times10^{-4} \text{ Amagat}^{-1},$$

with correlation coefficients

$$\rho_{01}=-0.9656,$$
$$\rho_{12}=-0.9849,$$
$$\rho_{20}=+0.9090,$$

whence

$$c_1'=A_0A_2=1.571\pm0.086.$$

Degree 3 (4 constants) gives

$$d_0= A_0=2988.4\pm7.8 \text{ Amagat},$$
$$c_0'=-A_1=0.639\pm0.071,$$
$$A_2=(13.7\pm2.0)\times10^{-4} \text{ Amagat}^{-1},$$
$$A_3=(-74\pm17)\times10^{-8} \text{ Amagat}^{-2},$$

with correlation coefficients

$$\rho_{01}=-0.9626,$$
$$\rho_{02}=+0.9084,$$
$$\rho_{03}=-0.8598,$$
$$\rho_{12}=-0.9864,$$
$$\rho_{13}=+0.9610,$$
$$\rho_{23}=-0.9931,$$

whence

$$c_1'=A_0A_2=4.10\pm0.18,$$
$$c_2'=-A_0^2A_3=6.6\pm1.6.$$

[16] A. Michels and L. Kleerekoper, Physica **6**, 586–590 (1939).

Either fit gives constants with the signs and orders of magnitude predicted by the various approximate forms of the theory.

The value of c_1' by degree 2, 1.571, is closer to the Böttcher value 2 than to the Kirkwood value (Eq. (1–4)) 15/16. It is therefore not surprising that a direct fit to Böttcher's formula is more successful than a fit to formula (1–4), giving $\sigma=0.00040$ against the latter's 0.00070. Going over to the quadratic formula (1–6) does not improve the fit in this case; the constants c_1 and c_2 of this formula are rather far from the values of c_1' and c_2' obtained by analysis of the data. All these formulas are more reliable than the Clausius-Mosotti, which is the polynomial of degree zero ($\sigma=0.0022$). Eykman's formula (1–2) gives $\sigma=0.0012$.

4. CONCLUSIONS

For future analyses of experimental data, it is recommended that not the Clausius-Mosotti function but its reciprocal, $(\epsilon+2)d/(\epsilon-1)$, be used. The departure of this quantity from the Clausius-Mosotti value d_0 is what one can hope to calculate directly from molecular distribution functions when they become known with sufficient completeness. In this recommendation the use of $\epsilon-1$ as denominator is more important than the use of $\epsilon+2$ in the numerator: the function $d/(\epsilon-1)$ or $\epsilon d/(\epsilon-1)$, or any linear combination of them, would do equally well.

It is further recommended that for the time being this function be merely expressed as a polynomial in the density, to as many terms as are significant. The weights to be assigned to the various experimental values should correspond to the estimated relative precisions of the measurements at various values of ϵ; and the numerical values of the polynomial coefficients should be accompanied by estimates of their uncertainties and of the coefficients of correlation between them (or of the mean squares and products of the errors), in order that when further quantities are calculated from them the uncertainties in these further quantities may be easily estimated. The coefficients in this polynomial can be given a fairly direct theoretical interpretation and can eventually be calculated from molecular theory.

Formulas of special form, such as Eykman's and Böttcher's, can be fitted to the data more or less successfully; but no one of these has either enough theoretical basis or (if the data analyzed here are representative) enough empirical reliability to justify its use in preference to the straightforward method recommended. Within the precision of present data, use of such special forms is equivalent to specification of auxiliary conditions to be imposed on the coefficients in the polynomial; and anything that can be accomplished by their use can also be accomplished by merely assigning fixed numerical values to one or more of the constants c_0', c_1', etc. Thus it may turn out upon analysis of all available data that the second-degree polynomial, i.e. Eq. (1–1) with $(d/d_0)^2$ neglected, gives sufficient precision for practical purposes if c_0' and c_1' are assigned fixed values, independent of the fluid (at least for a large class of fluids). From the limited number of data analyzed here, it appears that the best value of c_0' is probably somewhat larger than the value 1/4 based on a very crude model, and that the best value of c_1' may be intermediate between the Kirkwood value 15/16 and the Böttcher value 2.

Tables I–III show the actual deviations computed by some of the formulas, together with the experimental data and the constants used in the formulas. Formulas (1–3) (Böttcher), (1–4), and (1–5) yield somewhat different values of $d_0(=3m_0/4\pi\alpha)$ and $2\alpha/a^3$. Values of α and a^3 calculated from these are of the expected order of magnitude.

In a recent empirical study, Rosen[17] has fitted dielectric constant and refractive index data on a number of fluids (polar as well as non-polar) with a formula equivalent to the first two terms of Eq. (2–3). His use of $(\epsilon+2)/(\epsilon-1)$ rather than of its reciprocal is supported by the present analysis of data and by the theory of I; but it appears that a third term is already significant in some modern data. It will probably become more clearly significant as experimental techniques continue to improve.

[17] Joseph S. Rosen, J. Chem. Physics **17**, 1192–1197 (1949). Rosen's values of A_0 and A_1 (his m and b) for carbon disulfide at 30° differ slightly from those given here because of the different weights used.

THE JOURNAL OF CHEMICAL PHYSICS VOLUME 18, NUMBER 9 SEPTEMBER, 1950

The Vibration-Rotation Energies of the Plane Symmetrical $X_2Y_2X_2$ Molecular Model

ROBERT C. HERMAN
Applied Physics Laboratory, The Johns Hopkins University, Silver Spring, Maryland*

AND

WAVE H. SHAFFER
Mendenhall Laboratory of Physics, The Ohio State University, Columbus, Ohio

(Received June 12, 1950)

The quantum-mechanical calculation of the rotation-vibration energies of the plane symmetrical $X_2Y_2X_2$ molecular model is carried out to second-order approximation so as to include contributions arising from cubic and quartic anharmonic terms in the potential function, Coriolis interactions, centrifugal stretching, and changes in the rotational constants produced by vibration.

I. INTRODUCTION

THE plane symmetrical molecular model $X_2Y_2X_2$ which belongs to the point group $D_{2h}\equiv V_h$ is exemplified by ethylene, C_2H_4, tetrachloroethylene, C_2Cl_4, as well as other molecules. Many experimental and theoretical studies have been reported for molecules of this type and an extensive set of references has been collected by Herzberg.[1] The purpose of the present paper is to give a unified treatment of this molecular model and to derive the vibration-rotation energies. The calculations are extended to second-order approximation so as to include contributions arising from cubic and quartic anharmonic terms in the potential function, all types of Coriolis interactions, centrifugal stretching, and changes in the rotational constants produced by vibration.

II. THE CLASSICAL VIBRATION PROBLEM

The equilibrium configuration of the plane symmetrical $X_2Y_2X_2$ molecular model is shown in Fig. 1. A right-handed body-fixed rectangular coordinate system xyz, with origin at the center of mass of the molecule, is so oriented that the axes are the principal axes of inertia. The equilibrium coordinates and masses of the respective atoms are given in Table I.

In the equilibrium configuration the model belongs to the symmetry point group $D_{2h}\equiv V_h$. The instantaneous positions of the atoms are described during vibration by a right-handed body fixed rectangular coordinate system which coincides in the equilibrium configuration with the system described above. The instantaneous position of the rth atom is given by

$$(x_r, y_r, z_r)=(x_{0r}+x_r', y_{0r}+y_r', z_{0r}+z_r'),$$

where x_r', y_r', and z_r' denote components of displacement from the equilibrium position. There are 18 displacement coordinates of which only 12, corresponding to the number of vibrational degrees of freedom, are linearly independent since six linear relations are given by the Eckart conditions[2,3] that (a) the coordinate origin remains at the center of mass and (b) none of the modes of vibration results in angular momentum of rotation of the molecular framework as a whole inside the coordinate system. A suitable set of 12 linearly independent intermediate generalized coordinates, which are mutually orthogonal and of proper symmetry, is:

$$\Gamma_h=(f_6\pm f_5)/2, \tag{1a}$$

Γ_h being equal to σ_9 and ζ_{11} when f is equal to y' and z' respectively, using the + sign; and equal to η_5 and ξ_1 when f is equal to y' and z' respectively, using the minus sign;

$$\Gamma_h=[(f_3-f_1)\pm(f_4-f_2)]/2, \tag{1b}$$

Γ_h being equal to η_6 and ξ_3 when f is equal to y' and z' respectively, using the + sign, and equal to ρ_4, ζ_{12}, and σ_{10} when f is equal to x', y', and z' respectively, using the minus sign; and

$$\begin{aligned}\xi_2&=(y_2'-y_1'+y_4'-y_3')/2,\\ \theta_7&=\{(x_1'+x_2'+x_3'+x_4')-(M/m)(x_5'+x_6')\}/4,\\ \chi_8&=\{(x_1'+x_2'-x_3'-x_4')+[Ma_0/(mb_0)](x_6'-x_5')\},\end{aligned} \tag{1c}$$

where ξ denotes a coordinate belonging to symmetry

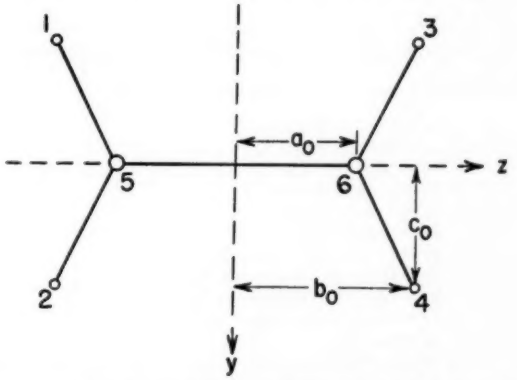

FIG. 1. Equilibrium configuration of the plane symmetrical $X_2Y_2X_2$ molecular model. The x-axis points upward, perpendicular to the plane of the molecule.

* A portion of the work described in this paper was supported by the U. S. Navy, Bureau of Ordnance under Contract N-Ord-7386.

[1] G. Herzberg, *Infrared and Raman Spectra of Polyatomic Molecules* (D. Van Nostrand Company, Inc., New York, 1945).

[2] C. Eckart, Phys. Rev. 47, 552 (1932).

[3] E. B. Wilson and J. B. Howard, J. Chem. Phys. 4, 260 (1936).

type A_g, η to B_{1g}, ζ to B_{3u}, σ to B_{2u}, ρ to A_u, θ to B_{1u}, and χ to B_{2g}. The particular numerical subscripts used for each of the symmetry types were chosen consistent with the notation for the normal frequencies given by Herzberg.[1] The above relations and the Eckart conditions make possible an inverse transformation giving the 18 displacement coordinates x_r', y_r', and z_r' in terms of the intermediate generalized coordinates defined in Eq. (1).†

The kinetic energy of vibration, T_v, is given in terms of the generalized coordinates by:

$$\begin{aligned}2T_v=&\mu_1\dot{\xi}_1^2+\mu_2\dot{\xi}_2^2+\mu_3\dot{\xi}_3^2+\mu_5\dot{\eta}_5^2+\mu_6\dot{\eta}_6^2+2\mu_{5,6}\dot{\eta}_5\dot{\eta}_6\\&+\mu_{11}\dot{\zeta}_{11}^2+\mu_{12}\dot{\zeta}_{12}^2+\mu_9\dot{\sigma}_9^2+\mu_{10}\dot{\sigma}_{10}^2\\&+\mu_4\dot{\rho}_4^2+\mu_7\dot{\theta}_7^2+\mu_8\dot{\chi}_8^2,\end{aligned}\tag{2}$$

where

$$\begin{aligned}&\mu_1=2M,\\&\mu_2=\mu_3=\mu_4=\mu_{10}=\mu_{12},\\&\mu_5=\mu_1+\mu_2\phi_5^2,\\&\mu_6=\mu_2(\phi_6^2+1),\\&\mu_7=\phi_7(M+2m),\\&\mu_8=\mu_2(1+2\phi_8^2\phi_9),\\&\mu_9=\mu_{11}=\phi_9^2\mu_7,\\&\mu_{5,6}=\mu_2\phi_5\phi_6,\end{aligned}\tag{2a}$$

with

$$\begin{aligned}&\phi_5=Ma_0/(mc_0),\\&\phi_6=b_0/c_0,\\&\phi_7=\phi_9^{-1}=\phi_{11}^{-1}=m/M,\\&\phi_8=mb_0/(Ma_0).\end{aligned}\tag{2b}$$

The quadratic potential function, U_0, is given by:

$$\begin{aligned}2U_0=&k_1\xi_1^2+k_2\xi_2^2+k_3\xi_3^2+2k_{1,2}\xi_1\xi_2+2k_{1,3}\xi_1\xi_3\\&+2k_{2,3}\xi_2\xi_3+k_5\eta_5^2+k_6\eta_6^2+2k_{5,6}\eta_5\eta_6+k_{11}\zeta_{11}^2\\&+k_{12}\zeta_{12}^2+2k_{11,12}\zeta_{11}\zeta_{12}+k_9\sigma_9^2+k_{10}\sigma_{10}^2\\&+2k_{9,10}\sigma_9\sigma_{10}+k_4\rho_4^2+k_7\theta_7^2+k_8\chi_8^2,\end{aligned}\tag{3}$$

in which the k's are generalized force constants.

The Lagrange secular determinant $|\lambda T_v-U_0|=0$ is of twelfth order but is factored by the foregoing procedure into seven steps each of which is associated with one symmetry type of the point group D_{2h}. The subscripts i, j, k, l, m, n, and s are employed throughout this paper to denote the normal frequencies belonging to each symmetry type in the following manner: $i=1, 2, 3$ for type A_g; $j=5, 6$ for type B_{1g}; $k=11, 12$ for type B_{3u}; $l=9, 10$ for type B_{2u}; $m=4$ for type A_u; $n=7$ for type B_{1u}; and $s=8$ for type B_{2g}. The transformation from the intermediate symmetry coordinates, defined in Eq. (1), to the normal coordinates Q_h are given by the following relations where the subscript t is used to designate the intermediate coordinates:

$$\Gamma_t=\sum_h n_{th}Q_h,\tag{4}$$

where for type A_g, $\Gamma=\xi$, $t=1, 2, 3$, $h=1, 2, 3$; for type B_{1g}, $\Gamma=\eta$, $t=5, 6$, $h=5, 6$; etc.

In terms of the normal coordinates

$$T_v=(1/2)\sum_{h=1}^{12}\dot{Q}_h^2,\tag{5}$$

and

$$U_0=(1/2)\sum_{h=1}^{12}\lambda_hQ_h^2=2\pi^2c^2\sum_{h=1}^{12}\omega_h^2Q_h^2,\tag{6}$$

where the roots λ of the secular determinant are related to the normal frequencies ω (cm^{-1}) by the expression $\lambda=4\pi^2c^2\omega^2$ if c is the velocity of light in cm/sec. The discussion of vibration-rotation energies is simplified by the use of dimensionless normal coordinates q_h defined by

$$Q_h=[h/(2\pi c\omega_h)]^{\frac{1}{2}}q_h.\tag{7}$$

The most general cubic portion, U_1, of the anharmonic potential function of the plane symmetrical $X_2Y_2X_2$ model is given by:

$$\begin{aligned}U_1/hc=&\sum_i\beta_{iii}q_i^3+\sum_i\sum_{i'}\beta_{iii'}q_i^2q_{i'}+\beta_{ii'i''}q_iq_{i'}q_{i''}\\&+\sum_j\sum_i\beta_{jji}q_j^2q_i+\sum_i\beta_{jj'i}q_jq_{j'}q_i\\&+\sum_k\sum_i\beta_{kki}q_k^2q_i+\sum_i\beta_{kk'i}q_kq_{k'}q_i\\&+\sum_l\sum_i\beta_{lli}q_l^2q_i+\sum_i\beta_{ll'i}q_lq_{l'}q_i\\&+\sum_i\beta_{mmi}q_m^2q_i+\sum_i\beta_{nni}q_n^2q_i+\sum_i\beta_{ssi}q_s^2q_i\\&+\sum_j\beta_{mnj}q_mq_nq_j+\sum_k\beta_{nsk}q_nq_sq_k\\&+\sum_l\beta_{msl}q_mq_sq_l+\sum_j\sum_k\sum_l\beta_{jkl}q_jq_kq_l.\end{aligned}\tag{8}$$

The quartic portion, U_2, of the anharmonic potential function which contributes to the allowed energies to second-order approximation is given by:

$$\begin{aligned}U_2/hc=&\sum_{h=1}^{12}\gamma_{hhhh}q_h^4+\sum_h\sum_{h'\neq h}\gamma_{hhh'h'}q_h^2q_{h'}^2\\&+\sum_h\sum_{h''}\gamma_{hhh''h''}q_h^2q_{h''}^2.\end{aligned}\tag{9}$$

In Eq. (8) primed and unprimed subscripts in a given

TABLE I.

atom	r	m_r	x_{0r}	y_{0r}	z_{0r}
X	1	m	0	$-c_0$	$-b_0$
X	2	m	0	c_0	$-b_0$
X	3	m	0	$-c_0$	b_0
X	4	m	0	c_0	b_0
Y	5	M	0	0	$-a_0$
Y	6	M	0	0	a_0

† The displacement coordinates are as follows:

$$\begin{aligned}x_1'&=(-\rho_4+\theta_7+\chi_8)/2,\\x_2'&=(\rho_4+\theta_7+\chi_8)/2,\\x_3'&=(\rho_4+\theta_7-\chi_8)/2,\\x_4'&=(-\rho_4+\theta_7-\chi_8)/2,\\x_5'&=-\phi_7\theta_7-\phi_8\chi_8,\\x_6'&=-\phi_7\theta_7+\phi_8\chi_8,\\y_1'&=(-\zeta_{12}-\xi_2-\phi_9\sigma_9-\eta_6)/2,\\y_2'&=(\zeta_{12}+\xi_2-\phi_9\sigma_9-\eta_6)/2,\\y_3'&=(\zeta_{12}-\xi_2-\phi_9\sigma_9+\eta_6)/2,\\y_4'&=(-\zeta_{12}+\xi_2-\phi_9\sigma_9+\eta_6)/2,\\y_5'&=\sigma_9-\eta_5,\\y_6'&=\sigma_9+\eta_5,\\z_1'&=(-\phi_{11}\zeta_{11}-\phi_5\eta_5-\xi_3-\phi_6\eta_6-\sigma_{10})/2,\\z_2'&=(-\phi_{11}\zeta_{11}+\phi_5\eta_5-\xi_3+\phi_6\eta_6+\sigma_{10})/2,\\z_3'&=(-\phi_{11}\zeta_{11}-\phi_5\eta_5+\xi_3-\phi_6\eta_6+\sigma_{10})/2,\\z_4'&=(-\phi_{11}\zeta_{11}+\phi_5\eta_5+\xi_3+\phi_6\eta_6-\sigma_{10})/2,\\z_5'&=\zeta_{11}-\xi_1,\\z_6'&=\zeta_{11}+\xi_1,\end{aligned}$$

where the ϕ are given in Eq. (2b).

summation denote coordinates of the same symmetry type. In Eq. (9) the unprimed and single primed subscripts refer to coordinates of the same symmetry type whereas the unprimed and double primed subscripts in the last summation denote coordinates of different symmetry types. Permutations of a given set of subscripts are not allowed. The most general anharmonic potential function contains many additional quartic terms which are of odd degree in one or more coordinates. These terms are not given since ordinarily they do not contribute to the allowed energies up to second-order approximation.

The components of internal angular momentum of vibration p_x, p_y, and p_z are defined as $p_x=\sum_r m_r(y_r'\dot{z}_r'-z_r'\dot{y}_r')$, etc., and may be expressed in terms of the dimensionless normal coordinates q_h and conjugate momenta p_h as follows:[3-6]

$$\begin{aligned}
p_x&=\sum_i\sum_j \xi_{ij}[(\omega_i/\omega_j)^{\frac{1}{2}}q_jp_i-(\omega_j/\omega_i)^{\frac{1}{2}}q_ip_j]\\
&\quad+\sum_k\sum_l \xi_{kl}[(\omega_k/\omega_l)^{\frac{1}{2}}q_lp_k-(\omega_l/\omega_k)^{\frac{1}{2}}q_kp_l],\\
p_y&=\sum_k \eta_{nk}[(\omega_n/\omega_k)^{\frac{1}{2}}q_kp_n-(\omega_k/\omega_n)^{\frac{1}{2}}q_np_k]\\
&\quad+\sum_l \eta_{lm}[(\omega_l/\omega_m)^{\frac{1}{2}}q_mp_l-(\omega_m/\omega_l)^{\frac{1}{2}}q_lp_m]\\
&\quad+\sum_i \eta_{si}[(\omega_s/\omega_i)^{\frac{1}{2}}q_ip_s-(\omega_i/\omega_s)^{\frac{1}{2}}q_sp_i],\\
p_z&=\sum_j \zeta_{js}[(\omega_j/\omega_s)^{\frac{1}{2}}q_sp_j-(\omega_s/\omega_j)^{\frac{1}{2}}q_jp_s]\\
&\quad+\sum_l \zeta_{ln}[(\omega_l/\omega_n)^{\frac{1}{2}}q_np_l-(\omega_n/\omega_l)^{\frac{1}{2}}q_lp_n]\\
&\quad+\sum_k \zeta_{mk}[(\omega_m/\omega_k)^{\frac{1}{2}}q_kp_m-(\omega_k/\omega_m)^{\frac{1}{2}}q_mp_k],
\end{aligned}\tag{10}$$

where the Coriolis parameters are given by

$$\begin{aligned}
\xi_{ij}&=n_{5j}(m\phi_5n_{2i}-\mu_1n_{1i})+n_{6j}(m\phi_6n_{2i}-mn_{3i}),\\
\xi_{kl}&=mn_{12,k}n_{10,l}-\mu_{11}n_{9l}n_{11,k},\\
\eta_{lm}&=mn_4n_{10,l},\\
\eta_{nk}&=(M+2m)n_{7n}n_{11,k},\\
\eta_{si}&=mn_{8s}[n_{3i}-(2b_0/a_0)n_{1i}],\\
\zeta_{js}&=mn_{8s}[n_{6j}-(2b_0/a_0)n_{5j}],\\
\zeta_{ln}&=(M+2m)n_{7n}n_{9l},\\
\zeta_{mk}&=mn_{4m}n_{12,k}.
\end{aligned}\tag{11}$$

III. VIBRATION-ROTATION ENERGIES

The quantum-mechanical Hamiltonian is set up according to the method of Wilson and Howard[3] and, after contact transformation of the Hamiltonian according to the method of Thomas,[7] Nielsen,[5] and Shaffer,[8] a perturbation calculation of the allowed energies is made.‡

For the vibrating rotating model the classical rotational Hamiltonian is

$$\begin{aligned}
H_R=(1/2)\{&\mu_{xx}(P_x-p_x)^2+\mu_{yy}(P_y-p_y)^2\\
&+\mu_{zz}(P_z-p_z)^2+2\mu_{yz}(P_y-p_y)(P_z-p_z)\},
\end{aligned}\tag{12}$$

where P_x, P_y, and P_z are the components of total angular momentum and the coefficients of inertia μ_{xx}, etc., are expressed as follows:[6] **

$$\begin{aligned}
\mu_{xx}&=I_{ex}^{-1}\{1-\textstyle\sum_i \omega_i^{-\frac{1}{2}}a_iq_i\\
&\qquad+\textstyle\sum_h \omega_h^{-1}(a_h^2-a_{hh})q_h^2+\cdots\},\\
\mu_{yy}&=I_{ey}^{-1}\{1-\textstyle\sum_i \omega_i^{-\frac{1}{2}}b_iq_i\\
&\qquad+\textstyle\sum_h \omega_h^{-1}(b_h^2-b_{hh}+d_h^2)q_h^2+\cdots\},\\
\mu_{zz}&=I_{ez}^{-1}\{1-\textstyle\sum_i \omega_i^{-\frac{1}{2}}c_iq_i\\
&\qquad+\textstyle\sum_h \omega_h^{-1}(c_h^2-c_{hh}+d_h^2)q_h^2+\cdots\},\\
\mu_{xy}&=\mu_{zz}=0,\\
\mu_{yz}&=(I_{ey}I_{ez})^{-\frac{1}{2}}\{\textstyle\sum_j \omega_j^{-\frac{1}{2}}d_jq_j+\cdots\}.
\end{aligned}\tag{13}$$

The equilibrium values of the moments of inertia I_{ex}, etc., are

$$\begin{aligned}
I_{ex}&=4m(b_0^2+c_0^2)+2Ma_0^2,\\
I_{ey}&=4mb_0^2+2Ma_0^2,\\
I_{ez}&=4mc_0^2.
\end{aligned}\tag{13a}$$

The coefficients a_i, a_{ii}, etc., in Eq. (13) are defined in the following equations in which $\tau=\hbar/(2\pi c)$; the quantities n_{th} are the transformation coefficients in Eq. (4); the quantities $\xi_{hh'}$, $\eta_{hh'}$, and $\zeta_{hh'}$ are the Coriolis parameters defined in Eq. (11) and the equilibrium rotational constants are $B_{ex}=h/(8\pi^2cI_{ex})$, $B_{ey}=h/(8\pi^2cI_{ey})$, and $B_{ez}=h/(8\pi^2cI_{ez})$:

$$\begin{aligned}
a_i&=4\tau^{-\frac{1}{2}}B_{ex}(\mu_1a_0n_{1i}+2\mu_2c_0n_{2i}+2\mu_3b_0n_{3i}),\\
b_i&=4\tau^{-\frac{1}{2}}B_{ey}(\mu_1a_0n_{1i}+2\mu_3b_0n_{3i}),\\
c_i&=8\tau^{-\frac{1}{2}}B_{ez}\mu_2c_0n_{2i},\\
a_h&=b_h=c_h=0,\quad h\neq i,\\
a_{ii}&=2B_{ex}(\mu_1n_{1i}^2+\mu_2n_{2i}^2+\mu_3n_{3i}^2-\xi_{i5}^2-\xi_{i6}^2),\\
b_{ii}&=2B_{ey}(\mu_1n_{1i}^2+\mu_3n_{3i}^2-\eta_{8i}^2),\\
c_{ii}&=2B_{ez}\mu_2n_{2i}^2,\\
a_{jj}&=2B_{ex}(\mu_5n_{5j}^2+\mu_6n_{6j}^2+2\mu_{5,6}n_{5j}n_{6j}-\xi_{1j}^2-\xi_{2j}^2-\xi_{3j}^2),\\
b_{jj}&=2B_{ey}(m\phi_5^2n_{5j}^2+m\phi_6^2n_{6j}^2+2\mu_{5,6}n_{5j}n_{6j}),\\
c_{jj}&=2B_{ez}(2Mn_{5j}^2+mn_{6j}^2-\zeta_{j8}^2),\\
a_{kk}&=2B_{ex}(\mu_{11}n_{11,k}^2+\mu_{12}n_{12,k}^2-\xi_{k,9}^2-\xi_{k,10}^2),\\
b_{kk}&=2B_{ey}(\mu_{11}n_{11,k}^2-\eta_{7k}^2),\\
c_{kk}&=2B_{ez}(\mu_{12}n_{12,k}^2-\zeta_{4k}^2),\\
a_{ll}&=2B_{ex}(\mu_9n_{9l}^2+\mu_{10}n_{10,l}^2-\xi_{11,l}^2-\xi_{12,l}^2),\\
b_{ll}&=2B_{ey}(\mu_{10}n_{10,l}^2-\eta_{l,4}^2),\\
c_{ll}&=2B_{ez}(\mu_9n_{9l}^2-\zeta_{l,7}^2),\\
a_{44}&=4B_{ex}\mu_4n_{44}^2,\\
b_{44}&=2B_{ey}(\mu_4n_{44}^2-\eta_{9,4}^2-\eta_{10,4}^2),\\
c_{44}&=2B_{ez}(\mu_4n_{44}^2-\eta_{4,11}^2-\eta_{4,12}^2),\\
a_{77}&=4B_{ex}\mu_7n_{77}^2,\\
b_{77}&=2B_{ey}(\mu_7n_{77}^2-\eta_{7,11}^2-\eta_{7,12}^2),\\
c_{77}&=2B_{ez}(\mu_7n_{77}^2-\zeta_{9,7}^2-\zeta_{10,7}^2),\\
a_{88}&=4B_{ex}\mu_8n_{88}^2,\\
b_{88}&=2B_{ey}(\mu_8n_{88}^2-\eta_{8,1}^2-\eta_{8,2}^2-\eta_{8,3}^2),\\
c_{88}&=2B_{ez}(\mu_8n_{88}^2-\zeta_{5,8}^2-\zeta_{6,8}^2),\\
d_j&=8\tau^{-\frac{1}{2}}B_{ey}{}^{\frac{1}{2}}B_{ez}{}^{\frac{1}{2}}(Ma_0n_{5j}+mb_0n_{6j}),\\
d_h&=0,\quad h\neq j.
\end{aligned}\tag{14}$$

The subscript notation is that used in Section I. Cross-product terms in Eq. (13) and the corresponding coefficients in Eq. (14) have been omitted for the sake of brevity since they do not ordinarily contribute to the energies up to second-order approximation.

[4] H. Margenau and G. M. Murphy, *The Mathematics of Physics and Chemistry* (D. Van Nostrand Company, Inc., New York, 1943).
[5] H. H. Nielsen, Phys. Rev. **60**, 794 (1941).
[6] R. C. Herman and W. H. Shaffer, J. Chem. Phys. **16**, 453 (1948).
[7] L. H. Thomas, J. Chem. Phys. **10**, 532, 538 (1942).
[8] Shaffer, Thomas, and Nielsen, Phys. Rev. **56**, 895, 1051 (1939).
‡ This calculation is greatly facilitated by tables given in reference 6.

** The subscript notation is that defined in Section II.

The zero-, first-, and second-order parts of the quantum-mechanical Hamiltonian operator, set up according to the method of Wilson and Howard,[3] are formally similar to those of the tetrahedral X_2YZ_2 molecular model.[9] A perturbation calculation yields the purely vibrational contribution E_v and a modified rotational Hamiltonian H_R in which the rotational constants B_{ez}, etc., are replaced by B_{ev}, etc., effective in the vibrational states.[5-8]

The purely vibrational contribution to the eigenvalues of the vibration-rotation Hamiltonian is $E_v=hcG$ where $G(\text{cm}^{-1})$ can be written in the form

$$G=G_0+\sum_{h=1}^{12}\omega_h(v_h+\tfrac{1}{2})+\sum_h[G_{hh}(v_h+\tfrac{1}{2})^2+\sum_{h'<h}G_{hh'}(v_h+\tfrac{1}{2})(v_{h'}+\tfrac{1}{2})], \quad (15)$$

and v_h denotes the vibrational quantum number which is associated with the hth normal frequency ω_h.

If for convenience the following abbreviations are introduced

$$\begin{aligned}
D_{hh'h''}&=[(\omega_h+\omega_{h'}+\omega_{h''})(\omega_h-\omega_{h'}-\omega_{h''})\\
&\quad\times(\omega_h-\omega_{h'}+\omega_{h''})(\omega_h+\omega_{h'}-\omega_{h''})]^{-1},\\
E_{hh'}&=[(8\omega_h^2-3\omega_{h'}^2)/(4\omega_h^2-\omega_{h'}^2)],\\
F_{hh'}&=[2\omega_h/(4\omega_h^2-\omega_{h'}^2)],\\
C_{hh'h''}&=[\omega_h(\omega_h^2-\omega_{h'}^2-\omega_{h''}^2)D_{hh'h''}/2],\\
K_{hh'}&=[(\omega_h/\omega_{h'})+(\omega_{h'}/\omega_h)],\\
H_{hh'}&=[\omega_{h'}/(4\omega_h^2-\omega_{h'}^2)],
\end{aligned}$$

then the quantities G_0, G_{hh}, and $G_{hh'}$ are given by the following relations:[6] ††

$$\begin{aligned}
G_{ii}&=(1/4)\{6\gamma_{iiii}-15\omega_i^{-1}\beta_{iii}^2-\textstyle\sum_{i'}\omega_{i'}^{-1}E_{ii'}\beta_{iii'}^2\},\\
G_{jj}&=(1/4)\{6\gamma_{jjjj}-\textstyle\sum_i\omega_i^{-1}E_{ji}\beta_{jji}^2\},\\
G_{kk}&=(1/4)\{6\gamma_{kkkk}-\textstyle\sum_i\omega_i^{-1}E_{ki}\beta_{kki}^2\},\\
G_{ll}&=(1/4)\{6\gamma_{llll}-\textstyle\sum_i\omega_i^{-1}E_{li}\beta_{lli}^2\},\\
G_{mm}&=(1/4)\{6\gamma_{mmmm}-\textstyle\sum_i\omega_i^{-1}E_{mi}\beta_{mmi}^2\},\\
G_{nn}&=(1/4)\{6\gamma_{nnnn}-\textstyle\sum_i\omega_i^{-1}E_{ni}\beta_{nni}^2\},\\
G_{ss}&=(1/4)\{6\gamma_{ssss}-\textstyle\sum_i\omega_i^{-1}E_{si}\beta_{ssi}^2\},\\
G_{ii'}&=\{\gamma_{iii'i'}-3\omega_i^{-1}\beta_{iii}\beta_{ii'i'}-3\omega_{i'}^{-1}\beta_{i'i'i'}\beta_{i'ii}\\
&\quad-\textstyle\sum_{i''}(\omega_{i''}^{-1}\beta_{iii''}\beta_{i'i'i''})-F_{ii'}\beta_{iii'}^2\\
&\quad-F_{i'i}\beta_{i'i'i}^2-\textstyle\sum_{i''}C_{i'i''i}\beta_{ii'i''}^2\},\\
G_{ij}&=\{\gamma_{iijj}-3\omega_i^{-1}\beta_{iii}\beta_{jji}-F_{ji}\beta_{jji}^2+K_{ij}\xi_{ij}^2B_{ez}\\
&\quad-\textstyle\sum_{j'}C_{j'ji}\beta_{ijj'}^2\},\\
G_{ik}&=\{\gamma_{iikk}-3\omega_i^{-1}\beta_{iii}\beta_{kki}-F_{ki}\beta_{kki}^2\\
&\quad-\textstyle\sum_{k'}C_{k'ki}\beta_{ikk'}^2\},\\
G_{il}&=\{\gamma_{iill}-3\omega_i^{-1}\beta_{iii}\beta_{lli}-F_{li}\beta_{lli}^2\\
&\quad-\textstyle\sum_{l'}C_{l'li}\beta_{ill'}^2\},
\end{aligned}$$

$$\begin{aligned}
G_{im}&=\{\gamma_{iimm}-3\omega_i^{-1}\beta_{iii}\beta_{mmi}-F_{mi}\beta_{mmi}^2\},\\
G_{in}&=\{\gamma_{iinn}-3\omega_i^{-1}\beta_{iii}\beta_{nni}-F_{ni}\beta_{nni}^2\},\\
G_{is}&=\{\gamma_{iiss}-3\omega_i^{-1}\beta_{iii}\beta_{ssi}-F_{si}\beta_{ssi}^2+K_{si}\eta_{si}^2B_{ey}\},\\
G_{jj'}&=\{\gamma_{jjj'j'}-\textstyle\sum_i C_{ijj'}\beta_{ijj'}^2\},\\
G_{jk}&=\{\gamma_{jjkk}-\textstyle\sum_l C_{ljk}\beta_{jkl}^2\},\\
G_{jl}&=\{\gamma_{jjll}-\textstyle\sum_k C_{klj}\beta_{jkl}^2\},\\
G_{kk'}&=\{\gamma_{kkk'k'}-\textstyle\sum_i C_{ikk'}\beta_{ikk'}^2\},\\
G_{kl}&=\{\gamma_{kkll}+K_{kl}\xi_{kl}^2B_{ez}-\textstyle\sum_j C_{jkl}\beta_{jkl}^2\},\\
G_{ll'}&=\{\gamma_{lll'l'}-\textstyle\sum_i C_{ill'}\beta_{ill'}^2\},\\
G_{mj}&=\{\gamma_{mmjj}-C_{nmj}\beta_{mnj}^2\},\\
G_{mk}&=\{\gamma_{mmkk}+K_{mk}\zeta_{mk}^2B_{ez}\},\\
G_{ml}&=\{\gamma_{mmll}+K_{lm}\eta_{lm}^2B_{ey}-C_{sml}\beta_{msl}^2\},\\
G_{mn}&=\{\gamma_{mmnn}-\textstyle\sum_j C_{jmn}\beta_{mnj}^2\},\\
G_{ms}&=\{\gamma_{mmss}-\textstyle\sum_l C_{lms}\beta_{msl}^2\},\\
G_{nj}&=\{\gamma_{nnjj}-C_{mnj}\beta_{mnj}^2\},\\
G_{nk}&=\{\gamma_{nnkk}+K_{nk}\eta_{nk}^2B_{ey}-C_{snk}\beta_{nsk}^2\},\\
G_{nl}&=\{\gamma_{nnll}+K_{ln}\zeta_{ln}^2B_{ez}\},\\
G_{ns}&=\{\gamma_{nnss}-\textstyle\sum_k C_{kns}\beta_{nsk}^2\},\\
G_{sj}&=\{\gamma_{ssjj}+K_{js}\zeta_{js}^2B_{ez}\},\\
G_{sk}&=\{\gamma_{sskk}-C_{nsk}\beta_{nsk}^2\},\\
G_{sl}&=\{\gamma_{ssll}-C_{msl}\beta_{msl}^2\}.
\end{aligned} \quad (16)$$

The effective rotational Hamiltonian, H_R, is given by

$$H_R=(hc/\hbar^2)\{B_{vx}P_x^2+B_{vy}P_y^2+B_{vz}P_z^2\}-H_{RC}, \quad (17)$$

in which H_{RC} contains the centrifugal stretching terms and has the form

$$\begin{aligned}
H_{RC}&=(hc/\hbar^4)\{\tau_1P_x^4+\tau_2P_y^4+\tau_3P_z^4\\
&\quad+\tau_5(P_yP_z+P_zP_y)^2+\tau_7(P_x^2P_y^2+P_y^2P_x^2)\\
&\quad+\tau_8(P_x^2P_z^2+P_z^2P_x^2)+\tau_9(P_y^2P_z^2+P_z^2P_y^2)\},
\end{aligned} \quad (18)$$

where

$$\begin{aligned}
\tau_1&=B_{ex}^2\textstyle\sum_i[a_i^2/(2\omega_i^2)],\\
\tau_2&=B_{ey}^2\textstyle\sum_i[b_i^2/(2\omega_i^2)],\\
\tau_3&=B_{ez}^2\textstyle\sum_i[c_i^2/(2\omega_i^2)],\\
\tau_4&=\tau_6=0,\\
\tau_5&=B_{ey}B_{ez}\textstyle\sum_j[d_j^2/(2\omega_j^2)],\\
\tau_7&=B_{ex}B_{ey}\textstyle\sum_i[a_ib_i/(2\omega_i^2)],\\
\tau_8&=B_{ex}B_{ez}\textstyle\sum_i[a_ic_i/(2\omega_i^2)],\\
\tau_9&=B_{ey}B_{ez}\textstyle\sum_i[b_ic_i/(2\omega_i^2)].
\end{aligned} \quad (18a)$$

The effective rotational constants are, to second-order approximation, as follows:

$$\begin{aligned}
B_{vx}&=B_{ex}\{1+\sum_{h=1}^{12}\alpha_h(v_h+\tfrac{1}{2})\},\\
B_{vy}&=B_{ey}\{1+\sum_{h=1}^{12}\beta_h(v_h+\tfrac{1}{2})\},\\
B_{vz}&=B_{ez}\{1+\sum_{h=1}^{12}\gamma_h(v_h+\tfrac{1}{2})\},
\end{aligned} \quad (19)$$

where if

$$J_{hh'}=[(3\omega_h^2+\omega_{h'}^2)/(\omega_h^2-\omega_{h'}^2)],$$

[9] W. H. Shaffer and R. C. Herman, J. Chem. Phys. **13**, 83 (1945).

†† The zero-point energy is given by

$$\begin{aligned}
G_0&=(1/4)\Sigma_h\{(a_{hh}+b_{hh}+c_{hh})-(3/8)(a_i^2+b_i^2+c_i^2)\\
&\quad+(1/4)(a_ib_i+b_ic_i+c_ia_i)-d_j^2+(3/2)\gamma_{hhhh}\}\\
&\quad-(1/16)\Sigma_h\{7\omega_i^{-1}\beta_{iii}^2+4\omega_i\omega_{i'}\omega_{i''}D_{ii'i''}\beta_{ii'i''}^2\\
&\quad+4\omega_i\omega_{j'}D_{ijj'}\beta_{ijj'}^2+4\omega_i\omega_k\omega_{k'}D_{ikk'}\beta_{ikk'}^2+4\omega_i\omega_l\omega_{l'}D_{ill'}\beta_{ill'}^2\\
&\quad+4\omega_m\omega_s\omega_lD_{msl}\beta_{msl}^2+4\omega_n\omega_s\omega_kD_{nsk}\beta_{nsk}^2\\
&\quad+4\omega_m\omega_n\omega_jD_{mnj}\beta_{mnj}^2+4\omega_j\omega_k\omega_lD_{jkl}\beta_{jkl}^2-3H_{ii'}\beta_{iii'}^2\\
&\quad-3H_{mi}\beta_{mmi}^2-3H_{ni}\beta_{nni}^2-3H_{si}\beta_{ssi}^2-3H_{ji}\beta_{jji}^2\\
&\quad-3H_{ki}\beta_{kki}^2-3H_{li}\beta_{lli}^2\}\\
&\quad-(1/2)\textstyle\sum_{h,h'}\{(\xi_{ij}^2+\xi_{kl}^2)B_{ez}+(\eta_{si}^2+\eta_{lm}^2+\eta_{nk}^2)B_{ey}\\
&\quad+(\zeta_{mk}^2+\zeta_{js}^2+\zeta_{ln}^2)B_{ez}\}.
\end{aligned}$$

and

$$A=[3\beta_{iii}+\sum_{i'}\beta_{ii'i'}+\beta_{iss}+\beta_{imm}+\beta_{inn}+\sum_j\beta_{ijj}+\sum_k\beta_{ikk}+\sum_l\beta_{ill}],$$

$$\alpha_i=\omega_i^{-1}\{a_i^2-a_{ii}+\omega_i^{-1}a_iA+2B_{ex}\textstyle\sum_j J_{ij}\xi_{ij}^2\},$$
$$\beta_i=\omega_i^{-1}\{b_i^2-b_{ii}+\omega_i^{-1}b_iA+2B_{ey}J_{is}\eta_{si}^2\},$$
$$\gamma_i=\omega_i^{-1}\{c_i^2-c_{ii}+\omega_i^{-1}c_iA\},$$
$$\alpha_j=\omega_j^{-1}\{-a_{jj}+2B_{ex}\textstyle\sum_i J_{ji}\xi_{ij}^2\},$$
$$\beta_j=\omega_j^{-1}\{d_j^2-b_{jj}\},$$
$$\gamma_j=\omega_j^{-1}\{d_j^2-c_{jj}+2B_{ez}J_{js}\zeta_{js}^2\},$$
$$\alpha_k=\omega_k^{-1}\{-a_{kk}+2B_{ex}\textstyle\sum_l J_{kl}\xi_{kl}^2\},$$
$$\beta_k=\omega_k^{-1}\{-b_{kk}+2B_{ey}J_{kn}\eta_{nk}^2\},$$
$$\gamma_k=\omega_k^{-1}\{-c_{kk}+2B_{ez}J_{km}\zeta_{mk}^2\},$$
$$\alpha_l=\omega_l^{-1}\{-a_{ll}+2B_{ex}\textstyle\sum_k J_{lk}\xi_{kl}^2\},$$
$$\beta_l=\omega_l^{-1}\{-b_{ll}+2B_{ey}J_{lm}\eta_{lm}^2\},\qquad(19a)$$
$$\gamma_l=\omega_l^{-1}\{-c_{ll}+2B_{ez}J_{ln}\zeta_{ln}^2\},$$
$$\alpha_m=-\omega_m^{-1}a_{mm},$$
$$\beta_m=\omega_m^{-1}\{-b_{mm}+2B_{ey}\textstyle\sum_l J_{ml}\eta_{lm}^2\},$$
$$\gamma_m=\omega_m^{-1}\{-c_{mm}+2B_{ez}\textstyle\sum_k J_{mk}\zeta_{mk}^2\},$$
$$\alpha_n=-\omega_n^{-1}a_{nn},$$
$$\beta_n=\omega_n^{-1}\{-b_{nn}+2B_{ey}\textstyle\sum_k J_{nk}\eta_{nk}^2\},$$
$$\gamma_n=\omega_n^{-1}\{-c_{nn}+2B_{ez}\textstyle\sum_l J_{nl}\zeta_{ln}^2\},$$
$$\alpha_s=-\omega_s^{-1}a_{ss},$$
$$\beta_s=\omega_s^{-1}\{-b_{ss}+2B_{ey}\textstyle\sum_i J_{si}\eta_{is}^2\},$$
$$\gamma_s=\omega_s^{-1}\{-c_{ss}+2B_{ez}\textstyle\sum_j J_{sj}\zeta_{js}^2\}.$$

The eigenvalues of H_R can be evaluated from a secular determinant which is a modified form of the one given by Wang[10] for the rigid asymmetric rotator and can be expressed in the form $E_R=hcF$, where F is the rotational term. The evaluation of F is facilitated by a method discussed by Shaffer and Nielsen[11] and Nielsen.[12] The non-vanishing matrix elements of the rotational Hamiltonian can be obtained from Eq. (16) of reference 9 using appropriate values of the τ_1, etc., defined in Eq. (18a) above.

For a discussion of selection rules for the $X_2Y_2X_2$ model the reader is referred to Herzberg.[1]

We wish to thank Dr. G. Herzberg for some valuable comments and Dr. H. H. Nielsen for his encouragement and interest in this work.

[10] S. C. Wang, Phys. Rev. **34**, 243 (1929).
[11] W. H. Shaffer and H. H. Nielsen, Phys. Rev. **56**, 188 (1939).
[12] H. H. Nielsen, Phys. Rev. **59**, 565 (1941).

THE JOURNAL OF CHEMICAL PHYSICS VOLUME 18, NUMBER 9 SEPTEMBER, 1950

Light Scattering and Spectrophotometry of Colloidal Solutions

PAUL DOTY AND ROBERT F. STEINER
Gibbs Memorial Laboratory, Harvard University, Cambridge, Massachusetts
(Received April 27, 1950)

During the past several years it has been demonstrated that the light scattered from dilute solutions of macromolecules or colloidal particles is intimately related to the weight, size, and interaction of the solute species. Theoretical developments and improved techniques have made possible the determination of the molecular weight, dimension and activity coefficient of a number of polymers and proteins in solution. In these investigations the intensity of light scattered at various angles from a monochromatic beam passing through the solution has been measured by means of specially designed photometers. However, it would appear that the equivalent information could be derived from a different means of observation—that of transmission measurements at various wave-lengths. If this possibility could be exploited the common techniques of spectrophotometry could replace the more specialized ones now used. The extent to which this is feasible is explored in this paper.

As a first step it is necessary to review some aspects of the scattering from small particles and the internal interference arising in the case of larger particles. This opportunity is taken to present a compilation of the scattering factors and the quantities derived from them, that is the dissymmetry and correction factor, in a more precise and convenient form than has appeared previously, because of the use to which they are put in the following sections. The calculations relating to the case of transmittance of solutions containing larger particles are then presented and in the final sections the application of both methods of observation to the determination of the molecular weight and size of samples of polystyrene and tobacco mosaic virus is reported.

I. SCATTERING AND TRANSMITTANCE BY SOLUTIONS OF SMALL PARTICLES

WE consider first the trivial case in which the solute molecules are small in comparison with the wave-length of incident light. Except when unusually large repulsions exist among solute molecules[1] the intensity of light scattered from these solutions, for the case of unpolarized incident light, exhibits an angular dependency given by

$$i_\theta=i_0(1+\cos^2\theta)/2,\qquad(1)$$

where θ is the scattering angle with reference to the forward direction of the incident beam and i_0 is the intensity of the scattered light at 0°. If r is the distance between the solution and the detector, the total light scattered from the illuminated volume, V, of solution is given by

$$\int_0^\pi i_\theta 2\pi r^2\sin\theta d\theta=\frac{8\pi}{3}i_0r^2.\qquad(2)$$

In this case the total light scattered (total flux emitted) can be characterized in terms of the intensity at any specified angle relative to the intensity of the incident

[1] P. Doty and R. F. Steiner, J. Chem. Phys. **17**, 743 (1949).

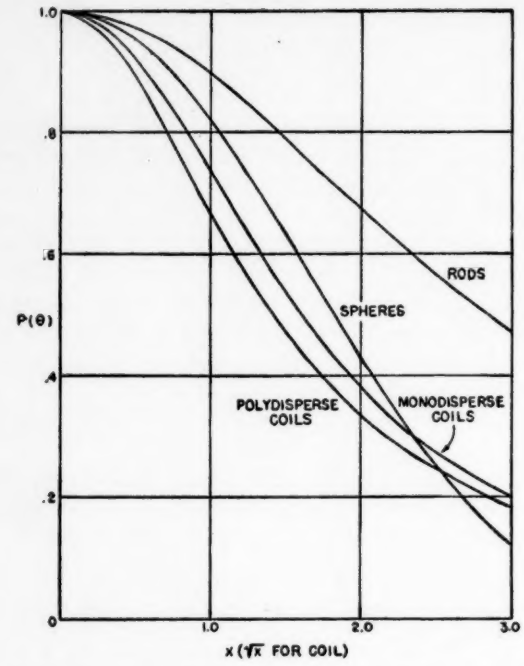

FIG. 1. Particle scattering factors for spheres, rods monodisperse and polydisperse randomly kinked coils.

light, I_0. However, the same information can be conveyed for *any* case, assuming non-absorbing solutions, by means of the turbidity. The turbidity is defined so that its product with the incident intensity and V is equal to the total light scattered. Hence

$$I_0 V\tau = (8\pi/3)i_0 r^2 = (16\pi/3)i_{90} r^2. \tag{3}$$

The turbidity is, of course expressible as an extinction coefficient. It is, therefore, clear that the total light scattered by a solution of small particles can be completely characterized by measuring either the ratio of the intensities of the scattered and incident light, i_θ/I_0, or the transmittance, I/I_0.

Throughout this discussion it should be noted that only the scattering due to fluctuations in concentration is treated, whereas scattering from density fluctuations (solvent scattering) and fluctuations in orientation of the solute also contribute to the total scattering. The effect of the former is eliminated in practice by subtracting the scattering due to the solvent alone or by using a cell filled with solvent in determining the transmittance. The latter contribution is usually negligible although correction can be made when warranted.[2]

The turbidity due to concentration fluctuations is related to the molecular weight according to the expression:[3,4]

$$H(c/\tau) = (1/M) + 2Bc, \tag{4}$$

where c denotes the concentration, B represents the deviation from van't Hoff behavior, and

$$H = 32\pi^2 n_0^2/3N\lambda^4(dn/dc)^2$$

The refractive index of the solvent is given by n_0, that of the solution by n; $N = 6.02\times10^{23}$ and λ = the wavelength of light in vacuum. Although the application of Eq. (4) implies that the experimental observations have been those in which the turbidity has been directly measured it has nevertheless been widely used in this form for the interpretation of scattering measurements by using Eq. (3) or some more general relation to evaluate the turbidity. In this paper Eq. (4) is reserved for use with direct turbidity measurements. For scattering at 90° from a beam of unpolarized incident light we have the corresponding expression

$$K(c/R_{90}) = (1/M) + 2Bc \tag{5}$$

where $K = 2\pi^2 n_0^2(dn/dc)^2/N\lambda^4$ and $R_{90} = i_{90}r^2/I_0$. The latter quantity is known as the reduced intensity or Rayleigh's ratio at the angle denoted in the subscript. The value of K, like that of H, depends only upon the system being measured.

II. SCATTERING BY SOLUTIONS OF LARGE PARTICLES

When the particle size is greater than that considered in the previous section interference will occur between light waves scattered from the same particle. This internal interference causes a diminution of the intensity of the scattered light which, at concentrations sufficiently low to eliminate external interference, is given quantitatively by the expression:

$$P(\theta) = \sum_i \sum_j \frac{\sin ksr_{ij}}{ksr_{ij}}, \tag{6}$$

where the double summation extends over all pairs of scattering elements, i and j: $k = 2\pi/\lambda'$, λ' = wavelength of light in solution, $s = 2\sin\theta/2$ and r_{ij} is the distance between the ith and jth scattering element. This general expression was derived originally[5] to treat the case of internal interference arising in x-ray diffraction by atoms: there it is known as the square of the atomic scattering factor; here it may be called properly the *particle scattering factor*. Equation (1) may now be revised to give for the general case:

$$i_\theta = i_0 \frac{1+\cos^2\theta}{2} P(\theta). \tag{7}$$

Rather simple, closed-form expressions have been obtained for the particle scattering factor for the most important particle shapes, i.e., sphere, rod, and random

[2] B. Zimm, R. S. Stein, and P. Doty, Polymer Bull. 1, 90 (1945).
[3] P. Debye, J. App. Phys. 15, 338 (1944).
[4] P. Doty, B. H. Zimm and H. Mark, J. Chem. Phys. 12, 144 (1944).
[5] P. Debye, Physik. Zeits., 28, 135 (1927).

coil[2,6] These expressions are:

$$\text{Sphere } P(\theta)=\left[\frac{3}{x^3}(\sin x - x\cos x)\right]^2 \qquad x=\frac{ksD}{2} \tag{8.1}$$

$$\text{Rod } P(\theta)=\frac{1}{x}\int_0^{2x}\frac{\sin w}{w}dw-\left(\frac{\sin x}{x}\right)^2 \qquad x=\frac{ksL}{2} \tag{8.2}$$

$$\text{Coil } P(\theta)=\frac{2}{x^2}[e^{-x}-(1-x)] \qquad x=\frac{k^2s^2R^2}{6}, \tag{8.3}$$

where D=diameter of sphere, L=length of rod and R=root mean square of the distance between ends of the random coil. These particle scattering factors are shown in Fig. 1. Since much of the current practice of light scattering as well as the extensions developed in this paper depend upon the accurate implementation of these expressions, tables of their values to three significant figures as functions of the argument x are given in the Appendix. This tabulation permits the large scale reproduction of Fig. 1 from which Figs. 2–5 and other useful graphs can be constructed with an accuracy sufficient for any foreseeable need.

The particle scattering factors serve two purposes in the most common method of interpretation of light scattering data, the method which we shall call the *dissymmetry method*. First, the measurement of the ratio of the intensities at any two angles permits the evaluation of the dimension (D, L, or R) if the particle shape is known or can be deduced. Second, the same measurement makes possible the correction of the observed intensity at 90° for the loss due to internal interference. It is this corrected intensity, or the turbidity calculated therefrom which must be employed in Eqs. (5) and (6). It has become fairly standard practice to choose the angles 45 and 135° for measurement and the ratio of these intensities is known as the dissymmetry, z. The dimension relative to the wave-length, λ', and the correction factor for the three particle shapes are shown in Fig. 2. A table of precise values of z and $1/P(90)$ for selected values of D/λ' is given in the Appendix.

The scattering factor for the random coil assumes uniform molecular weight: significant deviations are encountered for broad molecular weight distributions. The exponential distribution, $f(M)=aMe^{-bM}$ where M=molecular weight and a and b are constants, occurs frequently in polymers and approximates many other more complicated distributions. For this case, which is typical of unfractionated polymers, the scattering factor has the particularly simple form:[7]

$$P(\theta)=1-\langle x\rangle/(2+\langle x\rangle), \tag{9}$$

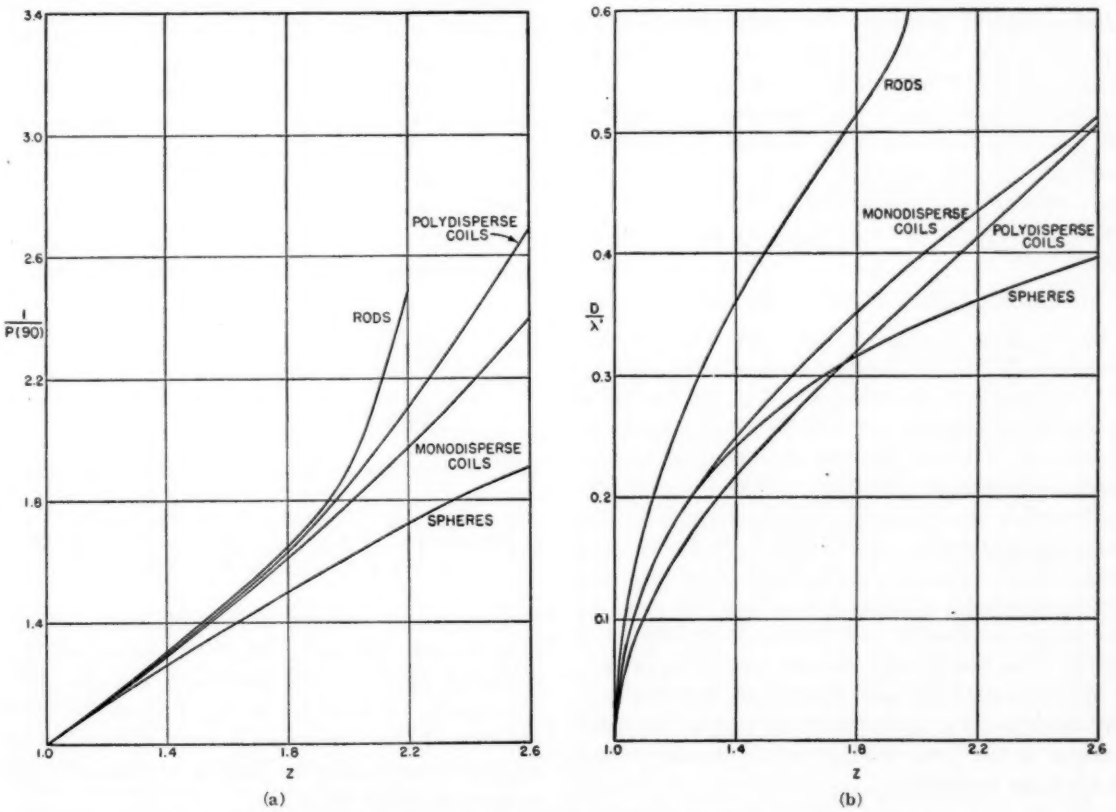

FIG. 2. Correction factors and particle dimensions as a function of the dissymmetry.

[6] P. Debye, J. Phys. Colloid Chem. **51**, 18 (1947).
[7] B. H. Zimm, J. Chem. Phys. **16**, 1093, 1099 (1948).

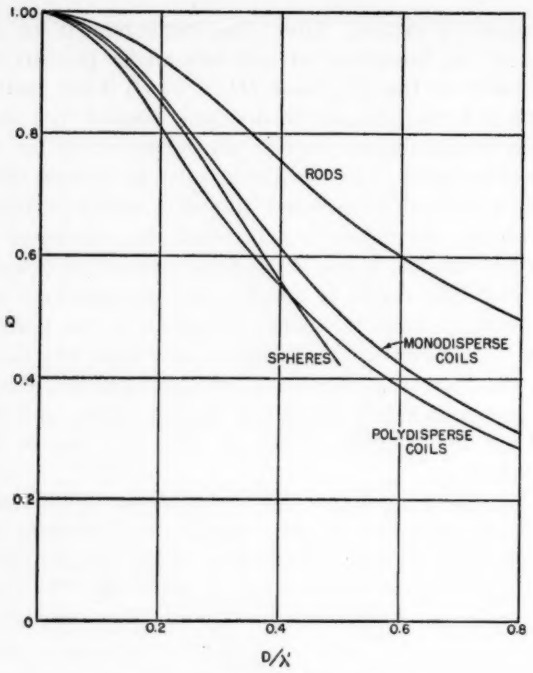

FIG. 3. Particle dissipation factors.

where $\langle x \rangle$ has the same meaning as x in Eq. (8.3) if the weight average value is used for R^2. The result obtained using this scattering factor is included in Fig. 2. This factor should generally be used instead of the corresponding one for monodisperse coils to interpret measurements made on unfractionated polymers.

At finite concentrations the intensity of scattered light is generally diminished by external interference, characterized by the quantity B, as well as by the internal interference. These dual effects cannot be rigorously resolved but to a good approximation it can be shown[8] that

$$K(c/R_{90})P(90)=(1/M)+2BP(90)c. \qquad (10)$$

In the implementation of Eq. (10) the intrinsic dissymmetry, $[z]$, is obtained by extrapolating a plot of $1/(z-1)$ against c to zero concentration. By the use of Fig. 2 the corresponding value of $P(90)$ can be determined and then a plot of Eq. (10) can be made directly.

Internal interference vanishes at 0° and correspondingly all particle scattering factors become unity. Consequently, an alternative method of dealing with light scattering from solutions containing large particles consists in obtaining scattering data over as great an angular range as possible and then extrapolating this data to 0°. The theory and practice of this approach, which may be called the *extrapolation method*, has been recently described by Zimm[8] and will not be discussed here except in the final sections where measurements of this kind are reported.

III. TRANSMITTANCE OF SOLUTIONS OF LARGE PARTICLES

Obviously the effect of internal interference will be to increase the transmittance, I/I_0, of the solutions over that which would have been observed in the absence of such interference because less light is being removed by scattering from the incident beam. The consequences of this interference can be treated quantitatively in the following way.

From Eqs. (2) and (3) the turbidity in the absence of internal interference may be expressed as

$$\tau=\frac{1}{I_0V}\int_0^\pi i_0(1+\cos^2\theta)\pi r^2\sin\theta d\theta=\frac{8\pi}{3}\frac{i_0r^2}{I_0}. \qquad (11)$$

But in the general case where internal interference may be present the observed turbidity will be given by

$$\tau=\frac{i_0\pi r^2}{I_0V}\int_0^\pi P(\theta)(1+\cos^2\theta)\sin\theta d\theta. \qquad (12)$$

Consequently we may define a factor, Q, so that the observed turbidity multiplied by its reciprocal will equal the turbidity that would have been observed in the absence of the interference, i.e., the turbidity required in Eq. (4). This factor will be the ratio of Eq. (12) to Eq. (11), thus

$$Q=\frac{3}{8}\int_0^\pi P(\theta)(1+\cos^2\theta)\sin\theta d\theta. \qquad (13)$$

It will be noticed that Q bears the same relation to the turbidity that $P(\theta)$ does to the intensity of scattering at the angle θ. It seems appropriate, therefore, to name Q the *particle dissipation factor* for it characterizes the ability of the particles to dissipate light from the incident beam just as the scattering factor denotes the corresponding ability to scatter light at a given angle.

The integration in Eq. (13) for the various forms of $P(\theta)$ leads to expressions which are too laborious to evaluate except in the case of polydisperse coils where

$$Q=\frac{3}{2}\left[\frac{A^2+2A+2}{A^3}\ln(1+A)-\frac{2+A}{A^2}\right]$$
$$A=4/3\pi^2(R/\lambda')^2. \qquad (14)$$

With monodisperse coils, for example, one obtains

$$Q=1-\frac{4\pi^2}{9}\left(\frac{R}{\lambda'}\right)^2+\frac{28\pi^4}{135}\left(\frac{R}{\lambda'}\right)^4-\frac{22\pi^6}{225}\left(\frac{R}{\lambda'}\right)^6+\cdots. \qquad (15)$$

Convergence is so gradual that the terms shown suffice only for very low values of R/λ'. Consequently graphical integration was used here and in the two other cases. The results are collected in Fig. 3 where Q is shown as a function of D/λ'. It is readily noticed that the variation of this function is quite similar to that of the particle scattering factor (Fig. 1).

We now turn to the utilization of the dissipation factor in a manner analogous to that described for the scattering factor. First let us define the quantity H' as equal to $H\lambda^4$. Equation (4) can then be rearranged to

give for the observed turbidity

$$\tau=\frac{H'cM}{(1+2BMc)}\frac{Q}{\lambda^4}. \tag{16}$$

From this one obtains the derivative

$$-\frac{d\log\tau}{d\log\lambda}=4-\frac{d\log Q}{d\log\lambda}=4-\beta. \tag{17}$$

The derivative $d\log Q/d\log\lambda$ will be used frequently and will be denoted as β. Clearly the value of $d\log Q/d\log\lambda$ for a given wave-length depends only on the dimension D. Thus an experimental determination of β establishes a certain value of D/λ' and this in turn corresponds to a unique value of Q as shown in Fig. 3. The reciprocal of the value of Q identified in this way is the turbidity correction factor. Therefore, the dependence of $1/Q$ and D/λ' on β can be obtained directly from a double logarithmic plot of Fig. 3. The results are shown in Fig. 4 and a tabulation is given in the Appendix.

The similarity between the scattering and turbidity of colloidal solutions with respect to their functional dependence is clearly seen by comparing Fig. 2 and Fig. 4. There is a direct correspondence between β, $1/Q$, and D/λ' and z, $1/P(90)$ and x respectively. Both β and z depend on the wave-length; consequently this should be designated in the measurement of either. The implementation of this method, *the transmission method*, is formally the same as the dissymmetry method. Instead of Eq. (10) we have the turbidity relation

$$H(c/\tau)Q=(1/M)+2BQc \tag{18}$$

with the corresponding qualifications mentioned previously. The details of the application of the transmittance method in practice are given in the following sections.

IV. CALIBRATION

In comparing the different light scattering methods the ratios $i_{90}r^2/I_0$ and I/I_0 must be measured with comparable accuracy. The rigorous demonstration that these ratios are being precisely measured in any given case requires a thorough analysis of the geometric optics involved and a critical inspection of every aspect of the experimental arrangement which can affect the final observation. These conditions have been generally satisfied in the case of transmittance due to the wide spread development and use of spectrophotometry.[7] In contrast there has been little comparable coordinated activity associated with the determination of ir^2/I_0. The precision attained has been approximately an order of magnitude less than in spectrophotometry; for example, values in the literature for benzene vary over a range of 15 percent and it now appears that this range is considerably displaced from the true value. Consequently, with the rapid ascendancy of light

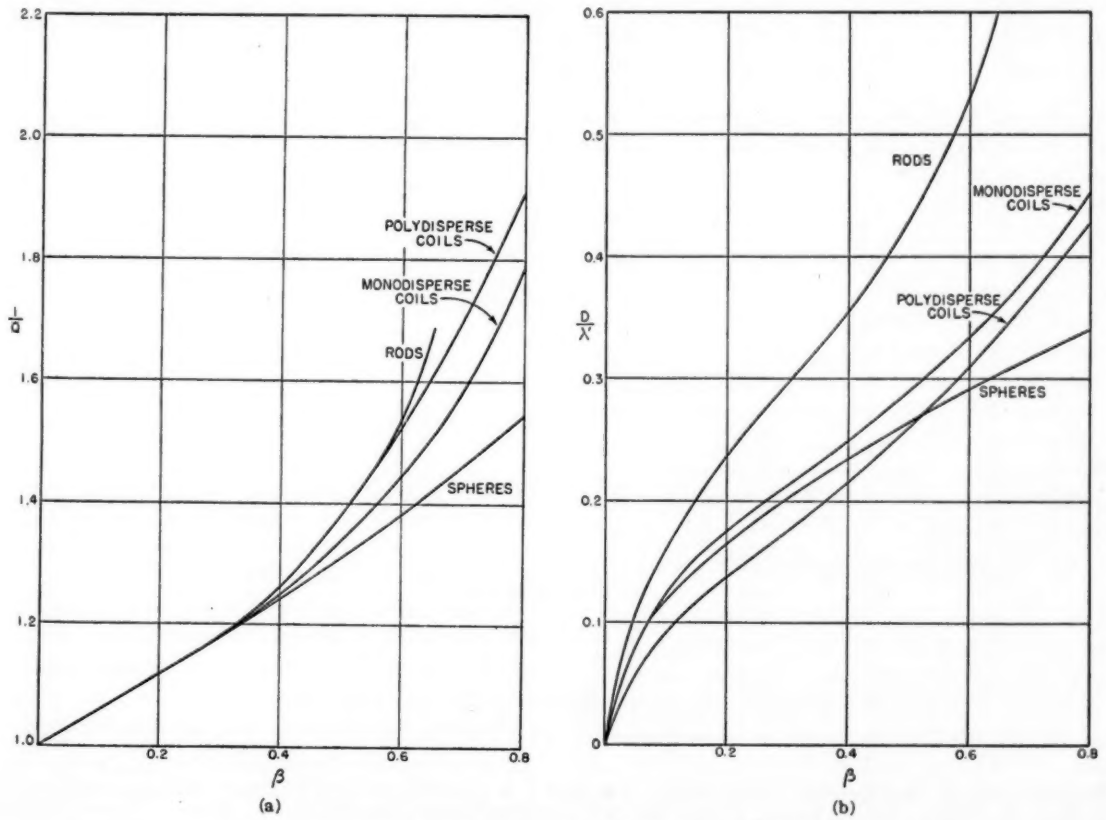

FIG. 4 Correction factors and particle dimensions as a function of β.

scattering techniques a determined effort has been made recently to establish precise methods for the evaluation of this ratio. Reports on some of this work will soon be available.[8,9] It should be noted in passing that an accurate absolute calibration cannot be based upon the scattering of any liquid nor upon the scattering of a solution of a substance of known molecular weight.

The basis of our calibration has been the measurement of both ratios on various solutions and the checking of one against the other by use of Eqs. (3) and (4). In order that the result correspond only to the scattering by the solute the scattering of the solvent was subtracted from that of the solution and in the transmittance measurement the solvent served as the blank. The identical solution and solvent was used for the determination of both ratios. The angular distribution of intensity was essentially symmetrical about 90° in the range of 30 to 150°.

The calibration of the scattering photometer was based upon an analysis by Dr. B. A. Brice.[9] This analysis provides for the dependence of ir^2/I_0 on the square of the refractive index of the solution in addition to a minor reflection correction also involving the refractive index. The diffuse transmittance of a properly compensated opal glass corrected to a perfect diffuser serves as a reference standard.

The transmittance measurements were made in a Beckman Spectrophotometer using 10 cm matched cells and observing the proper precautions.[10] The wavelength employed was 4370 and 5460A because these are the effective wave-lengths used in scattering measurements. In each case it was demonstrated that there was no significant absorption by the solute and that the transmittance was independent of the diameter of the aperture before the photo-tube, providing its diameter did not exceed 4 mm. Measurements made without limiting this aperture are about 2 percent too small due to the transmitted light being augmented by the light scattered at low angles. This correction has been applied to measurements made without a limited aperture.

The solutions were prepared from freshly distilled sol-

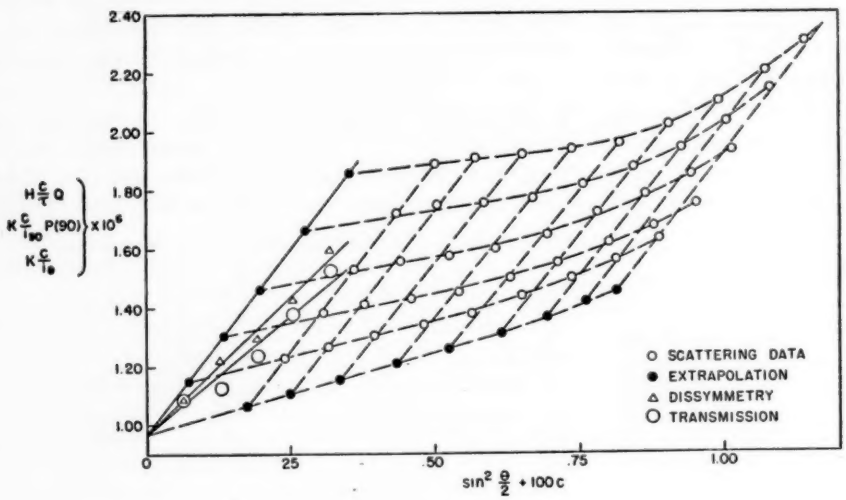

FIG. 5. Reciprocal reduced intensity and turbidity plots for polystyrene in butanone.

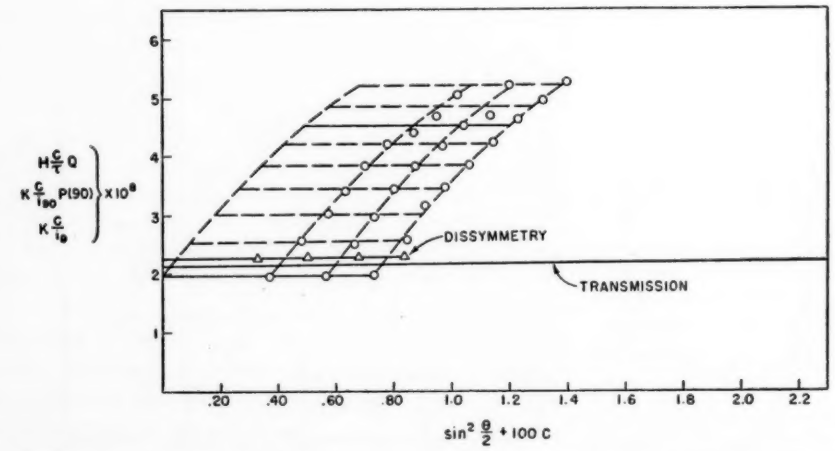

FIG. 6. Reciprocal reduced intensity and turbidity plots for tobacco mosaic virus in 0.1M phosphate buffer.

[8] B. H. Zimm and C. I. Carr (private communication). Thesis of C. I. Carr, University of California, Berkeley, California, 1949.
[9] B. A. Brice, M. Halwer, and R. Speiser, J. Opt. Soc. Am., (to be published).
[10] K. S. Gibson and M. M. Balcom, J. Opt. Soc. Am. **37**, 593 (1947).

TABLE I. Summary of calibration data.

Polymer sample	Conc. g/l	Solvent	Refractive index	Wave-length	$\frac{16\pi}{3}R_{90}\times10^3$	$\tau\times10^3$	Percentage difference
Polystyrene	5.0	toluene	1.498	4370	3.53	3.50	0 percent
—Cornell	5.0	toluene	1.519	5460	1.40	1.43	−2
—Cornell	5.0	ethylene dichloride	1.455	5460	2.95	2.95	0
—Cornell	5.0	butanone	1.389	4370	27.6	26.6	4
—Cornell	5.0	butanone	1.381	5460	10.68	10.34	4
Polystyrene	9.49	butanone	1.381	4370	27.3	26.3	4
—*IUC* Dow 1	4.76	butanone	1.381	4370	17.2	16.3	4
—*IUC* Dow 1	2.38	butanone	1.381	4370	9.84	9.64	2
—*IUC* Dow 1	10.0	ethylene dichloride	1.444	4370	5.01	5.37	−7
—*IUC* Dow 1	10.0	ethylene dichloride	1.444	5460	2.02	2.01	0
Polyvinyl alcohol-1	17.1	water	1.340	4370	5.55	5.86	−6
	17.1	water	1.334	5460	2.08	2.14	−3

vents. Both solution and solvent were centifuged at 20,000 g for one hour prior to measurement. The temperature was approximately 25°C for all measurements.

The two types of measurements on eight different solutions covering the range of refractive index usually encountered are summarized in Table I. It is estimated that a systematic error of 5 percent can enter into measurements of R_{90} due to uncertainties in geometrical factors contained in Brice's equation and a random error of 2 percent results from fluctuations and other variables encountered in actual measurements. Consequently, it is seen that the differences between the two measurements are in all cases within the probable experimental error. The measurements in butanone, where the precision of transmittance measurements was the greatest, suggest that the scattering method may be yielding values approximately 4 percent higher but this cannot be proven by the present data.

As a consequence of this agreement the working equation of Brice was accepted for determining R_{90}. With the use of this equation the values of R_{90} for benzene were found to be 48.2×10^{-5} at $\lambda=4370$ and 16.4×10^{-5} at $\lambda=5460$. These values compare favorably with those obtained by Carr and Zimm[9] and Brice *et al.*[10] However, they are considerably higher than other previously published values.

V. COMPARATIVE EXPERIMENTS WITH POLYSTYRENE

A fraction of polystyrene[11] distributed by the International Union of Chemistry[12] was used in butanone solution for this comparative investigation. The intrinsic viscosity of this sample in butanone at 25°C was 1.21. Solutions of five different concentrations were prepared and used for all measurements. Before use the solutions and solvent were centrifuged for one hour at 20,000 g.

For measurements by the dissymmetry method a glass cell having faces at 0, 45, 90, 135, 180, and 270° was used to hold the solution. A very small residual background correction was employed in the measurement of dissymmetry. The transmittance measurements were carried out as described in the previous section. Values were obtained at wave-lengths of 417, 427, 437, 447, 457 mu. These values were multiplied by the ratio of the value of $(dn/dc)^2$ at 437 to that at the wave-length in question, this being a very minor correction. β was then determined from a log log plot of this data and the corresponding value of Q obtained from Fig. 4. The limiting value of z, $[z]$, was obtained by extrapolating $1/(z-1)$ to zero concentration. The limiting value of β, $[\beta]$, was obtained by direct extrapolation. The values of R were then obtained from Figs. 2 and 4. The data are summarized in Table II and plotted in Fig. 5.

TABLE II. Light scattering data on Polystyrene IUC—Dow 1.

c(g/cc) $\times10^4$	z	$K\frac{c}{i_{90}}\times10^6$	$K\frac{c}{i_{90}}P(90)\times10^6$	β	$H\frac{c}{\tau}\times10^6$	$H\frac{c}{\tau}Q\times10^6$
6.38	1.329	1.38	1.09	0.40	1.36	1.085
12.76	1.295	1.50	1.22	0.30	1.435	1.14
19.14	1.271	1.65	1.30	0.25	1.57	1.24
25.4	1.240	1.82	1.43	0.15	1.75	1.38
31.8	1.213	2.03	1.60	0.15	1.93	1.53

$[z]=1.38$ $R=765\pm25$A $[\beta]=0.45$ $R=825\pm70$A

$\left[K\frac{c}{i_{90}}P(90)\right]=0.97\times10^{-6}$ $\left[H\frac{c}{\tau}\right]Q=0.97\times10^{-6}$

$M=1{,}030{,}000\pm30{,}000$ $M=1{,}030{,}000\pm70{,}000$

$\lambda=4370$A $n=1.389$ $dn/dc=0.222$ $T=25$°C

The agreement between the measured values of $K(c/R_{90})P(90)$ and $H(c/\tau)Q$ are seen to be quite good, well within probable experimental error. Consequently, the molecular weights derived from them are in essential agreement. As indicated in Table II the measurement of β is much less precise than z but the value of R derived from the two methods again is found to be within probable experimental error. The slopes of the

[11] This is fraction number 5 described in a forthcoming publication by E. A. Merz and R. W. Raetz in J. Polymer Sci.

[12] Through Professor H. Mark, Polytechnic Institute of Brooklyn, Brooklyn, New York.

TABLE III. Light scattering data on tobacco mosaic virus.

c(g/cc) $\times 10^3$	z	$K\frac{c}{i_{90}}$ $\times 10^8$	$K\frac{c}{i_{90}}P(90)$ $\times 10^8$	c(g/cc) $\times 10^3$	β	$H\frac{c}{\tau}\times 10^8$	$H\frac{c}{\tau}Q$ $\times 10^8$
0.0327	2.20	5.55	2.22	0.055	0.69	3.96	1.90
0.0510	2.19	5.53	2.21	0.187	0.69	4.31	2.12
0.0681	2.21	5.53	2.21	0.278	0.69	4.15	1.97
0.0840	2.21	5.55	2.22	0.413	0.70	4.34	2.04

$[z]=2.20$ $L=2500$A $[\beta]=0.69$ $L=2500$A

$\left[K\frac{c}{i_{90}}P(90)\right]=2.25\times10^{-8}$ $\left[H\frac{c}{\tau}Q\right]=2.04\times10^{-8}$

$M=44{,}500{,}000\pm1{,}000{,}000$ $M=49{,}000{,}000\pm3{,}000{,}000$

$\lambda=4370$A $n=1.340$ $dn/dc=0.176$ $T=25$°C

straight lines fitting these data are equal to $2BP(90)$ and $2BQ$ respectively. The value of B determined from these slopes is found to be 1.20×10^{-4} cc-moles/g^2 from the dissymmetry data and 1.05×10^{-4} cc-moles/g^2 from the turbidity data. Thus reasonably consistant values of M, R and B have been obtained by two different light scattering methods.

We turn now to the extrapolation method for further comparison. This method requires and makes use of more data than the other two methods and, providing the data are of commensurate precision, it permits a more reliable determination of M, R, and B. For the angular measurements a thin, hand-blown glass cell similar in size and shape to a 50-cc Erlenmeyer flask was used to contain the solution. It was selected and mounted so that no distortion of the scattering envelope occurred over the range of 40-135° as demonstrated by the constancy of the angular intensity (after multiplication by $\sin\theta$ to correct for the volume of solution viewed) of fluorescence from fluorescein solutions whose concentrations were varied so as to cover the range of intensities encountered in practice.

The data are shown in Fig. 5 as small open circles. The lines of constant angle were drawn so that there was only a gradual and continuous change in slope among neighboring lines. The extrapolated points ($c=0$) were located on these lines at a distance proportionate to the concentration. The curves of constant concentration were extrapolated linearly on the basis of the best straight line from $\theta=80°$ downward. Lines through the extrapolated points meet at the abscissa at an intercept of 0.97×10^{-6} thus giving a value of 1,030,000 for the molecular weight. The limiting slope of the other extrapolated line ($c=0$) is 0.54×10^{-6} which, being equal to $(8\pi^2/9M)(R/\lambda')^2$, yields a value of $R=790\pm10$A. These values are in satisfactory agreement with the other results and substantiate the previous estimates of probable error. Since the transmittance and dissymmetry are in agreement here, it appears that the actual difference in intercepts is possibly due to the error involved in establishing the absolute value of the intensity of scattering in the conical cell for this requires an additional measurement of the same solution in a square cell and thereby permits a 2 percent error to arise. The value of the interaction constant, B, is obtained directly from the slope of the plot in Fig. 5: it is 1.25×10^{-4} cc-moles/g^2.

The results obtained by these three methods still require correction for depolarization. Since it has been demonstrated that the depolarization is nearly constant in dilute polystyrene solutions in butanone[13] measurements were made at only one concentration. At a concentration of 4.45 g/1 $\rho_u=0.043$ and $\rho_v=0.00665$. The use of the value of ρ_u in the Cabannes correction factor $(6+6\rho)/(6-7\rho)$ would result in a 9.1 percent reduction in the molecular weights. However, it has been pointed out[2] that it is $2\rho_v(1-\rho_v)$ that should be employed in this factor. This leads to a 3.1 percent reduction in the value of the molecular weight determined by the dissymmetry method. The corresponding correction for the turbidity, $(6+3\rho)/(6-7\rho)$, causes a reduction of 2.2 percent in that value. Averaging the values obtained by the transmittance and dissymmetry methods with that obtained by the extrapolation method and applying the correction we obtain a final value of 980,000±30,000. (This value is in exact agreement with that given by Outer, Carr, and Zimm, J. Chem. Phys. **18**, 830 (1950) for this same sample.)

VI. COMPARATIVE EXPERIMENTS WITH TOBACCO MOSAIC VIRUS

In order to establish further the validity of the transmittance method measurements, all three methods were applied to 0.1M phosphate buffer solutions of a purified sample of tobacco mosaic virus.[14] Transmittance measurements were made on this sample a few days after its preparation and were found not to have changed appreciably when duplicated a year later, the solution having been stored at 4°C. Measurements by the other methods were made at this later date. Despite reports of the aggregation of this virus upon storage, it does not appear to have occurred to a significant extent in this sample. However, our principle interest here is to compare measurements made on a particular sample of the virus and not to establish accurately the physical constants of highly purified tobacco mosaic virus, this having been done[15] by light scattering methods. The claim[16] that the correct molecular weight of tobacco mosaic virus can be obtained by turbidity measurements without corrections such as we make here is considered to be untenable.

The procedure was similar to that described in Section V. The results are summarized in Table III and Fig. 6. Since the scale is too small to accommodate some of the transmittance points only the line they determine

[13] P. Doty and S. J. Stein, J. Polymer Sci. **3**, 763 (1948).

[14] The authors greatly appreciate the gift of this sample from Dr. Gerald Oster, formerly of the Rockefeller Institute for Medical Research, Princeton, New Jersey.

[15] G. Oster, P. Doty, and B. H. Zimm, J. Am. Chem. Soc. **69**, 1193 (1947).

[16] G. Oster, J. Gen. Physiol. **33**, 445 (1950).

is included in Fig. 6. Measurements at $\lambda = 5460$ were also used in the determination of this line.

Although the van't Hoff behavior displayed by this system should result in improving the accuracy in comparison with the polystyrene experiments, two other features more than compensate. The first is the use of different sets of solutions for the three different types of measurement; the second is the difficulty of assessing accurately the values of the dimension and correction factor for a rod-like molecule of this length. The extrapolation method is not subject to this latter difficulty until much longer particles are encountered. Consequently, it appears that here too the results of the extrapolation method must be considered the more reliable. This is particularly true for the determination of dimension where the values given in Table III can only be considered as lower limits. The value obtained from the limiting slope of the zero concentration curve in Fig. 6 is 2650 ± 100A. The extrapolation method yields a value of $51{,}000{,}000 \pm 1{,}000{,}000$. In addition to the possible causes for small discrepancies mentioned above the low value of M obtained by the dissymmetry method may be due to the existence of some larger particles (aggregated virus or impurities) which contribute significantly to the scattering only at scattering angles less than 45°. In any event the spread of values is understandable.

VII. DISCUSSION

The three methods of observation of the light scattering characteristics of colloidal solutions can now be summarized with particular reference to solutions of large particles. The extrapolation method is the least dependent upon assumptions of particle shape, makes use of more data and provides the most accurate and precise determinations of weight, size, and activity coefficient. Its proper execution requires a rather elaborate photometer, extreme care in preparing optically clear solutions, and some critical judgment in making the measurements and interpreting them.

The precision of the dissymmetry method depends to a greater extent on the correct choice of the proper particle shape. The method is relatively easy to apply. The demands of cleaning the solution are not quite as great as in the other two methods because large foreign particles may scatter predominately only at low angles. The results are quickly obtained with a relatively simple photometer. Interpretation is straightforward. However, because the $K(c/i_{90})P(90)$ *versus* c plot may be curved a relatively large number of concentrations need to be measured. The intrinsic dissymmetry serves as a very useful index of the overall size of the scattering particle having a more unique interpretation than the intrinsic viscosity, for example.

In the transmission method a considerable loss in accuracy results from the uncertainty of determining β. This is inherent in methods requiring the evaluation of derivatives of experimental data. Again extreme care must be taken to insure optical cleanliness and furthermore, the absence of real absorption must be shown. The great advantage of this method is the fact that the necessary measurement can be made with any of the widely available precision spectrophotometers. The method is practically limited to the study of solutions having turbidities greater than 0.02 cm^{-1} if observational errors of more than 1 percent are to be avoided. In contrast, the lower limit of intensity in the other two methods, assuming photo-multiplier photometers are used, is actually set by the completeness and reproducibility of the cleaning of the solvent and solutions, and not be the over-all sensitivity of the detector.

Of course, as the particle size diminishes the extrapolation and dissymmetry methods merge into one requiring only the determination of the ratio of the intensity at any angle, usually 90°, to the incident intensity. In the size range just larger than this, that is where $1 < [z] < 1.4$, the dissymmetry method is at no disadvantage with respect to the extrapolation method except perhaps in extremely polydisperse systems. This is clear from Fig. 2 where the curves in this range of z are practically coincident. It is here then that the simplicity and speed offered by the dissymmetry method recommend its use.

In conclusion, it should be pointed out that a still different method of observation is possible. Just as the transmission method is complementary to the dissymmetry method an observational scheme based on transmittance but complementary to the extrapolation method is readily imagined. The variable of angle in the latter would be replaced by the variable of wave-length. The extrapolation would then be carried out to infinite wave-length rather than zero angle. This method has been discussed[17] but it will probably be of limited applicability because of the rather short range of wave-length available. The limitation arises not so much from the limited range of transparency of the solution as from the fact that the turbidity generally falls to too low values at higher wave-lengths. Thus the accessible wave-length scale is small relative to the available range of scattering angles, except for very strongly scattering solutions.

In addition mention should be made of an experimental study[18] of the variation of β with the diameter of spherical particles larger than those considered here and an earlier report[19] in which the interdependence of z and β was shown in several cases.

VIII. ACKNOWLEDGMENT

The authors wish to acknowledge their indebtedness to Mrs. M. E. Doty for some of the calculations and

[17] W. M. Cashin and P. Debye, Phys. Rev. **75**, 1307 (1949).
[18] V. K. LaMer, J. Phys. Colloid Chem. **52**, 65 (1948).
[19] P. Doty, J. Chim. Phys. **44**, 242 (1947).

transmission measurements, to Dr. André Oth for some of the results reported in Section IV, and to Dr. Oth and Professor Bruno Zimm for helpful discussions. The award of a fellowship to one of us (R.F.S.) by the Standard Oil Company of California is greatly appreciated.

APPENDIX

TABLE IV. Particle scattering factors, $P(\theta)$, for spheres and rods [x is defined in Eq. (8)].

	$P(\theta)$			$P(\theta)$	
x	sphere	rod	x	sphere	rod
0.1	0.998	0.999	2.6	0.219	0.543
0.2	0.998	0.996	2.7	0.191	0.524
0.3	0.978	0.990	2.8	0.165	0.506
0.4	0.968	0.983	2.9	0.141	0.489
0.5	0.949	0.973	3.0	0.120	0.473
0.6	0.929	0.961	3.1	0.0999	0.547
0.7	0.906	0.948	3.2	0.0824	0.443
0.8	0.818	0.933	3.3	0.0671	0.430
0.9	0.848	0.916	3.4	0.0534	0.417
1.0	0.817	0.897	3.5	0.0420	0.406
1.1	0.781	0.878	3.6	0.0320	0.395
1.2	0.745	0.857	3.7	0.0237	0.384
1.3	0.707	0.835	3.8	0.0172	0.375
1.4	0.667	0.813	3.9	0.0117	0.366
1.5	0.627	0.790	4.0	0.00757	0.358
1.6	0.587	0.767	4.1	0.00453	0.350
1.7	0.546	0.745	4.2	0.00231	0.343
1.8	0.506	0.720	4.3	0.000930	0.336
1.9	0.465	0.696	4.4	0.000199	0.329
2.0	0.426	0.673	4.5	0.0000196	0.323
2.1	0.388	0.650	4.6	0.000216	0.317
2.2	0.350	0.627	4.7	0.000740	0.311
2.3	0.316	0.605	4.8	0.00147	0.306
2.4	0.282	0.584	4.9	0.00233	0.300
2.5	0.249	0.563	5.0	0.00336	0.295

TABLE V. Particle scattering factors, $P(\theta)$ for monodisperse and polydisperse randomly kinked coils [$(x$ is defined in Eq. (8)].

	$P(\theta)$			$P(\theta)$	
$(x)^{\frac{1}{2}}$	mono-disperse	polydisperse	(x)	mono-disperse	polydisperse
0.1	0.996	0.995	2.6	0.252	0.228
0.2	0.987	0.980	2.7	0.237	0.215
0.3	0.971	0.957	2.8	0.223	0.203
0.4	0.949	0.926	2.9	0.209	0.192
0.5	0.922	0.889	3.0	0.198	0.182
0.6	0.891	0.847	3.1	0.187	0.172
0.7	0.855	0.803	3.2	0.176	0.163
0.8	0.817	0.758	3.3	0.167	0.155
0.9	0.776	0.712	3.4	0.158	0.147
1.0	0.736	0.667	3.5	0.150	0.140
1.1	0.694	0.623	3.6	0.142	0.134
1.2	0.652	0.581	3.7	0.135	0.127
1.3	0.613	0.542	3.8	0.129	0.122
1.4	0.573	0.505	3.9	0.123	0.116
1.5	0.536	0.471	4.0	0.117	0.111
1.6	0.499	0.439	4.1	0.112	0.106
1.7	0.466	0.409	4.2	0.107	0.102
1.8	0.434	0.382	4.3	0.1025	0.0976
1.9	0.404	0.357	4.4	0.098	0.0936
2.0	0.377	0.333	4.5	0.094	0.0899
2.1	0.352	0.312	4.6	0.090	0.0864
2.2	0.328	0.292	4.7	0.086	0.0830
2.3	0.307	0.274	4.8	0.083	0.0799
2.4	0.287	0.258	4.9	0.080	0.0769
2.5	0.269	0.242	5.0	0.077	0.0741

TABLE VI. Dissymmetries and correction factors as a function of D/λ' (the dissymmetries correspond to the angles 45° and 135°).

	Rods		Coils (monodisperse)		Coils (polydisperse)		Spheres	
D/λ'	z	$\frac{1}{P(90)}$	z	$\frac{1}{P(90)}$	z	$\frac{1}{P(90)}$	z	$\frac{1}{P(90)}$
0.05	1.006	1.006	1.014	1.012	1.012	1.016	1.011	1.010
0.10	1.032	1.023	1.065	1.045	1.094	1.066	1.061	1.041
0.15	1.070	1.050	1.135	1.103	1.200	1.148	1.136	1.090
0.20	1.127	1.089	1.257	1.183	1.340	1.263	1.255	1.171
0.25	1.200	1.144	1.410	1.290	1.519	1.391	1.441	1.280
0.30	1.279	1.207	1.585	1.432	1.715	1.520	1.695	1.439
0.35	1.372	1.288	1.790	1.612	1.924	1.760	2.080	1.622
0.40	1.495	1.377	2.020	1.809	2.151	2.051	2.657	1.930
0.45	1.620	1.486	2.283	2.049	2.360	2.330	3.692	2.341
0.50	1.753	1.608	2.534	2.320	2.569	2.642	5.810	2.78
0.55	1.895	1.744	2.796	2.660	2.778	2.987		
0.60	1.971	1.860	3.060	2.982	2.980	3.365		
0.65	2.058	2.010	3.303	3.413	3.169	3.776		
0.70	2.106	2.193	3.521	3.814	3.354	4.218		
0.75	2.160	2.361	3.745	4.348	3.523	4.695		
0.80	2.200	2.500	3.915	4.776	3.681	5.205		

TABLE VII. Values of β and correction factors as a function of D/λ'.

	Rods		Coils (monodisperse)		Coils (polydisperse)		Spheres	
D/λ'	β	$1/Q$	β	$1/Q$	β	$1/Q$	β	$1/Q$
0.05	0.017	1.007	0.027	1.015	0.038	1.020	0.028	1.015
0.10	0.045	1.020	0.071	1.044	0.114	1.060	0.072	1.044
0.15	0.087	1.045	0.145	1.088	0.234	1.130	0.171	1.099
0.20	0.150	1.089	0.265	1.169	0.368	1.239	0.292	1.175
0.25	0.220	1.125	0.405	1.250	0.481	1.363	0.488	1.275
0.30	0.309	1.172	0.522	1.372	0.583	1.506	0.635	1.409
0.35	0.394	1.255	0.630	1.481	0.672	1.655	0.841	1.580
0.40	0.463	1.330	0.725	1.630	0.755	1.812	1.058	1.795
0.45	0.523	1.405	0.795	1.800	0.833	2.000	1.281	2.061
0.50	0.575	1.490	0.856	1.986	0.894	2.188		
0.55	0.615	1.579	0.937	2.173	0.941	2.390		
0.60	0.645	1.673	0.988	2.352	0.978	2.591		
0.65	0.690	1.761	1.039	2.550	1.017	2.815		
0.70	0.701	1.842	1.084	2.761	1.056	3.030		
0.75	0.701	1.931	1.120	2.985	1.099	3.270		
0.80	0.701	2.015	1.150	3.223	1.122	3.509		

Kinetics of OH Radicals from Flame Emission Spectra. I. Vibrational Transition Probabilities, Intensities, and Equilibrium in the $^2\Sigma^+ - {}^2\Pi$ Transition*

K. E. SHULER**
Applied Physics Laboratory, The Johns Hopkins University, Silver Spring, Maryland
(Received April 10, 1950)

The relative vibrational transition probabilities for the first four vibrational levels of the $^2\Sigma^+ - {}^2\Pi$ system of OH have been calculated. Anharmonic wave functions derivable from the Morse potential function were used and the electronic dipole moment matrix component appearing in this formulation has been evaluated. Relative intensities for the various bands have been calculated under the assumption of thermal equilibrium. Comparison of these calculated values with the data of Dieke and Crosswhite on the oxy-acetylene flame at one atmosphere indicate vibrational equilibrium with a vibrational temperature of ~3750°K in the outer cone which compares with a rotational temperatue of ~3000°K. The relationship between vibrational and rotational equilibrium for this case is discussed briefly.

INTRODUCTION

IN studying the kinetics of chemical reactions occurring in flames it is of great importance to ascertain whether the electronically excited species are in thermodynamic equilibrium. A spectroscopic study of the radiation emitted by a flame can give much information about the processes by which these excited species are formed. A non-equilibrium distribution or a lack of equipartition of the various degrees of freedom in the emitted radiation indicates that one is dealing with chemiluminescence, and the specific deviation from an equilibrium distribution can give a clue as to the chemical reaction responsible for it.[1,2] A state of complete thermodynamic equilibrium of the excited species indicates either that the radiation is purely thermal, or that the radiating species, which may have been formed in a non-equilibrium distribution by a chemical reaction, have been brought to a state of thermal equilibrium by collisions. This alternative may be resolved by further experiments at various pressures. This paper deals with a case of chemiluminescence where the electronically excited OH radicals do not appear to be in equilibrium as regards their nuclear motions.

It is intended here to discuss the various factors connected with the spectroscopic study of vibrational equilibrium such as vibrational transition probabilities and relative intensities on which, as pointed out by Gaydon,[3] not too much work has been done so far. While this paper deals specifically with the $^2\Sigma^+ - {}^2\Pi$ transition of OH, the methods discussed are of general utility and can be applied to any case for which sufficient spectroscopic data are at hand.

TRANSITION PROBABILITIES

Quantum-Mechanical Formulation

The intensity of a line due to a transition $n \rightarrow m$ is given by

$$I_{nm} = N_n A_{nm} h\nu_{nm}, \tag{1}$$

where A_{nm} is the radiative transition probability for the transition $n \rightarrow m$, and N_n is the number of molecules in the initial state. The Einstein transition probability coefficient for spontaneous emission, A_{nm}, is a molecular constant and is given by[4]

$$A_{nm} = \frac{32\pi^3 \nu_{nm}^3}{3c^3\hbar} |M_{nm}|^2, \tag{2}$$

where

$$|M_{nm}| = \int \Psi_n \mathbf{M} \Psi_m d\tau \tag{3}$$

is the matrix element of the electric moment $\mathbf{M}$. The complete wave function can be written as[5]

$$\Psi = \varphi_e(x, r)\psi_{ev}(r), \tag{4}$$

where x represents the electronic coordinates, r the nuclear coordinate (internuclear separation), which enters into the electronic wave function, φ_e, as a parameter, e and v are the electronic and nuclear quantum numbers respectively, and ψ_{ev} is the nuclear wave function.[6] Within this approximation Eq. (3) becomes

$$|M_{nm}| = \int \psi_{e'n}(r)\psi_{e''m}(r) M_{e'e''}(r) dr, \tag{5}$$

* The work described in this paper was supported in part by the Bureau of Ordnance, U. S. Navy under Contract NOrd-7386.
** This research was conducted while the author was an AEC Postdoctoral Fellow in the Physical Sciences of the National Research Council.

[1] See for example, A. G. Gaydon, *Spectroscopy and Combustion Theory* (Chapman and Hall, Ltd., London, 1948), Chapter III.
[2] A. G. Gaydon, Rev. Inst. Franc, Petrole et Ann. Combustibles liquides **IV**, No. 8, 405 (1949).
[3] A. G. Gaydon, Nature **165**, 170 (1950).
[4] See for example, Eyring, Walter, and Kimball, *Quantum Chemistry* (John Wiley and Sons, Inc., New York, 1947), p. 115.
[5] M. Born and J. R. Oppenheimer, Ann. d. Physik **84**, 457 (1927).
[6] Gibson, Rice, and Bayliss, Phys. Rev. **44**, 193 (1933), have shown that the values of the vibrational matrix components are practically independent of the rotational quantum number J. This is particularly true for the relatively low values of J likely to be encountered in flames or discharges. The rotational part of the wave function can therefore be neglected in the evaluation of the nuclear wave function $\psi_{ev}(r)$.

TABLE I. Spectroscopic data for OH (nnits in cm^{-1}).

State	ω_e	$x_e\omega_e$	B_e	γ_e	r_e(A)
$^2\Sigma^+$	3184.28	97.84	17.355	−0.00825	1.013
$^2\Pi$	3735.21	82.21	18.871	0.0035	0.971

where

$$M_{e'e''}(r)=\int \varphi_{e'}(x,r)M(x,r)\varphi_{e''}(x,r)dx \qquad (6)$$

is the electronic dipole moment matrix component.

It is usual in the application of these formulas to replace $M_{e'e''}(r)$ by an average value independent of r, so that the evaluation of Eq. (5) reduces to that of an overlap integral of the nuclear wave functions, ψ_{ev}, in the different states.[7] In the treatment to follow, it will however not be assumed that $M_{e'e''}(r)$ is a constant with respect to r, and an attempt will be made to evaluate it and investigate the effects of this procedure on the values of the transition probabilities.

Because of our lack of knowledge of the correct electronic wave functions of OH, it is not possible to evaluate $M_{e'e''}(r)$ explicitly as has been done for the case of H_2 by James and Coolidge.[8] However, following an earlier procedure of these authors,[9] one can expand $M_{e'e''}(r)$ in terms of r as

$$M_{e'e''}(r)=c(1+\rho r+\sigma r^2+\cdots), \qquad (7)$$

where the expansion coefficients are then determined by comparison with experimental intensity data. Since for OH there are only sufficient data to determine the first expansion coefficient, the expansion given in Eq. (7) was terminated at the second term.[10]

Potential Curves and Wave Functions

The best radial wave functions for the evaluation of Eq. (5) can be obtained from a Dunham series by the method of James, Coolidge, and Present,[9] but this rather laborious procedure does not seem worth while in this case. On the other hand, the usual procedure[11–16] of using harmonic oscillator wave functions and assuming $\rho, \sigma, \cdots=0$ is admittedly only a first approximation. Recent attempts by Gaydon and Pearse[17] and others[18,19] to obtain better approximations to the correct wave functions by empirically distorting harmonic wave functions to "fit" a Dunham potential curve are probably not very successful due to the error involved in locating the central nodes and maxima on the bisector of a harmonic oscillator parabola. (Compare Fig. 1 of reference 17 with Fig. 1 of this paper.) The very beautiful method worked out by Gibson, Rice, and Bayliss,[20] for continuous absorption spectra is not readily applicable to discrete spectra.

TABLE II. Calculated and experimental values for the rotational constants α_e and D_e.

State	α_e calc.	α_e exp.	D_e calc.	D_e exp.
$^2\Sigma^+$	0.748	0.807	0.00207	0.00204
$^2\Pi$	0.622	0.714	0.00193	0.00187

The method adopted here is to use the anharmonic wave functions obtained from the Morse potential function[21] in the form given by Dunham.[22] The accuracy with which an analytic wave function will represent the true wave function will depend upon the accuracy with which the potential, from which it is derived, will reproduce both the correct vibrational and rotational energy levels. The applicability of Morse wave functions for OH can be tested in this manner. According to Pekeris[23] the Morse equation leads to

$$\alpha_e=6B_e x_e[(B_e/x_e\omega_e)^{\frac{1}{2}}-B_e/x_e\omega_e] \qquad (8)$$

$$D_e=4B_e^3/\omega_e^2 \qquad (9)$$

for the rotation and rotation-vibration constants, where α_e and D_e are, respectively, $-Y_{11}$ and $-Y_{02}$ in the energy-level equation

$$E_{V,J}=\sum_{i,j} Y_{ij}(v+\tfrac{1}{2})^i J(J+1)^j. \qquad (10)$$

The spectroscopic constants for OH used in evaluating the above relation and others throughout this paper are taken from a report by Dieke and Crosswhite[24] who redetermined the fundamental spectroscopic data for most of the prominent OH bands. Their data are reproduced in Table I. Table II gives the calculated and experimental values[24] for α_e and D_e. The rather good agreement indicates that the Morse wave function is a good approximation to the true wave function.

Another test which can be made for the suitability of the Morse potential function is a comparison with

[7] E. U. Condon, Phys. Rev. **32**, 858 (1928); see also Am. J. Phys. **15**, 365 (1947) for Condon's views on the above approximation.
[8] H. M. James and A. S. Coolidge, Phys. Rev. **55**, 184 (1939).
[9] Coolidge, James, and Present, J. Chem. Phys. **4**, 193 (1936).
[10] The results of James and Coolidge indicate that the variation of $M_{e'e''}(r)$ with r is represented more accurately as a quadratic function of r. If sufficient experimental data is available expansion (7) thus should be carried out at least to the r^2 term.
[11] E. Hutchisson, Phys. Rev. **36**, 410 (1930); **37**, 45 (1931).
[12] K. Wurm, Zeits. f. Astrophys. **5**, 260 (1932).
[13] N. R. Tawde, Proc. Roy. Soc. **A137**, 575 (1932).
[14] W. G. Brown, Zeits. f. Physik **82**, 768 (1933).
[15] V. Kondratjew, J. Exp. Theor. Phys. (U.S.S.R.) **4**, 447 (1937).
[16] N. R. Tawde and V. S. Patankar, Proc. Phys. Soc. **55**, 396 (1943).
[17] A. G. Gaydon and W. B. Pearse, Proc. Roy. Soc. **A173**, 37 (1939).
[18] R. C. Parkhurst, Proc. Phys. Soc. **62A**, 191 (1949).
[19] M. E. Pillow, Proc. Phys. Soc. **62A**, 237 (1949).
[20] See reference 6; I wish to thank Professor Rice for private communication in regard to this paper.
[21] P. M. Morse, Phys. Rev. **34**, 57 (1929).
[22] J. L. Dunham, Phys. Rev. **34**, 438 (1929).
[23] C. L. Pekeris, Phys. Rev. **45**, 98 (1934).
[24] G. H. Dieke and H. M. Crosswhite, *The Ultraviolet Bands of OH, Fundamental Data*, Bumblebee Series, Report No. 87, November 1948, The Johns Hopkins University. The spectra were photographed in the second order of a 21-ft. concave grating (30,000 lines/inch) in a Paschen mounting with a linear dispersion of 0.6A/mm. The author wishes to thank Drs. Dieke and Crosswhite for their kind permission to use their data in this paper.

the Dunham potential function[25] which explicitly includes rotation and rotation-vibration interaction terms. The potential energy $V(\xi)$ is given by

$$V(\xi)=a_0\xi^2[1+a_1\xi+a_2\xi^2+\cdots], \quad (11)$$

where $\xi=(r-r_e)/r_e$ and the a's are functions of the Y_{ij} of Eq. (10). Evaluation of Eq. (11) using the data of Table I gives

$$^2\Sigma^+: V(\xi)=146{,}062\xi^2(1-2.422\xi+3.574\xi^2-4.539\xi^3) \quad (12)$$

$$^2\Pi: V(\xi)=184{,}831\xi^2(1-2.248\xi+3.413\xi^2-4.702\xi^3). \quad (13)$$

Since one is dealing with the lower vibrational states, the Morse equations $V(\xi)=D[1-\exp(-2\beta)]^2$ with $2\beta=(\omega_e x_e/B_e)^{\frac{1}{2}}$ were fitted around the equilibrium point r_e by using the experimental values of $\omega_e x_e$ and B_e rather than the dissociation energies. These Morse potential curves are shown in Fig. 1. In the region of validity of a finite polynomial expansion of the potential function, i.e., for small values of ξ, the Dunham curve coalesces completely with the Morse curve. For the first three vibrational levels, the potential curves of Fig. 1 are thus both Morse and Dunham potentials.

According to Dunham[22] the wave functions for the Morse potential curve are

$$R_n(r)=A_n\exp[-(yk)/2](ky)^{(k-2n-1)/2}L_{kn}(ky) \quad (14)$$

where

$$y=\exp[-a(r-r_e)]$$

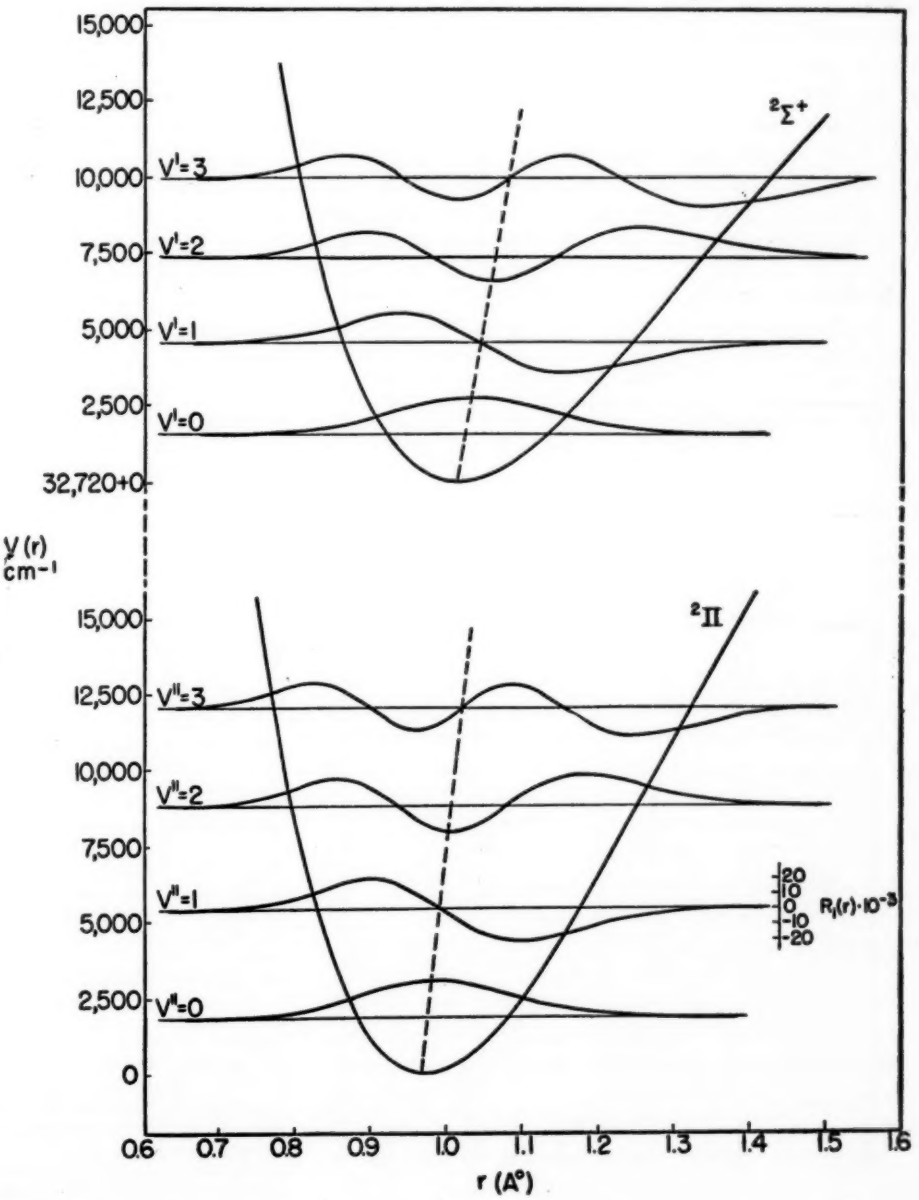

FIG. 1. Morse potential curves and Morse anharmonic wave functions for the $^2\Sigma^+$ and $^2\Pi$ states of OH.

[25] J. L. Dunham, Phys. Rev. 41, 72 (1932).

and

$$A_n=\left[\frac{a(k-2n-1)}{n!(k-n-1)\Gamma(k-n-1)}\right]^{\frac{1}{2}}. \quad (15)$$

L_{kn} is related to the generalized Laguerre polynomial and defined by

$$L_{kn}(z)=z^n-n(k-n-1)z^{n-1}+(2!)^{-1}n(n-1)(k-n-1)(k-n-2)z^{n-2}+\cdots \quad (16)$$

and a and k are given by

$$a=(\omega_e x_e/B_e)^{\frac{1}{2}}\cdot 1/r_e, \quad k=\omega_e/x_e\omega_e. \quad (17)$$

Equation (14) is the solution of the wave equation for $J=0$. The solution for the more general case $J\neq 0$ has been given by Pekeris.[23] As pointed out in reference (6), sufficient accuracy for comparison between experimental and calculated values can be achieved by using Morse wave functions ($J=0$) and experimental lines of low J.

The wave functions given by Eq. (14) are shown in Fig. 1. It may be noted that they are less "spread" in the steep part of the potential curve indicating that the oscillator spends less time in that configuration. It is also interesting to note that the central maxima and nodes fall on a straight line with a slope approximately proportional to the anharmonicity of the oscillator. A more detailed comparison between the harmonic and anharmonic oscillator OH is given in Fig. 2.

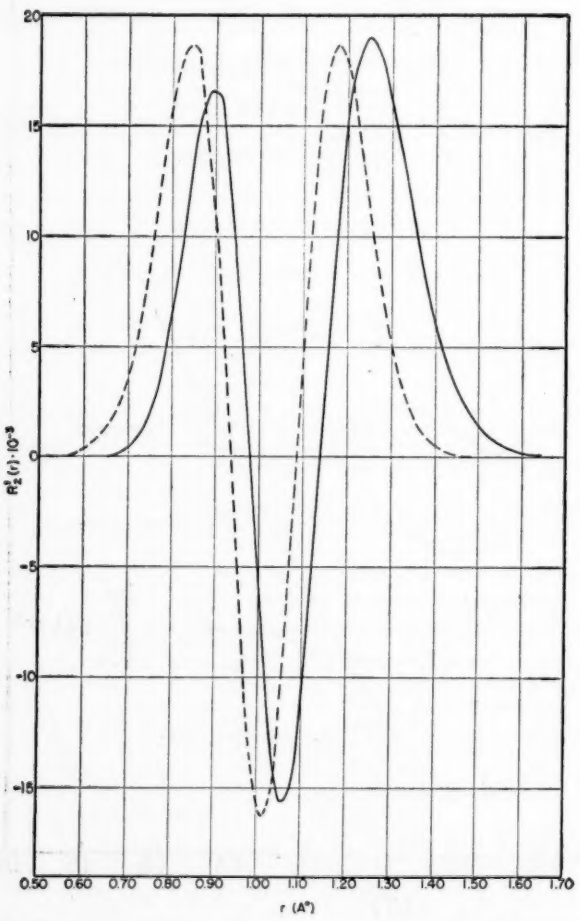

FIG. 2. Harmonic oscillator (dotted curve) and Morse anharmonic oscillator (full curve) for the $V'=2$ level of OH.

Evaluation of the Matrix Components and the Expansion Factor

It has so far not been possible to evaluate Eq. (5) with the wave functions of Eq. (14) in closed form.[26] The integrals of Eq. (5) (with $M_{e'e''}(r)$ given by Eq. (7) with $\sigma=0$) were therefore evaluated by numerical integration, i.e., by a summation of the products of ordinates in the case of integrals of the type $\int R'(r)R''(r)dr$ and a summation of the products of ordinates with the running variable r in the case of integrals $\int R'(r)R''(r)rdr$. Each summation extended over 80 intervals of 0.01A, each point having been calculated from Eq. (14) using the data of Table I. Since it is only the ratios $|M_{nm}|^2/|M_{0-0}|^2$ which are of interest, this method should be quite accurate.

The expansion coefficient ρ was determined by a comparison of the ratios $|M_{nm}|^2/|M_{np}|^2$, calculated from Eqs. (5) and (7), with the experimental values of these ratios determined by Dieke and Crosswhite.[27] Taking the ratio of intensities of bands from the same initial level, one can calculate the corresponding ratio of transition probabilities and matrix components independent of any vibrational temperature and irrespective of whether equilibrium exists.[28] The data of Dieke and Crosswhite give

$$|M_{1-1}|^2/|M_{1-0}|^2=1.625; \quad |M_{2-1}|^2/|M_{2-2}|^2=1.308; \quad |M_{3-2}|^2/|M_{3-3}|^2=2.700.$$

Substitution of these values into Eq. (5) gives $\rho=-0.80$, -0.75 and -0.71 with an average of $\rho=-0.75$.[29,30] This value of ρ for OH is reasonable in comparison with the value of $\rho=-0.3$ to -0.4 found by James and Coolidge[7] for H_2, the larger value of ρ being due to the

[26] The difficulty is that $r_e'\neq r_e''$ so that one has what virtually amounts to a shift of coordinate systems during integration. Since the Laguerre polynomials are generalized Hermite polynomials, one could use the method of Hutchisson (see reference 11). However, the resulting solutions are so laborious to evaluate that not much advantage is gained thereby.

[27] G. H. Dieke and H. M. Crosswhite, Quarterly Report, NOrd-8036, JHB-3, Problem A, October 1–December 31, 1949. These intensities were determined photoelectrically with photomultiplier tubes calibrated against a tungsten lamp. An accuracy of five percent is claimed for these measurements. The author wishes to thank Drs. Dieke and Crosswhite for permission to use these unpublished data.

[28] $I_{j-k}=c\nu_{j-k}A_{j-k}N_j$ where the unspecified N_j depends upon the excitation conditions. Analogously $I_{j-l}=c\nu_{j-l}A_{j-l}N_j$ with the same N_j. Then $I_{j-k}/I_{j-l}=(\nu_{j-k}/\nu_{j-l})(A_{j-k}/A_{j-l})$ where the ratio of intensities and frequencies is known experimentally.

[29] Dr. Crosswhite informed the author that I_{1-0} may not be quite accurate because of the difficulty of calibrating the phototube at this short wave-length region (2811A) with the tungsten lamp in use at present.

[30] Since ρ appears as a quadratic in the evaluation of $|M_{nm}|^2/|M_{np}|^2$ the solutions for ρ give double roots. The other set of roots with a $\rho_{Av}=-0.994$ must be rejected since its use results in physically meaningless negative values of some of the $|M_{nm}|^2$.

contribution of the permanent dipole of the heteronuclear OH. This rather large value of ρ indicates that the variation of $M_{e'e''}(r)$ with r cannot be neglected in the calculation of the vibrational transition probabilities of OH.*

The results of these calculations are summarized in Table III. Column 2 gives the values of $|M_{nm}|^2$ calculated by Kondratjew[15] by means of Hutchisson's formula using harmonic oscillator wave functions; blank spaces indicate that no value was given by Kondratjew for these transitions. Column 3 gives the values calculated from Eqs. (5) and (7) with $\rho=0$, using the anharmonic oscillator wave function of Eq. (14). Column 4 gives the values of $|M_{nm}|^2$ calculated for the case of a variable electronic dipole moment matrix component. Comparison of column 4 with columns 2 and 3 shows that the variation of $M_{e'e''}(r)$ with r is a more important factor in the calculation of transition probabilities for most of the transitions than is the use of more exact wave functions. Column 5 gives the relative transition probabilities as defined by Eq. (2). While it is difficult to make an estimate of their accuracy, one would probably be safe considering them accurate to about ten percent. Columns 6 and 7 give the relative and absolute radiative lifetimes τ of the several vibrational levels, where τ_i is defined by

$$\tau_i=1/\sum_k A_{ik}. \qquad (18)$$

The absolute radiative lifetimes were calculated from the value of τ_0 for OH determined by Oldenberg and Rieke[31] from absorption spectra. These figures indicate that the radiative lifetime of OH in the level $v'=2$ may be somewhat shorter than in the other levels.

VIBRATIONAL EQUILIBRIUM AND TEMPERATURE

Discussion of Results

The relative intensities of the various bands can be calculated for the case of thermal equilibrium by

$$I_{nm}/I_{0-0}=(A_{nm}/A_{0-0})(\nu_{n-m}/\nu_{0-0}) \times\exp[(E_0-E_n)/kT]. \qquad (19)$$

The calculated values of I_{n-m}/I_{0-0} are given for various temperatures by the curves of Fig. 3. The crosses are the experimental points of Dieke and Crosswhite[27] for the relative intensities of the various OH bands in the outer cone of an oxy-acetylene flame at atmospheric pressure. With the exception of the apparently bad (1–0) point (see reference 29) all the remaining points fall on a straight line indicating vibrational equilibrium with a temperature of ~3750°K. This compares with a rotational temperature of ~3000°K found by Dieke and Crosswhite[24] and a thermochemically calculated flame temperature of 3320°K[32] for a stoichiometric oxy-acetylene flame at one atmosphere.

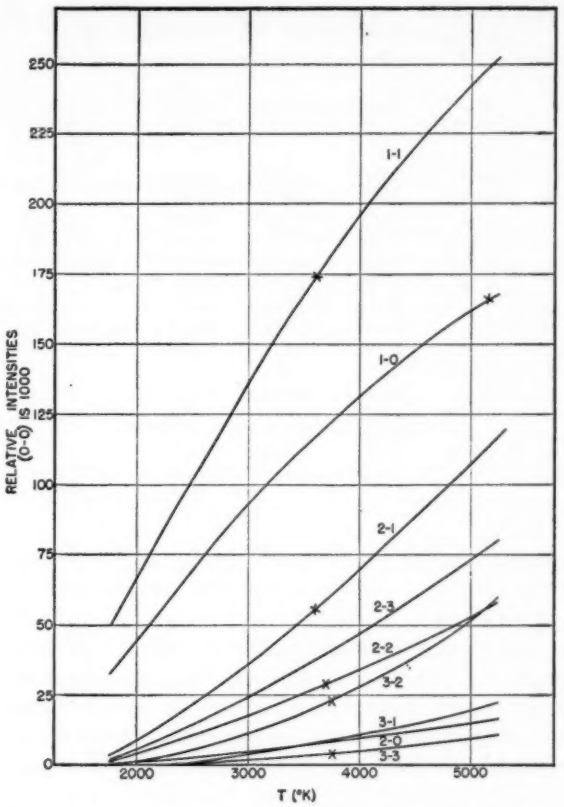

FIG. 3. Relative intensity of various OH bands (O→O is 1000) in the temperature range between 2000–5000°K under assumption of thermal equilibrium. Crosses are experimental points of Dieke and Crosswhite for the outer cone of an oxy-acetylene flame at atmospheric pressure.

This difference between the vibrational and rotational "temperatures" seems to indicate a lack of equipartition between the vibrational and rotational degrees of freedom. If the OH radicals are produced in the oxy-acetylene flame by chemical reactions, as is most probably the case, this lack of equipartition is due to the failure of the collisions to establish a state of complete equilibrium. The relative efficiency of collisions in the interchange of energy has been discussed in detail by Oldenberg and Frost.[33] They have pointed out that the persistence of the internal modes of motion under collision is more pronounced the larger the individual quantum is in comparison with kT. For OH in the lower vibrational levels the vibrational quanta are about 2000–3000 cm^{-1}, the rotational quanta are about 100–400 cm^{-1} while kT at 3000°K is about 2000 cm^{-1}. The

* *Note added in proof.*—As has been pointed out by G. Herzberg in *Spectra of Diatomic Molecules* (D. Van Nostrand Company, Inc., New York, 1950), p. 396, the variation of $M_{e'e''}(r)$ with r is particularly large when a transition is forbidden for the separated atoms but allowed in the molecule, as is the case for the $^2\Sigma^+-{}^2\Pi$ transition of OH. The large value of ρ found here is thus in good agreement with the small f value determined by Oldenberg and Rieke (see reference 31) for OH and attributed by them to the half-forbidden transition of OH.

[31] O. Oldenberg and F. F. Rieke, J. Chem. Phys. **6**, 439 (1938).

[32] A. G. Gaydon and H. G. Wolfhard, Proc. Roy. Soc. **A194**, 169 (1948).

[33] O. Oldenberg and A. Frost, Chem. Rev. **20**, 99 (1937).

TABLE III. Relative transition probabilities and lifetimes of excited states for the $^2\Sigma^+ - ^2\Pi$ transition of OH.

Transition $V'-V''$	$\lvert M_{nm}\rvert^2$ reference 15	$\lvert M_{nm}\rvert^2$ $\rho=0$	$\lvert M_{nm}\rvert^2$ $\rho=-0.75$	A_{n-m} $\rho=-0.75$	τ_{rel}	$\tau_{abs}\cdot 10^6$ sec.
0–0	1	1	1	1	1	3.8
0–1	0.090	0.103	0.005	0.004		
0–2	0.014	0.004	0.001	0.000		
0–3	0.002	0.000	0.000	0.000		
1–0	0.105	0.098	0.267	0.348	1.07	4.1
1–1	0.809	0.780	0.612	0.580		
1–2	0.147	0.220	0.004	0.003		
1–3		0.016	0.003	0.001		
2–0		0.007	0.041	0.067	0.76	2.9
2–1	0.204	0.199	0.432	0.526		
2–2	0.644	0.550	0.323	0.289		
2–3		0.324	0.686	0.442		
3–0	0.000	0.001	0.011	0.022	1.17	4.4
3–1	0.002	0.028	0.122	0.185		
3–2	0.294	0.278	0.478	0.543		
3–3		0.309	0.126	0.106		

rotational degrees of freedom are therefore brought more readily into complete thermal equilibrium with the other degrees of freedom than the vibrational ones; thus Oldenberg[34] finds no persistence of any abnormal rotation for OH. On the other hand, vibrational persistence is well known from sound dispersion experiments where one is also dealing with vibrational quanta comparable with kT. It is, however, possible as indicated by the above results that the vibrational modes will show an equilibrium distribution among themselves due to the relative ease of vibration-vibration energy interchange without being in equilibrium with the translational and rotational modes of motion. This point will be discussed in more detail in a later communication.

[34] O. Oldenberg, Phys. Rev. **37**, 1550 (1931); **46**, 210 (1934).

There is also the possibility that the discrepancy between the rotational and vibrational temperatures noted above is due to the various approximations which are involved in this comparison. These approximations are twofold: the empirical expansion of $M_{v'v''}(r)$ as a linear moment function and the partial neglect of vibration-rotation interaction in the calculation of both rotational[35] and vibrational transition probabilities. It is very difficult to estimate the effect of these approximations upon the accuracy of the calculated vibrational temperature, and further work will be necessary before it is possible to decide between the above alternatives as to the cause of this "temperature" discrepancy.

ACKNOWLEDGMENTS

The author wishes to express his appreciation to the National Research Council for the award of an AEC Postdoctoral Fellowship. He also wishes to acknowledge with thanks the hospitality of the Applied Physics Laboratory of The Johns Hopkins University during the tenure of this fellowship. Particular thanks are due the members of the Research Center for their kind interest. The writer is indebted to Dr. F. T. McClure and Dr. R. C. Herman of this Laboratory, Dr. G. H. Dieke and Dr. H. M. Crosswhite, The Johns Hopkins University, and Dr. Hugh M. Hulburt, The Catholic University of America, for stimulating discussions and helpful suggestions in connection with this work. Thanks are also due Miss K. E. Pace for assistance in the calculations and Miss S. Thomas for aid in the preparation of this manuscript.

[35] E. L. Hill and J. H. Van Vleck, Phys. Rev. **32**, 250 (1928); L. T. Earls, Phys. Rev. **48**, 423 (1935).

Diffusion of Lead Chloride Dissolved in Solid Silver Chloride

CARL WAGNER*
Ordnance Research and Development Division Suboffice (Rocket), Fort Bliss, Texas
(Received May 19, 1949)

A particular solution of the differential equation of diffusion involving a diffusion coefficient proportional to concentration is presented.

From previous experiments by Wagner and Zimens the diffusion coefficient for the exchange of lead and silver ions, extrapolated to the concentration of a saturated solution of lead chloride in solid silver chloride, is calculated to be $2.4 \cdot 10^{-9}$ cm²/sec. at 270°C. Therefrom it follows that the self-diffusion coefficient of lead ions equals $0.8 \cdot 10^{-9}$ cm²/sec. In contrast, the self-diffusion coefficient of silver ions, derived from conductivity measurements of Koch and Wagner, amounts to $9.2 \cdot 10^{-8}$ cm²/sec.

INTRODUCTION

In pure solid silver chloride, cationic conduction is due to the presence of interstitial silver ions and cation vacancies as suggested by Frenkel.[1] Addition of small amounts of lead chloride increases the conductivity greatly. According to Koch and Wagner,[2] the conductivity over a wide range is proportional to the concentration of lead chloride. If the concentration of lead chloride is much greater than the concentration of interstitial silver ions in pure silver chloride, interstitial silver ions can practically be disregarded and the number of cation vacancies equals the number of lead ions, each lead ion occupying a normal cation position and replacing two silver ions in accordance with its double electrical charge. Silver ions can move by jumping from normal lattice positions to adjacent cation vacancies, and the same holds true for lead ions.

On the basis of this disorder model, it is to be expected that the diffusion coefficient for the exchange of lead and silver ions in solid silver chloride as solvent is essentially proportional to the concentration of lead chloride, although the solution is a dilute one, the saturation concentration being as low as 0.63 mole percent at 270°C as found by Wagner and Zimens.[3]

To obtain the solubility of lead chloride in solid silver chloride, Wagner and Zimens put a set of three tablets of silver chloride between tablets consisting of a heterogeneous mixture of 90 percent of silver chloride and 10 percent of lead chloride. After annealing, the lead content of the middle silver-chloride tablet was determined. To ascertain the time required for practical establishment of equilibrium, different annealing periods were applied. Thus far the concentration of lead as a function of the annealing time has not been used to calculate the diffusion coefficient. This evaluation follows below.

MATHEMATICAL ANALYSIS

The general equation for non-stationary, one-dimensional diffusion reads

$$\frac{\partial c}{\partial t} = \frac{\partial}{\partial x}\left(D\frac{\partial c}{\partial x}\right). \tag{1}$$

Here c represents the concentration of the diffusing component, x the distance from a reference plane, t time, D the diffusion coefficient, which may vary with concentration, or be constant. If the diffusion coefficient is assumed to be proportional to concentration, we have

$$\frac{\partial c}{\partial t} = \frac{\partial}{\partial x}\left(D_0\frac{c}{c_0}\frac{\partial c}{\partial x}\right), \tag{2}$$

where D_0 represents the diffusion coefficient for a reference concentration which in the following text is equated to the saturation concentration c_0.

Under the conditions applied by Wagner and Zimens, the approach to equilibrium is represented by a solution of differential Eq. (2) with the initial condition

$$c=0 \quad \text{at} \quad t=0. \tag{3}$$

At the two borders of the silver chloride layer ($x=0$ and $x=\delta$), the concentration of lead chloride equals the saturation concentration c_0 at any time. Thus,

$$c=c_0 \quad \text{at} \quad x=0 \quad \text{and} \quad x=\delta \quad \text{if} \quad t>0. \tag{4}$$

According to the foregoing assumption $D=D_0(c/c_0)$, diffusion is extremely slow at small concentrations and the diffusion rate even becomes zero for $c=0$. Consequently, we must expect a peculiar form of the concentration-locus curve at low concentrations provided Eq. (2) holds true. This is the salient point of the following mathematical analysis, based on Eq. (2) as an interesting limiting case.

Actually, deviations from the presuppositions of this limiting case occur, for the diffusion coefficient in pure silver chloride is finite because of its finite conductivity, which is accounted for by the disorder model of Frenkel. Hence, the investigation of the limiting case $D=D_0(c/c_0)$ leads to a minimum value of the diffusion rate for a

* Present address: Department of Metallurgy, Massachusetts Institute of Technology, Cambridge, Mass.

[1] J. Frenkel, Zeits. f. Physik **35**, 352 (1926).
[2] E. Koch and C. Wagner, Zeits. f. physik. Chemie B **38**, 295 (1938).
[3] C. Wagner and K. E. Zimens, Acta Chem. Scandinavica **1**, 539 (1947).

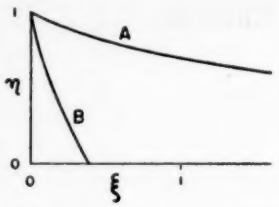

FIG. 1. Schematic solutions of differential Eq. (11).

given diffusion coefficient D_0 and thus yields a limit of error for the following evaluation of diffusion experiments.

The present problem may be resolved into two separate problems. First, we inquire into the concentration as a function of locus and time as long as the concentration in the central region of the silver chloride layer is negligible so that we have practically the problem of diffusion into a semi-infinite space. Then partial differential Eq. (2) can be transformed into an ordinary differential equation by introducing

$$\xi = x/2D_0^{\frac{1}{2}}t^{\frac{1}{2}} \tag{5}$$

as independent variable which is also used in the analysis for a constant diffusion coefficient. In addition, we introduce the ratio of the concentration c to the saturation concentration c_0,

$$\gamma = c/c_0. \tag{6}$$

Upon substitution of Eqs. (5) and (6) in differential Eq. (2) and the first of the pertinent boundary conditions in Eq. (4), we obtain

$$\gamma(d^2\gamma/d\xi^2)+(d\gamma/d\xi)^2+2\xi(d\gamma/d\xi)=0, \tag{7}$$

$$\gamma=1 \quad \text{at} \quad \xi=0. \tag{8}$$

According to Eq. (3) the concentration c shall vanish for $x>0$ and $t=0$. Thus

$$\gamma=0 \quad \text{at} \quad \xi=\infty. \tag{9}$$

Further simplification is achieved by substituting

$$\eta=\gamma^2, \tag{10}$$

whence Eqs. (7), (8), and (9) become

$$d^2\eta/d\xi^2=-2\xi\eta^{-\frac{1}{2}}(d\eta/d\xi), \tag{11}$$

$$\eta=1 \quad \text{if} \quad \xi=0, \tag{12}$$

$$\eta=0 \quad \text{if} \quad \xi=\infty. \tag{13}$$

Since analytical integration of differential Eq. (11) is not possible, numerical methods are to be used. Disregarding temporarily the second boundary condition (13), we can obtain a family of integrals by numerical integration from $\eta=1$, $\xi=0$ on with arbitrarily chosen values of $(d\eta/d\xi)_{\xi=0}\equiv\eta_0'$. Practically, only negative values of η_0' are to be taken into account because η must fall from $\eta=1$ on if one of the thus resulting integrals shall satisfy the second boundary condition (13). Then, according to Eq. (11), the second derivative of η with respect to ξ is essentially positive and the curve $\eta(\xi)$ levels off for increasing values of ξ. If $|\eta_0'|\ll 1$, a limiting value of η is reached as indicated schematically by curve A in Fig. 1. The behavior of the function $\eta(\xi)$ for large arguments can readily be derived from Eq. (11) by equating approximately η to the limiting value η_∞ and integrating analytically. Hence

$$\eta=\eta_\infty+C[1-erf(\xi\eta_\infty^{-\frac{1}{2}})] \tag{14}$$

where *erf* represents the error function and C is a constant of integration. A solution of this kind, however, does not apply in the case $\eta_\infty=0$ as required by Eq. (13) for the final solution of the present problem.

On the other hand, if $|\eta_0'|\gg 1$, integral curves result which approach the abscissa with finite slopes as schematically indicated by curve B in Fig. 1.

Tentatively, we may assume that a special value of $|\eta_0'|$ of the order of unity yields a solution $\eta(\xi)$ which vanishes at a certain argument ξ_0 and satisfies the additional condition

$$d\eta/d\xi=0 \quad \text{if} \quad \eta=0, \quad \xi=\xi_0, \tag{15}$$

which is equivalent to the condition that the transport rate shall vanish if the concentration c equals zero, for, in view of Eqs. (5), (6), and (10), the transport rate per unit cross-sectional area is

$$D_0\frac{c}{c_0}\frac{\partial c}{\partial x}=\frac{D_0^{\frac{1}{2}}c_0}{2t^{\frac{1}{2}}}\gamma\frac{d\gamma}{d\xi}=\frac{D_0^{\frac{1}{2}}c_0}{4t^{\frac{1}{2}}}\frac{d\eta}{d\xi}. \tag{16}$$

A function satisfying Eqs. (11), (12), and (15) for $0<\xi\leqq\xi_0$ can then be combined with the trivial solution $\gamma=0$ for $\xi\geqq\xi_0$ so that a solution for the whole range $\xi\geqq 0$ results.

Under the tentative assumption that condition (15) is satisfied at a finite value of $\xi=\xi_0$, the factor ξ on the right of differential Eq. (11) can approximately be replaced by ξ_0 if $\eta\ll 1$. Thus

$$d^2\eta/d\xi^2\cong-2\xi_0\eta^{-\frac{1}{2}}(d\eta/d\xi) \quad \text{if} \quad \eta\ll 1 \tag{17}$$

with the pertinent boundary conditions

$$\eta=0 \quad \text{at} \quad \xi=\xi_0, \tag{18}$$

$$d\eta/d\xi=0 \quad \text{at} \quad \xi=\xi_0. \tag{19}$$

Integration yields

$$\eta=[2\xi_0(\xi_0-\xi)]^2 \quad \text{if} \quad \eta\ll 1. \tag{20}$$

Consequently, in the vicinity of $\xi=\xi_0$, where $\eta\ll 1$, or $\gamma\ll 1$, or $c\ll c_0$, the function $\eta(\xi)$ is represented approximately by a parabola, and the concentration ratio $\gamma(\xi)=\eta^{\frac{1}{2}}$ by a straight line.

To obtain a solution of differential Eq. (11) for the whole range from $\xi=0$ to $\xi=\xi_0$, numerical integration is required. Since the boundary conditions (12) and (15) refer to different values of ξ, it is expedient to employ the further substitutions

$$z=\eta/\xi_0^4, \tag{21}$$

$$y=1-(\xi/\xi_0). \tag{22}$$

Upon introduction into Eqs. (11), (18) and (19), we have

$$d^2z/dy^2=2(1-y)z^{-\frac{1}{3}}(dz/dy) \quad (23)$$

$$z=0 \quad \text{at} \quad y=0 \quad (24)$$

$$dz/dy=0 \quad \text{at} \quad y=0. \quad (25)$$

To integrate differential Eq. (23) from $y=0$ on, the second derivative of z with respect to y at $y=0$ must be known. This value cannot be obtained directly from Eq. (23) because for $y=0$ the right member of Eq. (23) is indeterminate. Substituting Eqs. (21) and (22) in (20) and differentiating twice, we obtain

$$d^2z/dy^2=8 \quad \text{at} \quad y=0. \quad (26)$$

The numerical integration of Eq. (23) has been carried out with the aid of the method of Runge and Kutta. Thus we obtain $z(y=1)=z(\xi=0)=2.34$. Then it follows from Eqs. (21) and (12) that

$$\xi_0=[z(y=1)]^{-\frac{1}{4}}=0.81. \quad (27)$$

Transforming Eq. (22) and substituting Eq. (27), we have

$$\xi=\xi_0(1-y)=0.81(1-y). \quad (28)$$

Finally it follows from Eqs. (6), (10), (21), and (27) that

$$c/c_0=\gamma=\eta^{\frac{1}{3}}=z^{\frac{1}{3}}\xi_0^2=[z/z(y=1)]^{\frac{1}{3}}. \quad (29)$$

A graph of this function is shown as curve A in Fig. 2. For comparison, curve B shows the concentration ratio γ for a constant diffusion coefficient according to the well-known relation

$$c/c_0=1-erf(\xi)=1-erf(x/2D^{\frac{1}{2}}t^{\frac{1}{2}}). \quad (30)$$

Curve B approaches the abscissa asymptotically, whereas curve A reaches the abscissa at the finite value $\xi_0=0.81$ with a finite slope as inferred above from Eq. (20). Thus, in this special case, an advancing velocity of the diffusing component is strictly definable. From Eqs. (5) and (27) it follows that

$$(dx/dt)_{c=0}=\xi_0D_0^{\frac{1}{3}}/t^{\frac{1}{3}}=2\xi_0^2D_0/x=1.31D_0/x. \quad (31)$$

In the region $\xi\sim 0$, the two curves in Fig. 2 do not differ widely. The initial slope of curve A is obtained by differentiation of Eq. (29) and introduction of Eqs. (22) and (27)

$$(d\gamma/d\xi)_{\xi=0}=-\tfrac{1}{2}[z(y=1)]^{-\frac{1}{4}}(dz/dy)_{y=1}=-0.89, \quad (32)$$

and that of curve B by differentiation of Eq. (30),

$$(d\gamma/d\xi)_{\xi=0}=-2/\pi^{\frac{1}{2}}=-1.13. \quad (33)$$

Comparison of Eqs. (32) and (33) shows that the slopes differ only by a factor of 0.79. Since these expressions are proportional to the diffusion rates at $x=0$, we conclude that the substance passing a given cross-sectional area at $x=0$ within a given time for $D=D_0(c/c_0)$ is only 21 percent less than that in the conventional case of a constant diffusion coefficient.

Hence, the final approach to saturation of a finite region of thickness δ in the case of a diffusion coefficient proportional to concentration can approximately be described by the well-known solution of differential Eq. (1) with a constant diffusion coefficient D_0 and the boundary conditions (3) and (4). According to Barrer,[4] the solution reads

$$\frac{c(x,t)}{c_0}=1-\frac{4}{\pi}\sum_{m=0}^{m=\infty}\frac{1}{2m+1}\sin\frac{(2m+1)\pi x}{\delta}\times\exp\left[-\frac{(2m+1)^2\pi^2D_0t}{\delta^2}\right], \quad (34)$$

where m is an integral serial number. Practically, only the first term of the infinite series counts if approach to saturation corresponding to the condition $c\sim c_0$ is regarded.

In the investigation by Wagner and Zimens,[3] the average concentration c_{Av} of lead chloride in the middle silver-chloride tablet out of three, reaching from $x=\frac{1}{3}\delta$ to $x=\frac{2}{3}\delta$, was determined. Therefore we calculate from Eq. (34)

$$\left[\frac{c_{Av}}{c_0}\right]_{x=\frac{1}{3}\delta}^{x=\frac{2}{3}\delta}=1-\frac{3}{\delta}\int_{x=\frac{1}{3}\delta}^{x=\frac{2}{3}\delta}\frac{c}{c_0}dx=1-\frac{12}{\pi^2}\exp\left(-\frac{\pi^2D_0t}{\delta^2}\right) \text{ if } c_{Av}\sim c_0. \quad (35)$$

Furthermore, Eq. (23) may be integrated up to $y=-\infty$, or $x=-\infty$ with a limiting value of $z_1=6.82$. This calculation yields the solution of the following problem. We consider a semi-infinite space ($x<0$) with an initial uniform concentration c_1 and another semi-infinite space ($x>0$) with zero concentration. The

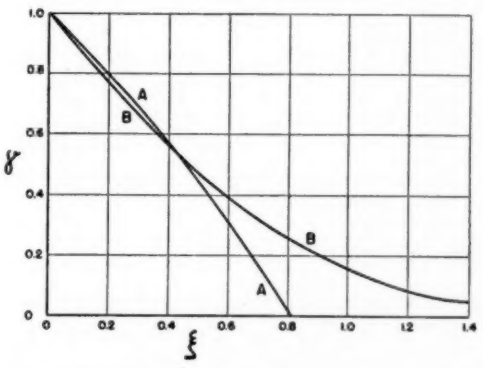

FIG. 2. Concentration ratio $\gamma=c/c_0$ versus auxiliary variable $\xi=x/2D_0^{\frac{1}{3}}t^{\frac{1}{3}}$. Curve A: Solution of differential Eq. (2) according to Eq. (29). Curve B: Solution of differential Eq. (1) with a constant diffusion coefficient, according to Eq. (30).

[4] M. Barrer, *Diffusion in and through Solids* (The Macmillan Company, New York, 1941), p. 15.

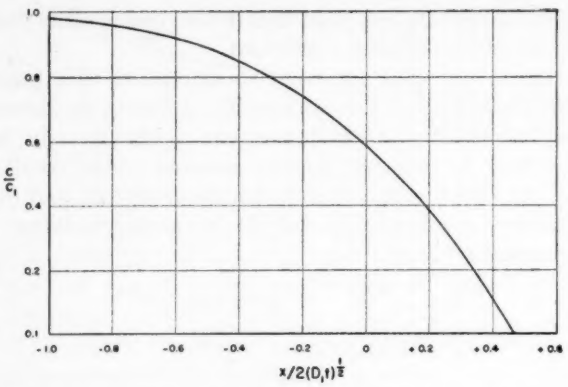

FIG. 3. Concentration ratio c/c_1 for diffusion between two semi-infinite spaces with initial concentrations c_1 for $x<0$ and zero for $x>0$ in the case of a diffusion coefficient proportional to concentration.

diffusion coefficient shall be proportional to concentration, $D=D_1(c/c_1)$, where D_1 is the diffusion coefficient for the concentration c_1. Then in view of Eqs. (6), (10), (21), and (22),

$$\frac{c}{c_1}=\left[\frac{z(y)}{z(y=\infty)}\right]^{\frac{1}{2}}=\left(\frac{z}{z_1}\right)^{\frac{1}{2}}. \tag{36}$$

This concentration ratio is to be related to the dimensionless group $x/2D_1^{\frac{1}{2}}t^{\frac{1}{2}}$, which equals because of Eq. (5)

$$\frac{x}{2D_1^{\frac{1}{2}}t}=\xi\left(\frac{D_0}{D_1}\right)^{\frac{1}{2}}=\xi\left[\frac{z(y=1)}{z(y=\infty)}\right]^{\frac{1}{2}}=0.585\xi, \tag{37}$$

where ξ is determined by y according to Eq. (28).

A graph of c/c_1 as function of $x/2(D_1t)^{\frac{1}{2}}$ is shown in Fig. 3, which may be useful in future investigations. The concentration at $x=0$ equals $0.59c_1$ instead of $\frac{1}{2}c_1$ as found in the conventional case of a constant diffusion coefficient.

CONCLUSIONS

Upon introduction of the values observed by Wagner and Zimens for diffusion periods of six and eight days into Eq. (35), there results a diffusion coefficient $D_0=2.4\cdot10^{-9}$ cm²/sec. for the exchange of lead and silver ions referred to a saturated solution of lead chloride in solid silver chloride at 270°C.

Since the mobility of cation vacancies derived from conductivity measurements is much greater than the diffusion coefficient for the exchange of lead and silver ions, diffusion of lead ions, coupled with motion of cation vacancies in the same direction, is supported by a diffusion potential. Theoretical analysis analogous to that used for other purposes[5] shows that the diffusion coefficient for the exchange of lead and silver ions equals three times the self-diffusion coefficient of lead ions. Thus the self-diffusion coefficient of lead ions in a saturated solution of lead chloride in silver chloride at 270°C is found to be $0.8\cdot10^{-9}$ cm²/sec.

In addition, we can calculate the self-diffusion coefficient of silver ions under the same conditions from conductivity measurements. Interpolating the data reported by Koch and Wagner,[2] we obtain a specific conductivity of $7.3\cdot10^{-3}$ ohm$^{-1}\cdot$cm^{-1}. Hence, with the aid of the Nernst-Einstein relation[6] between self-diffusion coefficient and electrical conductivity, the self-diffusion coefficient of silver ions in a saturated solution of lead chloride in silver chloride at 270°C is found to be $9.2\cdot10^{-8}$ cm²/sec., that is 115 times greater than the self-diffusion coefficient of lead ions under the same conditions. This divergence is understandable in view of the double electrical charge and the greater size of lead ions. According to Goldschmidt, the ionic radii of silver and lead ions respectively are 1.13 and 1.32A.

---

[5] C. Wagner, Zeits. f. physik. Chemie *B* **21**, 25 (1933); **32**, 447 (1936).

[6] W. Nernst, Zeits. f. physik. Chemie **2**, 613 (1888). A. Einstein, Ann. Physik (4) **17**, 549 (1905). C. Wagner, Zeits. f. physik. Chemie *B* **11**, 139 (1930).

Self-Diffusion of Sodium in Sodium Chloride and Sodium Bromide

DILLON MAPOTHER,* H. NELSON CROOKS,† AND ROBERT MAURER‡
Carnegie Institute of Technology, Pittsburgh, Pennsylvania
(Received May 22, 1950)

The self-diffusion coefficient of sodium in sodium chloride and sodium bromide has been measured as a function of temperature. A comparison of the self-diffusion coefficient with the electrolytic conductivity reveals that the Einstein relation is satisfied at high but not at low temperatures. The temperature dependence of the diffusion coefficient may be explained by the Schottky-Wagner vacancy theory if the presence of impurity ions is taken into account. A possible explanation for the failure of the Einstein relation in terms of association between multivalent foreign ions and vacancies is suggested.

IT is generally believed that lattice imperfections of the type known as Schottky defects are responsible for ionic mobility in the alkali halide crystals.[1] Schottky defects, as illustrated in Fig. 1, consist of vacant lattice sites. The migration of these vacancies, as neighboring ions jump into them, provides a mechanism for ionic self-diffusion and, in the presence of an electric field, for electrolytic conduction.

The transference number measurements of Tubandt show that, except at quite high temperatures, the electrical conductivity of sodium chloride is due entirely to migration of the sodium ion.[2] Presumably, the activation energy for the jump of a chloride ion into a chloride ion vacancy is much greater than that associated with the jump of a sodium ion into a sodium ion vacancy.

The vacancy mechanism of migration[1] leads to the following equations for the temperature dependence of the self-diffusion coefficient and of the electric conductivity of an alkali halide, such as sodium chloride, when it is assumed that the crystal is in thermodynamic equilibrium.

$$D=D_0\exp\left(-\frac{\epsilon+\epsilon'/2}{kT}\right), \tag{1}$$

$$\sigma=\frac{\sigma_0}{T}\exp\left(-\frac{\epsilon+\epsilon'/2}{kT}\right). \tag{2}$$

The quantities D and σ are the self-diffusion coefficient and conductivity, respectively. D_0 and σ_0 are constants. The activation energy for the jump of a sodium ion into a vacancy is represented by ϵ, while ϵ' is the work necessary to create a positive and a negative ion vacancy by moving the ions from the interior to the surface of the crystal. The ratio σ/D has the simple form

$$\sigma/D=Ne^2/kT, \tag{3}$$

which is known as the Einstein relation.[1] The number of sodium ions per unit volume of crystal is given by N while the other symbols have their usual significance.

The validity of the Einstein relation rests upon the assumption that both self-diffusion and conductivity are due to the same mechanism—in this case the migration of single vacancies. If a substantial fraction of the single positive and negative ion vacancies is paired as a result of the electrostatic attraction between them, the migration of these pairs affects the magnitude of the self-diffusion coefficient but not that of the conductivity since the pairs are electrically neutral.[1] Pairs are illustrated in Fig. 2. A calculation by Dienes[3] indicates that the pairs have an activation energy, ϵ_p, for diffusion about half as large as that of single, positive ion vacancies.

The present work is an experimental test of the Einstein relation for sodium chloride and sodium bromide. The self-diffusion coefficient and the conductivity have been measured over a range of temperature upon the same crystal samples. The conductivity of these salts has been investigated previously, notably by Lehfeldt.[4]

Single crystals in the form of cubes approximately 1 centimeter on edge were used for the measurement of the diffusion coefficient. A film of radioactive salt about 5×10^{-4} centimeter thick was deposited upon one face of each cube by evaporation in a vacuum from an electrically heated platinum boat. The faces of the crystals were masked during this operation so that the evaporated salt was deposited over a circular area whose

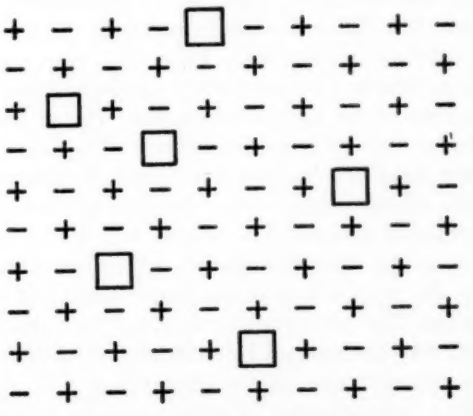

FIG. 1. Schottky defects.

* Now at the University of Illinois, Urbana, Illinois.
† Now at RCA, Camden, New Jersey.
‡ Now at the University of Illinois, Urbana, Illinois.
[1] N. Mott and R. Gurney, *Electronic Processes in Ionic Crystals* (Oxford University Press, London, 1940), Chapter II.
[2] C. Tubandt, *Handbuch der Experimental Physik*, Vol. II, Part 1.
[3] G. J. Dienes, J. Chem. Phys. **16**, 620 (1948).
[4] W. Lehfeldt, Zeits. f. Physik **85**, 717 (1933).

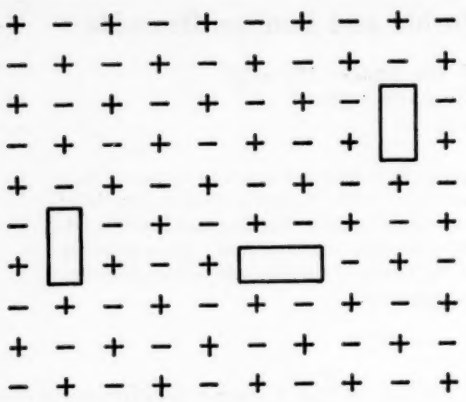

FIG. 2. Paired vacancies.

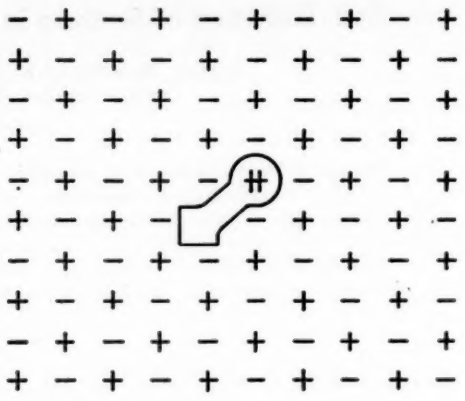

FIG. 3. Divalent ion-vacancy complex.

diameter was $\frac{11}{32}$ inches. The salt was activated by neutron irradiation at Oak Ridge, Tennessee. The chlorine activity was negligible in comparison with that of the Na^{24}.

Following the evaporation procedure, the crystals were transferred to constant temperature ovens where diffusion proceeded for a known time. During this process the crystals were sealed in Pyrex capsules at an air pressure of about 0.1 millimeter of mercury. At the higher temperatures, the crystals were placed in stainless steel cartridges, which, when sealed in Pyrex, prevented the Pyrex from collapsing about the crystals. Two crystals were placed in each capsule to provide a check upon the consistency of the data. The oven temperature was regulated to $\pm 0.5°C$ and the temperature of the crystals was determined with chromel-alumel thermocouples which were placed in contact with the outer surface of the capsule.

At the conclusion of a diffusion run, the crystals were removed from the capsules and sectioned with a microtome, slices being taken parallel to the face upon which the radioactive salt had been deposited. For this purpose, two microtomes were constructed. The first microtome which was used for the measurements upon sodium chloride was similar in principle to the second instrument but less elaborate in construction.

The microtome possessed a knife which was moved in a vertical direction by means of a precision screw which was calibrated by an interferometer. The crystal was attached to a carriage which was moved horizontally on precision ways by a motor-driven screw. In this manner, the knife edge was passed over the face of the crystal in the sectioning process. The crystal was held under the knife by a vise with micrometer adjustments for positioning the crystal face in the plane swept out by the knife edge. The proper placement of the crystal in this position was determined by reflection of a light beam from a mirror resting on the crystal face.

During the operation of sectioning the crystal, the knife and crystal were observed with a binocular microscope. The material removed from the crystal by the knife was in the form of a fine powder which was collected in the following manner. Before each passage of the knife over the crystal a strip of adhesive Cellophane tape was pressed to the crystal face. As the knife passed across the crystal the tape was removed carrying with it the sectioned material in the form of a fine powder which adhered to the tape. The samples were mounted on brass rings and the radioactive intensity of each was determined with conventional Geiger counters and scale of sixty-four circuits. The time of diffusion was limited to seven or eight half-lives of the Na^{24} and the depth of penetration of the radioactive sodium into the crystal was of the order of 10^{-2} cm. The thickness of individual slices taken with the microtome was about 5×10^{-4} cm.

The data obtained in the manner outlined was used to obtain diffusion coefficients by comparison with the equation

$$c(x,t)=\frac{c_0}{(\pi Dt)^{\frac{1}{2}}}\exp\left(-\frac{x^2}{4Dt}\right), \tag{4}$$

which is the solution of the diffusion equation appropriate to the geometry and boundary conditions of the present experiment. The concentration of radioactive sodium at time, t, and distance, x, from the face of the crystal is represented by $c(x,t)$. The initial surface concentration of radioactive sodium is represented by c_0 and D is the diffusion coefficient. In Fig. 4, which is a plot of typical data obtained from sodium chloride, the logarithm of the counts per minute obtained from a given slice is plotted against the square of the distance of the slice from the surface. In agreement with Eq. 4, the data, when plotted in this manner, yield straight lines, the slope of which is $(4Dt)^{-1}$. The precision of the determinations of the diffusion coefficients is rather difficult to estimate but is believed to be within 10 percent in the middle of the temperature range, rising to not more than 20 percent at the highest temperatures and 15 percent at the lowest temperatures. The self-diffusion coefficient of sodium in the two salts is shown as a function of temperature in Figs. 5 and 6.

The samples used for the diffusion measurements were cleaved into slabs about 2 millimeters on edge and less

than a millimeter thick for the measurement of the electrical conductivity. Electrodes were applied to the faces of the sodium chloride slabs by painting with a suspension of colloidal graphite in methyl alcohol. Sodium bromide is sufficiently hygroscopic to necessitate handling in a dry room. Graphite electrodes were applied by slightly roughing the surfaces and rubbing with a graphite pencil.

The crystal slabs were held in a constant temperature oven between nickel electrodes which were clad with platinum foil. The entire electrode assembly was mounted in a quartz tube through which a slow current of purified helium was passed. The electrically heated oven which surrounded the quartz tube was temperature-regulated to within ± 0.5°C. The temperature of the crystals was determined by a chromel-alumel thermocouple mounted in one of the nickel electrodes.

In order to avoid polarization of the crystals as a result of the passage of charge, the resistance was measured with the circuit illustrated in Fig. 7. The crystal, x, was subjected to single d.c. pulses of constant duration by means of the timing switch, T, and the resulting deflection of the ballistic galvanometer, G, observed. The pulse voltage was determined by the setting of the potentiometer, P, and measured with the voltmeter, V. The direction of the current through the crystal was reversed after each pulse with the switch, S. By means of the switch, C, the known resistance, R, was substituted for the crystal in the circuit and was adjusted to give the same deflection of the galvanometer.

The ballistic galvanometer had an undamped charge sensitivity of 3×10^{-10} coulomb per millimeter and a period of 27 seconds. The charge passed through the crystal during a single pulse varied from 10^{-8} coulomb at the lowest temperatures to 10^{-6} coulomb at the highest temperatures. The standard resistance, R, consisted of two four decade resistance boxes with a maximum series resistance of 22 megohms. At the lowest temperatures, the crystal resistance rose to 100 megohms. The maximum voltage applied to the crystal under these circumstances was 40 volts.

The timing switch, T, was a snap action switch actuated by a rotating cam. Pulse durations of 0.05, 0.091, and 0.20 second were used. A manually operated switch and relay, H, was used to allow the switch, T, which was periodically closed, to deliver isolated pulses to the crystal.

The measured crystal resistance was independent of the pulse duration indicating that polarization was avoided. Ohm's Law was verified by changing the magnitude of the applied voltage pulse. A typical result of such a check is shown in Fig. 8. Surface conduction over the sides of the crystals was shown to be negligible by the following procedure. After the resistance of a sodium chloride crystal had been measured it was split into halves along a plane perpendicular to the electrode faces and replaced between the electrodes. Although splitting the crystal increased the surface area of the sides by 50 percent, the measured resistance was unchanged over the entire temperature range within the experimental error of 5 percent.

The results of the conductivity measurements upon sodium chloride and sodium bromide are presented in Figs. 5 and 6. With the use of the Einstein relation (Eq. (3)) and the measured conductivity, a diffusion coefficient has been calculated and is shown as a function of the temperature. A typical curve obtained from a sodium bromide crystal is shown in Fig. 9. Four such curves, taken from four crystal samples, were averaged to obtain the data from which the calculated diffusion coefficient-temperature curve of Fig. 6 was drawn. The average deviation of the four individual curves from the average curve was less than 5 percent. The maximum deviation from the average curve occurred at the highest temperature where it was 13 percent.

The procedure used in obtaining diffusion and conductivity data was somewhat different for sodium chloride and sodium bromide. A fresh crystal sample was used for each diffusion experiment with sodium chloride. The conductivity of this sample was measured later at a temperature near that of the diffusion experiment. The sodium chloride samples were obtained at different times from the Harshaw Chemical Company

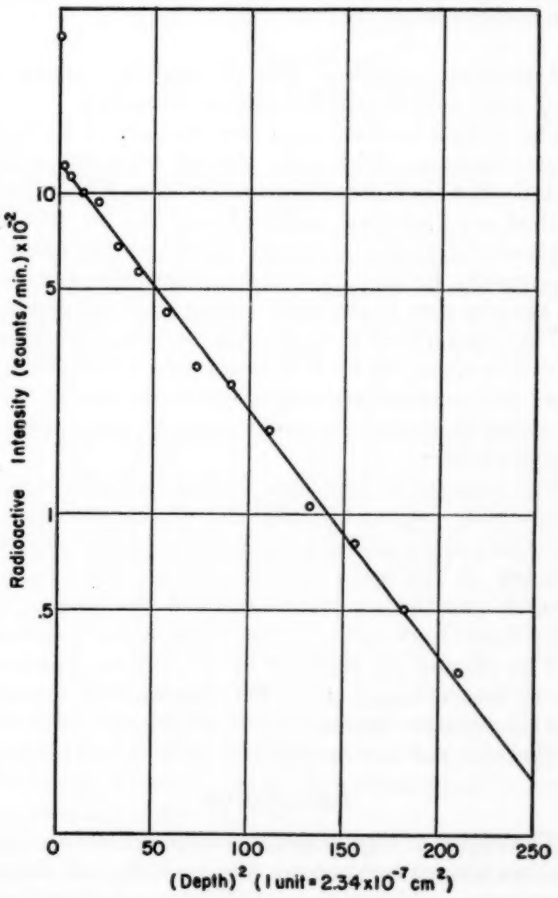

FIG. 4. Distribution of radioactive sodium in sodium chloride. $T=603$°C. $t=5.92$ hours. $D=1.52\times10^{-10}$ cm²/sec.

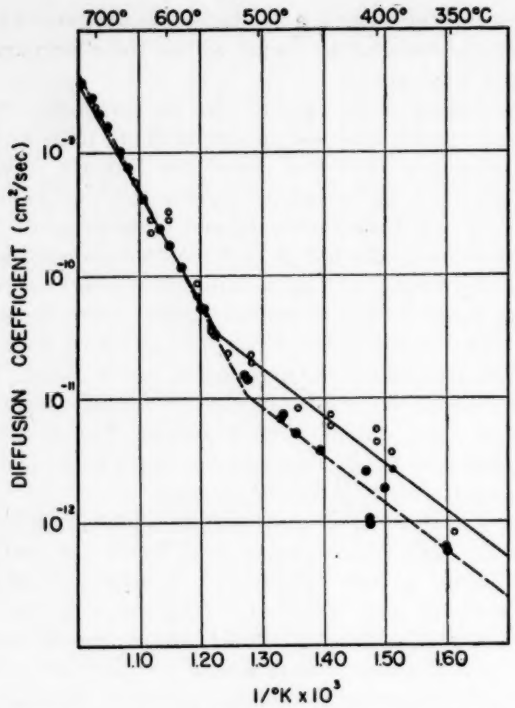

FIG. 5. Temperature dependence of self-diffusion coefficient of sodium in sodium chloride. ○ Directly measured. ● Calculated from measured conductivity.

and probably possessed different impurity contents. They were used as received without annealing.

The sodium bromide data was obtained from eight crystal samples, which were cleaved from one single crystal that had been grown by the Kyropolous[5] method in a platinum crucible. Eimer and Amend C.P. salt was used. Each sample was used for several diffusion experiments. Before each diffusion experiment, the crystal samples were annealed by raising their temperature to 720°C in a time of one hour. After holding the crystals at this temperature for four hours they were cooled to room temperature at a rate of 0.6°C per minute. This annealing procedure was conducted in an atmosphere of purified helium.

The radioactive Na^{24} used for the diffusion experiments with sodium bromide was evaporated upon a plane face of the crystal in the form of sodium chloride. Because of the small mobility of the chloride and bromide ions this procedure appeared unobjectionable.

In Table I are collected the values of the constants of Eqs. (1) and (5), obtained by fitting these equations to the data of Figs. 5 and 6. It is assumed that Eqs. (1) and (5) represent the behavior of the diffusion coefficient in the high and low temperature regions, respectively.

DISCUSSION

The curves of Figs. 5 and 6 possess well-defined high and low temperature regions. Above a fairly well-defined temperature which is about 550°C for sodium chloride and 425°C for sodium bromide the Einstein relation is satisfied by the data. Not only do the curves exhibit a change in slope at these temperatures but, below them, the Einstein relation is not valid.

In the high temperature region, the slope of the calculated diffusion coefficient curve appears to be slightly greater than that of the measured diffusion temperature curve. Extrapolation of Tubandt's transference number data indicates that this effect is due to the small contribution of the anions to the measured conductivity.

The low temperature behavior of the crystals appears to be due to the presence of multivalent cation impurities. The replacement of a sodium ion in the lattice by a divalent ion such as lead introduces a positive ion vacancy into the crystal in order that it remain electrically neutral. At low temperatures, the temperature independent concentration of these added positive ion vacancies is much larger than the temperature dependent concentration of "natural" vacancies. Under these circumstances the low temperature diffusion coefficient is given by the equation

$$D = D_0' \exp(-\epsilon/kT). \tag{5}$$

In support of this interpretation, there exist the experiments of Koch and Wagner[6] and others[4, 7, 8] which show that the low temperature conductivity is extremely

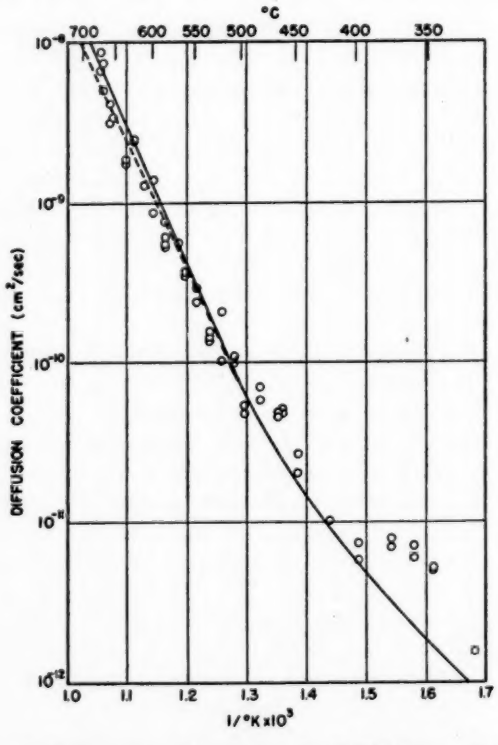

FIG. 6. Temperature dependence of self-diffusion coefficient of sodium in sodium bromide. – – ⊖ – – Directly measured. —— Calculated from measured conductivity.

[5] S. Kyropolous, Zeits. f. anorg. allgem. Chemie **154**, 308 (1926).

[6] E. Koch and C. Wagner, Zeits. f. physik. Chemie (B) **38**, 295 (1937).

[7] H. Etzel and R. Maurer, J. Chem. Phys. **18**, 1003 (1950).

[8] Z. Gyulai, Zeits. f. Physik **67**, 812 (1931).

sensitive to the presence of minute traces of divalent impurities, a few parts per million being sufficient to account for our data. We have found that the low temperature conductivity of Harshaw sodium chloride crystals varies from lot to lot even though subjected to identical annealing procedures. The same behavior is exhibited by crystals grown by us. Etzel and Maurer[7] found that the low temperature conductivity of sodium chloride was not affected by rather violent changes in annealing procedure.

These experiments argue against the suggestion by Schottky and Wagner that the low temperature behavior is due to a non-equilibrium state.[9] At low temperatures the mobility of the anion vacancies is assumed by these authors to become too small to permit the maintainance of the equilibrium vacancy concentration by diffusion to and from the crystal surface. If such an effect exists it appears that substantially purer crystals are needed for its observation.

An interpretation of the low temperature behavior in terms of a "frozen equilibrium" is inconsistent with an explanation of the failure of the Einstein relation in terms of pairs. The presence of pairs provides at low temperatures a mechanism for maintaining thermodynamic equilibrium. It appears dubious, however, that the low temperature failure of the Einstein relation is explainable in terms of pairs. An elementary treatment gives for the diffusion coefficient of the pairs the equation

$$D_p = (\text{constant}) \exp\left(-\frac{\epsilon_p - \epsilon_p' + \epsilon'}{kT}\right), \qquad (6)$$

where ϵ_p' is the binding energy of a pair. Using the theoretical estimates of $\epsilon_p = 0.4$ ev and $\epsilon_p' = 1$ ev for sodium chloride[1,3] and taking $\epsilon' = 2.06$ ev from Table I, the ratio of D_p to the diffusion coefficient of the single vacancies, D, is

$$D_p/D = (\text{constant}) \exp(0.34/kT). \qquad (7)$$

Assuming $(D_p/D) = 1$ at 500°C in order to account for the low temperature failure of the Einstein relation, the value of the ratio at 700°C is approximately 0.3. This result is in disagreement with the observed validity of the Einstein relation in the high temperature region.

The assumption that the low temperature behavior of the crystal is determined by the presence of excess positive ion vacancies resulting from the presence of impurities leads rather naturally to an explanation of the failure of Einstein's relation at low temperatures. It is to be expected that, as illustrated in Fig. 3, a fraction of the divalent impurity ions will be associated with vacancies to form a "complex" in which a positive ion vacancy is a nearest neighbor of the impurity ion.[10] Not only does there exist an electrostatic attraction between

[9] W. Jost, *Diffusion und Chemische Reaktion in Festen Stoffen* (Steinkopf, 1937), p. 77.
[10] O. Stasiw and J. Teltow, Ann. d. Physik (6) 1, 261 (1947).

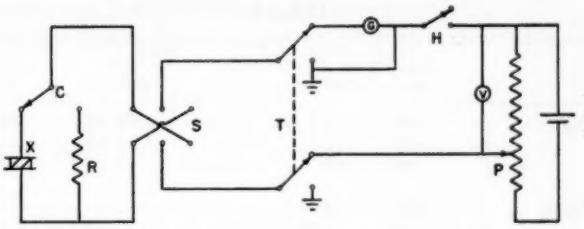

FIG. 7. Circuit for measurement of crystal resistance.

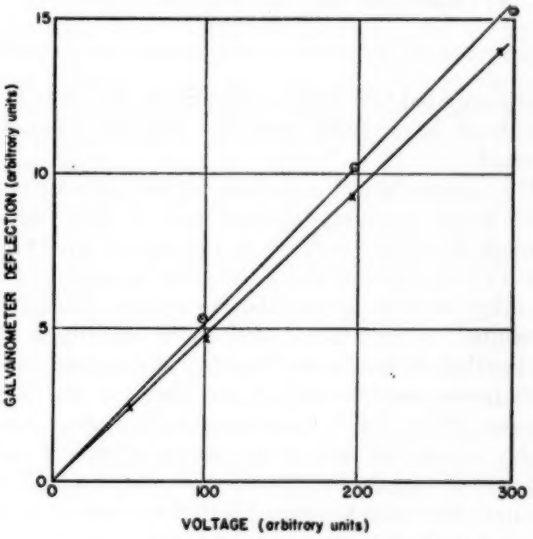

FIG. 8. Test of Ohm's Law for sodium chloride.
○ 721°C × 504°C.

a multivalent positive ion and a positive ion vacancy but also the stress in the lattice surrounding the foreign ion may be partially relieved by the vacancy.

Such complexes will contribute nothing to the measured conductivity. Assuming the presence of complexes, an elementary treatment following that of Seitz[11] gives for the self-diffusion coefficient of the sodium ion

$$D_m = d^2/3(\bar{\nu} n_v^f/n + \bar{\nu}_c n_v^c/3n), \qquad (8)$$

where d is the spacing of the lattice planes. The jump frequencies of the sodium ion into free and associated vacancies are $\bar{\nu}$ and $\bar{\nu}_c$ respectively. The concentration of free positive ion vacancies is n_v^f and of associated vacancies is n_v^c. The ratio of the measured diffusion coefficient to that calculated from the conductivity is now

$$D_m/D_c = 1 + \tfrac{1}{3}(\bar{\nu}_c/\bar{\nu})(n_v^c/n_v^f). \qquad (9)$$

Since, experimentally, D_m/D_c is approximately two at low temperatures the concentrations of associated and free vacancies are of the same order of magnitude. This conclusion assumes that the jump frequencies $\bar{\nu}_c$ and $\bar{\nu}$ are approximately the same.

It is clear that above the knee of the diffusion curve where the concentration of positive ion vacancies is

[11] F. Seitz, *Modern Theory of Solids* (McGraw-Hill Book Company, Inc., New York, 1940), p. 548.

TABLE I.

		$(\epsilon+\epsilon^{\frac{1}{2}})$ (ev)	D_0 (cm²/sec.)	ϵ (ev)	D_0' (cm²/sec.)	ϵ' (ev)
NaCl	*A*	1.80	3.1	0.77	1.6×10^{-6}	2.06
	B	1.89	14.	0.83	2.5×10^{-6}	2.12
	C	1.98	63.	0.78	$63.\times10^{-6}$	2.40
NaBr	*A*	1.53	0.67			
	B	1.68	5.98	0.84	$10.\times10^{-6}$	1.68
	C	1.85	63.	1.02	4.2×10^{-6}	1.66

(*A*) Self-diffusion data. (*B*) From conductivity data. (*C*) From Lehfeldt.

large compared with that of impurities, the effect of the complexes is negligible and the Einstein relation is satisfied.

The complexes will contribute to the diffusion coefficient in the manner discussed only if they migrate through the crystal as freely as the unassociated vacancies. This condition is met if the jump frequencies of the impurity ion and the neighboring sodium ions into the associated vacancy are of the same magnitude. This implies that the associated impurity ions migrate enormously faster than the sodium ions since the chance that a given sodium ion is a nearest neighbor of a vacancy is only (n_v/n), the ratio of the concentrations of vacancies and of ions in the lattice. According to Etzel and Maurer[7] this ratio is about 5×10^{-6} for "pure" sodium chloride in the low temperature region.

A simple experiment was performed to obtain an order of magnitude estimate of the diffusion coefficient of a divalent ion, cadmium, in sodium chloride. A one-centimeter cube of sodium chloride was packed in a finely ground powder of a solid solution of cadmium chloride in sodium chloride. The concentration of cadmium chloride in the powder was one part in six hundred. The assembly was held at 490°C for 24 hours. The crystal was then removed and the surfaces lightly scraped to remove traces of the powdered salt. Analysis of the crystal by the polarographic method showed a cadmium concentration of one part in five thousand.

The interpretation of this experiment is a bit difficult because the diffusion coefficient of the cadmium ion is expected to depend upon the cadmium concentration. The average cadmium diffusion coefficient is, however, several hundred times larger than the self-diffusion coefficient of the sodium ion in sodium chloride at this temperature.

The degree of association of cadmium ions and vacancies is probably smaller than in the case of other divalent ions whose ionic radii do not agree as well with that of the sodium ion. The data of Etzel and Maurer[7] indicate that less than 1 percent of the cadmium ions form complexes in sodium chloride at a temperature of 450°C and a cadmium concentration of a few parts per million.

Breckenridge[12,13] has discovered and investigated an anomalous low frequency dielectric loss in the alkali halides. This loss is interpreted by Breckenridge as a dipole relaxation phenomenon due to the presence of paired vacancies and complexes of foreign ions and vacancies. The concentrations of complexes and pairs deduced by Breckenridge are much too small to account for the low temperature failure of the Einstein relation as observed in our experiments.

It appears highly desirable to investigate further the problem of association between foreign ions and vacancies in the alkali halides. A promising method of attack appears to be the study of the concentration dependence of the diffusion coefficients of foreign ions in the alkali halides.

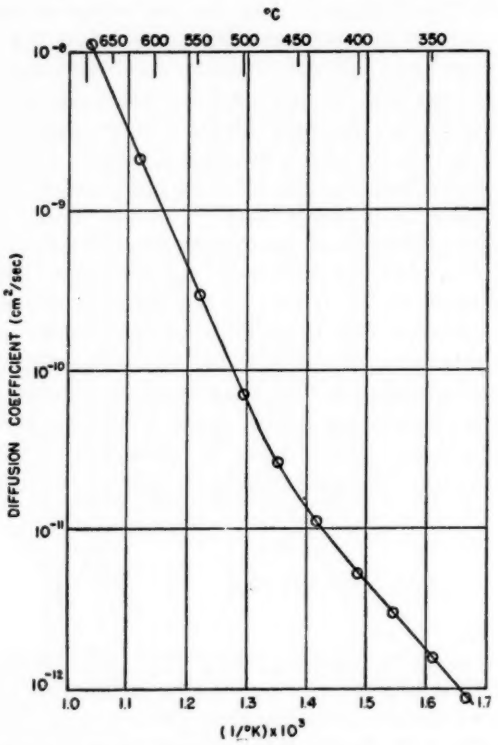

FIG. 9. Typical diffusion coefficient. Temperature curve for sodium bromide calculated from measured conductivity.

These experiments were given partial support by ONR. One of the authors (D.M.) was assisted by fellowships granted by the du Pont and Westinghouse Corporations.

The successful operation of the microtomes was in large measure due to their skillful construction by Mr. Frank Witt.

The advice and encouragement of Professor Frederick Seitz is gratefully acknowledged by the authors.

[12] R. G. Breckenridge, J. Chem. Phys. **16**, 959 (1948).
[13] R. G. Breckenridge, Technical Report 26, Laboratory for Insulation Research, MIT, 1949.

An X-Ray Investigation of the Shapes and Hydrations of Several Protein Molecules in Solution*

H. N. RITLAND,† PAUL KAESBERG, AND W. W. BEEMAN
Department of Physics, University of Wisconsin, Madison, Wisconsin
(Received May 10, 1950)

The x-ray scattering curves of five proteins in solution have been measured at small angles. The radii of gyration of the protein molecules are determined from the scattering curves. These data together with the known molecular weights, densities, and frictional ratios are used to estimate the axial ratios and hydrations of the molecules. Some possibilities and limitations of the method are pointed out.

INTRODUCTION

SINCE the first observation of the effect[1] in the early 1930's and the development of a quantitative[2] theory in 1937–39, the small angle scattering of x-rays has been used by a number of investigators as a tool in the study of finely divided materials. Most of this work has been concerned with the determination of particle sizes and particle size distributions in materials such as carbon black and catalysts.[3]

Small angle scattering is also an excellent tool for the study of the sizes and shapes of protein molecules in solution. The molecular sizes are in a convenient range and the uniformity of the molecules in a pure protein makes possible relatively unambiguous interpretation of the data. Little work has so far been reported in this field. Guinier has worked with egg white[2] and hemoglobin[4] and Kratky has reported preliminary results on edestin, hemocyanin, insulin, and tobacco mosaic virus.[5]

METHOD

In the present work the small angle x-ray scattering was measured as a function of scattering angle by means of a Geiger counter-slit system to be described in the *Journal of Applied Physics*. The protein solution sample to be studied was placed in a Lucite sample holder about one millimeter thick, with sides of 0.001 in. polyethylene film. It should be noted that polyethylene film has a slight fibrous structure and will itself give an appreciable small angle scattering unless properly oriented on the sample holder. The x-ray source was a copper-target tube used with a nickel-cobalt double filter to provide monochromatic copper K_α radiation of wave-length 1.54A.

A background counting rate was determined with distilled water in the sample holder. Counting rates with 5 or 10 percent protein solution samples were several times the background rate except at very small angles where slit edge scattering could be detected and at large angles where both the protein and water scattering approached room background.

In the analysis of the data, the theory developed by Guinier has been used.[2] According to this, the intensity scattered by a group of identical particles at sufficiently small angles is

$$I(\varphi) = Nn^2 I_e \exp(-4\pi^2 R^2 \varphi^2/3\lambda^2).$$

In this formula N is the total number of particles irradiated; n is the number of electrons per particle; I_e is the Thomson scattering at zero angle for one electron; R is the radius of gyration of the particle; φ is the scattering angle, and λ is the wave-length of the radiation. R is defined, of course, with respect to the electron density rather than the mass density. The radius of gyration may be obtained at once from the slope of a plot of $\log I(\varphi)$ *versus* the square of the scattering angle.

There are two ways of obtaining information as to particle shape. If we know the particle volume, we can calculate the axial ratio required to give the measured radius of gyration for an assumed shape, for example, cylindrical or ellipsoidal. In the case of protein molecules where the molecular weight is known, the molecular volume can be easily calculated with the aid of the specific volume of the protein. In Fig. 1, the quantity $R/M^{\frac{1}{3}}$ (M = molecular weight) is plotted as a function of the axial ratio for cylinders and ellipsoids of revolution. This calculation is for a specific volume of 0.75, and assumes that the molecules are of uniform electron density and are not swelled by internal water of hydration when in solution.

Another source of shape information is the scattering at larger angles, beyond, roughly, the angle of half-maximum intensity, where the Guinier approximate scattering function no longer is valid. In this region, the scattering depends explicitly on particle shape. The calculation of the scattering function for shapes other than spherical is rather tedious, and has been done only for certain shapes. Guinier[2] published curves for ellipsoids of revolutions for axial ratios both greater and less than one. Porod[6] has published tables of the scattering from cylinders, ellipsoids of revolution, and

* This work was supported in part by the joint program of the ONR and AEC and in part by the Wisconsin Alumni Research Foundation.
† Now at the University of Washington, Seattle, Washington.
[1] P. Krishnamurti, Ind. J. Phys. **5**, 473 (1930); B. E. Warren, J. Chem. Phys. **2**, 551 (1934).
[2] A. Guinier, Ann. de Physik **12**, 161 (1939).
[3] C. G. Shull and L. C. Roess, J. App. Phys. **18**, 295 (1947).
[4] A. Guinier and Fournet, Comptes Rendus **226**, 656 (1948).
[5] O. Kratky, J. Polymer Science **3**, 195 (1948).
[6] G. Porod, Acta Phys. Austriaca **2**, 255 (1948).

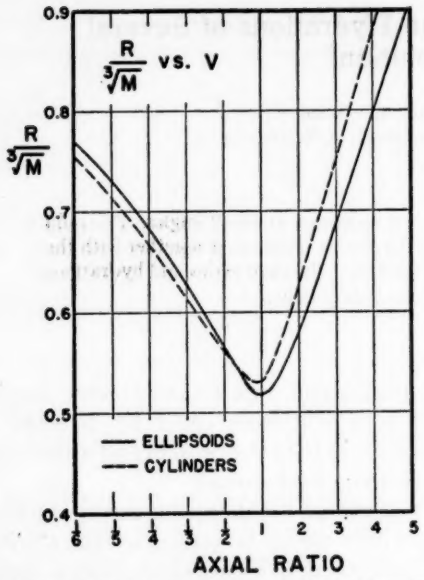

FIG. 1. Plots of the radius of gyration divided by the cube root of the molecular weight as a function of the axial ratio for ellipsoids of revolution and right circular cylinders. The curves are for a specific volume of 0.75. Of the proteins measured only lysozyme deviates sufficiently (v=0.72) from this value to necessitate a correction.

rectangular prisms, all for axial ratio greater than one. The theoretical curves used in this paper (see Fig. 3) were taken from Porod's work.

By comparing the experimental scattering curve with those calculated for ellipsoids or cylinders of various axial ratios, the shape of the particle can be determined. If the particle volume is not known, this gives the only information about shape. In the case of protein molecules of known molecular volume and radius of gyration, the larger angle scattering can be used to verify the general results given by R. It is very difficult, however, to choose between an ellipsoidal or cylindrical shape on this basis, as the scattering curves for the same volume and radius of gyration are quite similar.

In the derivation of the Guinier function, certain approximations are made which must be carefully examined for their effect on the experimental results. Among these is the assumption that the incident and detected radiation are perfectly collimated. In practice, slits are usually used, as in this investigation, to gain the necessary intensity. The collimation error introduced by the finite width of the slits is usually small, but the effect of slit height can be appreciable. Slit effects have been investigated theoretically by several authors.[3,4,7] The corrections can be fairly easily applied in the case of very high slits. An important result is that a Gaussian scattering curve, such as is given by the Guinier formula, is changed only by a numerical factor, regardless of slit heights.

In the present work, the slits were of intermediate height, so a rigorous correction of the experimental curves for slit effects would be extremely difficult. However, if the scattering curve deviates only slightly from a Gaussian within the angular range passed by the slits, the slope of the log$I$ *versus* φ^2 plot should not be altered appreciably. Thus if the straight line portion of the curve is fairly long, the error in R will be small. This was checked by taking data with several different slit heights, and in each case the data with the different slits agreed within experimental error.

In addition, Guinier assumes that the particles are randomly arranged so that no interparticle interference effects occur. Thus the scattered intensity from N particles is just N times that from a single particle. Actually, the presence of a minimum distance between particles and other particle correlations due to intermolecular forces produce interparticle interference effects, particularly in concentrated solutions. In order to evaluate this effect, a series of runs was made with different concentrations of bovine serum albumin solution. The results are shown in Fig. 2. It is seen that the interference is barely noticeable in a fifteen percent solution, but can become very serious in more concentrated solutions. In this work, the concentrations of the protein solutions were kept between five and ten percent to eliminate this source of error.

Finally, in order to obtain a unique value of R, the sample must be composed of identical particles. Thus purity of the protein is very important. Impurities of high molecular weight give a sharply upturning log$I$ *versus* φ^2 curve at small angles, as was found in the curve for uncentrifuged hemoglobin. With hemoglobin the impurity was of much higher molecular weight, of the order of a million or more, and its effect could be more or less uniquely separated from the desired scattering. However, if the impurity is of only slightly different radius of gyration, it is very difficult to separate out its effect. The R determined represents an average, weighted in favor of the larger particles because of their greater scattering power.

Even if the components of a mixture have quite different molecular weights the problem is much more difficult than the analysis of the decay curve of a radioactive mixture into its several half-lives since the scattering curve for a single component is Gaussian over but a limited angular range.

If the protein has undergone partial denaturation, it is practically impossible to get reliable data. The presence of large amounts of smaller denaturation products can completely invalidate the results, while small amounts can add excess scattering at larger angles and hence affect the shape determination there. A particular difficulty with small impurities is that they lessen the slope of the straight line part of the scattering curve without, however, betraying their presence by producing any deviations from linearity.

RESULTS

The results of this investigation of five common proteins with molecular weights ranging from 18,000 to

[7] K. L. Yudowitch, J. App. Phys. **20**, 174 (1949).

69,000 are given in Table I. They are further discussed under separate headings at the end of the paper.

The radii of gyration listed in Table I are independent of water of hydration bound to the surface of the molecule if the hydration layer has the same density as normal water. This assumption will be further discussed at the end of this section. There is evidence from the detailed x-ray analysis of single crystals of insulin, horse methemoglobin, and tobacco mosaic virus[8] that the internal hydration of protein molecules is not large.

In their independence of surface hydration effects the x-ray measurements complement, in a very useful way, the standard methods of size and shape determination. A review of the standard methods, as well as a critical survey of results for a number of proteins, has been given by Oncley.[9] A more detailed discussion will be found in the monograph of Cohn and Edsall.[10]

Column three of Table I lists values of the frictional ratio for the proteins under consideration. This is the ratio of the frictional resistance experienced by a protein molecule moving in the solvent to that which would be experienced by a spherical molecule (from Stokes' law) of the same volume. The frictional ratio as well as the molecular weight may be calculated from measurements of the sedimentation constant and the diffusion constant. It is found experimentally that the frictional ratio is always greater than one. However, the experiments are unable to determine whether the frictional excess is to be attributed to an asymmetry of the molecule (such effects have been calculated by Perrin[11]) or to water of hydration which, of course, increases the effective volume and the frictional resistance. Oncley[9] has published families of curves, calculated for ellipsoids of rotation, which give all combinations of axial ratio and hydration consistent with a given frictional ratio. The axial ratios of column four Table I, calculated from the data of columns one and two, are presumably characteristic of the hydration free molecule. One can, therefore, with the help of Oncley's curves and the frictional ratios, determine the hydrations. These are given in column five.

TABLE I[a]

	Radius of gyration in A units	Molecular weight	Frictional ratio	Axial ratios	Hydration in g of water per g of protein
Lysozyme	16.0	18,000	1.20	2.3 prolate	0.32 prolate
				$(2.8)^{-1}$ oblate	0.25 oblate
β-Lactoglobulin	24.6	35,400	1.25	3.6	0.20
				$(5.5)^{-1}$	0.00
Ovalbumin	24.0	44,000	1.16	2.9	0.15
				$(4.0)^{-1}$	0.00
Bovine Hemoglobin	23.9	66,700	1.16	2.1	0.28
				$(2.4)^{-1}$	0.20
Bovine Serum Albumin	26.6	69,000	1.27	2.7	0.42
				$(3.4)^{-1}$	0.30

[a] There is a strong evidence that hemoglobin cannot be treated as an ellipsoid of revolution. See discussion at the end of the paper. All of the axial ratios and hydrations of this table are based on the assumption that the molecules are ellipsoids of rotation. A single hydration layer calculates to about 0.5 g of water per g of protein for lysozyme down to 0.3 g for bovine hemoglobin and bovine serum albumin. For similar shapes it varies as the reciprocal of the cube root of the molecular weight.

The values obtained are of the same order of magnitude as those deduced from a variety of physical-chemical measurements (see Oncley[9]) and correspond to a hydration layer about one water molecule thick on the surface of the protein molecule. The measurements of the three lightest molecules give evidence for less than a complete hydration layer.

A further check on the validity of the assumption of negligible internal hydration could be obtained from an accurate scattering curve at larger angles where there is an explicit dependence on particle shape. One expects, since internal hydration will increase the volume occupied by the scattering material, that asymmetries will be exaggerated when they are calculated from the radius of gyration and the molecular weight (which is always stated for the unhydrated molecule). Asymmetries based on the scattering curve alone are, of course, truly representative of the spatial distribution of the scattering material. Unfortunately, in the experiments as we have been able to do them thus far, the advantage of direct interpretation is more than outweighed by the experimental uncertainty, due to low counting rates, of the larger angle part of the scattering curve.

In Fig. 3 the experimental points for three proteins are compared with theoretical curves (the solid lines) for prolate ellipsoids of revolution of different axial ratios. The axial ratios so obtained are in sufficiently good agreement with those of Table I to reassure us

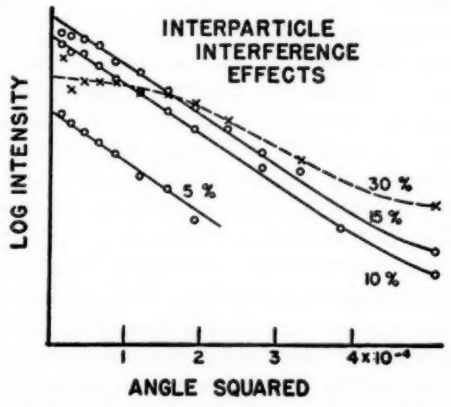

FIG. 2. Scattering curves for different concentrations of bovine serum albumin solution.

[8] M. F. Perutz, Research **2**, 52 (1949). M. A. Lauffer, J. Am. Chem. Soc. **66**, 1188 (1944).
[9] J. L. Oncley, Annals New York Acad. of Sci. **41**, 121 (1941).
[10] E. J. Cohn and J. T. Edsall, *Proteins, Amino Acids and Peptides* (Reinhold Publishing Corporation, New York, 1943).
[11] F. Perrin, J. de phys. et rad. **7**, 1 (1936).

that no gross errors of measurement or interpretation have occurred. However, there does appear to be a slight tendency for the axial ratios from the scattering curve to be smaller than those from the radius of gyration and the molecular weight. From the scattering curves the axial ratio for bovine serum albumin is about 2.2, lysozyme 2.0, and ovalbumin 2.5. The corresponding values from Table I are 2.7, 2.3, and 2.9. The accuracy of the present data does not warrant the attachment of much significance to these differences. It should be pointed out, however, that the radius of gyration and axial ratio furnished by an accurate scattering curve permit the calculation of the molecular volume. This volume, as has been mentioned, will be equal to or greater than that calculated from the molecular weight and the density of the unhydrated protein. The difference must be ascribed to internal hydration. The differences which we get, if real, would correspond to internal hydrations of the order of 0.15 to 0.20 g of water per g of protein.

We did not run an extended scattering curve for

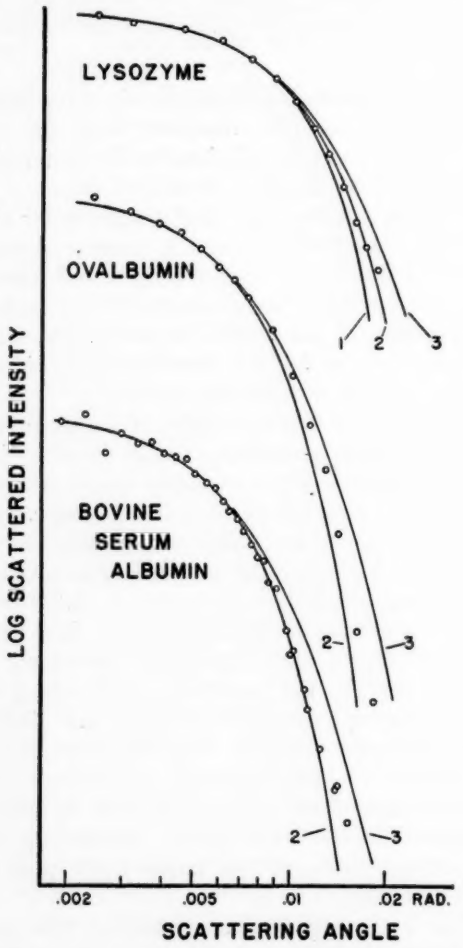

FIG. 3. The extended scattering curves of three proteins. The solid lines are theoretical curves for prolate ellipsoids of the indicated axial ratio. The experimental points span intensity ratios of about 6 for lysozyme, 35 for ovalbumin and 17 for bovine serum albumin.

β-lactoglobulin. Hemoglobin will be discussed separately since there is excellent reason to believe that this molecule is a flattened circular cylinder.

Finally we must say a few words on the dependability of the data of Table I. The radii of gyration can be determined from the plots of Fig. 4 to within 2 or 3 percent. Because of the difficulty of obtaining and keeping homogeneous protein preparations free of both aggregation and denaturation it is not certain that these values characterize the pure protein. An extended series of measurements on proteins from different sources and subject to different treatments would be necessary to settle this point. However, most of our proteins were carefully prepared. With some exceptions to be noted they are homogeneous in sedimentation and electrophoretic studies under the conditions of solution used in this investigation.

Besides its dependence on R the axial ratio depends also on the molecular weight and density. This dependence is less important than that on R since the molecular weight and density enter (in Fig. 1) as the cube roots. These several uncertainties introduce an error in $R/M^{\frac{1}{3}}$ which we estimate at about ± 6 percent; an estimate whose status is somewhat clouded by the uncertain effects of protein inhomogeneity. If $R/M^{\frac{1}{3}}$ is known to ± 6 percent the axial ratios are determined from Fig. 1 to ± 15 or 20 percent. The determination is the more accurate the more asymmetric the molecule.

Unfortunately in calculating hydrations from the axial ratio and the frictional ratio one finds the hydration to be a rapidly varying function of the frictional ratio. At a frictional ratio of 1.20 and an axial ratio of 2.0 a 15 percent uncertainty in hydration results from a 2 percent uncertainty in frictional ratio. Frictional ratios are not more accurately known than this. When the possible errors in axial ratio are also considered one must assign to the hydrations an uncertainty of ± 40 to 50 percent.

One must remember, too, that all of the above considerations are based on the assumption that protein molecules in solution are rigid ellipsoids of revolution. The evidence for their rigidity is considerable but the assumption of shape is motivated only by the mathematical ease with which ellipsoids may be treated. The latter assumption is standard in the protein literature. In its further defense it may be said that the experimental measurements, including those reported here, are not sufficiently accurate to justify their treatment with a more complicated model. It is expected that asymmetries and hydrations agreeing with the present within the probable error would be obtained on the basis of any reasonable shape assumption, that of cylinders for instance.

The model used in the present discussion is a considerable simplification of reality in another respect. Protein molecules in solution are not regions of uniform electron density at whose surface the electron density suddenly drops to that of water. In most cases, however,

significant errors do not seem likely to arise from this source. For instance the location in the molecule of the four iron atoms of hemoglobin will not affect the radius of gyration by more than a small fraction of one percent. The adsorption on the surface of heavier ions such as sodium or chlorine will change the radius of gyration by less than one percent for thirty chloride ions on the surface of a roughly spherical molecule of molecular weight 40,000. Thirty is about the maximum number of attached ions which Scatchard, Scheinberg, and Armstrong[12] found in their study of the interaction in solution of human serum albumin and sodium chloride.

The model may also be criticized for the assumption that the hydration layer has the same density as normal water. A compressed hydration layer will, of course, increase the measured radius of gyration and the axial ratio and decrease the estimated hydration. The radius of gyration of a spherical molecule of molecular weight 60,000 and hydration 0.3 g of water per g of protein would be increased about 11 percent if the hydration layer had the density of the protein. However this effect goes as the square of the density difference between the hydration layer and normal water. Thus the increase in density of the hydration layer must be an appreciable fraction of the density difference between protein and water if there is to be a large change in radius of gyration. The increase in radius of gyration is only slightly more than one percent for the above molecule if the hydration layer has a density of 1.1 g per cm^3.

The best evidence that such compressions are unlikely comes from the data on the electrostriction associated with the solvation of ions. It is found that the apparent molal volumes of the amino acids[10] are less than those of their uncharged isomers. If the difference is assigned to a compression of the hydration layer it is much too small to invalidate the simplified model we have used.

X-ray measurements of the present type should be capable of appreciable refinement. The use of a rotating anode tube would speed up data taking by a factor of five or ten and permit fairly dependable shape and molecular volume determinations from the scattering curve alone. Since the slit system is designed specifically for ionization chamber or Geiger counter measurements a comparison of incident and scattered intensities may be possible. Such a measurement would determine a function of molecular volume and electron density in the protein.

There is at present a good deal of interest among physical chemists in the problem of the hydration of proteins. Because of the fairly complicated dependence on the various directly measured quantities it seems unlikely that the hydrations of proteins can be determined nearly as accurately as can their molecular weights and radii of gyration. However, with the refinements in x-ray technique which seem easily obtainable and with the molecular weights, densities and frictional ratios known to 2 or 3 percent one should be able to determine internal and surface hydrations to within 20 or 25 percent. This is sufficient accuracy to answer such questions as whether significant deviations from a single surface hydration layer occur and to measure or place maximum upper bounds on the internal hydration.

[12] Scatchard, Scheinberg, and Armstrong, J. Am. Chem. Soc. 72, 535 (1950).

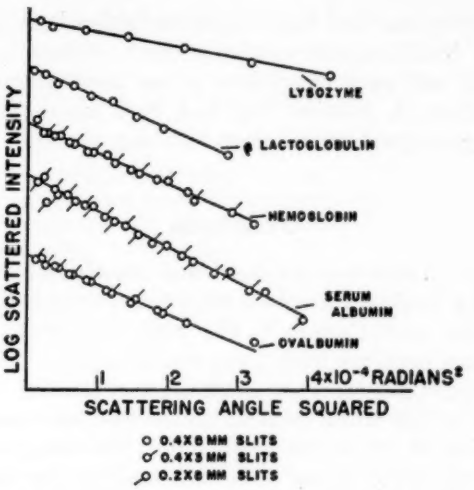

FIG. 4. The straight line portion of the scattering curves of five proteins. The experimental points span intensity ratios of between two and three.

DISCUSSION OF INDIVIDUAL PROTEINS

Lysozyme

This material was six times recrystallized from egg white by Mr. L. R. Wetter of the Department of Physiological Chemistry following the method of Alderton and Fevold.[13] Lysozyme from Armour Company gave much too small a slope indicating the presence of appreciable amounts of low molecular weight impurities. After recrystallization by Mr. Wetter this material gave results agreeing with the above.

The molecular weight, frictional ratio and density used in the calculations of Table I are from the unpublished work of Mr. Wetter. Earlier authors[14] found values of the molecular weight ranging from 14,000 to 17,500. These values would somewhat increase our estimate of the axial ratio.

β-Lactoglobulin

This material was prepared and six times crystallized by Professor Harold Deutsch of the Department of Physiological Chemistry following a method used by Cecil and Ogston.[15] The molecular weight and frictional ratio are from the work of Cecil and Ogston and from Cohn and Edsall (reference 10 p. 428).

[13] G. Alderton and H. L. Fevold, J. Biol. Chem. **164**, 1 (1946).
[14] Alderton, Ward and Fevold, J. Biol. Chem. **157**, 43 (1945); Palmer, Ballantyne, and Calvin, J. Am. Chem. Soc. **70**, 906 (1948).
[15] R. Cecil and A. G. Ogston, Biochem. J. **44**, 33 (1949).

Protein that had been frozen and dried from a 0.15-molar NaCl solution to give a dried product with 20 percent salt gave indications of low molecular weight impurities. A solution that had been frozen but not dried gave good results after dialyzing out most of the salt.

Ovalbumin

This protein was prepared and six times recrystallized by Professor Deutsch according to the method of Kekwick and Cannan.[16] The molecular weight and frictional ratio are from Cohn and Edsall.

Guinier[2] has reported small angle scattering experiments on egg white from which he deduces a radius of gyration of 20.3A for ovalbumin. The disagreement with our value seems somewhat outside the limit of error. Guinier does not describe his measurements in detail.

Ovalbumin shows two peaks in electrophoresis. It is not known that this corresponds to an inhomogeneity in size or shape.

Bovine Hemoglobin

This protein was obtained from Armour Company. It was used without recrystallization. Some difficulty was experienced with aggregation or impurities of high molecular weight which gave a sharp upturn to the scattering curve at the smallest angles. A solution which had been ultra-centrifuged to remove the heavier impurities gave the scattering curve of Fig. 4.

Horse methemoglobin has been very thoroughly investigated by Perutz.[17] From x-ray analysis of single crystals he found the molecule to be a cylinder 34A high and 57A in diameter. It is presumed that the bovine hemoglobin molecule will have very nearly the same dimensions. These dimensions give an axial ratio of $(1.7)^{-1}$ and a radius of gyration of 22.4A. Our result, 23.9A, is somewhat larger than can be explained by errors in measurement and probably indicates some remaining high molecular weight impurities in our sample. Guinier[4] measured the small angle scattering from horse methemoglobin in solution and reported a radius of gyration of 23.0A.

Perutz found that the molecules in the crystal were surrounded by one or more hydration layers. A single layer corresponds to a hydration of 0.3 g of water per g of protein. Our measurements of the extended scattering curve of hemoglobin (not shown) are consistent with a cylinder of axial ratio $(1.7)^{-1}$.

Bovine Serum Albumin

This was also an Armour preparation obtained through Professor Alberty of the Department of Chemistry. From Professor Alberty's electrophoretic investigations this protein appeared to be quite pure except for a small admixture of globulin. The molecular weight is from the osmotic equilibrium measurements of Scatchard, Batchelder, and Brown.[18] The frictional ratio (for horse serum albumin) is from Cohn and Edsall (reference 10, p. 428).

In conclusion we wish to thank Professors J. W. Williams, H. F. Deutsch, R. A. Alberty, and J. D. Ferry and the other members of the protein chemistry group on this campus for their invaluable aid in obtaining samples and for their frequent and much needed advice on the physical chemistry of proteins. We wish to thank, also, the Kimberly-Clark Corporation for their support of the Kimberly-Clark Fellowship held by one of us (H.N.R.) during the year 1948–49.

[16] R. A. Kekwick and R. K. Cannan, Biochem. J. **30**, 227 (1936).
[17] M. F. Perutz, Proc. Roy. Soc. **A195**, 474 (1949).
[18] Scatchard, Batchelder, and Brown, J. Am. Chem. Soc. **68**, 2320 (1946).

The Electroplating of Metallic Selenium*

A. VON HIPPEL AND M. C. BLOOM**
Laboratory for Insulation Research, Massachusetts Institute of Technology, Cambridge, Massachusetts

(Received May 23, 1950)

The electroplating of metallic selenium from acid baths has been achieved and reduced to practice. The paper discusses in succession the polymorphism of selenium; selenium ions in selenious acid solution; cathodic deposition as the amorphous and metallic phase; the nucleation characteristic and crystal growth of the metallic modification; the properties of various types of plating baths; a selenium-carbon anode for the stabilization of the bath composition; and finally a number of influences affecting the crystallization habit of the deposit. The current density of 200 amp./ft.² attainable in a well-balanced plating bath compares favorably with standard baths for true metals.

INTRODUCTION

WHILE the electroplating of true metals can be accomplished according to well-known procedures,[1] no definite disclosure seems to have appeared in the literature concerning the formation of a homogeneous metallic selenium electro-deposit. This is not due to a lack of interest in the subject; on the contrary a number of attempts have been made, starting in 1829 with Magnus[2] and continued by Berthelot,[3] Müller,[4] LeBlanc,[5] and others.[6] The technical importance of selenium rectifiers and photo-cells furthermore places a special emphasis on the solution of this problem. That previous attempts failed, is due to the fact that selenium is a non-metal of peculiar properties.

Selenium in the solid state can assume four allotropic modifications: a vitreous, two monoclinic, and a hexagonal metallic phase (Fig. 1).[7] The amorphous material seems, in general, to consist of a brushwork of chain molecules; the α- and β-phases of the monoclinic selenium have just been analyzed in detail by R. D. Burbank in our laboratory and found to be composed of Se ring molecules,[8] while the hexagonal form is built up from chain-molecule spirals.[9] The vitreous and the monoclinic modifications are insulators and conspicuous for their beautiful red color. The hexagonal material is a semiconductor, since the ordered arrangement of the chains makes electronic conduction possible.[10] This metallic phase is frequently gray in appearance and therefore called "gray" selenium. One of the main obstacles in electroplating Se lies in this polymorphism of the element. Unless special conditions are chosen, the material deposits as a non-conductor and interrupts the current flow.

The authors were engaged in this problem during the war under the sponsorship of the Federal Telephone and Radio Manufacturing Corporation and developed, in 1941 to 1944, with the help of various co-workers, a procedure of plating metallic selenium cathodically from acid solutions. The method is practical and not much more difficult to handle than the electroplating of nickel. It can also operate with corresponding current densities, even in excess of 200 amp./ft.² and has been used by us to produce selenium rectifiers and photo-cells.[11]

The selenium rectifier development has been continued in the laboratories of the sponsoring company; our research has so far been described only in patent applications. This delay in publication was caused partly by the right of the sponsor for protection and partly by the typical shortcomings of all war researches. Compelled to obtain practical results speedily, one has to leave the more subtle aspects of a problem unexplored and then feels disinclined to publish an obviously incomplete investigation.

One of the long-range projects of the Laboratory for

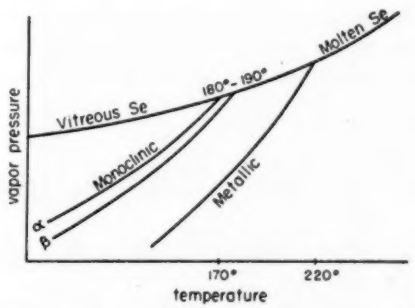

FIG. 1. Allotropic modifications of selenium (see reference 7).

* Sponsored by the Federal Telephone and Radio Manufacturing Corporation and later by the ONR, Signal Corps, and the Air Force under ONR Contract N5ori-07801.

** Dr. Bloom has been engaged elsewhere since 1945. Present address, Naval Research Laboratories, Washington, D. C.

[1] *Modern Electroplating* (Electrochemical Society, Inc., New York, 1942).

[2] G. Magnus, Pogg. Ann. **17**, 521 (1829).

[3] M. Berthelot, Ann. chim. phys. (3), **49**, 473 (1857).

[4] E. Müller, Ber. d. d. Chem. Ges. **36**, 4262 (1903); Zeits. f. physik. Chemie **100**, 346 (1922); E. Müller and R. Nowakowski, Ber. d. d. Chem. Ges. **38**, 3779 (1905); Zeits. f. Elektrochemie **11**, 931 (1905).

[5] M. LeBlanc, Zeits. f. Elektrochemie **11**, 813 (1905).

[6] A. Jílek and J. Lukáš, Chem. Listy **21**, 576 (1927); H. F. Schott *et al.*, J. Am. Chem. Soc. **50**, 721 (1928); F. C. Mathers and H. L. Turner, Trans. Am. Electrochem. Soc. **54**, 293 (1928); G. Sella, Ricerca Scient. **10**, 1193 (1939).

[7] Cf. J. W. Mellor, *Inorganic and Theoretical Chemistry* (Longmans, Green and Company, New York, 1940), Vol. X, p. 705.

[8] Acta Crystallographica, (to be published).

[9] A. J. Bradley, Phil. Mag. [6] **48**, 477 (1924); M. K. Slattery, Phys. Rev. **21**, 378 (1923); *ibid.* **25**, 333 (1925).

[10] A. von Hippel, J. Chem. Phys. **16**, 372 (1948).

[11] von Hippel, Schulman, and Rittner, J. App. Phys. **17**, 215 (1946).

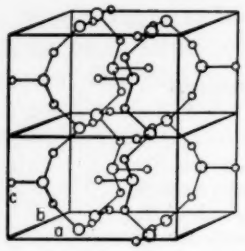

FIG. 2. Structure of SeO_2 (see reference 12).

Insulation Research concerns the transitions from insulators to metals. In this program the VI_b group of the periodic system, and with it selenium, play an important role.[10] We have consequently learned more about selenium lately and present now our old results, checked and re-evaluated in the light of new evidence.

SELENIUM IONS IN SELENIOUS ACID SOLUTIONS

Selenium belongs to one of the few elements of ambipolar character. In alkaline solutions its electronegativity is high enough to allow its existence as negative ions while in acid baths positive ions may be formed. Consequently it should be possible to electroplate selenium anodically or cathodically, and indeed we have been able to realize both possibilities. Since, however, the acid baths appeared to have greater promise, we concentrated on these using preferentially selenium dioxide as the starting material.

Solid SeO_2 forms tetragonal crystals consisting of flat chains oriented parallel to the c-direction (Fig. 2).[12] Each selenium atom is bound to two oxygen neighbors in the chain and to a third oxygen atom pointing at about 90° to its chain link. A neutral selenium atom with six outer electrons in the (s^2p^4) constellation can form only two covalent bonds with its two half-filled p-orbitals. The existence of the third oxygen suggests a strong resonance contribution of polar structures, in which the selenium is positively and the oxygen atoms, especially the third one, are negatively charged; the latter can thus also bond electrostatically to the Se atom of a neighboring chain. This agrees with the fact that the Se—O distance in the chain is somewhat shorter than a simple covalent bond (1.78A instead of 1.83A), and that the third bond is still shorter (1.73A) due to the joint action of covalent and electrostatic attraction.

With one water molecule per SeO_2 group the crystalline H_2SeO_3 structure results. By breaking one Se—O chain bond per Se atom and adding in its place one water molecule, Se—O_3 pyramids, linked by hydrogen bonds, are formed. Two of the oxygens of each pyramid are connected by one hydrogen bond to a neighboring SeO_3 group, and the third is attached by two bonds to two neighbors (Fig. 3).[13]

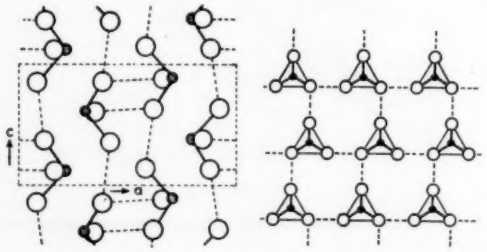

FIG. 3. Structure of H_2SeO_3 (see reference 13).

[12] J. D. McCullough, J. Am. Chem. Soc. **59**, 789 (1937).

In selenious acid solution, as Raman effect measurements indicate,[14] the SeO_3 pyramids will, in general, remain intact as neutral H_2SeO_3 molecules linked statistically by hydrogen bonds. By releasing some of the hydrogen atoms as protons, the solution obtains its weakly acidic character and preferentially $(HSeO_3)^-$ anions are formed. On the other hand, by the addition of a proton, the cation $(H_3SeO_3)^+$ may be obtained as Fig. 4 schematically indicates.

Thus we may assume that selenious acid solutions contain essentially three types of ions, produced by the reactions

$$H_2SeO_3 \rightleftarrows (HSeO_3)^- + H^+$$
$$H_2SeO_3 + H^+ \rightleftarrows (H_3SeO_3)^+.$$

The dissociation constant for the first reaction amounts to about 3×10^{-3} at room temperature.[15] Only a minor fraction of the protons will combine with H_2SeO_3 to $(H_3SeO_3)^+$ cations, hence their concentration in selenious acid solutions is small.

When voltage is applied, we would expect the discharge reactions:

Cathodic	*Anodic*
$H^+ + e^- \rightarrow H$	$4(HSeO_3)^- - 4e^- \rightarrow$
$(H_3SeO_3)^+ + 4e^- + 3H^+ \rightarrow Se + 3H_2O$	$4SeO_2 + 2H_2O + O_2$.

The end products of these reactions are observed. Selenium plates out cathodically already at very low voltage (Fig. 5); the charge transfer per selenium atom corresponds to four electrons as the equation requires. Hydrogen begins to discharge at the higher negative cathode potential of 1.2 volts. At the Pt anode oxygen evolves.

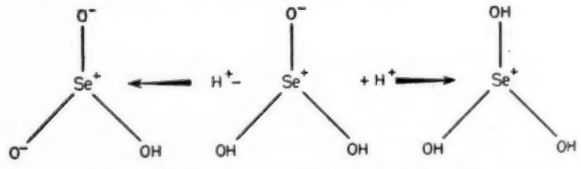

FIG. 4. Formation of $(HSeO_3)^-$ and $(H_3SeO_3)^+$ from selenious acid.

PRELIMINARY PLATING EXPERIMENTS

If one electroplates on Pt cathodes at room temperature from selenious acid solution below the discharge potential of hydrogen, a slowly falling current characteristic is observed while the cathode surface becomes

[13] A. F. Wells and M. Bailey, J. Chem. Soc. (London) 1282 (1949).

[14] J. H. Hibben, *The Raman Effect and its Chemical Applications* (Reinhold Publishing Corporation, New York, 1939), p. 389.

[15] Cf. Gmelin's *Handbuch der anorganische Chemie, Selen, Teil B* (Gmelin-Verlag, Clausthal-Zellerfeld, 1949), p. 57.

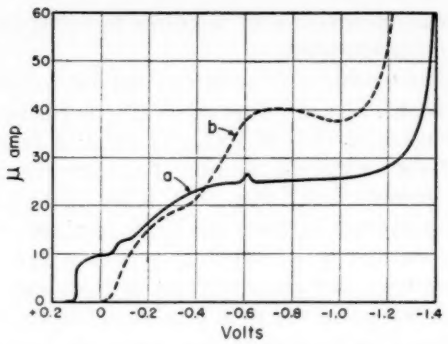

FIG. 5. Cathodic discharge characteristics: (a) polarogram (10^{-3} mole H_2SeO_3+0.12 mole HCl),[15a] (b) discharge at Pt electrodes (3 N H_2SeO_3).

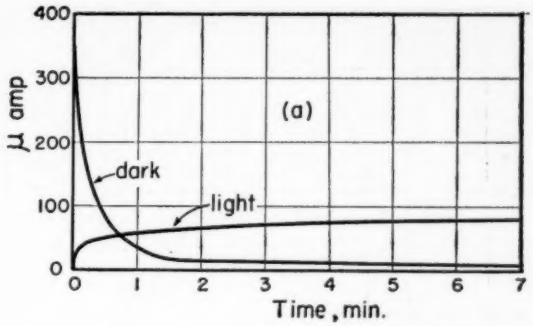

FIG. 6a. Current time characteristic for selenious acid solution at room temperature.

covered with a very thin layer of amorphous selenium. Under the conditions of Fig. 6a the current practically ceases in the dark when the layer has reached an average thickness of *ca.* 0.5×10^{-5} mm. Under a strong illumination, however, the deposition continues until an opaque layer of *ca.* 1.2×10^{-4} mm thickness has been formed.

Figure 6b illustrates the effect on a partly illuminated cathode and shows also the influence of the wave-length of the light on the plating process. Obviously the plating in the dark ceases when thickening of the layer has reduced the field between the solution and the metal cathode until no electrons can traverse the amorphous layer. Photo-effect in the selenium restores the transconductance, and the plating continues as long as the active radiation and the electrons can penetrate the deposit.

If the voltage is raised above the discharge potential of hydrogen, pitting results and additional red selenium, generated by the reduction of the selenious acid, may fall out in fluffy flakes, but no metallic selenium is observed.

This situation changes at elevated temperatures. At 55°C continuous plating is possible at low current densities, and a metallic deposit results. Once such a layer is formed, the metallic phase can be built up further even at room temperature by very slow deposition. However, in any holes of this layer the selenium discharges again as amorphous selenium. Thus a preformed metallic structure can be continued, but the metallic phase cannot be created at room temperature in this simple experiment.

NUCLEATION AND GROWTH OF METALLIC SELENIUM

The stability of the vitreous and monoclinic phases of selenium and the results just reported testify that the nuclei of the metallic modification are normally formed in a higher temperature zone. Obviously, control of the plating process presupposes accurate information on the speed of nucleation in its dependence on temperature.

To obtain this nucleation characteristic we coated Pt disks with selenium at about 340°C and transferred them without cooling to a hot plate held at about 180°C. In spite of the fact that this temperature lies *ca.* 40°C below the melting point of the metallic phase (*ca.* 219°C), no crystallization occurred in the course of one hour. If, however, such a disk was brought for a short time to an appropriate lower temperature or quenched to room temperature, a return to 180°C produced rapid crystallization. Consequently at these lower temperatures nuclei were formed which at high temperatures rapidly developed. Hence by keeping a selenium disk at a fixed temperature for a prescribed time interval, then developing the nuclei at high temperature to visible size, quenching and counting, the nucleation rate at a given temperature could be determined.

Figure 7 shows the result of such experiments. The nuclei of metallic selenium form from amorphous selenium according to a probability characteristic which has its maximum about 125°C below the melting point! The rate falls sharply towards higher and lower temperatures as may be expected: A stable nucleus can result only if a number of chain segments arrange themselves into the prescribed hexagonal pattern. The viscosity of the amorphous selenium must be sufficiently low to allow this organization of the chains, hence the rate of nucleation will initially rise with temperature. On the other hand, the segments have not only to be accumulated successively but held together until a

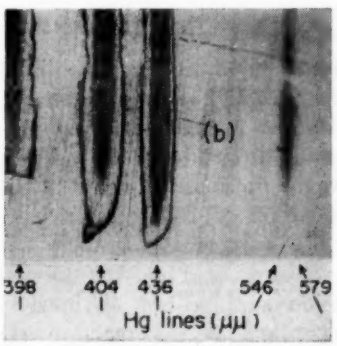

FIG. 6b. Cathode deposit as influenced by wave-length of illumination. (Yellow light, no effect. Green light less effective than blue.)

[15a] Cf. also J. J. Lingane and L. W. Niedrach, J. Am. Chem. Soc. 71, 196 (1949).

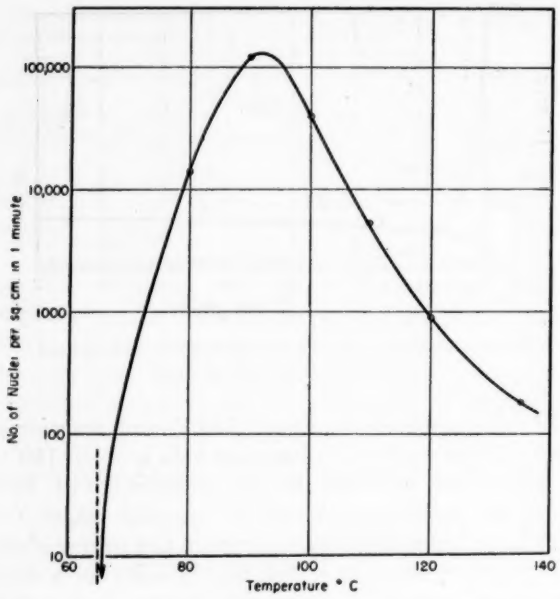

FIG. 7. Nucleation characteristic of metallic selenium (65° point obtained from x-ray data; 80 and 90° points estimated from speed of crystallization; remainder obtained by microscopic examination).

nucleus of stable size is formed. The probability that the incipient order is destroyed prematurely increases rapidly with temperature. Thus the nucleation characteristic traverses a maximum under the influence of these two opposing trends.

Once stabilized, the growth velocity of a nucleus depends on the speed with which new selenium segments can be added to continue the pattern. It therefore increases rapidly with temperature, that is, with decreasing viscosity of the amorphous phase, but not quite up to the melting point. Crystallization releases heat; the tip of the crystallite therefore reaches the melting temperature and stops growing before the over-all temperature is raised to this value. Thus the crystal-growth characteristic reverses its trend near 210°C under the conditions of our experiment (Fig. 8).

These results are in agreement with Tammann's classical investigations on other systems.[16]

PLATING BATHS

The discussion thus far has established three prerequisites which should be met to assure satisfactory plating conditions: (1) an ample supply of selenium cations; (2) no hydrogen ion discharge; and (3) a temperature near the optimum range of nucleation to permit fast deposition of the selenium in the metallic modification.

The weak selenious acid by itself does not provide an ample Se-cation supply, but obviously this can be increased according to the reaction $H_2SeO_3+H^+\rightleftarrows(H_3SeO_3)^+$ if the hydrogen ion concentration is raised by the addition of a strong acid. We experimented first with selenious-selenic acid mixtures to avoid the addition of other elements.

Selenious-selenic acid mixtures proved to be useful plating baths. Figure 9 shows the cathode efficiency and cell resistance of 18 N H_2SeO_4 at 55°C as a function of the SeO_2 content of the solution. The current density in this experiment was 8 amp./ft.^{2}. With increasing SeO_2 concentration the cathode efficiency rose steeply; that is, more current was carried by selenium and less by hydrogen ions, and the evolution of hydrogen ceased. At about 800 g/l of the 18 N acid the efficiency reached 100 percent; the total current of 8 amp./ft.^{2} was carried by selenium at the cathode if Se^{+4} ions are assumed to discharge. An analysis of the bath before and after plating indicated that at the Pt anode two reactions occur: the discharged oxygen partly escaped as gas bubbles and partly served for the oxidation of selenious to selenic acid.

At low cathode efficiency considerable gas polarization is observed and a badly pitted deposit of gray selenium results. The deposit is metallic at 55°C, as already mentioned previously for selenious acid; the nucleation characteristic for electrodeposition extends to lower temperature than the transformation characteristic of Fig. 7.

When the discharge of selenium at the cathode dominates, the fact that selenic can be reduced to selenious acid loses its importance. We therefore changed to sulfuric acid solutions, a substitution that proved completely successful (Fig. 9). The efficiency is practically identical, the deposits are smoother and more uniform, and the somewhat higher resistance of the sulfuric acid baths is of no consequence.

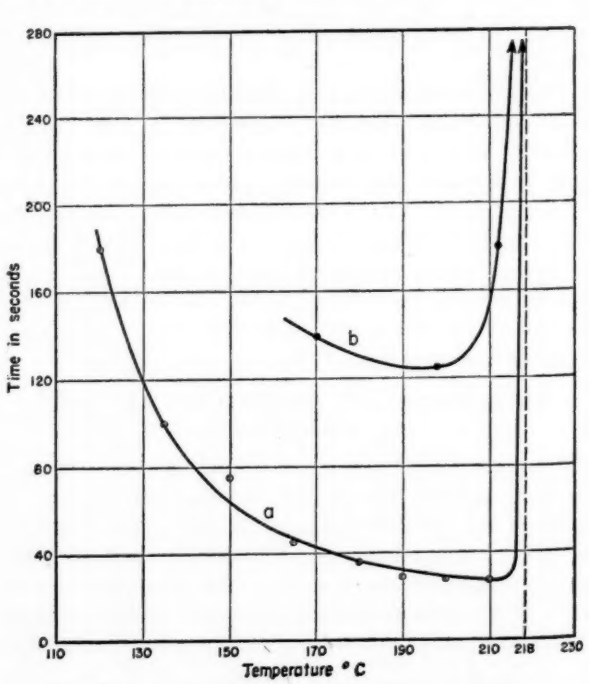

FIG. 8. Crystallization speed of two lots of selenium.

[16] G. Tammann, Zeits. f. physik. Chemie **25**, 441 (1898).

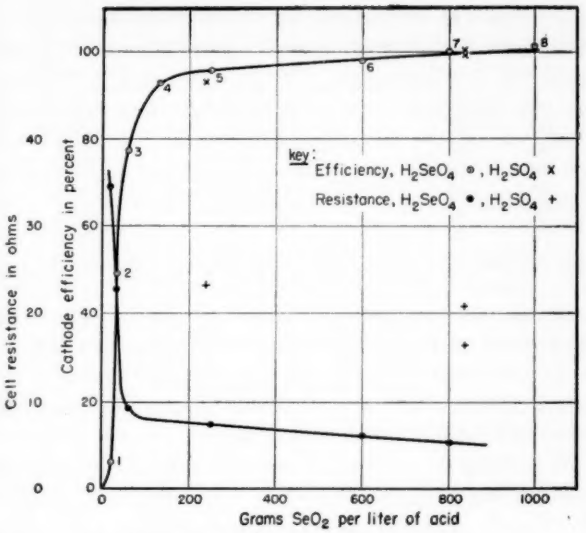
Cell resistance in ohms
Cathode efficiency in percent
Grams SeO_2 per liter of acid
key:
Efficiency, H_2SeO_4 ⊙, H_2SO_4 x
Resistance, H_2SeO_4 ●, H_2SO_4 +

FIG. 9. Effect of total Se concentration on cathode efficiency and cell resistance (18 N acid, 55°C, 8 amp./ft.²).

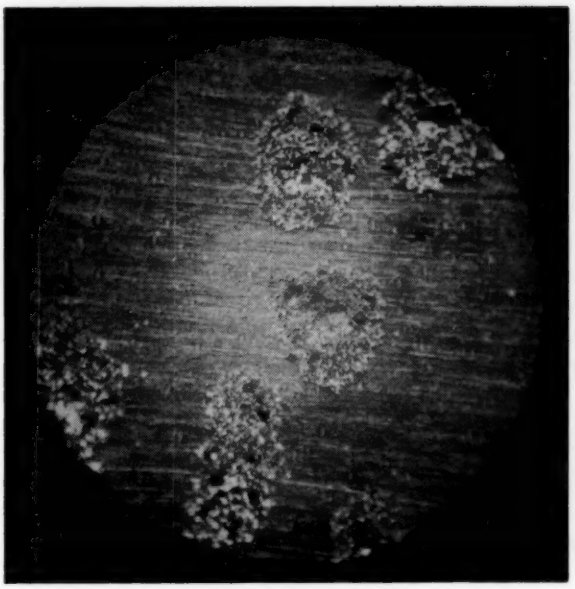

FIG. 11. Crystal clusters on untransformed background (10×).

At 55°C a concentration of 840 g SeO_2 per liter of 18 N selenic or sulfuric acid provided 100 percent cathode efficiency at 8 amp./ft.². Taking this bath composition as a starting point, we measured, as a function of temperature, the maximum permissible current density above which excessive hydrogen development and pitting of the deposit resulted (Fig. 10). While at room temperature a current density as low as 1 amp./ft.² proved excessive and red selenium discharged, at 100°C even 75 amp./ft.² did not produce any deleterious development of hydrogen. At 125°C, and more so at 150°C, the current density could be raised still further without producing bubble pits, but at these elevated temperatures a new phenomenon began to interfere. The selenium plated out initially as an intensely red film that did not cause a marked polarization. Then isolated nuclei of the metallic modification appeared and the subsequent deposit grew in star-like clusters from these spots until it covered the entire surface (Fig. 11).

This outcome was not unexpected (cf. Fig. 7). Raising the temperature led first into the region of improving nucleation. Simultaneously the viscosity of the solution rapidly decreased and successively higher current densities could be carried without hindrance by a sluggish transformation of the film or depletion of selenium ions in the cathodic region of the solution. However, at

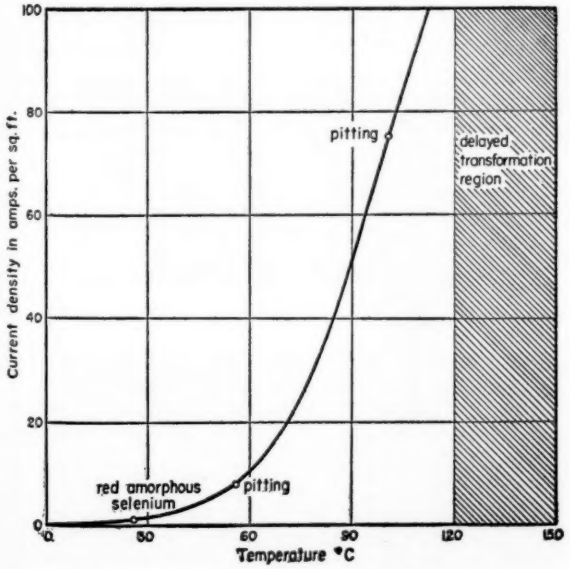

FIG. 10. Effect of temperature on permissible current density (18 N H_2SO_4, 840 g SeO_2 per liter of acid).

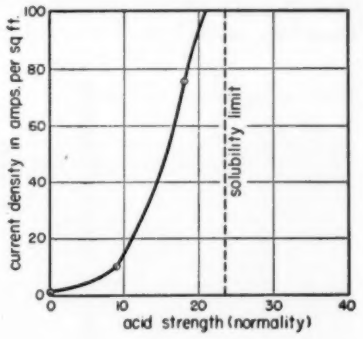

FIG. 12. Effect of acid strength at constant SeO_2 concentration (840 g SeO_2 per liter H_2SO_4, 100°C).

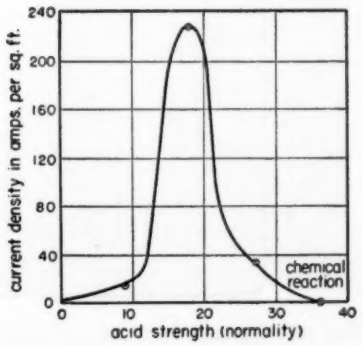

FIG. 13. Effect of acid strength in saturated solutions of SeO_2 in H_2SO_4 (100°C).

TABLE I. Solubility of SeO_2 in sulfuric acid at 100°C.

Acid	SeO_2 for saturation
0 N	5760 g/l
9	2580
20	2140
27	390

sufficiently high temperature one moved out of the region of rapid nucleation. The red selenium layer at this temperature was sufficiently conducting to allow transconduction, but the nuclei of the metallic form appeared only after a statistical waiting period.

Thus a bath temperature near 100°C appears most favorable for plating at high current densities. Once a metallic selenium coating has been formed, higher temperatures may be chosen because now every discharging selenium ion can deposit in its proper place in the hexagonal structure pattern.

With the temperature fixed at 100°C we next investigated the permissible current density as a function of the acid strength: (a) for a constant SeO_2 concentration of 840 g/l of H_2SO_4 (Fig. 12); and (b) for saturated solutions of SeO_2 in H_2SO_4 (Fig. 13). A comparison of the two characteristics shows that increase in SeO_2 concentration allows the passage of still higher currents without hydrogen evolution. For 18 N H_2SO_4 in saturated solution current densities of 200 amp./ft.^{2} can be employed, that is, a selenium rectifier of 3-mils layer thickness can be plated in 14 minutes.

That an optimum exists near 18 N is due to the fact that initially with increasing acid strength more hydrogen ions, hence more Se-cations, become available, but that in more concentrated solutions the SeO_2 molecules and hydrogen ions begin to compete for water molecules. Thus the solubility of SeO_2 decreases and the cation concentration traverses a maximum. Table I gives approximate solubility data for our solutions at 100°C.

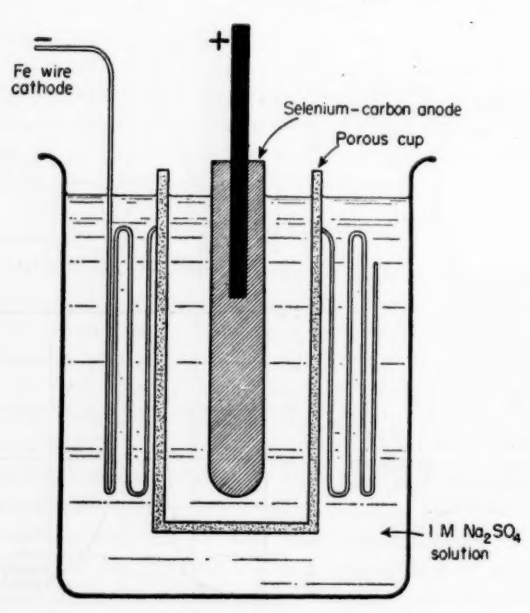

FIG. 14. Apparatus for testing efficiency of selenium-carbon anode.

TABLE II. Performance of selenium-carbon anodes.

Anode composition		Current density	Current efficiency
90% Se,	10% C	37 amp./ft.^{2}	83.3%
90	10	75	76.2
90	10	100	61.2
90	10	200	52.9
90	10	300	41.2
80	20	75	89.1
70	30	75	85.6

At very high acid strength, a chemical reaction between the sulfuric acid and the discharging selenium prevents the formation of a deposit.

A number of other acids have been tried more or less successfully.

SELENIUM-CARBON ANODES

In the preceding experiments platinum anodes were employed; carbon anodes disintegrated in our solutions. The plating bath could not be stabilized with either electrode type since oxygen develops anodically; thus SeO_2 was lost and some selenic acid formed in the overall process. A further drawback was that the gas bubbles drifting back to the cathode could cause a pitted deposit. These difficulties would be avoided if selenium could be dissolved at the anode.

Solid metallic selenium bars cannot serve as anodes because their resistivity is too high (*ca.* 10^5 ohm cm). This objection, however, may be overcome by the use of anodes prepared from selenium-carbon mixtures. Such electrodes we made from mixtures of selenium and carbon powders either by casting or by sintering under high pressure according to powder metallurgy procedures. Since these electrodes have to disintegrate as selenium is dissolved the released carbon particles must be trapped before they can enter the main solution.

To prove the final usefulness of the selenium-carbon anodes, it had to be established how far the anodic reaction product consisted of selenious or selenic acid and how the efficiency of the reaction depended on

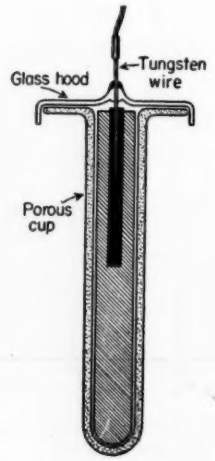

FIG. 15. Selenium-carbon anode.

anode composition and current density. For this study the arrangement of Fig. 14 was used with a 1 M Na_2SO_4 solution as the electrolyte. The porous cup *C* of unglazed porcelain prevented the diffusion of the electrolytically dissolved Se to the cathode where it would have been reduced to Se again. The composite electrode and the cup were washed thoroughly after the plating cycle, since both retained solution.

The known analytical procedures for determining selenious *vs.* selenic acid proved unreliable; it was therefore necessary to develop a new method of analysis. A double-indicator acidimetric titration was evolved which used bromcresol purple and alizarin yellow *R* as the indicators. The first-named changes color at the *p*H of the half neutralized selenious acid, while the color change of the second indicator is close to the *p*H of the completely neutralized selenious acid. If selenious acid is the only acid formed by the electrolysis, the second titration requires exactly twice as much alkali as the first one. If selenic acid is the only acid formed, the first and second titrations are equal. If both acids are formed, the second titration is less than twice the first one, and a simple calculation will give the percentage of each acid. The charge transfer was measured with a copper coulometer.

The result was that practically no selenic acid was formed over a wide range of current densities; the product of the electrolysis consisted of selenious acid and some oxygen. Table II gives current efficiencies in their dependence on current density and electrode composition.

Our final electrodes consisted of about 20 percent pure graphite and 80 percent selenium. The material was intimately mixed, cast into a glass tube, fitted with a spectroscopically pure carbon core, converted into metallic selenium and finally transferred into a porous porcelain cup. Figure 15 shows a typical anode of this type. The selenium and carbon used in these castings had to be carefully selected, since impurities are carried over from the anode into the cathodic deposit.

FIG. 16. Nodules of amorphous selenium (45×).

FIG. 17. Nodules breaking through top layer of selenium deposit (245×).

STRUCTURE OF THE SELENIUM DEPOSITS

Plating at room temperature from selenious acid solutions produces adherent layers of red selenium. If the voltage is raised and hydrogen discharged, the film may puncture and the current, concentrating in the breakdown spots, may discharge the selenium in odd, caterpillar-like, stratified structures (Fig. 16). With increasing voltage and current, more and more of these grayish, fibrous nodules appear, and fall off until the surface is converted into a crater field. The evolution of hydrogen creates simultaneously some brick-red selenium by the reduction of SeO_2 that only loosely adheres.

The gray appearance of the snails suggests metallic

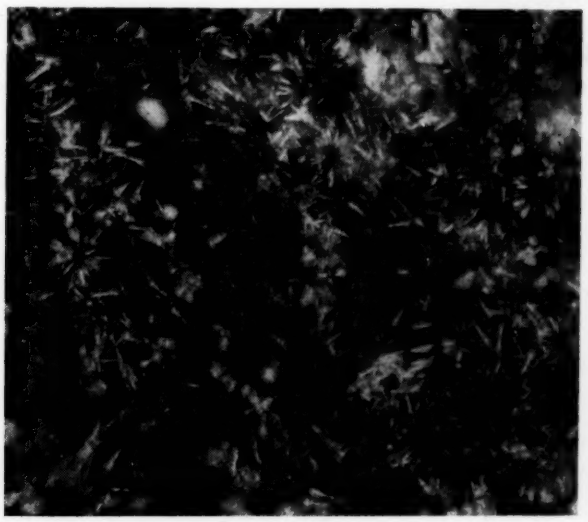

FIG. 18. Needle deposit of metallic selenium (220×).

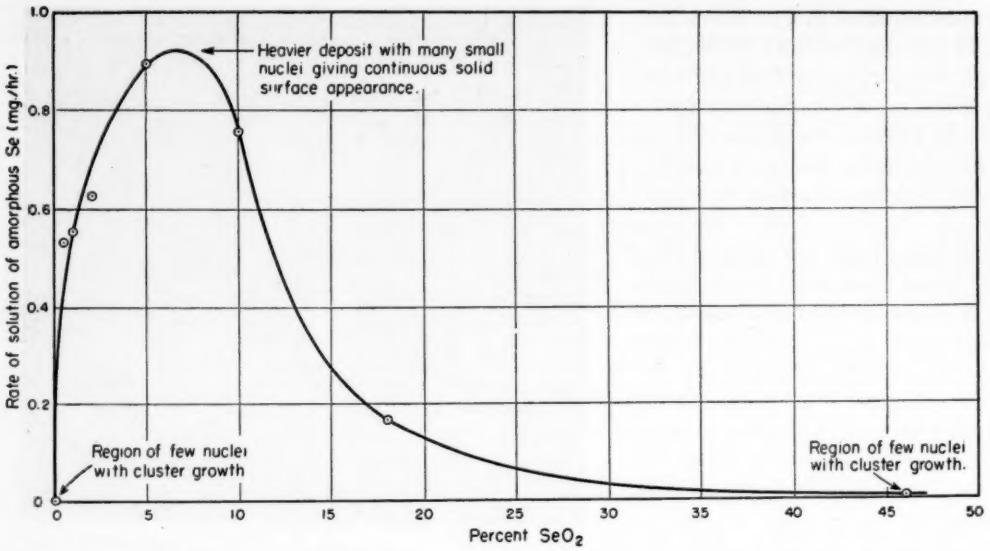
Heavier deposit with many small nuclei giving continuous solid surface appearance.
Region of few nuclei with cluster growth
Region of few nuclei with cluster growth.
Rate of solution of amorphous Se (mg./hr.)
Percent SeO_2
1.0
0.8
0.6
0.4
0.2
0
0 5 10 15 20 25 30 35 40 45 50

FIG. 19. Solubility of SeO_2 and nucleation behavior in concentrated HCl solution.

selenium, but this evidence is refuted by x-ray analysis. The material is completely amorphous at low currents; at high densities it may be converted into the metallic modification by Joule heat, but if the bath is kept cool, little evidence of conversion is obtained even at 175 amp./ft.^{2}. This conclusion is confirmed by the growth habit of the nodules (Fig. 17); they break through the top layer and grow by adding new layers of deposit as their base at the metal cathode, instead of growing from the tip as metallic dendrites would. When heated these nodules contract, soften, and collapse in a clump of metallic Se.

Our standard selenious acid-sulfuric acid bath at 100°C produces a velvety black deposit, in which the metallic selenium grows in star-like clusters of needles (Fig. 18). X-ray patterns parallel and perpendicular to the electrode surface show that these needles grow preferentially parallel to the hexagonal (c-) axis of the crystal, that is, in the direction of high electric conduction.

While no metallic selenium plates out on Pt from pure SeO_2 solutions at room temperature, a growth of metallic selenium, once obtained, may be continued at room temperature with low current densities, as mentioned above, and produce needles that stand practically perpendicular to the cathode surface.

FIG. 20a. Electropolished nickel sheet showing a few nuclei (300×).

The crystallization habit can be changed within wide limits by the type of acid used. Metallic selenium can be deposited from $HCl-SeO_2$, $H_2SO_4-SeO_2$ and to some extent from HNO_3-SeO_2 solutions at room temperature. The crystallites from the HCl bath are in general flat and form relatively hard and brittle deposits that may be stripped easily. From sulfuric acid solutions, round crystals are obtained which grow into space and lead to a softer and more adherent layer. Close inspection shows that in all cases first some red selenium plates out at room temperature and then transforms into the metallic phase by solvent action. Even simple immersion of red selenium in these acids produces a surface layer of metallic selenium by solution and redeposition: the speed of transformation parallels the solubility of amorphous selenium (Fig. 19).

Like acid type and concentration, the current density has a profound effect on the nature of the crystalline mat. For example, from the same bath (72 percent H_2SO_4 at 100°C) at 150 amp./ft.^{2} a deposit of very fine needles, like sheaves of wheat, grows nearly perpendicular to the base plate and produces a highly conducting deposit. At 10 amp./ft.^{2} the needles have broadened into leaf-like aggregates, not so well oriented and forming a mat of appreciably lower conductivity.

Finally, the structure of the base plate has a decisive influence on nucleation and the conductivity of the deposit. Pt or Ni cathodes of large grain size, in which the crystal structure is exposed by etching or electropolishing, are covered in the first stages of electrodeposition largely by a film of red selenium perforated only with a few incipient crystals of the metallic phase (Fig. 20a). The same surface, mechanically roughened, is covered under identical conditions by a fine-grained deposit of metallic selenium (Fig. 20b). The current, concentrated in the nucleated areas, builds up in the

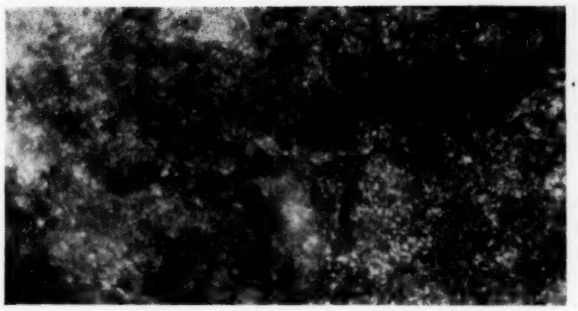

FIG. 20b. Nickel sheet, mechanically roughened, covered with metallic Se nuclei (300×).

FIG. 21. Cross section of Se plate on electropolished nickel sheet (300×).

former case a coarse layer of inferior conductivity; Fig. 21 shows a cross section of such a plate.

CONCLUSIONS

Electroplating of metallic selenium can be accomplished with a speed comparing favorably to that of any true metal. The bath composition can be stabilized to a large extent by the use of selenium-carbon anodes, and the structure of the deposit can be controlled in wide limits. It should be pointed out that the plating baths and deposits are sensitive against a variety of impurities, as may be expected from the polymorphism of the element and the semiconductor nature of its metallic phase. Consequently a number of unusual phenomena may be observed such as the formation of blocking layers during electroplating, acceleration or suppression of nucleation by addition agents, and the formation of deposits which lend themselves in varying degrees to applications as rectifiers and photo-cells. Detailed investigations of these phenomena will be concluded shortly.

ACKNOWLEDGMENT

In the course of this investigation, J. H. Schulman was engaged in the development of the selenium-carbon anode, F. G. Chesley in the x-ray studies, while J. P. Levy, M. Krulfeld, M. Albright, A. Boissevin, and B. Murray carried through various phases of the electroplating research. The authors want to express their indebtedness to these co-workers and to J. Kalnjs who recently took some polarograms and kindly checked a number of our earlier findings.

On Lattice Theories of the Liquid State*

H. Milton Peek† and Terrell L. Hill
Department of Chemistry, University of Rochester, Rochester, New York and Naval Medical Research Institute, Bethesda, Maryland

(Received May 23, 1950)

The Lennard-Jones and Devonshire theory of the liquid state has been modified by introduction of the quasi-chemical method to allow for both holes in the liquid and an expandable lattice. The essential step is to minimize the free energy with respect to a lattice expansion parameter. On the whole, critical constants obtained in this way are in appreciably better agreement with experiment than those of the Lennard-Jones and Devonshire theory. However, the equilibrium number of holes turns out to be much too small.

I. INTRODUCTION

ALTHOUGH considerable progress has been made using rigorous approaches to the theory of a classical liquid with spherically symmetrical molecules and a potential energy given by the sum of pair interactions,[1] owing to purely mathematical difficulties it has not proved possible to carry these investigations sufficiently far to predict quantitative thermodynamic properties, such as the equation of state. Pending solution of these mathematical problems, approximate theories of the liquid state remain of interest.

Perhaps the most successful approximate theory of liquids is that due to Lennard-Jones and Devonshire[2] (L.J.D.). Their model is the following: In a close-packed lattice, any given molecule is surrounded by $z_0=12$ nearest neighbors which lie, when in their equilibrium lattice positions, on the surface of a sphere. In the liquid state it is assumed that the z_0 molecules are, on a time average, "smeared" with uniform (surface) density over the surface of this sphere. The motion of the molecule of interest inside the "cell" is then determined by the potential energy of interaction of the interior molecule with its smeared shell of neighbors, the interaction energy being a function of the distance of the interior molecule from the center of the cell. The fact that a molecule can in due course escape from any particular cell and thus wander over the entire volume V of the container is recognized rather artificially and probably incorrectly by the insertion of a factor $N^N/N!$ in the partition function for the system of N molecules.

In the present theory we retain the fundamental cell and lattice (or solid→liquid rather than gas→liquid) point of view used by L.J.D. but introduce the quasi-chemical approximation[3] to allow for the obviously desirable refinement of an expandable lattice not all of whose sites are in general occupied.[4,5] This approach makes unnecessary the arbitrary introduction of an extra factor such as $N^N/N!$ mentioned above. Earlier approximate theories of liquids have taken into account an expandable lattice (Lennard-Jones and Devonshire)[2] or holes in the liquid (Cernuschi and Eyring,[3] for example) but not both. As will presently be clear, instead of assigning an arbitrary number of holes to the liquid we essentially let the liquid "choose" its own number of holes (by minimizing the free energy).

II. DERIVATION OF EQUATIONS

We use the notation of Fowler and Guggenheim[6] where convenient. We consider a close-packed lattice ($z_0=12$=number of nearest neighbor *sites*) with B sites, volume V, and nearest neighbor intersite distance $a(V=Ba^3/\sqrt{2})$. N molecules are distributed among the B sites, the fraction of sites occupied being $\theta=N/B$. The configurational entropy associated with the differ-

* From part of a Ph.D. thesis submitted by H. M. Peek to the University of Rochester.

† Present address: Los Alamos Scientific Laboratory, P. O. Box 1663, Los Alamos, New Mexico.

[1] See, for example, J. E. Mayer *et al.* J. Chem. Phys. **5**, 67, 74 (1937); **6**, 87, 101 (1938); **7**, 1025 (1939); **9**, 2, 626 (1941); J. G. Kirkwood, J. Chem. Phys. **3**, 300 (1935); J. G. Kirkwood and E. M. Boggs, J. Chem. Phys. **10**, 394 (1942); M. Born and H. S. Green, Proc. Roy. Soc. **188A**, 10 (1946); **189A**, 103 (1947).

[2] J. E. Lennard-Jones and A. F. Devonshire, Proc. Roy. Soc. **163A**, 53 (1937); **165A**, 1 (1938).

[3] This is not the first application of the quasi-chemical method to liquids though it appears to be the first such application which permits an expandable lattice.

F. Cernuschi and H. Eyring (J. Chem. Phys. **7**, 547 (1939)) applied to liquids the method introduced by Bethe in the theory of the order-disorder transition in alloys. But this method, though having an altogether different appearance, is actually identical with the quasi-chemical method (see reference 6, pp. 589–598). Cernuschi and Eyring did not take into account the effect of nearest neighbor lattice vacancies on the cell partition function.

The quasi-chemical approximation in the usual form was applied to the holes in a liquid in a paper by S. Ono (Memoirs of the Faculty of Engineering, Kyushu University, Vol. X, No. 4, 1947) which came to our attention during the course of this work. Ono uses a strictly empirical equation to take care of the effect of lattice vacancies on the cell partition function and determines the cell size from experimental data. Incidentally, the equation of state he obtains is formally identical with Eq. (1012,15) of reference 6.

Also, in their order-disorder theory of melting, Lennard-Jones and Devonshire (Proc. Roy. Soc. **169A**, 317 (1939)) used Bethe's method combined with their own earlier treatment of the cell partition function.

Note added June 19, 1950: In a paper just received (J. Phys. Soc. Japan **4**, 103 (1949)) Sato and Ono modify Ono's paper (above) by introducing the L.J.D. cell treatment. However, the empirical features mentioned above appear to be retained.

[4] That is, it is an experimental fact (see reference 5) that the average number of molecules z in the first coordination shell varies, as expected, with the temperature and density of the liquid. $z=z_0$ is a constant in the L.J.D. theory.

[5] See, for example, A. Eisenstein and N. S. Gingrich, Phys. Rev **62**, 261 (1942).

[6] R. H. Fowler and E. A. Guggenheim, *Statistical Thermodynamics* (Cambridge University Press, London, 1939). See pp. 336–350 for a discussion of the L.J.D. theory and pp. 429–430, 437–443 for a treatment of the quasi-chemical method in a closely related problem (localized monomolecular adsorption).

ent ways of distributing N molecules among B sites and the total potential energy of interaction of pairs of molecules in *equilibrium* positions on nearest neighbor sites are handled by the quasi-chemical approximation. The motion of each molecule within its cell is treated in the manner of L.J.D., except that the average number of nearest neighbor molecules is z and not z_0. Our use of $z<z_0$ in the L.J.D. model takes into account, approximately, the effect[7] of lattice vacancies on the "free volume."

We now outline the argument in detail. The partition function for the system of N molecules is[6]

$$Q=\sum_{N_A} g(N, N_A, B)j^N \exp[-N_A w(a)/kT], \quad (1)$$

$$\sum_{N_A} g=B!/N!(B-N)!=G, \quad (2)$$

where g is the number of ways of distributing N molecules among B sites so that there are exactly N_A nearest neighbor pairs, $w(a)$ is the potential energy of interaction of a pair of molecules at the nearest neighbor intersite distance a and j is the partition function for the motion of a molecule within its cell. In order to keep the equations tractable, we use a single *average* j for all molecules over all G configurations:

$$j=j(\bar{N}_A)$$

$$z=2\bar{N}_A/N$$

$$\bar{N}_A=[\sum_{N_A} N_A g \exp(-N_A w(a)/kT)]/\sum_{N_A} g \exp(-N_A w(a)/kT). \quad (3)$$

Hence j^N in Eq. (1) can be placed in front of the summation sign.

Equation (1) can now be written

$$Q=Gj^N \exp[-N_A^* w(a)/kT] \quad (4)$$

which defines N_A^*.

Introducing the quasi-chemical approximation[6] and the L.J.D. model,[6] we have

$$z=2\bar{N}_A/N=12\left[1-\frac{2(1-\theta)}{\beta+1}\right] \quad (5)$$

$$N_A^*=6B\theta+\frac{6BkT}{w(a)}\left[\theta \ln\frac{(\beta+2\theta-1)(1-\theta)}{\theta(\beta-2\theta+1)}+\ln\frac{(\beta-2\theta+1)}{(1-\theta)(\beta+1)}\right] \quad (6)$$

$$\beta=\{1-4\theta(1-\theta)[1-\exp(-w(a)/kT)]\}^{\frac{1}{2}} \quad (7)$$

[7] J. G. Kirkwood, J. Chem. Phys. **7**, 908 (1939). This paper criticizes the failure of Cernuschi and Eyring (see reference 3) to take this effect into account.

$$j=\left(\frac{2\pi mkT}{h^2}\right)^{\frac{1}{2}} 2\pi a^3 \int_0^s y^{\frac{1}{2}} \exp\left\{-\frac{z\epsilon}{kT}\left[\left(\frac{r^*}{a}\right)^{12} l(y)-2\left(\frac{r^*}{a}\right)^6 m(y)\right]\right\} dy \quad (8)$$

$$l(y)=(1+12y+25.2y^2+12y^3+y^4)(1-y)^{-10}-1 \quad (9)$$

$$m(y)=(1+y)(1-y)^{-4}-1. \quad (10)$$

Note that z from Eq. (5) is used in Eq. (8). The constants ϵ and r^* are the parameters of the assumed potential energy curve for the interaction of two molecules at a distance r,

$$w(r)=\epsilon(r^*/r)^{12}-2\epsilon(r^*/r)^6. \quad (11)$$

The upper limit s in the integral is determined by the consideration[8] that for a perfect gas

$$2\pi a^3 \int_0^s y^{\frac{1}{2}} dy=V/B=a^3/\sqrt{2}$$

or

$$s=(3/4\pi\sqrt{2})^{\frac{1}{3}}=0.30545. \quad (12)$$

We now define

$$\alpha=(r^*/a)^3 \quad \gamma=v/v^* \quad v^*=r^{*3}/\sqrt{2} \quad \theta=1/\alpha\gamma=N/B \quad v=V/N \quad \lambda=\epsilon/kT. \quad (13)$$

The Helmholtz free energy A can then be written

$$A/NkT=-(1/N)\ln Q$$

$$=\alpha\gamma \ln\left(1-\frac{1}{\alpha\gamma}\right)+\ln\frac{1}{\alpha\gamma-1}+6\alpha\gamma \ln\frac{[\beta-(2/\alpha\gamma)+1]}{[1-(1/\alpha\gamma)](\beta+1)}+6 \ln\frac{[\beta+(2/\alpha\gamma)-1][1-(1/\alpha\gamma)]}{(1/\alpha\gamma)[\beta-(2/\alpha\gamma)+1]}+6\lambda\alpha^2(\alpha^2-2)-\ln\left(\frac{2\pi mkT}{h^2}\right)^{\frac{3}{2}}-\ln(2\pi r^{*3}/\alpha)-\ln\Gamma, \quad (14)$$

$$\Gamma=\int_0^s y^{\frac{1}{2}} \exp\{\}\, dy, \quad (15)$$

$$\{\}=12\lambda\alpha^2\left[1-\frac{2(\alpha\gamma-1)}{\alpha\gamma(\beta+1)}\right][2m(y)-\alpha^2 l(y)], \quad (16)$$

$$\beta=\left[1-\frac{4(\alpha\gamma-1)}{\alpha^2\gamma^2}\{1-\exp[\lambda\alpha^2(2-\alpha^2)]\}\right]^{\frac{1}{2}}. \quad (17)$$

[8] In the liquid state the exact choice of the upper limit is of no practical consequence. In the gaseous state it would have an effect; but the model used here is presumably not very good for a dilute gas anyhow. In the calculations of Section III, at the largest volumes the contributions to j were in the range $0 \leqslant y \leqslant 0.28$. L.J.D. chose arbitrarily $s=0.25$.

TABLE I. Isotherm for $\lambda=0.80$.

$\gamma=v/v^*$	α	θ	Pv^*/kT	Γ
1.25	0.8012	0.9985	2.658	0.0021779
1.5	0.6724	0.9915	1.399	0.0065778
1.75	0.5838	0.9788	0.9079	0.014073
2.0	0.5242	0.9538	0.5661	0.022442
2.25	0.4829	0.9204	0.3878	0.029635
2.5	0.4510	0.8869	0.3086	0.035642
2.75	0.4231	0.8595	0.2724	0.041152
3.0	0.3977	0.8382	0.2568	0.046430
3.5	0.3526	0.8103	0.2438	0.056632
4.0	0.3162	0.7906	0.2327	0.065636

This gives A/NkT as a function of γ, λ, and α. Of course α is not an independent variable, since thermodynamically A/NkT is determined by γ and λ only; we choose α so that A is *minimized* for given N, V, T, and neglect fluctuations of α from this value.

From Eq. (14), after lengthy algebra, we find

$$\left(\frac{\partial[A/NkT]}{\partial\alpha}\right)_{\gamma,\lambda}=0=\gamma\ln\frac{\alpha\gamma-1}{\alpha\gamma}+\frac{1}{\alpha}+24\alpha\lambda(\alpha^2-1)+\frac{48(\alpha\gamma-1)(1-\alpha^2)\lambda}{\gamma(\beta+1)}+6\gamma\ln\frac{[\beta-(2/\alpha\gamma)+1]}{[1-(1/\alpha\gamma)](\beta+1)}-\frac{1}{\Gamma}\left(\frac{\partial\Gamma}{\partial\alpha}\right)_{\gamma,\lambda},\quad(18)$$

$$\left(\frac{\partial\Gamma}{\partial\alpha}\right)_{\gamma,\lambda}=24\lambda\alpha\int_0^s y^{\frac{1}{2}}\left\{\frac{1}{\gamma(\beta+1)}[\alpha^2l(y)-2m(y)]\times\left[\frac{1}{\alpha}-\frac{(\gamma\alpha-1)(\partial\beta/\partial\alpha)_{\gamma,\lambda}}{\beta+1}\right]-2\left[1-\frac{2(\alpha\gamma-1)}{\gamma\alpha(\beta+1)}\right]\times[\alpha^2l(y)-m(y)]\right\}\exp\{\}dy,\quad(19)$$

$$\left(\frac{\partial\beta}{\partial\alpha}\right)_{\gamma,\lambda}=\frac{2}{\beta\alpha^3\gamma^2}\{4\alpha^2\lambda(\alpha\gamma-1)(1-\alpha^2)\times\exp[\lambda\alpha^2(2-\alpha^2)]+(\alpha\gamma-2)(1-\exp[\lambda\alpha^2(2-\alpha^2)])\}.\quad(20)$$

Equation (18) thus gives $\alpha=\alpha(\gamma,\lambda)$ as the root of $\partial(A/NkT)/\partial\alpha=0$ associated with the minimum free energy A.

The equation of state is then, after another long calculation,

$$\frac{Pv^*}{kT}=\alpha\ln\frac{\alpha\gamma}{\alpha\gamma-1}+6\alpha\ln\frac{[1-(1/\alpha\gamma)](\beta+1)}{[\beta-(2/\alpha\gamma)+1]}+\frac{1}{\Gamma}\left(\frac{\partial\Gamma}{\partial\gamma}\right)_{\alpha,\lambda},\quad(21)$$

TABLE II. Isotherm for $\lambda=0.85$.

$\gamma=v/v^*$	α	θ	Pv^*/kT	Γ
2.0	0.5232	0.9557	0.5112	0.022560
2.25	0.4818	0.9225	0.3412	0.030067
2.5	0.4502	0.8885	0.2655	0.036266
2.75	0.4230	0.8597	0.2351	0.041831
3.0	0.3977	0.8382	0.2250	0.047280
3.25	0.3740	0.8227	0.2223	0.052698
3.5	0.3520	0.8117	0.2216	0.058044
4.0	0.3158	0.7916	0.2151	0.067307

$$\left(\frac{\partial\Gamma}{\partial\gamma}\right)_{\alpha,\lambda}=\frac{24\lambda\alpha}{\gamma(\beta+1)}\left[\frac{1}{\gamma}-\frac{(\gamma\alpha-1)(\partial\beta/\partial\gamma)_{\alpha,\lambda}}{\beta+1}\right]\times\int_0^s y^{\frac{1}{2}}[\alpha^2l(y)-2m(y)]\exp\{\}dy,\quad(22)$$

$$\left(\frac{\partial\beta}{\partial\gamma}\right)_{\alpha,\lambda}=\frac{2(\alpha\gamma-2)\{1-\exp[\lambda\alpha^2(2-\alpha^2)]\}}{\beta\alpha^2\gamma^3},\quad(23)$$

where α is to be found from Eq. (18) as discussed above. For a perfect gas ($\lambda=0$), Eqs. (18) and (21) give $Pv=kT$ as expected.

III. CALCULATION OF CRITICAL CONSTANTS

We have calculated $P-V$ isotherms for two temperatures, $\lambda=0.80$ and $\lambda=0.85$, the latter isotherm turning out to be almost exactly the critical isotherm.

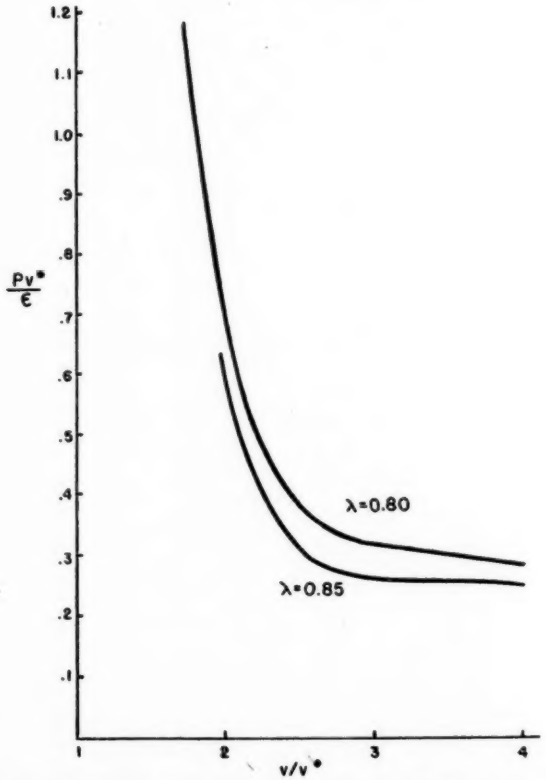

FIG. 1. Pressure-volume relations (Pv^*/ϵ *versus* v/v^*) in the critical region. $\lambda=0.85$ is the critical temperature.

TABLE III. Theoretical and experimental critical constants.*

	Neon	Nitrogen	Argon	Methane	van der Waals	L.J.D.	P. and H.
ϵ/kT_c	0.798	0.762	0.792	0.779	27/8=3.375	0.75	0.85
v_c/v^*	3.35	2.92	3.14	2.95	$2\pi\sqrt{2}$=8.88	~1.9	~3.25
P_cv^*/ϵ	0.111	0.131	0.117	0.126	$1/18\pi\sqrt{2}$= .0125	0.471	0.261
P_cv_c/kT_c	0.296	0.292	0.291	0.291	3/8= .375	~0.67	~0.72

* P_c, v_c, and T_c from International Critical Tables. r^* and ϵ for Ne, N_2, A from reference 6, based on work of Lennard-Jones and Buckingham; for CH_4 from Beattie and Stockmayer, J. Chem. Phys. 10, 473 (1942).

In these calculations, for given λ and γ, Eq. (18) is first solved for α as mentioned above. It should be pointed out in this connection that Eq. (18) may have two solutions, one corresponding to minimum A and the other to maximum A.

The results for $\lambda=0.80$ and $\lambda=0.85$ are given in Tables I and II, respectively, and in Fig. 1. The critical point is difficult to determine exactly (especially γ_c), but it is approximately $\lambda_c=0.85$, $\gamma_c=3.25$ and $P_cv^*/kT_c=0.222$. In Table III we compare experimental values of the critical constants for neon, nitrogen, argon and methane with theoretical values from the present paper, the work of L.J.D. and van der Waals' equation.[9] It will be noted that, while the L.J.D. theory is very successful in predicting the critical temperature, it gives a critical volume which is too small by a factor of about 1.6, and a critical pressure which is too large by a factor of about 3.9. Our theory is rather good, though not quite as good as L.J.D., on the critical temperature, but also gives almost the correct critical volume and improves the critical pressure by a factor of 1.8 over L.J.D. Van der Waals' equation gives poor values for the separate critical constants, but by a cancellation of errors actually gives the best of the three theoretical values for the combined quantity P_cv_c/kT_c.

In the absence of other information we would consider the above results on critical constants encouraging. However, if one calculates a_c and z_c (using $\gamma=3.25$, $\lambda=0.85$ and $\alpha=0.374$) one finds $a_c=5.3$A (argon) and $z_c=9.9$, both of which appear to be too large.[10] We have confirmed this difficulty by a calculation at $\lambda=1.42$, $P=0$, which should be in the neighborhood of the boiling point of the liquid. We find $\gamma=1.425$, $\alpha=0.7046$, $\theta=0.9959$, $z=11.95$, and for argon, $a=4.30$A. Experimental values for argon[5] are about $z=10.5$ and $a=3.8$A. Similar results are obtained at neighboring temperatures and densities.

We believe that the present theory is an improvement over the L.J.D. theory in that the critical constants are, on the whole, better and that an arbitrary constant number of holes (e.g., *no* holes, if $z_0=12$) is not assumed. However, in view of the wrong order of magnitude obtained for the number of holes, it is clear that further refinements are needed.[11] As a matter of fact, since completion of this work, we have learned of two independent and more general approaches to a cell or lattice theory of liquids using the method of minimizing the free energy.[12,13]

We have profited from an exposition by Dr. George Halsey of his related views on the theory of liquids.

[9] See, for example, J. E. Mayer and M. G. Mayer, *Statistical Mechanics* (John Wiley and Sons, Inc., New York, 1940), Chapter 12.

[10] X-ray diffraction measurements on argon are not available at the critical point, but from the *approximate* results *near* the critical point, obtained by Eisenstein and Gingrich (see reference 5), the rough experimental values $a_c=4.3$A and $z_c=4$ might be interpolated (using $v_c=12a_c^3/\sqrt{2}z_c$, which assumes a random distribution of molecules among sites, these latter values of a_c and z_c are somewhat inconsistent with the experimental value of v_c in Table III, whereas $a_c=5.3$A and $z_c=9.9$, by a cancellation of errors, are consistent).

[11] For example: (1) instead of, in effect, "smearing" a neighboring hole over the surface of a sphere, localize the hole in the spherical shell (this is necessary for diffusion)—this should increase the free volume and the equilibrium number of holes; (2) replace the quasi-chemical assumption by a better approximation; (3) improve the assumption of a single average $j(\bar{N}_A)$. We intend to examine refinement (1), which we believe to be important.

[12] J. G. Kirkwood, J. Chem. Phys. 18, 380 (1950).

[13] J. E. Mayer (to be published).

Paramagnetic Susceptibilities of Solid Solutions of MnF_2 and ZnF_2*

LESTER CORLISS, YVETTE DELABARRE, AND NORMAN ELLIOTT
Chemistry Department, Brookhaven National Laboratory, Upton, Long Island, New York

(Received May 29, 1950)

The paramagnetic susceptibilities of solid solutions of MnF_2 and ZnF_2 have been measured as a function of temperature. The Curie-Weiss law $X=C/T+\Delta$ is obeyed by all the solutions examined over the temperature range 76°–295°K. The constant Δ was found to be a linear function of the mole fraction of MnF_2. This behavior is consistent with the assumption that the magnetic interaction energy associated with a given ion is proportional to the number of its paramagnetic neighbors.

THE existence of exchange forces in paramagnetic salts has been inferred from the fact that a large number of substances have magnetic susceptibilities which follow the Curie-Weiss law

$$X=C/(T+\Delta).$$

An attempt has been made to study the magnetic behavior of a paramagnetic salt as it is diluted with an isomorphous diamagnetic salt, since the interaction effects presumably responsible for the Δ term should disappear on sufficient dilution.[1]

The system chosen was manganous fluoride, MnF_2, and zinc fluoride, ZnF_2. The manganous ion, Mn^{++}, which is responsible for the paramagnetism, is in a $^6S_{\frac{5}{2}}$ ground state, and to a first approximation the susceptibility of its salts should not show a crystalline field effect.[2] It is also to be noted that the electrical environment of the Mn^{++} ion is substantially unchanged when MnF_2 is diluted with ZnF_2. These two compounds have the rutile structure. Each metal ion is surrounded octahedrally by fluoride ions in the first coordination zone and by ten other metal ions in the second zone. The lattice dimensions of the two salts differ by only three percent.

The magnetic susceptibility of manganous fluoride has been reported by Bizette and Tsai[3] to follow a Curie-Weiss law. It has also been measured by De Haas, Schultz, and Koolhaas[4] who found some deviation from this law. The results reported here are based on measurements made with C.P. materials which were analyzed chemically and spectroscopically, particularly for paramagnetic impurities; none of which were found in significant concentration. The magnetic susceptibilities agree with those obtained with a sample of manganous fluoride kindly given by Dr. Stout and Dr. Griffel at the Institute of Metals, the University of Chicago. The results of the various investigations are shown in Fig. 1.

Samples of C.P. MnF_2 and C.P. ZnF_2 were weighed out, intimately mixed, and fused in a closed platinum crucible inside a nickel reaction vessel. An atmosphere of anhydrous HF was maintained in the container. The fused mixtures were ground to fine powders for the magnetic measurements, which were made by the Gouy method. X-ray powder photographs were taken, and the fused samples were determined to be homogeneous in composition and to have lattice spacings which obeyed Vegard's rule.

Magnetic susceptibilities were measured at liquid nitrogen, dry ice, and room temperatures. Three or more samples of each composition were used and the data averaged with an average deviation of ±1 percent. The results are shown in Fig. 2. The dotted line passing through the origin in the graph is calculated for the free ion, and represents the situation approached by manganous fluoride on dilution with zinc fluoride.

From the susceptibility data were calculated values of the Curie constant C, the magnetic moment μ, and

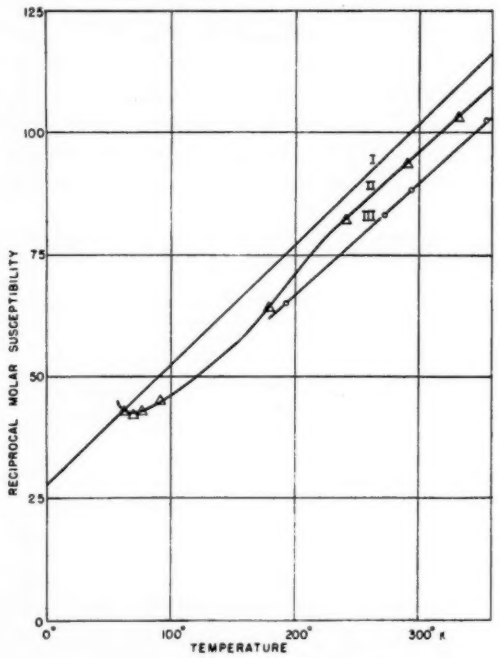

FIG. 1. Magnetic susceptibility of MnF_2 as a function of temperature. I. Bizette and Tsai (empirical formula); II. De Haas, Schultz and Koolhaas; III. Corliss, Delabarre and Elliott.

* Research carried out under the auspices of the AEC.

[1] For other experiments see P. W. Selwood, *Magnetochemistry* (Interscience Publishers, Inc., New York), pp. 89, 110; and Michel and Pouillard, Comptes Rendus **227**, 194 (1948).

[2] For a discussion of the effect of crystal fields on magnetic behavior see J. H. Van Vleck, *Theory of Electric and Magnetic Susceptibilities*, Oxford University Press, London, 1932), p. 286. Application of the theory to magnetically dilute manganous salts is given by J. H. Van Vleck and W. G. Penney, Phil. Mag. **17**, 961 (1934).

[3] H. Bizette and B. Tsai, Comptes Rendus **209**, 205 (1939).

[4] De Haas, Schultz, and Koolhaas, Physica **VII**, No. 1, 57 (1940).

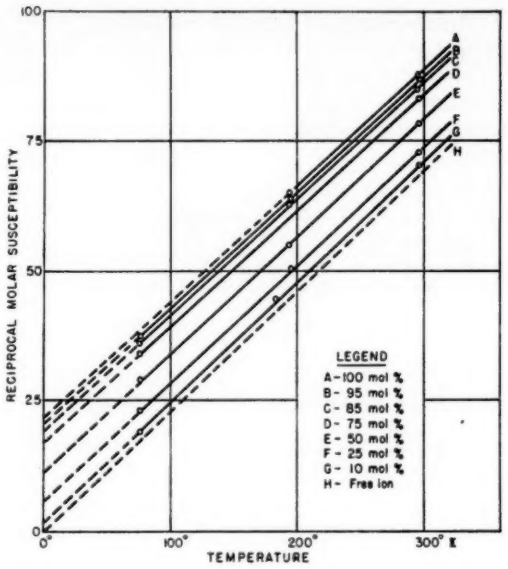

FIG. 2. Magnetic susceptibility of MnF_2 as a function of temperature and concentration (Mole percent MnF_2).

the paramagnetic Curie temperature Δ. These are given in Table I.

The magnetic moments found are in good agreement with the calculated value, 5.92 Bohr magnetons for the $^6S_{\frac{5}{2}}$ state.

In Fig. 3 the paramagnetic Curie temperatures are plotted against the mole percent of MnF_2 in the samples. Except for a small deviation in the neighborhood of pure MnF_2, the experimental curve is linear and passes through the origin. These results suggest a simple and admittedly naive interpretation. Let us assume that the exchange interaction energy for any one Mn^{++} ion is proportional to the number of nearest neighbors. This is analogous to Stoner's approximation in the theory of ferromagnetism.[5] We can then divide the Mn^{++} ions into groups having 0, 1, $\cdots z$ nearest neighbors ($z=10$ in this case). The average value of Δ will then be given by

$$\bar{\Delta}=\sum_{k=0}^{k=z} f_k k\delta,$$

where f_k is the fraction of the Mn^{++} ions having k Mn^{++} nearest neighbors and δ represents the contribution to

[5] Edmund C. Stoner, *Magnetism and Matter* (Methuen and Co. Ltd., London), p. 358.

TABLE I.

Mole % MnF_2	C	Δ	μ (Bohr Magnetons)
5%	4.33	5.5°K	5.90
10%	4.33	9.5°	5.90
25%	4.40	25.5	5.95
50%	4.40	49.5	5.95
75%	4.47	76.5	5.98
85%	4.47	85.0	5.98
95%	4.47	93.0	5.98
100%	4.47	97.0	5.98

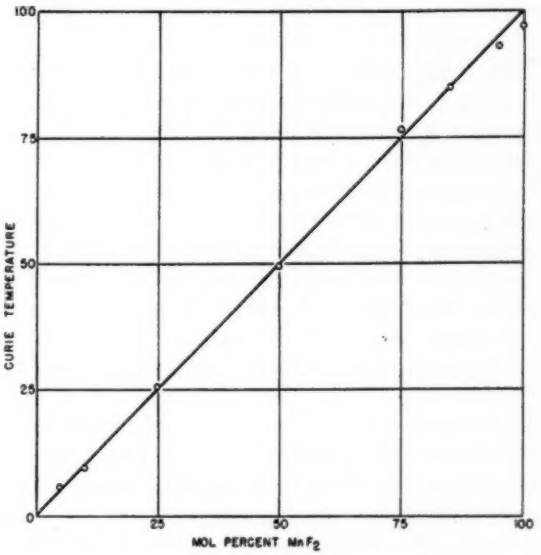

FIG. 3. Paramagnetic Curie temperature as a function of molar concentration of MnF_2.

the total Δ of one of the equivalent nearest neighbors. The fraction f_k is the probability that a given Mn^{++} ion will have k nearest neighbor positions occupied by Mn^{++} ions and $z-k$ positions occupied by Zn^{++} ions. Thus,

$$f_k=\frac{z!}{k!(z-k)!}x^k(1-x)^{z-k},$$

where x is the mole fraction of MnF_2. From this in turn it follows by direct summation that

$$\bar{\Delta}=xz\delta=x\Delta_{\text{pure } MnF_2}$$

which is the desired relationship.

We wish to thank Dr. Bigeleisen, Dr. Freed, Mr. Slavin, and Dr. Stoenner for their help during the course of this experiment.

THE JOURNAL OF CHEMICAL PHYSICS VOLUME 18, NUMBER 9 SEPTEMBER, 1950

Polarization of the Singlet-Singlet and Triplet-Singlet Luminescence of Chelate Compounds

S. I. WEISSMAN
Department of Chemistry, Washington University, St. Louis, Missouri
(Received April 13, 1950)

The polarizations of the luminescence of the dibenzoylmethane complexes of lithium, potassium, aluminum, lanthanum, and gadolinium have been determined. The first excited singlet state of the univalent chelates has symmetry B_1. The triplet states have not been uniquely classified. The nature of the perturbation of the triplet state introduced by the magnetic gadolinium ion seems qualitatively different from the perturbations introduced by non-magnetic ions.

THE luminescence of a series of metal ion complexes with dibenzoylmethane has been found to consist, in common with the luminescence of many other substances, of two parts: an emission of very short lifetime and one of comparatively long duration.[1] The rapidly decaying portion has been ascribed to a transition from the first excited singlet state to the normal state, while the portion of long duration has been ascribed to a transition from the first excited triplet state to the normal state. For further characterization of these states the polarization of the luminescence has been determined.

Observations have been made on the luminescence of the lithium, potassium, aluminum, lanthanum, and gadolinium complexes with dibenzoylmethane. Excitation was accomplished by polarized light absorbed in the intense near ultraviolet absorption band (3000A–4000A) of these molecules. The polarization of a pencil of luminescence in a direction parallel to the exciting beam was observed.

The assumption is made throughout the following discussion that depolarization through molecular rotation and intermolecular reasonance transfer is unimportant in the rigid glass solutions used. Experience with other substances[2,3] has demonstrated that the rotation of large molecules in such media is small during times of the order of the lifetimes of the excited states. Further, there was no change of polarization with temperature in the range 77–90°K. That intermolecular energy transfers were not important is indicated by the fact that no changes in polarization with concentration were observed to concentration as low as 10^{-6} molar. One other possible source of depolarization-saturation effects through maintenance of an appreciable fraction of the molecules in long lived excited states also may be eliminated. The light intensities employed were not sufficient for achievement of this effect. The fact that at least part of the luminescence from each substance was highly polarized further eliminates these possibilities.

[1] P. Yuster and S. I. Weissman, J. Chem. Phys. **17**, 1182 (1949).
[2] G. N. Lewis and J. Bigeleisen, J. Am. Chem. Soc. **65**, 520 (1943).
[3] G. N. Lewis and J. Bigeleisen, J. Am. Chem. Soc. **65**, 2102 (1943).

EXPERIMENTAL OBSERVATIONS

The polarizations were observed photographically. Light from a quartz General Electric A-H-6 high pressure mercury arc was passed through cupric sulfate and Corning 9863 and 5863 filters. A horizontal slit, about 1-mm wide and 20-mm long, was uniformly illuminated by this source; light from the slit passed through a Wollaston prism whence it was focused on the sample. Two horizontal strips of luminescence, one above the other, excited by mutually perpendicular polarizations, resulted. Luminescence from these strips passed through an analyzing Polaroid and was then focused on the slit of a stigmatic spectrograph. The analyzing Polaroid was oriented so that the electric vector of the light transmitted by it was parallel to the electric vector of one of the exciting beams. Polarization of the luminescence is revealed as an intensity difference between the two adjacent spectra which appear on the photographic plate. Since the singlet-singlet and triplet-singlet luminescences are well separated spectrally, a single photograph under steady illumination yields the polarization of both.

The luminescent solutions were contained in carefully annealed Pyrex cells twenty mm wide and one mm deep. The cells were maintained at liquid oxygen or liquid nitrogen temperature in a square cross section Dewar flask. The entire arrangement, including the rigid solvent, was tested for depolarization; no significant amount was found.

Absolute alcohol was used as the solvent. Highly rigid clear solutions were formed at the temperatures used. In most of the experiments the concentration of chelate was 10^{-4} molar.

The photographs were usually taken with the analyzing Polaroid set to transmit light with its electric vector horizontal. This direction was chosen because it is the direction of maximum transmission of the Steinheil spectrograph which was employed. A few photographs were made with the vertical polarization to demonstrate that no adventitious effects were responsible for the observed intensity differences.

The results are conveniently described in terms of the ratio I_U/I_L, where I_U and I_L are the intensities of the adjacent spectral strips. This ratio is easily seen to be

equal to the ratio $I_{\parallel}/I_{\perp}$ which would have been observed had a single strip been examined with the analyzing Polaroid parallel to the exciting polarization ($I_{\parallel}$) and perpendicular to the exciting polarization ($I_{\perp}$).

The experimental results, obtained by visual intensity matching, follow:

For all the chelate compounds the singlet-singlet emission is highly polarized with $I_{\parallel}/I_{\perp}\sim 2.5$. For the triplet-singlet emission the results vary from compound to compound and may be summarized in Table I.

TABLE I.

Metal ion in chelate	$I_{\parallel}/I_{\perp}$
Li^{+}	1.2
K^{+}	1.2
Al^{+++}	1.0*
La^{+++}	1.0–1.1
Gd^{+++}	2.0–2.5

* There seems to be a small variation in $I_{\parallel}/I_{\perp}$ in the various vibrational bands of the phosphorescence of the aluminum compound.

DISCUSSION OF RESULTS

The singlet-singlet luminescence is in all likelihood the reverse of the absorption by which excitation was accomplished. The univalent complexes, such as $(C_6H_5COCHCOC_6H_5)Li$, are of symmetry C_{2v}; no degenerate states are permissible under this symmetry. It may be shown that for transitions between non-degenerate states, with emission the reverse of absorption, the anticipated value of $I_{\parallel}/I_{\perp}$ is three.[4] Hence the observed results for the singlet-singlet emission of the univalent complexes are to be expected.

In order to make the results for the singlet-singlet emission of the univalent and trivalent complexes consistent with each other, the electric dipole transition moment in the univalent complexes must be assigned to the oxygen-oxygen (x axis) direction. This is demonstrated in the following manner: coordinate axes are chosen in the single chelating groups as follows: z along the twofold axis, x perpendicular to z and in the plane of the chelate ring, y perpendicular to the plane of the ring. The allowed electric dipole transitions from an A_1 state and their directions are

$$A_1 \rightarrow A_1(z)$$
$$A_1 \rightarrow B_1(x)$$
$$A_1 \rightarrow B_2(y)$$

The normal state is most probably A_1; the first excited singlet state is either A_1, B_1, or B_2.

For the trivalent complexes of symmetry D_3 three kinds of states are permitted—two non-degenerate varieties A_1 and A_2, and one doubly degenerate variety E. The selection rules are

$A_1 \rightarrow A_2$ (along the trigonal axis)
$A_1 \rightarrow E$ (perpendicular to the trigonal axis).

Corresponding to an $A_1 \rightarrow E$ transition, polarization with $I_{\parallel}/I_{\perp}=1.33$ is anticipated.[5] Since the observed polarization ratios far exceed this value the excited singlet state of the trivalent chelate responsible for the fluorescence must be of symmetry A_2.

It is now necessary to relate the states of the univalent chelates with those of the trivalent chelates. It is supposed that the ground state of the trivalent chelate results from the union of three univalent complexes, each in its ground state. The excited states are thought of as arising from the union of one excited and two unexcited univalent molecules.

The choice of wave functions for the excited states of the trivalent complexes requires a decision as to whether the excitation is localized in one of the chelating groups or whether it belongs to the entire molecule. The former alternative could explain the polarization of the luminescence of the trivalent molecules but is not in accord with what is known about migration of excitation energy.[6–12] The latter alternative is capable of explanation of the polarizations and does not suffer from the above mentioned defect.

The experimental and theoretical works referred to in the previous footnote reveal that electronic excitation energy is transferred between molecules in solution at separations of 50A–100A in times comparable with fluorescence lifetimes. According to the theoretical analysis by Foerster[10] the rate constant for this energy migration is inversely proportional to the sixth power of the intermolecular separation. In the trivalent chelates, with a separation of a few angstroms between chelating groups, the transfer by the above mechanism would be rapid compared with emission lifetimes. Overlap effects might change the nature of the transfer mechanism, but presumably would not decrease the rate. It will be assumed, then, that in excited states of the trivalent complexes the excitation energy cannot be localized in single groups.

The correlations between the various possible states of excitation of the single chelating groups and the excited trivalent chelates may be found as follows. Label the three chelating groups I, II, and III. Let the wave function of the normal state of a single chelating group be called η; of an excited group ϵ. In the absence of energy migration the excited state of the trivalent molecule formed from groups I and II in normal states and III in an excited state would be approximated by $\eta(I)\eta(II)\epsilon(III)$. The variables I, II, III refer to the space coordinates of the three groups. (The

[4] See, for instance, P. Pringsheim, *Fluorescence and Phosphorescence* (Interscience Publishers, 1949, New York), p. 370.

[5] This result is obtained under the assumption that there is no memory by the emitting molecule of which direction in the plane perpendicular to the trigonal axis was initially excited.

[6] F. Perrin, Ann. d. physique **12**, 169 (1929).
[7] F. Perrin, Ann. d. physique **17**, 283 (1932).
[8] S. Vavilov, J. Phys. U.S.S.R. **7**, 141 (1943).
[9] P. Feofilov and B. Sveshnikov, J. Phys. U.S.S.R. **3**, 493 (1940).
[10] Th. Foerster, Ann. d. Physik **2**, 55 (1948).
[11] Th. Foerster, Zeits. f. Natürforschung **4A**, 321 (1949).
[12] Th. Foerster, Zeits. f. Elektrochemie **53**, 93 (1948).

functions may be antisymmetrized with respect to permutation of electrons but this need not be carried out explicitly in this case.) To take account of the energy migration, appropriate linear combinations of the above expression with $\eta(I)\epsilon(II)\eta(III)$ and $\epsilon(I)\eta(II)\eta(III)$ are used.

These combinations are chosen to transform according to irreducible representations of the symmetry group of the united molecule. The linear combinations are given in the appendix. The classifications of the states arising from combinations of two unexcited A_1 chelating groups and one excited group are given below.

States of single excited chelate	States of trivalent chelates
A_1	A_1, E
A_2	A_1, E
B_1	A_2, E
B_2	A_2, E

In view of the selection rules and polarization data the excited state mainly responsible for the singlet-singlet luminescence of the trivalent chelate must be of symmetry A_2. An A_2 state of the trivalent complex can arise only from a B_1 or B_2 state of the univalent complex. Each of these states will also contribute an E state.

Because of the great similarity in spectra of the univalent and trivalent complexes it may be assumed that the A_2 and E states arising from the interaction are close to each other, and both participate in the absorption and luminescence. The choice between B_1 and B_2 excited states of the univalent complexes may be made in terms of the relative intensities of the $A_2 \rightarrow A_1$ and $E \rightarrow A_1$ transitions which would arise in the trivalent complexes.

The relative intensities are obtained from a calculation of the correct linear combinations of the functions $\eta(I)\eta(II)\epsilon(III)$, $\eta(I)\epsilon(II)\eta(III)$ and $\epsilon(I)\eta(II)\eta(III)$ for the ϵ function of symmetry B_1 or B_2. From these combinations the transition moments along the trigonal axis and in the plane perpendicular to it may be obtained in terms of the transition moments of the single chelating groups. With the choice of a B_1 function for ϵ, the $A_1 \rightarrow A_2$ transition has four times the intensity of either of the two $A_1 \rightarrow E$ transitions. For the B_2 choice, the result is that the transition moments for $A_1 \rightarrow A_2$ and $A_1 \rightarrow E(X)$, $A_1 \rightarrow E(Y)$ are all equal with the consequence that no polarization would be anticipated. The observed polarization leaves only the B_1 possibility.[13]

The results for the relationships between the transition moments in the univalent and trivalent complexes are summarized in Table II.

[13] A simple valence bond picture involving resonance between the states 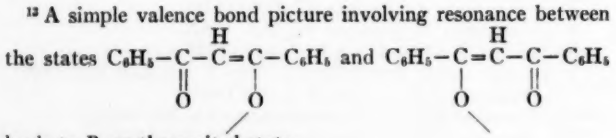 leads to B_1 as the excited state.

TABLE II. Squares of transition moments of trivalent complexes for various excitations of single groups.

Moment \ State	A_1	A_2	B_1	B_2
m_T^2:	0	0	$2m_x^2$	m_y^2
$m_{L_1}^2$:	$3/2m_x^2$	0	$1/2m_x^2$	m_y^2
$m_{L_2}^2$:	$3/2m_x^2$	0	$1/2m_x^2$	m_y^2

TRIPLET STATES

The polarizations of singlet-triplet transitions are determined by the selection rules already given for singlet-singlet transitions. The symmetry of the complete wave function (spin and orbit) rather than the symmetry of the orbital factors alone must be used.[14] The total symmetries for the triplet states under the symmetries here being considered follow.[15,16]

Univalent chelates (C_{2v})		Trivalent chelates (D_3)	
Orbital	Total	Orbital	Total
A_1	A_2, B_1, B_2	A_1	A_2, E
A_2	A_1, B_1, B_2	A_2	A_1, E
B_1	A_1, A_2, B_2		
B_2	A_1, A_2, B_1	E	$A_1, A_2, 2E$

Thus in C_{2v} symmetry $^3A_1 \rightarrow {}^1A_1$ may proceed by $B_1 \rightarrow A_1$ (x polarized) and $B_2 \rightarrow A_1$ (y polarized) transitions. ($A_2 \rightarrow A_1$ is forbidden.) The triplet splitting cannot be resolved; the degree of polarization in the observed radiation from oriented molecules in the example given would depend on the relative values of the coefficients of the B_1 and B_2 singlet constituents of the $^3A_1$ state.

The triplet-singlet emission of the univalent complexes has a small positive polarization. Since the singlet state through which excitation was accomplished is of symmetry B_1, the triplet state, to yield positive polarization, must have a B_1 component. $^3B_1$ is thus eliminated (provided only totally symmetric vibrations are involved). All the others are possible and further work is necessary for a unique assignment.

In the trivalent molecules the possible classifications of the triplet states are numerous. By a procedure similar to the one already described the correlations between triplet states of the univalent and trivalent chelates may be established. These are given below.

State of single excited chelate	States of trivalent chelate
$^3A_1$	$A_1, 2A_2, 3E(^3A_1, {}^3E)$
$^3A_2$	$A_1, 2A_2, 3E(^3A_1, {}^3E)$
$^3B_1$	$2A_1, A_2, 3E(^3A_2, {}^3E)$
$^3B_2$	$2A_1, A_2, 3E(^3A_2, {}^3E)$

The first excited triplet state of the trivalent chelates contains components of all symmetries. Since the triplet-singlet luminescence is but little polarized except in the case of the gadolinium compound, at least two of

[14] For states involving non-totally symmetric vibrations, the vibrational symmetries must be included.

[15] D. S. McClure, J. Chem. Phys. **17**, 665 (1949).

[16] S. I. Weissman, J. Chem. Phys. **18**, 232 (1950).

these varieties must contain singlet constituents with amplitudes which lead to comparable intensities of emission.

The gadolinium compound is qualitatively different from the others. The vibrational structure of the triplet-singlet luminescence is quite clean, containing only transitions to those vibrational levels which appear in the singlet-singlet luminescence. The polarization is high and positive. Both observations lead to the conclusion that the principal constituents of the triplet state are those of symmetry A_2.

The explanation of why the gadolinium ion with its seven unpaired but well shielded electrons introduces a qualitatively different perturbation from that produced by the other ions with no unpaired electrons is not apparent to the author. However a rather formal suggestion appears through classification of the states of the entire molecule.[17] The states formed by union of chelating groups in singlet or triplet states with singlet metal ions are singlet or triplet respectively. The states formed by chelation of gadolinium ion are octet for combination with singlet organic molecules, and sextet, octet, and decet for combination with triplet organic groups. The fluorescent state of the gadolinium compound is classified as octet while the phosphorescent states are classified sextets, octets, and decets. A perturbation which could yield the observed luminescence mixes the octet fluorescent wave function with the octet component of the phosphorescent levels. It may be that detailed calculation will reveal that this type of perturbation, a mixing between states of the same multiplicity, occurs more readily than the spin-orbit mixing between states of different multiplicity.

Although because of the unfortunately large number of possibilities for the phosphorescent states of the molecules here considered no unique assignment of their symmetry has been feasible, similar polarization studies may lead to more definite information concerning other molecules. For instance, McClure's deduction[18] that the triplet state of aliphatic ketones is perturbed principally by the singlet state at 51000 cm^{-1} requires that the phosphorescence, when excited by 51000 cm^{-1} polarized radiation, should be highly polarized. Also, the negative polarization of the phosphorescence of Trypaflavin and other substances observed by Pringsheim and Vogels[19] probably arises through perturbation of the phosphorescent state by an excited singlet state corresponding to a transition moment perpendicular to the one involved in the excitation.

APPENDIX

Consider the chelating groups I, II, III, situated in a cartesian coordinate system XYZ with the x, y, z axes of the individual groups chosen in the manner previously described. The individual groups may be placed in the XYZ system with the x, y, z directions of the individual molecules possessing the following direction cosines:

$$I(x)\ \frac{1}{\sqrt{2}}\ \frac{1}{\sqrt{2}}\ 0;\quad I(y)\ 0\ 0\ 1;\quad I(z)\ \frac{-1}{\sqrt{2}}\ \frac{1}{\sqrt{2}}\ 0$$

$$II(x)\ 0\ \frac{1}{\sqrt{2}}\ \frac{1}{\sqrt{2}};\quad II(y)\ 1\ 0\ 0;\quad II(z)\ 0\ -\frac{1}{\sqrt{2}}\ \frac{1}{\sqrt{2}}$$

$$III(x)\ \frac{1}{\sqrt{2}}\ 0\ \frac{1}{\sqrt{2}};\quad III(y)\ 0\ 1\ 0;\quad III(z)\ \frac{1}{\sqrt{2}}\ 0\ -\frac{1}{\sqrt{2}}.$$

A more convenient coordinate system is the one in which the trigonal axis T and two directions perpendicular to it, $\perp_1$ and $\perp_2$, are used.

In the XYZ system T has direction cosines $1/\sqrt{3}\ 1/\sqrt{3}\ 1/\sqrt{3}$; $\perp_1$ and $\perp_2$ are taken with direction cosines $1/\sqrt{2}\ -1/\sqrt{2}\ 0$ and $1/6^{\frac{1}{2}}\ 1/6^{\frac{1}{2}}\ -2/6^{\frac{1}{2}}$.

In the T, $\perp_1$, $\perp_2$ system the x, y, z directions of the individual molecules have direction cosines:

	T	$\perp_1$	$\perp_2$
$I(x)$	$\frac{2}{6^{\frac{1}{2}}}$	0	$\frac{2}{12^{\frac{1}{2}}}$
$II(x)$	$\frac{2}{6^{\frac{1}{2}}}$	$-\frac{1}{2}$	$-\frac{1}{12^{\frac{1}{2}}}$
$III(x)$	$\frac{2}{6\frac{1}{2}}$	$\frac{1}{2}$	$-\frac{1}{12^{\frac{1}{2}}}$

	T	$\perp_1$	$\perp_2$
$I(y)$	$\frac{1}{\sqrt{3}}$	0	$-\frac{2}{6^{\frac{1}{2}}}$
$II(y)$	$\frac{1}{\sqrt{3}}$	$\frac{1}{\sqrt{2}}$	$\frac{1}{6^{\frac{1}{2}}}$
$III(y)$	$\frac{1}{\sqrt{3}}$	$-\frac{1}{\sqrt{2}}$	$\frac{1}{6^{\frac{1}{2}}}$

	T	$\perp_1$	$\perp_2$
$I(z)$	0	−1	0
$II(z)$	0	$\frac{1}{2}$	$-\frac{3}{12^{\frac{1}{2}}}$
$III(z)$	0	$\frac{1}{2}$	$\frac{3}{12^{\frac{1}{2}}}$.

Linear combinations of the products $\eta(I)\eta(II)\epsilon(III)$, $\eta(I)\epsilon(II)\eta(III)$, $\epsilon(I)\eta(II)\eta(III)$ which transform properly in symmetry D_3 are given below.

Symmetry of ϵ is A_1 or A_2

$$A_1: \frac{1}{\sqrt{3}}\{\eta(I)\eta(II)\epsilon(III)+\eta(I)\epsilon(II)\eta(III) + \epsilon(I)\eta(II)\eta(III)\} \quad (1)$$

[17] This suggestion was originally made by the referee of the paper by Yuster and Weissman (reference 1).

[18] D. S. McClure, J. Chem. Phys. 17, 905 (1949).

[19] P. Pringsheim and H. Vogels, Acta phys. pol. 4, 341 (1935).

$$E:\ \frac{1}{\sqrt{2}}\{\eta(I)\epsilon(II)\eta(III)-\eta(I)\eta(II)\epsilon(III)\} \quad (2)$$

$$(2/3)^{\frac{1}{2}}\{\epsilon(I)\eta(II)\eta(III)-1/2[\eta(I)\epsilon(II)\eta(III)+\eta(I)\eta(II)\epsilon(III)]\}. \quad (3)$$

Symmetry of ϵ is B_1 or B_2

The A_2 function is of form (1).

The E functions are of form (2) and (3).

The transition moments for the various choices of ϵ are obtained from the preceding linear combinations and the geometrical relations. (They are worked out for cases where a vanishing moment is expected for the trigonal molecules as a check on the computation.)

If ϵ has the symmetry A_1, the only non-vanishing transition moment in the individual chelating groups is in the z direction. For the excited A_1 state of the trivalent molecule the moments m_T, $m_{\perp 1}$, $m_{\perp 2}$ are determined in terms of m_z the moment per molecule.

$m_T=0$ (since all m_z's have zero component along T)

$$m_{\perp 1}=\frac{m_z}{\sqrt{3}}(-1+1/2+1/2)=0$$

$$m_{\perp 2}=\frac{m_z}{\sqrt{3}}\left(0-\frac{3}{12^{\frac{1}{2}}}+\frac{3}{12^{\frac{1}{2}}}\right)=0.$$

For the E state, the wave function (2) yields

$$m_T=0$$

$$m_{\perp 1}=\frac{m_z}{\sqrt{2}}(1/2-1/2)=0$$

$$m_{\perp 2}=\frac{m_z}{\sqrt{2}}\left(-\frac{3}{12^{\frac{1}{2}}}-\frac{3}{12^{\frac{1}{2}}}\right)=-\frac{3}{6^{\frac{1}{2}}}m_z;\quad m_{\perp 2}^2=(3/2)m_z^2.$$

The wave function (3) yields

$$m_T=0$$

$$m_{\perp 1}=(2/3)^{\frac{1}{2}}m_z\{-1-1/2(1/2+1/2)\}=-(3/2)^{\frac{1}{2}}m_z;\quad m_{\perp 1}^2=(3/2)m_z^2$$

$$m_{\perp 2}=(2/3)^{\frac{1}{2}}m_z\left\{0-1/2\left(\frac{-3}{12^{\frac{1}{2}}}+\frac{3}{12^{\frac{1}{2}}}\right)\right\}=0.$$

If ϵ has the symmetry A_2 all moments vanish, since the individual moments vanish by the selection rules for a C_{2v} molecule.

If ϵ has the symmetry B_1, only m_x is non-vanishing. For the A_2 combination arising from ϵ of symmetry B_1

$$m_T=\frac{m_x}{\sqrt{3}}\left(\frac{2}{6^{\frac{1}{2}}}+\frac{2}{6^{\frac{1}{2}}}+\frac{2}{6^{\frac{1}{2}}}\right)=\sqrt{2}m_x;\quad m_T^2=2m_x^2$$

$$m_{\perp 1}=\frac{m_x}{\sqrt{3}}(0-1/2+1/2)=0$$

$$m_{\perp 2}=\frac{m_x}{\sqrt{3}}\left(\frac{2}{12^{\frac{1}{2}}}-\frac{1}{12^{\frac{1}{2}}}-\frac{1}{12^{\frac{1}{2}}}\right)=0.$$

For the E combinations, the function (2) yields

$$m_T=\frac{m_x}{\sqrt{2}}\left(\frac{2}{6^{\frac{1}{2}}}-\frac{2}{6^{\frac{1}{2}}}\right)=0$$

$$m_{\perp 1}=\frac{m_x}{\sqrt{2}}(-1/2-1/2)=-\frac{m_x}{\sqrt{2}};\quad m_{\perp 1}^2=\frac{m_x^2}{2}$$

$$m_{\perp 2}=\frac{m_x}{\sqrt{2}}\left(-\frac{1}{12^{\frac{1}{2}}}+\frac{1}{12^{\frac{1}{2}}}\right)=0.$$

The function (3) yields

$$m_T=m_x(2/3)^{\frac{1}{2}}\left\{\frac{2}{6^{\frac{1}{2}}}-\frac{1}{2}\left(\frac{2}{6^{\frac{1}{2}}}+\frac{2}{6^{\frac{1}{2}}}\right)\right\}=0$$

$$m_{\perp 1}=m_x(2/3)^{\frac{1}{2}}\{0-1/2(1/2-1/2)\}=0$$

$$m_{\perp 2}=m_x(2/3)^{\frac{1}{2}}\left\{\frac{2}{12^{\frac{1}{2}}}-\frac{1}{2}\left(-\frac{1}{12^{\frac{1}{2}}}-\frac{1}{12^{\frac{1}{2}}}\right)\right\}=\frac{m_x}{\sqrt{2}};\ m_{\perp 2}^2=\frac{m_x^2}{2}.$$

If ϵ has the symmetry B_2, m_y is the only non-vanishing transition moment.

For the A_2 combination

$$m_T=\frac{m_y}{\sqrt{3}}\left(\frac{1}{\sqrt{3}}+\frac{1}{\sqrt{3}}+\frac{1}{\sqrt{3}}\right)=m_y;\quad m_T^2=m_y^2$$

$$m_{\perp 1}=\frac{m_y}{\sqrt{3}}\left(0+\frac{1}{\sqrt{2}}-\frac{1}{\sqrt{2}}\right)=0$$

$$m_{\perp 2}=\frac{m_y}{\sqrt{3}}\left(\frac{2}{6^{\frac{1}{2}}}+\frac{1}{6^{\frac{1}{2}}}+\frac{1}{6^{\frac{1}{2}}}\right)=0.$$

For the E combination, (2) yields

$$m_T=\frac{m_y}{\sqrt{2}}\left(\frac{1}{\sqrt{3}}-\frac{1}{\sqrt{3}}\right)=0$$

$$m_{\perp 1}=\frac{m_y}{\sqrt{2}}\left(\frac{1}{\sqrt{2}}+\frac{1}{\sqrt{2}}\right)=m_y;\quad m_{\perp 1}^2=m_y^2$$

$$m_{\perp 2}=\frac{m_y}{\sqrt{2}}\left(\frac{1}{6^{\frac{1}{2}}}-\frac{1}{6^{\frac{1}{2}}}\right)=0.$$

(3) yields

$$m_T=m_y(2/3)^{\frac{1}{2}}\left\{\frac{1}{\sqrt{3}}-\frac{1}{2}\left(\frac{1}{\sqrt{3}}+\frac{1}{\sqrt{3}}\right)\right\}=0$$

$$m_{\perp 1}=m_y(2/3)^{\frac{1}{2}}\{0-1/2(1/2-1/2)\}=0$$

$$m_{\perp 2}=m_y(2/3)^{\frac{1}{2}}\left\{-\frac{2}{6^{\frac{1}{2}}}-\frac{1}{2}\left(\frac{1}{6^{\frac{1}{2}}}+\frac{1}{6^{\frac{1}{2}}}\right)\right\}=m_y;\quad m_{\perp 2}^2=m_y^2.$$

THE JOURNAL OF CHEMICAL PHYSICS VOLUME 18, NUMBER 9 SEPTEMBER, 1950

Infra-Red and Ultraviolet Spectra of Sulphur Monoxide*

A. VALLANCE JONES**
Division of Physics, National Research Council, Ottawa, Canada
(Received June 5, 1950)

The infra-red spectrum of sulphur monoxide, prepared by the method of Schenk, has been examined between 400 cm^{-1} and 2000 cm^{-1}. Bands were observed at 679 cm^{-1} and 1165 cm^{-1}.

The ultraviolet absorption band system discovered by Schenk in the region 3500A to 2500A has been obtained under high resolution (21-ft. grating). A very sharp predissociation occurs at 31,702 cm^{-1} leading to an upper value for a dissociation limit of 91 kcal. $mole^{-1}$. A ground state vibration frequency of 679 cm^{-1} was deduced from a partial analysis of the electronic absorption band system.

It has been shown that the molecule cannot be diatomic SO, but probably has the formula S_2O_2, as suggested by Kondrat'eva and Kondrat'ev. The spectroscopic evidence supports the structure .

A. INTRODUCTION

IN 1933 Schenk[1] obtained evidence of the existence of a new oxide of sulphur prepared by streaming SO_2 at low pressure through a high voltage electric discharge; when sulphur vapor was present in the discharge tube, greater yields were obtained. The product was shown to possess a strong system of absorption bands from 2500A to 3400A. Schenk showed by quantitative analysis of the gaseous product collected in a liquid air trap[2] that the ratio of sulphur to oxygen atoms was unity. This conclusion was confirmed later by Kondrat'eva and Kondrat'ev.[3]

Schenk assumed that the substance was identical with diatomic sulphur monoxide which gives an electronic band system in emission from 2400–4000A when SO_2 is subjected to a high voltage condensed discharge.[4] This emission band system was later analysed in detail by Martin[5] who showed that the emitter was the diatomic molecule SO. On the other hand Cordes[6] fitted the absorption bands of the discharge tube product to a vibrational level scheme on the assumption that the bearer of the spectrum was an excited diatomic sulphur molecule. Kondrat'eva and Kondrat'ev criticized[3] both this hypothesis and that of Schenk and concluded that the substance probably had the formula S_2O_2. Kondrat'eva and Kondrat'ev showed that the absorption spectrum obtained by Schenk did not correspond to the emission spectrum observed by Henri and Wolff, and by Martin. In order to investigate the problem further it was decided to obtain the infra-red absorption spectrum of the substance and to examine its ultraviolet absorption band system under high resolution with a 21-ft. grating.

B. PREPARATION OF THE SULPHUR MONOXIDE

Sulphur dioxide from a cylinder was dried over P_2O_5 and liquefied. A middle fraction of the liquid was used to fill a reservoir to a pressure of about 40 cm. The discharge tube, shown in Fig. 1, was 70 cm long with an internal diameter of 20 mm and had Duralumin electrodes. A 25,000-volt transformer maintained the discharge at pressures of SO_2 up to 4 mm mercury in the presence of sulphur vapor. In order to increase the vapor pressure of the latter the walls of the discharge tube were heated by an Alumel winding to a temperature of 150°. Considerable trouble was at first experienced from the discharge puncturing the glass by striking through to the heater winding. This was finally overcome by winding the heating wire on to an outer glass jacket which was also utilized as an air thermometer to indicate the temperature of the discharge tube. The bulb, *G*, contained sulphur heated to 200°C. Finally the gases from the discharge tube were led into a one-meter absorption cell.

The procedure used was as follows. After the apparatus had been evacuated and flamed to remove adsorbed gases the stopcock at the outlet of the absorption cell was closed, the discharge turned on and SO_2 admitted until the total pressure rose to the value desired. The current corresponded to four amperes in the 110-volt primary of the transformer.

A series of preliminary experiments was carried out under a variety of conditions, and the sulphur monoxide yield compared by means of the intensity of the ultraviolet absorption band system and of the SO_2 infra-red absorption band at 1361 cm^{-1}. It was found that the yield of sulphur monoxide was almost independent of the type of discharge but was very sensitive to the temperature of the walls of the discharge tube. A temperature of 150° gave maximum yield. In agreement with Schenk's observations it was found that the yield of

---

* Contribution from the National Research Council, Ottawa, Canada.
** Postdoctorate Fellow, National Research Council of Canada.
[1] P. W. Schenk, Zeits. f. anorg. allgem. Chemie **211**, 150 (1933).
[2] P. W. Schenk, Zeits. f. anorg. allgem. Chemie **233**, 385 (1937).
[3] E. Kondrat'eva and V. Kondrat'ev, J. Phys. Chem. U.S.S.R. **14**, 1528 (1940).
[4] V. Henri and F. Wolff, J. de Phys. et Rad. **10**, ser. 6, 81 (1929).
[5] E. V. Martin, Phys. Rev. **41**, 167 (1932).
[6] H. Cordes, Zeits. f. Physik **105**, 251 (1937).

monoxide increased with higher vapor pressures of sulphur although greater voltages become necessary to obtain a discharge. Analysis of the product in the absorption tube was carried out by measuring the total pressure with a monometer and estimating the partial pressure of sulphur monoxide by difference from the intensity of the 1361 cm^{-1} SO_2 band. It was found that the average yield so measured was from 30–40 percent sulphur monoxide.

C. INFRA-RED SPECTRUM

A one-meter glass absorption cell was provided with potassium bromide windows for measurement of the infra-red absorption spectrum with a Perkin-Elmer Model 12C spectrometer fitted with a Golay cell. The region between 2000 cm^{-1} and 400 cm^{-1} was investigated with rocksalt and potassium bromide prisms. Two absorption bands were found at 679 cm^{-1} and 1165 cm^{-1}. These bands are plotted in Fig. 2. No bands were found below 600 cm^{-1} although the region was examined with total pressures of up to 30 mm of gas in the tube. This pressure was sufficient for the 679 cm^{-1} band to show an absorption of about 50 percent. At these pressures the decomposition of the gas proceeded very rapidly. The high pressures were obtained as described by Schenk[7] using a rubber balloon as a Toepler pump.

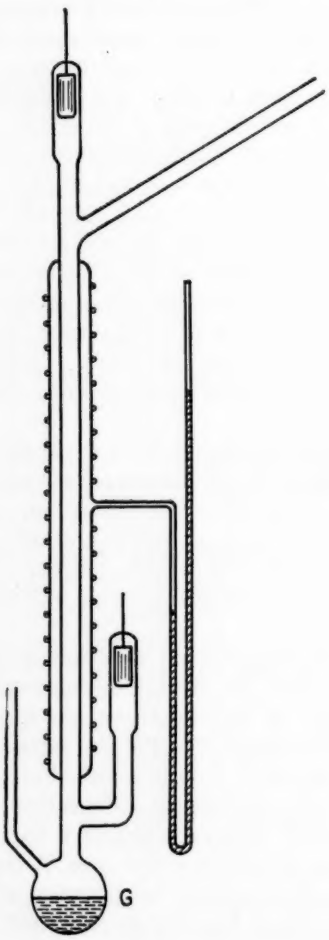

FIG. 1. Discharge tube for preparation of sulphur monoxide.

Since the meter cell did not pass a beam of the full aperture of the spectrometer the energy available from 500 cm^{-1} to 400 cm^{-1} was small. Of the two observed bands the 679 cm^{-1} band shows a *P*, *Q*, *R* structure with a *PR* spacing of about 18 cm^{-1} while the 1165 cm^{-1} band appears as an unsymmetrical doublet. The separation of the two maxima of the latter band is 15 cm^{-1}.

D. ULTRAVIOLET ABSORPTION SPECTRUM

The ultraviolet absorption between 2500A and 3500A was examined using the second order of a 21-ft. grating spectrograph having a dispersion of 1.2A/mm. A Corning 7–54 filter was used to isolate the second-order spectrum. The sulphur monoxide was in this case streamed continuously through a one meter cell with quartz windows at pressures ranging from 0.1 to 1.0 mm mercury. The continuous flow method was chosen to avoid decomposition of the monoxide during the course of an exposure and so to minimize the sulphur dioxide absorption which occurs in the same spectral region. Five minute exposures were taken with Kodak 103a–0 plates. The source was a Beckman hydrogen lamp.

Part of the spectrum is reproduced in Fig. 3a. All bands at wave-lengths less than 3193.13A are diffuse, whereas those at longer wave-lengths show clear rotational fine structure with the exception of the band at 3222.52A.

Cordes[6] attempted an analysis of the electronic absorption band system. However his spectra were obtained with low resolution and he assumed that the absorbing molecule was diatomic sulphur. While no attempt will be made here to present a complete vibrational analysis of the system, certain valuable information may be obtained from the bands with wave-lengths greater than 3190A. The wave-lengths and wave numbers of these bands are listed in Table I.

As noted by earlier workers,[1,7] the most prominent feature of the spectrum is a long progression which has a spacing of 400 cm^{-1} at the long wave-length end of the system. The spectrum at wave-lengths greater than 3193.13A consists of three progressions with sharply defined band heads which are indicated as A, B, and C on Fig. 3a and in Table I. Kondrat'eva and Kondrat'ev[3] observed that the intensity of the 3307.02A and 3263.97A bands increased with temperature. They compared the intensities of these bands with those of the adjacent bands at 3321.33A and 3277.07A at temperatures from −60°C to +60°C and so calculated a ground state vibration frequency of about 450 cm^{-1}.

The bands at 3321.33A and 3277.07A belong to the progression, *A*, the thirty-two bands of which may be followed easily through the whole band system. Kon-

[7] H. Cordes and P. W. Schenk, Zeits. f. Elektrochemie **39**, 594 (1933).

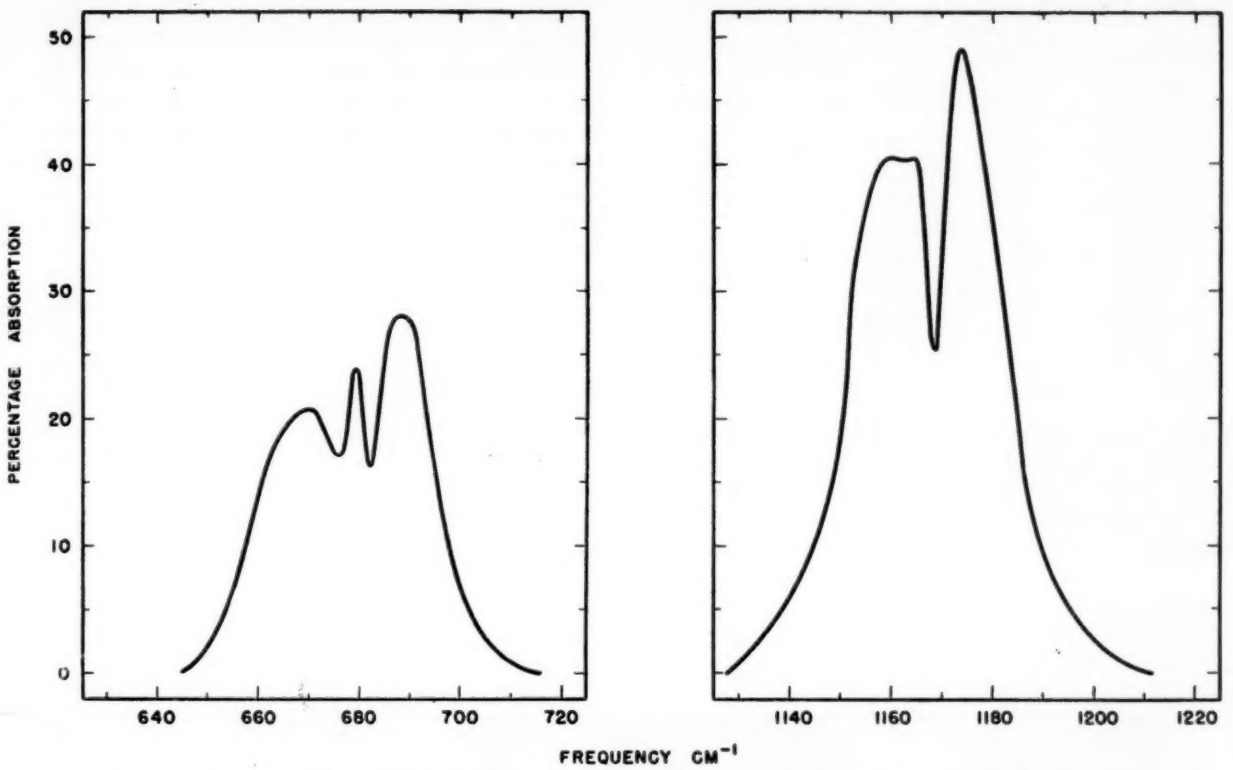

FIG. 2. Infra-red absorption bands of sulphur monoxide. Path length 100 cm. Estimated partial pressure of sulphur monoxide; 1165 cm^{-1} band, 0.8 mm; 679 cm^{-1} band, 2.0 mm.

drat'eva and Kondrat'ev found that the absolute intensity of these bands did not vary with temperature. The bands belonging to this progression may therefore be assigned to transitions from the lowest vibrational level of the ground state to successive vibrational levels of a particular mode in the upper state. The second progression, B, to which the temperature sensitive bands belong may be assigned to transitions from a singly excited vibrational level of the ground state to the same set of upper state vibrational levels which give rise to progression A.

The wave numbers of the band heads of progressions A and B with wave-lengths greater than 3190A (the limit of sharp band heads) fit the following scheme of Table II within the accuracy of measurement.

Since the 0, 0 band was not identified the absolute numbering of the vibrational levels of the upper state cannot be given. The upper state vibrational levels are therefore numbered arbitrarily relative to an unknown integer k.

The frequency deduced for the ground state vibration is the same for each pair of bands; alternative numberings for the temperature sensitive progression, B, do not lead to a constant value for the ground state frequency and so cannot be correct.

The onset of diffuseness in the v', 1 progression (B) at 3222.52A ($v'=k+3$), corresponds to its appearance in the v', 0 progression (A), at the 3153.8A band, ($v'=k+3$). This is in itself good evidence of the correctness of the above scheme since the diffuseness may then be interpreted as a predissociation of the $k+3$th vibrational level of the upper state.

The third progression, C, does not yield constant differences with the bands of the v', 0 progression. It probably corresponds to transitions from the ground state to combination levels in the upper state.

The sharpness of the transition from bands showing rotational fine structure to diffuse bands is well illustrated by the enlargement of the 3222.52A and 3234.27A bands in Fig. 3b. Since the onset of predissociation in polyatomic molecules usually occurs over a range of several 100A,[8] the spectrum of sulphur monoxide provides an unusually clear-cut example of the phenomenon. In this respect it resembles nitrogen dioxide.[9] A predissociation at 31,702 cm^{-1} corresponds to an upper limit for the dissociation of the sulphur monoxide molecule of about 91 kcal. $mole^{-1}$.

The electronic absorption system of sulphur monoxide is very intense. Schenk[2] showed that the absorption could be detected at pressures of S_2O_2 of 10^{-3} mm mercury with a path of one meter. This strongly suggests that the band is due to an allowed electronic transition. The S_2O_2 absorption is certainly between ten and one hundred times more intense than the allowed SO_2 absorption band system which falls in the same

[8] H. Sponer and E. Teller, Rev. Mod. Phys. 13, 101 (1941).
[9] V. Henri, Trans. Faraday Soc. 25, 765 (1929).

TABLE I. Wave-lengths and wave numbers of band heads of sulphur monoxide.

Wave-length A	Wave number cm^{-1}	Progression
3193.13	31,308.2	*A*
3206.84	31,174.5	*C*
3222.52	31,022.7	*B*
3234.37	30,909.0	*A*
3248.23	30,777.1	*C*
3263.97	30,628.7	*B*
3277.07	30,506.3	*A*
3291.14	30,375.9	*C*
3307.02	30,230.0	*B*
3321.33	30,099.8	*A*
3351.69	29,827.2	*B*

spectral region (3400A−2600A).[10] Moreover there is no evidence at the long wave end of the system of any bands which might indicate, as in the case of benzene and formaldehyde, that the electronic transition is forbidden.

The length of the v', 0 progression, *A*, indicates[8] that the upper state vibrational mode involved is totally symmetrical with respect to the common symmetry elements of the upper and lower states. The vibrational selection rules,[8,11] for an allowed electronic transition then require that the excited vibrational level of the ground state responsible for the v', 1 progression, *B*, must also be totally symmetrical with respect to the common symmetry elements of the upper and lower state configurations.

The analysis of the ultraviolet spectrum presented above shows that an excited vibrational level of the ground state lies 679 cm^{-1} above the lowest vibrational level. This value corresponds exactly with the frequency of one of the two infra-red bands. It is unlikely in so small a molecule that this agreement is due to a chance coincidence of the frequencies of vibrational modes of different symmetry type. Therefore it is almost certain that the vibrational mode giving rise to

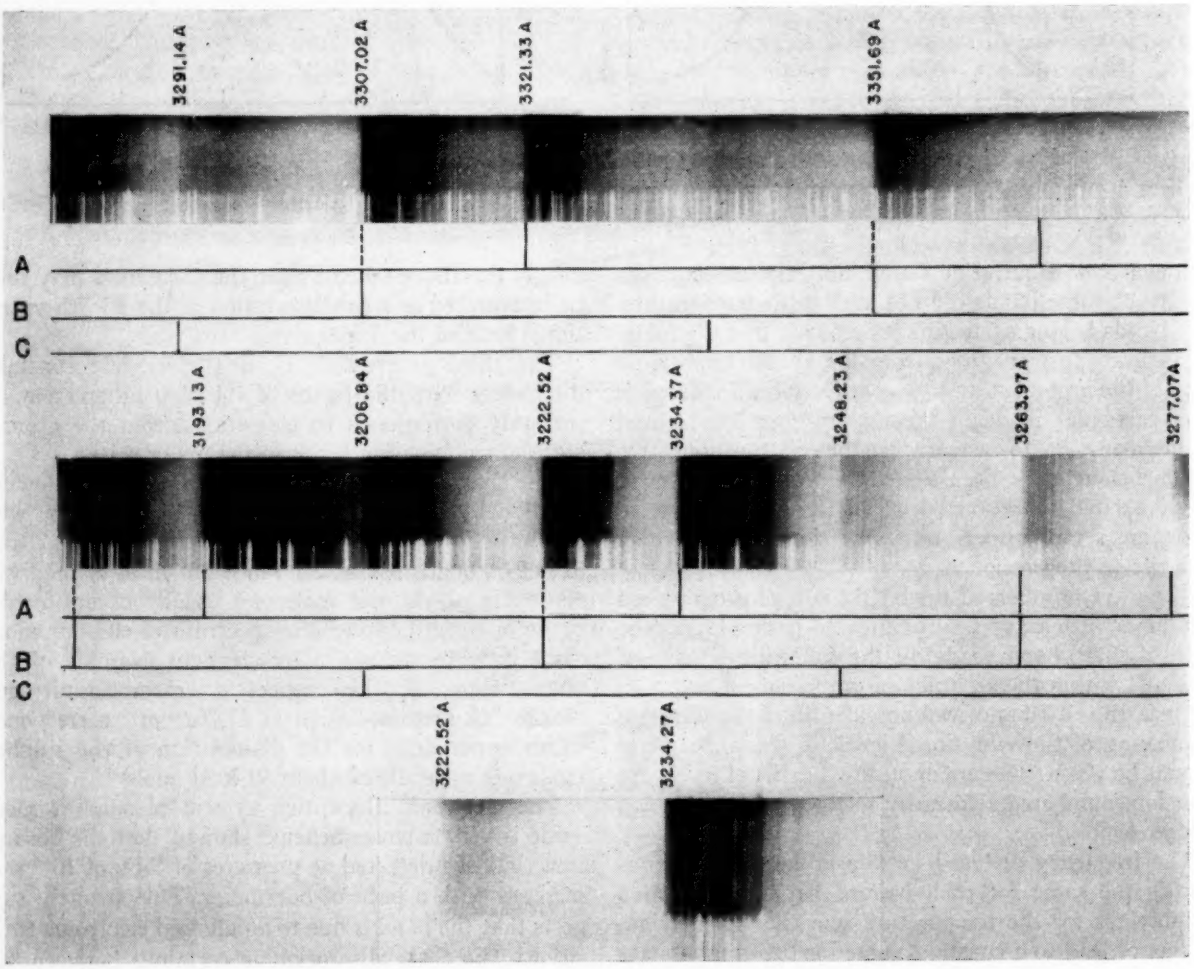

FIG. 3. Ultraviolet absorption spectrum of sulphur monoxide, obtained with 21-ft. grating spectrograph. (a) 3150A to 3370A. (b) Enlargement of 3222.52A and 3234.27A bands.

[10] N. Metropolis, Phys. Rev. **60**, 295 (1941).
[11] G. Herzberg and E. Teller, Zeits. f. physik. Chemie **B21**, 410 (1933).

TABLE II.

v'' / v'	0	1	Difference
k	30506.3	29827.2	679.1
$k+1$	30909.0	30230.0	679.0
$k+2$	31308.2	30628.7	679.5
$k+3$	Diffuse	31022.7 (Diffuse)	—

the 679 cm^{-1} infra-red band is totally symmetric with respect to the common symmetry elements of the upper and lower electronic states.

If the electronic band system of sulphur monoxide were to be a forbidden one the evidence that the 679 cm^{-1} mode is totally symmetric would be less conclusive. However even in this case, the similarity of the fine structure (Fig. 3a) of the bands of the v', 0, and v', 1 progressions supports the conclusion that both have ground states of the same symmetry type. This again would lead to the conclusion that the 679 cm^{-1} vibration is totally symmetrical since the wave function of the lowest vibrational level is certainly symmetrical.

It has not been assumed that the 679 cm^{-1} vibrational mode of the ground state is the same mode which is excited in the upper electronic state and gives rise to the progression A. However the upper state vibrational frequency is about 400 cm^{-1} which would correspond very satisfactorily with 679 cm^{-1} for the same vibration mode in the ground state. If this identification is made it follows immediately that the ground state vibrational mode is totally symmetrical since the length of the progression, A, leaves no doubt that the upper state mode is totally symmetrical.

E. CONSTITUTION AND STRUCTURE OF SULPHUR MONOXIDE

The possibility that sulphur monoxide is a diatomic molecule is immediately ruled out since more than one strong infra-red band is observed. Moreover the *PR* spacing expected from the B'' value found by Martin[5] is 34 cm^{-1} compared to the 15–18 cm^{-1} observed. No absorption was found at 1111.5 cm^{-1} which is the frequency of the fundamental of SO calculated from Martin's data.

The spacing of the rotational lines of the electronic absorption spectrum, Fig. 3b, is also too close to correspond to the diatomic SO molecule. The emission bands of the latter were well resolved by Martin with line spacings up to 20 cm^{-1} near the band tails, whereas the absorption spectrum does not show anywhere a spacing wider than 2 cm^{-1}. Moreover the line spacing is not regular as it should be for a diatomic molecule, but seems to show some sub-structure such as is characteristic of a more complicated molecule.

The most probable alternative to the diatomic formula, SO, is the dimeric formula, S_2O_2, proposed by Kondrat'eva and Kondrat'ev.[3] A molecule of this size gives a *PR* spacing of the right order. A number of arrangements of the atoms which seem likely to be chemically stable are set out below. Arrangements which would require a terminal sulphur atom with an incomplete octet have been omitted.

(I) O=S=S=O

(II)
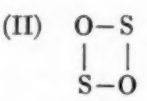

(III)
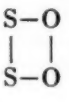

(IV)
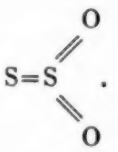

Arrangement I which is akin to SO_2 should be stable because sulphur may have covalencies greater than two. Arrangements II and III both demand abnormal bond angles for the sulphur atoms and are therefore, *a priori*, less likely. Structure IV seems reasonable chemically and is analogous to SO_3.

The excited states of structures I, II, and III are most unlikely to have less symmetry than point group C_2, so that the common symmetry elements of the upper and lower electronic states must be at least those of this point group. Therefore it is at least necessary that the vibrational mode corresponding to the 679 cm^{-1} infra-red band is totally symmetrical with respect to the symmetry elements of point group C_2.

The following conditions must therefore be fulfilled by the correct structure: (1) The 679 cm^{-1} vibration mode must be both infra-red active and totally symmetrical (in the way described above). (2) The direction of the change in dipole moment associated with the 679 cm^{-1} vibration mode must be such as to account for the Q-branch observed in the infra-red band.

Condition (1) requires that this vibrational mode must belong to symmetry type A_1, A_u or B_{2g} if the ground state configuration has respectively the symmetry of point group C_{2v}, C_{2h} or V_h. If the upper electronic state has the same symmetry as the lower, configurations belonging to point groups C_{2h} and V_h are ruled out since the totally symmetric classes of these groups are not infra-red active. Condition (2) requires that the twofold axis of a configuration of point-group C_{2v}, C_{2h} or C_2 must also be the axis of least moment of inertia.

These two conditions make it possible to reject many of the possible structures.

Several configurations are possible for *arrangement* I; namely, (a) linear form of point group $D_{\infty h}$, (b) planar form of point group C_{2h} (zig-zag), (c) planar form of point group C_{2v}, (d) non-planar form of point group C_2.

The *linear* model, (a), is ruled out by the observed *PR* spacing of 15–18 cm^{-1}; this spacing would lead to abnormally short SO and SS bond lengths. If the ratio of SO to SS bond lengths is taken to be 1.5/1.9 from

those in S_2 and SO[12] then to explain the *PR* spacing of 15 cm^{-1} requires the SO bond length in S_2O_2 to be 1.09A and the SS bond length 1.37A. In comparison with the values obtained from the triple bond radii, given by Pauling,[13] namely 1.37A for S≡0 and 1.74A for S≡S, these bond lengths are impossibly short.

For the *planar zig-zag* form, (b), of arrangement I, condition (2) is satisfied since the twofold axis is that of greatest moment of inertia. Condition (1) is satisfied only if the symmetry is lower in the excited electronic state. Even then this would require that the vibrational mode responsible for the 679 cm^{-1} band was of symmetry type A_u, that is, an out-of-plane bending mode. It is unlikely that such a mode would have a frequency as high as 679 cm^{-1}.

The *planar* C_{2v} form, (c), of arrangement I is inconsistent with condition (2) since for all configurations possible with normal bond lengths the twofold axis is the axis of intermediate moment of inertia.

The *non-planar* C_2 form, (d), of arrangement I again satisfies conditions (1) and (2) provided that it does not deviate so far from the C_{2h} configuration that the twofold axis becomes the axis of intermediate moment of inertia. This very restriction again raises the objection that 679 cm^{-1} is a rather high frequency for what is virtually an out-of-plane bending mode.

Only the *planar forms* of *arrangements II and III* are likely since these rings would be highly strained and any departure from planarity would lead to an even greater departure from normal bond angles. These structures would have the symmetries of point groups V_h and C_{2v} respectively. The same objections then apply to these structures as to structures Ic and Ib, respectively. Moreover in the case of II the strained nature of the ring makes it especially likely that the excited state would also be planar. Then condition (1) would not be fulfilled.

Arrangement IV (point group C_{2v}) satisfies both conditions 1 and 2. This model will have three infra-red active modes of type A_1, two of type B_1 and one of type B_2. The three infra-red active modes A_1 may be classified approximately as a symmetrical breathing mode and two modes which will consist of mixtures of the SS stretching and the symmetrical SO_2 bending modes. The observed infra-red band at 679 cm^{-1} may be assigned to one of the two latter modes. The 1165 cm^{-1} band may be assigned to the B_2 mode derived from an antisymmetric SO_2 stretching motion. This would account for the *PR* structure. The symmetrical A_1 breathing frequency might well be too weak to be observed at the concentrations available.

Structure IV, 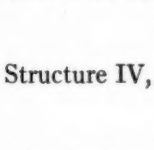 , is strongly favored by the spectroscopic evidence since all the other structures discussed either violate the spectroscopic evidence directly or can be reconciled with it only by making certain unlikely assumptions. Structure IV would also be in agreement with Schenk's observation of the production of thiosulphuric or polythionic acid as a product of the reaction between condensed sulphur monoxide and water. Nevertheless on account of the uncertainties in their interpretation of the electronic spectra of polyatomic molecules it would be desirable to have further confirmatory evidence perhaps from electron diffraction or from microwave spectra.

ACKNOWLEDGMENTS

The author wishes to acknowledge his indebtedness to Dr. G. Herzberg for suggesting the problem and for much helpful discussion; to Dr. A. E. Douglas for continued valuable advice in experimental matters.

[12] G. Herzberg, *Molecular Spectra and Molecular Structure*, I, (D. Van Nostrand Company, Inc., New York, 1950), second edition, pp. 566, 573.

[13] L. Pauling, *The Nature of the Chemical Bond* (Cornell University Press, Ithaca, New York, 1945), p. 164.

Compressibility of Gases at High Temperatures. IV. Carbon Dioxide in the Temperature Range 0°–600°C, and Pressures up to 50 Atmospheres

K. E. MacCormack* and W. G. Schneider
Division of Chemistry, National Research Laboratories, Ottawa, Canada

(Received June 19, 1950)

The compressibility of carbon dioxide has been measured in the temperature range 0°–600°C, at pressures up to 50 atmospheres, by a method employing gas expansion. Data are presented for the virial coefficients of the series equation, PV (Amagat Units) $=A_T+B_TP+C_TP_1^2+D_TP_1^4+\cdots$ and values of PV (Amagat) at integral values of pressure and temperature.

INTRODUCTION

THE principal features of the method and apparatus used in the present work have been fully presented in two earlier papers[1,2] by workers in this laboratory. Essentially, this consists of the accurate measurement of the pressure of a gas maintained at constant temperature in a stainless steel pipet. The gas is then expanded to a second pipet of smaller dimensions and the new pressure is determined. Further expansions are performed after evacuating the small pipet. It is possible to relate the ratio of the initial and final pressures to a virial series in powers of pressure, without the necessity of making precise volume measurements.

EXPERIMENTAL

(A) Design

The volumes of the pipets used in this work were made approximately three times larger than those used for the measurements on helium, for example, 200 cc and 56 cc, the volume ratio thus being reduced to approximately 1:1.3, thereby allowing a greater number of expansions to be made during the course of one experiment. Furthermore, the corrections to be applied respecting dead-space volumes became appreciably less important. A number of tests were performed to determine the extent of oxidation by CO_2 of the steel used (Carpenter Type 304) in the construction of the pipets. Several types of stainless steel were tested under pressure at temperatures in the region of 620°C, and though all showed a surface darkening due to oxidation, it was shown that further treatment, over periods far in excess of those required to make each compressibility experiment, produced no apparent progression in the oxidation. It can be safely assumed that the initial film of oxide which is produced will largely inhibit further oxidation, and the reproducibility of high temperature compressibility measurements was sufficiently good to indicate no possibility of error arising from this source.

(B) Purification of Gas

The carbon dioxide was prepared by heating chemically pure sodium bicarbonate which had been previously evacuated for 24 hours. Water was removed by passing through a trap cooled in a solid CO_2-acetone bath, a tube containing $CaCl_2$ and finally over P_2O_5. The gas was condensed in a bulb cooled in liquid air and then evacuated for 10–15 minutes. The solid was then allowed to evaporate slowly, whilst chilled in a solid CO_2-acetone bath, and recondensed in a second bulb cooled in liquid air. The evacuation and distillation procedure was repeated three times before final condensation into a storage cylinder.

(C) Temperature and Pressure Measurements

Temperatures were measured by a platinum resistance thermometer in conjunction with a Leeds and Northrup G-2 Mueller Bridge, the sensitivity being 0.001°. Thermostatting was achieved using a stirred distilled water-ice bath at 0°C, oil up to 150°C, and a molten mixture of lithium, sodium, and potassium nitrates for higher temperatures. All temperatures were automatically controlled, within the limits of ±0.005°, by a photo-cell relay circuit. In view of the large heat capacity of the steel vessels and the rapid alternation of the measured temperature, it can be assumed that the gas temperature remained constant to ±0.002°.

Pressures were measured by a dead weight piston gauge of the type designed by F. G. Keyes.[3] The sensitivity was 0.2 g, for example, 2×10^{-4} atmosphere, the calibration having been made using the vapor pressure of pure CO_2 at 0°C,[4] as a standard. Details of corrections to be applied in the use of this instrument have been described previously.[2]

SERIES EVALUATION OF DATA

The P-V-T relations of a non-ideal gas may be expressed in the form of a series equation of the following type

$$PV=n(A_T+B_TP+C_TP^2+D_TP^4+\cdots)$$

at constant temperature T. Odd powers of P beyond the first are omitted as suggested by Kamerlingh Onnes. It follows, therefore, with reference to the present experimental procedure, that,

$$P_1V_1=n(A_T+B_TP_1+C_TP_1^2+D_TP_1^4+\cdots) \quad (1)$$

$$P_2(V_1+V_2)=n(A_T+B_TP_2+C_TP_2^2+D_TP_2^4+\cdots), \quad (2)$$

* National Research Council (Canada), Postdoctoral Fellow.
[1] W. G. Schneider, Can. J. Research **27B**, 339 (1949).
[2] W. G. Schneider and J. A. H. Duffie, J. Chem. Phys. **17**, 751 (1949).
[3] F. G. Keyes, Ind. Eng. Chem. **23**, 1375 (1931).
[4] O. C. Bridgeman, J. Am. Chem. Soc. **49**, 1174 (1927).

TABLE I. Values of the coefficients in the series $y=a+bp+cp^2+dp^4+\cdots$ ($a=1.28892$ from He measurements).

T°C	$b\cdot10^3$	$c\cdot10^5$	$d\cdot10^8$	Max. devtns. $y_{calc.}-y_{obs.}$
0	−2.015490	−1.304329	−1.809340	0.00025
50	−1.118109	−0.455200	−0.065676	0.00010
100	−0.677926	−0.098956	···	0.00005

TABLE II. Virial coefficients for CO_2 (Amagat units).

T°C	A_T	$B_T\cdot10^3$	$C_T\cdot10^6$	$D_T\cdot10^9$	Max. devtns. $\left(\frac{P_1}{P_2}\right)_{calc.}-\left(\frac{P_1}{P_2}\right)_{obs.}$
0	1.007050	−7.025	−24.88	−28.80	0.00020
50	1.191383	−4.611	−10.41	−1.38	0.00015
100	1.375717	−3.228	−2.93		0.00007
150	1.560050	−2.273			0.00005
200	1.744383	−1.531			0.00005
300	2.113050	−0.610			0.00005
400	2.481717	−0.071			0.00005
500	2.850384	+0.272			0.00005
600	3.219050	+0.544			0.00005

where P_1, P_2, V_1, and (V_1+V_2) refer to pressures and volumes respectively, before and after expansion of n moles of gas; A_T, B_T, C_T, and D_T are the virial coefficients at the temperature T. The volumes are expressed in Amagat units, so that at 0°C and 1 atmosphere,

$$PV=1=A_0+B_0+C_0+D_0. \quad (3)$$

A detailed account of the evaluation of series equations for CO_2 has been presented by Michels,[5] showing that a density series represents the data more satisfactorily at pressures above 500 atmospheres. One series was inadequate for fitting both liquid and gas data over a range of pressure extending to 3000 atmospheres. The present work, however, is confined entirely to the gaseous region with a maximum pressure of 50 atmospheres, and it is thus considered satisfactory to use the pressure series written above.

By combining Eqs. (1) and (2) it can be shown that,

$$\frac{P_1}{P_2}=N+(N-1)\frac{B_T}{A_T}P_1+\left(N-\frac{P_2}{P_1}\right)\frac{C_T}{A_T}\cdot P_1^2 +\left(N-\frac{P_2^3}{P_1^3}\right)\frac{D_T}{A_T}\cdot P_1^4, \quad (4)$$

where the volume ratio, $N=(V_1+V_2)/V_1$. Introducing the relation that

$$A_T=A_0T/273.16, \quad (5)$$

where the temperature of the ice-point on the absolute scale is taken as 273.16°K,[6] it becomes evident that the coefficients at 0°C may be found from (3) and (4), and at other temperatures from (4) and (5), following the evaluation of B_T/A_T, C_T/A_T, and D_T/A_T described below. An accurate value for N may be found from preliminary measurements with helium, making use of a modified Eq. (4), *viz.*,

$$P_1/P_2=N+(N-1)B_T/A_T\cdot P_1. \quad (6)$$

Terms involving higher powers of P_1 are negligible in this case, and the linear form of the equation lends itself to simple least means squares analysis from a given set of P_1/P_2 *vs.* P_1 data.

The direct computation of the coefficients B_T/A_T, C_T/A_T, and D_T/A_T in Eq. (4) is not readily accomplished. The following outline of the method finally adopted was simple compared with other techniques and proved to be sufficiently accurate for the present purpose.

The pressure ratio, P_1/P_2, is assumed to approximate closely to a power series in P_1. Thus,

$$y=P_1/P_2=a_T+b_TP_1+c_TP_1^2+d_TP_1^4+\cdots. \quad (7)$$

The series written in Eqs. (4) and (7) are each close approximations to the true relation between P_1/P_2 and P_1, but it should be pointed out that each coefficient in one series is not necessarily identical with its counterpart in the other. At zero pressure, however, P_1/P_2, must be equal to N, and therefore a_T of Eq. (7) is identical with N. Using the previously determined value of N, which effectively fixes the zero pressure point on the isotherm, the experimental data was fitted by the method of least mean squares, and coefficients b_T, c_T,

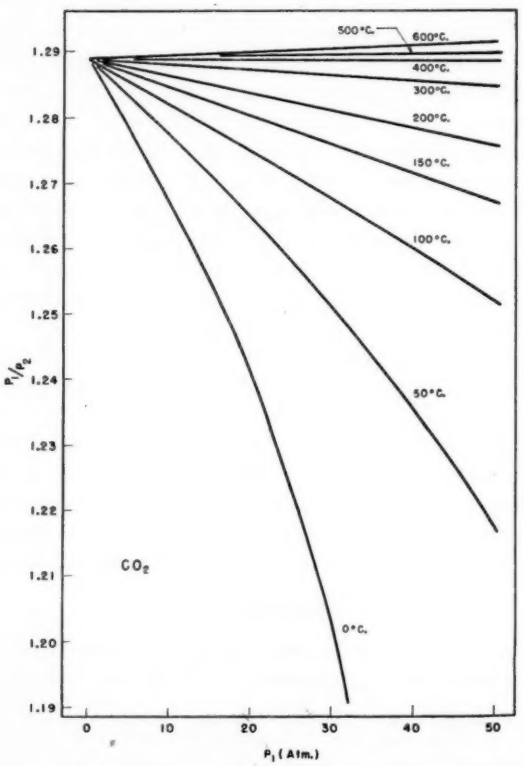

FIG. 1. Plots of pressure ratio P_1/P_2 *vs.* initial pressure P_1.

[5] A. Michels and C. Michels, Proc. Roy. Soc. **A160**, 348 (1937).
[6] H. F. Stimson, J. Research Nat. Bur. Stand. **42**, 209 (1949).

TABLE III. Values of B_T (Amagat units) calculated from series Eq. (8).

T°K	$B_T \cdot 10^3$	$(B_{obs.} - B_{calc.}) 10^3$
273.16	−6.911	−0.114
323.16	−4.620	+0.009
373.16	−3.189	−0.039
423.16	−2.222	−0.051
473.16	−1.531	0
573.16	−0.624	+0.014
673.16	−0.072	+0.001
773.16	+0.287	−0.015
873.16	+0.526	+0.018

d_T, presented in Table I, were computed. These series gave values of P_1/P_2 not differing from the experimental values by more than 0.02 percent in the worst case. At 150°C and above, the isotherms showed the linear form represented by Eq. (6) and were analyzed by the simple linear mean square method.

In order to compute the values of B_T/A_T, C_T/A_T, and D_T/A_T from the coefficients of Eq. (7), the assumption was made that

$$b_T=(N-1)B_T/A_T$$

on the basis of close analogy in the forms of Eqs. (4) and (7). By a process combining solution of two simultaneous equations containing two unknowns, with successive approximation, the coefficients C_T/A_T and D_T/A_T were computed from Eq. (4), substituting into the right-hand side, computed values of $P_2/P_1=y^{-1}$ obtained from Eq. (7). Values of A_T, B_T, C_T, D_T, and (P_1/P_2) obs., when resubstituted into Eq. (4), showed that the series was adequate to represent the experimental data within the limits ±0.017 percent at 0°C and ±0.005 percent at 100°C. The final column in Table II shows the maximum deviations from experimental data.

RESULTS

Figure 1 shows typical plots of P_1/P_2 *vs.* P_1. Experimental points have been omitted since the scatter about the lines on this scale is imperceptible. Qualitatively these are of the same form as PV *vs.* P plots, and the sign of the second virial coefficient at once becomes evident from the initial slope of the isotherms.

The virial coefficients for CO_2 at nine temperatures between 0° and 600°C inclusive, are presented in Table II. These coefficients are expressed in units of Amagat volume and may be converted to units of cm³/mole by multiplying by the normal volume, V_N, of CO_2. This may be calculated from the standard volume of a perfect gas, *viz.*, 22414.6±0.6 cm³/mole,[7] using the relation,

$$V_N=\frac{22414.6}{A_0}\ \text{cm}^3/\text{mole}.$$

In choosing a value for A_0, consideration has been given to the use of compressibility data obtained in the pressure range 0–1 atmosphere, where the $PV-P$ isotherm for 0°C is linear. A review[8] of such data indicates the best value to be 1.0067, giving a value of V_N equal to 22265 cm³/mole. If the value of A_0 deduced from the present high pressure data is used, the value of $V_N=22257.7$ cm³/mole.

An attempt was made to represent the second virial coefficient, B_T, by a temperature power series. The following equation was found to be the best representa-

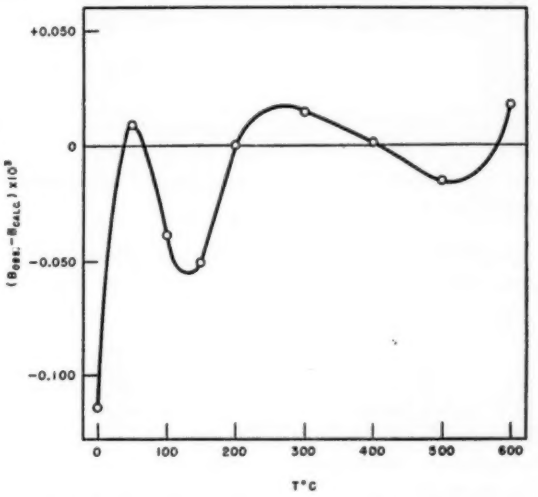

FIG. 2. Deviation curve for values of B_T (calc.).

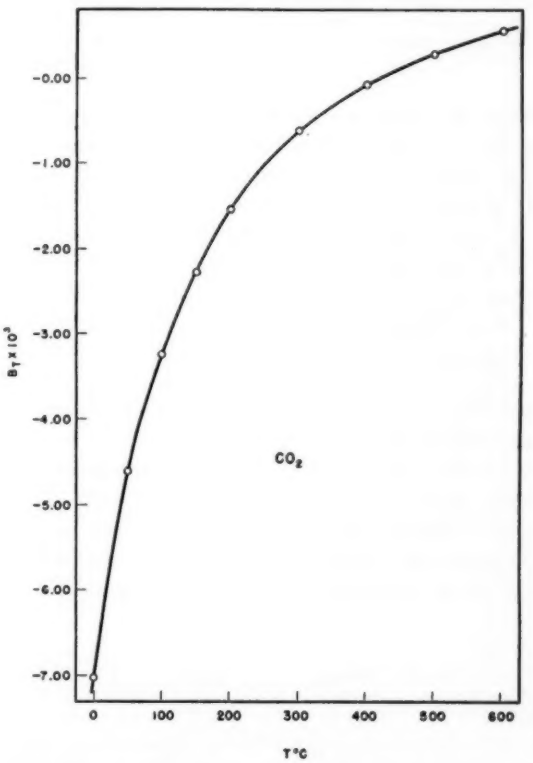

FIG. 3. The second virial coefficients (B_T) for CO_2.

[7] J. W. Dumond and E. R. Cohen, Rev. Mod. Phys. **20**, 82 (1948).

[8] W. Cawood and S. Patterson, J. Chem. Soc., Part I, 619 (1933).

TABLE IV. Values of PV (Amagat units) calculated from data in Table II.

Pressure (atmos.)		1	10	20	30	40	50
0°C	Present data	1.00000	0.93402	0.85199	0.75058	—	—
	Michels (interp.)	1.00000	0.93518	0.85270	0.74928	—	—
	Amagat (I.C.T.)	1.0000					
50°C	Present data	1.18676	1.14422	1.09478	1.04257	0.99238	0.92619
	Michels*	1.18646					0.92517
	Amagat (I.C.T.)						0.9200
100°C	Present data	1.37249	1.34314	1.30998	1.27623	1.24189	1.20697
	Michels*	1.37211					1.20578
	Amagat (I.C.T.)						1.2065
150°C	Present data	1.55778	1.53732	1.51459	1.49186	1.46913	1.44640
	Michels*	1.55735					1.44421
200°C		1.74285	1.72907	1.71377	1.69846	1.68315	1.66785
300°C		2.11244	2.10696	2.10086	2.09476	2.08867	2.08257
400°C		2.48165	2.48101	2.48031	2.47960	2.47889	2.47818
500°C		2.85065	2.85310	2.85583	2.85855	2.86128	2.86400
600°C		3.21959	3.22449	3.22993	3.23537	3.24081	3.24625

* See reference 8.

TABLE V. Comparison of second virial coefficient data.

	Present data		A. Michels*	
T°C	A	$10^3 \cdot B$ calc.	A	$10^3 \cdot B$ exp.
0	1.007050	−7.025	1.006824	−6.791
49.712	1.190322	−4.621	1.190062	−4.611
99.767	1.374858	−3.233	1.374563	−3.285
150.140	1.560566	−2.271	1.560237	−2.347

* See reference 8.

tion of the data, where T is the absolute temperature.

$$B_T \text{ (Amagat units)} = 3.9386\times10^{-3} - 1.0790\times10^{-6}T - 2.0787T^{-1} - 0.6002\times10^{5}T^{-3}. \quad (8)$$

Table III presents values of B_T calculated from this equation and also shows the deviations from experimental values which are plotted in Fig. 2. Within the limits of experimental error, estimated to be 0.5 percent at 0°C, and 1 percent at 600°C, the above equation is therefore not satisfactory, but may be useful for interpolation purposes used in conjunction with the deviation curve. Figure 3 shows a plot of experimental values of B_T against the temperature in °C. In view of the large curvature at low temperatures, it is not surprising that an equation could not be fitted accurately to cover the whole temperature range.

From data presented in Table II, values of PV in Amagat units have been computed (Table IV) for integral values of pressure and temperature, and show good agreement with the results of other workers in the region where comparative figures are available.

Although these values agree to at least 0.15 percent with those of A. Michels and S. R. de Groot,[9] it is noteworthy that values of the second virial coefficient differ in some instances by 1 or 2 percent.[5] The comparative figures were computed from the coefficients of the density series using the relation that,

$$B_P = B_\rho / A_\rho,$$

where subscripts P and ρ designate the coefficients of pressure and density series, respectively. These are compared in Table V.

It becomes evident, therefore, that care must be taken in attempting to assess intermolecular force fields from such data. Series equations involving powers of P or ρ higher than the first may be perfectly adequate to fit experimental data, but the physical significance of the second virial coefficient tends to become lost in the coefficients of the higher powers. It is suggested that where an investigation of intermolecular force fields is proposed, it would be advantageous to make compressibility measurements over a wide temperature range, and wherever possible, to confine working pressures to the region where the isotherms are linear or nearly so.

ACKNOWLEDGMENTS

We wish to express our thanks to Mr. Y. Lupien and Mr. A. Stevenson for assistance in the measurements.

[9] A. Michels and S. R. de Groot, App. Sci. Res. **A1**, 103 (1948).

Thermodynamic Properties of Gaseous Carbon Dioxide at Temperatures from 0°–600°C, and Pressures Up to 50 Atmospheres

K. E. MacCormack* and W. G. Schneider
Division of Chemistry, National Research Laboratories, Ottawa, Canada
(Received June 19, 1950)

Compressibility data presented in a previous paper have been used in conjunction with spectroscopically determined zero pressure specific heat data for CO_2, to calculate thermodynamic properties over the temperature range 0°–600°C at pressures up to 50 atmospheres.

INTRODUCTION

THE compressibility data presented in the preceding paper[1] have been employed to derive the thermodynamic properties of carbon dioxide in the temperature range from 0°–600°C, and at pressures up to 50 atmospheres. The required partial derivatives were in nearly all cases evaluated algebraically from the PV series equation corresponding to each temperature. Originally, a method employing graphical integration and differentiation was employed, but in order to maintain the desired accuracy, this was discarded in favor of computation on the basis of the equation of state.

In addition to compressibility data, computation of thermodynamic properties involves a knowledge of the specific heat as a function of temperature at a fixed pressure, and the most reliable values at present have been calculated from spectroscopic data. Recently, S. Gratch[2] has carried out a very accurate computation of the zero pressure specific heat for carbon dioxide, taking into account corrections for anharmonicity, centrifugal stretching and rotation-vibration level interaction; the zero pressure thermodynamic properties given in Table I have been obtained by five-point Lagrangian interpolation from this data.† Thermodynamic properties of carbon dioxide from 0°C to 150°C and pressures up to 3000 atmospheres have been published by Michels and de Groot,[3] using zero pressure specific heat data calculated on the basis of a linear harmonic oscillator approximation.

The value of R, the gram molecular gas constant, and the absolute temperature of the ice-point used in the present work differs slightly from the values employed by Michels and de Groot (see references 4 and 5).

1. Specific Heat at Constant Pressure, C_p. For a given temperature, T, and pressure, P,

$$C_p = C_p^0 - T\int_0^P \left(\frac{\partial^2 V}{\partial T^2}\right)_P dp. \qquad (1)$$

The appropriate value of C_p^0 is selected from values in Table I. The series equation of state is written as follows,

$$PV = A_T + B_T P + C_T P^2 + D_T P^4, \qquad (2)$$

where A_T, B_T, C_T, and D_T, are the virial coefficients for a given T. It was found that B_T could be represented as a function of temperature by the equation,

$$B_T \text{ (Amagat units)} = 3.9386\times10^{-3} - 1.0790\times10^{-6}T - 2.0787T^{-1} - 0.6002\times10^{5}T^{-3}.$$

Evaluation of the first and second derivatives with respect to temperature could thus be performed with greater accuracy than that offered by graphical differentiation. The derivatives of C_T and D_T with respect to temperature could be found only by graphical methods as insufficient values were available to fit them to a mathematical series. From Eq. (2),

$$-T\int_0^P \left(\frac{\partial^2 V}{\partial T^2}\right)_P dp = -T\int_0^P \left[\frac{d^2B}{dT^2} + P\frac{d^2C}{dT^2} + P^3\frac{d^2D}{dT^2}\right]dp$$

$$= -T\left[P\frac{d^2B}{dT^2} + \frac{P^2}{2}\frac{d^2C}{dT^2} + \frac{P^4}{4}\frac{d^2D}{dT^2}\right].$$

At temperatures of 150°C and above, terms involving derivatives of C_T and D_T became negligible, as explained in reference 1. Compressibility data presented in Amagat units were converted to units of cal./mole, using the relation that 1 Amagat unit of energy

$$= RT_0/A_0 = 539.02 \text{ cal./mole}$$

where $A_0 = 1.00705$ Amagat units,[1] $R = 1.98718$ cal./mole-deg.K[4] and $T_0 = 273.16$°K.[5] The values of C_P are

TABLE I. Zero pressure properties of carbon dioxide.

T°K	C_p^0 cal./mole-deg.K	ΔH^0 cal./mole	ΔS^0 cal./mole-deg.K
273.16	8.5712	0	0
323.16	9.1179	442.45	1.4862
373.16	9.6095	910.86	2.8330
423.16	10.0485	1402.52	4.0689
473.16	10.4419	1914.95	5.2131
573.16	11.1181	2994.06	7.2800
673.16	11.6779	4134.69	9.1132
773.16	12.1452	5326.62	10.7632
873.16	12.5364	6561.20	12.2644

* National Research Council (Canada), Postdoctoral Fellow.
[1] K. E. MacCormack and W. G. Schneider, J. Chem. Phys. **18**, 1269 (1950).
[2] S. Gratch, Trans. A.S.M.E. (Nov. 1949), p. 897.
† We are indebted to S. Gratch for supplying the data given in Table I.
[3] A. Michels and S. R. de Groot, App. Sci. Res. **A1**, 94 (1948).
[4] J. W. Dumond and E. R. Cohen, Rev. Mod. Phys. **20**, 82 (1948).
[5] H. F. Stimson, J. Research Nat. Bur. Stand. **42**, 209 (1949).

TABLE II. Isobaric specific heat, C_p, cal./mole-deg.K.

Pressure (atmos.)	1	10	20	30	40	50
273.16°K	8.671	9.602	10.745	12.138		
323.16	9.175	9.711	10.353	11.052	11.824	12.692
373.16	9.646	9.991	10.415	10.879	11.385	11.933
423.16	10.073	10.295	10.541	10.787	11.033	11.280
473.16	10.460	10.620	10.797	10.975	11.152	11.330
573.16	11.129	11.222	11.327	11.431	11.535	11.639
673.16	11.685	11.746	11.815	11.883	11.951	12.020
773.16	12.150	12.194	12.242	12.290	12.339	12.387
873.16	12.540	12.571	12.605	12.640	12.674	12.709

TABLE III. C_p-C_v, cal./mole-deg.K.

Pressure (atmos.)	1	10	20	30	40	50
273.16°K	2.052	2.722	3.730	5.231		
323.16	2.026	2.409	2.924	3.556	4.339	5.318
373.16	2.012	2.256	2.565	2.920	3.325	3.783
423.16	2.005	2.165	2.351	2.544	2.744	2.953
473.16	2.000	2.116	2.250	2.387	2.529	2.674
573.16	1.995	2.062	2.139	2.217	2.297	2.378
673.16	1.992	2.035	2.083	2.132	2.181	2.230
773.16	1.990	2.019	2.050	2.082	2.114	2.146
873.16	1.989	2.008	2.030	2.051	2.072	2.094

TABLE IV. Constant volume specific heat, C_v, cal./mole-deg.K.

Pressure (atmos.)	1	10	20	30	40	50
273.16°K	6.619	6.880	7.015	6.907		
323.16	7.149	7.302	7.429	7.496	7.485	7.374
373.16	7.634	7.735	7.850	7.959	8.060	8.150
423.16	8.068	8.130	8.190	8.243	8.289	8.327
473.16	8.460	8.504	8.547	8.588	8.623	8.656
573.16	9.134	9.160	9.188	9.214	9.238	9.261
673.16	9.693	9.711	9.732	9.751	9.770	9.790
773.16	10.160	10.175	10.192	10.208	10.225	10.241
873.16	10.551	10.563	10.575	10.589	10.602	10.615

TABLE V. Enthalpy, H_{TP}, cal./mole.

Pressure (atmos.)	1	10	20	30	40	50
273.16°K	0	−116.1	−255.1	−413.1		
323.16	446.3	366.5	273.6	175.7	72.0	−38.7
373.16	917.0	858.4	791.2	721.8	650.3	576.6
423.16	1410.1	1366.0	1316.9	1267.8	1218.7	1169.7
473.16	1923.6	1889.1	1850.8	1812.5	1774.1	1735.8
573.16	3004.1	2979.5	2954.8	2930.1	2905.5	2880.8
673.16	4145.6	4130.9	4114.6	4098.3	4079.9	4065.7
773.16	5338.1	5328.5	5317.9	5307.3	5296.6	5286.0
873.16	6573.1	6567.4	6561.2	6554.9	6548.6	6542.3

presented in Table II. Since compressibility measurements were not carried out in the liquid phase, data for 0°C at 40 and 50 atmospheres are omitted throughout the paper.

2. C_p-C_v. These values, presented in Table 3 were computed from the relation

$$C_p-C_v=-T(\partial V/\partial T)_P^2(\partial V/\partial P)_T^{-1}.$$

From Eq. (2)

$$C_p-C_v=-T\left[\frac{\left(\frac{1}{P}\frac{dA}{dT}+\frac{dB}{dT}+P\frac{dC}{dT}+P^3\frac{dD}{dT}\right)^2}{-\frac{A}{P^2}+C+3DP^2}\right].$$

Since by definition,

$$A_T=A_0T/T_0$$

$$\frac{1}{P}\frac{dA}{dT}=\frac{A_0}{PT_0}=\frac{3.6867\times10^{-3}}{P}\text{ Amagat units.}$$

The other derivatives were calculated as described earlier.

3. The specific heat at constant volume, C_v, is presented in Table IV and is computed from the corresponding differences of values in Tables II and III.

4. The enthalpy, H_{TP}, is given in Table V. In compliance with present general agreement, the reference point at which H_{TP} is zero has been chosen to be 0°C, and 1 atmosphere. The enthalpy at a given temperature, T, and pressure, P, is then expressed by the relation,

$$H_{TP}=\int_{273.16}^{T}C_p^0dT+\int_0^P[V-T(\partial V/\partial T)_P]dp-H_{01},$$

where H_{01} is a reference point adjustment term given in the following relation.

$$H_{01}=\int_0^1\left[V-T\left(\frac{\partial V}{\partial T}\right)_P\right]dp=-12.5_3\text{ cal./mole.}$$

The specific heat integral,

$$\int_{273.16}^{T}C_p^0dT,$$

is shown in Table I, for the several temperature intervals. From Eq. (2), the compressibility integral from zero pressure to pressure, P, becomes equal to

$$P\left[B-T\frac{dB}{dT}\right]+\frac{P^2}{2}\left[C-T\frac{dC}{dT}\right]+\frac{P^4}{4}\left[D-T\frac{dD}{dT}\right].$$

5. The internal energy, E_{TP}. Values of the internal energy have been derived from the relation, $E=H-PV$. It should be noted, however, that since the zero point is to be fixed at 0°C and 1 atmosphere, the values, E_{TP}^*, presented in Table VI, are greater than E in the above relation by an amount equal to the value of PV at 0°C and 1 atmosphere.

Therefore,

$$E^*=H-PV+539.02\text{ cal./mole.}$$

TABLE VI. Internal energy, E_{TP}^*, cal./mole.

Pressure (atmos.)	1	10	20	30	40	50
273.16°K	0	−80.5	−175.3	−278.7		
323.16	345.6	288.8	222.5	152.8	76.1	1.1
373.16	716.2	673.4	624.1	572.9	519.9	465.0
423.16	1109.4	1076.4	1039.5	1002.7	965.8	929.1
473.16	1523.2	1323.2	1466.1	1436.0	1405.9	1375.8
573.16	2404.5	2382.8	2361.4	2340.0	2318.7	2297.3
673.16	3347.0	3332.6	3316.7	3300.8	3282.7	3268.9
773.16	4340.6	4329.6	4317.6	4305.5	4293.3	4281.3
873.16	5376.7	5368.4	5359.2	5350.0	5340.8	5331.5

TABLE VII. Entropy, S_{TP}, cal./mole-deg.K.

Pressure (atmos.)	1	10	20	30	40	50
273.16°K	0	−4.873	−6.611	−7.835		
323.16	1.499	−3.254	−4.839	−5.895	−6.674	−7.373
373.16	2.853	−1.838	−3.348	−4.292	−5.007	−5.600
423.16	4.092	−0.562	−2.026	−2.919	−3.578	−4.108
473.16	5.239	0.606	−0.835	−1.704	−2.340	−2.847
573.16	7.308	2.699	1.284	0.441	−0.168	−0.648
673.16	9.143	4.546	3.154	2.316	1.719	1.253
773.16	10.794	6.204	4.811	3.990	3.402	2.943
873.16	12.295	7.710	6.322	5.506	4.924	4.470

6. The entropy, S_{TP}. Values of the entropy at the specified temperatures and pressures, have been evaluated using the relation,

$$S_{TP}=\int_{273.16}^{T} C_p^0\frac{dT}{T}-\int_0^P\left(\frac{\partial V}{\partial T}\right)_p dp-S_{01},$$

where S_{01} is a reference point adjustment term given by the following relation.

$$S_{01}=-\int_0^1\left(\frac{\partial V}{\partial T}\right)_P dp=-0.032 \text{ cal./mole-deg.K.}$$

The term involving zero pressure entropy change is selected from values listed in Table I, and from Eq. (2), the compressibility integral is given by,

$$\int_0^P\left(\frac{\partial V}{\partial T}\right)_P dp=R\ln P+P\frac{dB}{dT}+\frac{P^2}{2}\frac{dC}{dT}+\frac{P^4}{4}\frac{dD}{dT}.$$

The final values are presented in Table VII.

TABLE VIII. Helmholtz free energy, A_{TP}^*, cal./mole.

Pressure (atmos.)	1	10	20	30	40	50
273.16°K	0	1250.6	1630.6	1861.5		
323.16	−138.8	1340.4	1786.3	2057.8	2232.9	2383.8
373.16	−348.4	1359.3	1873.4	2174.5	2388.3	2554.7
423.16	−622.2	1314.2	1896.8	2237.9	2479.9	2667.4
473.16	−955.7	1036.5	1861.2	2242.3	2513.1	2722.9
573.16	−1784.2	835.8	1625.5	2087.2	2415.0	2668.7
673.16	−2807.7	272.4	1193.6	1741.8	2125.5	2425.4
773.16	−4004.9	−467.1	597.9	1220.6	1663.0	2005.9
873.16	−5358.8	−1363.7	−160.9	542.4	1041.4	1428.5

TABLE IX. Gibbs free energy, F_{TP}, cal./mole.

Pressure (atmos.)	1	10	20	30	40	50
273.16°K	0	1215.0	1550.8	1727.1		
323.16	−38.1	1418.1	1837.4	2080.7	2228.8	2344.0
373.16	−147.6	1544.3	2040.5	2323.4	2518.7	2666.3
423.16	−321.5	1603.8	2174.2	2503.0	2732.8	2908.0
473.16	−555.3	1602.4	2245.9	2618.8	2881.3	3082.9
573.16	−1184.6	1432.5	2218.9	2677.3	3001.8	3252.2
673.16	−2009.1	1070.7	1991.5	2539.3	2922.7	3222.2
773.16	−3007.4	531.8	1598.2	2222.4	2666.3	3010.6
873.16	−4162.4	−164.7	1041.1	1747.3	2249.2	2639.3

7. The Helmholtz free energy, A_{TP}, is computed from the relation,

$$A=E-TS.$$

Since the zero point for this property has been chosen at 0°C and 1 atmosphere, the values A_{TP}^*, presented in Table VIII, are greater than A in the above relation by 539.02 cal.

Thus

$$A^*=E^*-TS \text{ cal./mole.}$$

8. The Gibbs free energy, F_{TP}, is presented in Table IX, evaluated from the relation,

$$F=H-TS.$$

Since H and S have already been evaluated with the common zero point at 0°C and 1 atmosphere, F_{TP} also becomes zero in the same reference state.

Motions of Molecules in Condensed Systems. VII. The Infra-Red Spectra for Single Crystals of Ammonium Nitrate and Thallous Nitrate in Polarized Radiation*

ROGER NEWMAN** AND RALPH S. HALFORD
Department of Chemistry, Columbia University, New York, New York

(Received July 21, 1949)

Infra-red spectra in plane polarized light for properly oriented, thin sections from single crystals of NH_4NO_3 (IV), NH_4NO_3 (III), and $TlNO_3$ (γ) are described and interpreted. The selection of proper orientations for such work is indicated for crystals in general and potential difficulties with some types are noted.

Spectra for the first two crystals show (1) that absorptions by molecular modes of nitrate ion, and their combinations, are strongly polarized in directions predicted for these structures by the general theory of crystalline spectra; (2) that envelope structure resulting from combinations between molecular modes and lattice modes is present but not uniquely polarized, again in agreement with the general theory; (3) that absorptions by molecular modes of ammonium ion appear to be unpolarized, indicating that these ions are disordered from rotation or other causes.

Spectra for the third substance are used to complete the determination of its crystal structure. One band in this substance has a remarkable envelope consisting of a strongly polarized central branch and, at room temperature, three pairs of symmetrically distributed, virtually unpolarized satellites. The satellites become more numerous at lower temperature (see accompanying article).

The spectra for the several substances suggest that optical branches of their lattice mode distributions are located between about 35 and perhaps 200 cm^{-1}.

INTRODUCTION

THE infra-red absorption spectrum for a single crystal, or other anisotropic specimen, in plane polarized radiation will depend upon the orientation of the specimen relative to both the plane of polarization and the direction of incidence of the light. It is convenient to recognize this situation by saying that the spectrum of the anisotropic substance is polarized.

The systematic study of polarized infra-red spectra offers promise of making significant contributions to the identification of crystal structures, molecular structures, and their respective modes of vibration. Such studies can serve also as a source of detailed information about crystalline and molecular dynamics, as a testing ground for general theories of crystalline and molecular spectra.

Pioneer investigations[1] of polarized infra-red spectra, stemming from the invention of a suitable polarizer by Pfund[2] in 1906, were severely hampered by difficulties with instrumentation, and by the lack of any fundamental theory of crystal spectra that might guide the detailed interpretation and thereby increase the value of these truly hard-won observations. As a result, the use of polarized infra-red radiation was, for the time being, almost abandoned.

Recent advances (1) in the field of general purpose infra-red instrumentation;[3] (2) in the construction[4] of convenient, efficient polarizers for infra-red radiations; (3) in the development of a fundamental theory[5,6] for interpretation of crystalline spectra, all may be expected to quicken interest in polarized spectra and to greatly enhance their value. At the present time the major obstacle to such work is the difficulty of obtaining suitable specimens, and even this one seems[7] upon the verge of becoming relieved. A growing interest in the polarized spectra of crystals has indeed become evident,[8] especially in England where a number of preliminary reports[9] have appeared while our own work was in progress. An equally great interest is being shown[10] also toward polarized spectra of plastics and natural or synthetic fibers, but results with these materials pose some problems of interpretation that will become apparent in the next section.

In the present article we shall describe in detail the methods and results of a study of polarized infra-red spectra for three crystalline nitrates: NH_4NO_3 (IV) and (III), $TlNO_3$ (γ). In the course of our discussions we shall have opportunities to illustrate the value of this and similar studies by indicating some of the variety of questions whose answers may be sought from polarized spectra. Specific questions that we touch upon here are (1) the general theory of crystalline spectra, (2) verification of the assignment of frequencies to molecular modes of vibration, in this case the ones for nitrate ion, (3) the degree of disorder, resulting from rotation or otherwise, of ammonium ions in two of the

* Publication assisted by the Ernest Kempton Adams Fund.
** University Fellow for the academic year 1948–49.
[1] R. E. Nyswander, Phys. Rev. **28**, 291 (1909). For reviews of other investigations see, C. Schaefer and F. Matossi, *Das Ultrarote Spektrum* (Julius Springer, Berlin, 1930), pp. 329–330; and J. Lecomte, *Le Spectre Infrarouge* (University of France Presses, Paris, 1928), pp. 177 f.
[2] A. H. Pfund, Astrophys. J. **24**, 19 (1906).
[3] V. Z. Williams, Rev. Sci. Inst. **19**, 135 (1948).
[4a] R. Newman and R. S. Halford, Rev. Sci. Inst. **19**, 270 (1948).
[4b] Elliot, Ambrose, and Temple, J. Opt. Soc. Am. **38**, 212 (1948).
[4c] N. Wright, J. Opt. Soc. Am. **38**, 69 (1948).
[5] H. Winston and R. S. Halford, J. Chem. Phys. **17**, 607 (1949).
[6] D. F. Hornig, J. Chem. Phys. **16**, 1063 (1948).
[7] Bauer, Cole, and Thompson, Nature **163**, 198 (1949).
[8] W. E. Keller, Dissertation, Harvard University (1948).
[9] J. Mann and H. W. Thompson, Nature **160**, 17 (1947), and Proc. Roy. Soc. **192A**, 489 (1948); D. A. Crooks, Nature **160**, 17 (1947); G. B. B. M. Sutherland and A. V. Jones, Nature **160**, 567 (1947); and others.
[10] See for example: L. Glatt and J. W. Ellis, J. Chem. Phys. **15**, 880 (1947), **15**, 884 (1947), and **16**, 551 (1948); Ambrose, Elliot, and Temple, J. Chem. Phys. **16**, 877 (1948), Nature **163**, 859 (1949); and others.

crystals examined, (4) verification of the complete crystal structures for two of the substances and a partial determination of that for a third one, (5) evaluation of some properties of the distributions of frequencies among lattice modes in the several crystals. Although the discussion is organized, for convenience, around the observations, all of the foregoing questions will be found to have prominent places and to receive significant, if incomplete answers in it.

Before presenting our observations we shall discuss briefly some conditions governing their interpretations, conditions that have an important bearing upon the planning of the most significant experiments.

SELECTION OF ORIENTATIONS

The general theory of crystalline spectra, including polarized ones, has been thoroughly discussed elsewhere.[5,6] It should suffice to say here that any fundamental mode of motion which is capable of absorbing radiation must be accompanied by an oscillating electric moment. This latter, because it is a vector quantity, will develop along a well-defined direction in the medium, a direction that is specified in the general theory, and will be incapable of absorbing radiation that is polarized in the plane perpendicular to that direction. This is the origin of polarized spectra, whose significances lie in the possibilities of identifying the characteristic direction associated with an absorption, correlating the latter with a mode of motion, and of interpreting these directions for different modes in terms of molecular and crystalline structures.

In order to realize the possibilities just noted we must first solve a crucial problem: the structurally significant directions are defined inside the absorbing medium whereas the plane of polarization of the radiation, and its direction of propagation, are easily identified only outside the medium. If we are to translate the latter directions, determined outside the medium, into knowledge of the former ones, defined inside the medium, we must, if possible, select orientations for our crystal such that plane polarized radiation may traverse it without suffering either refraction or change of polarization character (plane to elliptical, etc.). Otherwise, if plane polarized radiation is incident upon a plate of anisotropic crystal in an entirely arbitrary way, it will[11] suffer refractions not in accordance with any simple law and, furthermore, for a non-absorber at least, the electric vector of the light will be resolved along directions in the medium peculiar both to the directions of propagation of the light through the crystal and to the frequency of the light.

In certain special orientations, however, the requirements we must impose upon the behavior of the light inside the medium can† be met. These occur[11] for a non-absorber when the light is incident normal to a plate, whose surface is parallel with a plane containing two principal axes of the dielectric ellipsoid of the crystal, and when the electric vector strikes parallel with one or the other of those principal axes. The orientation of the principal axes within the medium can depend, however, upon the frequency of the light. For an absorber we must[11] replace the real, dielectric tensor by the sum of it and an imaginary, conductivity tensor. Unless we can specify that the eigenvectors of these two tensors are parallel, which we sometimes can, the situation becomes highly involved. In the situations noted below where the two sets of eigenvectors are parallel, it is still necessary to say that the resolution of the electric vector of arbitrarily incident light takes place "along" two ellipses rather than definite directions. But, when the previously prescribed conditions of incidence are met, and the eigenvectors of the two tensors are parallel, the requirements we have had to place upon the light as it enters the medium will then be fulfilled. It is clear that severe difficulties may attend the interpretation of polarized spectra when they are obtained with crystal mosaics or partially oriented microcrystals.

As was noted above, the directions of the eigenvectors for the dielectric and conductivity ellipsoids can depend upon the frequency of the light. This circumstance may give rise to difficulties, especially if the two sets of eigenvectors depend differently upon the properties of the light, but also even when they change directions together. For example, suppose that the characteristic directions for monochromatic, visible light, normally incident, are determined with crossed Nicol prisms. It could happen, when we get into the region of infra-red absorption, that the principal axes would become rotated by some large undetermined angle from the positions observed with visible light. If the angle were near to 45° and infra-red spectra were observed with light polarized first along one, then along the other of the axes found in the visible light, these spectra would appear to be identical. In contrast, spectra properly obtained might show extreme differences.

For many forms of crystals, fortunately, the directions of the aforementioned, polarization axes are fixed by symmetry and become independent of the frequency of the light. In uniaxial crystals of the hexagonal, trigonal, and tetragonal systems, and for biaxial crystals of the orthorhombic system, all distinguishable polarization axes are symmetry fixed along crystallographic axes. Spectra observed along these axes will assume a fundamental significance, the ones for other conditions of incidence being representable as superpositions of them. For crystals of the regular system there are, of course, no polarized spectra.

For monoclinic crystals, one axis is symmetry fixed but the other two are unrestricted. There are no

[11] M. Born, *Optik* (Julius Springer, Berlin, 1933).

† Met in theory but not strictly so in practice. The actual light is neither entirely parallel, nor perfectly polarized, nor all incident normal to the crystal face. However, the distribution of light across the beam, the placement and small size of the specimen, all make for a good practical approximation to the ideal.

restrictions upon the axes of a triclinic crystal, and perhaps none upon the axes in some kinds of fibers, films, and other quasicrystalline materials. Particular pains will be required, when working with these latter kinds of substances to resolve the potential difficulties.

In the investigations that we shall now describe, all substances crystallize in the orthorhombic system. Their achromatic polarization axes were oriented in the light beam so as to satisfy all of the foregoing specifications.

EXPERIMENTAL PROCEDURES

The experimental program, in the case of each substance examined, consisted of the following steps: (1) the growing of suitable single crystals of the substance in question, (2) the locating of their axes by well-known techniques of optical or x-ray crystallography, (3) the producing of thin sections whose principal faces exhibited the desired crystallographic planes, (4) the obtaining of their spectra with radiation polarized successively along the several crystal axes. These steps will be described in appropriate detail in this section under the subheadings that follow.

Specimens

NH_4NO_3 (IV), stable from $-16°$ to 32°C, was obtained by slow evaporation of an aqueous solution at 25°C in the form[12] of orthorhombic prisms, with (110) and ($\bar{1}10$) planes parallel to the principal faces, greatly elongated in the direction of the c axis. Preliminary observations with a petrographic microscope disclosed how the crystals should be cut in order to produce the desired thin sections, ones with principal faces parallel to the (100) and (010) planes. The usual mineralogical sectioning techniques were found to be unsuitable in our hands for these soft crystals. Instead, a crystal ($2\times2\times10$ mm) was (1) secured with pyroxilin mucilage, edge upward, into a long, shallow, right-angled V-groove in the face of a metal block, (2) polished down flush with the face of the block, (3) removed from the groove and attached, newly formed face down, on a glass flat, (4) polished down again parallel to the surface of the flat. Polishing was effected with absorbent cotton moistened with water, or with ethanol for finishing operations, as the abradant. Uniformity of thickness could be figured during finishing operations by observation of the polarization colors, seen with the aid of the petrographic microscope. The finished section, having a thickness in the range from 35 to 100 microns, uniform to within an estimated 5 microns through the useful region, was removed from the flat, washed exhaustively to remove mucilage, and dried. It was then attached to a suitably constructed mask, whose open area it covered completely, the mask being designed to facilitate mounting of the section immediately adjacent to the entrance slit of the spectrometer, long axis vertical. After it had been studied spectroscopically, the section was subjected to thorough crystallographic examination on the stage of the petrographic microscope, including refractive index measurements with polarized light, in order to establish beyond doubt its crystallographic orientation. Efforts to produce much thinner specimens, which would have been highly desirable for spectroscopic study, were unsuccessful with this technique because of severe fragmentation occurring at the edges of the section whenever its thickness was reduced much below 40 microns.

NH_4NO_3 (III), stable from 32° to 84°C, was obtained, by slow evaporation of a solution in methanol at 60°C, also in the form[13,14] of orthorhombic prisms with (110) and ($\bar{1}10$) faces, greatly elongated in the direction of the c axis. All operations with these crystals, from beginning to end, were carried out while they were held at temperatures near 60°C, but otherwise the procedure resembled the one that has already been described. Essential innovations were the immediate transfer of a crystal from the mother solution into isoamyl acetate, in order to forestall the phase transition, induced by cooling that accompanied the rapid evaporation of methanol from the surface of the crystal, and, for the same reason, the use of water only during the operations of abrasion. Sections were prepared by working intermittently in a laboratory oven in which the crystals had been grown and the necessary apparatus, other than the microscope, were preheated. During microscopic observations the crystal was transferred to a hot stage, and during spectroscopic observations it was mounted in a small specially constructed oven that served to maintain its elevated temperature while the masked section rested immediately adjacent to the slit.

$TlNO_3$ (γ), stable below 75°C, was obtained, by slow evaporation of an aqueous solution at 55°C, as orthorhombic plates, not larger than $10\times10\times0.5$ mm, whose principal faces were subsequently identified as (010) planes. The fresh solution, prepared with Eimer and Amend Reagent Grade material, contained an appreciable amount of thallic salt which hydrolyzed immediately, forming a brown sludge. By heating the solution to boiling, and then filtering, this impurity was effectively removed. The resulting solution, if evaporated at room temperature, was prone to initiate dendritic growths but this habit was broken by proceeding to 55°C. Preliminary crystallographic examination of the plates was inconclusive and cursory, inasmuch as the optical constants of this substance are unknown and because the shapes of the plates were unfavorable anyhow for producing oblique sections having sufficient width to allow spectroscopic examination. Thin sections were prepared by securing the plates to glass flats and abrading them parallel to their principal faces with a

[12] C. D. West, J. Am. Chem. Soc. **54**, 2256 (1932).

[13] T. H. Goodwin and J. Whetstone, J. Chem. Soc. 1455 (1947).

[14] Hendricks, Deming, and Jefferson, Zeits. f. Krist. **85**, 145 (1933).

felt buffing wheel, about 1 inch in diameter, powered by a small, motor driven hand tool of the kind used by hobbyists. The periphery of the wheel was continually moistened by holding a water saturated piece of cotton against it, about a quarter turn back from the point of contact with the crystal. By varying the amount of water, the speed of the wheel, and the pressure applied to the crystal, a rather delicate control could be exercised over the rate of abrasion. This technique, adopted because the crystals were hard, brittle, and poorly soluble in water, should be applicable to any fairly hard crystal, provided that a suitable solvent can be found, but was unsatisfactory for the soft NH_4NO_3. Finished sections were mounted so as to have each of the two directions of extinction for polarized, visible light parallel in successive observations to the plane of vibration of the polarized infra-red beam. Different sections were observed to have similar spectra, their only differences being attributable to variations of thickness. Subsequently, a fragment was taken from the section whose spectra accompany this article and used to obtain x-ray photographs with the crystal rotating about either of the two directions of extinction contained in its principal face. These photographs yielded lattice spacings of 6.25 ± 0.1 and 3.99 ± 0.05 AU, rough because of imperfect alignment ($\pm5°$) between axes of extinction and rotation but satisfactory for purposes of comparison with the lattice parameters[15] $a=6.19$, $b=12.27$, $c=3.98$ AU, showing that the principal face was a (010) plane. While still attached to the camera mounting, these spacings were correlated with the axes of fast and slow extinction in the fragment, thus permitting their identification in the parent section and, in turn, labeling of the spectra. Once again, specimens much thinner than the ones used could not be obtained because of the onset of severe fragmentation. Moreover, because the original plates were rather thin, perpendicular sections prepared from them were correspondingly too narrow and yielded spectra of such poor quality that we have elected to omit the b spectrum from this report.

Spectra

Absorption spectra were obtained with a Perkin-Elmer Infra-red Spectrograph, Model 12B, equipped with the silver chloride polarizer described[4a] by us previously, a Golay Detector with modified[16] accessories permitting either single-beam or double-beam operation as desired, and a Brown Electronik Recording Potentiometer. The crystal section, containing in every case two crystallographic axes at right angles in its principal face, was supported inside the entrance port of the monochromator immediately adjacent to the slit. It was arranged as well as possible so as to have the principal face parallel to the plane of the slit, with one of its crystallographic axes vertical and the other axis horizontal, whereupon the third crystallographic axis would become aligned with the optic axis of the spectrometer. Specimens ranged in area from 0.5×4 mm on upward to 3×10 mm with average thicknesses in the range from 35 to 100 microns. With the radiation polarized either vertically or horizontally, a spectrum was obtained by the conventional method of single-beam spectroscopy; the blanks were obtained in each case under the same conditions of polarization, aperture, and slit schedule as used in the corresponding absorption runs. Dispersion was effected in the range from 700 to 1600 cm^{-1} with a rocksalt prism, from 1600 to 3400 cm^{-1} with a fluorite prism. The monochromator was calibrated against known absorption bands of ammonia, methane, carbon dioxide, and water vapor. Calibration was checked periodically.

Records for both blank and absorber were scrutinized thoroughly for evidences of interference fringes and suspect ones were discarded. Such fringes can originate either in the polarizer or in the specimen and occasionally are observed. Simple considerations show that fringes, if caused by interference between internally reflected and directly transmitted beams, will appear with wave number intervals $\Delta\nu=(2nd)^{-1}$ where d is the crystal thickness measured in cm and n is its refractive index. Moreover, the total amplitude of fluctuation about the mean intensity of the emergent beam may approach the fraction $2(n-1)^2/(n+1)^2$ of the beam. To illustrate the magnitude of this effect we may take $n=2$ and $d=0.01$, representative of either AgCl in a polarizer or $TlNO_3$ as a specimen, whereupon we find that fringes occur at intervals of 25 cm^{-1} with heights equal to 22 percent of the mean beam intensity. Such effects, if present and unrecognized, could obscure or distort the envelope structure appearing in our spectra, structure that may become of considerable interest. Fortunately, except for occasional instances, successive sheets of AgCl and their separations in the polarizer were sufficiently non-uniform, likewise our crudely cut specimens, so that the fringes did not appear. Irregularities of the order of 5 microns are probably sufficient to obliterate them.

RESULTS AND INTERPRETATIONS

It is to be expected, inasmuch as intraionic forces in these crystals are more powerful than interionic ones, and it has been verified[17] previously, that the nitrate and ammonium ions retain much of their dynamical individualities, that there are modes of vibration in these crystals which can be correlated with motions of the hypothetical, isolated ions. Accordingly, the description and interpretation of our present observations will be organized for each substance separately upon this basis.

The nitrate ion, known to be a centered equilateral

[15] L. Rivoir and M. Abbad, Anal. Fis. Quim. **39**, 306 (1943).
[16] A. Savitsky and R. S. Halford, Rev. Sci. Inst. **21**, 203 (1950).
[17] W. Keller and R. S. Halford, J. Chem. Phys. **17**, 26 (1949).

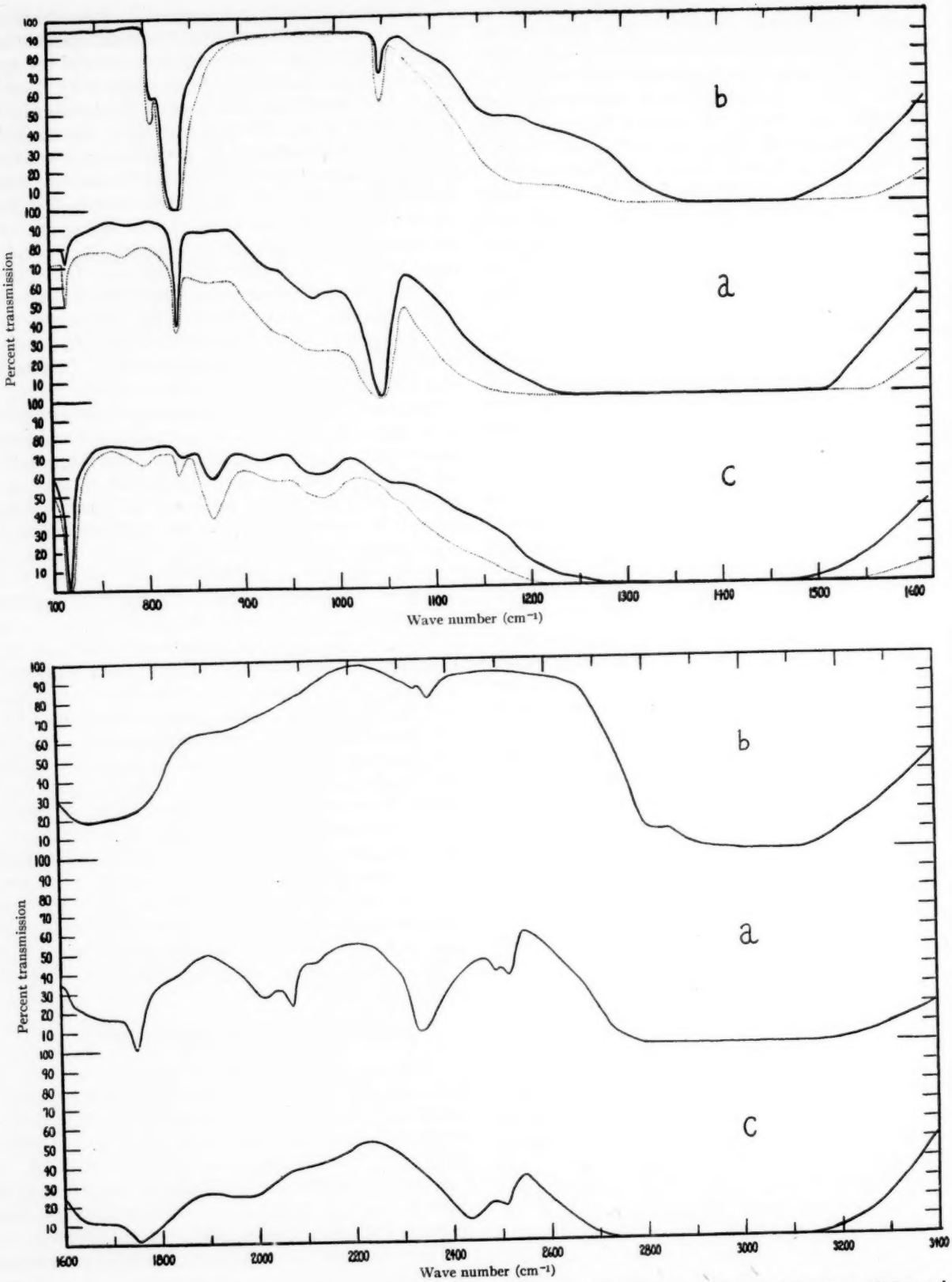

FIGS. 1 and 2. Polarized spectra for single crystals of NH_4NO_3 (IV). Electric vector of the light beam is parallel to axis indicated. Dotted curve is for sample 80 microns thick, solid curve for sample 35 microns thick. Axes are identified in Fig. 3.

triangle having symmetry D_{3h}, would, if isolated, have[17,18] four fundamental frequencies of vibration: ν_1, near 1050, the totally symmetric stretching mode (forbidden in the infra-red spectrum for the isolated ion); ν_2, near 830, the out-of-plane bending mode; ν_3, near 1390, the doubly degenerate, predominantly stretching mode; ν_4, near 715, the doubly degenerate, predominantly bending mode. This assignment of frequencies is the customary one and, as the polarized absorptions will be seen presently to be consistent with it, we do, in some measure, independently verify this assignment.

The ammonium ion, assumed to be a centered tetrahedron having symmetry T_d, would likewise, if isolated, have [17,18] four fundamental frequencies: ν_1', near 3033, the totally symmetric stretching mode; ν_2', near 1685, the doubly degenerate bending mode; ν_3', near 3134, the triply degenerate stretching mode; and ν_4', near 1397, the triply degenerate bending mode (ν_1' and ν_2' would be forbidden to appear in the spectrum for the isolated ammonium ion). This assignment of frequencies, analogous to the well-established one for methane, is undoubtedly correct but we were unable, for reasons that will emerge during the discussion, to independently verify it.

It is to be expected also that the spectra obtained for the several different crystals may show marked differences in detail, depending upon the crystal structures. Selection rules governing absorption by the isolated ions, and strict degeneracies prevailing therein, will be relaxed[5,6] or removed in ways that are peculiar to each crystal structure. In particular, transitory electric moments generated by the vibrations must develop along characteristic directions in a crystal and, depending upon its structure, may have components along only one or along several of the crystallographic axes. Thus, a mode having always the same molecular origin may appear completely polarized in the spectra for one crystal but not so in those for another. Moreover, it will be seen that the resolved bands appearing in our spectra have envelopes more or less rich in detail. These envelopes include many unresolved, composite absorptions, involving simultaneous changes in the molecular mode and various ones of the lattice modes, and thus assume appearances that are peculiar to the crystal structures. These matters will be considered, and interpreted wherever possible, during the course of the ensuing discussion.

NH_4NO_3 (IV)

The spectra, designated as *a*, *b*, and *c* to denote the crystallographic axis along which the light was polarized, are shown for this crystal in Figs. 1 and 2 supplemented by Table I wherein we have tabulated the locations for all components of absorption that appear to have been resolved.

TABLE I. Frequencies (cm^{-1}) observed for NH_4NO_3 (IV).

a	*b*	*c*	Assignment[a]
715	—	715	ν_4
780	—	—	−50
—	—	792	−38
—	807	—	$\nu_2(N^{16}O_3)$?
830	830	830	ν_2
865	—	865	+35
—	—	915	−131
~930	—	—	~−116
975	—	975	−70
1046	1046	1046	ν_1
—	~1095	—	~+50
—	—	~1125	~+80
—	~1170	—	~+125
—	—	~1180	~+135
1250 to 1550	1370 to 1470	1280 to 1470	ν_3, ν_4', $2\nu_4$
1700	1700	1700	ν_2'
1750	—	1750	$\nu_1+\nu_4$
2016	~1900	~2000	
2074	to	2060	$2\nu_1$, $\nu_4+\nu_3$, $\nu_2+\nu_3$, $3\nu_4$
2130		to	
—	~2200	2200	
2330	2330	—	$2\nu_2+\nu_4$
—	2360	—	
—	—	2434	$2\nu_4+\nu_1$
2490	—	2508	$\nu_1+\nu_2+\nu_4$
2520	—	—	
—	2830	—	$2\nu_1+\nu_2$
2800 to 3160	3000 to 3140	2740 to 3140	ν_1', ν_3', $\nu_2'+\nu_4'$, $3\nu_1$

[a] Unprimed, boldface symbols denote fundamental modes of nitrate ion, primed ones those for ammonium ion. Positive numbers show spacing from nearest fundamental of lower frequency, negative numbers show spacing from nearest fundamental of higher frequency. Absolute values of these numbers are thought to be indicative of groups of frequencies for optical branches in lattice mode distribution.

The crystal structure,[12,19] space group V_h^{13} with two molecules per unit cell, site[20] groups C_{2v} for both kinds

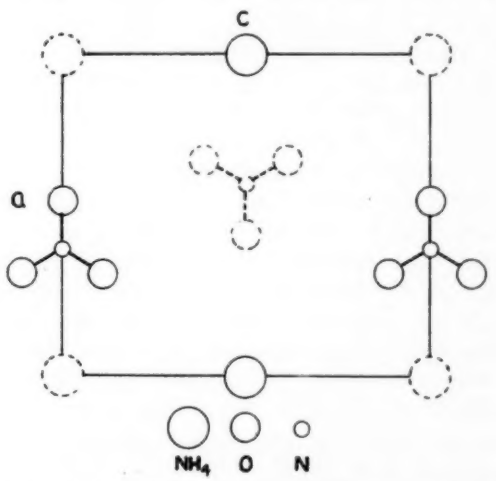

FIG. 3. Unit cell of NH_4NO_3 (IV) projected onto (010) plane. Full lines depict atoms or ammonium ions whose centers are in upper and lower faces of unit cell, broken lines depict ones that are halfway between. Sites for both kinds of ions have symmetries C_{2v}, with C_2 axes along *a*, symmetry planes parallel with (010) and (001). Axes are labeled according to West (reference 12).

[18] G. Herzberg, *Infrared and Raman Spectra of Polyatomic Molecules* (D. Van Nostrand Company, Inc., New York, 1945), pp. 167, 178.

[19] Hendricks, Posnjak, and Kracek, J. Am. Chem. Soc. **54**, 2780 (1932).

[20] R. S. Halford, J. Chem. Phys. **14**, 8 (1946).

TABLE II. Binary combinations involving lattice modes, allowed in spectra for NH_4NO_3 (IV).[a]

a	*b*	*c*
$\nu_{1g}\pm t_{au}$	$\nu_{1g}\pm t_{bu}$, R_{cu}	$\nu_{1g}\pm t_{cu}$, R_{bu}
$\boldsymbol{\nu_{1u}\pm t_{ag}}$	$\nu_{1u}\pm t_{bg}$, R_{cg}	$\nu_{1u}\pm t_{cg}$, R_{bg}
$\nu_{2g}\pm t_{bu}$, R_{cu}	$\nu_{2g}\pm t_{au}$	$\nu_{2g}\pm R_{au}$
$\nu_{2u}\pm t_{bg}$, R_{cg}	$\boldsymbol{\nu_{2u}\pm t_{ag}}$	$\nu_{2u}\pm R_{ag}$
$\nu_{3ag}\pm t_{au}$	$\nu_{3ag}\pm t_{bu}$, R_{cu}	$\nu_{3ag}\pm t_{cu}$, R_{bu}
$\boldsymbol{\nu_{3au}\pm t_{ag}}$	$\nu_{3au}\pm t_{bg}$, R_{cg}	$\nu_{3au}\pm t_{cg}$, R_{bg}
$\nu_{3cg}\pm t_{cu}$, R_{bu}	$\nu_{3cg}\pm R_{au}$	$\nu_{3cg}\pm t_{au}$
$\nu_{3cu}\pm t_{cg}$, R_{bg}	$\nu_{3cu}\pm R_{ag}$	$\boldsymbol{\nu_{3cu}\pm t_{ag}}$
	ν_4 is like ν_3	

[a] Boldface symbol identifies fundamental mode allowed in that spectrum without combination.

of ions, is depicted in Fig. 3. The crystallographic information is subject to the reservation that it describes the arrangement of heavier atoms only, the positions of the hydrogen atoms being unknown. The spectra furnish evidence, to be reviewed presently, that the hydrogen atoms are disoriented with respect to the elements of symmetry at the sites C_{2v}.

The selection rules for nitrate ion under the site group C_{2v} show[5,6,20] that all modes are permitted to absorb, with ν_1 polarized along *a*, ν_2 polarized along *b*, ν_3, and ν_4 each split into two components polarized along *a* and *c*, respectively. Lattice modes of translatory origin t_a, t_b, and t_c will be active and polarized along *a*, *b*, and *c*, respectively, while lattice modes of rotatory origin R_a, R_b, and R_c will involve librations about *a*, *b*, and *c*, respectively, with R_a inactive, R_b polarized along *c* and R_c polarized along *b*. The physical basis for these selection rules becomes apparent upon inspection of Fig. 3. The lattice modes, which can be correlated with motions of the free ion by inspection of Fig. 3, will have frequencies too low to appear as fundamentals in the range covered by our observations but could conceivably become the source of envelope structure by entering into combinations with molecular modes. Under the factor group, each of the foregoing modes gives rise[5] to two, symmetric or antisymmetric under the crystallographic inversion, respectively. These will be distinguished henceforth, when necessary, by appending the subscripts *g* and *u* to the symbols defined previously. The binary combinations between molecular modes and lattice modes allowed under the factor group, a conceivable basis for interpreting envelope structure, are presented in Table II.

ν_1(**1046**) appears strongly in the *a* spectrum where it is allowed. It appears also, but more weakly, in the *b* spectrum where it is forbidden except in combinations. We believe that this should be attributed tentatively to the crudity of our sectioning technique, that the section being observed was not accurately a (100) plane but was tilted sufficiently to admit an appreciable component of *a*. It is possible, of course, that the band results from combinations between the molecular mode and an acoustical branch of the lattice spectrum.

ν_2(**830**) appears strongly in the *b* spectrum where it is allowed, to a lesser extent in the *a* spectrum and very weakly in the *c* spectrum. Its appearance in the *a* spectrum we attribute again to inaccuracy of sectioning. Its appearance in the *c* spectrum might be caused by incomplete polarization and lack of parallelism in the incident light, but then we should expect to find a residual of similar strength for ν_1 in *c* where none is observed. It appears probable therefore that the weak component of ν_2 in the *c* spectrum arises from its combinations with lattice modes.

The weak satellite at 807 appears also in the spectra for NH_4NO_3 (III) and $TlNO_3$ and it is found[22] to be intensified, if anything, at low temperatures, showing that it is not a difference band involving ν_2. A frequency 808 is predicted[18] for ν_2 in the isotopic molecule wherein N^{15} replaces N^{14}. The ratio of extinctions was determined with powdered specimens of $TlNO_3$, whose thickness could be adjusted to afford such a measurement, to be 1/150 which stands in some agreement with the known[21] isotopic abundance ratio of 1/350. Nevertheless, and although we shall have no other suggestion to offer, we are somewhat hesitant about accepting this interpretation for the satellite because the intensities of it and the main band are inverted,[22] perhaps as an unrelated coincidence, in the spectrum of $Pb(NO_3)_2$.

ν_3(**1390?**)[17,18] may appear in the *a* and *c* spectra but is forbidden to appear in the *b* spectrum. This band remains unresolved from the neighboring overtone $2\nu_4$ and the ammonium ion fundamental ν_4' at 1397, all of which produce together the intense, broad absorption occurring in our spectra. We are probably observing the disappearance of ν_3 from the *b* spectrum in the form of a narrowing of the region of intense absorption, especially on the low frequency side. The complicating absorption by ammonium ion involves a triply degenerate mode and, accordingly, is most likely unpolarized, while the overtone $2\nu_4$ would be more likely to affect the high, rather than the low frequency side of the absorption. In addition, it would require but little inaccuracy of sectioning, already suggested in connection with ν_1 and ν_2, to cause an appreciably broad residual of a highly absorptive ν_3 to appear in the *b* spectrum.

ν_4(**715**) may appear in both the *a* and the *c* spectra but should be absent from the *b* spectrum as is seen to be the case. It is surprising, perhaps, that there should be such a disparity in the intensities of the two allowed components of a degenerate mode when their frequencies are so nearly alike. Moreover, this is the mode

[21] D. Yost and H. Russell, *Systematic Inorganic Chemistry* (Prentice-Hall, Inc., New York, 1944), p. 4.

[22] See R. Newman and R. S. Halford, J. Chem. Phys. 18, 1291 (1950).

that has been found[17] to disappear anomalously from the spectra for NH_4NO_3 (II) and (I). In spite of these seeming aberrations, which might be attributed to an erroneous assignment, we feel that the behavior of this band in the several nitrates we have examined is consistent with its assignment to a degenerate mode, that the behavior in question must be more or less accidental. Although this motion is permitted to absorb in the isolated ion, it is not necessary that it should do so. Indeed, it is possible to construct normal coordinates for the degenerate bending mode such that it would generate little or no transitory electric moment. Then, the capacity of this mode to absorb when it occurs in a crystal would be largely an acquired characteristic, sensitive to details of the environment, anisotropic along with the latter. We know[23] from experience that the environment can induce an appreciable absorption intensity without much alteration of frequency. At any rate, the behavior of this absorption is strictly correct as regards its disappearance from the *b* spectrum, a characteristic that marks it unequivocally as an in-plane motion.

The nitrate ion fundamentals, in summary, appear to have been correctly assigned by previous investigators and to behave in accord with selection rules characteristic of their environment in NH_4NO_3 (IV). Uncertainties regarding the positions of hydrogen atoms in this crystal do not materially effect these conclusions.

The selection rules for ammonium ion will depend upon the unknown positions taken by the hydrogen atoms. If these are distributed with a pair in each of the reflection planes at the site C_{2v}, so as to be consistent with the space symmetry found for the heavier atoms, all modes will be permitted[20] to absorb, with ν_1' polarized along *a*, ν_2' split into two components, one inactive and one polarized along *a*, ν_3' and ν_4' each split into three components, polarized along *a*, *b*, and *c*, respectively. If, instead, the ammonium ion is now rotated around *b* so that the *ac* plane remains the only one of symmetry, ν_1' will acquire a component along *c*, ν_2' along both *b* and *c*. If, to the contrary, it were rotated only about *c*, ν_1' would acquire a component this time along *b*, ν_2' again along both *b* and *c*. If the ion is rotated about both axes *b* and *c* together, or about *a* alone, all modes are permitted to have components along all axes. Thus, the polarization of the absorptions attributable to ν_1' and ν_2' furnishes us with a clue to the positions of the hydrogen atoms in this crystal. Unfortunately, none of these highly absorptive vibrations were resolved at all distinctly in the polarized spectra, our conclusions must be entertained with some reservations.

ν_1'**(3033?)**[17,18] is proximate to, and unresolved from ν_3' and several bands attributable to nitrate ion, which latter may be seen clearly in our spectra for $TlNO_3$.

[23] O. A. Shaeffer and R. S. Halford, J. Chem. Phys. **14**, 141 (1946).

TABLE III. Frequencies (cm^{-1}) observed for NH_4NO_3 (III).

a	*b*	*c*	Assignment[a]
—	—	716	ν_4
720	720	—	ν_4
—	—	750	−80, +30?
808	808	—	$\nu_2(N^{15}O_3)$?
830	830	830	ν_2
—	—	∼850	∼+20
—	855	—	+25
880	—	—	+50
925	925	—	−122, +95?
—	—	927	−120, +97?
—	—	964	−84
—	—	988	−60
995	—	—	−48
—	—	1005	−43
1048	1048	1048	ν_1
∼1100	∼1100	—	+52
—	—	∼1120	∼+72
1140	—	∼1140	∼+92
1240 to 1530	1250 to 1480	1230 to 1580	ν_3, ν_4', $2\nu_4$
1660	1660	1660	ν_2'
1766	1766	1766	$\nu_1+\nu_4$
2005	2052	2052	
2055	—	2100	$2\nu_1$, $\nu_4+\nu_3$, $\nu_2+\nu_3$
—	2160	—	$3\nu_4$
—	—	2390	
2405	2405	—	$2\nu_4+\nu_1$
2530	2530	2530	$\nu_1+\nu_2+\nu_4$
2840 to 3200	2800 to 3320	2800 to 3300	ν_1', ν_3', $\nu_2'+\nu_4'$, $3\nu_1$ $2\nu_1+\nu_2$

[a] See Table I.

Observations, not shown here, with extremely thin, sublimed films of NH_4NO_3 showed the bands clearly resolved, with ν_1' but slightly less intense than ν_3', the latter having about the same intensity as ν_2 at 830. Basing our judgment upon the knowledge gained from these observations and upon the course of the envelope as it rises at higher frequencies, we are of the opinion that a disappearance of ν_1' from the *b* or *c* spectrum, especially the former, should have been discernible in the region from 2900 to 3000. We see, however, that absorption remains intense in this region, even in the *b* spectrum where the total range of absorption has become markedly narrower, a circumstance that is entirely attributable to loss of the contributions from nitrate ion. Indeed, the appearance of the *b* spectrum is rather suggestive of the presence of two, highly absorptive bands with envelope structure beginning to be partly resolved in the lower lying one. Nevertheless, we are not justified in reaching any conclusions beyond the cautious one that ν_1' could have been, and more probably was present in all three spectra although this last is by no means certain.

ν_2'**(1685)** is seen to be a broad region of incomplete absorption in all cases, with a sharp band at 1750 superimposed upon it in the *a* and *c* spectra. The sharp band has both the proper frequency and the proper polarization for the combination of nitrate ion frequencies $\nu_1+\nu_3$; moreover, a similar, polarized band appears in the $TlNO_3$ spectra, confirming this assignment. The residual, surely attributable to ammonium ion by virtue of its absence from the spectra of $TlNO_3$,

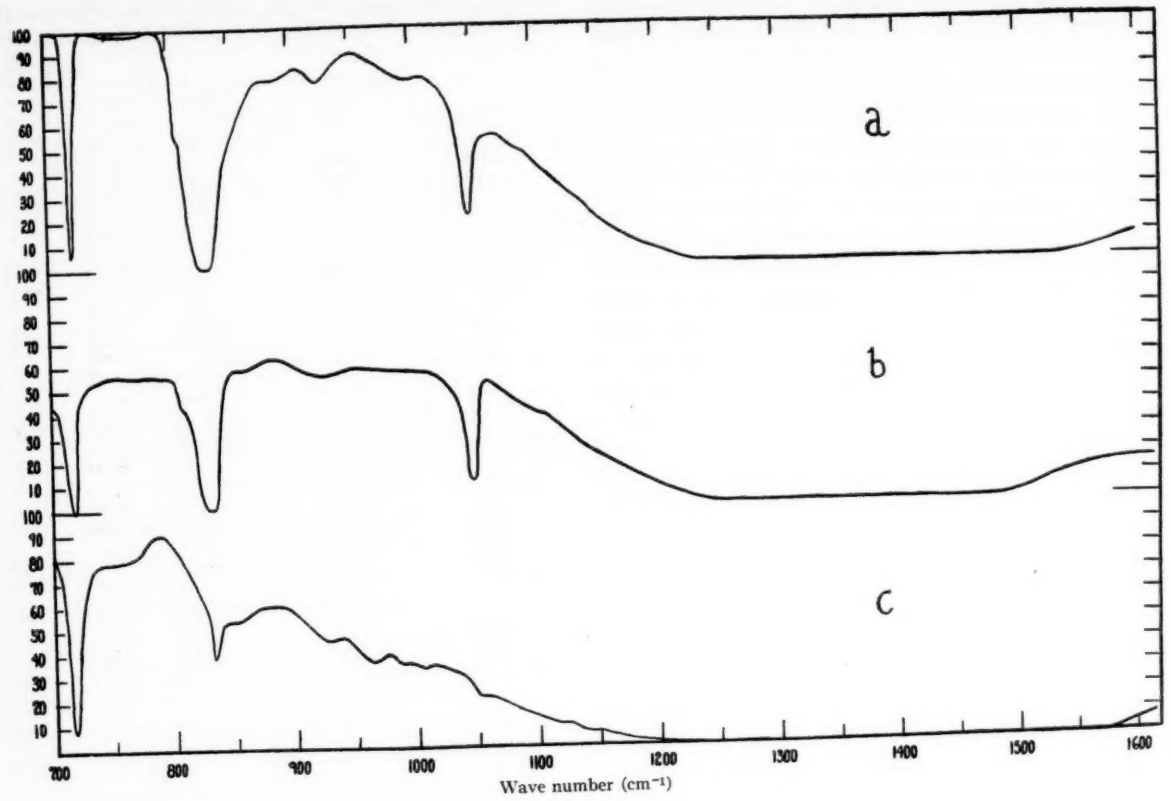

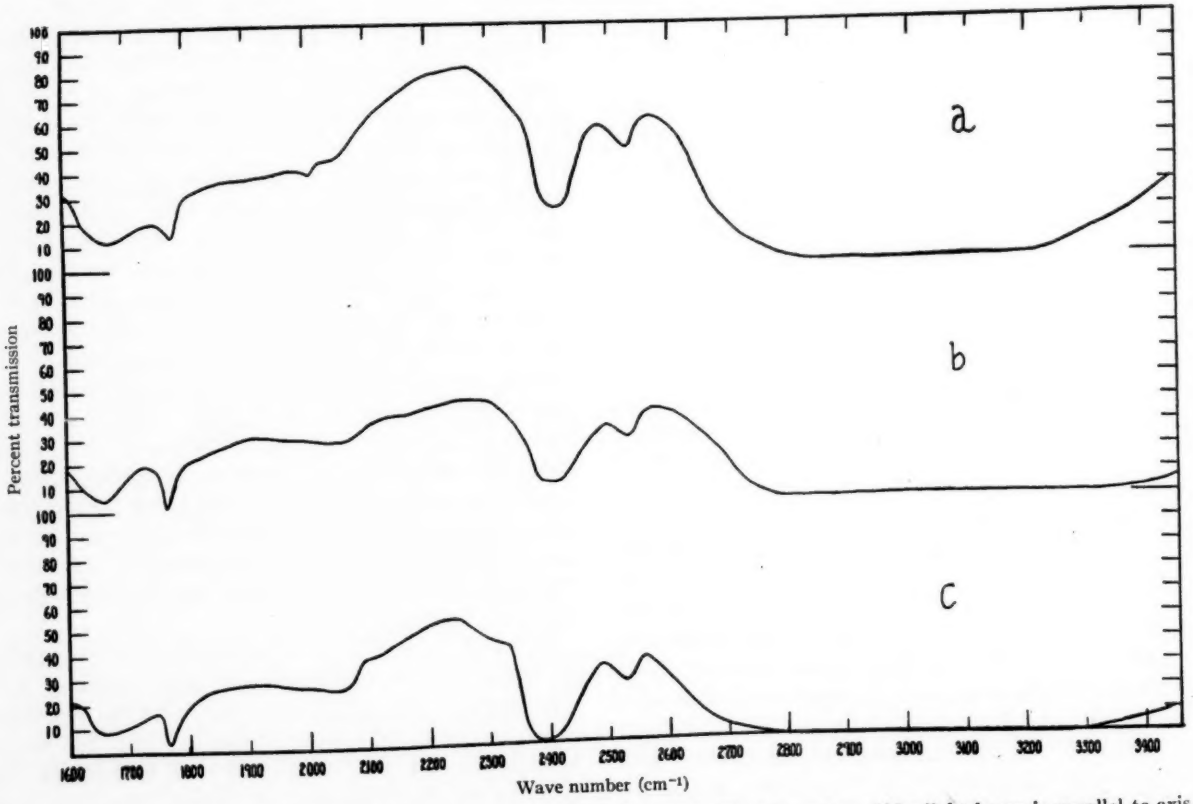

FIGS. 4 and 5. Polarized spectra for single crystals of NH_4NO_3 (III). Electric vector of the light beam is parallel to axis indicated. *a* and *c* spectra are from a sample about 75 microns thick, *b* spectrum from a sample about 40 microns thick. Axes are identified in Fig. 6.

presumably ν_2', exhibits no appreciable polarization, contrary to the behavior expected of ammonium ions oriented so as to preserve the site symmetry C_{2v}. At the same time, the appearance of this absorption seems odd, its unusual width for incomplete absorption suggesting the presence of a complex of unresolved bands, possibly connected with the circumstances of disorientation. The alternative to this interpretation would assign the unpolarized residual to a combination of ν_4' or ν_2' with lattice modes, which, because of the triply degenerate origin of ν_4', and for other reasons,[5] would not be expected to be polarized. In view of the great intensities of absorption by the other ammonium ion fundamentals, including the here allowed but sometimes forbidden ν_1', we think it unlikely that ν_2' would fail to appear in our spectra.

ν_3'**(3134?)**[17,18] has been considered previously in our discussion of ν_1'. Its triply degenerate origin makes it of little interest in the present study.

ν_4'**(1397?)**[17,18] appears, unresolved from the neighboring ν_3, in all three spectra. Again, its triply degenerate origin detracts from its interest.

Disorientation of ammonium ions seems to be indicated by our observations, although not conclusively. Taking all things into consideration, the probable behavior of ν_1', the definitely unpolarized nature of what is probably ν_2', and the marked contrast between these observations and the pronounced polarizations observed with the numerous bands attributable to nitrate ion, the conclusion is somewhat forcefully indicated. It is confirmed, to be sure, by other sorts of observations.[24]

Overtones and combinations involving internal modes of nitrate ion give rise to a number of sharp, polarized bands in the region from 1600 to 3400, in addition to ones that may not have been resolved. The assignments listed in Table I were chosen so as to give the correct polarization behavior and a frequency reasonably close to the one observed. We have ignored the possibilities for combinations involving one molecular mode from nitrate ion, one from ammonium ion, inasmuch as all bands in question have counterparts in the spectrum of $TlNO_3$. In a few instances we have included alternative assignments that give a superior fit to the observed frequency but are not entirely in accord with the observed polarization.

Combinations of lattice modes with internal modes of nitrate ion are presumed to be the source of weaker, but clearly discernable components, not otherwise explicable, falling in the region below 1200. Reference to the tabulation given earlier for fine structure components allowed under the factor group selection rules shows that a large number of these may be expected. One would suppose, for the lower lying lattice frequencies at least, that any additive combination would be accompanied by a subtractive one, the two having approximately equal intensities and being symmetrically disposed about the fundamental. However, if a number of these satellites are present, not well resolved, and if additive combinations with one molecular mode are superimposed upon subtractive ones with another, individual components may become badly obscured and symmetry of envelopes may be destroyed. This possibly may account for our inability to find any correlation between the fine structure components observed and the ones predicted. On the other hand, factor group selection rules for combinations are known[5] to be woefully incomplete with vastly many more being allowed under the complete space group selection rules. Probably, then, our hope of finding such a correlation represents little more than mere wishful thinking. For the present we have merely indicated in Table I the molecular mode from which each such component seems to us to be derived. This element of identification is based mainly upon an expectation of symmetrical envelopes, realized as we shall see with $TlNO_3$. Low temperature spectra[22] also have been consulted, but these are of dubious significance with NH_4NO_3 where a phase transition intervenes.

NH_4NO_3 (III)

The spectra, again designated as *a*, *b*, and *c* with unchanged significance, are shown for this crystal in Figs. 4 and 5 supplemented by Table III.

The crystal structure,[13,14,19] space group V_h^{16} with four molecules per unit cell, site groups C_s for both

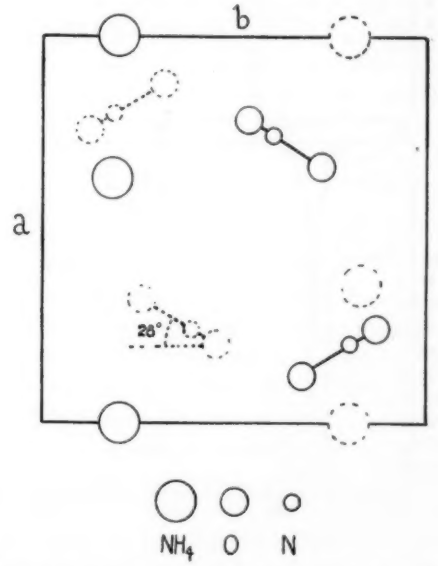

FIG. 6. Unit cell of NH_4NO_3 (III). Full lines depict ions centered in upper and lower faces of unit cell, broken lines depict ones centered halfway between. Both kinds of ions occupy sites with symmetries C_s, with planes of symmetry parallel to (001). The ammonium ions have been displaced slightly from their actual positions in the planes of symmetry for sake of clarity. Axes are labeled according to reference 14 (see footnote to text).

[24] J. L. Crenshaw and I. Ritter, Zeits. f. physik. Chemie **B16**, 143 (1932). G. E. Pake and H. S. Gutowsky, J. Chem. Phys. 16. 1164 (1948).

kinds of ions, is shown‡ in Fig. 6. The crystallographic information is again subject to the reservation noted previously for NH_4NO_3 (IV).

The selection rules for nitrate ion under the site group C_s show that all modes are permitted to absorb, with ν_1 and ν_2 polarized along a and b, ν_3 and ν_4 each split into two components, one polarized along both a and b, the other polarized along c. The analysis for lattice modes will be omitted in consequence of its demonstrated unsuitability for interpretation of the previous case.

ν_1**(1048)** is forbidden to appear in the c spectrum and is not observed there. Intensities for the a and b spectra should be in the ratio of one to three, respectively, as can be deduced from the disposition of nitrate ion planes depicted in Fig. 6. Inasmuch as the two spectra were obtained with sections of unequal thickness, direct verification of this prediction is impossible. Using the measured thicknesses and amounts of absorption at the band center, assuming an exponential law for absorption, one obtains for the ratio of extinction coefficients the result 1/2.8. Considering the crudity of the calculation, this may be a fortuitous check.

ν_2**(830)** is forbidden to appear in the c spectrum where, however, a weak residual is observed. We interpret this, as we did the corresponding band in the c spectrum for NH_4NO_3 (IV), to be the result of combination between ν_2 and low lying lattice modes, a proposal that seems in accord with the diffuse background accompanying this band. For the allowed components appearing in the a and b spectra, the expected apportionament of intensities seems to hold qualitatively, that is, $a>b$. The completeness of the absorptions precludes any attempt to examine the quantitative check by the means used for ν_1.

The weak satellite at 808 appears less well resolved than formerly, its frequency becoming correspondingly more uncertain. Once again it has the proper location and something like the proper intensity for assignment to the isotopic ion.

ν_3**(1390?)**[17,18] is again completely obscured by neighboring bands. Expected to appear in all three spectra, it seems this time to do so. At least, the b spectrum stands in contrast with the corresponding one for the previous substance where a marked narrowing of absorption was seen to occur.

ν_4**(720, 716)** is allowed in all three spectra and appears in all of them. In gratifying agreement with

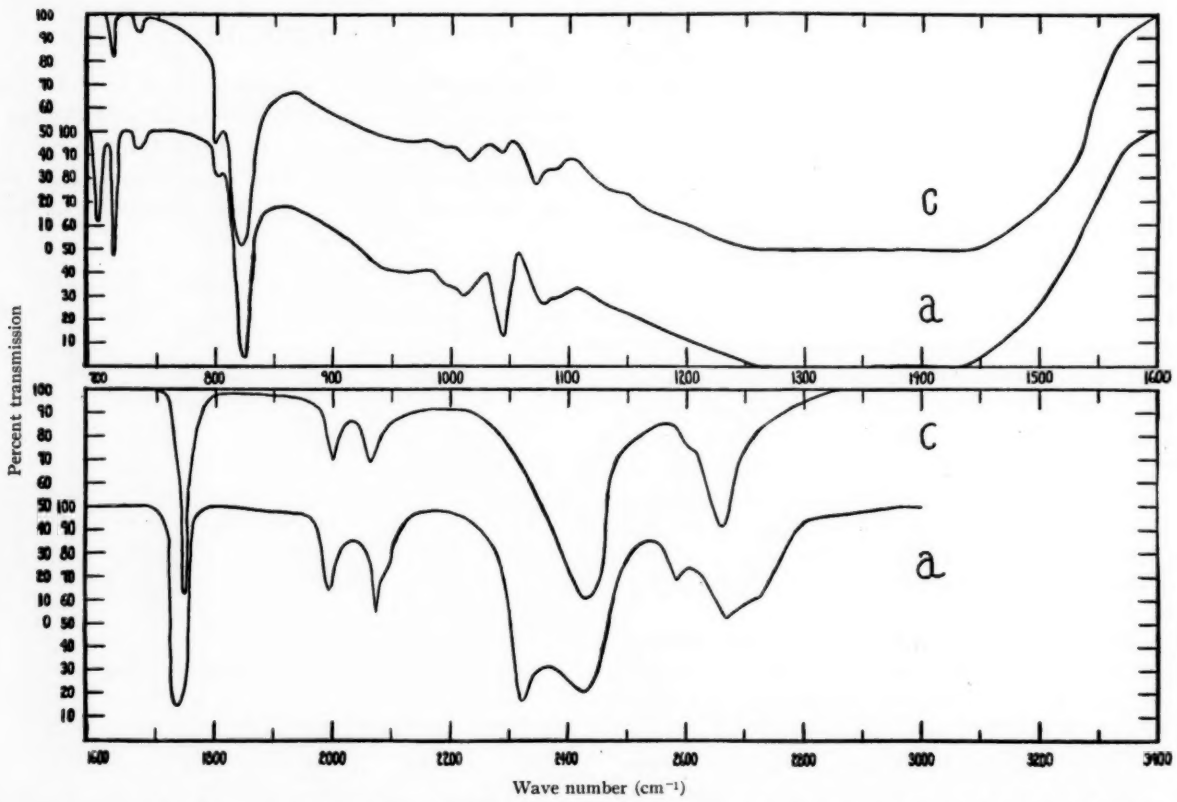

FIG. 7. Polarized spectra for single crystal of $TlNO_3$ (γ). Electric vector of the light beam is parallel to axis indicated, sample about 60 microns thick. Axes are labeled according to reference 15.

‡ It should be noted that references 13 and 14 differ, as far as the present work is concerned, in the assignment of the a and b periods relative to the angles of the NO_3 planes. The labeling of the spectra (Figs. 4, 5) and the crystal diagram (Fig. 6) is in accordance with reference 14. In as much as both sets of authors are in agreement as to the relation of the angles of the nitrate planes and the directions appropriate to the principal refractive indices, it would perhaps have been better to have labeled the spectra and diagram α, β, and γ, the measured quantities, rather than a, b, and c as was done.

expectations, the same frequency 720 appears in both *a* and *b* spectra with a qualitatively correct apportionment of intensities ($b>a$) while a new frequency 716 appears in the *c* spectrum. This difference in frequencies is well beyond experimental precision in this region. Moreover, we should note that the anomaly of intensities encountered with NH_4NO_3 (IV) no longer confronts us, tending to confirm some of the views expressed there.

The nitrate ion fundamentals, in summary, absorb in a manner that seems to dispel all doubt concerning the correctness of their previous identifications, one that is in good accord with selection rules characteristic of their environment in this crystal.

The ammonium ion fundamentals will not be discussed again here, inasmuch as the bands show no polarization and the remarks offered for the previous case will hold as well for this one.

Combinations among molecular modes and between molecular modes and lattice modes will not be treated separately for this case. In general, all remarks made for the previous case will apply here as well. Assignments appear in Table III.

$TlNO_3$ (γ)

This substance will be treated as an example to show how polarized spectra might be used in conjunction with the established methods of x-ray crystallography to identify a crystal structure when it is difficult to obtain by the latter method alone. The example is a valid one because the orientations of the nitrate ions in this crystal must be deduced from features of the x-ray diffraction that are overshadowed by the preponderant scattering from the heavy thallous ions. To this end, we shall depart from the previous order of presentation to describe first the spectra, next the selection rules that might be indicated by them, and last the implications of this information toward the crystal structure.

The spectra, only two of them because of our failure to produce sections capable of exhibiting satisfactorily the third one, are shown in Fig. 7 and Table IV, wherein they have been designated as *a* and *c* according to our previously explained conventions.

ν_1(**1044**) appears prominently in the *a* spectrum, probably¶ likewise along *b*, and just perceptibly along *c*. The remarkable envelope structure accompanying this band will be treated in another paragraph dealing with combinations between molecular modes and lattice modes.

ν_2(**824**) appears in both the *a* and *c* spectra, but broadens asymmetrically upon passing from *a* to *c*. That is, it appears as though another absorption were added in the *c* spectrum at a slightly lower frequency than the one appearing along *a*. Occasionally, under conditions of best resolution, a small shoulder appeared at about 821. The effect was never great enough, however, relative to noise, to establish its reality. The spectra of powdered specimens at low temperatures showed[22] the band sharpened and shifted slightly toward higher frequency but did not produce any resolution into two bands. Whatever be the case, a multiplicity of frequencies, a number not exceeding the population of the unit cell, is permissible[5,6] for a fundamental under the complete space group selection rules. It is significant, though, that this band appears prominently in both *a* and *c* spectra.

The weak satellite, now at 800, has shifted frequency parallel with ν_2, behaving properly for an isotopic shift. We remark again, however, that the appearance of this pair in[22] $Pb(NO_3)_2$ casts some doubt upon this assignment.

ν_3(**1390?**),[17,18] although no longer complicated by the absorption in ammonium ion, remains concealed in a broad region of complete absorption. It is probably obscured in part by the overtone $2\nu_4$ and, although the fundamental would be expected to behave like ν_4, no significant changes in the envelope were detected. The study of this fundamental and the possible Fermi resonances between components of it and the degenerate overtone must await the preparation of much thinner sections.

TABLE IV. Frequencies (cm^{-1}) observed for $TlNO_3$ (γ).

a	*c*	Assignment[a]
700	—	ν_4
713	713	ν_4
735	735	+35
800	800	$\nu_2(N^{15}O_3)$?
824	822	ν_2
—	960	−84
965	—	−79
—	~988	~−56
~1000	—	~−44
1010	—	−34
—	1015	−29
1044	1044	ν_1
—	1072	+28
1078	—	+34
~1085	~1085	~+41
—	~1130	~+86
—	~1180	~+136
1260 to 1430	1260 to 1440	ν_3, $2\nu_4$
1736	—	$\nu_1+\nu_4$
—	1750	
1994	—	
—	2000	
—	2064	$2\nu_1$, $\nu_3+\nu_4$, $3\nu_4$
2074	—	
~2080	—	
2320	—	$2\nu_2+\nu_4$
2430	2430	$\nu_1+\nu_3$
2584	—	$\nu_1+\nu_2+\nu_4$
—	2610	
2670	2660	$2\nu_2+\nu_1$
~2720	—	

[a] See Table I.

¶ Although we were unable to produce sections that would be altogether satisfactory for observations at longer wave-lengths, we conducted observations with a small fragment having the proper orientation and obtained what we believe was a partial *b* spectrum containing this and other principal bands. See Table V.

ν_4(**696, 700, 713**) is involved in absorptions at these places, at 735, and probably at lower frequencies as well. The band at 700 appears in the *a* spectrum only, the one at 713 in both spectra but is noticeably weaker along *c*, the one at 735 in both spectra with about the same intensity. The bands at 700 and 713 are sharp, whereas the one at 735 is comparatively broad. Upon the basis of their strengths and sharpness we assign the bands at 700 and 713 to the now separate components of the originally degenerate mode ν_4. The band at 735 we believe to be a combination of one component of ν_4 with some branch of the lattice spectrum and we prefer to attribute it to the component at 700, rather than 713, because the former is polarized like ν_1, the latter more like ν_2, and ν_1 is evidently prone to enter into such combinations. This would place the difference combination at 665 where it would be masked by an atmospheric absorption and thus account for our lack of success when searching‖ for this companion at lower frequencies. Observations[22] with a powder specimen at low temperature served to eliminate the possibility that 735 is a difference frequency involving any of the other fundamentals and disclosed, at the same time, that the situation is rather more complicated than it thus far appears. In the powder spectra at room temperature the band noted here at 700 appears instead at 697, noticeably broadened, while 713 and 735 appear unchanged. When the powder is cooled with liquid air, the band at 735 is unaffected, the one at 713 is sharpened and shifted upward to 714, while the third band becomes[22] resolved into two components at 696 and 700, respectively. The latter is evidently the one we have seen in our polarized spectra whereas the former, since we have not found it along either *a* or *c*, must be virtually completely polarized along *b*. This multiplicity of frequencies arising out of ν_4 is, as we remarked before, evidence for a plural number of molecules per unit cell. We are unable at this time, however, to better clarify the situation that we have been describing.

Combinations and overtones involving molecular modes of nitrate ion give rise to a number of bands, more or less sharp, falling at higher frequencies, and, in several instances, appearing to be virtually excluded from the spectrum as seen along *c*. Assignments, based upon gaining agreement with frequencies and tending to be confirmed by polarization properties observed in the other crystals, are included in Table IV.

Combinations between molecular modes and lattice modes produce the truly remarkable envelope structure observed in the vicinity of ν_1. As can be seen in Fig. 7, and spectacularly so in the original records, three pairs of branches, whose members are distributed symmetrically above and below another central one, were more or less well resolved. When examined in detail it is found that (1) the most immediate satellites move from 1015 and 1072 in the *c* spectrum to 1010 and 1078 in the *a* spectrum, changing thus from ± 28 to ± 34, (2) the proximate shoulders at 1000 and 1085 appear to become intensified upon passing from *c* to *a*, as does the broad, outermost satellite at 960 and probably also its companion at 1145. While these effects may denote the presence of some polarized components contributing to the fine structure, we must bear in mind that the first two could be caused in some part, if not altogether, by the introduction of the strongly polarized central branch which is absent from *c* but appears along *a*. We are left to conclude that the resolved components of the fine structure are not strikingly polarized, a conclusion that is in accord[5] with the general theory and bespeaks against any attempt at this time to identify the resolved increments with particular branches of the lattice mode distribution. Especially striking is the sharp contrast between the behavior of the central branch and that of the satellites. It is possible, of course, that the small shift of spacing described above results from the substitution, in the combinations, of lattice modes polarized along *a* for ones polarized along *c* but, if so, the case needs to be more convincingly demonstrated. The complexity of these satellites, as well as the correctness of identifying them with combinations, is indicated by the low temperature spectra.[22]

Selection rules appear to be operating in this crystal although, from the standpoint of strict logic, we cannot be absolutely certain that crystallographic symmetry is their cause. The evidence for selection rules is summarized in Table V, where we show the presence or absence of each fundamental absorption by + or − respectively, and in the untabulated behaviors of several combinations at higher frequencies. When assembling this evidence we have ignored small residuals such as the trace of ν_1 that remains along *c*. The significance of these empirical selection rules is discussed below.

The crystal structure of this substance will now be discussed from the standpoint of ascertaining, insofar as possible from our spectra, the orientations of the nitrate ions. For this purpose we shall find it convenient to make use of the knowledge[15] that the crystal is orthorhombic with four molecules per unit cell, and illuminating to carry the argument as far as possible without resorting to any other crystallographic information.

Orthorhombic space groups include the classes C_{2v}^n, V^n, V_h^n. The maximum symmetry that is common[20] to any of these and to the molecular group D_{3h} is C_{2v}. Accordingly, C_{2v} and its subgroups C_2 and C_s are the only possible non-trivial site groups for nitrate ion. Referring to Table V and recalling the selection rules for nitrate ion under the group C_{2v}, described in connection with NH_4NO_3 (IV), we see that the rotation axis, if it exists, cannot lie along *c*. Furthermore that,

‖ Although not shown in Fig. 7, the region below 680 was searched as well as possible with the rocksalt prism, handicapped as we were by the light losses attending use of the polarizer and the inferior aperture presented by the crystal.

if the ions do occupy sites having symmetry C_{2v}, the axis at some of them must lie along a (ν_1 is in a), at others along b (ν_2 is in a). Moreover, for either of the two axial orientations, the plane of the molecule might lie in either of two crystallographic planes, yielding four possible arrangements in all, and the entirety of Table V cannot be accounted for unless at least three of these possibilities are invoked. These three possibilities are all non-equivalent under the operations of any orthorhombic space group. The class V_h^n is now ruled out, because it would demand[20] two equivalent sites of each kind, a total of six in all, exceeding the known population of the unit cell. The classes C_{2v}^n and V^n are likewise impossible; the former because we would require rotation axes along both a and b, the latter because it lacks planes of symmetry. Thus, we have shown that the site group cannot, under any likely circumstances, have the symmetry C_{2v}.

If we suppose instead that the site group is C_s, and recall that ν_1 must develop its transitory electric moment entirely in the plane of symmetry, we find that the only possibility for this plane is the one of a and b. Again, however, in order to account for all of Table V we must arrange the plane of the molecule sometimes parallel with a and b, sometimes perpendicular to them, to produce arrangements that are non-equivalent. Space groups of class V_h^n are now ruled out, on ground of population, and those of class V^n, because they contain no plane of symmetry. Space groups of class C_{2v}^n are possible wherein the nitrate ions occupy non-equivalent sites as described above, but in this case are restricted to ones having not more than one glide plane, ones whose rotational element lies along a or b but never along c.

If we suppose next that the site group is C_2, and compare the observed occurrences of ν_1 and ν_2 with ones permitted by the appropriate selection rules, we find it necessary to invoke sites with the C_2 axis sometimes along a, sometimes along b, but never along c. Because these sites are non-equivalent, space groups of class V_h^n are eliminated on ground of population, while ones of class C_{2v}^n are eliminated because they do not contain the required, two, rotation axes. Space groups of class V^n are possible wherein the nitrate ions occupy non-equivalent sites C_2 described above, provided that they contain not more than one screw axis which, if it exists, must have the direction of c.

In both of the foregoing instances, where we have been able to find acceptable arrangements of nitrate ions at sites with non-trivial symmetry, we have had to invoke duplicate, non-equivalent[20] sets of sites. Although there is no clearly stated principle in our knowledge that forbids such occurrences they are nevertheless quite rare, and when they are observed there is usually some recognizable reason whereas none seems evident in this substance. We would, accordingly, regard both of these possibilities for site groups as highly unlikely and expect to find the nitrate ions in general positions, ones having the trivial symmetry C_1, an expectation that can be tested objectively by examination of the systematic x-ray extinctions.

TABLE V. Observed behaviors of fundamentals.

	a	b[a](?)	c
ν_1 1044	+	+	−
ν_2 824	+	+	+
ν_3 696, 700	+	+	−
ν_3 715	+	+	+

[a] See footnote ¶ under discussion of ν_1.

If we suppose finally that the nitrate ions are in general positions, space groups of class V_h^n are eliminated immediately on ground of population, classes V^n and C_{2v}^n remain acceptable without restriction upon their symmetry elements. We must, however, explain the apparent exclusions to be found in Table V. For this latter purpose it is instructive to compare the acceptable, if unlikely arrangements we have described in the preceding paragraphs. The sites of kind C_s, whose common plane of symmetry is required to be the one of a and b, will have always one molecular C_2 axis in that plane. These sites will effect the exclusions of ν_1 and one component of ν_4 from the spectrum along c, independent of the direction given to the molecular C_2 axis in that plane. On the other hand, sites of kind C_2, whose axes are required to lie along both a and b, will effect the same exclusions, independent of the amount of rotation of the molecular plane around those axes. At each kind of site the selection rule is preserved during an operation that would destroy the symmetry of the other kind of site, an operation that in either case would do so without removing the molecular axis from the plane of a and b. This latter restriction upon the directions taken by molecular C_2 axes, rather than the existence of any actual symmetry at the site, is evidently a sufficient and more likely cause for the observed selection rules.

Summarizing our conclusions concerning the crystal structure: when the crystal is viewed along its c axis (1) the nitrate ions each will be seen to have one of their molecular C_2 axes lying in a plane that contains only a and b, (2) these axes in the different nitrate ions will be pointing in four directions, necessarily intermediate between a and b, that are equivalent under the operations of the orthorhombic space group, (3) the molecular planes will appear tilted, by equivalent rotations about these molecular C_2 axes only. The four directions for molecular C_2 axes must have equal absolute values for their corresponding direction cosines. These values could be estimated by comparing the intensities for ν_1 along a and b, respectively, if the latter spectrum were available. The angles of tilt given to the molecular planes must correspond in a similar way, and these can be estimated by comparing the intensities for ν_2, or for the persistent component of ν_4, along a

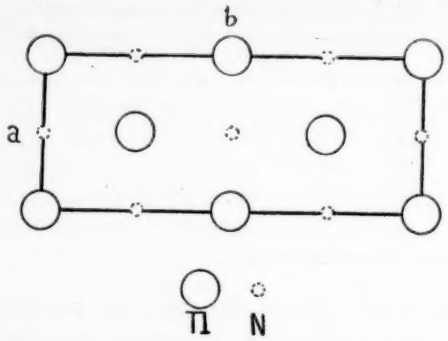

FIG. 8. Unit cell of $TlNO_3$ (γ) showing occupied sites according to Rivoir and Abbad. Full lines depict thallous ions in upper and lower faces, broken lines depict nitrogen atoms in plane exactly halfway between. Positions of oxygen atoms, which determine both space symmetry of lattice and point symmetries of sites, are described in accompanying text.

and *c*. The former, although too intense for satisfactory measurement, suggests by its widths an angle in the neighborhood of $\pm 30°$; the latter an angle near $\pm 22°$.

Employing the conventional methods for structure determination, Rivoir and Abbad[15] obtained the lattice of occupied sites which we show in Fig. 8. It will be seen that this partial lattice, into which the oxygen atoms have yet to be introduced, is tetragonal, with completely equivalent axes *a* and *b*, that the sites assigned to nitrate ions have in this incomplete lattice a higher kind of symmetry than will the finished nitrate ion itself. Thus, when the nitrate ions are completed by addition of their oxygen atoms, the symmetry of their sites, and of the complete lattice, will be lowered thereby to an extent depending solely upon the orientations given to these ions. In this way a variety of space groups, with corresponding site symmetries, could be generated. Rivoir and Abbad attacked the problem of determining the complete structure upon the basis of how best to accommodate the dimensions of nitrate ions, as determined in other crystals, into the spaces available in the readily ascertained partial lattice of thallous ions. They concluded that the space group is either V^2 or V^3, more probably the latter. In the structure selected finally by them the nitrate ions meet our specifications in all respects save one. They show the molecular C_2 axes all aligned with *a*, the molecular planes tilted by rotation about this direction. We hold to our conclusion that these axes must have directions intermediate between *a* and *b*, for otherwise ν_2 would not be seen along *a*. Moreover, since these two directions are equivalent before introducing oxygen atoms, it would seem remarkable if these atoms should show any preference between them. From this point of view it appears probable that the four axial directions would be exactly midway between *a* and *b*, along the lines of closest approach for nitrate ions. This would be compatible with our incomplete spectroscopic information.

Lattice Frequencies

On the basis of the observations made, it is felt that certain tentative conclusions may be drawn as to the range of frequencies of the low lying lattice modes. If the various assignments of the fine structure as combinations of lattice and internal modes are correct, then it would appear that optical branch lattice frequencies in these crystals have a lower limit at about 35–50 cm^{-1} and range upward to perhaps between 100–200 cm^{-1}. It is, for the moment, impossible to determine whether a band is a result of a simple transition, wherein the quantum number of the associated lattice mode changes by one, or whether it results from more complicated transitions involving overtones of lattice frequencies or combinations of them.

It is interesting to note that the Raman spectrum of single crystals of $NaNO_3$ showed[25] anti-Stokes lines at 100 and 185 cm^{-1}, which are presumably caused by excited lattice modes. Other Raman investigations on ionic single crystals have shown similar magnitudes for the frequencies of the lattice modes. Again, of course, it is not known whether the observed lines are simple transitions.

Perhaps when microwave or other techniques are suitably perfected for work in the 100 cm^{-1} range, they will yield sufficient information on lattice frequencies to make data, such as have been obtained here, somewhat more intelligible.

---

[25] Shaefer, Matossi, and Adelhold, Physik. Zeits. **30**, 581 (1929).

Motions of Molecules in Condensed Systems. VIII. Infra-Red Spectra for Ammonium Nitrate, Thallous Nitrate, and Plumbous Nitrate at −160° and 25°C*

ROGER NEWMAN** AND RALPH S. HALFORD
Department of Chemistry, Columbia University, New York, New York
(Received July 21, 1949)

Envelope structure in the spectra of these substances is shown to depend upon temperature in a way that indicates the presence of both additive and subtractive combinations of lattice modes with molecular modes. At −160°C there are no less than seven distinct satellites on the high frequency side of one band in thallous nitrate with damped out counterparts on the low frequency side. The possibility is considered that a second-order phase transition, as well as a first-order one, may be influencing envelope structure in ammonium nitrate. The spectra for plumbous nitrate contain several features of interest.

IN connection with another investigation, described in an accompanying article,[1] we found it desirable to consult infra-red spectra for some powdered, crystalline nitrates at low temperatures. Our objective in obtaining these low temperature spectra was primarily to ascertain which ones of numerous, weak components, appearing at lower frequencies in the spectra of our substances at ordinary temperatures, might be assigned to subtractive combinations of lattice modes with molecular modes. Because such combinations originate from excited states of the lattice, their intensities will be diminished by lowering its temperature; because the energies required for lattice excitation are low, drastic cooling is required in order to produce an easily discernible effect. We found that refrigeration with liquid air was adequate for our purpose, although further cooling would probably have been advantageous.

We are presenting the low temperature spectra here, along with a few comments that seem appropriate, in order to avoid too frequent digressions from the main subject of our other article. Further remarks concerning the significances of the low temperature spectra will be found in the text of that article.

EXPERIMENTAL METHOD

The specimen, a fine powder or microcrystalline mass, was deposited as a uniformly thick, adhering layer upon a sheet of silver chloride. This might have been done, depending upon the substance, by one of several familiar methods, such as sublimation, cooling of a melt, evaporation of solution or slurry, and the like.

The low temperature cell consisted of an ordinary cylindrical glass tube, about four inches long, closed with salt windows, wrapped with aluminum foil, fitted with a narrow side arm near one end and a wide, vacuum jacketed, vertical, side arm at the center. A rubber stopper served to seal the wide side arm. From the stopper a closed, copper can was suspended by means of two copper tubes, passing through holes in the former and entering into the latter. These tubes served as liquid air inlet and vent, respectively, for the can. From the bottom of the can emerged a U-shaped loop of copper tubing, whose ends terminated in the can. This loop was supplied with clamps to hold the silver chloride mounting and specimen tightly against it, positioned so that the light beam, incident normal to the plane of the loop, would pass through that portion of the specimen framed by the loop. Before fixing it in place, an edging of lead foil was pressed tightly onto the mounting with the pious hope that it would improve thermal contact. A spring loaded thermocouple was held in contact with the center of the specimen. After the whole had been assembled and sealed, the space interior to the glass envelope, exterior to the copper can and tubing, was evacuated through the narrow side arm to a pressure of about 0.1 mm Hg with a mechanical pump, and liquid air was introduced when desired into the copper can and tubing. The temperature of the thermocouple fell to −160°C, an upper limit for the sample temperature, and, if unwanted radiation was removed from the light beam with filters of MgO or sulfide-coated AgCl, this temperature could be maintained steadily during observations at the expense of about 600 cc of liquid air per hour, much of which was wasted in overflow and other extravagances of transport.

The spectrograph, its accessories, and the operating procedures were described in the companion article.

RESULTS

The spectra, at 25° and −160°C, for the same specimen of NH_4NO_3 are shown in Fig. 1 and Table I, those likewise obtained for $TlNO_3$ and $Pb(NO_3)_2$ in Fig. 2 and Tables II and III.

In all instances the specimens consisted of finely divided material. Accordingly, the observed transmittances may be affected by variations of scattering as well as absorption. The consequences of scattering will be unimportant except for possible Christiansen Filter Effects, which could be caused[2] by anomalous dispersion in the neighborhoods of the individual absorption bands.

The classical theory of the Christiansen Effect, as

* Publication assisted by the Ernest Kempton Adams Fund.
** University Fellow for the academic year 1948–49.
[1] R. Newman and R. S. Halford, J. Chem. Phys. **18**, 1276 (1950).
[2] For a recent discussion of this phenomenon, see W. C. Price and K. S. Tetlow, J. Chem. Phys. **16**, 1157 (1948).

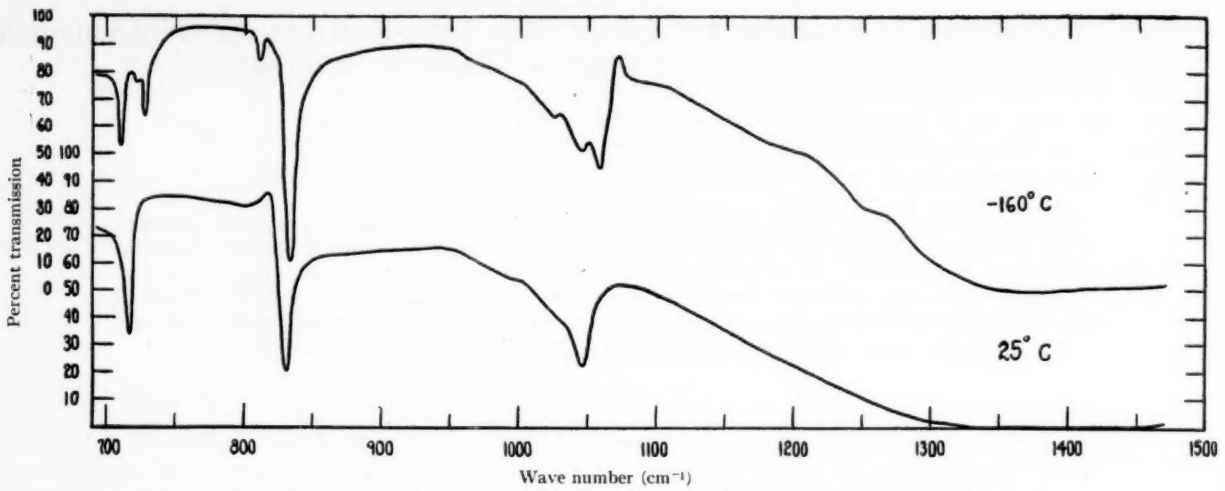

FIG. 1. Spectra of powdered NH_4NO_3 at 25°C and −160°C. Sample thickness about 50 microns.

presented[2] by Price and Tetlow, predicts that it will cause abnormally powerful scattering (low transmittance) at frequencies below, and abnormally weak scattering (high transmittance) at frequencies above the ones being absorbed. The abnormalities will diminish rapidly in magnitude upon moving in either direction away from a center of absorption. The consequence of these abnormalities of scattering usually will be to produce an unsymmetrical envelope of apparent absorption, including a peak of transmittance on the high frequency wing of the band, with the minimum transmittance displaced from the center of absorption always toward lower frequencies. The envelopes shown for $Pb(NO_3)_2$ in Fig. 2 are typical, in the vicinity of 725, of a small contribution of the expected effect.

Our concern with the Christiansen Effect is occasioned by the possibility that it could give rise to spurious components of envelope structure. In this regard, it seems altogether safe to say that the effect is in no way responsible for structure observed in the room temperature spectrum for $TlNO_3$, since the same structure was obtained with a polished, single crystal (see the *a* spectrum for this substance in Fig. 7 of the companion article[1]). The powder spectrum differs at most from the crystal spectrum by a slight asymmetry of envelope in the band at 715, an asymmetry that is too minor to be regarded as a source of spurious structure. The alterations produced in the spectrum of $TlNO_3$ at the lower temperature are not accompanied by any correspondingly spectacular onset of anomalous scattering and accordingly, are to be regarded as real manifestations of structure in the absorption.

In the case of $Pb(NO_3)_2$, except for the previously noted band at 725, the spectra appear otherwise free of asymmetries that would indicate the occurrence of anomalous scattering.

With NH_4NO_3 the envelopes near 716 in the spectra for both temperatures show only slight asymmetries, having similar magnitudes in bands with otherwise strikingly different structures. Comparison of these envelopes affords the conclusion that anomalous scattering cannot be responsible for the marked differences of structure at this place. In the envelope near 1050 we observe in Fig. 1 a peculiar asymmetry, including a peak of transmittance on the high frequency side, in the low temperature spectrum only. On the other hand, the recovery of transmittance on the low frequency side is more rapid and more complete in the low temperature spectrum than in the high temperature one, although the latter shows no striking amount of asymmetry. Accordingly, we conclude again that the increase of structure observed near 1050 at the low temperature manifests a real change of absorption, although the relative intensities and perhaps also the locations of the components of this structure may be in some measure spurious. Finally, the appearance of the envelope near 830 in the room temperature spectrum is inexplicable in terms of anomalous scattering. The asymmetry here is as peculiar as any previously noted but, because of the permutation of low and high transmittances, it cannot be attributed to anomalous scattering without contradicting the fundamental theory that has been invoked to account for the Christiansen Effect. Moreover, throughout the room temperature spectrum shown here for powdered NH_4NO_3, the frequencies of all the major centers of absorption are the same within experimental error as the ones found in the spectra for single crystals.

After weighing all of the evidence we believe that our conclusions are not likely to be erroneous on account of any spurious effects caused by anomalous scattering. We shall continue our remarks by referring to some significant details of the spectra for each substance individually.

NH_4NO_3

The spectra for this substance are strikingly, and surprisingly, different. Although this is not an unlikely

consequence of a phase transition[3] of the first order, and perhaps also another[3] of the second order, that intervenes between 25° and −160°, the degree of difference is surprising in view of results reported in another investigation. Keller and Halford[4] found seemingly identical spectra at −40° and −65°, both differing significantly with respect to intensities from the one found then and now at 25°, but not differing with respect to multiplicities from the one at room temperature. Although the resolving power employed by them was lower than the one we are now using, it was capable of indicating structure in the envelopes for $TlNO_3$ near both 715 and 1050, structure whose spacings at the former place are comparable with what we now find in the spectrum for NH_4NO_3. It seems, accordingly, that significant changes must occur in the spectrum of NH_4NO_3 at temperatures intermediate between −65° and −160°, whereas the phase transitions are reported[3] to occur at about −60° (second order) and −18° (first order). An investigation is being initiated to determine whether these discrepancies are instrumental only, or whether we are here presented with an opportunity to follow some new details in the thermal history of a second-order phase transition.

The two envelopes in Fig. 1 have enough resemblance near 1050 so that the one might be merely a better resolved version of the other, with spurious relative intensities resulting from anomalous scattering. It seems more likely, however, that the envelopes differ here also because of dissimilar internal configurations for the crystals at the two temperatures.

In view of the tendency exhibited at the lower temperature for broadening of the apparent envelope of absorption (1) by multiplication of structure and (2) by a more prominent contribution from anomalous scattering, it is significant that there is substantially

TABLE I. Frequencies (cm^{-1}) observed for powdered NH_4NO_3.

25°C	−160°C	Assignment[a]
—	710	
716	—	ν_4
—	~722	
—	728	
—	810	$\nu_2(N^{15}O_3)$?
830	833	ν_2
~990	~990	~−55
~1025	1025	
1046	1046	ν_1
—	1058	
—	~1100	~+55
—	~1190	~+145
—	~1260	~+215
1350 to 1450	1360 to 1400	ν_3, ν_4', $2\nu_4$

[a] Unprimed, boldface symbols denote fundamental modes of nitrate ion, primed ones those for ammonium ion. Positive numbers show spacing from nearest fundamental of lower frequency, negative numbers show spacing from nearest fundamental of higher frequency. Absolute values of these numbers are thought to be indicative of groups of frequencies for optical branches in lattice mode distribution.

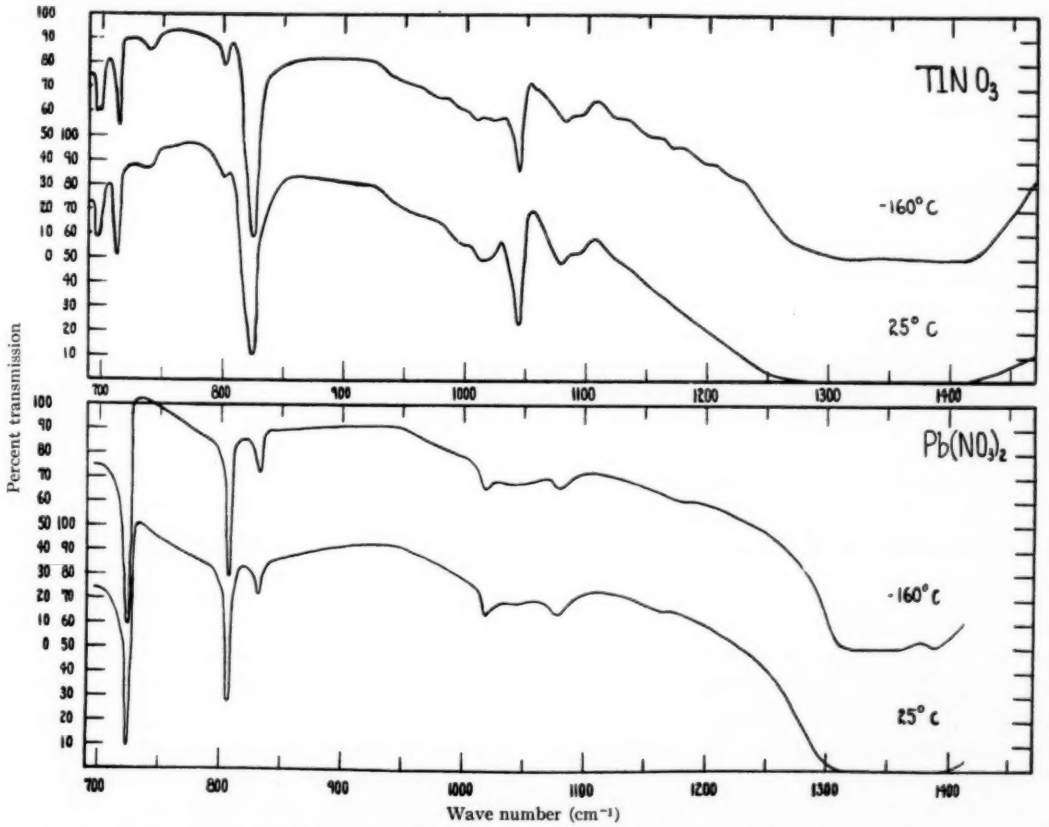

FIG. 2. Spectra of powdered samples of $TlNO_3$ and $Pb(NO_3)_2$ at 25°C and −160°C. Sample thickness about 50 microns.

[3] See reference 24 of accompanying article.
[4] See reference 17 of accompanying article.

TABLE II. Frequencies (cm^{-1}) observed for powdered $TlNO_3$ (γ).

25°C	−160°C	Assignment[a]
—	690	
697	—	ν_4
—	700	
713	714	
735	735	+35
800	800	$\nu_2(N^{15}O_3)$?
822	824	ν_2
960	960	−84
—	∼980	∼−64
—	∼997	∼−47
∼1000	—	∼−44
—	∼1008	∼−36
1015	—	−29
—	∼1024?	∼−20?
1044	1044	ν_1
1078	1078	+34
∼1085	∼1085	∼+42
∼1130	∼1128	∼+84
—	∼1155	∼+110
—	∼1170	∼+125
—	∼1200	∼+155
—	∼1225	∼+180
1280 to 1410	1320 to 1410	ν_3, $2\nu_4$

[a] See Table I.

TABLE III. Frequencies (cm^{-1}) observed for powdered $Pb(NO_3)_2$.

25°C	−160°C	Assignment[a]
723	723	ν_4
807	807	ν_2
831	831	ν_2
1018	1018	ν_1-31
1080	1080	ν_1+31
1190	1190	ν_1+140
1310 to 1400	1320 to 1360	ν_3, $2\nu_4$
—	1390	

[a] See Table I.

greater transmission between major bands at the lower temperature. This is what we would expect to observe if the major bands were superimposed upon a weak, diffuse background of combinations involving lattice modes, including combinations formed by difference. We conclude, accordingly, that such combinations are contributing to the envelopes at both temperatures, with the subtractive ones especially becoming less intense at the lower temperature.

The weak satellite at 810 is, if anything, intensified at the lower temperature. The intensification may be illusory, however, and result merely from removal of background accompanied by sharpening of absorption at this place.

$TlNO_3$

The spectra for this substance resemble each other very closely except for the improvement of resolution that is achieved by lowering the temperature. No phase transitions are known[5] to occur for this substance at any intervening temperature.

In the envelopes near 1050 we find unmistakable evidence for subtractive combinations. Whereas at the lower temperature there now appear to be no less than seven distinctly resolved satellites in the high frequency branch of this band, with similar intensities for the ones appearing at both temperatures, the satellites on the low frequency side have become weakened and, although more numerous at the lower temperature, they damp out as we proceed away from the band center.

The band appearing at 697 in the spectrum for the higher temperature becomes distinctly resolved into two, at 696 and 700, respectively, at the lower temperature. The significance of this observation is considered in our other article.[1]

The small bands at 735 and 800 appear to become intensified, if anything, at the lower temperature. This rules out the possibility that they originate with subtractive combinations although, as we mentioned before, their apparent intensifications may be illusory.

$Pb(NO_3)_2$

The spectra for this substance are included here because they contain several features of interest, ones that contrast strikingly with the other nitrates we have been considering. They were examined along with ones for the isomorphous $Ba(NO_3)_2$, wherein barium ion has a complete valence shell of electrons, in an effort to see whether the incomplete valence shell of thallous ion, isoelectronic with plumbous ion, might be responsible in any way for the remarkable fine structure observed in $TlNO_3$. The spectrum of the barium salt, not shown, was found to be quite similar to the one for the lead salt with the exception that the absorption and structure near 1050 was weaker This is indicative but, in view of the scarcity of fine structure in both substances, not very conclusive.

With $Pb(NO_3)_2$ we find in the band at 1050 that the central branch is now missing, that the fundamental is evidently forbidden to appear under the selection rules appropriate for this cubic crystal. There are, however, two side branches along with apparently diffuse absorption at the center and wings, indicating[6] the presence of numerous combinations with lattice modes in this vicinity.

A pair of bands is observed again at 807 and 831, almost exactly the same locations as for a pair in NH_4NO_3 (IV), but with the intensities radically altered from the previous ones. This seems to rule out the possibility[1] that the one at lower frequency belongs to an isotopic nitrate ion, but there may be a weak band of still lower frequency lurking in the shoulder that appears on the one at 807, inasmuch as this absorption is weaker now than heretofore.

The band at 1350, still very intense, is weaker than the corresponding ones shown for the other nitrates as is also the one at 807. On the other hand, the one at 723 is more intense here than in the spectra we have shown heretofore, illustrating once more the peculiar sensitivity[3,7] of the absorption by this latter fundamental to the environment of the nitrate ion.

[5] W. M. Latimer and J. E. Ahlberg, J. Am. Chem. Soc. **54**, 1900 (1932).

[6] See reference 5 of accompanying article.

[7] See also text of accompanying article.

Letters to the Editor

THIS section will accept reports of new work, provided these are terse and contain few figures, and especially few half-tone cuts. The Editorial Board will not hold itself responsible for opinions expressed by the correspondents. Contributions to this section should not exceed 600 words in length and must reach the office of the Managing Editor not later than the 15th of the month preceding that of the issue in which the letter is to appear. No proof will be sent to the authors. The usual publication charge ($8.00 per page) will not be made and no reprints will be furnished free.

A Test of Ideal Solution Laws for H_2, HD, and D_2. Vapor Pressures and Critical Constants of the Individual Components*

ROBERT D. ARNOLD AND HAROLD J. HOGE
National Bureau of Standards, Washington, D. C.
July 10, 1950

IN order to determine the approximate magnitude of the deviations from the law of ideal solutions in mixtures of H_2, HD, and D_2, dew-point pressures of several mixtures were observed at various temperatures. In these measurements a two-component gaseous mixture of known composition was forced in measured increments into an adiabatic calorimeter operated as a thermostatted container. The pressure in the container was then plotted as a function of the quantity of material admitted. These plots took the form of two straight lines of different slope, one in the gas-phase region and one in the gas-liquid region of the isotherm, joined by a rounded segment. The dew-point pressure of the mixture is taken to be the pressure at the junction of the two straight-line segments extrapolated to intersect. Table I contains the results.

The ortho-para-compositions were assumed to correspond to equilibrium at high temperature since no catalyst was used. This assumption is supported by the single-component condensation pressures (runs *E* and *H*) observed with this apparatus. Compositions shown in Table I were determined by measuring the pressure in the mixing vessel after the first gas was admitted and then again after the second. Mass spectrometric determinations of composition differed slightly from the values in Table I but were within the deviations shown. Traces of a third component in the binary mixtures were present as impurities (D_2 in HD and HD in D_2) and their amounts were determined by mass spectrometric analysis of the appropriate component before mixing.

Calculated pressures are based on the equation for the dew-point pressure of a mixture forming ideal solution, $1/P_d = Z_1/P_1 + Z_2/P_2 + Z_3/P_3$, which follows directly from the basic assumption that for a given component the mole fraction Z_i in the saturated vapor is proportional to x_iP_i, the product of the mole fraction in the liquid phase and the vapor pressure of the pure component, provided that the total pressure of saturated vapor is Σx_iP_i. Vapor pressures of the pure components are from the report by Woolley *et al.*[1] Principal sources of error are (1) in P_{calc} the uncertainty in the composition and (2) in P_{obs} the uncertainty in extrapolating the two straight lines to their intersection. Observed pressures are about three percent above those calculated from the equation. The estimated error in these deviations is about ±50 percent. Significant deviations from the law of ideal solutions in mixtures of ortho- and para-H_2 have been reported by Woolley *et al.*[2]

TABLE I. Dew-point pressures of mixtures of H_2, HD, and D_2.

Run	*E*	*F*	*G*	*H*	*J*	*K*	*L*
T(°K)	20.04	19.00	20.00	18.01	18.005	17.03	18.00
$Z_1(H_2)$	0	0.499	0.440	1.00	0.503	0.503	0.752
Z_2(HD)	0.008	0.004	0.004	0	0.496	0.496	0.248
$Z_3(D_2)$	0.992	0.497	0.556	0	0.001	0.001	0
P_{calc}(mm Hg)	224.3	224±2	313±2	347.2	234±2	154±2	279±2
P_{obs}(mm Hg)	223.5	234±2	322±2	348.2	240±1	158±1	286±1
ΔP (mm Hg)	−0.8	10±4	9±4	1.0	6±3	4±3	7±3
$100\Delta P/P$	−0.35	4.4	2.8	0.3	2.5	2.6	2.5

TABLE II. Vapor pressures and critical constants of $e-H_2$, HD, and $e-D_2$.

Property	$e-H_2$	HD	$e-D_2$
P at 25°K (atmos.)	3.242	2.124	1.457
P at 30°K (atmos.)	8.108	5.883	4.441
P at 35°K (atmos.)	—	—	10.286
P_c (atmos.)	12.77	14.64	16.28
T_c (°K)	33.00	35.91	38.26
V_c (cm³ mole⁻¹)	65.5	62.8	60.3
P_cV_c/RT_c	0.309	0.312	0.312

Vapor pressures and critical constants of H_2, HD, and D_2 (single-component systems only) were observed in a different apparatus capable of withstanding higher pressures. This apparatus and the methods of using it are described in a recent publication.[3] All measurements made thus far with this apparatus have been on material catalyzed to ortho-para-equilibrium at 20.4°K (except for HD, which has no ortho- and para-varieties). The prefixed symbol *e* is used to indicate material in equilibrium at this particular temperature. The catalyst was Nd_2O_3, a pale blue powder furnished by Dr. Raleigh Gilchrist and Mr. Ernest Weise of this Bureau. Complete conversion to ortho-para-equilibrium at 20.4°K appeared to take place in less than the time required to condense a sample on the catalyst and pump it off again. Table II contains the critical constants derived from the measurements, and also a few selected vapor pressures obtained from smooth curves representing the data. The critical pressures, temperatures, and volumes of HD and $e-D_2$ are thought to be the first experimental values to be reported. It is planned to make measurements on normal hydrogen ($n-H_2$) such as have now been made on $e-H_2$, HD, and $e-D_2$, after which complete reports covering all our work on dew points of mixtures, vapor pressures, and critical constants will be submitted for publication in *J. Research NBS*. The critical constants in Table II were derived after plotting isotherms of log$P$ *vs.* log$V$ for the critical region of each modification. The three sets of curves were superposed in such a way as to form one single family of isotherms, after which a single reduced critical point was determined simultaneously for the entire family. Accepting the law of corresponding states $\log(P/P_c)$ should, for any given value of T/T_c, be a universal function of $\log(V/V_c)$. The relative displacements of the three sets of curves take into account the differences in the values of logP_c and logV_c for the various modifications. It is thought that the use of this procedure substantially improved the accuracy of the critical constants in Table II. Correlation with isotherms of $n-H_2$ may subsequently lead to minor changes in the values now being reported; also the data in Table II have not been corrected for the presence of the small amounts of isotopic impurities detected by the mass spectrometer. Effects of such corrections will probably be no more than a few units in the last decimal place. In the V_c values the last decimal place is significant only on a relative basis.

The HD was prepared, and the HD and D_2 purified, by A. Fookson, P. Pomerantz, and E. H. Rich of this Bureau by methods to be described in *Science* and in *J. Research NBS*. Mass spectrometer analyses were made by the Mass Spectrometry Section of this Bureau.

* Supported in part by the AEC.
[1] Woolley, Scott, and Brickwedde, J. Research Nat. Bur. Stand. **41**, 379 (1948), RP1932.
[2] See reference 1, p. 454.
[3] Harold J. Hoge, J. Research Nat. Bur. Stand. **44**, 321–45 (1950), RP2081.

Cerium Oxyfluoride and Its Lattice Structure

WOLFGANG FINKELNBURG AND ADAM STEIN
Engineer Research and Development Laboratories, Fort Belvoir, Virginia
June 29, 1950

SOME years ago, Klemm and Klein[1] published a note according to which lanthanum oxyfluoride LaOF can be produced by heating a mixture of LaF_3 and La_2O_3 for one hour at 900°C in high vacuum. They found that the new compound crystallizes in a cubic lattice with a lattice constant $a=5.756\pm0.003$A. This lattice constant increases up to 5.82A if an excess of fluorine is dissolved in the LaOF.

In a still unpublished investigation, H. Stintzing at Darmstadt (1942–1944) confirmed these results and extended them by studying also high intensity carbon cores in which fluorides and oxides of the rare earths are used after extensive baking. Diffraction patterns of these cores revealed two lines indicating a cubic lattice with a lattice constant 5.70 ± 0.01A, i.e., somewhat smaller than that of the pure LaOF. While Stintzing assumed that this diminished lattice constant was caused by the participation of cerium in the oxyfluoride lattice, he was not able to find more than traces of two CeOF lines when he started with pure CeF_3 and baked it in a rarified atmosphere at high temperatures with or without carbon. He concluded that CeOF was of low stability and that, in contrast to LaF_3, CeF_3 has little inclination to form CeOF in the presence of oxygen.

Without detailed knowledge of Stintzing's results, a complete report of which has become available only after the main part of our studies had been carried out, we have made extensive x-ray diffraction studies of the rare earth oxides and fluorides in isolated form and in carbon mixtures, after they had been subjected to different heat treatments. The investigation was carried out with a General Electric x-ray diffraction instrument using a copper tube and a camera of 71.6 mm radius. Apparently our resolving power was higher than that of Stintzing as, in contrast to his statement, we could easily resolve the lines of substances with a lattice constant difference of as little as 0.03A. In further contrast to Stintzing who could not discover any graphite lines and only two LaOF lines, we found all the 14 oxyfluoride lines of cerium and lanthanum which are expected theoretically for scattering angles below 120°, in addition to the six strongest graphite lines (in mixtures with graphite) which, being very sharp, could be used as calibration lines. For the purpose of checking this calibration, or whenever graphite was not present or not in sufficient concentration in the samples, small amounts of pure CeO_2 or TlCl were added to the substances under investigation. As samples, tiny cylinders of 0.15 to 0.2 mm diameter were used which were made from the material under investigation, with a small amount of Duco cement as binding material.

The essential result of this study is that cerium oxyfluoride CeOF exists as a stable compound. It has a face-centered cubic lattice of the CaF_2 type with a lattice constant which, depending on the amount of fluorine dissolved in the lattice, varies from 5.66 to 5.73 ± 0.01A, with reference to the CuK_α line 1.539A.

We succeeded in producing pure cerium oxyfluoride by baking mixtures of CeO_2 and CeF_3 in a small carbon arc furnace from 5 to 30 minutes at temperatures which are believed to be of the order of 3000°K. Quantitative transformation could be obtained if the mixture was chosen correctly. However, in agreement with Stintzing, we were not able to produce CeOF by oxidation of CeF_3. There is, consequently, a marked difference in the chemical behavior of the corresponding compounds of lanthanum and cerium. Whereas LaOF could be produced, by Stintzing, by oxidation of LaF_3, cerium oxyfluoride CeOF apparently can be produced only by reduction of CeO_2 with fluorine. Oxidation of CeF_3, on the other hand, always led directly to CeO_2. The influence of oxygen on the two oxyfluorides is very different also. Whereas baking at 1200°C for two hours in oxygen did not affect LaOF appreciably, temperatures above 300°C were sufficient for quantitative transformation of CeOF into CeO_2. To check this result in more detail, samples of CeOF were heated for one hour each at different temperatures in air. Whereas at 200°C only slight indications of CeO_2 lines could be found in addition to the strong CeOF lines, the strength of CeOF and CeO_2 lines was approximately the same after baking for one hour at 260°C. After baking at temperatures above 320°C, finally, only traces of CeOF lines were found besides the CeO_2 lines.

We appreciate greatly the help of Mr. S. M. Segal in the final experiments, particularly after one of us (A.S.) had to give up the work prematurely.

[1] W. Klemm and H. A. Klein, Zeits. f. Anorg. Chemie **248**, 167 (1941).

The Magnetic Susceptibility of Tungsten Bronzes

F. KUPKA AND M. J. SIENKO
Baker Laboratory of Chemistry, Cornell University, Ithaca, New York
June 28, 1950

STRAUMANIS *et al.*[1] have assumed that the yellow sodium tungsten bronzes of composition $NaWO_3$ contain tungsten in the pentavalent state and that the red, violet, and blue bronzes, which are deficient in sodium, correspond to solid solutions of WO_3 in $NaWO_3$ with varying ratio of W(V) to W(VI). We have determined the magnetic moment of several bronzes in order to cast more light on the probable oxidation state of tungsten in these systems.

Sodium and potassium tungsten bronzes were prepared by reduction with hydrogen of a molten mixture of tungstic oxide (WO_3) and the corresponding alkali metal tungstate (M_2WO_4). The composition of the sodium bronzes was determined by x-ray analysis as suggested by Straumanis;[1] that of the potassium bronze, by chemical analysis for potassium and for tungsten. Magnetic susceptibilities were measured by the Gouy method using an electromagnet at field strength 9000 gauss. The field strength was determined by calibration with standard nickelous chloride solution. The observed values for the susceptibility per gram atom of alkali metal are given in the first line of Table I.

In calculating the theoretical susceptibility expected for a mixture of W(V) and W(VI), it is assumed that the orbital contribution to the magnetic moment is *not* quenched and, therefore, the "spin-only" treatment does not hold. Such non-perturbation of the multiplet structure seems to be fairly common with the heavier transition metals,[2] especially in octahedrally symmetrical crystalline fields such as obtain in these bronzes. Assuming Russell-Saunders coupling of the orbital and spin contributions, the expected moment for the W(V) ion is 1.55-bohr magnetons. The susceptibilities given in line 2 of Table I include corrections for the diamagnetic contribution of Na^+, K^+, $O^=$, W^{+5}, and excess WO_3. It is evident that the observed susceptibilities are considerably lower than those predicted on the assumption these bronzes contain pentavalent tungsten. Similarly, the observed susceptibilities are lower than those predicted for a mixture of W(IV) and W(VI).

The low magnetic susceptibility reported here together with the striking electrical properties described by Straumanis and Dravnieks[3] leads us to suggest that the alkali metal tungsten bronzes are actually solutions of the alkali metal in WO_3 with the alkali metal more or less completely dissociated into diamagnetic ions and free electrons. In such case, the magnetic behavior should

TABLE I. Magnetic susceptibility of tungsten bronzes per gram atom of alkali metal.

	$Na_{0.554}WO_3$ (21°C)	$Na_{0.936}WO_3$ (27°C)	$K_{0.93}WO_3$ (21°C)
Observed	5.8×10^{-6}	15.3×10^{-6}	194×10^{-6}
Calculated for W(V)	960×10^{-6}	940×10^{-6}	940×10^{-6}
Calculated for W(IV)	510×10^{-6}	510×10^{-6}	500×10^{-6}
Calculated for an electron gas	-10.9×10^{-6}	-5.8×10^{-6}	$-18.6\times10^{-}$

be predictable on the basis of an electron gas. Using Pauli's well-known equation[4] for the magnetic susceptibility of an electron gas and correcting for the Landau diamagnetism[5] we predict, after correcting for diamagnetic alkali metal ions and WO_3, the values given in line 4 of Table I for the magnetic susceptibility of the tungsten bronzes per gram atom of alkali metal.

The correspondence between the observed and calculated values is remarkably good, considering that even slight binding of the free electrons to the alkali metal ion introduces a paramagnetic correction to the values calculated on the basis of completely free electrons. The large disagreement, observed in the case of the potassium bronze, may be due to the greater polarizability of the potassium ion with consequent greater binding of the free electrons. The agreement in the case of the sodium bronzes is fully as good as that found for the pure alkali metals and better than that found for a saturated solution of sodium in liquid ammonia.[6]

Further work on these and other bronzes is in progress.

We are indebted to Dr. E. O. Brimm of Linde Air Products Company for sending us samples of the yellow and blue sodium bronzes. These bronzes were prepared by reduction with tungsten of a mixture of WO_3 and Na_2WO_4. Measurements on them are included in our results.

[1] M. E. Straumanis, J. Am. Chem. Soc. **71**, 679 (1949). This paper contains references to earlier work.
[2] J. H. Van Vleck, *The Theory of Electric and Magnetic Susceptibilities* (Oxford University Press, London, 1932), p. 312.
[3] M. E. Straumanis and A. Dravnieks, J. Am. Chem. Soc. **71**, 683 (1949).
[4] W. Pauli, Zeits. f. Physik **41**, 81 (1927).
[5] L. Landau, Zeits. f. Physik **64**, 629 (1930).
[6] Yost and Russell, *Systematic Inorganic Chemistry* (Prentice-Hall, Inc., New York, 1946), p. 143.

Chemical Reactions in a Magnetic Field

SONIA COLLINS AND W. A. BRYCE
Department of Chemistry, University of British Columbia, Vancouver, Canada
July 7, 1950

THE possible effects of applied magnetic fields on chemical reactions have been investigated in some detail[1,2] and in general it has been concluded that such effects, if they exist at all, are not great. Bhatnagar reported that the rates of certain inorganic reactions could be altered by approximately one percent by fields of the order of 10,000 gauss. However, Schmid, Muhr, and Marek[3] have reported that when styrene was polymerized at 80°C in a field of 16,000 gauss, an eightfold reduction in rate was observed. An explanation has been suggested for this phenomenon based on an orientation by the field of the spin moments of the unpaired electrons.[4]

The experiment reported above has been reinvestigated in this laboratory and the investigation has been extended to other reactions. An electromagnet was used which could provide a field of 14,000 gauss across a 1-in. pole space. The reactions in the field took place in a flat Pyrex cell under an inert atmosphere. This cell and a control removed from the field were maintained at a temperature of 80±0.3°C in a suitable thermostat. A field of 12,000 gauss was used for all experiments reported here.

Benzoyl peroxide is an effective catalyst for the polymerization of styrene and accordingly the effect of the field on the decomposition of this substance was investigated. Two grams of the peroxide were dissolved in 100 g of toluene and the reaction was followed until the peroxide was 70 percent decomposed. No measurable effect of the field could be observed, a result which agrees with that reported recently by Leffler[5] for a field of 7518 gauss. The catalyzed polymerization was then studied using 2.00 g of peroxide per liter of styrene. The results are given in Table I. The uncatalyzed polymerization of styrene was studied under the conditions described and also in a number of experiments in which carefully purified styrene was sealed in ampoules in the absence of air. In none of these experiments on the polymerization of styrene in a field of 12,000 gauss was any measurable effect of the field observed. A similar result has recently been reported by Breitenbach and Richter.[6]

The decomposition of hydrogen peroxide in a field of 12,000 gauss was also examined and no significant effect of the field on the rate of the reaction could be detected.

TABLE I. The polymerization of styrene in a magnetic field of 12,000 gauss.

Time (hr.)	Percent conversion in field	Percent conversion in control
1	11.2	11.4
2	19.9	20.0
3	28.1	28.2
4	35.7	35.9

[1] Selwood, Chem. Rev. **38**, 41 (1946).
[2] Bhatnagar, Mathur, and Kapur, Phil. Mag. **78**, 457 (1929).
[3] Schmid, Muhr, and Marek, Zeits. f. Electrochemie **51**, 37 (1945).
[4] J. E. Leffler and M. J. Sienko, J. Chem. Phys. **17**, 215 (1949).
[5] J. E. Leffler, J. Chem. Phys. **17**, 741 (1949).
[6] Breitenbach and Richter, Monats. f. Chem. **80**, 315 (1949).

The Barrier to Internal Rotation in Methylfluoroform

H. S. GUTOWSKY AND H. B. LEVINE*
Noyes Chemical Laboratory, University of Illinois, Urbana, Illinois
July 27, 1950

SOME uncertainty exists in published values[1–4] for the barrier to internal rotation in methylfluoroform, CH_3-CF_3. We have re-examined its infra-red spectrum, particularly the critical long wave-length region to 300 cm^{-1}. Measurements were also made of the temperature dependence of several of the lower frequency bands as an aid in frequency assignment. Possible indirect values for the torsional frequency were obtained from combination and difference bands. The corresponding barriers were then compared with the statistical values for the barrier, computed from the fundamental frequencies in conjunction with recent structural data[5–7] and the calorimetric entropy.[1] Two internally consistent sets of frequency assignments are proposed. They lead to barriers of 1740, 2000 and 3210, 2800 cal./mole; the value 3000±200 cal./mole is considered more probable.

The spectrum of the gas was observed to 400 cm^{-1} with a Perkin-Elmer 12B spectrometer. The KRS-5 region from 400 to 300 cm^{-1} was run on a similar instrument at M.I.T. through the courtesy of Dr. M. Kent Wilson of Harvard and Mr. R. S. McDonald of M.I.T. The sample of methylfluoroform was furnished by Dr. A. F. Benning, du Pont and Company. The spectrum observed agrees in most regards with that reported previously.[2] The temperature dependence of absorption listed in Table I was obtained in a sealed 7-cm gas cell[8] at a room-temperature pressure of 45 cm.

The various assignments of fundamentals are given in Table II and the Raman and infra-red spectra below 1200 cm^{-1} are given in detail in Table III. Concerning the A_1 assignments, the CH_3 bending, ν_2, is 1375[-1] in ethane[9] and 1378 cm^{-1} in methylchloroform,[9] CH_3-CCl_3. Of the two bands, 1279 and 1410 cm^{-1}, nearest these values, 1410 cm^{-1} is most likely ν_2. This leaves the 1279

TABLE I. Temperature dependence† of some infra-red bands of CH_3-CF_3.

Band cm^{-1}	Percent transmission 20°C	130°C	190°C	Assignment
818	20	26	35	fundamental
829	12	13	17	fundamental
842	18	27	32	fundamental
910	62	46	32	difference band
1013	19	14	12	difference band
1090	40	30	19	difference band

† Qualitative observations of the weak 541 and 732 cm^{-1} bands revealed an increase in transmission over the same temperature range, indicating that they are not difference bands.

TABLE II. Assignments of fundamental frequencies for CH_3-CF_3.

Species	Description		Reference 1	Reference 2	This research
A_1	C−H stretching	ν_1	2974 cm^{-1}	2974 cm^{-1}	2974 cm^{-1}
	CH_3 bending	ν_2	1450	1278	1410
	C−F stretching	ν_3	968	1135	1279
	C−C stretching	ν_4	829	828	829
	CF_3 bending	ν_5	603	540	605
A_2	torsion	ν_6	—	—	(172; 218)
E	C−H stretching	ν_7	3040	3040	3041
	CH_3 deformation	ν_8	1450	1412; 1450	1450
	C−F stretching	ν_9	1279	1230	1230
	CH_3 rocking	ν_{10}	1025	606	(1185; 966)
	CF_3 deformation	ν_{11}	541	968	(966; 541)
	CF_3 rocking	ν_{12}	368	368	370

cm^{-1} band for the C−F stretching, ν_3, for which the corresponding frequencies in fluoroform,[7] CHF_3, and perfluoroethane,[10] C_2F_6, are 1209 and 1420 cm^{-1}. Similarly, for the CF_3 bending, ν_5, the assigned values in fluoroform and perfluoroethane are 509 (or 703) and 809 cm^{-1}; the strong methylfluoroform band at 605 cm^{-1} has an attractively close value.[11]

Perhaps the least certain part of the assignment concerns the 541, 966, and 1185 cm^{-1} bands from which the E fundamentals ν_{10} and ν_{11} must be chosen. The vibrational mode in methylchloroform equivalent to ν_{10} has been assigned as 1179 cm^{-1}, and in ethane the E_u and E_g assignments are 821.5 and 1190 cm^{-1}. While part of the absorption by methylfluoroform about 970 cm^{-1} may be the combination 605+370 cm^{-1}, the complex band structure suggests overlapping with what must be a fundamental. If 1185 cm^{-1} is taken as ν_{10}, then ν_{11} is 966 cm^{-1}. On the other hand, in perfluoroethane the values assigned to the E_u and E_g vibrations similar to ν_{11} are 522.5 and 620 cm^{-1}, strongly suggesting 541 cm^{-1} as ν_{11}. The only factor against this interpretation is the uncertain band structure and weakness of the infra-red absorption.

TABLE III. Assignments of frequencies below 1200 cm^{-1} in CH_3-CF_3.

Raman[1] cm^{-1}	Infra-red Reference 2	Infra-red This research	Assignment
368 (2)		356, 371, 379 m	ν_{12}
541 (2s)	540	543 mw	172+ν_{12} or ν_{11}
603 (2s)	593, 606, 616 s	593, 605, 616 s	ν_5
	733?	732 w	$2\nu_{12}$
		747 vw	ν_3−541 or 966−219
829 (5s)	818, 828, 840 s	818, 831, 843 s	ν_4
	889, 900 s		impurity?
968 (3)	910, 953, 964, 971, 978	910 w, 962, 967, 974, 980 vs	$\nu_3-\nu_{12}$; ν_{11} or ν_{10}; overlapped by $\nu_8+\nu_{12}$
	1004 w		impurity?
	1013	1013 w	1185−172 or ν_9−217
1025 (2d)?		1030 vw	$\nu_3-\nu_{12}$
		1090 w	$\nu_8-\nu_{12}$
	1125, 1135, 1143 s		impurity
	1177, 1184, 1191	1173, 1187, 1198 m	ν_{10} or 966+219

The recent structural data[5-7] give a value for Sr of 22.16 e.u. at 224.40° and 0.9330 atmos. Combining this with the previous data and using the same methods[1] for calculation, the two sets of fundamentals give statistical values of 2000 and 2800 cal./mole for the barrier. The indirectly inferred torsional frequencies of 172 and 218 cm^{-1} yield barrier heights of 1740 and 3210 cal./mole from the relation $V_0 \cong 8\pi^2 I_A \nu_t^2/3^2 h$. Both methods assume the usual $(V_0/2)(1-\cos 3\phi)$ potential curve.[4] Since the second assignment is considered more likely, the barrier value of 3000±200 cal./mole is preferred.

* Department of Chemistry, University of Chicago, Chicago, Illinois.

[1] Russell, Golding, and Yost, J. Am. Chem. Soc. **66**, 16 (1944).
[2] H. W. Thompson and R. B. Temple, J. Chem. Soc. **1948**, 1428 (1948).
[3] Dailey, Minden, and Schulman, Phys. Rev. **75**, 1319 (1949). In a recent private communication, Dr. Dailey stated that new results indicate an upward revision of the torsional frequency to 230±20 cm^{-1}, indicating a barrier of 3120±550 cal./mole.
[4] E. Blade and G. E. Kimball, J. Chem. Phys. **18**, 630 (1950).
[5] W. F. Edgell and A. Roberts, J. Chem. Phys. **16**, 1002 (1948).
[6] L. G. Smith, J. Chem. Phys. **17**, 139 (1949).
[7] H. J. Bernstein and G. Herzberg, J. Chem. Phys. **16**, 30 (1948).
[8] F. A. Miller and S. D. Koch, Jr., J. Am. Chem. Soc. **70**, 1890 (1948).
[9] K. W. F. Kohlrausch, *Ramanspectren* (Becker and Erler, Leipzig, 1943), p. 173.
[10] Nielsen, Richards, and McMurry, J. Chem. Phys. **16**, 67 (1948).
[11] In a private communication, Professor J. Rud Nielsen suggested an assignment of fundamentals identical with our second except for the torsional frequency. His results include Raman polarization data so ν_5 is undoubtedly 605 cm^{-1}.

Infra-Red Data on Epoxy Structures

J. E. FIELD, J. O. COLE, AND D. E. WOODFORD
Research Laboratory, Goodyear Tire and Rubber Company, Akron, Ohio
June 30, 1950

OUR interest in the identification of epoxy groups by infra-red absorption methods was initiated by our studies of the structural changes resulting from oxidation of GR-S. One of these studies was an attempt to follow the structural changes resulting from the reaction of the double bonds in GR-S with perbenzoic acid.[1] Another concerned the hydroperoxide theory of autoxidation of Gr-S and other elastomers in which the epoxy group is involved.[2]

According to the results of other investigators,[3,4] it has been shown that absorption frequencies resulting from the epoxy group in ethylene oxide occur at approximately 865 cm^{-1}, 1165 cm^{-1}, and 1265 cm^{-1}. Since these frequencies result from absorptions by relatively simple molecules, it was thought that more reference data should be obtained from more complicated hydrocarbon compounds containing the epoxy structure. Accordingly, the authors have investigated the absorption spectra of the following compounds:

propylene oxide	styrene oxide
tetramethylethylene oxide	cyclohexene oxide
trimethylethylene oxide	butadiene monoxide
isobutylene oxide	sym. dimethylethylene oxide.

Although absorption bands were found in the spectra of the above compounds at the frequencies indicated for the epoxy group in the simple ethylene oxide molecules, only the 1250 cm^{-1} band could be identified with reasonable certainty as being characteristic of this molecular group. In the spectra of the eight compounds investigated an absorption band was consistently found in the frequency range 1240 cm^{-1} to 1260 cm^{-1}. Although bands were found in the other spectral regions, their use for identification purposes is less certain because of the increased number of possible C−C vibrational frequencies and C−H rocking frequencies arising from these larger molecules.

[1] Field, Cole, and Woodford, private communication to Rubber Reserve, December, 1947.
[2] J. O. Cole and J. E. Field, Ind. Eng. Chem. **39**, 174 (1947).
[3] G. Herzberg, *Infra-Red and Raman Spectra* (D. Van Nostrand Company, Inc., New York, 1945), p. 172.
[4] L. G. Bonner, J. Chem. Phys. **5**, 704 (1937).

Observation of Discrete Bands in the Near Ultraviolet Absorption Spectrum of Liquid Ethylene

C. REID
National Research Council, Ottawa, Canada
July 19, 1950

THE absorption spectrum of liquid ethylene at a temperature of about 120°K, in the region 2000 to 4000A, has been examined with optical paths up to 2.5 meters using a medium Hilger quartz spectrograph. With a path of 1.25 meters, the continuous absorption, which was followed in the vapor phase by Allsop and Snow[1] up to about 2200A, extends to about 2600A and here is overlapped by diffuse bands which have been followed up to 3400A by increasing the path length to 2.5 meters (four traversals through a 62-cm column). These bands are shown in Fig. 1. The slow decrease in intensity with increasing wave-length makes it very probable that, even with 2.5-m path length, we are still far from the O—O band of the system.

The bands have an average spacing of 995 cm^{-1} and show no appreciable convergence. The band centers (± 40 cm^{-1}) are at 29,802, 30,758, 31,729, 32,710, 33,698, 34,686, 35,610, 36,583, 37,540, and 38,476 cm^{-1}. The last of these bands is faint, and its position only approximately estimated. At much shorter wavelengths (just below 2000A) Wilkinson and Johnston[2] have recently observed bands showing very similar structure to the ones we have found.

Careful investigation of the region below 2600A, with shorter path lengths, showed no trace of structure. In the banded region the absorption coefficient $(1/lc)\log(I_0/I)$ is approximately 10^{-4}. This means that the transition is a highly forbidden one. The most probable interpretation is that the bands belong to the $T \leftarrow N$ electronic transition (Mulliken's notation[3,4]) from the ground state N to the lowest triplet level T. This transition is not only forbidden by the non-intercombination selection rule, but is also quite strongly Franck-Condon forbidden in the region observed.

Following the considerations of Mulliken and co-workers[3,4] we assume that the triplet state is stable in the perpendicular form. Accordingly the potential curve relationships are as shown in Fig. 2. Application of the Franck-Condon principle then shows immediately that the C=C twisting vibration will be strongly excited. Therefore, we may interpret the observed band separation of 995 cm^{-1} as the upper state twisting frequency. It is clear from Fig. 2 that the O—O transition is so highly forbidden that we are very unlikely to reach it.

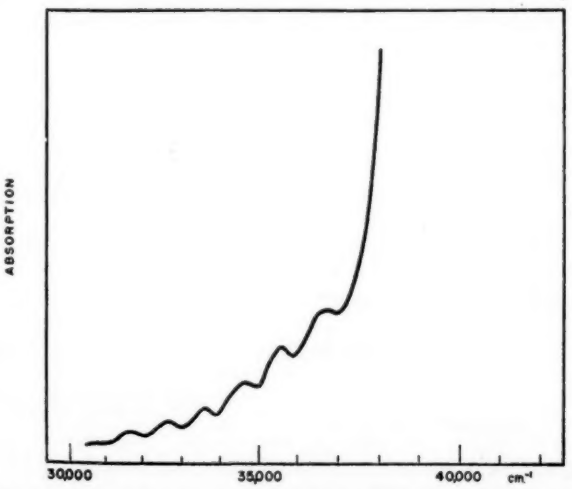

FIG. 1. Densitometer trace of part of the banded region of absorption in ethylene. Path length 1.4 meters of liquid.

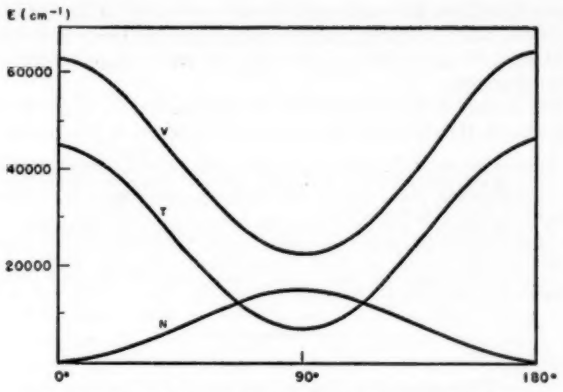

FIG. 2. Potential diagram for N, T, and V states of ethylene (after Mulliken).

Although some considerations[5,6] put the energy of the O—O transition to the lowest triplet level quite close to our observed bands (around 4000A), the weight of evidence suggests that the energy of the triplet state in its perpendicular equilibrium form is only about 20 kcal. above the ground state.[7]

An attempt was made to detect the transition from the upper state of the new bands to the ground state, using the low temperature glass phosphorescence technique of Lewis and Kasha.[8] No emission was observed in the region from 3000A to 10,000A which was examined. This negative result is consistent with a low lying triplet state from which emission would be in the infra-red beyond the photographic region.

It has been pointed out to the author by M. Kasha and R. S. Mulliken that the observed bands may not be due to the $T \leftarrow N$ transition but instead to a $V \leftarrow N$ transition.[3,4] Such a transition is not forbidden by the non-intercombination selection rule, but since the V state is also stable in the perpendicular form it may be seen from Fig. 2 that transitions in the observed energy range are extremely highly Franck-Condon forbidden.

Although it is not possible unambiguously to decide which interpretation is correct without more accurate intensity measurements throughout the range 2000 to 3500A, the first explanation seems the more probable. If the banded region is part of the $T \leftarrow N$ transition then the continuous absorption from 2000 to 2600A must be the "tail" of the $V \leftarrow N$ absorption band which has its maximum at 1630A.

Very rough intensity considerations support this view. An examination of Fig. 2 shows that if absorption to the V state occurs at 2500A it must do so from a non-equilibrium ground state position in which the molecule is twisted through an angle of 45 to 50°. A simple harmonic oscillator approximation shows that at this angle the ground state wave function has decreased from its value at the position of zero twist by a factor $\simeq 10^3$. Since the transitions under consideration are to upper states with quite high vibrational quantum numbers we may assume in first approximation that the wave functions in these upper states all make approximately equal contributions to the transition probability integrals. Thus the transition probability from a ground state with a given angle of twist becomes proportional to the square of the value of ground state wave function at that angle of twist. It is to be noted that twisting does not alter the symmetry selection rules, since the group V remains throughout the common point group of the upper and lower states. The intensity at 2500A will therefore be reduced from its value at zero twist by a factor 10^6. The observed value, $\epsilon = 10^{-3}$, in this region is in fact lower by a factor of about 10^7 than the value observed at the maximum by Wilkinson and Johnston.[2]

Similar considerations show that the observed bands of the $T \leftarrow N$ transition are produced by absorption from a ground state with angle of twist 20 to 30°, and put the reduction of intensity from the maximum value as about 100 to 1000. At its maximum

value, therefore, the molar absorption coefficient is between 0.1 and 0.01. Since in this region the intensity of the $V \leftarrow N$ transition is at least 10 times greater than this we cannot hope to observe this maximum.

The author is indebted to Dr. M. Kasha, Dr. R. S. Mulliken, and Dr. G. Herzberg for illuminating discussions of this problem.

[1] C. P. Snow and C. B. Allsop, Proc. Roy. Soc. London **A200**, 272 (1950).
[2] P. G. Wilkinson and H. L. Johnston, J. Chem. Phys. **18**, 190 (1950).
[3] R. S. Mulliken, Phys. Rev. **41**, 751 (1932); J. Chem. Phys. **7**, 14 (1939); Rev. Mod. Phys. **14**, 265 (1942).
[4] R. S. Mulliken and C. C. J. Roothan, Chem. Rev. **41**, 219 (1947).
[5] D. P. Craig, Proc. Roy. Soc. London **A200**, 272 (1950).
[6] G. N. Lewis and M. Kasha, J. Am. Chem. Soc. **66**, 2100 (1944).
[7] See, for example, reference 4, and also Magee, Shand, and Eyring, J. Am. Chem. Soc. **63**, 677 (1941).

Ultrasonic Absorption in the Critical Temperature Region

W. G. SCHNEIDER
National Research Council, Ottawa, Canada
June 30, 1950

IN the course of an investigation of the behavior of the sound velocity in the critical temperature region, a high acoustic absorption has been observed which is believed to be characteristic of this region. Figure 1 shows a plot of both the sound velocity curve and the absorption curve for sulfur hexafluoride in the neighborhood of the critical point. The absorption coefficient plotted is the absorption coefficient per wave-length defined by

$$A = A_0 e^{-\alpha\chi/\lambda},$$

where A_0 is the initial amplitude and A the amplitude at a distance χ measured in wave-lengths. The critical temperature, T_c, is the temperature of meniscus disappearance. At this temperature the sound velocity curve has a minimum, and the absorption coefficient reaches a maximum value. It is noteworthy that the region of anomalous absorption extends over a temperature interval of roughly one degree, and begins approximately 0.3° below the temperature of meniscus disappearance.

The velocity curve below the critical temperature is that for the liquid phase and the measurements were made at a point at least 2 cm below the meniscus. All measurements were made with a single filling of the interferometer, the filling corresponding to the critical density. The meniscus disappeared at the center, i.e., halfway up the tube in which the measurements were made. Each measurement was made only after thermostatting at a given temperature to within ±0.002°C for at least 12 hr. Taking readings in this manner at successively higher temperatures gave the points indicated by the upright triangles on the absorption curve. After the highest temperature above T_c was reached, the temperature was then lowered in steps, and at each temperature readings were

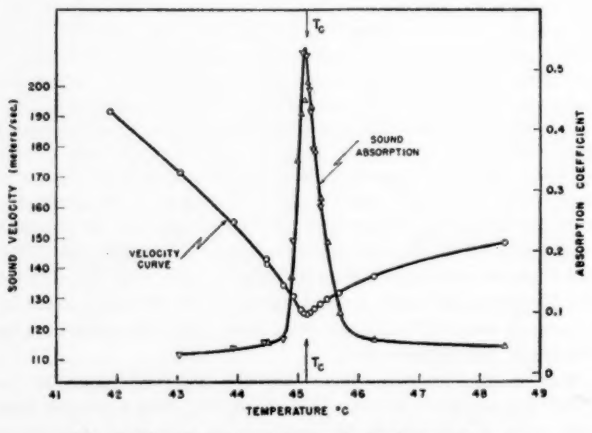

FIG. 1. Plot of sound velocity and sound absorption as functions of temperature.

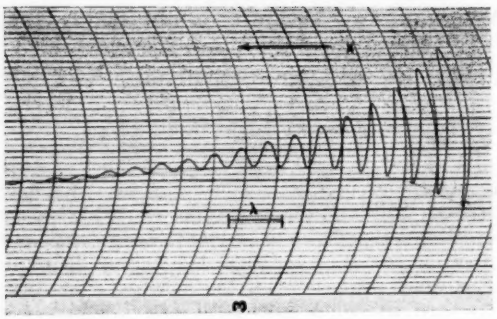

FIG. 2. Resonance peaks close to T_c.

taken only after thermostatting 24 hr. These points are indicated by the upside-down triangles. Accordingly, the absorption measurements carried out in this manner appear to be reversible with respect to temperature. The temperature of reappearance of the meniscus was approximately 0.02° lower than the temperature of meniscus disappearance.

The measurements were carried out with a double crystal acoustic interferometer at a frequency of 600 kc. The acoustic chamber consisted of a heavy walled glass cylinder to permit observations of the meniscus and the positions of the transmitting and receiving crystals. The receiving crystal was moved along the chamber by means of a synchronous motor drive and the voltage on the receiving crystal was amplified and automatically recorded by a pen and paper recorder. Figure 2 shows a record of the resonance peaks obtained at a point very close to T_c.

Several interpretations are possible for the absorption curve shown in Fig. 1. These will be discussed in a forthcoming publication.

The Angle-Angle Interaction in the Vibration Potential Function of Pyramidal Molecules

LOUIS BURNELLE AND JULES DUCHESNE
Department of Chemical Physics, University of Liège, Belgium
July 17, 1950

RECENTLY Duchesne and Ottelet[1] computed with accuracy the most general valence-force potential function controlling the fundamental vibrations of the NH_3 and AsH_3 pyramidal molecules. It was shown, in particular, that the constant g_4 for the angle-angle interaction is negative and very small. However, in contrast to the various studies devoted to the length-length and length-angle interactions,[2] very little attention has in fact been devoted to g_4. We therefore considered it of interest to extend the former analysis to include such structurally related molecules as PF_3 and AsF_3, with the main aim of studying the changes appearing in g_4 when fluorine is substituted for hydrogen.

In the present investigation, however, no isotopic frequencies are available which would provide additional data from which all the interaction constants might be determined. Thus, the four frequencies at our disposal[3] are not sufficient to evaluate the six parameters of the potential function[1]

$$2U = f_1 \sum_i \langle \Delta l_i^2 \rangle_{Av} + f_2 \sum_{i<j} \Delta l_i \Delta l_j + g_3 l^2 \sum_{i,j} \langle \Delta\theta_{ij}^2 \rangle_{Av} + g_4 l^2 \sum_{i,j,k} \Delta\theta_{ij}\Delta\theta_{ik} + g_5 l \sum_{j \text{ and } k \neq i} \Delta l_i \Delta\theta_{jk} + g_6 l \sum_{\substack{i,j,k \\ j<k}} [\Delta\theta_{ij} + \Delta\theta_{ik}]\Delta l_i.$$

Δl_i and $\Delta\theta_{ij}$ are respectively the changes of the PF and AsF bond lengths and of the FPF and FAsF angles from their equilibrium position.

TABLE I.

	f_1	f_2	g_2	g_4	g_5	g_6
PF_3	6.0	+0.91	0.86	+0.22	−1	+1
AsF_3	4.3	+0.70	0.41	+0.15	−0.69	+0.79

In order to overcome the difficulty, we have selected solutions for f_1, f_2, g_2, and g_4 corresponding to a range of values adopted for the g_5 and g_6 constants, the limits of which are taken to be -1.5 to $+1.5\times10^5$ dynes/cm. This is a method which has been found very successful in other cases.[4] This analysis shows clearly that the constant for the angle-angle interaction is positive in both molecules. It is to be noted that the interaction constants are fairly sensitive to the value adopted for the angles. For FPF and FAsF we have chosen respectively 104° and 100° which should not be considered as very accurate.[5] This dependence of the potential function upon the molecular dimensions does not, however, invalidate our general conclusions.

It is now well established that a difference in sign for g_4 may be caused by substitution ($AsH_3\rightarrow AsF_3$). A similar fact has already been observed and explained for other types of cross-terms in some molecules[6] (HCN→ClCN and $C_2H_4\rightarrow C_2Cl_4$). However, it is to be noticed that Torkington[7] has recently shown the existence of alternative solutions for C_2Cl_4 in terms of which the sign of these cross-terms remains unaffected on passing from C_2H_4 to C_2Cl_4. Consequently, in this particular case, some indetermination remains. However, the present analysis as well as recent theoretical considerations[2] seem to reinforce the validity of the earlier view.

In the case of PF_3 and AsF_3, g_4 presumably depends, to a large extent, on the interactions between the non-bonded atoms, which should give a positive sign. On the other hand, for the corresponding hydrogenated compounds, changes of hybridization at the P and As atoms during the vibrations are probably the decisive factor, and this may be shown to be a possible explanation of the negative sign. Of course, the H−H interactions have also to be considered as contributing to g_4, but by analogy with the well-known behavior of the length-length cross-terms,[1,2] it is to be expected that a negative sign might also occur.

As far as the exact magnitude of g_4 is concerned, no definite value can yet be put forward. This arises from the fact that variations of g_5 and g_6 within reasonable limits appreciably modify g_4. The very small values* which Howard and Wilson[8] have calculated for a set of pyramidal molecules are based on a limiting potential function and cannot therefore be accepted as entirely conclusive. Even the detailed study of Meister, Rosser, and Cleveland[9] on some tribromomethanes rests on assumptions which might affect considerably the values proposed for the same type of cross-term in the CBr_3 group. The only statement at present possible is that g_4 should have the essential property of being small with respect to other types of cross-terms.

A final decision for the other constants of PF_3 and AsF_3 must be left until further data are available. However, as regards f_2 and g_6, a positive sign can be considered as practically certain. Table I gives tentative solutions expressed in 10^5 dynes/cm units which show how the force constants may be associated.

A detailed account of this work will be published elsewhere.

[1] J. Duchesne and I. Ottelet, J. Chem. Phys. **17**, 1354 (1949); J. d. phys. et rad. **T.11**, 119 (1950).
[2] J. Duchesne, Mém. Soc. Roy. Sc. Liége **11**, 429 (1943); Coulson, Duchesne, and Manneback, V. Henri Mem. Vol., Desoer, Liége (1948), p. 33; J. Duchesne and A. Monfils, J. Chem. Phys. **17**, 586 (1949).
[3] Ta-You Wu, *Vibrational Spectra and Structure of Polyatomic Molecules* (Michigan, 1946), p. 201.
[4] J. Duchesne, Physica, La Haye, **IX**, 249 (1942).
[5] L. Pauling, J. Am. Chem. Soc. **57**, 2684 (1935); L. O. Brockway, J. Am. Chem. Soc. **56**, 2373 (1934).
[6] J. Duchesne, V. Henri Mem. Vol., Desoer, Liége, (1948), p. 47.
[7] P. Torkington, J. Chem. Phys. **18**, 773 (1950).
[8] J. B. Howard and E. B. Wilson, J. Chem. Phys. **2**, 630 (1934).
* On account of a slight difference in the expression of the potential functions used, the values of our cross-terms have to be divided by two in order to be compared with those of Howard and Wilson.
[9] Meister, Rosser, and Cleveland, J. Chem. Phys. **18**, 346 (1950).

General Form of the Force Constant Matrix for Harmonic Vibrations*

WILLIAM J. TAYLOR
Cryogenic Laboratory and Department of Chemistry, Ohio State University, Columbus, Ohio
July 10, 1950

IN the normal coordinate treatment of the vibrations of a molecule one is confronted with the problem of finding a set of force constants consistent with the mass or kinetic energy matrix of the molecule and with the observed frequencies of vibration. In general this problem is indeterminate unless assumptions are made which reduce the number of force constants, or additional data, such as the frequencies of isotopic or related molecules, are available. For this reason there is some value in considering the general forms which the solution may assume. Torkington[1] has given a general treatment of the secular equation of second degree, and Glockler and Tung[2] have considered the third degree equation. In the present note it is pointed out that there exists an explicit expression for the most general force constant matrix consistent with a given mass matrix and a given set of frequencies. In principle this expression enables one to obtain all possible sets of force constants satisfying the conditions of the problem *without solving the secular equation.*

Denote by G the reciprocal mass or kinetic energy matrix of Wilson,[3] and by Λ the diagonal matrix whose elements are $\lambda_i=(2\pi\nu_i)^2$, where the $\nu_i (i=1, 2, \cdots, n)$ are the observed frequencies. There exists a real orthogonal matrix A, unique except for the ordering and sign of its columns, which reduces the real symmetric matrix G to diagonal form,

$$A'GA=\Gamma, \tag{1}$$

where A' is the transpose of A. The elements, γ_i, of the diagonal matrix Γ are the latent roots of G, and are positive, since G is positive definite. The matrices A and Γ may be obtained by solving the secular equation,

$$|G-\gamma I|=0. \tag{2}$$

From Eq. (1) one easily obtains,

$$\Gamma^{\frac{1}{2}}A'G^{-1}A\Gamma^{\frac{1}{2}}=I, \tag{3}$$

where I is the unit matrix of order n. The elements of $\Gamma^{\frac{1}{2}}$ are $\gamma_i^{\frac{1}{2}}$.

Now consider the form the force constant or potential energy matrix, F, must have in order that the secular equation,

$$|F-\lambda G^{-1}|=0, \tag{4}$$

have the required roots, λ_i. In view of Eq. (3), Eq. (4) is equivalent to,

$$|\Gamma^{\frac{1}{2}}A'FA\Gamma^{\frac{1}{2}}-\lambda I|=0, \tag{5}$$

and there must therefore exist a real orthogonal matrix, B, such that

$$B'\Gamma^{\frac{1}{2}}A'FA\Gamma^{\frac{1}{2}}B=\Lambda. \tag{6}$$

Equation (6) may be solved for F, and the result put in the form,

$$F=K\Lambda K', \tag{7}$$

where

$$K=A\Gamma^{-\frac{1}{2}}B. \tag{8}$$

The matrix $A\Gamma^{-\frac{1}{2}}$ is a constant matrix for any given problem, and need be computed only once. The columns of the matrix K are the normal coordinates. It should be noted that K is not orthogonal.

Equations (7) and (8) show that in order to determine the force constants and normal coordinates it is sufficient to specify the real orthogonal matrix B.[4] Actually it is not necessary to specify B completely, since F is unaffected by a change in sign of any column of B, and the normal coordinates are merely changed in sign. It is easy to show that $n(n-1)/2$ parameters are sufficient to specify the general orthogonal matrix of order n, if the signs of its columns are left indeterminate. This is consistent with the fact that F has $n(n+1)/2$ distinct elements while n frequencies

are known. As the matrix B ranges over the real orthogonal n-dimensional (rotation) group all the possible solutions are obtained. The present method provides a systematic approach to the study of these solutions in indeterminate cases. It may then be possible to select the optimum solution on the basis of other considerations.

* This work was supported in part by the ONR under contract with the Ohio State University Research Foundation.
[1] P. Torkington, J. Chem. Phys. **17**, 357 (1949).
[2] G. Glockler and J. Y. Tung, J. Chem. Phys. **13**, 388 (1945).
[3] E. B. Wilson, Jr., J. Chem. Phys. **7**, 1047 (1939); **9**, 76 (1941).
[4] The order in which the "frequencies," λ_i, are arranged on the diagonal of Λ is immaterial, since F is invariant to a permutation of the λ_i's *accompanied by an equivalent permutation of the normal coordinates* (i.e., the columns of K, or B).

Use of Radiotracers to Measure Surface Adsorption from Mixtures

C. M. Judson, Ann A. Argyle, D. J. Salley, and J. K. Dixon
Stamford Research Laboratories, American Cyanamid Company, Stamford, Connecticut
July 27, 1950

A METHOD for using a radiotracer to measure the adsorption of a soluble surface-active agent at the solution-air interface has been developed in this laboratory[1,2] and has since been used elsewhere.[3] The method depends upon the fact that the radiation counted at the surface of a solution containing a soft beta-ray emitter is principally radiation from atoms which are near the surface of the solution. The measurements previously reported have been an adsorption isotherm for di-*n*-octyl sodium sulfosuccinate (Aerosol OTN)[1,2] and a single measurement for sodium octadecyl sulfate.[3] In both cases the agent was tagged with S^{35}.

A considerable number of measurements have now been carried out determining the adsorption of Aerosol OTN from solutions containing mixtures of Aerosol OTN with various inorganic salts and with alcohols, esters, or acids related to Aerosol OTN. The amount of Aerosol OTN adsorbed was not changed very much except when the second compound was also a surface-active agent.

The study of mixtures of Aerosol OTN with another similar surface-active agent, di-(2-ethyl hexyl) sodium sulfosuccinate (Aerosol OT), has provided some interesting data which are presented in Fig. 1. Varying amounts of Aerosol OT were added to solutions containing 3.2×10^{-6} molar Aerosol OTN (a concentration below the knee of the isotherm[1,2] and below the micelle point), and the surface adsorption was measured at 24°C. As the Aerosol OT concentration was increased, the Aerosol OTN on the surface was reduced, apparently being replaced by Aerosol OT. The equilibrium concentration of Aerosol OTN after formation of the surface layer varied from 2.3×10^{-6} molar to 3.2×10^{-6} molar. While the comparison should preferably have been made at constant equilibrium concentration of Aerosol OTN rather than at constant initial concentration, the experiment shows how

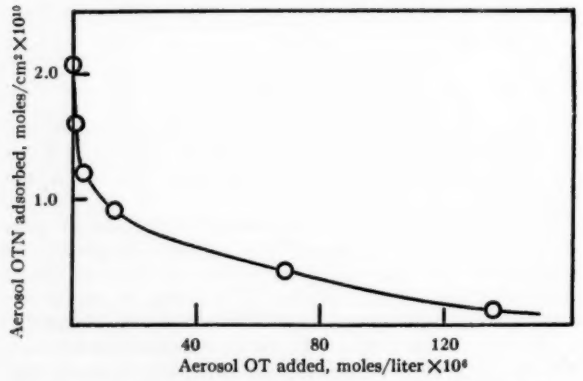

FIG. 1. Aerosol OTN adsorbed from mixtures with Aerosol OT containing 3.2×10^{-6} molar Aerosol OTN.

the radioactive tracer method can be used to measure the surface adsorption of one or more species in a mixture of surface-active agents. Surface tension measurements, conventionally used to measure surface adsorption, do not permit ready interpretation of results obtained in mixtures.

[1] Dixon, Weith, Argyle, and Salley, Nature **163**, 845 (1949).
[2] Salley, Weith, Argyle, and Dixon, Proc. Roy. Soc. (to be published).
[3] Aniansson and Lamm, Nature **165**, 357 (1950).

The Isothermals of Rocksalt from Its Thermal Expansion

Bisheshwar Dayal
Department of Physics, Indian Institute of Science, Bangalore and Department of Physics, Banaras Hindu University, India
July 3, 1950

THE usual calculations of the equation of state of solids are based on some pre-assumed form of the potential curves between pairs of atoms.[1,2] It would, however, be much simpler to use the thermal expansion data for this purpose as this would obviate the necessity of any assumption regarding the accuracy of the Debye theory or of the potential expression. The isothermals of rocksalt drawn on this basis are reproduced in Fig. 1. The

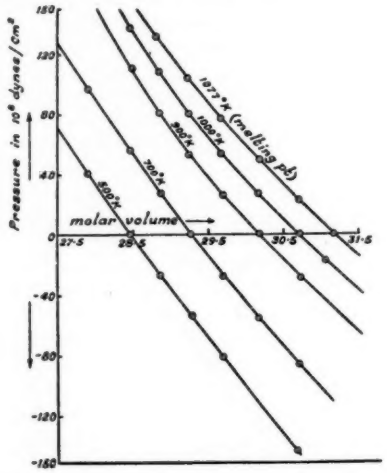

FIG. 1. Isotherms of rocksalt calculated from the thermal expansion.

method used by the writer is based on the evaluation of p_2, the part of the pressure due to the thermal vibrations from the Gruneisen constants at the appropriate volumes. The values of p_1, i.e., $\partial(N\phi/2)/\alpha V$ the part of pressure due to a static lattice, are obtained from the condition that at the volumes observed at different temperatures, $p_1+p_2=0$. For evaluating volumes at different temperatures, V_0 is assumed to be equal to 26.72. The Gruneisen constants at different volumes have been calculated from the thermal expansion data of Walther[3] by the usual relation,[4]

$$\gamma=\frac{\alpha V_0}{C_v K_0}\left(1-\frac{m+n+3}{6}\gamma\frac{K_0 E}{V_0}\right)^2. \quad (1)$$

For evaluating the quantity within the brackets we have used $E=RT$, $(m+n+3)/6=2$ and the mean value of $\gamma=1.65$ as given in Gruneisen's article.

Compressibilities have been calculated from the slope of the curves and show a fair agreement with experimental values[5] (Table I). The agreement is liable to some improvement by a suitable modification of the evaluation of the bracket quantity in Eq. (1).

The values of p_1 calculated from the expansion data as indicated above are less than those evaluated from the expression for potential due to Huggins and Mayer.[6]

TABLE I. Compressibility of rocksalt at different temperatures in 10^{-13} cm²/dyne.

Temperature °K	Experimental k Adiabatic	Isothermal	k calculated from curves
500	47.6	52.6	50
600	50.1	56	52
700	54.1	62	56
800	59.3	68	58
900	61.4	72	63
1000	65.7	85	73
1070	63.7	89	76

The method can be used at low temperatures where the bracket quantity is unimportant. The experimental values of C_v, E, and α can be used, so that the results become independent of any theory of crystal vibration. The values of p_1 can then be used in obtaining an accurate expression for the potential energy as a function of the volume. Such calculations are in progress.

I wish to thank Professor R. S. Krishnan for his interest in this investigation.

[1] Herzfeld and Mayer, Phys. Rev. **49**, 995 (1935).
[2] Kane, J. Chem. Phys. **7**, 603 (1939).
[3] Walther, Haschkowsky, and Stvelkow, Physik. Zeits. d. Sowjetunion 12, 35 (1937).
[4] Gruneisen, *Handbuch der Physik*, Vol. X.
[5] Hunter and Seigel, Phys. Rev. **61**, 84 (1942).
[6] Huggins and Mayer, J. Chem. Phys. **1**, 643 (1933).

Ultrasonic Velocity of Sound at 12 Mc in Liquid Sulfur

O. J. KLEPPA
Institute for the Study of Metals, University of Chicago, Chicago, Illinois
July 26, 1950

IN other communications[1,2] the author has reported the application of the pulse-circuit technique to measure the ultrasonic velocity of sound in liquid metals. The present communication refers to the application of the same technique for the measurement of the velocity of sound in liquid sulfur. Over a period of about four days a total of 29 separate measurements at temperatures from 115° to 315°C was carried out on a sample of liquid sulfur prepared from "Sulfur Sublimed, U.S.P. XII" (Mallinckrodt). The results of these measurements are plotted in Fig. 1. The data recorded in Table I were obtained from the smooth curve drawn through the experimental points.

It will be seen that there is no simple linear relationship between sound velocity and temperature. In fact, it appears that the curve in Fig. 1 has an inflection point in the transition region 160°–220°C, where the maximum viscosity is found. It should be pointed out that it was never possible to detect any hysteresis in the measured values for sound velocity during heating or cooling through this region.

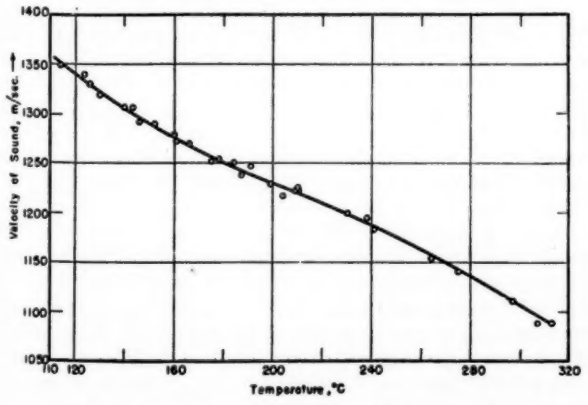

FIG. 1. Sound velocity as function of temperature.

TABLE I. Velocities of sound in liquid sulfur.

Temperature, °C	Sound velocity (m/sec.)
115	135_0
150	129_0
200	123_0
250	117_8
300	110_8

Adiabatic and isothermal compressibility of liquid sulfur:—International Critical Tables' report for the density of liquid sulfur at 115°C, $\rho=1.808$ g cm^{-3}, for the specific heat, $C_P=7.27$ cal. deg.$^{-1}$ and for the coefficient of thermal expansion, $\alpha=4.3\times10^{-4}$ deg.$^{-1}$. Making use of these data we compute for liquid sulfur at 115°C:

Adiabatic compressibility, $K_S=30.4\times10^{-6}$ bar^{-1}
Isothermal compressibility, $K_T=34.6\times10^{-6}$ bar^{-1}.

Thus, $C_P/C_V=1.14$ and specific heat, $C_V=6.3_8$ cal. deg.$^{-1}$. The compressibility data may be compared with the isothermal compressibility of orthorhombic sulfur at 20°, which by I.C.T. is reported to be 13.1×10^{-6} bar^{-1}. The data thus indicate a very large increase in compressibility on fusion compared to what is found in the case of metals. These, in general, show an increase on fusion of about 15 percent only, while the same figure for sulfur appears to be of the order of 100 percent or more.

[1] O. J. Kleppa, J. Chem. Phys. **17**, 668 (1949).
[2] O. J. Kleppa, J. Chem. Phys. (to be published).

Proton Magnetic Resonance in Polyethylene

ROGER NEWMAN*
Lyman Laboratories, Harvard University, Cambridge, Massachusetts
June 23, 1950

IN the course of some studies of the proton magnetic resonance in high polymers, a line-width transition was observed in polyethylene. Figure 1 summarizes the results. Figure 1a shows the line shape of the resonance at −186° and 25°C. Figure 1b shows the line width[1] as a function of temperature. As can be seen from the figure the midpoint of the line-width transition lies at about −38°C.

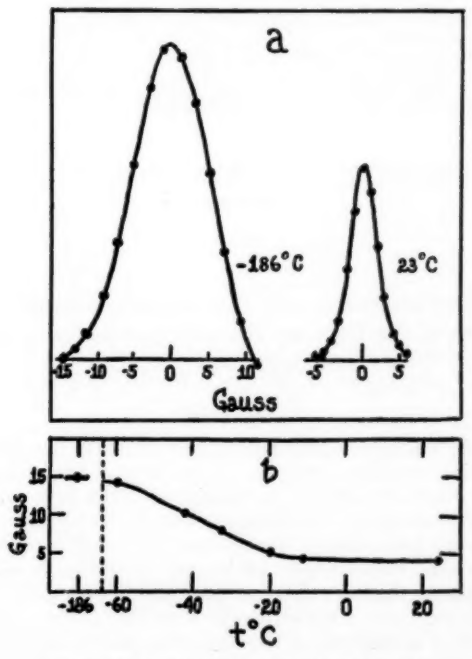

FIG. 1. Line shape data for polyethylene.

It will be recalled that a transition, as shown by a change in the coefficient of expansion, has been reported at −40°C for this polymer.[2] The line-width transition reported here occurs at very closely the same temperature. However, the coincidence of the two effects may be accidental. Hunter and Oakes have described their effect as being due to a "freezing in" of the motion of the polymer segments. That is, at temperatures below the transition point, the mean thermal energy is presumably insufficient to allow passage of the chain segments with sufficient frequency over whatever potential barriers separate their equilibrium positions. Such a description would of course account for the line-width transition as observed here.[3]

Using a procedure described elsewhere,[3] a rough estimate of the height of the aforementioned potential barriers can be made. It should of course be appreciated that for something whose motions are as complicated as those of a polymer a measured "barrier height" must be a rather loosely defined term. Any number, such as that obtained here, probably represents no more than some sort of suitably weighted average. With this reservation in mind, the present data suggest a barrier height of about 7 kcal./mole. A more accurate value probably could have been obtained from a nuclear relaxation time study, but the latter was precluded by instrumental difficulties. It is of some interest to note that in polyethylene sebacate, the dielectric dispersion data indicated a barrier height of 12 kcal./mole.[4] In the sebacate it might be expected that the interactions of the strong polar groups would tend to raise the existing potential barriers over what they would be for polyethylene, which is perhaps borne out by the data.

The resonance line shows no suggestion of structural features down to liquid nitrogen temperatures. This is in agreement with the results of Andrew, who studied several long chain paraffins.[5] Polyethylene is, of course, simply a paraffin molecule of tremendous length.

The second moment of the polyethylene resonance at −186°C is 28±2 gauss². On the basis of a zig-zag chain structure the intermolecular contribution to the second moment would be about 19 gauss². A reasonable maximum value for the contribution due to intramolecular or folded chain interactions would be about 8 gauss².[5] The maximum total second moment would then be about 27 gauss², which is of the same order as the observed moment. A closer comparison of the two values does not seem justified.

I should like to thank Drs. Buchdahl and Nielson of Monsanto for a helpful discussion of this work.

* Du Pont Postdoctoral Fellow in Chemistry (1949–50).
[1] H. S. Gutowsky and G. E. Pake, J. Chem. Phys. **16**, 1164 (1948).
[2] E. Hunter and W. Oakes, Trans. Faraday Soc. **41**, 49 (1945).
[3] H. S. Gutowsky and G. E. Pake, J. Chem. Phys. **18**, 162 (1950).
[4] W. A. Yager and W. O. Baker, J. Am. Chem. Soc. **64**, 2164 (1942).
[5] E. R. Andrew, J. Chem. Phys. **18**, 607 (1950).

The Development and the Surface Energy of the Planes of the Primary Rhombohedron in α-Quartz

B. D. Saksena and L. M. Pant
Department of Physics, University of Allahabad, India
May 2, 1950

QUARTZ shows a large development of form. The three principal development forms are the faces of the primary and inverse rhombohedra and the hexagonal prism faces which are found in most crystals. Of these, the faces of the primary rhombohedron are found highly developed even in small specimens. To explain this, Beckenkamp[1] located the Si−O bonds along the edges joining the faces of the primary and inverse rhombohedra, but this prediction is not verified by x-ray data. By projecting the unit cell of α-quartz on a rhombohedral pattern, we have been able to show that the silicon-oxygen bonds in quartz lie very close to the planes of the primary rhombohedron, and it appears likely that this is the cause of the large development of these planes.

The coordinates of the atoms in the unit cell of left quartz with respect to the hexagonal axes (a, a, and c) are (Wyckoff)[2]:

Silicons (1, 2, 3, 4, 5, 6)—$(u, 0, 0)$, $(1-u, 1-u, \frac{1}{3})$, $(0, u, -\frac{1}{3})$, $(\overline{1-u}, 0, 0)$, $(\bar{u}, \bar{u}, \frac{1}{3})$, $(0, \overline{1-u}, -\frac{1}{3})$

Oxygens (7, 8, 9, 10, 11, 12)—(x, y, z), $(y, x, \bar{z}+\frac{2}{3})$, $(\bar{y}, x-y, z-\frac{1}{3})$, $(\bar{x}, y-x, \bar{z}+\frac{1}{3})$, $(y-x, \bar{x}, z-\frac{2}{3})$, $(x-y, \bar{y}, \bar{z})$.

To represent the atoms on a rhombohedral pattern we take three equal axes inclined at angles of 93°57′ to one another, and then find the corresponding hexagonal axes. These are seen from Fig. 1 to be OF, OB, OD, and OO′ where OF=OB=OD=a and

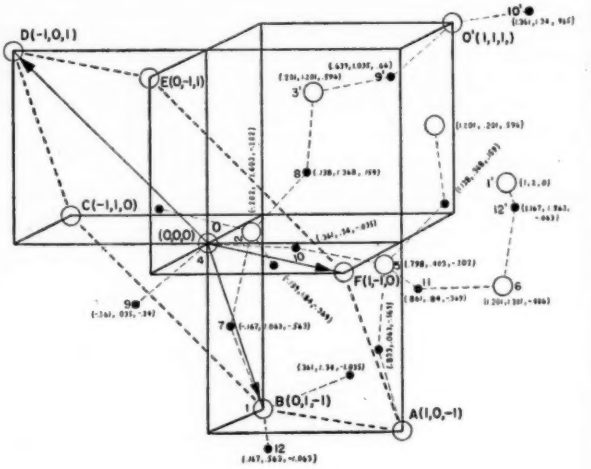

FIG. 1. Positions of the atoms in left quartz.

OO′=c, the ratio c/a being equal to 1.1. The silicon atoms situated at the center and the corners of the hexagon ABCDEF and at the point O′ are equivalent atoms. By joining the point O′ to the corners of the hexagon, we get the hexagonal pyramid of quartz whose alternate planes O′AF, O′BC, O′DE are the rhombohedral planes (1, 0, 0) (0, 1, 0), and (0, 0, 1). It is easy to see that if the hexagonal axes are taken in the order OF, OB, and OD (OF facing the observer), the above planes are also the planes of the primary rhombohedron for left quartz. Since we may locate the origin of the coordinates in the unit cell on either OF, OB, or OD, we suppose it to lie between the points O and B at a distance "u" from B. The hexagonal coordinates (e, f, g), referred to the axes parallel to OB, OD, and OO′ through this origin, may now be converted into rhombohedral coordinates (p, q, r), having their origin at the point (0, 0, 0), by the relations given below

$$p=-f+g, \quad q=(1-u)+e+g, \quad r=f+g-e-(1-u).$$

The rhombohedral coordinates of the atoms in the unit cell, using the x-ray data of Wei,[3] $u=0.465a$, $x=0.417a$, $y=0.278a$, $z=0.111c$, are shown in Fig. 1. It is seen that two of the Si−O bonds at each silicon atom lie very close to the planes of the primary rhombohedron. If we slightly alter the coordinates to $u=0.47a$, $x=0.42a$, $y=0.31a$, and $z=0.11c$, the bonds are found to lie exactly in these planes. Thus the two Si−O bonds joining the silicon O′ to the oxygen atoms 9′ and 10′ now have the direction-ratios (1, 0, 1) and (1, 1, 0) respectively, and therefore lie in the planes (0, 1, 0) and (0, 0, 1) of the primary rhombohedron for left quartz, along the lines joining the point 0′ to the middle points of the lines CB and DE. On changing the sign of the z coordinate, i.e., considering the case of right quartz, we obtain the same result. It is noticed that the same bonds now lie in the planes of the inverse rhombohedron for left quartz and, therefore, in the planes of the primary rhombohedron for right quartz.

The binding forces between the silicon and oxygen atoms in quartz are very strong (Saksena).[4] Therefore, the energy needed to form a given plane in the initial stages of crystallization would depend largely on the orientation of the plane with respect to Si−O bond and would be smallest when the given plane contains the bond. Since the Si−O bonds lie very close to the planes of the primary rhombohedron, it may be expected that the energy of these planes would be much smaller than the surface tension of the liquid with the result that these faces will always be well-formed.

The surface energy of the various faces in quartz may be obtained by the method used by Harkins[5] for diamond. If E is the energy required to break one mole of bonds, and A is the area of the plane perpendicular to the bond-direction, the surface energy is given by $(E/2A)/(6.06\times10^{23})$ ergs/cm². For quartz the areas of the planes of the primary and inverse rhombohedra "r" and "z" and the hexagonal prism faces "m" are $1.4a^2$, $1.4a^2$, and $1.1a^2$, and from Fig. 1 it is seen that the minimum number of bonds cut by these faces is 1, 2, and 1 respectively. Since the dissociation energy of the Si−O bond is 180 kcal. per mole (Gaydon),[6] the surface energies of the "r," "m," and "z" faces are found to be 1895, 2368, and 3790 ergs/cm². These values are the upper limits. For the "r" faces, the energy is reduced to 1340 ergs/cm² since the normal to this plane makes an angle of 45° with the Si−O bond. One consequence of the small surface energy of the planes of the primary rhombohedron is that the cleavage in quartz occurs along these planes.

Cristobalite is a cubic crystal of the diamond structure, the side of the unit cell being 7.12A (Bragg).[7] The silicon atoms occupy the same positions as the carbon atoms in diamond. As each oxygen atom is linked to two silicon atoms, there are twice as many Si−O bonds per mole in cristobalite as there are C−C bonds in diamond, and the dissociation energy per Si−O bond is, therefore, $90/6.06\times10^{23}$ kcal. The surface energies of the (1, 1, 1) and (1, 0, 0) planes are found to be 1420 and 2460 ergs/cm².

Lennard-Jones and Dent[8] have calculated the energies of the (1, 0, 0) planes in MgO and CaO (both having NaCl structure) to be 1362 and 1032 ergs/cm². The values found for Si−O are of the same order.

We are thankful to the Council of Scientific and Industrial Research for a research grant and a scholarship to one of us (L. M. P.).

[1] Beckenkamp, *Structure and Properties of Silica* (by Sosman), p. 237.
[2] Wyckoff, *Structure of Crystals, Part 1.*
[3] P. H. Wei, Zeits. f. Kryst. **92**, 356 (1935).
[4] B. D. Saksena, Proc. Ind. Acad. Sci. **A19**, 357 (1944).
[5] W. D. Harkins, J. Chem. Phys. **10**, 268 (1942).
[6] Gaydon, *Dissociation Energies*, p. 214.
[7] W. L. Bragg, *Atomic Structure of Minerals*, p. 89.
[8] Lennard-Jones and Dent, Phil. Mag. **8**, 530 (1929).

The Relation of the Frequency of Ultraviolet Absorption to the Reduction Potential of Aromatic Hydrocarbons

A. T. WATSON
Humble Oil & Refining Company, Baytown, Texas
AND
F. A. MATSEN
Departments of Chemistry and Physics, The University of Texas Austin, Texas
July 27, 1950

IT has been shown by Maccoll[1] that the reduction potential $(-E)$ for a series of polynuclear aromatic compounds is proportional to the coefficient of the molecular orbital resonance integral in the expression for the energy of the lowest unoccupied orbital. This statement is based on the assumptions that (a) the potential-determining step is $R+e\rightarrow R^-$; (b) that the electron goes into lowest unoccupied molecular orbital; (c) that the entropy change for this electron transition will be the same for various aromatic molecular species, and that the change in reduction potential will be equal to the change in heat content; and (d) that the change in heat content is equal to the energy required to place an electron from outside the molecule into the first unoccupied orbital.

The frequency of the long wave-length absorption of these molecules is given by the difference in energy between the highest occupied and the lowest unoccupied LCAO molecular orbital.[2] For molecules with a relatively high degree of symmetry, e.g., naphthalene and anthracene, these energies are, neglecting overlap, $\alpha+a_1\beta$ and $\alpha-a_1\beta$[3], respectively. For molecules with a lower symmetry one may write $\alpha+a_1\beta$ and $\alpha-Xa_1\beta$, respectively, where X is generally a number quite close to one. Then $h\nu\equiv-(1+X)a_1\beta$. A plot of $(-E)$ against ν in electron volts should give a series of points which cluster about a line of slope two. This comparison is independent of the value of β assigned to each compound. In Fig. 1 are plotted the frequencies in electron volts

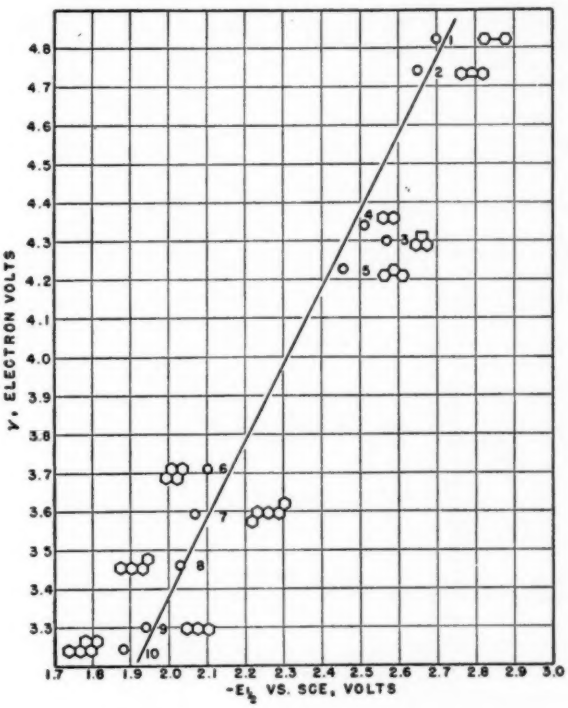

FIG. 1. The frequency of the major long wave-length absorption band of some aromatic hydrocarbons *vs.* their reduction potentials. The compounds referred to are:

1. Diphenyl
2. Fluorene
3. Acenaphthene
4. Naphthalene
5. Phenanthrene
6. Pyrene
7. 1,2,5,6-Dibenzanthracene
8. 1,2-Benzanthracene
9. Anthracene
10. 1,2-Benzpyrene.

against the reduction potential of all compounds for which both data are available.[4,5] The data used are the first strong absorption peak and the lowest reduction potential.

The conclusions reached in this paper and that of Maccoll's should apply only to compounds possessing conjugated unsaturation since only these systems possess well-defined orthogonal molecular wave functions of low energy.

[1] A. Maccoll, Nature **163**, 178 (1949).
[2] If either of these levels is degenerate in this approximation, splitting may occur in a higher approximation which will invalidate the above statement unless the splitting is small.
[3] Here α and β are the π-electron Coulomb and resonance integrals on carbon.
[4] W. V. Mayneord and E. M. F. Roe, Proc. Roy. Soc. **A152**, 299 (1935); **A158**, 634 (1937).
[5] S. Wawzonek and H. A. Laitenen, J. Am. Chem. Soc. **64**, 2365 (1942).

Raman Spectra and Normal Coordinate Treatment of Methylchlorosilanes

TAKEHIKO SHIMANOUCHI*
Chemical Laboratory, Faculty of Science, Tokyo University
ISAO TSUCHIYA
Electrotechnical Laboratory, Agency of Industrial Science and Technology, Tokyo
AND
YUKIO MIKAWA
Laboratory of Nihon Chemical Industrial Company, Tokyo, Japan
July 3, 1950

IN continuing the work concerning the vibrational spectra of methane, silane, and their derivatives,[1,2] the following Raman lines (cm^{-1}) have been observed.

TABLE I. The vibrational frequencies of methylchlorosilanes (cm^{-1}).[a]

		$SiCl_4$ Obs.		$SiCl_3CH_3$ Obs.	Calc.		$SiCl_2(CH_3)_2$ Obs.	Calc.		$SiCl(CH_3)_3$ Obs.	Calc.		$Si(CH_3)_4$ Obs.
$\delta(Cl-Si-Cl)$	E	150	E	164	165	A_1	169	173	E	—	—	E	—
$\delta(CH_3-Si-CH_3)$		—		—	—	A_2	177	186	A_1	187	187	T	202
$\delta(Cl-Si-Cl)$	T 221		A_1	229	229	A_1	232	215	E	242	250		239
$\delta(Cl-Si-CH_3)$			E	229	234	B_1	241	245		242	257		
$\delta(CH_3-Si-CH_3)$				—	—	B_2	?	304[b]		—	—		
$\nu(Si-Cl)$	A	424	A_1	450	446	A_1	465	497	A_1	467	517		
$\nu(Si-Cl)$	T	608	E	576	608	B_2	533	594		—	—	A	598
$\nu(Si-CH_3)$		—	A_1	761	765	A_1	691	753	A_1	637	696		696
$\nu(Si-CH_3)$		—		—	—	B_1	804	791	E	760	781	T	863

[a] As the values of $H(Cl-Si-CH_3)$, $F'(Cl\cdots CH_3)$, $F(Cl\cdots CH_3)$, and κ we take the mean values of $H(Cl-Si-Cl)$ and $H(CH_3-Si-CH_3)$, $F'(Cl\cdots Cl)$ and $F'(CH_3\cdots CH_3)$, $F(Cl\cdots Cl)$ and $F(CH_3\cdots CH_3)$, and $\kappa(SiCl_4)$ and $\kappa(Si(CH_3)_4)$, respectively.
[b] According to the private communication of Mr. H. Murata, he has found a very weak Raman line which can be assigned as $\epsilon-300$ cm^{-1}. This is in good agreement with the line calculated as B_2.

$SiCl_3(CH_3)_2$	169(8) $e\pm,k,i$	465(10) $e\pm,k,i,f,g$	1265(1) e,k
	177(5b) $e\pm,k,i$	533(2b) e,k	1401(4) e,k
	232(7) $e\pm,k,i$	691(7) $e\pm,k,i$	2910(9b) e,k,i,o,p,q
	241(5b) $e\pm,k,i$	804(4) e,k	2980(8b) e,k,i,o,p,q
$SiCl_3CH_3$	164(9b) $e\pm,k,i,f$	576(4b) e,k	1405(2) e,k
	229(9b) $e\pm,k,i,f$	761(5) e,k,i	2912(8) e,k,i,o,p,q
	450(9) $e\pm,k,i$	1265(1) e,k	2983(6) e,k,i,o,p,q

These vibrations and those of $SiCl(CH_3)_3$ observed by Duchesne[3] give a series of frequencies of methylchlorosilanes which is similar to that described in the case of chlorobromomethanes.[4] Using the method[1] and force constants[2] given in the preceding papers, we have calculated the skeletal vibrations of these molecules. The calculated frequencies are in good agreement with the observed, if the assignment of these frequencies is made adequately as shown in Table I. Although all the force constants were taken from the normal vibrations of $SiCl_4$ and $Si(CH_3)_4$ the mean difference between the observed and the calculated amounted only to 4.4 percent. Therefore, there seems to be little doubt in concluding that the Urey-Bradley field is also reasonable for these molecules.

* Formerly Takehiko Simanouti.
[1] T. Shimanouchi, J. Chem. Phys. **17**, 245 (1949).
[2] T. Shimanouchi, J. Chem. Phys. **17**, 848 (1949).
[3] J. Duchesne, J. Chem. Phys. **16**, 1006 (1948).
[4] Lecomte, Volkringer, and Tchakirian, Comptes Rendus **204**, 1927 (1937).

The Thermal Decomposition of Nitromethane

T. L. COTTRELL AND T. J. REID
Research Department, Imperial Chemical Industries Limited, Nobel Division, Stevenston, Ayrshire, Scotland
June 29, 1950

THE thermal decomposition of nitromethane was investigated several years ago by Taylor and Vesselovsky,[1] who stated that the reaction was first order. However, rate constants calculated from their published values of quarter- and half-lives of the reaction show a significant decrease in going from the quarter- to the half-life, and their experiments were all carried out at pressures below 200 mm. We have reinvestigated the reaction, also using a static method, and found that it is largely homogeneous. First-order constants were calculated from the initial rate of pressure increase and it was found that the rate constant increased with pressure up to about 200 mm. The rate constant, from experiments using 200 to 350 mm nitromethane, in the range 380 to 430°C, is given by $k=10^{14.36}\exp(-52{,}700/RT)$ $sec.^{-1}$; the activation energy being rather less than that found previously. The main gaseous products are CH_4, CO, and NO, with some CO_2 and H_2.

$\Delta H_{298.1}°$ for the reaction $CH_3NO_2(g)\rightarrow CH_3(g)+NO_2(g)$ is found to be 52.3 kcal., using the values 32.0 and 8.1 kcal. for the heats of formation of CH_3 and NO_2, respectively,[2] and the new value of −12.2 kcal. for the heat of formation of gaseous nitromethane.[3] With the usual assumption of zero activation energy for the reverse reaction, the activation energy is thus about 52 kcal., in good agreement with the experimental activation energy for nitromethane pyrolysis. The identification of the activation energy with the energy of dissociation to CH_3 radicals and NO_2 molecules depends on the assumption that the reorganization energy for the change NO_2 radical→NO_2 molecule is zero, or nearly so. The fact that the energy of activation for the dissociation of N_2O_4 is the same as the heat of dissociation[4] shows that this is reasonable. The assumption that the heat of reaction at 298.1° is about the same as at 700°K is also likely to be sufficiently accurate. It is therefore suggested that the initial step is the fission of the C−N bond, of energy 52–53 kcal. The mechanism of the reaction is being further investigated.

[1] Taylor and Vesselovsky, J. Phys. Chem. **39**, 1095 (1935).
[2] "Selected values of chemical thermodynamic properties" (National Bureau of Standards, 1949).
[3] Holcomb and Dorsey, Ind. Eng. Chem. **41**, 2788 (1949).
[4] Richards and Reid, J. Chem. Phys. **1**, 114 (1933).

Color of Diketo-Pyrazolidine Derivatives

SUNAO IMANISHI
Faculty of Science, Kyushu University, Fukuoka, Japan
July 24, 1950

IN order to contribute to the knowledge of the effect of chemical constitution on the color of dye-like organic compounds we have determined, using a "Spekker"-type spectrophotometric device and a medium-size quartz spectrograph, absorption curves of ethyl alcohol solutions (concentration 10^{-4}~10^{-5} mole/liter, cell length 1 cm) of 1,2-diphenyl- and 1-phenyl-3,5-diketo-pyrazolidine,[1]

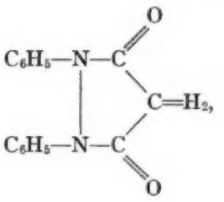

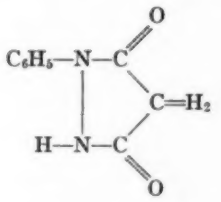

and their derivatives having different divalent radicals attached to the 4-carbon atom.

The general bathochromic shifts can qualitatively be understood by assuming resonating structures

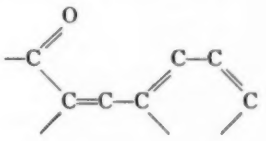

(a)

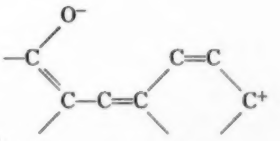

(b)

for the benzylidene derivatives, and similar structures for the cinnamylidene or the furfurylidene derivatives, and also by taking into consideration the electron-donating tendencies of various substituents on the benzene ring participating in the resonance path. A substituent capable of sending more electron into the ring and attached to a position more favorable therefore should assist the above resonance to occur and hence enhance the bathochromic effect. The hypsochromic action of an NO_2 substituent can be

TABLE I.

Radicals	First absorption peak $\lambda_1(m\mu)$	Extinction coefficient for λ_1 $k_1(10^4$ liter $\cdot mole^{-1}\cdot cm^{-1})$
Diphenyl compounds		
$=CMe_2$	<220	—
$=H_2$	<220	—
=CH— 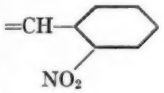	251	2.7
=CH— 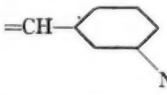	257	4.4
=CH— 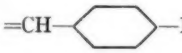	259	2.1
=CH— 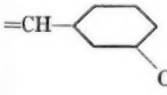	334	1.9
=CH— 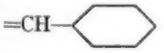	336	2.6
=CH—	352	3.8
=furfurylidene	382	4.7
=CH— 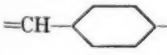	388	4.4
=CMe— 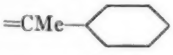	390	1.1
=CH— 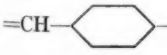	395	4.1
$=CH\cdot CH_2\cdot CH_3$	403	4.0
=CH— 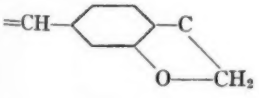	406	2.6
=CH— 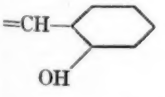	410	1.3
=CH— 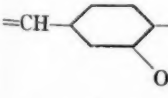	417	4.4
=CH— 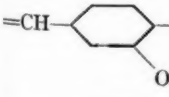	421	3.1
=CH— 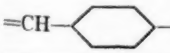	479	9.0

TABLE I.—(*continued*)

Radicals	First absorption peak $\lambda_1(m\mu)$	Extinction coefficient for λ_1 $k_1(10^4$ liter $\cdot mole^{-1}\cdot cm^{-1})$
Monophenyl compounds		
$=H_2$	<220	—
=CH— 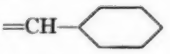	320	2.3
=CH—CH=CH— 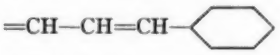	372	3.7
=furfurylidene	365	2.6
=CH— 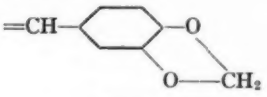	387	2.4
=CH— 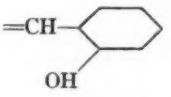	396	1.4
=CH— 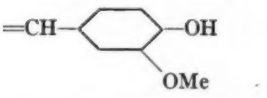	401	2.0

explained by the positive charge on the N atom inhibiting the resonance. Hypsochromic shifts of about 10~20 mμ are noticed in the transition from diphenyl to monophenyl derivatives. However, this effect cannot be accounted for by the simple scheme indicated above.

Applying the electron gas model[2] as a very crude approximation to these molecules, we obtain $\lambda_{1,\text{calc}}$ 340 mμ and 430 mμ for the simple diphenyl-benzylidene and the monophenyl-cinnamylidene derivatives, respectively. The coincidence of the former value with the experimental 336 mμ is rather too good, as the electron gas model assumes complete resonance between the two extreme structures (as obtains in a symmetrical cyanine ion), which is not the case in our molecules.

[1] First prepared by T. Tsumaki, Bull. Chem. Soc. Japan **6**, 1 (1931); *ibid.* **7**, 48 (1932).
[2] H. Kuhn, J. Chem. Phys. **17**, 1198 (1949).

The Infra-Red and Raman Spectra of COClF

E. A. Jones and T. G. Burke
*Carbide and Carbon Chemicals Division, K-25 Plant, Oak Ridge, Tennessee**
June 26, 1950

THE infra-red spectrum of gaseous carbonyl chlorofluoride and the Raman spectrum of the liquid have been investigated. Table I lists the frequencies of the observed infra-red bands and Raman lines.

Table I. Infra-red and Raman frequencies of COClF.

Infra-red bands (gas) cm^{-1}	Raman lines (liquid) cm^{-1}	Assignment
415	410	ν_6
501	506	ν_3
665	665	ν_5
776	765	ν_1
910		$\nu_3+\nu_6$
1004		$2\nu_3$
1095	1085	ν_4
1164		$\nu_3+\nu_5$
1182		$\nu_1+\nu_6$
1330		$2\nu_5$
1508		$\nu_4+\nu_6$
1867	1832	ν_2
	1858	$\nu_1+\nu_4$
2063		$\nu_3+2\nu_1$
2179		$2\nu_4$
2647		$\nu_1+\nu_2$
3743		$2\nu_2$

COClF is probably a planar molecule belonging to the point group C_s. This model has six non-degenerate vibrations all of which are Raman and infra-red active. Six fairly strong bands observed in the infra-red spectrum were found to be in agreement with six Raman lines and consequently have been designated as the fundamentals of the molecule. The assignments of the overtone and combination bands given in column 3 appear to be reasonable on the basis of these fundamentals. The infra-red bands at 665, 776, and 1095 cm^{-1} have *P*, *Q*, and *R* structure and the 501 cm^{-1} band appears to be a doublet at this resolving power. The contour of the 410 cm^{-1} band could not be determined because it occurs near the limit of the KBr region. Two Raman lines separated by 26 cm^{-1} were observed in the C=O region at 1832 and 1858 cm^{-1}. This doubling can be attributed to a Fermi resonance between ν_2 and the combination band $\nu_1+\nu_4$. As the selection rules do not in this case forbid the occurrence of either of these bands in the infra-red spectrum, this region was studied under high resolution. Two bands with a separation of approximately 20 cm^{-1} were observed in good agreement with the Raman lines.

A more detailed analysis of this molecule will be reported later.

* This document is based on work performed for the AEC by Carbide and Carbon Chemicals Division, Union Carbide and Carbon Corporation, at Oak Ridge, Tennessee.

The Raman Spectra of Ethylchlorosilanes

Hiromu Murata
The Osaka Municipal Technical Research Institute
Rokuro Okawara and Takeo Watase
Department of Industrial Chemistry, Faculty of Engineering, Osaka University, Osaka, Japan
June 29, 1950

RECENTLY T. Shimanouchi, I. Tsuchiya, and Y. Mikawa[1] have observed the Raman spectra of methylchlorosilanes and calculated the normal vibrations of these tetrahedral molecules using the Urey-Bradley field. Consulting their results we have tentatively assigned the skeletal frequencies of ethylchlorosilanes, assuming ethyl groups as one particle.

The Raman spectra of tetrachlorosilane and tetraethylsilane have been reported by several investigators.[2] We have measured the Raman spectra of ethyltrichlorosilane, diethyldichlorosilane,

Table I. Raman spectra of ethylchlorosilanes (cm^{-1}).

Modes of vibration		$SiCl_4$		$C_2H_5SiCl_3$		$(C_2H_5)_2SiCl_2$		$(C_2H_5)_3SiCl$		$(C_2H_5)_4Si$
τ(Si−C)*				125(4*s*)(*ek*)						
	E	150(5)	*E*	152(3*s*)(*ek*)	A_1	157(4*b*)(*ek*)	*E*	160(5*b*)(*ek*)	*E*	160(4)
δ(Si−Cl)					A_2	—				
δ(Si−C_2H_5)	F_2	221(5)	A_1	187(5*s*)(*e*)	A_1	190(4*b*)(*e*)	A_1	221(5*b*)(*ek*)	F_2	303(6)
			E	224(5*s*)(*ek*)	B_1	241(3*b*)(*ek*)	*E*	295(4*b*)(*ek*)		
					B_2	299(5*b*)(*ek*)				
δ(C−C)				328(6*s*)(*ek*)		371(2*b*)(*e*)		345(2*b*)(*ek*)		
	A	424(10)	*A*	447(10*s*)(*ek*)	*A*	458(8*b*)(*ek*)	*A*	464(6*b*)(*ek*)	*A*	553(10)
ν(Si−Cl)	F_2	608(1)	*E*	580(2*b*)(*ek*)	B_2	650(3*b*)(*ek*)	A_1	592(4*b*)(*ek*)	*F*	736(3)
ν(Si−C_2H_5)			A_1	715(3*b*)(*ek*)	A_1	695(1*b*)(*ek*)	*E*	739(3*b*)(*ek*)		
					B_1	746(1*b*)(*ek*)				
ν(C−C)				979(2*s*)(*ek*)		979(3*b*)(*ek*)		979(4*b*)(*ek*)		978(5)
				1013(2*s*)(*ek*)		1013(3*b*)(*ek*)		1013(4*b*)(*ek*)		1021(5)
				1241(3*s*)(*ek*)		1241(2*b*)(*ek*)		1241(2*b*)(*k*)		1200(7)
				1309(4*b*)(*ek*)		1309(4*b*)(*ek*)		1309(6*b*)(*ek*)		
δ(C−H)				1359(1*b*)(*e*)		1359(4*b*)(*ek*)		1359(6*b*)(*ek*)		1423(7)
				1407(2*b*)(*ek*)		1407(4*b*)(*ek*)		1407(5*b*)(*ek*)		1467(8)
				1460(3*s*)(*ek*)		1460(4*b*)(*ek*)		1460(8*b*)(*ek*)		
				2892(7*b*)(*ek*)		2890(10*b*)(*ek*)		2807(3*b*)(*e*)		2734(1)
								2870(10*b*)(*ek*)		2813(3)
ν(C−H)				2935(6*b*)(*ek*)		2930(8*b*)(*ek*)		2909(9*b*)(*ek*)		2885(10)
				2978(5*s*)(*ek*)		2970(7*b*)(*ek*)		2960(8*b*)(*ek*)		2912(6)
										2950(5)

* τ denotes the internal rotation around the axis of Si−C bond.

and triethylchlorosilane. The ethyltrichlorosilane (b.p. 97.5°C) and diethyldichlorosilane (b.p. 128.9°C) used were prepared by the direct reaction of C_2H_5Cl upon silicon metal, and triethylchlorosilane (b.p. 146°C) by Grignard reagent upon diethyldichlorosilane, purified by careful fractional distillation, and confirmed by the analysis of chlorine content. The results for these compounds together with the data available for the two compounds $SiCl_4$ and $Si(C_2H_5)_4$ are given in Table I. Taking into account the result obtained for methylchlorosilanes, we have assigned the observed lines as shown in Table I, where A denotes totally symmetric, B antisymmetric, E twofold degenerate, and F threefold degenerate vibrations of the tetrahedral molecule, respectively. Thus it is seen that the Raman spectra of ethylchlorosilanes provide with another typical example of a sequence of $XY_4 \rightarrow XZ_4$.[3]

[1] Shimanouchi, Tsuchiya, and Mikawa, J. Chem. Phys. **18**, 1356 (1950).
[2] J. F. Anderson, J. Chem. Phys. **4**, 161 (1936).
[3] Lecomte, Volkringer, and Tchakirian, Comptes Rendus **204**, 1927 (1937).

On the Time Lag in the Precipitation of Ice by Silver Iodide Crystals

R. S. BRADLEY
University of Leeds, England
July 20, 1950

IN a paper by H. Reiss[1] the time lag in the precipitation of ice by silver iodide, as described by B. Vonnegut[2], is ascribed to the time factor in precipitation on particles below the critical size. It seems to the writer that there is another possibility, not mentioned by H. Reiss or B. Vonnegut (the latter favors the deposition of silver iodide particles on the walls); this is the coagulation of the cloud of silver iodide particles, so that initially deposition occurs on the large particles and then, as coagulation proceeds, more large particles appear and act as immediate nuclei. Of course the simple Gibbs theory cannot apply to the large particles, which will probably be aggregates and not single particles; this will be true even at the start of the experiment with a polydisperse cloud. However, it might well be expected that an aggregate would be more likely to act as a nucleus the larger the size.

[1] H. Reiss, J. Chem. Phys. **18**, 529 (1950).
[2] B. Vonnegut, Chem. Rev. **44**, 277 (1949).

Adsorption of Carbon Dioxide on Reduced Nickel

TAKAO KWAN
The Research Institute for Catalysis, Hokkaido University, Sapporo, Japan
July 24, 1950

THE present author recently investigated the adsorption of carbon monoxide[1] on platinum catalyst statistical mechanically with special reference to its state on platinum, concluding that it was dissociated into statistically independent atoms. Developing the method further, carbon dioxide adsorption was not investigated on reduced nickel.

Adsorption isotherms of carbon dioxide are derived, introducing a set of functions, p, q, and θ (due to Horiuti[2]), respectively, for the undissociative adsorption, $CO_2 \rightleftarrows CO_2(a)$, the partially dissociative one, $CO_2 \rightleftarrows CO(a)+O(a)$ and for the completely dissociative one into three statistically independent atoms, $CO_2 \rightleftarrows C(a)+O(a)+O(a)$ as

$$\frac{\theta}{1-\theta}=\frac{q^{CO_2(a)}}{p^{CO_2}} \tag{1.1}$$

$$\left(\frac{\theta}{1-2\theta}\right)^2=\frac{q^{CO(a)}q^{O(a)}}{p^{CO_2}} \tag{1.2}$$

$$\left(\frac{\theta}{1-3\theta}\right)^3=\frac{q^{C(a)}q^{O(a)}q^{O(a)}}{p^{CO_2}} \tag{1.3}$$

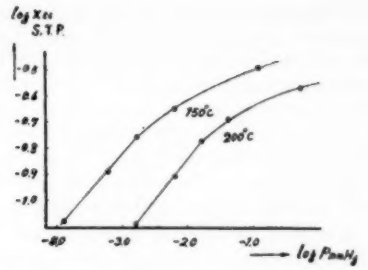

FIG. 1. Plot of log volume adsorbed against log pressure.

where $q^{CO_2(a)}$, $q^{CO(a)}$, $q^{C(a)}$, and $q^{O(a)}$ are the partition functions of the absorbed tsates of $CO_2(a)$, $CO(a)$, $C(a)$, and $O(a)$ expressed as

$$q^{CO_2(a)}=\prod^{i}(1-\exp(-h\nu_i/kT))^{-1}\exp(-\epsilon_0+\tfrac{1}{2}h\nu_i/kT), \text{ etc.,}$$

and p^{CO_2} is related with the ordinary partition function, Q, of gaseous carbon dioxide and its concentration N, as

$$p^{CO_2}=Q/N.$$

Equations (1.1), (1.2), and (1.3) are expressed for the case $\theta \ll 1$ as

$$\theta=\frac{q^{CO_2(a)}\exp[T\partial \log q^{CO_2(a)}/\partial T]}{Q_0}Pe^{\Delta\epsilon/RT} \tag{2.1}$$

$$\theta^2=\frac{q^{CO(a)}q^{O(a)}\exp[T\partial \log q^{CO(a)}q^{O(a)}/\partial T]}{Q_0}Pe^{\Delta\epsilon/RT} \tag{2.2}$$

$$\theta^3=\frac{q^{C(a)}q^{O(a)}q^{O(a)}\exp[T\partial \log q^{C(a)}q^{O(a)}q^{O(a)}/\partial T]}{Q_0}Pe^{\Delta\epsilon/RT} \tag{2.3}$$

where

$$Q_0=kT\frac{(2\pi mkT)^{\frac{3}{2}}}{h^3}\frac{8\pi^2 IkT}{sh^2}\prod^{i}(1-e^{-h\nu_i/kT})^{-1}e^{7/2}$$

$\Delta\epsilon$: differential heat of adsorption per gram mole
P: equilibrium pressure.

The investigation of the factors, $q^{C_2O(a)}\exp[T\partial \log q^{CO_2(a)}/\partial T]$ etc., in the above equations shows that every one of them is generally greater than 1 and approaches 1 as $h\nu_i \gg kT$. Assuming that the latter condition is fulfilled, we have

$$\left.\begin{matrix}\theta \\ \theta^2 \\ \theta^3\end{matrix}\right\}=P\frac{e^{\Delta\epsilon/RT}}{Q_0}. \qquad \begin{matrix}(3.1)\\(3.2)\\(3.3)\end{matrix}$$

The above equations give relations between θ and P, respectively, appropriate to the three different adsorbed states affording a method of experimental determination of them.

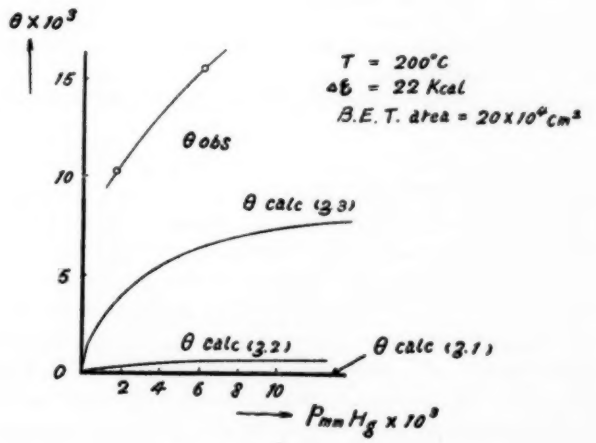

FIG. 2. Plot of θ against pressure.

* ▾ denotes the internal rotation around the axis of Si–C bond.

Adsorption isotherms of carbon dioxide were determined with special precaution for securing the thermodynamical equilibrium as described in the previous paper[3] at 150° and 200°C and for the equilibrium pressure ranging from 1×10^{-4} to 0.1 mm Hg.

The adsorbed quantities x were found to be proportional to about $\frac{1}{3}$ power of the equilibrium pressure at a very low degree of adsorption, the exponent decreasing as the adsorption proceeded further as shown in Fig. 1. The differential heat of adsorption calculated from the isotherms at the two temperatures according to the usual expression, $\Delta\epsilon=RT^2(\partial \log P/\partial T)_x$, was found almost constant at 22 kcal./mole over the range of the smaller adsorption.

Using the heat of adsorption, the covered fraction θ_{calc} was now calculated at 200°C, respectively, according to Eqs. (3.1), (3.2), or (3.3) and compared in Fig. 2 with θ_{obs} derived from the adsorbed quantities and the B.E.T.[4] area of the adsorbent assuming that 10^{15} nickel atoms per cm² were available each for adsorbing $CO_2(a)$, $CO(a)$, $C(a)$, or $O(a)$.

It is evident that θ_{obs} agrees fairly well with θ_{calc} derived from Eq. (3.3) and not with that from Eq. (3.1) or (3.2), hence showing that carbon dioxide molecule dissociates into three independent atoms at much the lower degree of adsorption. Somewhat too small value of θ_{calc} may be attributed to the simplification that $h\nu_i \gg kT$ in q's.

The investigation of carbon dioxide adsorption was carried out on reduced cobalt as well, leading to a similar conclusion. The details of these investigations will be given in the *Journal of the Research Institute of Catalysis* in the near future.

[1] Kwan, J. Res. Inst. Catalysis **I**, No. 2, 110 (1949).
[2] Horiuti, J. Res. Inst. Catalysis **I**, No. 1, 8 (1948).
[3] Kwan, J. Res. Inst. Catalysis **I**, No. 2, 81 (1949).
[4] Brunauer, Emmett, and Teller, J. Am. Chem. Soc. **60**, 309 (1938).

Erratum: The Raman Spectrum of Vinylidene Fluoride

WALTER F. EDGELL AND WILLIS E. BYRD
Department of Chemistry, University of Iowa, Iowa City, Iowa
[J. Chem. Phys. **18**, 892 (1950)]

THE G matrix for the A_1 vibrations of vinylidene fluoride appearing in the Appendix of the above article should read:

$$A_1: \quad \begin{matrix} \mu_H+2\mu_c\cos^2\delta & 0 & \sqrt{2}\mu_c\cos\delta & 0 & \sqrt{3}\mu_c\tau\sin2\delta \\ & \mu_F+2\mu_c\cos^2\gamma & \sqrt{2}\mu_c\cos\gamma & \sqrt{3}\mu_c\sigma\sin2\gamma & 0 \\ & & 2\mu_c & (6)^{\frac{1}{2}}\mu_c\sigma\sin\gamma & (6)^{\frac{1}{2}}\mu_c\tau\sin\delta \\ & & & 3\sigma^2(\mu_F+2\mu_c\sin^2\gamma) & 0 \\ & & & & 3\tau^2(\mu_H+2\mu_c\sin^2\delta). \end{matrix}$$

The **PREVENTION OF DETERIORATION ABSTRACTS,** published by the National Research Council (Prevention of Deterioration Center, Room 204), 2101 Constitution Avenue, Washington 25, D. C., are offered for subscription on a yearly basis. Abstracts are classified under the headings: Biological agents; Electrical and electronic equipment; Fungicides and other toxic compounds; Lacquers, paints, and varnishes; Leather; Lubricants; Metals; Miscellaneous; Optical instruments and photographic equipment; Packaging and storage; Plastics, resins, rubbers, and waxes; Textiles and cordage; and Wood and paper. One volume of approximately 2000 looseleaf pages is published each year in monthly issues. Subject and author indexes are compiled annually to cover abstracts issued from July through June. The yearly rate of $50.00 includes two sturdy binders and index tabs.

An **ADVANCE LIST,** a monthly bibliography of all reports received in this field, is available for $10.00 a year.